THE EFFECT OF ADSORBED POLY (VINYL ALCOHOL)
ON THE PROPERTIES OF MODEL SILICA
SUSPENSIONS

BY

CHANDRA KHADILKAR

A DISSERTATION PRESENTED TO THE GRADUATE SCHOOL
OF THE UNIVERSITY OF FLORIDA IN
PARTIAL FULFILLMENT OF THE REQUIREMENTS
FOR THE DEGREE OF DOCTOR OF PHILOSOPHY

UNIVERSITY OF FLORIDA

1988

ACKNOWLEDGEMENTS

I would like to express my sincere gratitude to Dr. M.D. Sacks for his invaluable guidance and financial support during the course of this study. I would like to thank him for allowing me to work in the area of colloid science and for demonstrating the importance of reproducibility and hard work in scientific research.

I am also grateful to Dr. C.D. Batich, Dr. L.L. Hench, Dr. D.O. Shah, and Dr. E.D. Whitney, members of supervisory committee, for their helpful suggestions.

I would like to thank Mr. H.W. Lee, Mr. O.E. Rojas, Mr. G.W. Scheiffele, Mr. S.D. Vora, and Mr. T.S. Yeh for their help during the course of this work. Thanks are also due to Professor B. Moudgil for allowing me to use spectrophotometer and Gel Permeation Chromagraphy apparatus. I would like to thank Ms. Hazel Feagle for typing, editing, and compilation of this dissertation.

I also wish to convey my sincere gratitude to my parents and to my wife for their encouragement and support during the course of this work.

TABLE OF CONTENTS

LIST OF TABLES

LIST OF FIGURES

Abstract of a Dissertation Presented to the Graduate School
of the University of Florida in Partial Fulfillment of the
Requirements for the Degree of Doctor of Philosophy

THE EFFECT OF POLY (VINYL ALCOHOL) ON THE
PROPERTIES OF MODEL SILICA SUSPENSIONS

By

Chandra S. Khadilkar

December 1988

Chairman: Dr. Michael D. Sacks
Major Department: Materials Science and Engineering

The effect of interparticle interactions on the properties of model
suspensions of monosized, spherical silica particles was investigated.
The electrostatic interactions between particles were controlled by
changing suspension pH. The effect of adsorbed polymer was investigated
using water soluble poly (vinyl alcohol), PVA. The adsorption was
dependent on a variety of factors including the overall polymer
concentration in suspension, PVA molecular weight, PVA degree of
hydroxylation, silica surface hydroxylation, and suspension pH. The
adsorption characteristics were correlated with the state of particulate
dispersion in suspension using rheological measurements. Suspension and
green compact properties were highly dependent upon the fraction of
silica surface covered by the adsorbed polymer and the thickness of the
adsorbed polymer layer. Suggestions are made for selecting polymer

molecular weight to prepare stable suspensions with higher solids

loading.

CHAPTER I
GENERAL INTRODUCTION AND AIM OF THE STUDY

Particle/liquid suspensions are prepared in various ceramic processing operations such as mixing, milling, spray granulation of powders, slip casting, tape casting, extrusion, etc. The control of rheological behavior of suspensions is important to maximize the processing efficiency and also to obtain the desired properties of the final products. The rheological behavior of particle/liquid suspensions can be modified by changing (1) particle characteristics (e.g., size and shape distribution), (2) liquid characteristics (e.g., viscosity), (3) particle concentration (solids loading of the suspensions), (4) interparticle forces in suspension, and (5) additives like dispersants, polymers, etc.

The interparticle interactions in suspensions can be broadly classified into two categories: (1) electrostatic interactions and (2) interactions due to adsorbed polymer. The electrostatic interactions arise due to development of charge at the solid/liquid interface. The electrically-charged interface leads to the formation of diffuse "electrical double layer" surrounding each particle. The overlap of two electrical double layers during Brownian encounter gives rise to repulsive forces between the particles which can overcome the Van der Waal's attraction. The effects of surface potentials (or charge) and ionic concentrations on the stability of dispersions can be quantitatively described using the "DLVO" theory (Chapter III).

1

Organic polymers are extensively used as processing aids in ceramic forming operations. In addition to acting as binders and plasticizers, polymers are often used to control the rheological properties of dispersions. The interactions between particles with added polymer are highly dependent on the adsorption behavior of polymer on particle surfaces. Generally, at low polymer concentrations in solution, suspensions can be destabilized (i.e., particles are aggregated) due to "bridging flocculation" where a polymer molecule can adsorb simultaneously onto two or more particles. At sufficiently high polymer concentrations in solution, under certain conditions, stable suspensions (i.e., in which primary particles are well separated) can be prepared. Two important factors controlling the interactions between the particles are (1) the fractional coverage of the particle by adsorbed polymer (which affects the bridging flocculation) and (2) the thickness of the adsorbed layer (which governs the stability at complete coverage in a good solvent).

A model ceramic powder (i.e., well-characterized, agglomerate-free, spherical, narrow-sized silica) was used in this investigation. The electrostatic interactions between particles were modified by varying the suspension pH and ionic strength. The effect of surface potentials on the flow curve parameters (i.e., extrapolated yield stress, relative plastic viscosity, etc.) were analyzed using the "elastic floc" model.

Water soluble poly (vinyl alcohol), PVA, was used to investigate the effect of adsorbed polymer on the suspension properties. PVA being a neutral polymer, the effects of electrostatic interactions and the effects of adsorbed polymer on the dispersion stability can be studied

less ambiguously. The concentration of PVA in solution can be readily determined; hence, the adsorbed amounts of PVA could be determined easily. The polymer adsorption behavior and rheological properties on the same system are rarely reported in literature. The adsorption experiments are generally carried out using dilute suspensions of high surface area, agglomerated powders, whereas rheological measurements are conducted on concentrated suspension where adsorption behavior and interparticle interactions are not very well defined. In this study, most of the rheological measurements and adsorption experiments were carried out at the same solids loading ($\approx$ 20 vol. %). The adsorption of PVA onto the silica surface was dependent on a variety of factors including the overall solution concentration, polymer characteristics (PVA molecular weight and degree of hydroxylation), silica surface nature, suspension pH, etc. The adsorption characteristics were correlated with the state of particulates in suspension using rheological measurements. Suspension rheological properties and green compact properties (e.g., relative density, median pore radius, etc.) were highly dependent on the fraction of silica covered by the adsorbed polymer and the thickness of the adsorbed layer.

A floc structure (i.e., floc compactness, strength, etc.) consistent with the rheological behavior and green compact characteristics is proposed. (Experimental techniques to obtain this information are not yet readily available). Finally, some suggestions regarding selection of polymers to achieve stable suspensions with high solids loading are made.

In the first part of thesis, we deal with general and theoretical concepts related to this work. In Chapter II, we describe the polymer

adsorption behavior at solid/liquid interface. Chapter III deals with the electrostatic interactions between colloidal particles, and Chapter IV deals with the effect of adsorbed polymer on dispersion stability. The effect of interparticle interactions on the state of particulate dispersion in suspension is described in Chapter V. The correlation between suspension structure and rheological behavior is discussed in Chapter VI. The silica preparation and characterization is described in Chapter VII. PVA fractionation and characterization is also described in Chapter VII. In Chapter VIII, we discussed experimental results obtained in this study. First, we describe the effect of electrostatic interactions on the rheological behavior of 20 vol.% silica suspensions. Subsequently, PVA adsorption behavior on silica particles is correlated with the rheological properties of suspensions and green compact characteristics.

CHAPTER II
ADSORPTION OF POLYMER AT SOLID/LIQUID INTERFACE

Introduction

Adsorbed polymer at solid/liquid interface has a profound effect on the stability behavior of suspensions. Typically, at low polymer dosages, flocculation of particles in the suspension can occur, while at the high polymer concentration, stable suspensions can be prepared. Polymer adsorption behavior has been extensively studied because of the present and the potential applications in industry, technology, and medicine. The polymer adsorption behavior is important in various processes (tape casting, slip casting, extrusion of ceramic parts, adhesion, separation of polymers, soil improvement, etc.) and various products (paints, cosmetics, magnetic tapes, pharmaceuticals, dyes, foods, lubricants, etc.). Theoretical interests in the polymer adsorption process stems from the fact that insight can be gained into the nature of the forces acting between polymer segments and surfaces and between particles coated with the adsorbed polymer. From the ceramic processing point of view, by the optimization of the adsorption process, one can control both the suspension properties as well as consolidated microstructures obtained from these suspensions.

The adsorption behavior of the polymer is different from the adsorption behavior of the small molecules (e.g., gas adsorption at solid/gas interface, surfactant adsorption, etc.). This difference

arises because polymers have a large number of internal degrees of freedom (i.e., flexibility).

Polymer molecules have a random coil type of arrangement in the solution. A full description of the shape of a molecule requires the description of the relative positions of each atom of the molecule (the configuration, see Flory 69). It is common to assume that a polymer chain consists of a number of connected chain segments for the theoretical treatments. Then, the conformation of the adsorbed polymer is described by specifying the relative positions of the endpoints of these segments (Kuhn 34). To understand the adsorption behavior of polymers, one needs to consider both the energetics and kinetics of the adsorption process. Polymer molecules experience short-range attractive forces near the adsorbing interfaces. For each polymer segment adsorbed on the surface, there is a decrease in the free energy of the system. At the same time, upon adsorption, the random coil structure of the polymer molecule in the solution will be distorted, which will lead to a decrease in the number of conformations of the adsorbed polymer. This entropic factor will oppose the adsorption process. Final conformation of the adsorbed polymer depends on this subtle balance between the entropic and the enthalpic terms. Also, though there is a small energy decrease due to adsorption process per segment of the polymer molecule, large number of segments per molecule can be adsorbed, and the total energy decrease per molecule can be quite large. Actual bonding mechanism between the polymer segment and the surface may involve various interactions such as electrostatic interactions, Van der Waal's interactions, hydrogen bonding or hydrophobic bonding.

The actual conformation of the adsorbed polymer near solid-liquid interface depends upon various factors such as solid-liquid, polymer-liquid and polymer-solid interactions, flexibility of the polymer molecule, concentration of the polymer in the solution, etc.

Experimentally, it has been found that the adsorption isotherm (i.e., adsorbed amount of polymer as a function of equilibrium concentration of polymer in solution at fixed temperature and pressure) of high molecular weight polymers display high affinity type of character, i.e., a steep initial part of the adsorption isotherm followed by a pseudo-plateau region. Adsorbed amounts at the plateau region are typically on the order of approximately one to four mg/m^2. This amount is much more than that can be accommodated in a close-packed monolayer of the polymer segments. This led early investigators to propose the conformation of the adsorbed polymer as shown in Figure 2.1 (Jenkel and Rumbach, 51). From Figure 2.1, it is clear that not all of the segments of the adsorbed polymer are in direct contact with the surface. This type of conformation is commonly called as "train-loop-tail" conformation. "Train" is defined as a sequence of consecutive segments in direct contact with the surface. "Loop" is defined as a sequence of segments with the end segments in direct contact with the surface, and remaining segments are in contact with the solution. "Tail" is defined as the portion of the chain with end segments in contact with the surface. From this type of conformation, it is clear that there is a significant change in the polymer conformation upon adsorption compared to the random coil arrangement in the solution and that the adsorbed polymer has sufficient extension in the solution. Actual details of the

Train-Loop-Tail conformation of Adsorbed Polymer

Tail

Loop

Liquid

Train

Solid
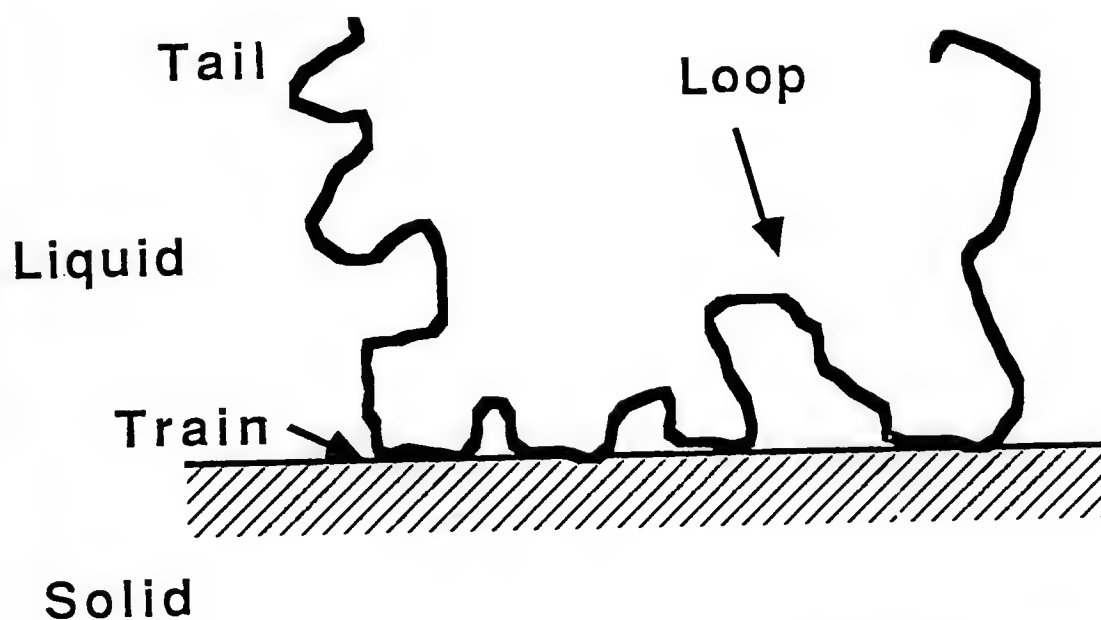
Figure 2.1   Schematic representation of an adsorbed polymer molecule.

conformation are dependent on the various factors mentioned previously. Some other types of conformations of the isolated adsorbed polymer molecules are shown in Figure 2.2 (Sato and Ruch 80).

Description of Adsorbed Polymer

The adsorption behavior of the polymers at the solid/liquid interface is commonly characterized using the following parameters.

Adsorbed Amount of Polymer (A)

This is the most commonly measured parameter in any adsorption experiment and is usually obtained by "solution depletion" techniques. Adsorbed amounts are commonly expressed in the units of mg of polymer adsorbed per unit area of the solid surface. It is also common to define the dimensionless adsorbed amount or adsorbance, γ, as the number of segments adsorbed per surface site or the number of (equivalent) complete monolayers than can be formed from the adsorbed amounts (Cohen Stuart 80a). This means that γ is the ratio between the adsorbed weight per unit area and the weight adsorbed per unit area in a complete monolayer, A_{mon}.

$$\gamma = A/A_{mon} \tag{2.1}$$

As we have seen earlier, there is a conformational change upon the adsorption of the polymer. Hence, for a complete description of polymer adsorption, it is not sufficient to measure only the adsorbed amount of polymer, as similar adsorbed amounts could be obtained for the thick adsorbed layer of polymer with low segment concentrations or thin adsorbed layer with high segment concentration.
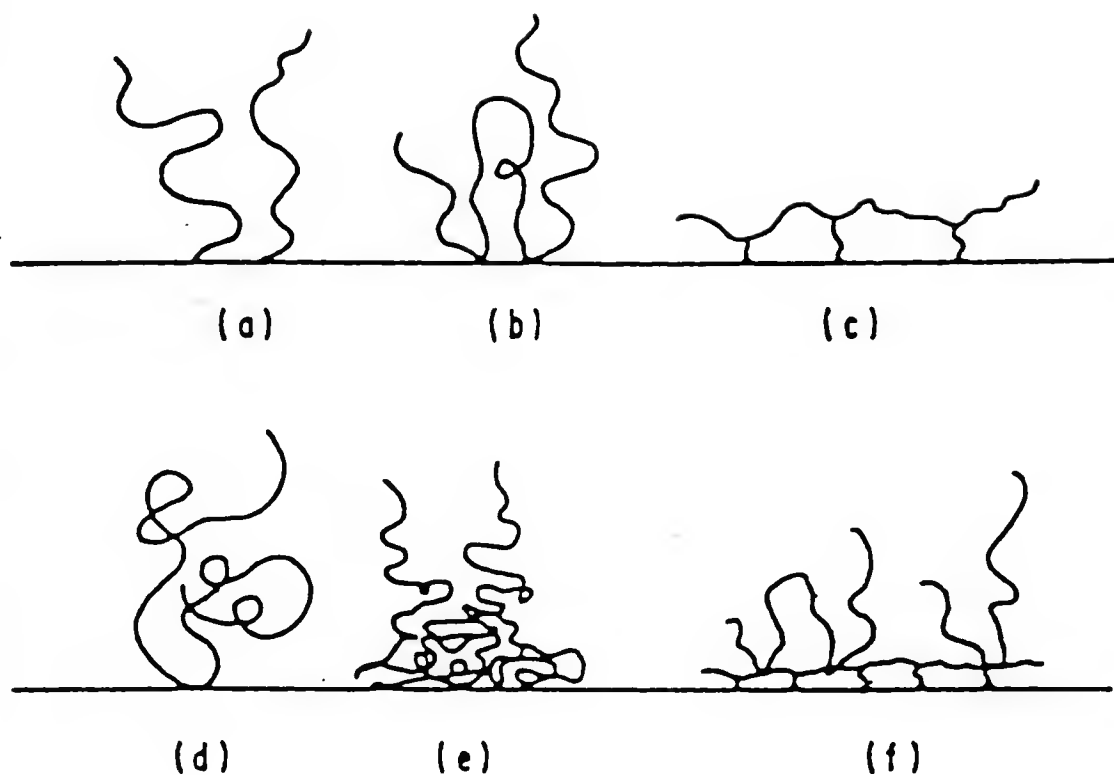
Figure 2.2   Conformations of adsorbed polymer molecules (a) single
point attachment, (b) train-loop-tail adsorption,
(c) flat multiple site attachment, (d) random coil,
(e) nonuniform segment distribution, and (f) multilayer
(Sato and Ruch, 1980).

Bound Fraction (p)

This is defined as the fraction of adsorbed amount of polymer in direct contact with the surface, i.e.,

$$p = A_{tr}/A \tag{2.2}$$

where A_{tr} is the amount of polymer adsorbed per unit area in trains. The bound fraction measures the change in the conformation upon adsorption. The p close to one indicates the polymer lies flat on the surface having two-dimensional structure; on the other hand, p close to 0 indicates polymer has essentially random coil shape with no significant change in conformation (Figure 2.c).

Direct Surface Coverage (θ)

This is defined as the fraction of the available surface sites occupied by polymer segments.

$$\theta = A_{tr}/A_{mon} \tag{2.3}$$

where A_{tr} and A_{mon} as defined previously and from the definition of θ and p, it follows that

$$\gamma = \theta/p \tag{2.4}$$

Segment Density Distribution ρ (X, Y, Z)

Segment density is the time-averaged volume fraction of segments per unit volume in the vicinity of the polymer molecule. In solution, many polymers adopt random coil conformation. For such a random coil, the segment density averaged on all conformations is usually Gaussian in any direction passing through the center of the molecule. (More accurately, the distribution is better represented by a prolate ellipsoid of revolution, see Flory 53.) Upon adsorption, there is a significant change in the conformation of the polymer molecules. At low adsorption

density (i.e., isolated polymer molecules) the segment density

distribution will be dependent upon Z (i.e., distance from the adsorbing

surface) and also on X, Y (ie., position parallel to the surface). At

higher adsorption densities, there will be a significant lateral

interpenetration of the molecules (since the volume percent occupied by

the segments is approximately ten percent at typical segment densities,

i.e., there is enough empty space in a given polymer molecule) and the

segment density distribution will be dependent on Z only. This segment

density distribution is the most important feature of the adsorbed

polymer in the theory of steric stabilization. Various types of segment

density distributions have been proposed for the adsorbed polymer and

will be reviewed later (Napper 83). The segment density distribution

determines the extension of the adsorbed polymers into the solution

phase. This extension of the adsorbed polymer layer can be expressed in

terms of a thickness parameter such as the root mean square layer

thickness δ, which is defined as follows:

$$\delta^2 = \int_0^\infty Z^2 \rho (Z) \, dZ / \int_0^\infty \rho (Z) \, dZ \qquad (2.5)$$

Theoretical Models

The adsorption behavior (and hence, conformation) of polymers at

solid-liquid interface is governed by various factors including polymer

segment-surface, surface-solvent, and segment-solvent interactions. The

driving force for the adsorption is the reduction in the net free energy

due to bonding of a polymer segment to the surface. This binding process

involves the removal of the solvent molecule from the surface and

replacement with the polymer segment. Energy change associated with this

process is denoted by the dimensionless adsorption energy parameter, X_S. This polymer adsorption process is opposed by the entropy changes associated with the changes in conformation upon adsorption. Polymer molecules have three-dimensional random coil structure in solution, and upon adsorption, some of the segments (i.e., train) are restricted to two dimensions.

This process is associated with considerable loss of entropy per molecule, and the magnitude depends on the chain length and flexibility. At equilibrium, the distribution of polymer molecules between the surface and the solution is essentially determined by the following five independent parameters: concentration of the polymer in solution, chain length (molecular weight), flexibility, adsorption energy parameter, and polymer-solvent interaction parameter. Variables, such as temperature, time (kinetics), and polydispersity, may also play an important role. Below, we will define some of these variables and discuss the effect of these independent variables on the adsorption.

Adsorption Energy Parameter (X_S)

As mentioned earlier, the bonding between the surface and the segment is the driving force for adsorption. A precise definition of X_S is due to Silberberg (Silberberg 68). The energy change (i.e., net enthalpy change) associated with the transfer of a polymer segment in a pure polymer from a bulk site to a surface site, minus the corresponding energy change for a solvent molecule in pure solvent, is denoted by $-X_S kT$. By choosing proper reference states (i.e., pure polymer and pure solvent), X_S is made independent of solvent-segment interactions and

depends only on the nature of the surface. It is clear from the definition that for $x_s > 0$ indicates segments are preferred over the solvent by the surface. Due to adsorption, polymer loses part of its conformational entropy and will oppose the adsorption. Hence, a certain minimum adsorption energy, denoted by x_{sc}, is required for the adsorption to take place.

Segment-Solvent Interaction Parameter (χ)

Linear, flexible polymer molecules have a random coil shape in the solution. For an "ideal" chain (i.e., polymer molecule represented as chain consisting of volumeless, non-interacting statistical units), this random coil conformation can be described by random walk in three dimensions. For an ideal chain, it can be shown that the radius of gyration is proportional to the molecular weight of the polymer and can be represented by the following equation:

$$<r^2>^{1/2} \alpha M_w^{0.5} \tag{2.6}$$

where $<r^2>$ is the root mean square radius of gyration and M_w is the molecular weight of the polymer (Flory 53). However, real chain segments have volume and interact with each other, and this effect is usually represented by the excluded volume effect, which can be defined in terms of either segment-segment interaction energy or in the framework of the Flory-Huggins theory of polymer solutions as the segment-solvent interaction parameter, χ. The parameter χ represents the quality of the solvent. Theoretically, $\chi < 0$ for a very good solvent, $\chi = 0$ for an athermal solvent, and $\chi = 1/2$ for an ideally poor or a θ solvent. χ represents an exchange process (and in such a way that), χkT represents

the difference in energy of a solvent molecule immersed in a pure polymer compared with one surrounded by pure solvent molecules. For $\chi > 0$, the solvent is poor and segment-segment contacts are preferred over segment-solvent contacts. The adsorption of polymer at the solid-liquid interface leads to an increase in the concentration of the segments near the surface, and the segment-segment or the segment-solvent interaction parameter has a profound effect on the adsorption. In poor solvents, adsorbed amounts of polymer are larger due to the fact that segments prefer other segments over solvent molecules. The χ parameter is one of the basic parameters of the polymer solution thermodynamics, and hence, plays an important role not only in the polymer adsorption behavior but also in the theories of steric stabilization.

Polymer Adsorption Theories: General Framework

The aim of polymer adsorption theories is to try to relate the conformations of the adsorbed polymer molecules to independent variables (such as adsorption energy parameter, χ_S, solvent-segment interactions, χ, molecular weight of the polymer, M, its concentration in solution, etc.). Various investigators have paid a lot of attention to the theoretical development of these models (for e.g., see Eirich 77; Hoeve 65,66,70,71; Silberberg 62,67,68; Scheutjeans and Fleer 79,80; deGennes 80,82,87). Since a large number of polymer molecules are involved, a statistical thermodynamic approach is usually employed. Contributions of the entropy and the energy of many chains in a given concentration gradient near the surface are evaluated. To evaluate these contributions, the thermodynamic theory of polymer solutions, as

developed by Flory and Huggins, is often employed (Flory 53). More
recently, scaling concepts have been applied to the polymer adsorption
(deGennes 87).

To describe polymer adsorption behavior, according to the methods of
statistical mechanics, the partition function of the system is set up
(see, Cohen Stuart 80a).

$$Q = \Sigma \ \Omega \ e^{-U/kT} \tag{2.7}$$

where Ω is the degeneracy, i.e., the number of different ways of
arranging systems having energy, U.

To evaluate Ω and U, appropriate reference states are chosen
(usually unmixed pure components). To evaluate Q, all possible energy
states of the system are considered. To determine the equilibrium state
of the system, Q is maximized. For example, Q is related to the free
energy of the system by

$$G = -kT \ Ln \ Q \tag{2.8}$$

and hence, G should be at minimal for equilibrium. To evaluate and
maximize Q, one needs to make certain assumptions, and the quality of
these assumptions leads to differences between various theories.

The earlier polymer adsorption theories (for e.g., Hoeve, Roe,
Silberberg, etc.) were formulated to describe the conformations of
isolated polymer chains. In these theories, train-loop-tail type of
polymer conformation was assumed. The chain conformation statistics,
such as average train, loop sizes, and tail, loop size distributions were
computed (but, tails were ignored). The segment-surface interaction was
taken into account using the adsorption energy parameter, X_S, (i.e.,
first layer interactions), but the solvent-segment interaction was
ignored. Since these early theories ignored solvent-segment interactions

and formulated for isolated chains (i.e., non-interacting with other adsorbed polymer molecules), their usefulness is limited.

Later theories employed Flory-Huggins polymer solution model to account for segment-segment and segment-solvent interactions (Hoeve, Silberberg, Roe, Scheutjeans and Fleer). The theories of Hoeve and Silberberg start with the train-loop model of the adsorbed polymer (i.e., tails were neglected) and the conformation probabilities of the adsorbed chains were computed. To evaluate U, assumptions were made regarding the shape of the segment density profile. Hoeve assumed the exponential profile for the evaluation of U (i.e., segment-segment, segment-solvent interactions) while Silberberg assumed step function for the segment density profile (Silberberg 68). This assumption regarding segment density profile to evaluate U has been avoided in the recently developed theories of Roe, Scheutjeans and Fleer (Roe 74, Scheutjeans and Fleer 79,80). These theories do not assume a model for the mode of polymer adsorption of an individual molecule. They derive the partition function for the mixture of free and adsorbed polymer chains and solvent molecules; a number of ways of arranging polymer chains and solvent molecules in a given (arbitrary, but fixed) concentration gradient near the surface was determined. Maximization of the partition function gives the equilibrium concentration profile (Scheutjeans and Fleer 79,80). To evaluate U, segment-segment and segment-solvent interactions were calculated using Flory-Huggins theory. Roe neglected the tails in evaluation of the energy term and his model predicts overall segment density profile. Later theory (SF) gives the complete distribution of polymer conformation near the surface and gives information about train,

loop, and tail distributions. The important difference between the Roe and the SF theory is the contribution of the long dangling tails to the overall segment density profile at relatively large distances from the interface, and these long tails can play an important role in the flocculation and stabilization of the system. Unfortunately, no simple analytical expressions are available with these theories and substantial computational time is required to calculate the conformation of the adsorbed polymer.

The scaling relation applicable to semi-dilute polymer solutions has been extended for the polymer adsorption problem by deGennes (see, deGennes 87). This theory is limited to athermal solvent (good solvent with $\chi = 0$) with moderate adsorption energies. Though this theory is analytical, the results are in the form of power-laws without exact coefficients.

In the next section, some of the predictions of these polymer adsorption theories will be discussed. These theories are mostly applicable for mono-dispersed homopolymers polymer on a homogeneous substrate. Other complications arising due to inhomogeneous surface structure and charge at the interface are not taken into account.

Results of the Polymer Adsorption Theories

In this section, the dependence of properties of the adsorbed polymer layer (such as total surface coverage (i.e., the adsorbed amounts A), direct surface coverage (i.e., occupancy in the first layer θ), bound fraction (p), root mean square layer thickness (δ), segment density distribution) on various independent variables (such as solution

concentration, chain length, χ and χ_S) will be reported. Only general trends will be reported. For detailed comparison between various theories, recent reviews are recommended (Fleer 87, Fleer and Lyklema 83).

Effect of Adsorption Energy Parameter (χ_S)

All theories predict that the adsorption energy parameter should exceed a certain critical (non-zero) adsorption energy, i.e., $\chi_S > \chi_{SC}$ for the adsorption of polymer to take place. This critical adsorption energy parameter χ_{SC} corresponds to the minimum energy necessary to compensate the unfavorable entropy loss of the segment, upon adsorption, compared to segment in solution. If the $\chi_S > \chi_{SC}$, then the surface coverage increases sharply with increasing χ_S. At high χ_S values, the surface becomes saturated and the total surface coverage θ, becomes independent of χ_S. For lattice theories, the critical value of χ_{SC} is related to the lattice type employed (Scheutjeans and Fleer 79,80).

Effect of Solvent-Segment Interaction Energy Parameter (χ)

The effect of solvent on adsorption behavior is pronounced. The adsorbed amount of polymer increases while bound fraction p decreases with decreasing quality of the solvent (i.e., as the solvent becomes poorer). (Though the adsorbed amount and the direct surface coverage are increased, the ratio, the bound fraction p is decreased.) Average loop and tail size are increased with decreasing the quality of solvent (Scheutjeans and Fleer 79,80).

Effect of Polymer Concentration and Molecular Weight

Adsorption isotherms for high molecular weight polymers are the high affinity type. Adsorbed amounts are high for higher molecular weight

polymer. For a good solvent, adsorbed amounts tend to reach a limiting value for high molecular weights, but from a poor solvent, various theories predict different trends. The increased amounts of adsorbed polymer with increasing molecular weight (and concentration in solution) are accommodated by increases in the average size of the loop and tails. This leads to an increase in the thickness of the adsorbed layer with increasing polymer concentration and molecular weight. For a low polymer concentration (typically, $\phi_p <$ .01, where ϕ_p is the volume fraction of polymer in the solution), the adsorbed amount in a θ-solvent increases linearly with log Mw. This dependence, as predicted by SF theory, is different from the empirical power law relations, i.e., $A \propto M_w^a$, where A is the plateau adsorbed amount of polymer (mg/m^2) and a is an empirically determined constant. For dilute concentration, the bound fraction decreases with increasing molecular weight. Root mean square thickness also increases with the molecular weight and the concentration.

The effect of tails, ignored in the earlier theories, is important at finite polymer concentrations. (At extremely low polymer concentrations, the adsorbed polymer lies in relatively flat configuration). These tails will affect the average layer thickness and the segment density profile at the outer region of the adsorbed layer, and hence, will be very important for colloidal stability.

The segment density distributions predicted by various theories are very important in various theories of steric stabilization. As mentioned earlier, Hoeve assumed an exponential segment density distribution (Hoeve 65) whereas Silberberg assumed it to be step function (Silberberg 68). Roe and SF theory can calculate segment density distributions without any

assumptions (Roe 74; Scheutjeans and Fleer 79,80). Both theories predict
an approximately exponential segment density distribution near the
surface. At larger distances, S.F. theory predicts a high density
compared to Roe's theory. This higher density is due to long dangling
tails. These long tails can dominate interparticle interactions and the
hydrodynamics of coated particles. The tail length increases with
increase in the molecular weight almost linearly for high molecular
weight polymer (Cohen Stuart 80a). Hence, molecular weight of the
polymer is among the most important variables for controlling rheological
and other properties of the dispersion. In the next section, various
experimental techniques used to characterize polymer adsorption will be
briefly described.

Experimental Techniques

An excellent review is available for the details of various
techniques (Cohen Stuart, et al. 86a). Adsorbed amount A, direct surface
coverage θ, bond fraction p, layer thickness δ, and segment density
distribution (Z), can be characterized experimentally.

The Adsorbed Amount of Polymer

Generally, a "solution depletion" technique is used to determine the
adsorbed amount of polymer. In this method, from the equilibrium and
initial known concentrations of polymer in solution, the adsorbed amount
of polymer is determined. Centrifugation is commonly used to separate
particles from the suspension, and the supernatant is analyzed. Various
analytical techniques are used to determine the solution such as
gravimetric, complex formation to give species which adsorb in the UV or

visible part of the electromagnetic spectrum (Zwick 65), etc. In certain cases, direct determination of the adsorbed amount is possible (e.g., IR, ellipsometry).

Trains, Bound Fraction, Direct Surface Coverage

Techniques to determine these parameters are broadly classified into spectroscopic methods, electrochemical methods, and calorimetric methods.

(1) Spectroscopic Techniques: Spectroscopic techniques include infrared (IR), electron spin resonance (ESR), and nuclear magnetic resonance (NMR). Due to specific interactions between polymer segments and solid surface, shifts in a characteristic band, either for the adsorbate (e.g., the carbonyl or benzene group in a polymer) or the adsorbent (e.g., the hydroyl group on an oxide) is utilized to determine the bound fraction using IR spectroscopy (for e.g., see Killmann 76; Takahashi et al. 80; Fontana et al. 61,63,66; Korn et al. 80a,80b, etc.). ESR can only be used for spin labeled polymers (Robb and Smith 74). Mobility criteria are used to distinguish between adsorbed and non-adsorbed segments. Segments having different mobility will give different magnetic relaxation times and hence mobility. NMR technique is also based on the mobility criterion to estimate p.

(2) Electrochemical Methods: Adsorbed neutral polymer affects the electrical double layer properties (such as change in the double layer capacitance and shift in the point of zero charge, PZC). These properties can be utilized to determine the fraction of surface area occupied by segments, θ (Koopal 78).

(3) Microcalorimetric Approach: In this method, the heat of immersion of adsorbent is measured at various adsorbed amounts of polymer.

Calibration can be achieved from the heat of immersion of a monomeric

analog compound of the adsorbed group (Korn et al. 80a,80b; Cohen Stuart

et al. 82; Killmann et al. 71; Hair 77).

There are several problems associated with these techniques, such as

distinguishing between contributions due to adsorbed and non-adsorbed

polymer, differentiation between train and loop segments, etc.

Thickness of the Adsorbed Layer

Methods to determine the thickness of the adsorbed polymer layer can

be divided into two broad categories: (1) ellipsometry and

(2) hydrodynamic methods.

(1) Ellipsometry: In this method, change in the properties of the

elliptically polarized light upon reflection, due to the adsorbed

polymer, is measured. From the measured phase shift and the amplitude of

the reflected light, under the assumption of homogeneous polymer layer,

the ellipsometric thickness and the refractive index of the film can be

calculated (e.g., see Killmann 76,77). Clearly, the assumption of

homogeneous segment density distribution leads to ambiguity in the

measured thickness. Also, this method is suitable for flat surfaces with

good reflectivity, and hence, limited mostly to bulk metal substrates and

some oxide films.

(2) Hydrodynamic Methods: These methods measure the extent of outward

shift of the slip plane due to the adsorbed polymer layer. Essentially,

they measure the drainage characteristics of the adsorbed layer, and

since the drainage characteristics of the adsorbed polymer layer (i.e.,

consisting of loops and tails) are not known, an exact definition of the

hydrodynamic thickness is not possible. Also, if the adsorbed polymer

layer is not homogeneous (e.g., at low adsorption densities), this method may over estimate the thickness. To measure the hydrodynamic thickness, several techniques have been employed.

(i) <u>Capillarity</u>: In this method, the inside wall of the fine capillary is coated with the adsorbed polymer layer, and the decrease in the flow rate due to adsorbed layer is measured (i.e., the effective decrease in the diameter of the capillary is determined). In this method, homogeneous coating of the capillary is critical (e.g., see Rowland and Eirich 66; Priel and Silberberg, 78).

(ii) <u>Viscometry</u>: In this method, the increase in the viscosity of the suspension of dispersed particles due to adsorbed polymer layer is measured. Due to the adsorbed polymer layer, there is an increase in the effective radius of the particle, hence, higher effective volume fraction solids in the suspension. For dilute dispersions, the intrinsic viscosity, [η], is measured (Barsted et al. 71; Dawkins and Taylor 80) while, for the concentrated suspensions, the high shear viscosity is determined (Dobroszkowski and Lambourne 66). To get information about the adsorbed layer, other parameters affecting the viscosity must be taken into account. Factors such as electroviscous effects, aggregation of particles, effect of shear on the thickness of the adsorbed layer, polymer degradation, etc. can complicate the interpretation. In this study, the adsorbed polymer thicknesses are determined from the high shear rate viscosities. The effect of PVA molecular weight on the adsorbed layer thickness will be reported later.

(iii) <u>Photon Correlation Spectroscopy</u>: In this method, the diffusion coefficients of the particles with and without adsorbed polymer are

measured using "Doppler" broadening of an incident laser line (for e.g., see van den Boomgaard et al. 78; Kato et al. 81; Garvey et al. 76; Killmann et al. 85,86,88, etc.). From the measured diffusion coefficients, the particle radius, and hence, the adsorbed layer thickness, is calculated using the Stokes-Einstein equation:

$$D = kT/6\pi\eta_o R_h \qquad (2.9)$$

where R_h = hydrodynamic radius of the particle, η_o = viscosity of the suspension medium, T = absolute temperature, and k = Boltzmann constant. This method is limited to monosized, spherical particles.

To obtain accurate values of the adsorbed layer thickness, diffusion coefficients are determined at various solid concentrations and the plot of diffusion coefficient vs. solid concentration is extrapolated to zero solids concentration. This procedure then eliminates the effects of interparticle interactions on the diffusion coefficient. As the adsorbed polymer layer is usually a small fraction of the particle radius, it is essential to obtain accurate values of particle radii with and without polymer.

(iv) <u>Electrokinetics</u>: In this method, the decrease in the electrokinetic potential (Zeta potential) of the charged particles, due to adsorption of neutral polymer, is measured to estimate the hydrodynamic thickness. Essentially, this method measures the outward displacement of the slip plane due to adsorbed polymer. Again, several complications are present in interpreting this data and the measured thickness is very sensitive to the ionic strength of the solution (Koopal 78; Cohen Stuart et al. 84a,84b,85).

(v) <u>Other Methods</u>: Sedimentation rate (i.e., change in the sedimentation coefficient due to the adsorbed polymer layer), (Garvey et al. 74) direct force-distance measurements (i.e., half the distance at which a certain minimum force is observed between two approaching surfaces, coated with the adsorbed polymer), etc., have been used to measure the thickness of the adsorbed layer (Sonntag et al. 82; Lubetkin 88; Gotze and Sonntag 87,88).

From the above discussion, it is clear that there are several techniques available to measure the layer thickness, but due to uncertainty about the effect of the tail-loop conformation of the adsorbed polymer on the properties of measured layer thickness, each technique gives some kind of average property of the adsorbed layer. Recently, it has been shown that the hydrodynamic thickness is essentially determined by the tails and that the loop contribution is negligible (Cohen Stuart 86a).

<u>Segment Density Distribution</u>

Small angle neutron scattering (SANS) has been used to obtain the segment density distribution for the adsorbed polymer. In this technique, the ability of neutron to distinguish between hydrogen and deuterium atoms, due to different coherent scattering cross sections, is utilized. By using a suitable mixture of H_2O/D_2O, particles can be contrast matched, and by measuring scattering intensity at various angles, information about the adsorbed polymer can be obtained. Unfortunately, the method is not sensitive enough yet to detect small concentrations of the tail segments at larger distances (Barnett et al. 82).

Adsorption Energy Parameter

As mentioned earlier, X_s represents the energy change associated with the exchange process of replacing solvent molecule from the surface with the polymer segment. Cohen Stuart has proposed a method to measure this parameter (Cohen Stuart 80a). In this method, a second solvent having strong affinity for the surface is added to the solution. With increasing concentration of the solvent (displacer), eventually polymer can be desorbed completely from the surface, and from this critical displacer concentration, X_s can be determined.

Adsorption of Polydisperse Polymers

Polymers used in practical application are mostly polydisperse, and polydispersity has an important effect on the adsorption behavior. This effect arises due to the difference in the adsorption behavior of long and short molecules. Long molecules are preferentially adsorbed over short molecules. As discussed earlier, the adsorption process is controlled by the various free energy changes related to adsorption process. The energy decrease due to adsorption of polymer segments is opposed by the entropy loss. The decrease in entropy arises from two contributions: (1) the loss of configurational entropy due to the unmixing of polymer molecules and solvent molecules and (2) the decrease in conformation entropy due to the decrease in number of different possible arrangements of the polymer as a result of the attachment of segments to the solid surface. In dilute solutions, which is of practical interest in most adsorption studies, the conformational entropy losses for one large chain compared to two shorter chains, each half the

length of the loner chain length, are similar. However, the decrease in
configurational entropy for the two short chains is twice that of the
longer chain. Hence, adsorption of the long chain is preferred over the
two short chains. Also, the long chain can displace the short chains
from the surface. Theory based on the above principles has been
developed, and it is successful in explaining various effects arising due
to the polydispersity of polymers (Cohen Stuart 80a,80b,84a; Koopal 81).

(1) Rounding of the adsorption isotherms: All polymer theories and
experiments using monodispersed polymers exhibit sharp adsorption
isotherms, whereas polydisperse samples lead to more rounded isotherms.

(2) Irreversibility: The observed irreversibility of adsorption
isotherms can be explained from the above theory.

(3) The effect of amount of adsorbent on the amount adsorbed and
the shape of the adsorption isotherm: Experimentally, it has been found
that the adsorption isotherms are sharper and the plateau adsorbed
amounts larger if the adsorption isotherms were determined using dilute
dispersions (i.e., small surface area/volume of the solution ratio)
(Koopal 81).

Preferential adsorption of the high molecular weight polymer over
the low molecular weight leads the fractionation of the polymer. The
molecular weight distribution in the adsorbed layer is shifted to higher
molecular weight as compared to that in the solution (Furusawa et al.
82). Also, from the practical processing point of view, the
preferentially adsorbed high molecular weight fraction may dominate the
properties of the dispersions, such as the rheology and the consolidation
behavior.

Additional factors, such as the charge on the solid surface and the effect of the solid surface structure, will be discussed in the experimental section.

Experimental Results for PVA-Water System

Properties of Poly (Vinyl Alcohol), PVA

PVA is a commonly used polymer as a steric stabilizer in aqueous media. PVA is prepared by alcoholysis of poly (vinyl acetate), PVAc, and is generally <u>not</u> hydrolysed fully. (Often the degree of hydrolyses is on the order of 88 mole percent or greater). It is, therefore, a copolymer of PVAc and PVA. This can be represented as follows:

$$CH_2 = CHOAc \xrightarrow{\text{Polymerization}} -CH_2-CH-CH_2-CH-CH_2- \\ \hspace{6cm} | \hspace{1cm} | \\ \hspace{6cm} OAc \hspace{0.6cm} OAc$$

vinyl acetate

poly (vinyl acetate)

$$\xrightarrow{\hspace{3cm}} -CH_2-CH-CH_2-CH-CH_2-CH- \\ \hspace{3.5cm} | \hspace{1.2cm} | \hspace{1.2cm} | \\ \hspace{3.5cm} OH \hspace{0.8cm} OAc \hspace{0.7cm} OAc$$
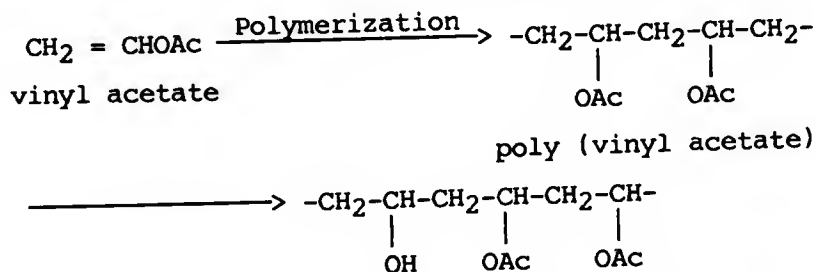
poly (vinyl alcohol) containing acetate groups.

where symbol OAc represents acetate groups, -COOH. Copolymers have been shown to be the best steric stabilizer for the following reasons: Usually, they consist of two types of segments having contrasting solubilities in a given aqueous or non-polar dispersion media. Less soluble segments of the copolymer will preferentially attach themselves to the solid surface, and thus, the polymer is firmly anchored to the surface. Thus, such a copolymer then consists of two types of segments, anchoring moieties and stabilizing moieties. Strong attachment of the polymer with the surface will prevent desorption of polymer or lateral movement of the polymer on the surface when two particles coated with

with adsorbed polymer will be encountered during Brownian collisions. In good solvents, the stabilizing moieties will offer repulsion, due to overlap of segments (i.e., due to osmostic effects).

This copolymeric nature of PVA makes direct comparison between experimental results and theoretical predictions difficult and only qualitative trends will be discussed. Also, the previously discussed theories were mainly developed for the monosized, homopolymers, while commercial polymers are usually polydispersed. In this section, available literature on the PVA adsorption behavior on various substances will be reviewed.

Two types of PVA's, i.e., partially hydrolysed, PVA88, (approximately 88 percent hydrolysed) and completely hydrolysed, PVA98, (greater than 98 percent hydrolysed) have been employed in various experimental investigations. Boomgaard et al. fractionated as-received polymer by sequential addition of acetone (i.e., a non-solvent) to approximately five wt.% PVA solution (van den Boomgaard et al. 78). Garvey et al. used preparative scale Gel Permeation Chromatography (GPC) to obtain narrow molecular weight fractions (Garvey et al. 74). These investigators did not measure the polymer molecular weight distribution or the polydispersity index M_w/M_n, where M_n is number average molecular weight and M_w is the weight average molecular weight. Acetone fractions gave fractions of varying molecular weights, but the degree of hydrolysis was also different for different fractions. (The degree of the hydrolysis decreased from the approximately ninety to approximately eighty mole percent with the decrease in the molecular weight) (van den Boomgaard et al. 78). Other studies used as-received commercial polymer.

PVA Characterization

From IR and UV spectra, Koopal concluded that the commercial samples used in his study were atactic and contained no or very little impurities (impurities, such as 1,2 glycol units and one or two conjugated groups if present are present as the end groups) (Koopal 78). The acetate group distribution is "blocky" for the PVA88, and acetate groups were distributed more or less "randomly" for the PVA98. Dunn (Dunn 80) and Barnett et al. (Barnett et al. 82) assumed that for the PVA88, the average block consists of three acetate groups. They assumed that the average acetate block size increases and the width of the acetate block size distribution increases with increasing PVA molecular weight.

The Mark-Houwink-Sakurada (MHS) equation was generally used to determine the viscometric average molecular weight, M_υ of the polymer.

$$[\eta] = kM_\upsilon^a \qquad \text{(MHS)} \qquad\qquad (2.10)$$

where $[\eta]$ is the intrinsic viscosity and k and a are MHS empirical constants. The values of the constants k and a used by various investigators are different. This can lead to different values of M_υ for the same polymer (i.e., same $[\eta]$). The values of k and a are dependent on the temperature, the acetate content, and the polydispersity of the sample. The value of constant a was in the range of 0.64 to 0.60 for PVA98 and was in the range of 0.71 to 0.63 for PVA88 (e.g., see Koopal 78). The PVA solution properties (i.e., the segment-solvent interaction parameter χ) and polymer molecule dimensions in solution (i.e., radius of gyration, end to end distance, etc.) were determined from the measured intrinsic viscosity and molecular weight for a series of samples with varying molecular weights. If these two quantities are not independently

available, then the MHS equation (Equaiton 2.9) was used to determine M_υ from the measured intrinsic viscosity. Hence, the values of solution properties and polymer molecule dimensions were influenced by the values of constants k and a used. For this reason, these values (i.e., χ, $<r>^2$, etc.) should be compared with caution since different values of constants k and a are employed by various investigators.

(1)   The Segement-Solvent Interaction Parameter: χ

Detailed comparison of the available values of χ parameter has been made by Koopal (Koopal 78). At 25°C in aqueous solutions, the χ values were in the range of 0.462 to 0.488 for PVA88 and in the range of 0.475 to 0.499 for PVA98. Thus, the degree of hydrolysis does not have significant effect on the solvent quality for typical PVA polymers. It should be noted that the aforementioned values of the χ parameter indicate that water is a relatively poor solvent for PVA. This also suggests that intersegmental interactions occur in the polymer chain (Koopal 78). van den Boomgaard et al. have determined the effect of temperature on the χ parameter (van den Boomgaard et al. 78). With increase in the temperature from 25°C to 50°C, the χ value changed from 0.464 to 0.485, indicating worsening of the solvency for PVA. Tadros and Vincent and Barker and Garvey have determined the effect of type and electrolyte concentration on the solvency (Tadros and Vincent 79; Barker and Garvey 80). With increase in the electrolyte concentration, the solvency decreases. They also found that Na_2SO_4 has greater effect on solvency compared to NaCl, i.e., lower concentration can change solvent quality.

(2) The X_S Parameter:

One needs to measure the adsorption energy parameter for both acetate and alcohol groups since the PVA adsorption mechanism may involve adsorption of these two groups. Heat of adsorption of low molecular weight analogues may be useful with this respect, but X_S values are not available for the various systems investigated. Typically, values in the range 1 - 2 kT have been assumed for X_S (Barnett et al. 82).

The Adsorbed Amount of Polymer

The Nature of Solid

PVA adsorption behavior has been studied on AgI solid particles (Fleer 71), AgI particles and sol (Koopal 78), silicas of various types (e.g., precipitated, Cab-o-sil, Ludox, Tadros 78), polystyrene latex particles (made by emulsion and dispersion stabilization, Garvey, et al. 74,76), montmorillenite clays (Greenland 62, Heath and Tadros 83). Due to differences in the chemical nature and surface heterogeneities (e.g., silica powder calcined at various temperature leads to various types of surface groups and the concentration of each group is dependent on the thermal history; polystyrene latex particles made by dispersion polymerization technique have more hydrophobic surface, etc.), it is not possible to compare adsorption data on the same basis. Also, other variables, such as solid concentration, aging time, polydispersity of the polymer samples, and the method of sample preparation, etc., can have an important effect. The detailed comparison with the literature results will be made in the results and discussion section. Here, we will briefly describe the important results.

The Effect of Acetate Content

The plateau adsorbed amounts (i.e., "saturation adsorbed amount" or adsorbed amounts at "complete" surface coverage) are generally more for PVA88 (i.e., partially hydrolysed PVA) than PVA98 (i.e., fully hydrolysed PVA) of similar molecular weights. This effect have been found on various substrates (e.g., AgI, Koopal 78; silica, Tadros 78; PS latex, Barnett, et al. 82). The larger adsorbed amount for PVA88 can be due to (i) increase in the adsorbed amount in the first layer (i.e., A_{mono}) or due to (ii) the formation of larger loops and tails. The adsorbed amount differences in the monolayer between these two polymers cannot account for this difference, hence, the contribution of the first layer to this difference is small (Koopal 78). The increase in adsorption with increasing acetate content has been attributed to greater adsorption in loops and tails. As explained earlier, χ (PVA98) and χ (PVA88) are only slightly different, and the difference in adsorption behavior cannot be explained by the solvency effect. The preferential adsorption of acetate groups onto AgI particles has been determined by Koopal from the electrochemical method (i.e., from the shift in the point of zero change) (Koopal 78). The preferential adsorption of acetate groups leads to accumulation of acetate groups in the first layer and gives an important contribution to the gain in the free energy of adsorption (i.e., χ_{s1}, the adsorption energy parameter for acetate groups is expected to be larger than the adsorption energy parameter for alcohol groups, χ_{s2}). The differences in flexibility of these two polymers (i.e., it can be assumed that the flexibility of PVA88 is relatively lower due to bulky acetate groups) will have effect on the size of the trains and loops. The train

size is limited by the length of the acetate blocks and lower flexibility of PVA88 can set constraints on the minimum loop size (i.e., the average loop size is expected to be larger for PVA 88). The preferential adsorption of acetate groups has been confirmed by NMR studies on PS latex particles (Barnett, et al. 82).

The Effect of Molecular Weight of PVA

As expected from the theoretical results, increased plateau adsorption with increasing molecular weight of PVA has been observed. Generally, this effect is represented by the following power law relation:

(2.11)

$$A = KM_w^a$$

where A is the plateau adsorbed amount of polymer and K and a are empirical constants. (Please note that the Equation 2.11 is empirical in nature. Modern adsorption theories (for e.g., SF, Roe) predict A α log M_w which is an entirely different type of functional relation). For the adsorption of PVA98 on the PS latex (made by dispersion polymerization), a = 0.5 has been reported (Garvey et al. 74). Weak molecular weight dependence has been observed for adsorption on AgI particles, a = 0.1 for PVA98 and a = 0.2 for PVA88 (Koopal 78). The hydrodynamic thickness of the adsorbed polymer layer increases with the molecular weight (Garvey et al 74; Killmann et al 88). The hydrodynamic thickness has been measured using various techniques (Electrophoresis, Viscometry, PCS, ultra centrifugation, slow speed centrifugation, direct force measurements, etc.). Again, the relation between the hydrodynamic thickness and molecular weight is represented by a power law. Generally, the measured hydrodynamic thicknesses were comparable to the random coil dimensions in solution.

The Effect of Solvency

Increases in temperature (van den Boomgaard et al. 78) and additions of electrolyte (Tadros and Vincent 79; Barker and Garvey 80) increased the plateau adsorbed amounts. This has been related to the worsening of solvent quality with temperature and electrolyte. Decreases in the measured hydrodynamic thickness with increasing temperature and electrolyte concentration were observed.

Adsorbed Layer Properties and Adsorbed Amounts

It has been suggested from theoretical results (e.g., see Fleer 87) that, although adsorbed layer properties such as θ, p, adsorbed layer thickness, etc. are dependent on M_w and solution concentration, it is still possible to express the adsorbed layer properties as a function of the adsorbed amount only (i.e., the properties of the adsorbed layer are the same for the high molecular weight polymer at low concentrations and for the low molecular weight polymer at high concentrations provided the adsorbed amount is the same). Based on the above hypothesis, Koopal plotted adsorbed layer properties, such as the first layer occupancy θ, and effective layer thickness δ (measured experimentally), as a function of adsorbed amount (Koopal 78). His results are shown in Figure 2.3. As expected from the theoretical and other experimental results, the root mean square thickness increased with increasing adsorbed amounts. The results for PVA98 and PVA88 are plotted on the same graph since no significant difference was found in χ (PVA98) and χ (PVA88) values. From the above results, he concluded that the acetate content and molecular weight influenced the adsorbed layer properties through adsorbed amounts only.
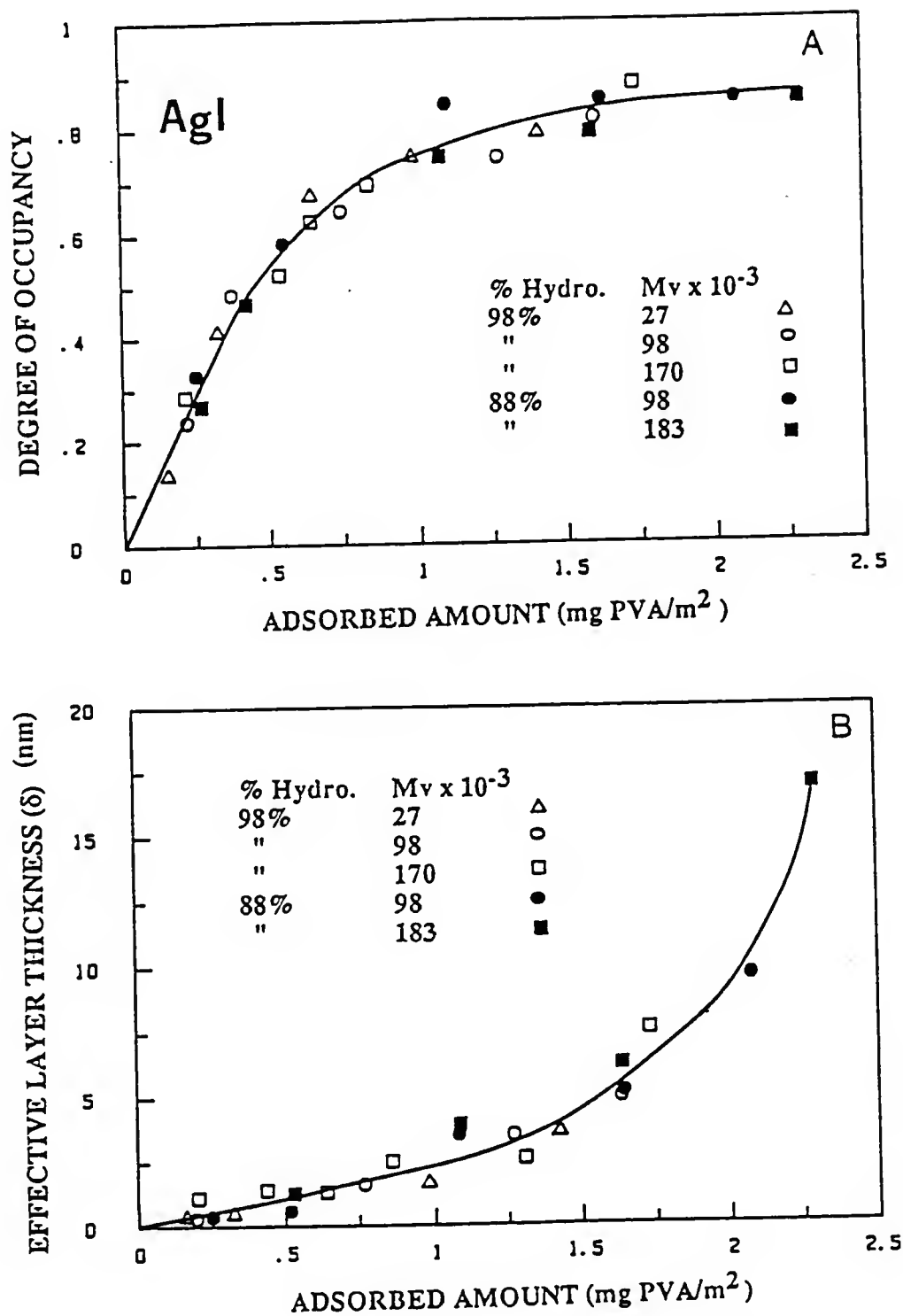
Figure 2.3   Plots of (a) degree of occupancy, θ, and the effective layer thickness, δ, as a function of the adsorbed amount of PVA on AgI and (b) the fraction of segments adsorbed in trains as a function of the total adsorbed amount (Koopal, 1978).

The Segment Density Distribution

The segment density distributions have been determined (Figure 2.4) using SANS for adsorbed PVA on PS latex particles (Barnett et al. 82). Typically, an exponential segment density distribution was observed near the surface. (This would be expected by the polymer adsorption theory of Hesselink in which the conformation consists of loops and trains, but no tails--Hesselink 71a.) However, higher segment density at the intermediate distances were related to longer "slightly folded" tails (Barnett et al. 82). This type of segment density distribution was different from the homopolymer PEO adsorbed on PS latex, where more or less exponential decay in the segment density was observed. In the study of PVA adsorbed on PS, the root mean square thickness calculated from the segment density distribution was smaller than results obtained by PCS. It was concluded that the SANS results were not sensitive enough to detect tails (which are present in low concentration) and the tails are responsible for the higher measured hydrodynamic thickness determined by PCS (Barnett et al. 82).

The Effect of Particle Radius

The effect of particle radius on adsorption behavior and the hydrodynamic thickness has been studied by Garvey et al. (Garvey et al. 76) and Ahmed et al. (Ahmed et al. 84). The former investigators related the increasing hydrodynamic thickness with decreasing particle radius to a geometric factor (Garvey et al. 76). Other groups correlated this observation to change in the conformation of the adsorbed polymer due to the change in the particle radius (Ahmed et al. 84).
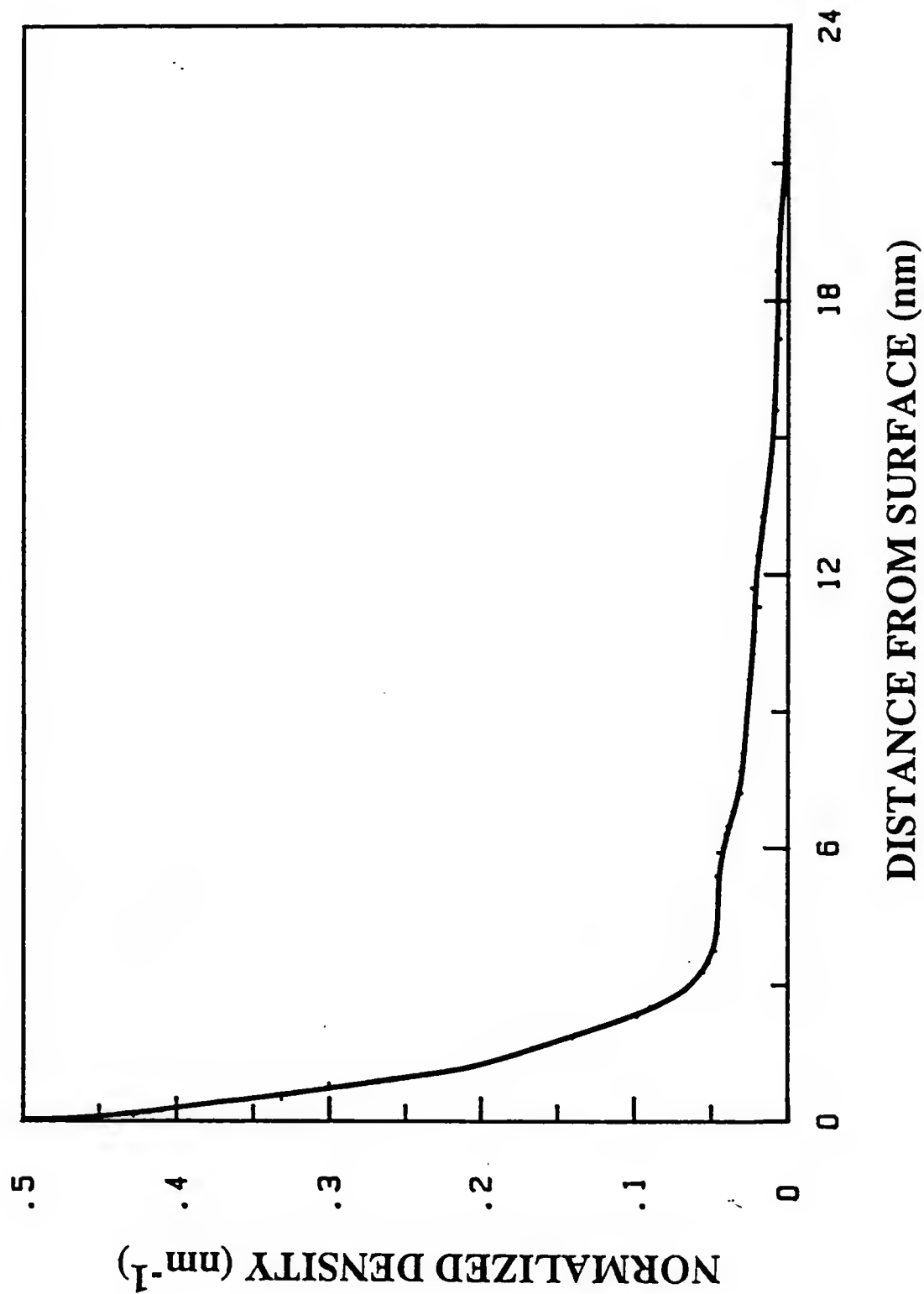
Figure 2.4   Plot of segment density as a function of distance from a surface for adsorbed
PVA on PS-latex (Barnett et al., 1982).

PVA Adsorption on Silica

Tadros has investigated the PVA adsorption behavior on various types of silicas (Tadros 78). Here, we will state the results from his investigation. A detailed comparison of his results and the results in this study are made in Chapter VIII.

(1) The Effect of Silica Calcination Treatment:

It was observed that the plateau adsorbed amount is a strong function of silica surface characteristics. The maximum in the plateau adsorbed amounts was observed for approximately 700°C calcined silica. This observation was correlated with the optimum density of isolated silanol groups on 700°C calcined silica.

(2) The Effect of Surface Charge:

The maximum adsorption occurs at the point of zero change, p.z.c., of the oxide and progressive decrease in the adsorption was observed above p.z.c (Tadros 78). (This effect was not observed for AgI particles and sol--Koopal 78, Fleer 71).

Summary

From the above discussion, following general trends have been established regarding adsorption behavior of PVA.

- Water is a relatively poor solvent for PVA (χ is close to 0.5).
- Partially hydrolysed PVA is blocky, while for fully hydrolysed PVA, acetate groups are randomly distributed.
- Partially hydrolysed polymer adsorbs more than fully hydrolysed PVA.
- Adsorption density increases with increase in the molecular weight.

- NMR and electrochemical methods suggest that the acetate segments are preferentially adsorbed.

- Adsorbed layer properties such as bound fraction (p) and effective thickness are functions of amount adsorbed only for PVA adsorption on AgI.

- Segment density distribution is exponential near the surface and relatively higher density (compared to an exponential distrituion) observed at the intermediate distances is related to the presence of slightly folded tails for PVA adsorption on PS.

- Hydrodynamic layer thickness is substantial (five to fifty nm) and, it is primarily the tails which are responsible for these large measured thicknesses.

- Calcination temperature and pH are among the most important variables controlling PVA adsorption behavior onto silica.

In the next Chapter, we will review the electrostatic interactions between colloidal particles.

CHAPTER III
ELECTROSTATIC INTERACTIONS BETWEEN COLLOIDAL PARTICLES

Introduction

Properties of the colloidal dispersion are directly influenced by the interparticle interactions. A colloidal dispersion is a two-phase mixture consisting of dispersed particles (solid) in a continuous dispersion medium (liquid). Particles are said to be colloidal in character if at least one of its dimensions is in the size range 1 nm to 10^4 nm (1 μm). In this size range, specific surface area is large (usually few m^2/gram up to 1000 m^2/gram), and hence, the interparticle interactions are dominated by the solid-liquid interface characteristics. Also, in this particle size range, the gravitational force is not important, and particles are moving randomly in the dispersion media due to thermal energy, i.e., Brownian motion. Particle encounters due to Brownian motion either leads to either formation of doublets (or higher order multiplates) or particles remain as individual units depending on the interparticle interactions. In the absence of any repulsive interactions, these random collisions lead to permanent contacts between particles and this reduces the free energy of the system. (The free energy is lowest when the particles are all clumped together). The origin of attractive interactions between particles is in the Van der Waal's attraction between the atoms of the colloidal particles. The characteristics of the aggregates formed also depend on the interparticle

forces. To prevent such aggregation of particles during collisions, there are two mechanisms available to overcome attraction.

(1) Electrostatic Interactions: If the colloidal particles can be given an electric charge (either positive or negative) and if all particles have the same sign of charge, particles will repel one another during approach.

(2) Interactions of Adsorbed Polymer: Under certain conditions (i.e., depending on the coverage of particle surfaces with adsorbed polymer, thickness of the coating, solvency for polymer, etc.), adsorbed polymer layer can prevent close approach of the particles.

These two repulsive interactions impart stability to the colloidal dispersion. The dispersion is said to be stable if the dispersed phase (colloidal particles) remains essentially as distinct single particles on a long time scale (e.g., days, months, years). Such a dispersion may be stable either due to kinetic (e.g., in the case of electrostatic interactions) or thermodynamic reasons (e.g., stabilization with adsorbed polymer). It is clear from the above definition that the stability criteria is essentially based on the state of particulates in the dispersion. The time scale is employed as a reference because, in the absence of repulsive interactions, the number of particles (kinetic units) in moderately concentrated suspensions can be reduced to half in a matter of seconds due to encounters arising from Brownian motion (von Smoluchowski 16a,16b,17).

The stability criterion based on the time scale (for e.g., time it takes to reduce the particle concentration to half, etc.) may not be useful to evaluate the stability of ceramic dispersions. The reasons are

two fold: (i) typically particles in the size range of 0.05 μm to 5-10 μm are often employed in various ceramic processing operations, and hence, suspensions are not strictly colloidal in nature. Also, the density of particles is usually greater than the density of suspending media leading to sedimentation of particles although particles are well dispersed. (ii) the particle concentration is also quite high, and usually, it is not possible to determine the change in particle concentration. Other techniques, such as rheological behavior, sedimentation behavior, properties of the sediment (porosity, average pore size, etc.) can be used to evaluate the stability of these dispersions.

Although interatomic attractive interactions are short range ($\alpha\ r^{-6}$ where r is the distance between the atoms), their summation over colloidal particle sizes leads to long range attraction. To overcome this attraction, the repulsion must also be long range.

In this chapter, we will review two components of interactions (1) Van der Waal's attraction between colloidal particles, and (2) electrostatic interactions.

Summation of these two components, under the assumption of additivity, leads to well known theory developed by Deryagin and London and independently by Verwey and Overbeek (commonly known as "DLVO" theory) to explain the stability behavior of the electrostatically stabilized dispersions (e.g., see Verwey and Overbeek 48). Excellent monographs are available to discuss various aspects of this theory, hence only the basic principles will be outlined here (e.g., see, Hiemenz 77, Hunter 87, Overbeek 82a,82b, Lyklema 68, etc.).

Development of Charge at Solid-liquid Interface

There are basically four different methods by which the charge can be developed at the solid/liquid interface (Hunter 87).

Dissociation of Surface Groups

This method is the charge determination mechanism for several oxides (e.g., alumina, silica, etc.). The surface of these oxides is hydroxylated to various extents. (For example, for precipitated silica used in this investigation, the surface is almost completely hydroxylated, i.e., the surface is nearly fully covered with silanol groups, Si-OH). Dissociation of surface silanol groups leads to surface charge development, as described by the following reactions:

$$-SiOH_{(surface)} + H^+_{(liquid)} \longrightarrow SiOH^+_{2(surface)} \qquad (3.1)$$
$$-SiOH_{(surface)} + OH^-_{(liquid)} \longrightarrow SiO^-_{(surface)} + H_2O_{(liquid)}$$
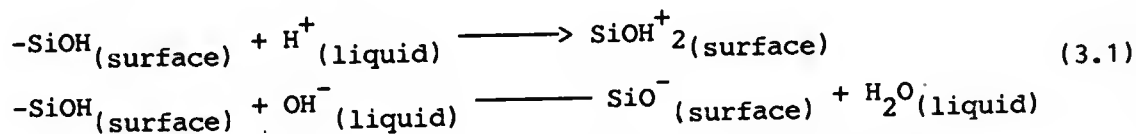
From the above reactions, it is clear that the silica surface can develop a positive or a negative surface charge.

A zero point of charge, (p.z.c.), is defined as a pH at which the surface charge is zero. Another important characteristic of the oxide material is its isoelectric point, i.e.p., which is defined as the pH at which the electrophoretic mobility is zero. H^+ and OH^- ions are called the potential determining ions. In the absence of specific adsorption of ions, the p.z.c. and the i.e.p. are the same. Below the i.e.p., the silica surface is positively charged, and above the i.e.p., negative charge is developed and its magnitude can be increased by increasing pH of the solution.

Adsorption of Potential Determining Ions

A familiar example is silver iodide particle/water suspensions in which the particles can preferentially adsorb an Ag^+ or I^- ions, rendering them positive or negative charge, respectively.

Adsorption of Ionized Surfactants

In this case, the charge is produced by the preferential adsorption of the ionic surfactants on the surface, for example, the preferential adsorption of $C_{12}H_{25}SO_4^-$ ions from sodium dodecyl sulfate, $C_{12}H_{25}SO_4^-Na^+$ surfactant.

Isomorphic Substitution

This charge development mechanism is important in the case of clay minerals (e.g., sodium montmorillenite). Inside the solid lattice, lower valent ions may replace higher valent ions (e.g., Al^{+3} replaced a Si^{+4} ion in the "tetrahedral silica layer," resulting in a deficit positive charge on the particle surface.

For the present investigation, dissociation of surface silanol groups on the silica particles is the important mechanism of charge development. The silica used in this study has an i.e.p. near pH ≈ 3.7. Hence, at high pH's, the silica surface develops negative surface charge, and at pH near 3.7, no net charge is present on the silica particles. (Hence, there is no net electrostatic repulsion between two approaching particles at pH ≈ 3.7.)

Electrical Double Layer

The development of surface charge is not yet a sufficient condition for stability because electroneutrality requires that the particle and

its immediate surroundings should have no net charge. In other words, the surface charge must be balanced by an equal but opposite counter charge in the solution. The rigid alignment of counter ions in the solution is implausible because of thermal agitation, which causes the counter ions to diffuse throughout the solution. To understand the stability, it is of crucial importance to understand the distribution of counter ions in the solution.

The stability of the charged particles can be understood qualitatively as follows: If the counter charge is very diffusely distributed and extends far from the particle surface, then when two particles having the same sign of charge (and hence, same sign of the counter ions in the diffuse layer) start approaching each other due to Brownian motion (or due to an applied shear field), the diffuse layer starts to overlap (even though the particles are far apart), thus giving rise to an electrostatic repulsive force. On the other hand, when the double layer is compressed (i.e., the counter ions are crowded close to the particle surface), particles can approach closer before they feel the electrostatic repulsion, and at that distance, the strong Van der Waal's attraction leads to flocculation of the particles.

To explain the stability behavior quantitatively, a description of the potential (or charge) distribution around the colloidal particles is required. To describe the variation of the potential with the distance from the charged surface, the Poisson equation is used as shown below:

$$\nabla^2 \Psi = \frac{-\rho}{\epsilon_o \epsilon_r} \tag{3.2}$$

where Ψ is the potential, ∇^2 is the Laplace operator, ϵ_r is the relative permittivity, ϵ_o is the permittivity of the free space, and ρ is the

local charge density (i.e., number of charges per unit volume). To solve
this equation, one needs to know the charge density as a function of
potential.

The work required to bring an ion to a position where the potential
Ψ is given by $Z_i e \Psi$. The probability of finding an ion at that position
is given by the Boltzmann factor:

$$\frac{n_i}{n_{io}} = \exp \left(\frac{-Z_i e \Psi}{kT} \right) \tag{3.3}$$

where T is the temperature, k is the Boltzmann constant, n_i is the number
of ions of type i per unit volume, and n_{io} is the concentration far from
the surface (i.e., the bulk concentration). The valance number Z_i is
either a positive or negative integer and e is the charge on the
electron. The charge density is related to the ion concentrations, as
follows:

$$\rho = \sum_i n_i e Z_i = \sum_i Z_i e n_{io} \exp \left(\frac{Z_i e \Psi}{kT} \right) \tag{3.4}$$

Substituting for the charge density, one obtains the Poisson-Boltzmann
equation, as follows:

$$v^2 \Psi = \frac{1}{\epsilon_o \epsilon_r} \sum_i n_{io} Z_i e \exp \left(\frac{-Z_i e \Psi}{kT} \right) \tag{3.5}$$

The following assumptions were made in solving the above equation:
(1) The surface charge on the particle and the space charge in the
solution are considered as smeared out. (2) The ions are considered as a
point charges, their distribution in the solution being determined by
their valancy and not by their volume, shape or polarizability. This
assumption makes the theory non-specific (e.g., the difference between

Li^+ and Na^+ ions cannot be distinguished). (3) The solvent is considered as homogeneous and continuous, and the solvent affects the charge distribution through its dielectric constant ϵ_r.

It is clear from the above equation that the potential distribution depends in a complex way on the ionic composition of the solution. This equation does not have an explicit general solution and has been solved for certain limiting cases (e.g., low surface potentials) and for simple geometries (i.e., flat plate, spherical particle, etc.).

At room temperature, the exponent $Z_i e\Psi/kT \approx Z_i\Psi/25.4$ if Ψ is expressed in millivolts.

Debye-Huckel solved the above equation for flat plate geometry and for low surface potentials, (i.e., $Z_i\Psi < 25.4$ mV). Under these conditions, they showed that the potential decays exponentially (Hunter 87):

$$\Psi = \Psi_o \exp(-\varkappa x) \tag{3.6}$$

where x is the distance from the interface and the $\varkappa$, the Debye-Huckel parameter, is defined as follows:

$$\varkappa = \left(\frac{e^2 \Sigma n_{io} Z_i^2}{\epsilon_r \epsilon_o kT}\right)^{1/2} \tag{3.7}$$

$\varkappa$ has the units of reciprocal length, i.e., $\varkappa^{-1}$ has the units of length. The exponential rate of the potential decay is controlled by $\varkappa$ (Equation 3.6). If the double layer thickness is defined as the distance over which the potential drops to (1/e) of its value at the surface, then $\varkappa^{-1}$ becomes the measure of the "double layer thickness." At 25°C in water, the value of $\varkappa$ is given by:

$$\varkappa = 3.288 \sqrt{I} \quad (nm^{-1}) \tag{3.8}$$

where I is the ionic strength ($= 1/2 \ \Sigma \ C_i Z_i^2$ where C_i is the ionic concentration in mole/liter). Table 3.1 shows calculated values of $\varkappa^{-1}$ (i.e., the double layer thickness) for several different electrolyte concentrations and valences for aqueous solutions at 25°C.

From the table, it is clear that the valency of the counter ions and the electrolyte concentration are important parameters to the control double layer thickness, and hence, the electrostatic interactions between colloidal particles.

Figure 3.1 shows the variation of the potential with the distance from the surface. The drop is dramatic for the higher electrolyte concentrations or valances.

The Poisson-Boltzmann equation has been solved for flat plates without the Debye Huckel approximation (i.e., $Z_i \Psi < 25$ mV) by Gouy-Chapman. The results are applicable only to symmetrical electrolyte, i.e., Z+ = Z-. According to the Gouy-Chapman, the variation of potential within the double layer can be described by the following equations (Hunter 87):

$$\Upsilon = \Upsilon_0 \ \exp \ (-\varkappa x) \tag{3.9}$$

where Υ is defined by the relationship

$$\Upsilon = \frac{\exp \ (Ze\Psi/2kT) - 1}{\exp \ (Ze\Psi/2kT) + 1} \tag{3.10}$$

and Υ_0 is calculated from the above equation when $\Psi = \Psi_0$. From Equations 3.9 and 3.10, it is clear that it is the complex ratio Υ that varies exponentially with x in the Gouy-Chapman theory. For the low potentials, as expected, the above equation reduces to the Debye-Huckel approximation (i.e., Equation 3.6).

TABLE 3.1

Effect of Ionic Strength and Valency on the Electrical Double Layer Thickness, κ^{-1}

Ionic Strength (moles/liter)	Symmetrical Electrolyte $Z_+ : Z_-$	κ^{-1} (nm)
1×10^{-4}	1:1	30.41
	2:2	7.60
	3:3	3.36
1×10^{-3}	1:1	9.61
1×10^{-2}	1:1	3.04
1×10^{-1}	1:1	0.96

52

Figure 3.1

Fraction of double
layer potential
versus distance
from a surface:
(a) curves for 1:1
electrolyte at
three concentra-
tions and (b)
curves for 0.001 M
symmetrical
electrolytes of
three different
valance types.
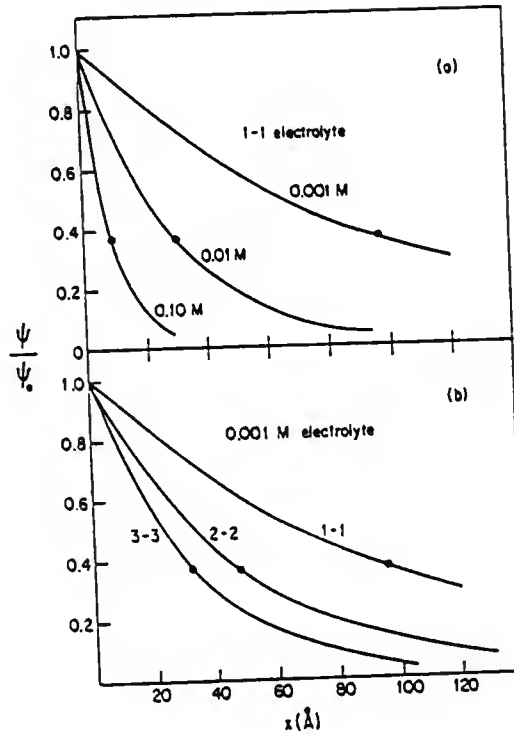
Figure 3.2
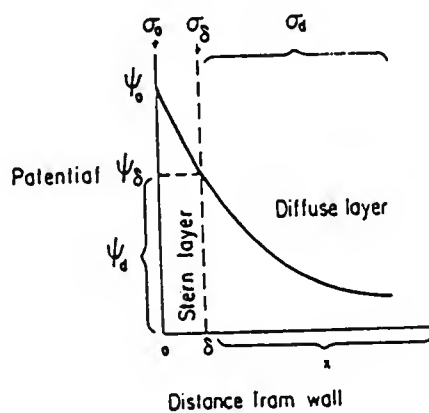
Schematic
illustration of
the variation of
potential as a
function of
distance from a
charged surface in
the presence of a
stern layer,
subscripts o at
wall, δ at stern
surface, d in
diffuse layer.

To describe the potential variation as a function of distance from the interface for spherical particles, the Poisson-Boltzmann equation should be solved in spherical coordinates. For the case of low surface potentials, analytical solution is available and given by the following equation:

$$\Psi(r) = \Psi_o \frac{a}{r} e^{-\varkappa(a-r)} \tag{3.11}$$

where $\Psi(r)$ is the potential at a distance r from the particle center and a is the particle radius.

In the theoretical development of the above equations, Debye-Huckel and Gouy-Chapman treated ions as point charges, i.e., the effect of ion size was ignored. To account for the finite volume of the ions, Stern divided the aqueous part of the double layer by a hypothetical boundary known as the Stern surface (Hunter 87). The Stern surface is situated at a distance δ from the actual surface as shown in Figure 3.2.

The Stern theory is difficult to apply quantitatively because it introduces several parameters into the picture of double layer which cannot be evaluated experimentally. There are several other models available to describe the charge and the potential variation at the charged interface, but they suffer the same problem as the Stern's model (Hunter 87).

It is important to note that the existence of the Stern layer does not invalidate the expressions for the diffuse part of the double layer, but one needs to use a potential at the Stern layer, Ψ_δ. This Stern layer potential is usually equated with the zeta potential, which is the potential measured using an electrokinetic method. The exact location of

at which the zeta potential is determined is not known, but it is assumed to be close to the Stern layer.

In summary, in this section, we looked at the various charge development mechanisms at the solid-liquid interface. The charge on the solid surface leads to the distribution of the counter ions in the solution. This model of the charged interface is often called the electrical double layer model. The potential variation as a function of distance from the interface can be obtained by solving the Poisson-Boltzmann equation. Under the assumptions of low potentials (Debye-Huckel approximation) and simple geometries, analytical solutions can be obtained. The parameter of great importance is κ (the Debye-Huckel parameter), which can be used to describe the effect of the concentration and valence of the counter ions on the potential distribution near the charged surface. To describe the stability behavior of the electrostatically stabilized dispersions, calculations are often made of the interaction energy as a function of distance of separation between particles. In the next section, expressions for the interaction energy due to overlap of the electrical double layers will be developed.

Double Layer Interactions

When two particles approach each other, overlap of the double layer occurs. The rate of approach of the two particles compared with the relaxation time of the diffuse double layer to adjust to the new situation is an important parameter. But, generally, two cases can be distinguished. They are denoted as the "constant potential" and the "constant charge" interactions.

In the first case, it is assumed that during the encounter of two colloidal particles, the surface potential Ψ_O remains constant. Under these conditions, analysis shows that, to keep the surface potential constant, the surface charge density, σ_O, should decrease. In the second case, it is assumed that during the encounter the surface charge density remains constant, and in this case, the overlap of the diffuse double layer leads to an increase in Ψ_O. The condition in which both Ψ_O and σ_O are not constant is also possible and has been called a charge regulation (Hunter 87).

The repulsive interactions due to the overlap of the double layer can be analyzed using two approaches (Lyklema 68).

(a) the free energy change involved when the overlap occurs, or

(b) the increase in the osmotic pressure due to accumulation of the ions between the particles.

Following the free energy change approach, there is an increase in the free energy of the double layer upon interaction, hence, work must be performed to bring the particles closer. In other words, the overlap of the double layer leads to repulsion between particles.

The repulsion energy $V_R(d)$ represents the work necessary to bring the particle surfaces from infinity to a distance d. To calculate $V_R(d)$, the free energy of the system as a function of the distance of separation should be known. It is clear that V_R can be represented by the following equation:

$$V_R(d) = 2 [G(d) - G(\infty)]$$

(3.12)

where $G(d)$ represents the free energy at the distance d and $G(\infty)$ represents the free energy at the infinite separation, i.e., for the

isolated double layer. The factor 2 results from the fact that two double layers are involved. On the basis of the above scheme, DLVO theory formulates the repulsive interaction energy. The exact solution is available only for simple shapes (e.g., flat plate) and under certain approximations (e.g., low potentials). For two flat plates, V_R as a function of distance d has been tabulated by Overbeek for any given value of the surface potential Ψ_0 and concentration of ions in solution (Overbeek 52).

The following approximate analytical equations are often used to represent V_R.

Interaction Between the Two Flat Plates

Under the assumption of the linear superposition[1] principle, and under the condition of the constant surface potential during the double layer overlap, the potential energy is given by the following equation

$$V_R(d) = \frac{64 n_0 kT \gamma^2}{\varkappa} \exp(-\varkappa d) \tag{3.13}$$

where V_R is the repulsive interaction energy per unit area (J/m^2) and n_0 is the ion concentration (total number of ions/m^3), and the other symbols have been previously defined.

The above expression is also valid for the constant charge case. Comparison of the above expression with the exact results (Overbeek 52) show that over a considerable range of overlap, the above equation is a

---

[1] The assumption is that the potential between two interacting particles is equal to the sum of potentials of individual double layers at the same distances from the surface. This is valid in the case of low surface potentials, i.e., for $d > 1/\varkappa$, the diffuse layer thickness, $\varkappa^{-1}$.

good approximation, though the approximation tends to overestimate the value of V_R (Hunter 87).

A more elaborate expression, valid for higher surface potentials under the conditions of the constant charge, is also available (Gregory 73).

Interaction Between Two Spherical Particles

This case is more important in the case of colloidal dispersions. (1) For large values of κa: Large values of κa means that the particle radius, a, is relatively large compared to the thickness of the diffuse layer, κ^{-1}. Under the conditions of low potentials and thin diffuse double layer, the repulsion energy can be calculated by Deryaguin procedure (see Hunter 87). Following this procedure, it is possible to calculate the interaction energy between two spherical particles if the interaction energy as a function of distance of separation is available for the flat plate case under similar conditions. For the case of two identical spherical particles, the energy of interaction can be calculated from the following equation:

$$V_R(d) \text{ (sphere)} = \pi a \int_{d}^{\infty} V_R(d) \text{ (flat plate) } dD \qquad (3.14)$$

where a is the radius of the particle.

Substituting for V_R (flat plate), the approximation valid for low potentials is given by:

$$V_R(d) \text{ (sphere)} = 2\pi \epsilon_r \epsilon_o^2 a \Psi_o \ln (1 + \exp (-\kappa H)) \qquad (3.15)$$

Note that Equation 3.15 gives the total repulsive energy between two spherical particles (in Joules) whereas flat plate expression (Equation

3.13) gives the energy per unit surface area (in Joules/m^2). For the
case of somewhat higher surface potential, the interaction energy is
given by the following equation:

$$V_R(d) \text{ (sphere)} = \frac{64\pi a n_o kT\gamma_o^2}{\kappa^2} \exp(-\kappa d)$$ (3.16)

For the spherical particles at high potentials, no analytical formula is
available, but a graphical solution is available (Overbeek 52).
(2) For the case of low κa, i.e., when the thickness of the diffuse
layer, κ^{-1}, is large compared to particle radius, a, the interaction
energy is given by the following equation:

$$V_R = \frac{4\pi \epsilon_r \epsilon_o a \Psi_o^2}{2a+d} \beta \cdot \exp(-\kappa d)$$ (3.17)

where β is a factor which allows for the loss of spherical symmetry in
the double layer and has been defined by Verwey and Overbeek (Overbeek
52).

From the above equations, it is clear that the repulsion is
determined by the ionic strength (through Debye-Huckel parameter κ) and
the surface potential, Ψ_o. For the case of spherical particles, the size
of the particle (i.e., radius a) is also important.

In the above equations, the finite size of counter ions (i.e.,
presence of the Stern layer) was ignored, and hence, these expressions
are not valid for the distances comparable to atomic dimensions.
Additional interactions due to solvation and hydration of ions and
hydrophobic interactions have been reported (Israelachvili and Pashley
82,83; Pashley and Quirk 84; Pashley et al. 82). Theses short range

interactions have been related to repeptization phenomenon (Overbeek 82b).

As mentioned earlier, the other term in DLVO calculations is the attraction energy term arising due to the Van der Waal's interaction between the colloidal particles leading to the flocculation of particles. This attraction energy term will be discussed in the next section.

Van der Waal's Interactions

The Van der Waal's interactions between neutral molecules may originate from three possible sources: permanent dipole-permanent dipole (Keesom), permanent dipole-induced dipole (Debye), or induced dipole-induced dipole (London) interactions. The distance dependence of these interactions can be represented as a power law, i.e., potential energy of interaction α r^{-x} where $x = 6$ and all interactions lead to attraction between molecules. In the case of non-polar molecules as the dipole moment is zero, Debye and Keesom interactions are absent. On the other hand, London interactions, also known as dispersion forces, are always present. The London dispersion force is attributed to correlated electronic motion in the atoms under consideration. This correlated motion of electrons leads to a decrease in the potential energy of the system (i.e., attraction). This attraction energy is short range since it is inversely proportional to the sixth power of the separation, but the total interaction energy between two colloidal particles (i.e., a collection of a large number of atoms) is quite large and of long-range order and comparable to electrostatic repulsion energy under certain conditions. The contributions to total interaction energy from the Debye

and Keesom interaction is usually small since dipolar contributions tend to average out when large number of atoms are considered.

There are two methods of calculating the magnitude of Van der Waal's attraction energy between two colloidal particles, (i) microscopic and (ii) macroscopic procedure.

Microscopic or Van der Waal's Method

The classical procedure adopted by Hamaker was based on two principles

(1) the additivity of London dispersion forces: The total interaction energy between two colloidal particles was calculated using summation of pairwise interactions between all the atoms or molecules of the two macroscopic bodies.

(2) The summation of these interaction energies between atoms or molecules can be replaced by an integration provided that the distance between the particle surface is large compared with the atomic distances. Under these assumptions, the Van der Waal's attraction energy between the two colloidal particles can be represented as follows:

$$V_A = - \Lambda(A) \cdot H(G) \tag{3.18}$$

Hence, $\Lambda(A)$ is a function of so-called Hamaker-Van der Waal's constant of the material and $H(G)$ is determined by the geometry of the system. For example,

Flat Plates

For two flat plates of substance 1, the Van der Waal's attraction energy is given by (Hamaker 37):

$$V_A = - \frac{A_{11}}{12 \pi d^2} \tag{3.19}$$

where A_{11} is the Hamaker constant for the substance 1, d is the distance between two flat plates, and the negative sign indicates that the energy is attractive. The Hamaker constant A_{11} for substance 1 is defined by

$$A_{11} = \pi \, q_1^2 \beta_{11} \tag{3.20}$$

where q_1 is the density of atoms in the colloidal particle and β_{11} is the constant in the London equation:

$$V_{11} = \frac{-\beta_{11}}{r^6} \tag{3.21}$$

describing interaction energy V_{11} between atoms or molecules. β_{11} is proportional to the polarizability of the atoms, and hence, increases with the size of the atom. From the above equation, it is clear that the Van der Waal's attraction energy V_A increases with square of the density of the substance and the interaction is of long range. (Note $V_A \, \alpha \, d^{-2}$ for "bulk" materials, compared to $V_{11} \, \alpha \, r^{-6}$ for molecular interactions.)

Spherical Particles

For two unequal spheres of radius a_1 and a_2 separated by a distance d in vacuum (d is the distance between two surfaces), the Van der Waal's attraction energy is given by the following equation (Hamaker 37):

$$V_A \text{ (sphere)} = \frac{-A_{11}}{12} \left[\frac{y}{x^2+xy+x} + \frac{y}{x^2+xy+x+y} + 2 \ln \left(\frac{x^2+xy+x}{x^2+xy+x+y} \right) \right] \tag{3.22}$$

where $x = d/2a_1$ and $y = d/2a_2$

For two spherical particles, having same radius a, it can be shown that for large separations, V_A decreases with the sixth power of d as in the London expression, but for short distances (i.e., $d \ll a$) V_A decreases slowly with the distance:

$$V_A = \frac{-A_{11}}{12} \; \frac{a}{d} \tag{3.23}$$

This distance dependence of the attractive (as well as the repulsive) energy of interaction is of great importance. As it will be shown later, at short and at long distances, the Van der Waal's attraction energy dominates the total interaction energy while at the intermediate distances of separation, electrostatic repulsion, which decay exponentially with the distance, may dominate the total energy of interaction. The above equation indicates that, for a small distance, V_A tends to assume very large negative value. However, the above equations are no longer valid for very short distances (i.e., dimensions comparable to the atomic dimensions) because strong Born repulsive interactions (usually represented as $V_{Born} \propto d^{-12}$), which arise from the overlap of electronic orbitals of approaching molecules, are operative.

Retardation Effect

The equations given above for V_A were derived under the assumption of the additivity of interactions between atoms. The origin of the London-Van der Waal's interaction is the electromagnetic interactions between atoms and molecules. The above equations for V_A do not allow for the finite time of propagation of electromagnetic waves from one atom to the other, and the induced-dipole becomes retarded against the inducing one when the distance between the atoms becomes comparable to the wave length of the London frequency. This leads to reduction in the London dispersion force between atoms. Casimir and Polder have shown that due to retardation the inverse sixth power law [Equation (3.21)] gradually changes into an inverse seventh power law with increasing distance

(Casimir and Polder 48, Gregory 69, and Visser 72). The retardation correction is negligible when the distances between the atoms are comparable to the atomic dimensions. However, for the interactions between the colloidal particles at the distances of the order of ten to one hundred nm, the retardation effect can be significant. Equations are available to correct for the retardation effect for the flat plates and for the spherical particles (Gregory 67). The retardation effect leads to reduction in the attraction energy and makes the dispersion force much longer range.

Effect of Medium on the Van der Waal's Attraction

The equations derived above for the Van der Waal's attraction energy can be used for the case of two colloidal particles interacting in vacuum.

In most practical cases, colloidal particles are embedded in a medium (e.g., water). To get the interaction energy V_A in this case, the Hamaker content A_{11} is replaced by the effective Hamaker constant. The effective Hamaker constant, A_{131}, now depends not only on A_{11} (particle-particle attraction) but also on A_{13} (particle-medium attraction) and A_{33} (medium-medium attraction) where subscript 1 refers to particle and 3 refers to medium. The effective Hamaker constant is defined as:

$$A_{131} = A_{11} + A_{33} - 2A_{13} \tag{3.24}$$

where $A_{11} = \pi q_1^2 \beta_{11}$, $A_{33} = \pi q_3^2 \beta_{33}$ and $A_{13} = \pi q_1 q_3 \beta_{13}$, and it is generally assumed that $\beta_{13} = (\beta_{11}\beta_{33})^{1/2}$, and hence,

$$A_{131} = (A_{11}^{1/2} - A_{33}^{1/2})^2 \tag{3.25}$$

Thus, to account for the medium, A_{11} should be replaced by A_{131} in all the previous equations for V_A. From the above equation, it is clear that the effective Hamaker constant is always positive (i.e., there is always net attraction between two particles) and the magnitude of the Van der Waal's attraction is reduced due to the presence of the medium (i.e., the medium imparts a certain measure of stability to the dispersed particles). By choosing A_{33} close to A_{11}, the Van der Waal's attraction can be substantially reduced and at $A_{11} = A_{33}$, there is no net attraction between particles. Thus, to evaluate Van der Waal's attraction energy, the Hamaker constants should be available for the materials under consideration.

Macroscopic Approach

One of the main drawbacks of the microscopic or the Hamaker theory is the assumption regarding additivity of interactions. The Van der Waal's attraction V_A has been calculated using a different approach by Lifshitz and collaborators using the "macroscopic" approach. In this theory, the interacting bodies are treated macroscopically, i.e., interacting bodies are considered as two semi-infinite phases separated by the distance d. The bodies are characterized by their complex dielectric constant. The interaction is evaluated using fluctuation theory. The spontaneous electromagnetic fluctuation in one body induces a fluctuation polarization in the other body. The correlation between the fluctuating fields in the two objects decreases the free energy of the system, and hence, leads to attraction. The Lifshitz theory has some advantages over the classical microscopic theory. The assumption

regarding additivity is avoided and contributions of bonding between the atoms and the molecules to the interactions are taken into account. The Lifshitz approach is more accurate to calculate V_A, but mathematics involved is quite complicated and requires dielectric constant data over a wide frequency range of the materials of interest. Due to these difficulties, the Hamaker microscopic approach is generally used in practice.

Hamaker Constants

To calculate the Van der Waal's attraction energy for practical systems, the values of the Hamaker constants should be available. In principle, there are two ways to estimate the Hamaker constants (see for e.g., Visser 72, Gregory 69, Lyklema 68):

(1) Direct Calculations: In this case, the Hamaker constant can be calculated by the microscopic approach (e.g., see equation 3.20) using molecular properties such as polarizability or by the macroscopic approach using dielectric constant data.

(2) Indirect Evaluation From the Experimental Data on Colloidal Stability: In this method, the Hamaker constant will depend on the experimental tool used to determine stability and the stability criteria used. The Hamaker constant can be experimentally determined from various techniques such as (i) flocculation experiments on dispersion of colloidal particles, (ii) from the measurements of direct force of interactions between crossed wires, (iii) from equilibrium film thickness measurements, (iv) surface tension measurements, and (v) from rheological data, etc. (Visser 72).

Table 3.2 shows the list Hamaker constants for the present system under investigation (i.e., silica-water-PVA). Data for other materials can be found in the above references.

The effective Hamaker constant will be also influenced by the electrolyte concentration, surface contamination, and adsorbed polymer layers. The effect of the adsorbed polymer layer will be discussed next.

The Effect of Adsorbed Polymer Layer on Van der Waal's Attraction

The effect of adsorbed polymer layer of thickness δ on the attractive force can be compared at (i) constant center-to-center distance of spheres, h (see Figure 3.3) or (ii) at constant separation of outer surfaces, d.

If one makes comparison at the constant center-to-cetner distance, then the adsorbed layer usually leads to an increase in attraction between particles. This is due to an effective increase in the particle size and decrease in the distance of separation between particles. If comparison is made at the constant distance of separation d, the adsorbed layer usually reduces the attraction between particles. In this case, the original spheres are separated by a greater distance and generally the adsorbed material has lower Hamaker constant. The attraction energy between two equal spheres of radius a, separated by distance d with the adsorbed layer thickness δ, is given by the following equation:

$$V_A(d) = -\frac{1}{2}[H_{11}(A_{11}^{1/2} - A_{22}^{1/2})^2 + H_{22}(A_{22}^{1/2} - A_{33}^{1/2})^2 +$$

$$2 H_{12}(A_{11}^{1/2} - A_{22}^{1/2})^2 (A_{22}^{1/2} - A_{33}^{1/2})]$$

(3.26)

TABLE 3.2

Compilation of Hamaker Constants for Silica-Water-PVA System

Material	Hamaker Constant $\times 10^{-20}$ J	Technique	Reference
Silica	6.6	Macroscopic	Hunter 87
(A_{11})	14.8	"	Visser 72
	50.0	Microscopic	"
	16.4	Surface Tension	"
Water	3.7	Macroscopic	Hunter 87
(A_{33})	4.4	Lifshits	Visser 72
	3.3-6.4	Microscopic	"
	3.0-6.1	Macroscopic	"
	4.8-3.0	Colloid Chemistry	"
	5.5-6.4	Surface Tension	"
PVA (A_{22})	6.8-8.8	Microscopic	Visser 72

Material	Hamaker Constant in Water $\times 10^{-20}$ J	Technique	Reference
Silica (A_{131})	0.85	Macroscopic	Hunter 87
PVA (A_{232})	0.50	Microscopic	Visser 72
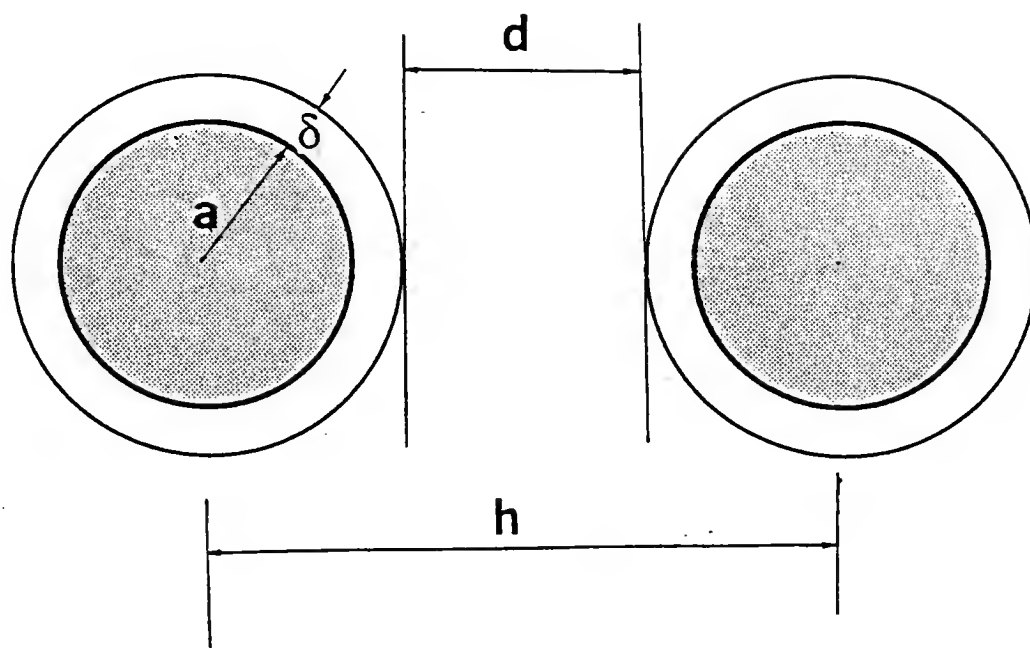
Figure 3.3   Schematic illustration of the effect of adsorbed polymer
layer on Van der Waal's attraction.

where A_{11}, A_{22}, A_{33} are Hamaker constants in vacuum for solid, polymer and liquid, respectively and H_{11}, etc. are geometric functions defined as:

$$H(x,y) = \frac{y}{x^2+xy+x} + \frac{y}{x^2+xy+x+y} + 2 \ln (\frac{x^2+xy+x}{x^2+xy+x+y})$$ (3.27)

where for H_{11}, $x = (d+2\delta)/2a$ and $y = 1$, for H_{22}, $x = d/2(a+\delta)$ and $y = 1$, and for H_{12}, $x = (d+\delta)/2a$ and $y = (a+\delta)/a$. It can be shown from Equations 3.26 and 3.27 that if the adsorbed layer is sufficiently thick and when $A_{22} = A_{33}$, the attraction between particles virtually disappears. To evaluate the Hamaker constant A_{22} for the adsorbed layer, two additional features need to be considered: (i) the adsorbed layer will be a composite, i.e., it will consist of polymer segments plus solvent molecules and (ii) the segment density will not be uniform. Both of these effects on the attraction energy have been discussed by Vincent (Vincent 74).

Potential Energy Curves and the DLVO Theory

Since the electrostatic repulsion and the Van der Waal's attraction are assumed to operate independently and since both are being scalar quantities, they can be added to give the total interaction energy, V_{total}. This is the basis of DLVO theory. The total interaction energy can be represented as:

$$V(d)_{total} = V_R(d) + V_A(d)$$ (3.28)

where V_R is the electrostatic repulsion energy and V_A is the Van der Waal's attraction energy term. Substituting for V_R and V_A from the previously developed equations, the total interaction energy as a

function of distance of separation between the particles can be plotted.
In this type of plot, the attraction energy term is represented as a
negative term and the repulsive energy by a positive term. Figure 3.4
shows schematically the total interaction energy as a function of the
distance of separation between two surfaces. The shape of the total
interaction energy curve is important in determining the stability of
colloidal dispersions and can be used pictorially to show the influence
of various relevant parameters on the stability. The type of curve shown
in Figure 3.4 results because of the different distance dependences of
the interaction energy terms V_R and V_A. The Van der Waal's attraction
energy term is important at close approach since at close approach $V_A \propto$
$1/d$ and also at large distances when $V_A \propto d^{-7}$ due to the retardation
effect. At the intermediate distance of separation, the electrostatic
repulsion (which decreases exponentially with the distance) is more
important. The summation of these two interaction energy terms having
different distance dependences leads to a total attraction energy curve
having a maxima in a potential energy separating two minimas. The
primary minima results from the strong Van der Waal's attraction at the
short distances and the Born repulsion due to overlap of electron clouds.
At such close distances of approach, recent experiments indicate that an
additional energy term, V_S, arising due to solvent structural effects,
should be included (e.g., see Israelachvili and Pashley 82,83). Due to
these additional complications, the exact location and depth of the
primary minima cannot be determined quantitatively. The secondary minima
results from the long-range Van der Waal's attraction and the rapid decay
of the electrostatic repulsion. The depth of the secondary minima is
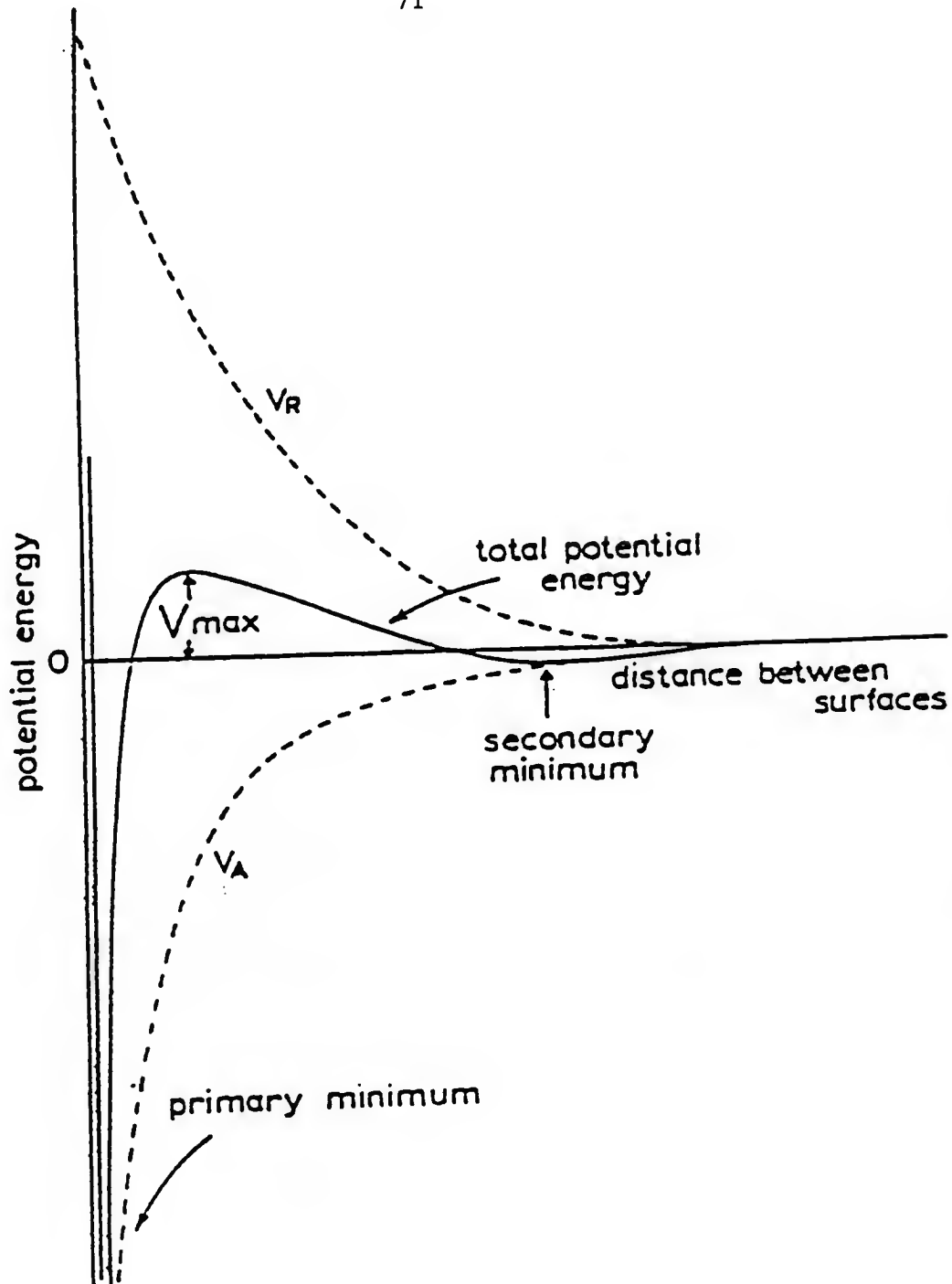
Figure 3.4   Total potential energy of interaction $V(d)_{total} = V_R(d) + V_A(d)$ where $V_R(d)$ is the potential energy of repulsion due to double-layer interactions and $V_A(d)$ is attractive potential due to Van der Waal's interactions (Overbeek, 1952).

usually not significant compared to the thermal energy of the particles.
Hence, flocculation of particles in the secondary minima tends be weak.
The other important characteristic of the total interaction energy curve
is the presence of the potential energy maxima. If the height of the
potential barrier, V_{max}, is greater than the thermal energy of the
particles (i.e., $V_{max} \gg kT$) then the potential barrier can prevent
flocculation of the colloidal particles and the dispersion is stable in a
colloid chemical sense. The fraction of particles that can surmount such
a potential barrier is given by Boltzmann's law. The fraction decreases
exponentially with increasing height of the potential barrier. V_{max} of
the order of 5-15 kT has been considered sufficient to achieve long-term
stability (Overbeek 82b). It should be noted that, in the case of flat
plates, the potential energy per unit area is plotted. In these cases,
the total interaction energy is obtained by multiplying by the
appropriate cross sectional area of the particles. In the case of
spherical particles, the net interaction energy is plotted. To
understand the stability behavior, factors influencing the repulsion
energy term V_R, and the attraction energy term V_A should be considered.

The Effect of Hamaker Constant

The range of values of Hamaker constant for substances (ignoring
retardation effects) immersed in water can be given as follows (Hunter
87):

A_{131} 30 - 10 for metal particles

3 - 1 for oxides and halides, and

$\approx 0.3 \times 10^{-20}$ J for hydrocarbons.
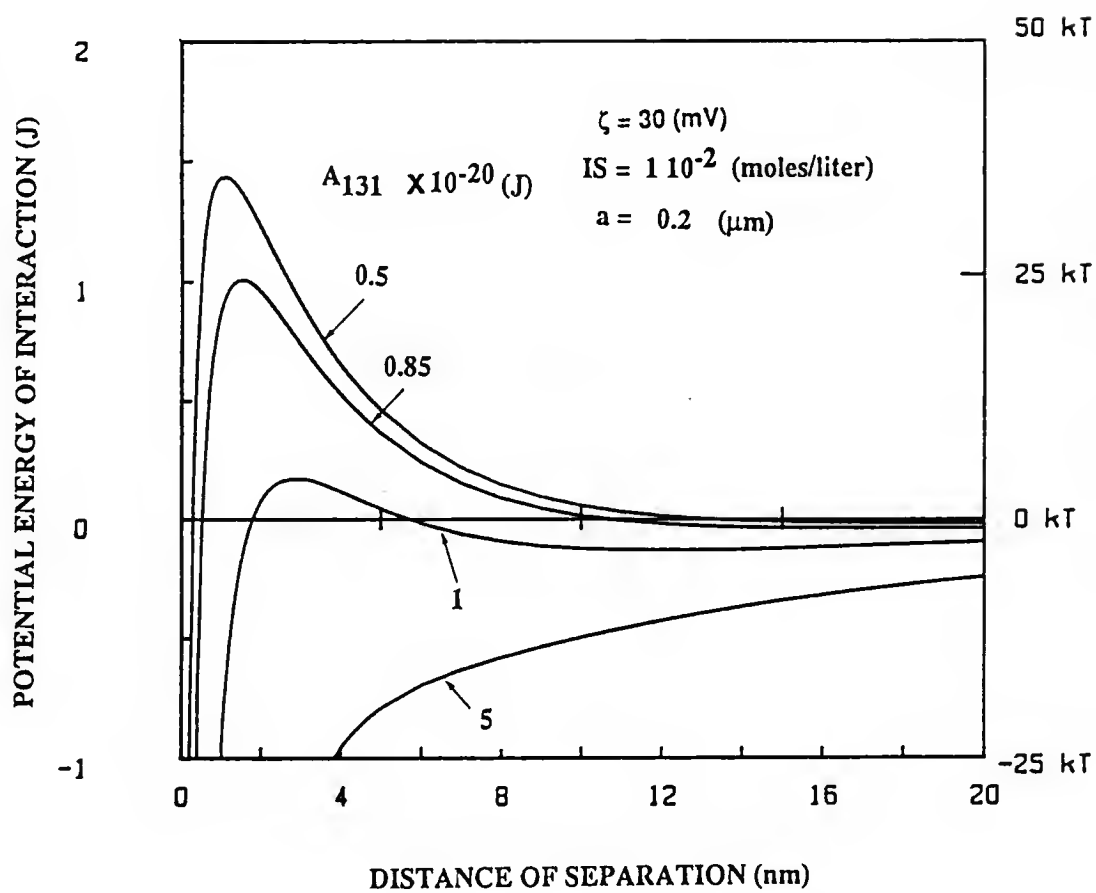
Figure 3.5   The effect of the Hamaker constant on the total
              interaction energy curves.

As discussed earlier, this difference essentially arises due to differences in the polarizability of these materials. Figure 3.5 shows the effect of the Hamaker constant on the total interaction energy curve. All other factors (i.e., the surface potential Ψ_O and the Debye-Huckel parameter κ) were kept constant. As expected with increasing values of A_{121}, the height of the potential barrier decreases and the depth of the secondary minima increases.

The Effect of Surface Potential, Ψ_O

The electrical double layer repulsion term V_R is usually dominated by two parameters (a) the near surface potential Ψ_O and (b) the thickness of the double layer, $1/\kappa$. Figure 3.6 shows that the height of the potential barrier increases as Ψ_O increases. (For oxide materials, such as silica, Ψ_O can be adjusted by varying the pH of the solution.) The exact value of Ψ_O is difficult to determine experimentally due to complications, such as specific ion adsorption and presence of the Stern layer, etc., so usually the near-surface potential, i.e., the zeta potential, ζ is used. This experimentally determined zeta potential does establish a lower limit of Ψ_O.

The Effect of Electrolyte Concentration

The Debye-Huckel parameter, κ, which represents the thickness of the electrical double layer, depends on both the concentration and the valance of the indifferent electrolyte (See Equation 3.7). Figure 3.7 shows the effect of concentration of a 1:1 electrolyte on the total potential energy curve. The potential energy barrier decreases with increasing electrolyte concentration, and above a certain concentration, the barrier vanishes. Thus, the addition of an indifferent electrolyte
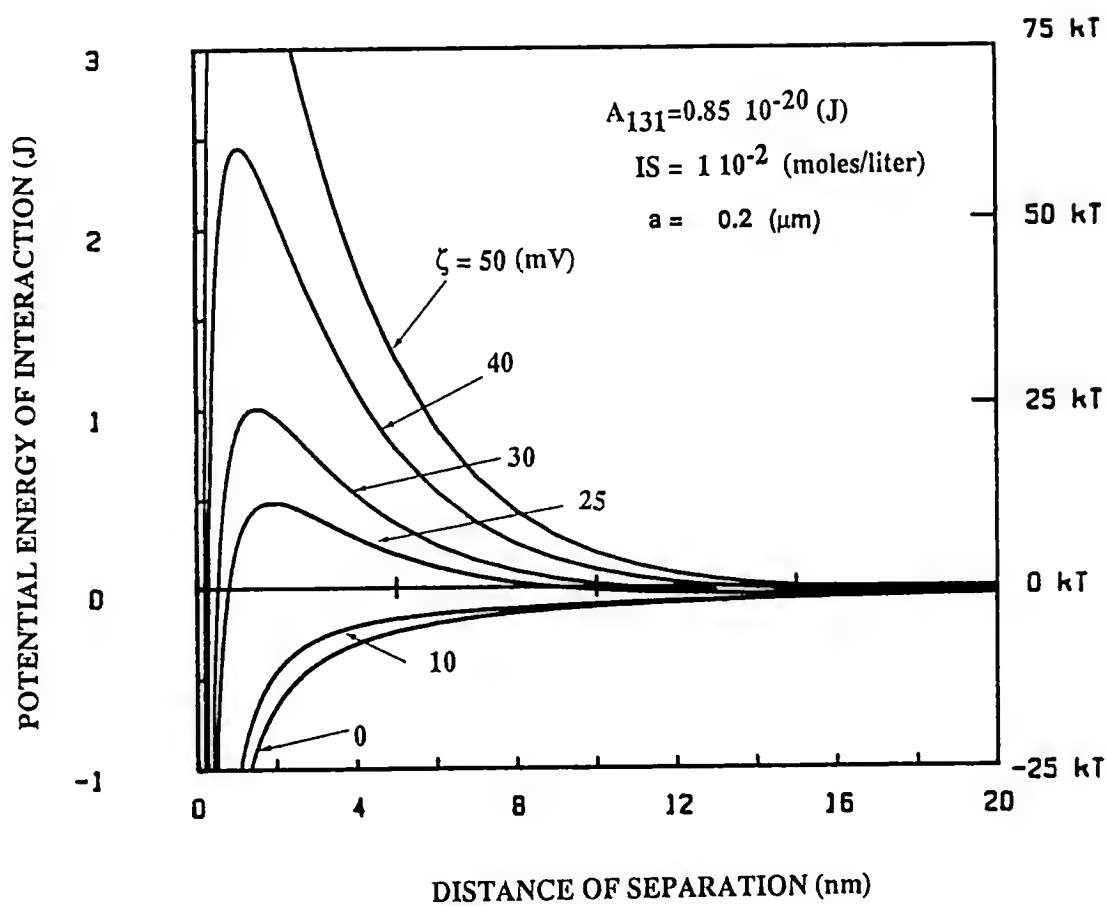
Figure 3.6   The effect of zeta potential on the total interaction
energy curves.
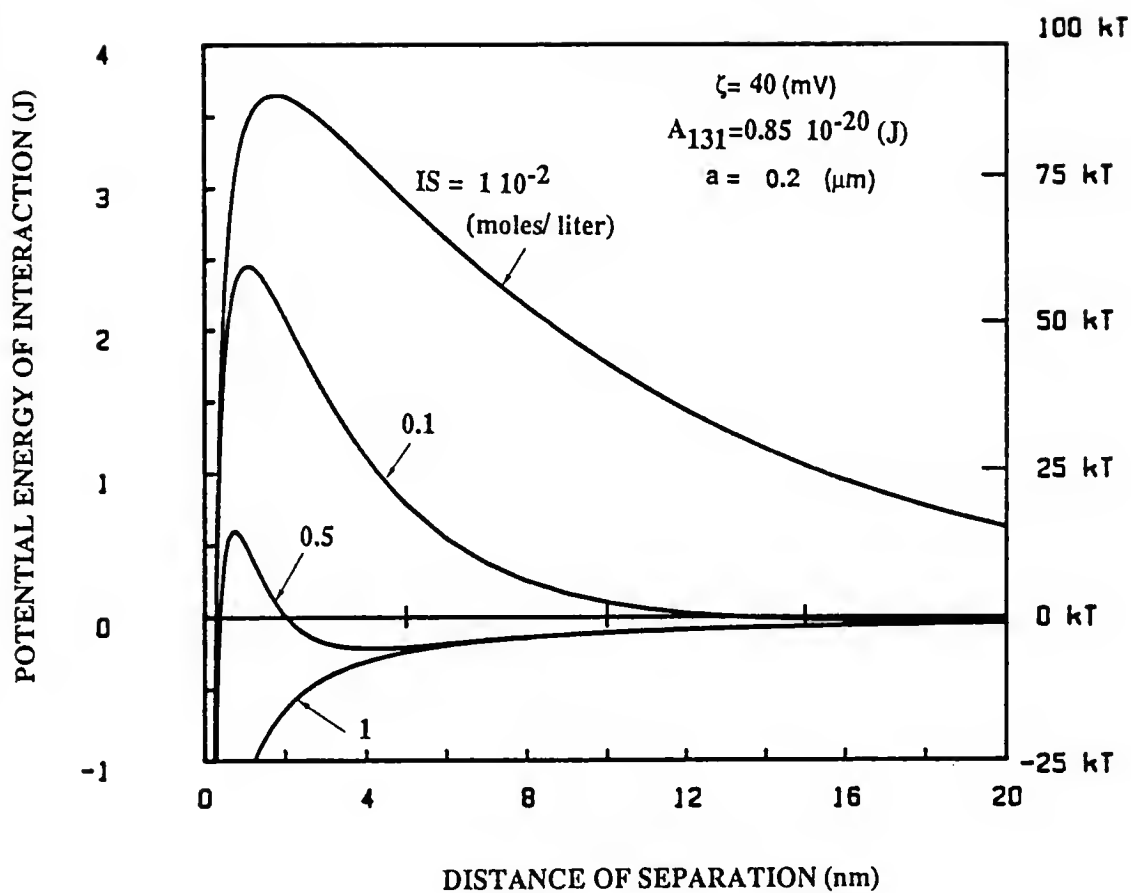
Figure 3.7   The effect of concentration of 1:1 electrolyte on the potential energy curves.

can cause a hydrophobic colloid to undergo flocculation. For a given salt, the critical concentration needed to induce aggregation can be predicted quantitatively by DLVO theory.

Effect of Particle Radius

The total interaction energy is influenced by the particle radius as follows. The Van der Waal's attraction energy is proportional to radius, a, and the electrical double layer repulsion is proportional to a^2, hence, the potential energy barrier increases with a. Thus, the bigger particles are more likely to be stabilized by the electrostatic repulsion (Figure 3.8).

In summary, for preparing electrostatically stabilized dispersions, one should operate under the conditions of high zeta potentials and low ionic strengths. We will examine the effect of electrolyte concentration in more detail as it proves the validity of the DLVO theory.

The Stability - Instability Approach

From the above discussion, it is clear that the form of the total potential energy curve gives an explanation for the stability behavior of lyophobic dispersions. When the potential energy barrier has a large positive value (usually greater than $\approx 10kT$), the system is kinetically stable due to large activation energy opposing transition from the secondary minima to the primary minima. With decreasing height of the potential barrier, V_{max}, the transition from stable to unstable dispersion is facilitated. Theoretically, the onset of instability can be defined by the following condition (Overbeek 52):

$$V(d)_{total} = 0 \text{ and } dV(d)_{total}/dd = 0 \tag{3.29}$$
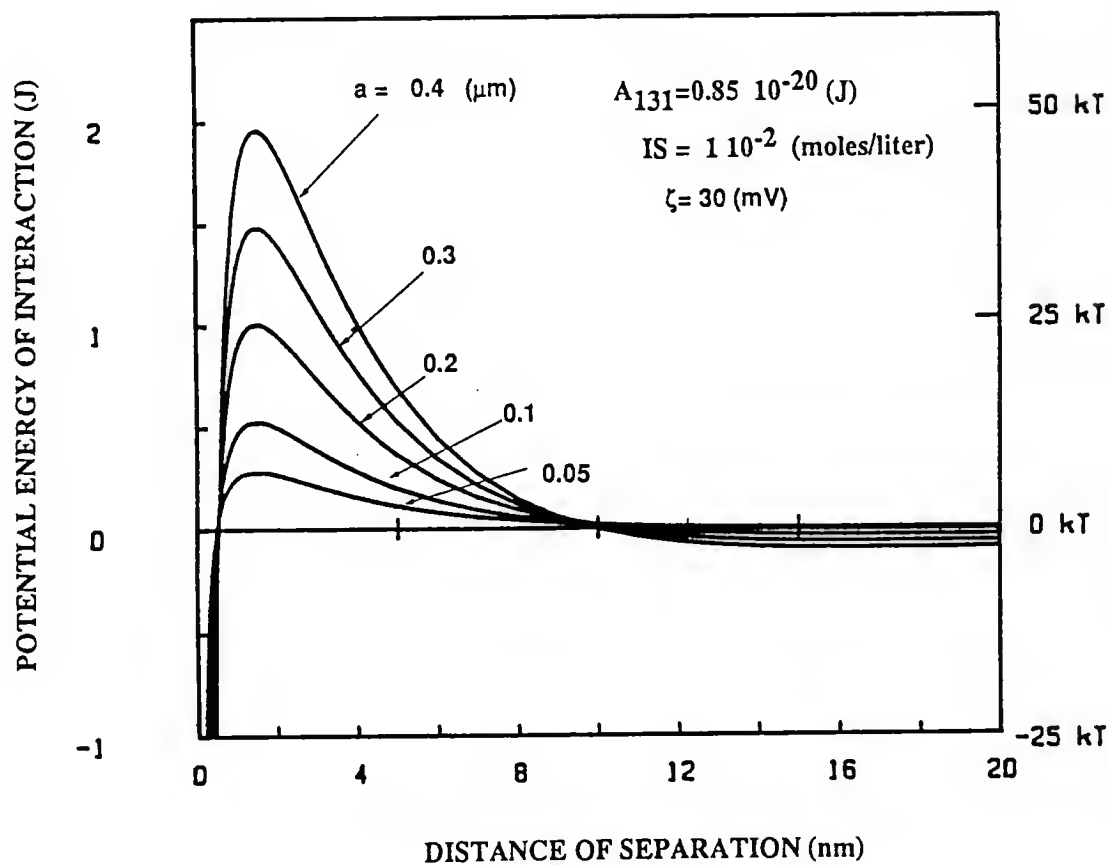
Figure 3.8   The effect of particle radius on the total interaction energy curves.

and the electrolyte concentration at which these conditions are fulfilled gives a theoretical critical coagulation concentration. The experimentally observed dependence of the critical coagulation concentration on the sixth power of the valence of the counter ions for high surface potentials and on the second power of the valence of the counter ions at low surface potentials can be explained using the above criteria. The successful explanation of the dependence of the critical coagulation concentration on the valence is one of the important contributions of the DLVO theory. The DLVO theory explains the stability criterion with the help of interaction energy plots while experimental determination of the stability involves some additional approximations. The effects of electrolyte concentration and the valence can be controlled experimentally, and the change in the particle concentration is measured using various techniques (i.e., direct particle counting, light scattering, etc.). To correlate the stability to instability transition to the critical coagulation concentration, the kinetics of coagulation should be considered.

Kinetics of Coagulation

The rate of coagulation in the absence of any potential barrier was first examined by von Smoluchowski (Smoluchowski 16a,16b,17). The rate of disappearance of primary particles in the initial stages of the coagulation could be written as:

$$-\frac{dN}{dt} = K_o N_o^2 \tag{3.30}$$

where N_o = the number of particles per unit volume present at time $t = 0$ and K_o is a rate constant. It was shown that, for the case of rapid

coagulation (i.e., coagulation with no potential barrier), $K_O = 8\pi aD$, where D = the diffusion coefficient of a single particle and a = the collision radius. In the presence of an energy barrier, the flocculation rate is slower and characterized by a rate constant, K, where $K = K_O/W$ and W is called the stability ratio. The above equation can be written as:

$$\frac{-dN}{dt} = KN_O^2 = (K_O/W)N_O^2 \qquad (3.31)$$

and W = 1 corresponds to rapid coagulation and W > 1 indicates a slow rate of coagulation. Experimentally, the rapid coagulation rate, K_O, is determined using either direct particle counting or light scattering technique. From the experimentally determined values of K_O and K, the stability ratio W under various electrolyte concentrations can be obtained. Typically, log W versus log C is plotted, and the sharp change of gradient at a particular electrolyte concentration establishes the critical coagulation concentration (see Figure 3.9).

According to DLVO theory, the stability ratio W is related to the potential energy maxima V_{max} by the following equation

$$W = 2a \int_0^\infty \exp (V_{max}/kT) \, dh/ (d + 2a)^2 \qquad (3.32)$$

where a is the particle radius and d is the distance between particle surfaces. Reerink and Overbeek showed that the slope of the log W versus log C curve is given by the following equation (Reerink and Overbeek 54):

$$d \log W/ d \log C = - 2.06 \times 10^7 (a\gamma^2 / z^2) \qquad (3.33)$$

where Z is the valance of electrolyte, and γ was previously defined (Equation 3.10). The above equation has been confirmed experimentally for various systems, but the dependence of slope on the particle radius
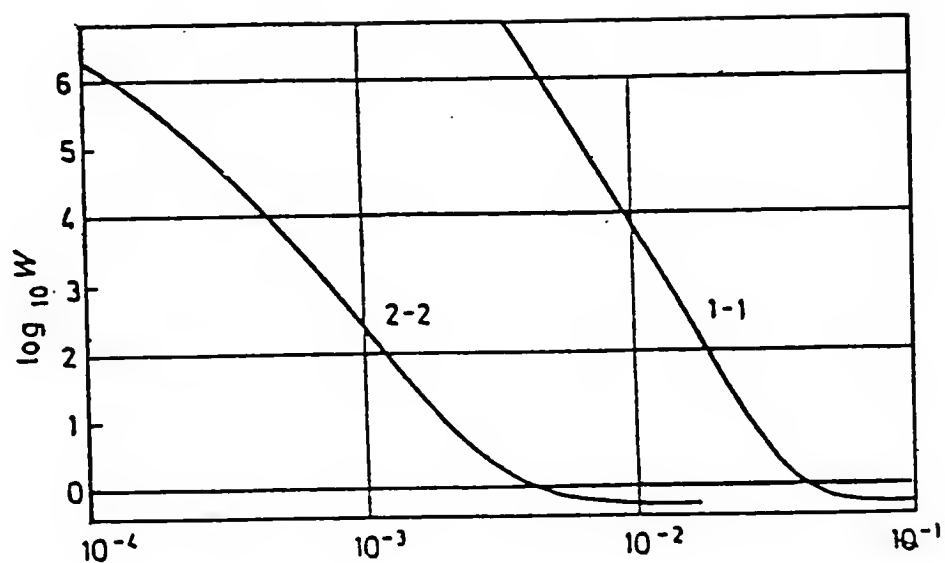
Figure 3.9   Theoretical dependence of stability ratio of electrolyte
concentration (Overbeek, 1952).

has not confirmed. The above theory has been modified to account for a hydrodynamic correction (e.g., see Honig et al. 71). The hydrodynamic correction attempts to take into account the fact that the particles are slowed down in the final stages of approach due to difficulty in removing the remaining liquid film between the particles. This treatment shows that the diffusion coefficient D is also a function of distance of separation between the particles and D approaches zero as 2d/a approaches zero, and that the rate of rapid coagulation can be reduced to a little less than half of the K_O value predicted by von Smoluchowski's equation.

Summary

The following comments can be made regarding the DLVO theory and the electrostatic stabilization:

- The origin of the charge on colloidal particles is well understood.
- The effect of valence of the electrolyte on the critical coagulation concentration can be understood from the Debye-Huckel parameter κ.
- The slopes of d log W/d log C have correct order of magnitude.

But, still there are certain weak points in this theory. They are as follows:

- The effect of the finite volume of the ions have been taken into account by the Stern's theory, but the pertinent parameters are difficult to measure experimentally.
- The surface potential Ψ_O cannot be measured experimentally due to the presence of the Stern layer. Often, experimentally measured zeta potential is substituted for Ψ_O.

- The expected dependence of d log W/d log C on particle radius is not confirmed, and whether this discrepancy is due to experimental problems or to a serious flaw in the theory is not yet known (Overbeek 82b).

- The minimum distance of closest approach of two particles is not known.

- The time scale of various relaxation processes occurring in the double layer are not incorporated in the theory (i.e., whether to use the constant charge or constant potential case).

- The recent direct force measurements between two macroscopic surfaces have confirmed the validity of the DLVO theory at the distances larger than 5 to 10 nm. But, the additional short range (1 to 10 nm) repulsive interactions due to changes in the liquid structure near the charged surface and attraction due to hydrophobic forces need to be considered. Quantitative treatments of these interactions are not yet available.

CHAPTER IV
EFFECT OF ADSORBED POLYMER ON DISPERSION STABILITY

Introduction

There are essentially two methods to impart stability to the dispersion of colloidal particles. In the last chapter, we reviewed the DLVO theory of electrostatic interactions between two charged particles, and potential energy versus distance diagrams were used to explain the stability behavior. In the case of electrostatic stabilization, the overlap of the electrical double layers around the charged particles give rise to repulsive interactions.

Absorbed polymer can affect two particle interactions in the following ways. It can increase the stability by increasing electrostatic repulsion between particles and/or decreasing the Van der Waal's attraction. The adsorbed polymer can also impart stability due to the additional "steric" component of repulsion. In this case, the overlap of the adsorbed polymer layers give rise to repulsive interactions. The protective action of the adsorbed polymer is often called "steric stabilization," (especially for the effects of non-ionic polymers on colloid stability) (Napper 83). The term 'steric stabilization' was introduced by Heller and Pugh (Heller and Pugh 54). As pointed out by Napper, the term 'steric' used in this context is a misnomer, and it has little in common with steric effects present in organic chemistry (Napper 83). The phenomenon of steric stabilization has a general thermodynamic basis. Steric interactions are of two major

kinds namely "entropic" and "mixing" interactions. Entropic interactions result from the loss of configurational freedom of the adsorbed polymer on approach of a second particle. The configuration entropy is decreased because less total volume is available for each chain due to "compression" of the chains. This effect is also called the "volume restriction" or the "elastic effect." The mixing interaction arises due to interpenetration of the adsorbed layers. This leads to a build up in the segment concentration in the interaction zone, and hence, an increase in the osmotic pressure. Hence, this mixing term is also known as the "Osmotic Repulsion" effect. The microscopic origin of these interactions will be considered later. As in the case of polymer adsorption behavior (Chapter II), interactions with adsorbed polymer will involve various interactions such as polymer-solvent, solvent-surface, and surface-polymer and as such is a very complicated problem.

Factors Influencing Steric Stabilization

Excellent reviews are available in this area, and hence, only a brief discussion will be attempted (Vincent 74; Tadros 82; Sato and Ruch 82; Napper 83; Lyklema 68; Vincent and Whittington 81). The principle factors governing the stability of particles with adsorbed layer are:

The Adsorbed Amount of Polymer

The adsorbed amount of polymer is related to the average thickness of the adsorbed layer (or, more importantly, to the segment density distribution). The adsorbed polymer should completely cover the particle surface to prevent "bridging flocculation." Generally speaking, in the absence of electrostatic interactions, at low polymer concentrations

(usually 0-1000 ppm), the dispersion is destabilized due to bridging flocculation, and at higher polymer dosages, the dispersion can be stabilized under certain conditions due to the steric interactions. To prepare stable dispersions, the adsorbed layer should have sufficient thickness to overcome the Van der Waal's attraction.

The Solvent-Segment Interaction Parameter, X

The origin of the steric stabilization is in the polymer solution thermodynamics. For the case of thick adsorbed polymer layers, the stability behavior can be related to the solvent-segment interaction parameter, X (i.e., it is independent of particle size, Hamaker constant, etc.) (Napper 83). The interactions between adsorbed polymer molecules are very similar to the interactions between the molecules in solution and directly related to the stability of long chains in solution.

The Effective Hamaker Constant and the Size of the Particles

These parameters are important when the thickness of the adsorbed polymer layer is small compared with the particle radius. For the case of thin adsorbed layers on the large particles, the Van der Waal's interactions are important.

The above factors can be controlled to influence the stability of polymer coated particles. For example, the adsorbed amount of polymer can be varied by changing the molecular weight of the polymer, chemical nature of the polymer, polymer concentration, etc. The solvency for the polymer molecules can be changed, for example, by changing electrolyte concentration or change in the temperature. As in the case of electrostatic stabilization, the effect of various parameters can be explained using the total interaction energy curves.

Applications and Advantages of Steric Stabilization

Steric stabilization has been used in a variety of technological applications and products (for example, paints, inks, glues, dispersion of latex particles, ceramic particulates, etc.) because it can offer several distinct advantages over electrostatic stabilization. These advantages will be discussed below:

(1) Relative Insensitivity to the Presence of Electrolytes

The thickness of the adsorbed layer (in the case of non-ionic polymer) is relatively insensitive to the presence of electrolyte, and hence, can overcome the Van der Waal's attraction. This is in sharp contrast with the effect of electrolyte concentration on the thickness of the electrical double layer. As discussed in the last chapter, the thickness of the electrical double layer, κ^{-1}, decreases with increasing electrolyte concentration. This effect can lead to the coagulation of electrostatically stabilized dispersion on the addition of high concentrations of electrolytes.

With a suitable steric stabilizer, coagulation can be prevented at high salt concentrations and dispersions of high solid volume fractions can be prepared. At low electrolyte concentrations, the thickness of the electrical double layer can be quite substantial. Concentrated dispersions of charged particles at low ionic strengths can have very high viscosities because of electroviscous effects (for e.g., see, von Smoluchowski 16a, Booth 48, Chan and Goring 66a, Chan et al. 66b, Stone-Masui and Watillon 68). In certain cases, this effect cannot be overcome by the addition of salt due to coagulation.

(2)   <u>Equally Effective in Aqueous and Non-aqueous Dispersion Medias</u>

From the practical experience, it can be concluded that the electrostatic stabilization is less effective in non-aqueous dispersion media than it is in aqueous media (Napper 83, Vincent 74). This is primarily due to the low relative dielectric constant of most non-aqueous media. Steric stabilization is equally effective in both aqueous and non-aqueous media, and for this reason, steric stabilization is often employed in non-aqueous dispersion media.

(3)   <u>Reversibility of Flocculation</u>

A sterically stabilized dispersion can be flocculated by adding non-solvent to the dispersion (or by changing the temperature). This behavior can be reversed by adding more solvent to the system (or by reversing the temperature change). In contrast to this behavior, the dispersion stabilized solely by an electrostatic mechanism can be coagulated by the addition of electrolyte, but that coagulation is usually irreversible to subsequent dilution. The difference in behavior between electrostatically and sterically stabilized dispersions may be due to the fact that the latter dispersions are thermodynamically stable, while the former dispersions are kinetically stable (Napper 83). The difference between these two cases will become clear when we consider the difference between the total interaction energy diagrams under these two stabilization mechanisms. In the latter case, the coagulation state is the lowest energy state, and it can be reversed only if additional work is done on the system (Overbeek 82b). One important consequence of the thermodynamic stability of sterically stabilized dispersion is that

particles redispersed spontaneously after drying (Napper 83). Sterically stabilized dispersions also often display good freeze-thaw stability.

Thermodynamic Basis of Steric Stabilization

The stability of sterically stabilized dispersion is thermodynamically limited provided that the following three requirements are fulfilled: (a) strong anchoring of polymer, (b) complete coverage of the surface, and (c) sufficiently large thickness of the adsorbed polymer layers. Under these condition, the thermodynamic limit of stability is largely dependent on the chemical nature of both the stabilizing moieties and the dispersion medium (i.e., solvent-polymer interactions). The stability is usually independent of particle nature and size and is independent of the chemical nature of the anchor polymer. The stability to instability transition can be induced in at least three different ways: by changing the temperature, by increasing the pressure, and by adding to the dispersion a miscible non-solvent medium for the stabilizing moieties (Napper 83). All of the above methods decrease the solvency of the dispersion medium for the stabilizing moieties. The transition from long-term stability to catastrophic flocculation occurs at the critical flocculation point (UFPT). This may be a critical flocculation temperature (CFT), a critical flocculation pressure (CFP), or a critical flocculation volume (CFV) of non solvent. It is possible to induce instability by increasing the temperature or cooling the dispersion. When the flocculation is induced by heating, CFT is usually called an upper critical flocculation temperature (UCFT), and when flocculation is induced by cooling, it is said to occur at a lower

critical flocculation temperature (LCFT). In principle, all sterically stabilized dispersions show a LCFT and a UCFT although both are not always experimentally accessible.

The thermodynamic limit is set by the polymer-solvent interactions, and hence, there is a strong correlation between the critical flocculation point and the theta point (θ point) of the stabilizing moieties. The theta point represents a transition point with respect to segment-solvent interactions. At this point, the interaction between two polymer segments changes from net repulsive to attractive. To understand this correlation between θ point and the stability, we will review briefly polymer solution thermodynamics.

Polymer Solution Thermodynamics

The best known theory of polymer solution was as developed by Flory and Huggins (Flory 53). The Flory-Huggins theory is based on statistical thermodynamics and describes the free energy changes associated with mixing of pure solvent and pure polymer. This is accomplished the separate calculations of the entropy of mixing and the enthalpy of mixing. Then, these two terms are combined to calculate the free energy change associated with the mixing processes as follows:

$$\Delta G_m = \Delta H_m - T\Delta S_m \tag{4.1}$$

where m denotes mixing.

The Entropy of Mixing

To calculate the configurational entropy, the lattice model was employed. In the model, a polymer molecule was assumed to consist of x segments and the size of each segment was assumed to be equal to the size

of solvent molecules. The total configurational entropy of the polymer

solution arises from the variety of ways of arranging the polymer and

solvent molecules. This was accomplished by placing a chain molecule

segment by segment on an empty or partially filled lattice. This

sequence of steps constitutes a three-dimensional random walk. A step in

such a walk is possible if the lattice site towards which it was directed

is unoccupied. To calculate the probability of finding a vacant lattice

site, the mean field approximation was made. It was assumed that all the

previously placed segments are uniformly distributed so that the solution

is a completely random mixture and local concentration was replaced by an

average segment concentration. Due to this assumption, the Flory-Huggins

theory is valid for relatively high polymer concentrations when the

polymer coils overlap extensively. With the above assumptions, the

configuration in entropy of mixing n_1 solvent molecules and n_2 polymer

molecules is given by the following expression[1]:

$$\Delta S_m = -k \ (n_1 \ \ln \ v_1 + n_2 \ \ln \ v_2) \tag{4.2}$$

where v_1 and v_2 are the volume fractions of solvent and solute,

respectively, and are defined as:

$$v_1 = n_1/(n_1 + xn_2) \text{ and } v_2 = (n_2 \cdot x)/(n_1 + xn_2) \tag{4.3}$$

and x is defined as:

$$x = \frac{\text{Molar volume of solute}}{\text{Molar volume of solvent}} \tag{4.4}$$

The above expression for the configurational entropy of mixing is

analogous to the expression for mixing of small molecules:

---

[1] It should be noted that the expression for the configurational
entropy of mixing can be arrived at following free volume theories (Flory
53).

$$\Delta S^m = -k \ (n_1 \ \ln x_1 + n_2 \ \ln x_2) \tag{4.5}$$

where x_i = mole fraction of species i.

The primary difference between the entropy of mixing expressions for small molecules (Equation 4.5) and for polymer solutions (Flory-Huggins Equation 4.2) is that mole fraction statistics is replaced by volume fraction statistics. This difference arises due to the dissimilarity in the sizes of solvent and polymer molecules. Since the values of volume fractions v_1 and v_2 are smaller than the unity, the entropy of mixing is always a positive quantity and mixing is spontaneous unless opposed by the enthalpy of mixing, ΔH_m. We will examine the enthalpy of mixing in the next section.

The Enthalpy of Mixing

Mixing can be considered as a quasi-chemical reaction between solvent contacts and segment contacts. Following Flory's lattice model, it can be represented as:

$$(1-1) + (2-2) \longrightarrow 2(1-1) \tag{4.6}$$

where 1 and 2 refer to solvent molecules and polymer segments, respectively, and the change in the enthalpy of formation of 1-2 contacts is given by:

$$\Delta \omega_{12} = \omega_{12} - \frac{1}{2} \ (\omega_{11} + \omega_{22}) \tag{4.7}$$

where ω_{11}, ω_{22}, and ω_{12} are the enthalpies associated with the respective pair contacts. For the case of random mixing of n_1 solvent molecules and n_2 polymer molecules, it can be shown that (Flory 53):

$$\Delta H_m = Z \Delta \omega_{12} n_1 v_2 \tag{4.8}$$

where Z is the coordination number of the lattice site and v_2 is the volume fraction of polymer. Now, if we write:

$$\Delta H_m = kT \chi n_1 \nu_2 \qquad (4.9)$$

Then, we have $\chi = \dfrac{\Delta H_m}{kTn_1\nu_2} = \dfrac{Z\Delta\omega_{12}}{kT}$ \qquad (4.10)

The parameter χ is called the Flory-Huggins interaction parameter. It is defined in such a way that χkT represents the difference in energy of a solvent molecule immersed in a pure polymer compared with that in pure solvent.

The expression for the total free energy of mixing can be obtained by combining equations for the enthalpy and entropy changes and is given as follows:

$$\Delta H_m - T\Delta S_m =$$
$$\Delta G_m = kT \{n_1 \ln \nu_1 + n_2 \ln \nu_2 + n_1 \nu_2 \chi\} \qquad (4.11)$$

As mentioned earlier, ΔS_m is always positive, hence, it contributes to a negative value of ΔG_m. The ΔH_m contribution can be either positive or negative depending on the sign of χ. For non-aqueous solvents, χ is often positive (i.e., mixing is endothermic), and hence, contact dissimilarity often opposes mixing. Note that χkT was originally introduced as a change in internal energy, but the above treatment will be essentially the same if χkT is considered as a free energy change for the process (Flory 53). In this way, χ determined experimentally incorporates both enthalpy and entropy change associated with the dissimilar contact formation.

The χ Parameter

From the above expression for the free energy of mixing, the chemical potential of the solvent and solute can be determined. The

chemical potential difference is related to the osmotic pressure as follows:

$$\pi = - (\mu_1 - \mu_1{}^o) / \bar{V}_1 \qquad (4.12)$$

where π is the osmotic pressure, $(\mu_1 - \mu_1{}^o)$ represents the change in the chemical potential of the solvent and $\bar{V}_1$ is the solvent molar volume. It can be shown that the osmotic pressure can be represented as (see Flory 53):

$$\pi/C_2 = RT \{B_1 + B_2C_2 + B_3C_2{}^2 + \dots \} \qquad (4.13)$$

where C_2 is the polymer concentration. B_1 is the first viral coefficient and B_1 is related to the number average molecular weight (i.e., $\pi/C_2 = RT/<Mn>$ according to van't Hoff osmotic pressure equation).

B_2 and B_3 are second and third viral coefficients. According to the Flory-Huggins theory, B_2 is given by the following equation:

$$B_2 = (\tfrac{1}{2} - \chi) \, \bar{V}_2{}^2 / \, \bar{V}_1{}^2 \, M^2 \qquad (4.14)$$

where $\bar{V}_i$ are the molar volume of solute and solvent and M is the molecular weight of the polymer.

Thus, the χ parameter is related to the osmotic pressure of the solvent. As mentioned earlier, the interaction parameter χ can be considered as a contact dissimilarity free energy, i.e., it contains both enthalpic and entropic contributions. Flory has defined enthalpy $(\varkappa_1)$ and entropy (Ψ_1) of dilution parameters as follows (Flory 53):

$$\Delta\bar{H}_1 = RT\varkappa_1\nu_2{}^2 \quad \text{and} \quad \Delta\bar{S}_1 = \Psi_1\nu_2{}^2 \qquad (4.15)$$

Here $\Delta\bar{H}_1$ and $\bar{\Delta}S_1$ are partial molar enthalpy and entropy. It can be shown that χ is related to $\varkappa_1$ and Ψ_1 as follows:

$$(\tfrac{1}{2} - \chi) = (\varkappa_1 - \Psi_1) \qquad (4.16)$$

and this important result allows the interaction free energy to be related to its enthalpic and entropic contributions.

The Theta Point

The equation for the second viral coefficient (B_2) shows that its value becomes zero when $\chi = 1/2$ (Equation 4.14). The point at which the second viral coefficient B_2 vanishes is known as the theta (θ) point. It has been also called the Flory point. In polymer/solvent systems, the second viral coefficient becomes equal to zero at some temperature, called the theta temperature. Then, the theta temperature is defined as follows:

$$\theta = \frac{\kappa_1 T}{\Psi_1} \text{ so that } \Psi_1 - \kappa_1 = \Psi_1 (1-\theta/T) = (\frac{1}{2} - \chi) \tag{4.17}$$

Clearly, if $T = \theta$, then, $\chi = 1/2$. The parameter χ can be used to compare different solvents at a single temperature, while the θ temperature can be used to describe changes in solvent goodness arising due to temperature changes. At the theta conditions (i.e., $\chi = 1/2$ or $T = \theta$), polymer solutions behave ideally. Under θ solvency conditions, high molecular weight polymer molecules behave as if they were ideal small molecules. At θ conditions, the excluded volume effects and intermolecular attractions are canceled out. Thus, the θ point represents the transitional point with respect to solvent-segment interactions. At $\theta = T$ or $\chi = 1/2$, the free energy of interaction is zero, i.e., there is no preference for the solvent or segment. When $\theta < T$ or $\chi < 1/2$, this case corresponds to the position derivation from the ideality. Under these conditions, dissimilar contacts are favored. For

a given system of solvent and polymer, the value of $\chi < 1/2$ indicates that the solvent is a good solvent. $\chi = 0$ is called an athermal solvent for which the enthalpy of mixing is zero. When $\theta > T$ (or $\chi > 1/2$), there is a negative derivation from the ideality, and under these conditions, there is a mutual attraction between polymer segments.

The value of χ is not predicted by the Flory-Huggins theory and must be measured experimentally. According to this theory, experimentally determined values should be independent of the concentration of the polymer. Measured values of χ parameter are usually concentration dependent, and for many systems, the free energy change associated with the exchange process is predominantly entropic in origin, and enthalpic contribution is relatively small. Also, the observation of phase separation upon heating non-aqueous polymer solutions cannot be explained by the original Flory-Huggins theory. To account for phase separation upon heating, free volume theories have been proposed (see Flory 70, Napper 83).

These theories account for the differences in the free volumes for the solvent and solute molecules at higher temperatures. Flory has developed an elaborate equation-of-state theory for non-aqueous polymer solutions that incorporates the changes in free volume of mixing as well as the combinational and contact dissimilarity contributions (Flory 70). The concepts underlying the theory can be used to describe microscopic processes that generate steric stabilization in both non-aqueous and aqueous dispersions. The free volume of the solvent near its critical point is much larger than the free volume of the polymer molecules. Near the critical point, solvent molecules essentially behave like a gas,

while due to the covalent bond constraints, there is no substantial increase in the free volume of the polymer molecules. When polymer molecules are placed in contact with solvent vapor, these segments can act as condensation sites. This condensation of solvent molecules provides a negative contribution to mixing entropy and, if sufficiently large, can promote phase separation. The enthalpy change associated with condensation is positive and opposes phase separation. The free volume dissimilarity provides the rationale for the following observations: (1) the observed phase separations on heating, (2) the strong entropic contribution to χ that opposes mixing, and (3) the concentration dependence of χ as an increase in the polymer concentration provides more condensation sites for the solvent molecules.

To explain the microscopic origin of the steric stabilization, the free energy changes associated with the combinational (as described earlier), contact dissimilarity and free volume dissimilarity should be considered (Napper 83). At normal temperatures, combinational entropy is responsible for the stability of non-aqueous dispersion. During the Brownian encounter of two colloidal particles, the adsorbed polymer layers will interpenetrate. This leads to an increase in the concentration of polymer segments in the interaction zone and transfer of solvent molecules into the dispersion media. Thus, there is a decrease in the entropy of mixing between polymer segments and solvent molecules on close approach of particles. The loss of entropy generates the observed steric stabilization. At high temperatures, the contribution due to the differences in free volume can become more important, and

thus, flocculation can occur at the critical temperature of the dispersion medium.

At present, there is no satisfactory theory for the thermodynamics of aqueous polymer solutions. The strong interactions between polar water molecules and water soluble polymers makes description speculative (Napper 83). The contributions of combinational and free volume dissimilarity terms to free energy are essentially the same as in non-aqueous dispersions. The main contribution to stability arises from the contact dissimilarity term due to the specific interactions (such as hydrogen bonding) between water molecules and polar stabilizing moieties (for example, hydroxyl groups of PVA). During the interpenetration of the adsorbed polymer layers, the bound water is released from the interaction zone into the bulk dispersion media. This process of removal of bound water is associated with the positive enthalpy change that opposes flocculation. This enthalpic stabilization is more common in aqueous dispersions (Napper 83).

Classification of Steric Stabilization

Three different types of steric stabilization can be classified as enthalpic, entropic, or combined enthalpic-entropic. This classification is based on the overall free energy change during the encounter of two sterically stabilized particles and can be represented as follows:

$$\Delta G_F = \Delta H_F - T\Delta S_F \tag{4.18}$$

where ΔG_F represents the free energy of flocculation of a pair of particles, and ΔH_F and ΔS_F are the enthalpic and entropic contributions, respectively. A positive value of ΔG_F indicates the particles are

sterically stabilized. The sign and the magnitude determines the type of steric stabilization as shown in the Table 4.1.

In enthalpic stabilization, the enthalpy changes associated with the overlap promotes stabilization whereas the corresponding entropy change promotes flocculation. At room temperature, the enthalpic contribution is dominant, and hence, promotes stabilization. In entropic stabilization, the entropy change promotes stability, whereas it is disfavored by the enthalpy change. In this case, the overall contribution of the entropy change prevails. In the case of combined enthalpic-entropic stabilization, both the enthalpic and the entropic changes contribute to stability.

At room temperature and pressure, entropic stabilization is more common in non-aqueous dispersion media, and enthalpic stabilization is more common in aqueous media. However, there are several examples contradicting the above statement (Napper 83).

Quantitative Theories of Steric Stabilization

In order to discuss the stability of colloidal particles, it is essential to know the pairwise interactions between two particles. In the case of two charged particles, the stability behavior can be explained from the well-known DLVO theory (See Chapter II). In the case of steric stabilization, no such general quantitative theory is available. The reasons for this are two-fold. One is the lack of quantitative theory of polymer solution thermodynamics which is the foundation of any theory of steric stabilization. Second, in order to calculate the distance dependence of steric interactions, it is necessary

TABLE 4.1

Classification of Steric Stabilization Depending on the Sign and
the Magnitude of Enthalpic and Entropic Contributions

ΔG_F	ΔH_F	ΔS_F	$|\Delta H_F|/|T\Delta S_F|$	Stabilization Type	Flocculation
≥0	+	+	≥1	Enthalpic	Heating to UCFT
≥0	−	−	≤1	Entropic	Cooling to LCFT
≥0	+	−	≶1	Combined Enthalpic-Entropic	Not accessible

to predict the conformation of the adsorbed polymer sandwiched between two flat plates. It is not possible to predict quantitatively the conformation of free polymer molecules in solution except for the limiting case such as θ solvent. Hence, a general quantitative description is not available. Despite these difficulties, various models have been developed to predict the distance dependence of steric interactions (Mackor 51; Fisher 58; Clayfield and Lumb 66,68; Meier 67; Dolan and Edwards 74; Ottewill and Walker 68; Napper 77; Scheutjeans and Fleer 85; Hesselink 77; Hesselink et al. 71b; Bagchi and Vold 72; Bagchi 74a,74b; deGennes 82,87).

The Three Domains of Close Approach

Figure 4.1 shows two parallel flat plates separated by a distance d and coated by the adsorbed polymer layer of thickness L. The three domains at close approach are classified as follows:

(a) d > 2L: This is called non-interpenetrational domain. In this case, the plates are too far apart for the adsorbed layers to overlap, and there is no steric interaction.

(b) L ≤ d ≤ 2L: This is called the interpenetrational domain. Once the distance of separation is less than twice the thickness of the adsorbed layer, the polymers attached to opposing surfaces undergo interpenetration. The increased segment concentration in the overlap region forces solvent molecules into the bulk dispersion media, and thus, reduces mixing between the polymer segments and the solvent molecules. In a good solvent ($\chi < 0.5$), the demixing of segments and solvents raises the free energy of the system leading to steric stabilization. In worse
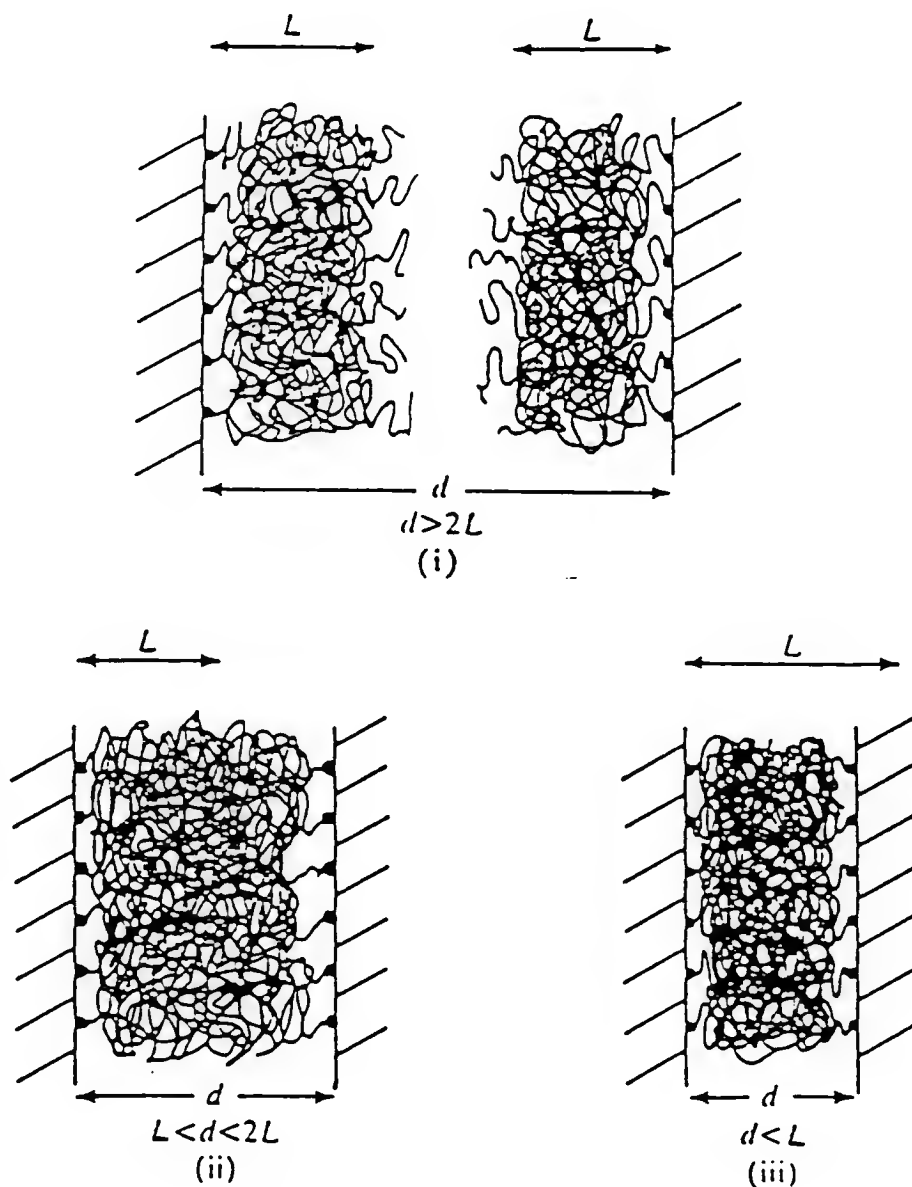
Figure 4.1   The three domains of close approach of sterically
              stabilized flat plates, (i) Noninterpenetration (d > 2L);
              (ii) Interpenetration (L ≤ d ≤ 2L);
              (iii) Interpenetration plus compression (d < L) (Napper,
              1983).

than θ solvent, overlap leads to attraction. The repulsion arising due to interpenetration is known as the "mixing" or "osmotic" effect.

(c) d < L: This is called interpenetrational-plus-compression domain. The free energy change in this case is derived from two components: a solvent-segment mixing term (as above) and an elastic component. The elastic effect arises due to the compression of the adsorbed layer by the opposing surfaces. This would reduce the volume available for the adsorbed molecules, and hence, restrict the number of possible configurations. This reduces the configurational entropy and, irrespective of the solvent quality, leads to repulsion between two surfaces. This effect is also called the "volume restriction" or "elastic" effect.

The classical approach for calculating steric interactions has been to consider two limiting cases: (1) interpenetration without compression and (2) compression without any interpenetration. These two terms are added to calculate total steric interactions. We will consider these two limiting cases in more detail.

The Interpenetration Domain

The free energy of mixing of polymer segments with solvent molecules in a small volume dV is given by the Flory-Krigbaum theory as follows:

$$\delta(\Delta G^M) = kT \ (\delta n_1 \ln \nu_1 + \delta n_1 \nu_2 \chi) \tag{4.19}$$

where δn_1 = number of solvent molecules in the volume element, and ν_1 and ν_2 are the volume fractions of solvent and solute. $\nu_1 = 1 - \nu_2 = 1 - \rho_2 V_s$, where ρ_2 = segment density distribution function of the polymer, V_s is the volume of the polymer segment. On expanding the logarithmic

function and ignoring terms higher than second order, the above equation

becomes:

$$\delta(\Delta G^M) = (kT/V_1) \{ - (1-\chi) \rho_2 V_s + (1/2-x_1) \rho_2^2 V_s^2 \} dV \qquad (4.20)$$

where V_1 is the volume of the solvent molecule.

This equation is applicable to all domains of approach.

The mixing free energy change for the approach of two sterically

stabilized particles, ΔG^M, is given by the following equation:

$$\Delta G^M = \Delta G(d) - \Delta G(\infty) \qquad (4.21)$$

where $\Delta G(d)$ = the mixing free energy at distance = d, and $\Delta G(\infty)$ = the

mixing free energy when the particles are separated by infinite distance.

After substituting the Equation 4.19 into Equation 4.20, the following

result is obtained:

$$\Delta G^M = kT \ (V_s^2/V_1)(\frac{1}{2} - \chi) \ [\int_V \rho_2^2(d)dV - \int_V \rho_2^2(\infty)dV] \qquad (4.22)$$

Thus, to evaluate the mixing free energy change, the following

quantitives should be known:

(i) The distance dependence of the segment density distribution, i.e.,

when the particles are separated by a distance d and when they are

infinitely separated, and

(ii) Geometry of the interacting bodies: Usually, two flat plates or

spherical particles are considered. Various treatments of steric

stabilization can be classified based on the assumptions regarding the

segment density distribution.

(1) Theoretically Derived Segment Density Distributions: Various

theoretical models are available to predict the segment density

distribution of the adsorbed polymer with or without the presence of

other interfaces. Meier (Meier 67) calculated the segment density

distribution for the isolated adsorbed polymer, and Hesselink (Hesselink 71) derived the segment density distributions for the case of isolated loop and tail conformation. Segment density distributions also have been derived from lattice models (SF) (Scheutjeans and Fleer 85) and from scaling concepts (deGennes 80). Napper has called these theories ab initio theories (Napper 83).

(2) <u>Experimentally Determined Segment Density Distributions</u>: Recently, it has become possible to obtain segment density distribution from the small angle neutron scattering, (SANS) technique (Barnett et al. 82). (The segment density distribution is exponential near the surface of the physically adsorbed polymer, but this technique is not sensitive enough to pick up the signal from the dilute tails far away from the interface.) It is then possible to use the experimentally determined segment density distribution to carry out necessary integration. Also, from experimentally determined force vs. distance curves, it may be possible to deduce the information about the segment density distribution.

(3) <u>Assumption Regarding the Segment Density Distribution</u>: This class of theories has been called the pragmatic theories of steric stabilization by Napper (Napper 83). Various types of segment density distributions can be assumed, such as constant segment density, exponential, the radial Gaussian, etc.

Only two equations for interactions between polymer-coated spherical particles will be reported here. According to the HVO theory (Hesselink et al. 71b), the mixing free energy for spheres is given by the following equation:

$$\Delta G^M = [2\pi^{5/2}/27] \, \nu^2 \, kT \, a \, <r^2>^{3/2} \, (\alpha^2-1) \, S^M \qquad (4.23)$$

where a = particle radius, d = the minimum distance of surface separations of the spheres, ν = the number of tails (loops) per unit area, and α is the expansion factor defined as $\alpha = \langle r^2 \rangle^{1/2} / \langle r^2 \rangle_o^{1/2}$. Where $\langle r^2 \rangle_o^{1/2}$ refers to unpurturbed dimensions (i.e., under θ conditions), $\langle r^2 \rangle^{1/2}$ is the r.m.s. end to end length of the polymer molecule in solution.

The distance dependence of S^M is given by the following equation for equal tails $S_T^M = 1.2\pi d^2 / \langle r^2 \rangle^{1/2} \exp \{- 1.2d^2 / \langle r^2 \rangle\}$.

And for equal loops, $S_L^M = 3\pi d^2 / \langle r^2 \rangle^{1/2} \exp \{- 3d^2 / \langle r^2 \rangle\}$. α is related to $(1/2 - \chi)$ by the following equation (Flory 53):

$$\alpha^5 - \alpha^3 = \frac{(9/2\pi)^{3/2} \, v_s^2 \, (\frac{1}{2} - \chi)}{v_1 \, \langle r \rangle_o^2 \,^{3/2}} \tag{4.24}$$

For the case of constant segment density distribution with the adsorbed layer thickness δ, Fisher gave the following expression (Fisher 58):

$$\Delta G^M = 4\pi a w^2 N_A \, (\bar{v}_2^2/\bar{v}_1)(\frac{1}{2} - \chi) \, kT \, (1 - d/2\delta)^2 \tag{4.25}$$

where w = weight of stabilizing moieties attached per unit area, N_A = Avogadro's number, $\bar{V}_1$ and $\bar{V}_2$ are the molar volumes of the solvent and polymer, respectively, and $\bar{v}_2 = \bar{V}_2/M$ is the partial specific volume of polymer.

From the above two equations, it is clear that the free energy of mixing (hence, steric stabilization) is controlled by the following factors: (i) particle size a, (ii) amount adsorbed (w or ν), (iii) solvent quality as determined by χ or α, (iv) molecular weight of the

polymer (through r.m.s. end to end distance or δ, the adsorbed layer thickness), and (v) segment density distribution.

The effect of the above parameters on the interparticle particle interactions will be reviewed in detail later. From Equations 4.23 and 4.25, it is clear that at θ conditions (x = 0.5 or α = 1), the net free energy of mixing is zero, and in a good solvent (x < 0.5 and α > 1), repulsion prevails, while in a poor solvent, attraction between particles leads to catastrophic flocculation.

Interpenetration Without Mixing (Elastic Repulsion)

This is the second term arising due to the compression of the adsorbed layer upon closer approach of two coated particles during the Brownian collision. This term becomes particularly important when the separation distance is less than the adsorbed layer thickness, i.e., (L < d). This leads to the reduction in the available volume to adsorbed molecules, and hence, restricts the number of possible configurations for adsorbed polymer chains. Thus, the loss in number of configurations on the approach of the second particle can be related to the decrease in the configurational entropy, ΔS, using the Boltzmann equation:

$$\Delta S = k \ln \frac{\Omega(d)}{\Omega(\infty)} \qquad (4.26)$$

where Ω is the total number of possible configurations when the second interface is present at a distance d, and Ω(∞) is the total number of possible configurations when the two particles are infinite distance apart. Evaluation of Ω(d), and Ω(∞) is model dependent. Usually, the effect of solvent is ignored. Mackor first attempted to evaluate these terms assuming a simple model based on inflexible rods terminally

attached, but freely jointed to a flat interface (Mackor 51). Clayfield and Lumb used Monte Carlo computations to calculate steric repulsion for flexible, terminally attached macromolecules (Clayfield and Lumb 66). Meier (Meier 67), and subsequently Hesselink (Hesselink 71a), applied random flight statistics to evaluate loss in configurational entropy for equal size loops and tails. A free energy change from the elastic effects for two flat plates is given by:

$$\Delta G^{VR} = 2\nu kTV(d) \tag{4.27}$$

where ν is the adsorbed amount of tails (loops) per unit area, and $V(d)$ determines the distance dependence of the elastic free energy contribution. The value of $V(d)$ needs to be evaluated numerically for the case of equal loops and equal tails. Approximate analytical expressions are also available (Hesselink et al. 71b). Subsequently, the effect of tail size distribution on the elastic free energy change has been considered, and it was shown that, with the wider tail size distribution, the repulsion curves becomes less steep (Hesselink 77). Bagchi (Bagchi 74a,74b) has proposed that, at high surface coverage, the adsorption layers will be dense and mixing will be improbable. On close approach of the two particles, the polymer layers will be compressed with the exclusion of solvent from the adsorption layer. This mechanism is called the "denting mechanism." The denting hypothesis has been criticized by Napper on the grounds that volume fraction of segments in the interactional zone rarely exceeds 0.1, and denting puts severe constraint on the conformation of stabilizing polymer, and hence, interpenetration is strongly favored over denting (Napper 83).

To evaluate the distance dependence of the elastic free energy contribution to steric stabilization, Hesselink assumed a theoretically derived segment density distribution, while Bagchi assumed a constant segment density. Evans et al. have shown that the elastic free energy change for spherical particles is given by (Evans et al. 77):

$$\Delta G^{VR} = 2\pi a \nu kTS_E \tag{4.28}$$

where $\nu = wN_A/M$, w = weight of stabilizing chains per unit area of surface, M = molecular weight of the polymer, and S_E is the distance dependent function for elastic repulsion. The S_E is a function of adsorbed layer thickness δ and the minimum distance between surfaces of the spheres, and it is a very sensitive function of the form of segment density distribution. The specific case of polystyrene latex spheres carrying adsorbed poly (vinyl alcohol) and dispersed in water has been considered by Smitham and Napper (Smitham and Napper 79). The effect of the assumed form of the segment density distribution on the elastic free energy repulsion is shown in Figure 4.2. It can be seen that, in the region, $\delta < d < 2\delta$, G(uniform) > G(Gaussion) $\approx$ G(radial Gaussian) >>> G_S(exponential), and at $d < \approx \delta/3$ G(exponential) > G(uniform).

Flory's classical lattice theory of polymer solutions has been used to evaluate interpenetration and elastic interactions, and hence, has a number of limitations discussed previously. The possible use of free volume theories (Flory 69) to evaluate mixing interactions have been considered by Evans and Napper (Evans et al. 77), but the mathematics is quite involved. The separation of steric interactions into elastic and mixing terms is open to criticism. To avoid this artifact, Dolan and Edwards (Dolan and Edwards 74) proposed a theory based on a self-
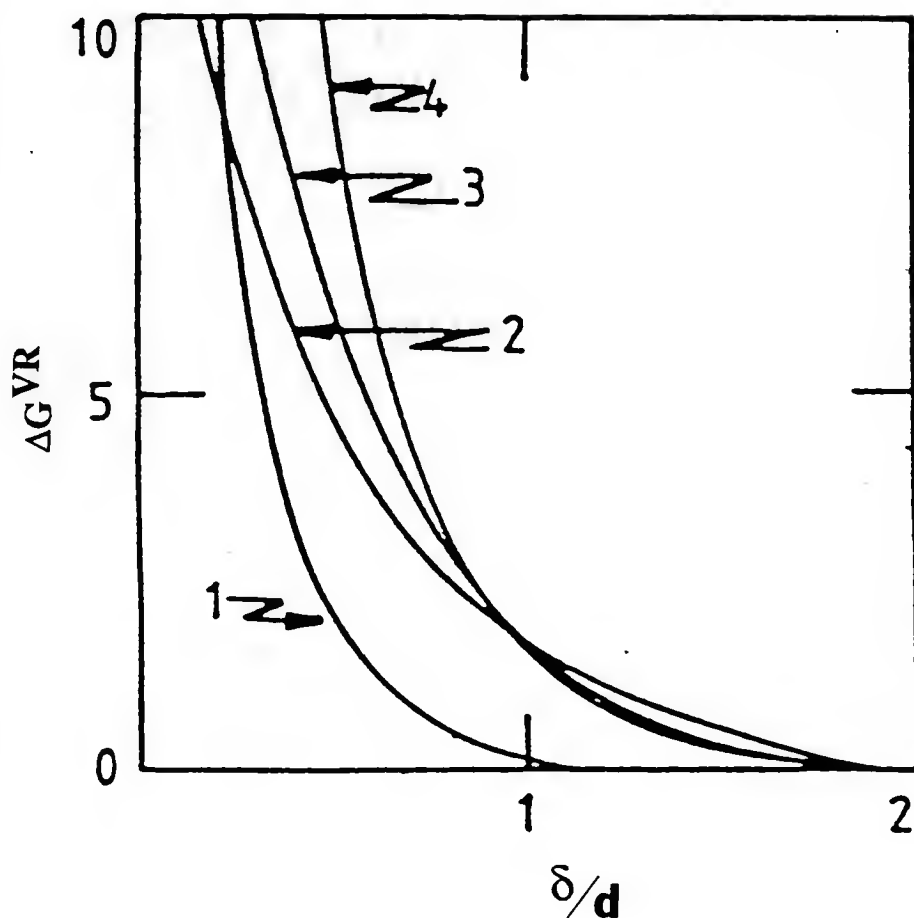
Figure 4.2   The distance dependence of the steric
interaction energy for two equal spheres of
radius a, stabilized by polymer layers with
different segment density distribution
functions. (1) exponential; (2) constant;
(3) Gaussian; (4) radial Gaussian. d is
the minimum distance between surfaces of
the spheres, δ is the barrier thickness,
and ΔG^S is the interaction energy (Smitham
and Napper, 1979).

consistent field approach. They evaluated the free energy term as a configurational term by treating the interactions between all polymer segments (i.e., intermolecular as well as intramolecular interactions). Then, calculations are limited to the good solvent regime, and as expected, predict strong repulsive interactions as predicted. Levine et al. have applied the self-consistent field approach to treat polymer adsorption process (Levine et al. 78). Scheutjeans and Fleer have extended this approach to polymer adsorption (Scheutjeans and Fleer 79,80) and to calculate the potential energy diagrams for steric interactions under variety of conditions (Fleer and Scheutjeans 86). That is the topic of the next section.

The Potential Energy Diagrams

The two factors contributing to steric stabilization are the loss of configurational entropy of two adsorbed polymer layers and the free energy of mixing. To describe the interactions, it was assumed that the particles were uniformly coated with the adsorbed polymer layer (i.e., complete surface coverages). This situation is valid at high polymer concentrations.

Time Scale of Approach of the Second Interface

Generally, two cases are considered (a) full equilibrium and (b) restricted equilibrium. (This situation is similar to constant potential and constant change case with the electrostatically stabilized dispersions.) In full equilibrium, the polymer is allowed to leave the gap between two particles during the Brownian encounter. Increased

polymer segment concentration in the overlap region puts severe entropical restriction on the adsorbed polymer if it cannot leave the gap. Polymer desorption, being a very slow process, is questionable to what extent the full equilibrium condition is applicable. The time, τ_{en}, it takes for two spherical colloidal particles of radius a to travel to distance δ corresponding to the thickness of an adsorbed layer during Brownian collision is given by (Hesselink et al. 71b):

$$\tau_{en} = 3\pi\eta a\delta^2 \ / \ 2kT \tag{4.29}$$

where the symbols have their usual meanings.

For example, in the case of 0.5 μm particles with the adsorbed layer thickness of 50 nm dispersed in water (i.e., viscosity $\eta \approx 1$ cp), the time of encounter is approximately 3 milliseconds. We can introduce the ratio (Lyklema 85):

$$D = \frac{\tau_{en}}{\tau_{des}}. \tag{4.30}$$

where τ_{des} equals the time of desorption. In practice, τ_{des} is usually very high, and depending upon conditions, it may be of the order of hours (Cosgrove and Fergie-Woods 87). Hence, D << 1 means that the polymers have no time to desorb. From the scaling theory, deGennes has proved that in full equilibrium (i.e., D >> 1), only attraction is found between two particles, and hence, steric stabilization cannot be explained (deGennes 82). This has also been proved from the self-consistent field lattice theory (Fleer and Scheutjeans 86). In this case, desorption of the polymer develops empty sites on the surface which can be bridged by the polymer molecules adsorbed on the other particles. Therefore, the case in which the amount of polymer is assumed to be constant during

particle encounter is more important (i.e.., D << 1). In this case, "local" or "restricted" equilibrium is assumed, and the segment density distribution and the distribution of trains, loops, and bridges adjust to a variable particle separation. This assumption has been used by all theories described earlier (e.g., Hesselink et al., Bagchi, Fisher, etc.).

The Potential Energy of Interaction

The total interaction between two polymer-coated particles is given by:

$$\Delta G^T = \Delta G^E + \Delta G^A + \Delta G^S \qquad (4.31)$$

where ΔG^E is the electrical double layer repulsion, ΔG^A is the Van der Waal's attraction, and ΔG^S is the steric interaction energy which consists of two additive contributions, i.e.,

$$\Delta G^S = \Delta G^{VR} + \Delta G^M \qquad (4.32)$$

where ΔG^{VR} is the elastic or volume restriction on entropic contribution, and ΔG^M is the mixing energy term. Both ΔG^E and ΔG^A are modified due to the presence of the adsorbed polymer layer (Vold 61, Vincent 74). First, we will consider a case where ΔG^E is negligible, and the adsorbed polymer layers have no effect on ΔG^A. (This approximation is usually valid as the concentration of segments in the adsorbed layer is generally quite low, and the Hamaker constant of the adsorbed polymer layer is similar to that of the dispersion media--e.g., see Bagchi 74a,74b). Under these assumptions, the total interaction energy as a function of distance between two flat plates is given by the following equations:

$$\Delta G^T = \Delta G^{VR} + \Delta G^M - \frac{A_{131}}{12\pi d^2} \tag{4.33}$$

and substituting for ΔG^{VR} and ΔG^M from the HVO theory, we obtain (Hesselink 77):

$$\Delta G^T = 2\nu kTV(d) + 2(2\pi/9)^{3/2} \nu^2 kT(\alpha^2-1)<r^2> M(d) - \frac{A_{131}}{12\pi d^2} \tag{4.34}$$

Thus, the main parameters determining the total free energy change of interaction, ΔG^T, on the approach of two flat plates, each carrying an adsorbed polymer layer are:

1. The adsorbed amount of polymer through ν, where ν is the number of tails (loops) per unit area and $w = \nu M/N_{av}$, where w is the adsorbed amount of polymer per unit area, and M is the molecular weight and N_{av} is Avogadro's number.

2. The dimensions of the adsorbed tails: where $<r^2>$ is the mean square end to end distance of the tail in solution.

3. The solvent quality χ as expressed in terms of the expansion factor α.

4. The mode of attachment of the polymer, i.e., tails or loops. $V(d)$ and $M(d)$ are the volume restriction and osmotic repulsion functions that give the dependence of ΔG^T on the distance d between the surfaces. $M(d)$ and $V(d)$ are extremely dependent on the mode of adsorption (i.e., conformation of the adsorbed polymer). Generally, the values of $M(d)$ and $V(d)$ are tabulated (Hesselink et al. 71b), and simple analytical approximate expressions are also available (Hesselink 77) and dependent on the form of the segment density distribution assumed.

Figure 4.3 shows the schematic of the total interaction energy as a function of distance of separation between two plates with the adsorbed polymer layer. Various contributions to the total interaction energy are also shown. At large values of d > 2L (where L is the adsorbed layer thickness), the Van der Waal's attraction predominates, but at close approach, very steep repulsion prevents further approach. The mixing interactions, ΔG^M, starts at higher values of d (usually $L \leq d \leq 2L$) than elastic interaction, ΔG^{VR} (usually $L \leq d$). This is expected since the mixing interactions start as soon as the polymer layers overlap, whereas the elastic repulsion starts after further closer approach of the two surfaces. Unlike the total interaction energy plots for the electrostatically stabilized system, the sterically stabilized system does not display the characteristic maxima and primary minima. Sterically stabilized systems display only one minima, ΔG_{min}, over the whole range of d and the stability/flocculation behavior is controlled by the magnitude of ΔG_{min}. Depending on the shape of the total interaction energy curve, the dispersion stability can be classified into various categories. The sign and magnitude of various contributions to the total interaction energy diagram are determined by the parameters, such as solvent quality, molecular weight, polymer concentration in solution, etc. Sterically stabilized dispersions can be classified into the following general categories:

Thermodynamically Limited Stability

The stability/instability transition of the sterically stabilized dispersions provides an insight about the thermodynamic factors controlling the stability. This type of steric stabilization is
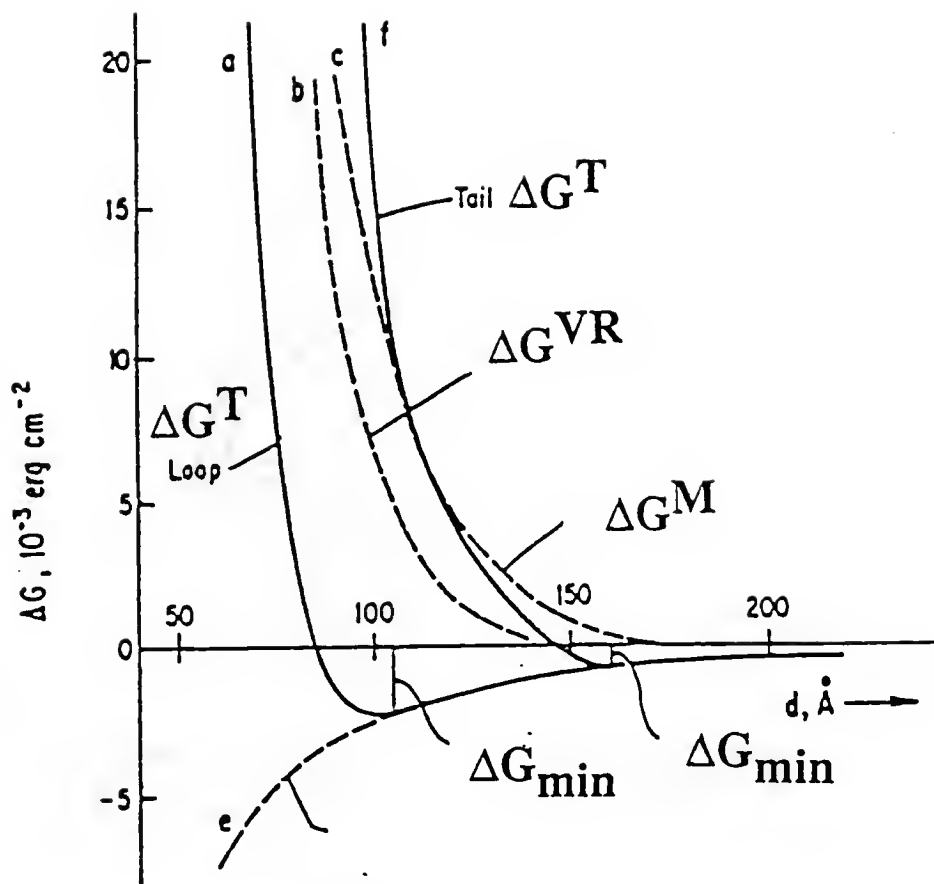
Figure 4.3   The free energy of interaction between particles covered
by equal tails (f) and equal loops (a). For particles
covered by equal tails, (b) gives the volume restriction
effect and (c) the osmotic repulsion; (f) is the
resultant of adding (b), (c), and (e) (Hesselink et al.
1971).

exhibited by colloidal particles with a firmly anchored polymer layer of sufficient thickness. In this case, the Van der Waal's interactions between the particles are unimportant, hence, the size of the particles has no significant effect on the stability. The stability behavior is essentially determined by the polymer solution thermodynamics, i.e., entropic and enthalpic interactions between the adsorbed polymer layer during the Brownian encounter. Hence, it is not surprising that the strong correlation exists between the CFT (i.e., critical flocculation temperature), CFV (i.e., critical flocculation volume of the non-solvent), and the theta conditions for the polymer chains in solution. As discussed earlier, the theta condition represents the thermodynamic limit of stability for an infinite molecular weight polymer. Above θ temperature (or in a poor solvent with $\chi > 0.5$), there is a net segment-segment attraction, and below θ temperature (or in a good solvent with $\chi < 0.5$), net segment-segment repulsion exists. At the θ temperature, there is no net free energy change associated with the overlap. The effect of the solvent-segment interaction parameter χ on the potential energy diagram is shown in Figure 4.4.

As shown in Figure 4.4A, in a poor solvent, the depth of the potential energy minima ΔG_{min} is sufficient to cause the flocculation of the particles. In this case (note that the depth of ΔG_{min} is much larger than the Van der Waal's attraction at a distance of separation of the order of 2L), the sign of mixing term is negative since there is a net segment-segment attraction. (This can be also seen from the Equations 4.23 and 4.25, when for the poor solvent, $\alpha < 1$ or $\chi > 0.5$ and ΔG^M is negative.) At the θ conditions, Figure 4.4B, $\Delta G^M = 0$ (since $\alpha = 1$ at $\chi =$

118
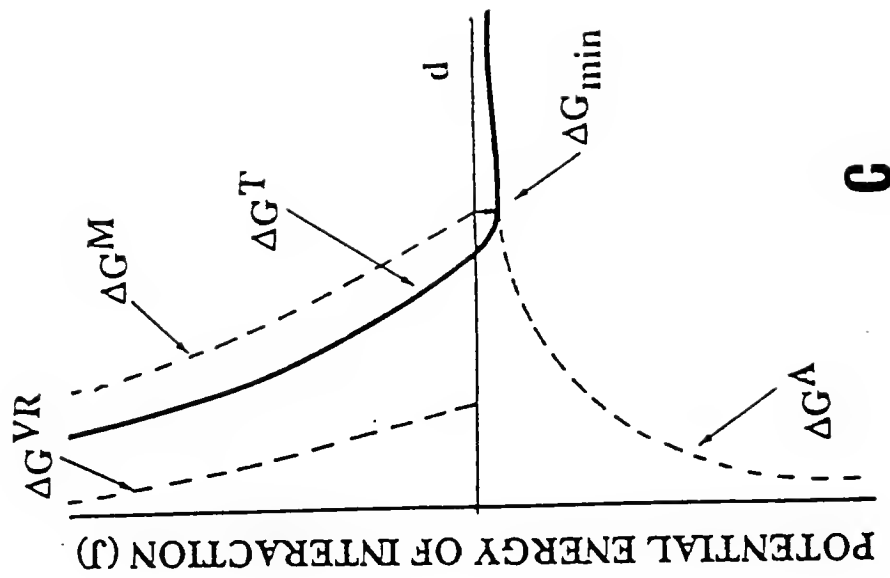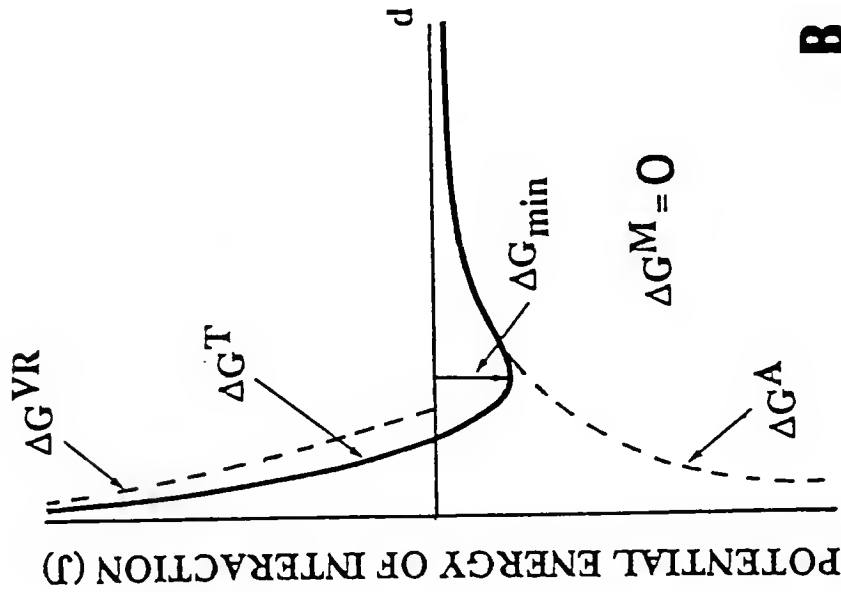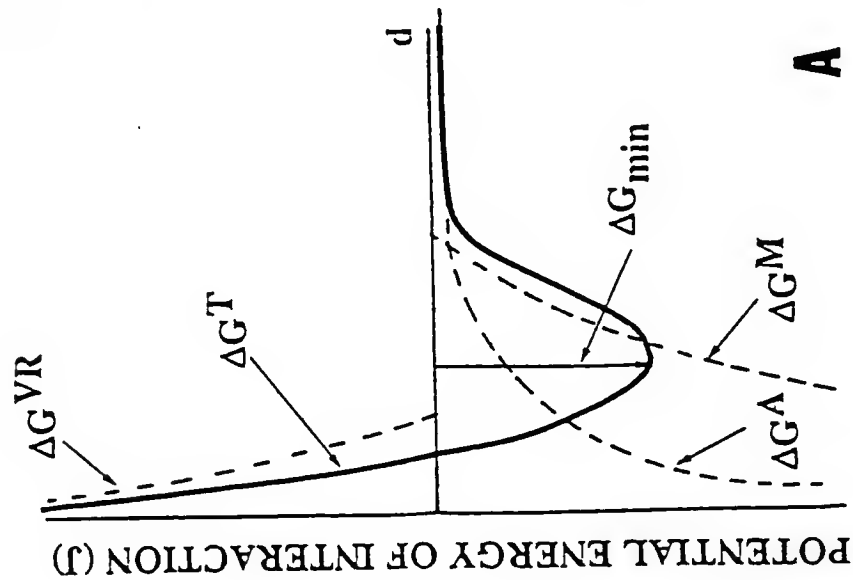
Figure 4.4   Schematic illustration of the effect of segment-solvent interaction parameter, x, on the potential energy diagram (A) poor solvent, x > 0.5, (B) theta solvent, x = 0.5, and (C) good solvent, x < 0.5.

0.5), and the elastic contributions impart stability to the dispersion. The elastic contribution, which is related to the decrease in the conformational entropy of the adsorbed polymer molecules upon approach of the second particle, is always repulsive. In a good solvent, Figure 4.4C, the mixing and the elastic interaction energy contribute to steric stabilization.

It has been experimentally observed that the CFT is independent of the molecular weight of the polymer (if sufficiently thick adsorbed layer is present) and the chemical nature of the polymer (as CFT is related to segment-solvent interactions) (e.g., see Napper 83). Exceptions to the above obeservations have also been reported in the literature (Napper 83). In this case, the stability in worse than θ solvent has been observed and referred to as "enhanced steric stabilization." The exact mechanism is not clearly understood but has been related to the loop-tail adsorption of the polymer.

Non-thermodynamically Limited

In this case, the flocculation is observed in better than θ solvents. The molecular weight of the polymer and the Van der Waal's attraction play an important role in determining the flocculation behavior. Usually, large particles coated with the low molecular weight polymers are less stable, i.e., the relative thickness of the adsorbed layer (δ/a) is an important parameter. The effect of molecular weight on the total interaction energy plots is shown in Figure 4.5.

If the adsorbed layer thickness is relatively small, then, an appreciable attraction exists between two particles. But with increase in the adsorbed layer thickness, the depth of ΔG_{min} is reduced
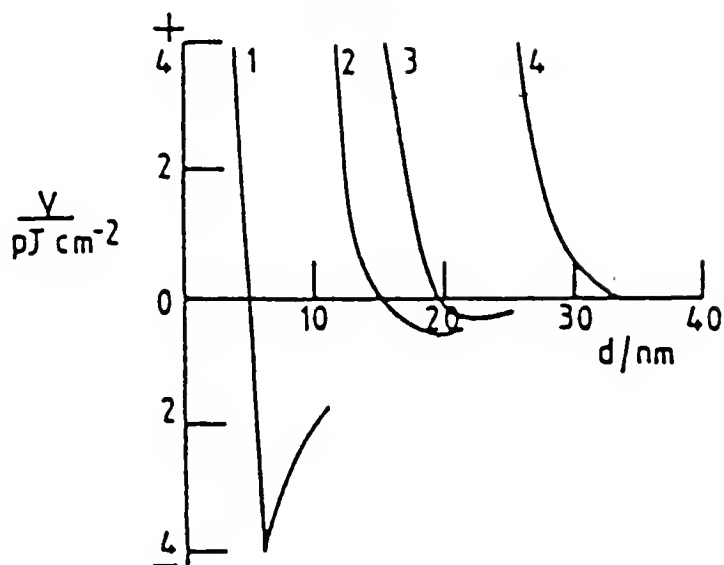
Figure 4.5   The free energy of interaction of polystyrene latex
              particles stabilized by poly (vinyl alcohol) according to
              Hesselink, Vrij, and Overbeek (1971); stabilizer
              molecular weight 1, 8,000; 2, 17,000; 3, 28,000;
              4, 43,000 (Tadros, 1982).
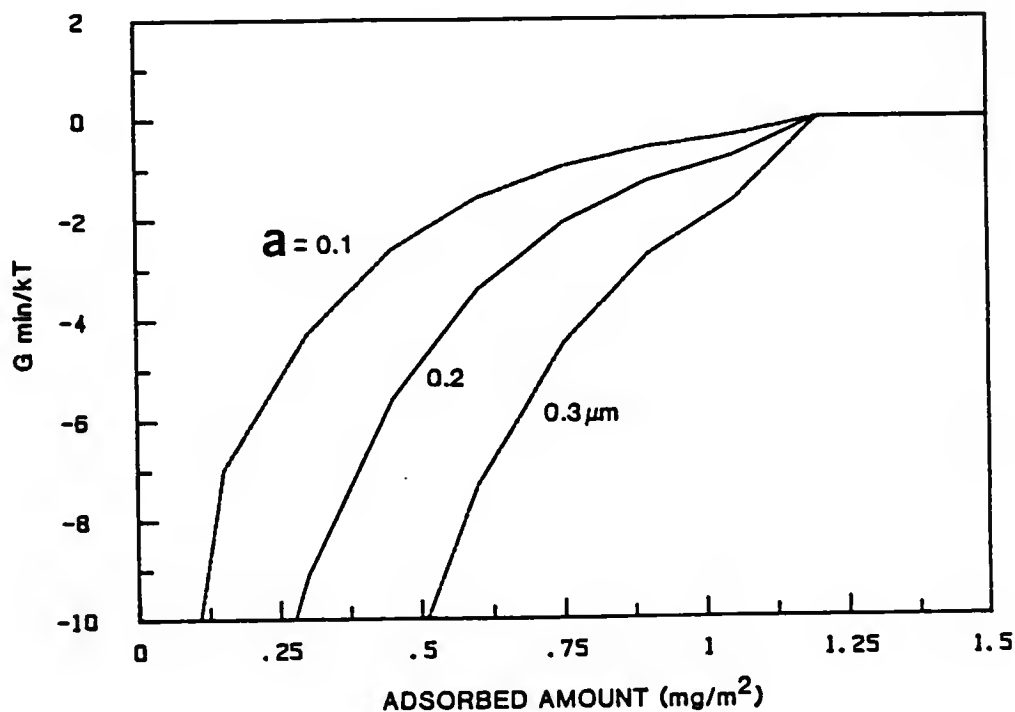
Figure 4.6   Plots showing the effect of particle size and adsorbed
              amount on the depth of the minima in the total potential
              energy of interaction.

considerably. Hence, above certain critical molecular weight (or the absorbed layer thickness), the dispersion stability will be thermodynamically limited (i.e., determined by the solvent quality). The effect of particle size and the adsorbed amount (or the thickness) on the depth of the minima in the total potential energy of interaction is shown in Figure 4.6. At a given distance of separation, the depth of ΔG_{min} increases with increase in the particle size since the Van der Waal's attraction increases with the size of the particles. Similar trends can be expected with the increase in the effective Hamaker constant of the materials involved. The critical molecular weight of the polymer required to stabilize the dispersion will increase with the Hamaker constant of the material (e.g., silica < alumina < zirconia < metal powders).

It should be noted that the origin of the minima in the total interaction energy curves is different in the above two cases. In the case of a thin adsorbed polymer layer, the depth of ΔG_{min} is controlled by the Van der Waal's interactions (through thickness and particle size), while in the case where flocculation is induced due to thermodynamic reasons (i.e., poor solvent), the magnitude of ΔG_{min} is usually large. If the flocculation is induced by thermodynamic factors, then, the flocculation behavior can be reversed, for example, by decreasing the temperature or adding more solvent to the dispersion, and volume fraction of solids, ϕ, does not play any role. If the depth of ΔG_{min} is determined by the Van der Waal's attraction, then, the resulting flocculation is usually weak since the magnitude of ΔG_{min} is usually small. In this case, the existence of a critical volume fraction solids

ϕ_C has been observed below which flocculation cannot be observed (Long et al. 73). The existence of a critical flocculation volume fraction solids ϕ_C has been related to the configurational entropy loss of the particles due to flocculation (Long et al. 73). The change in the configurational entropy due to flocculation (i.e., $\Delta S = S_{floc} - S_{dispersed}$) decreases with increasing volume fraction of solids. At the critical volume fraction ϕ_C, the decrease in the configurational entropy is balanced by the gain in energy due to flocculation.

Bridging Flocculation

During a Brownian collision, an adsorbed polymer chain from one particle and can attach itself to the empty sites on the other particle as shown in Figure 4.7. This process of destabilization of dispersions at low polymer concentrations has been called "bridging flocculation." If the dimensions of the flocculent polymer molecules are comparable to the dimensions of colloidal particles, then, a polymer molecule can attach itself to several particles. This phenomenon was first pointed out by Ruehrwein and Ward (Ruehrwein and Ward 54). The process of bridging flocculation is employed in various operations, such as water purification, selective flocculation in the mineral industry, etc. It has been experimentally found that, for a given polymer, there is an optimum concentration beyond which poorer flocculation is observed. This observation is quite consistent with the bridging hypothesis, which requires that the particle surface should be partially covered with the adsorbed polymer, so that attachments with other polymer segments can be formed. Thus, the fractional surface coverage is one of the important
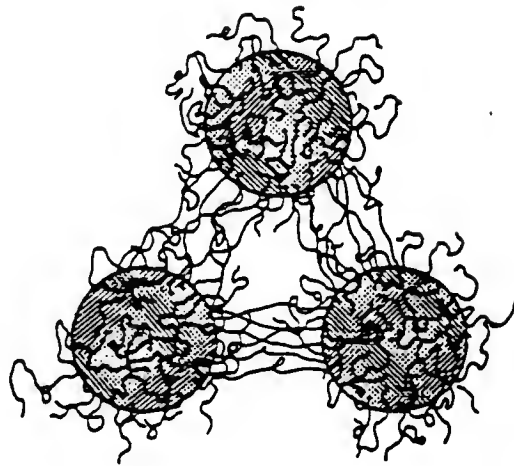
Figure 4.7   Schematic illustration of bridging flocculation with
              adsorbed polymer.

parameters controlling the phenomenon of bridging flocculation. Typically, high molecular weight polyelectrolytes of the same sign as the dispersed particles or polyelectrolytes of opposite sign of the dispersed particles are used in application. This area has been reviewed extensively by Vincent (Vincent 74 and Vincent and Whittington 81). Non-ionic PVA was used in this study, hence, we will focus on the effect of non-ionic polymers on bridging flocculation.

The important parameters controlling the stability behavior are: (i) polymer concentration, (ii) molecular weight and structure, (iii) electrolyte concentration, and (iv) particle concentration.

The following general trends are observed (Vincent 74). The optimum polymer concentration decreases with increase in the molecular weight of the polymer, and the concentration range over which the increased flocculation efficiency is observed decreases with increase in the molecular weight (Vincent 74). The chemical structure of the polymer does not play an important role with regard to their flocculating capacity. (It was observed that homopolymer PEO or co-polymer PEO-polypropelene oxide had no first order effect on flocculating capacity. Also, PVA88 and PVA98 were equally effective in flocculating dispersions.) But the chemical nature of the polymer has a pronounced effect on the stability at high polymer concentrations. (This effect may be due to the stronger anchoring and improved adsorption in the case of co-polymers.) (Vincent 74).

In the case of charged particles, it has been observed that the salt additions favor flocculation. The effect of ionic strength on flocculation behavior is shown in Figure 4.8. With increasing ionic

Low   Ionic Concentration
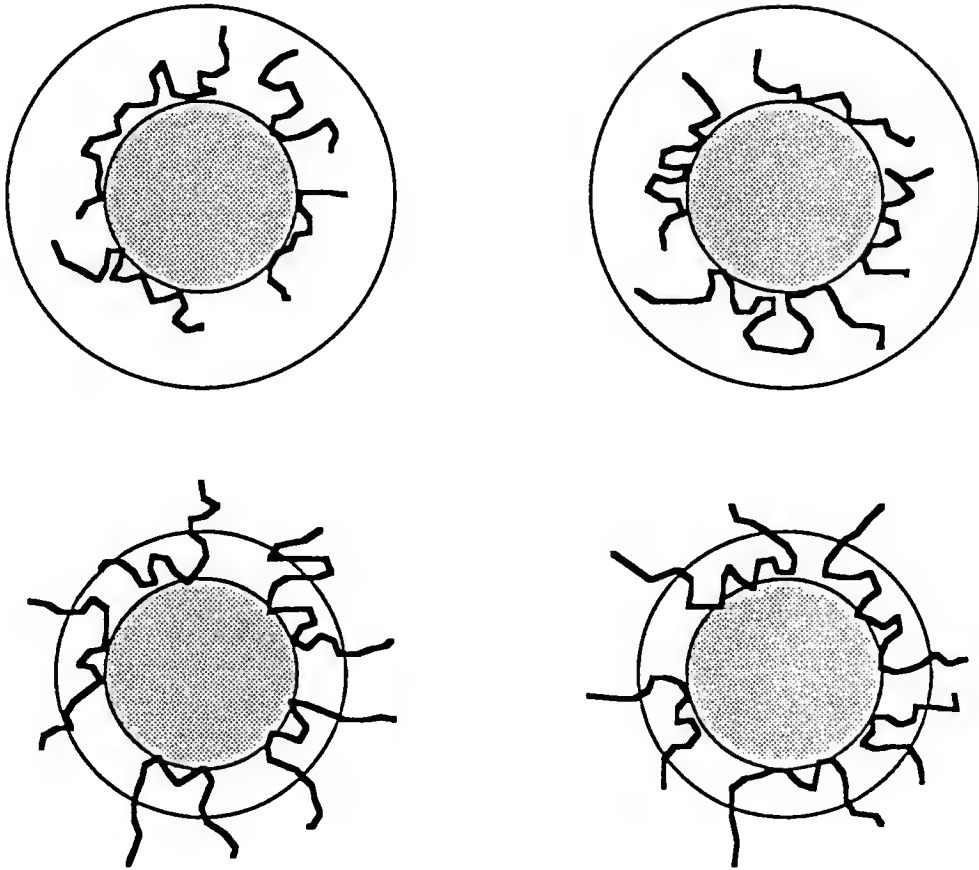
High Ionic Concentration

Figure 4.8   The effect of thickness of the electrical double layer on
               bridging flocculation.

strength, the electrical double layer thickness decreases (i.e., the Debye-Huckel parameter, κ^{-1} decreases, as discussed in Chapter II). Hence, the distance of closest approach between two spherical particles (approximately $2/\kappa$) will also be decreased. To form polymeric bridges between two approaching particles, the extension of the adsorbed polymer molecules (tails or loops) should be greater than the thickness of the electrical double layer. At higher ionic strengths, the electrical double layer is less extensive and bridging is more likely.

The above trends with regard to the efficiency of flocculation are measured using various experimental techniques, such as light scattering (turbidity), refilteration rates, sedimentation behavior, etc., and experiments are usually carried out at low particle concentrations. Additional effects due to possible differences in the method of mixing, rates of polymer adsorption and particle collision in the system studied makes quantitative comparison impossible. Fleer has compared the relative merits of two methods of mixing, i.e., the so-called "one portion" and "two portion" methods (Fleer 71). In the former method, dispersion is added to the polymer solution all at one time. In the latter method, a given portion of the dispersion is added to the polymer solution (the polymer concentration and the volume of the dispersion chosen so as to give complete coverage of the particles) and mixed together, and the remainder of the dispersion (containing bare particles) is added subsequently. Thus, in the two portion method, bridging flocculation takes place between sterically stabilized particles and bare particles. It has been speculated that this method may improve the reproducibility of the flocculation process, and hence, process control

at the same added polymer concentration (Lyklema 85). These two ways of mixing can lead to a dramatic difference in the final flocculation results. This shows that the kinetics play an important role in the flocculation experiment.

Kinetic Aspects of Bridging Flocculation

The rate of coagulation in the case of electrostatically stabilized dispersions was considered in Chapter II. At the moment of addition of polymers to a dispersion, several rate processes are initiated (Figure 4.9) (Akers 75, Gregory 88).

(i) Mixing of polymer molecules among the particles. (ii) Diffusion of polymers and attachment to the particles, i.e., adsorption.

(iii) Rearrangement of the adsorbed polymer chains towards equilibrium arrangement (reconfiguration). (iv) Collisions between coated particles resulting in aggregate formation.

In the case of polymer flocculation, the rate of polymer adsorption should be considered. Generally, two limiting cases are considered: (i) the time required (or rate) for adsorption and reconformation is longer than the collision between two particles and (ii) the adsorption and reconformation processes is much faster than the collision between approaching particles (Gregory 88).

It is usually assumed that the added polymer distributes itself instantly and uniformly throughout the dispersion.

To estimate the rate of polymer adsorption, Gregory treated the adsorption of polymer molecules as a process of heteroflocculation and assumed that each polymer particle contact leads to permanent attachments
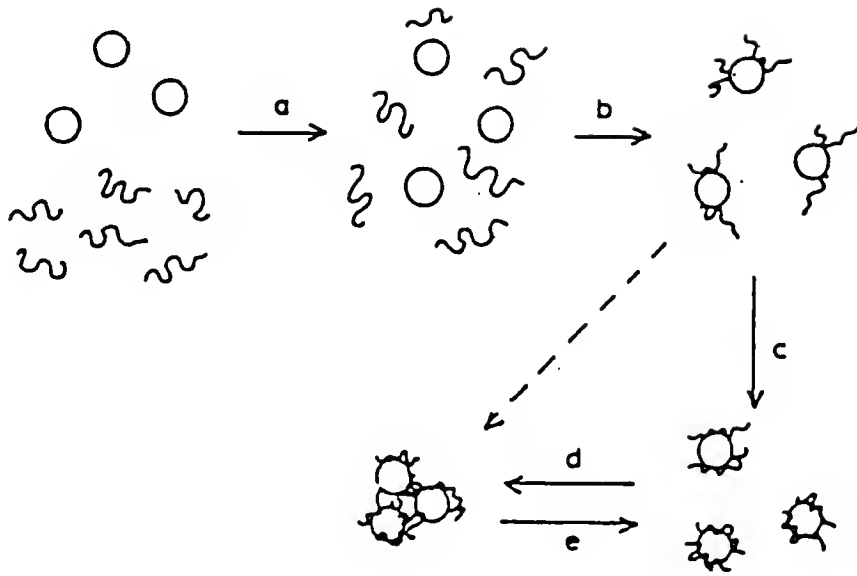
Figure 4.9   Schematic diagram showing mixing, adsorption, and
flocculation upon addition of polymeric flocculent
(Gregory, 1988).

(Gregory 88). Assuming that the particles and polymer molecules as spherical particles with radius a_1 and a_2 and the rate constants for particle-polymer molecule and particle-particle collisions are given by the Smoluchowski's theory. The ratio between the adsorption time, t_A, and collision time, t_f, is given by (Gregory 88):

$$t_A/t_f = -4 \, [\ln \, (1-f)] \, a_1 a_2 / \, (a_1 + a_2)^2 \qquad (4.35)$$

where f is the fraction of the added polymer adsorbed at time t_A. It can be shown from the above equation that, for very different values of a_1 and a_2, the adsorption step is faster (i.e., $t_f \gg t_A$). Also, if $t_A \gg t_f$, there might be an observable time lag between the addition of polymer and the onset of flocculation.

If one assumes that, at the moment of polymer adsorption, the conformation of the adsorbed polymer is similar to its random coil solution conformation, then, the time required for a polymer to achieve its equilibrium configuration is largely a matter of guesswork. Times of the order of hours or days may be involved (Cosgrove and Fergie-Woods 87). The reconformation rate will a have significant effect on bridging flocculation. As discussed in Chapter II, at extremely low polymer concentrations at equilibrium, the adsorbed polymer has flatter conformation (i.e., short sizes of loops and no tails), and hence, will be less effective than random coil adsorption (Scheutjeans and Fleer 79,80). This non-equilibrium random coil conformation of the adsorbed polymer will extend farther from the surface and will also cover less surface area and the particle may enhance the bridging flocculation. It can be expected that, at high volume fraction of solids in suspension, the rate of collisions between particles will be high, i.e., there may be

a considerable number of collisions between particles in the time period
of the reconformation step. At low particle concentrations, the
reconformation step may be faster and the extent of flocculation will be
less. Although there is very little experimental evidence on this point,
it can be concluded that "non-equilibrium flocculation" may be occurring
at high particle concentrations, where the time of flocculation is very
short (usually a fraction of a second) (Gregory 88).

Kinetics of Flocculation

We have already discussed the aggregation kinetics of
electrostatically stabilized dispersions in Chapter III. Smoluchowski's
second order kinetic equation for irreversible aggregation in the absence
of long-range particle interactions is given as:

$$\frac{dN_1}{dt} = -KN_1^2 \qquad (4.36)$$

where K is rate constant for the process, and dN_1/dt is the rate of
disappearance of primary particles N_1. Bridging flocculation is also an
example of irreversible flocculation, and the above equation is modified
and given as follows (Smellie and LaMer 58, Healy and LaMer 62):

$$\frac{dN_1}{dt} = -\theta (1-\theta) KN_1^2 \qquad (4.37)$$

where θ is the fraction of surface covered by the polymer. LaMer called
$E = \theta (1-\theta)$ an efficiency factor. It represents the probability that the
surface of one of the particles is covered by polymer (θ) and that the
other particle has bare patch ($1-\theta$) during collision. In this
derivation, it has been assumed that the polymer adsorption reaches
steady state very rapidly compared to the rate of particle collision.

From the Equation 4.37, it is clear that at extremely low fractional coverates (i.e., $\theta \to 0$), and near complete coverages (i.e., $\theta \to 1$), dN_1/dt will approach zero. This can be represented as follows:

$$\frac{dN_1}{dt} \to 0 \text{ as } \theta \to 0 \text{ as } \theta \to 1 \qquad (4.38)$$

and that dN_1/d_t is maximum at $\theta = 0.5$ (i.e., half surface coverage). Usually, θ is defined as $\theta = $ (adsorbed amount)/(plateau adsorbed amount), i.e., fraction plateau coverage. By defining θ this way, the conformation change of the adsorbed polymer with the surface coverage (or polymer concentration) is ignored. Hogg has modified the collision efficiency factor to account for the reorientation of particles during collision (Hogg 84). This model predicts that the collision efficiencies are very high (close to approximately 100%) over a broad range of surface coverages ($\theta = 0.1$ to 0.9, typically) for the flocculation of large particles with low molecule weight polymers (i.e., $\langle r^2 \rangle \ll a$, where $\langle r^2 \rangle$ is the root mean square radius of gyration of the polymer molecule in solution and a is the particle radius.)

The observed initial rate of flocculation, K, is often higher than the rate predicted by Smoluchowski for diffusion-controlled aggregation (i.e., $K = 8kT/3\eta$, where η is the viscosity of the dispersion media). This has been attributed to (1) reduced hydrodynamic interactions between the particles and (2) an increase in the effective collision radius of the particles when they have an adsorbed polymer layer. Walles has shown that the ratio of number of collisions per unit time Z, between the bare and covered particles, to the number of collisions, Z_0, between bare particles is given by (Walles 68):
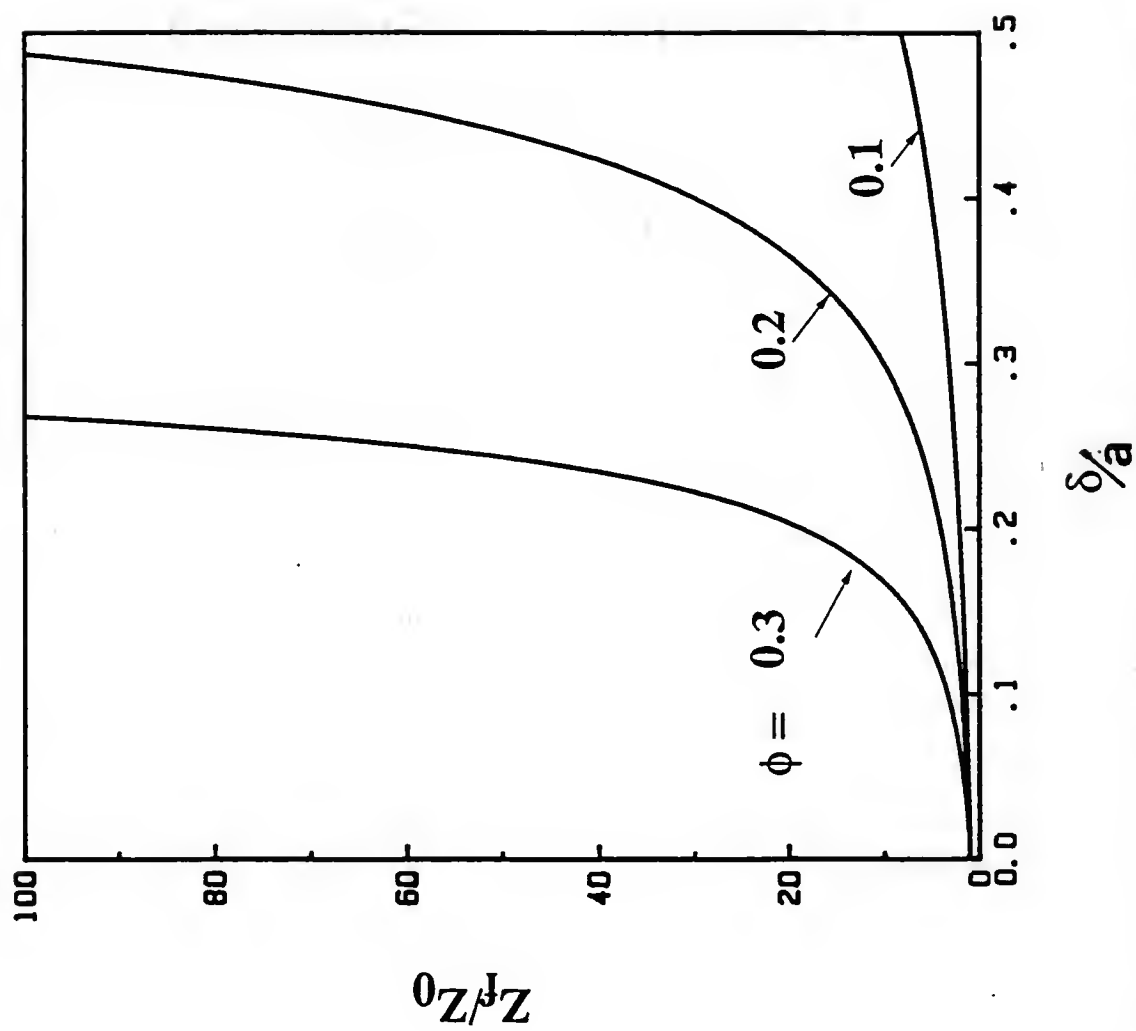
Figure 4.10   The effect of solids loading ϕ and δ/a on collisions z_f/z_0 (Walles, 1968).

$$\frac{Z}{Z_o} = \frac{(2 + \delta/a)^2 \ (1.69q - 2)^4}{4 \ (1.69q - 2 - \delta/a)^4} \text{ and } q = \phi^{-1/3} \tag{4.39}$$

This ratio increases with the adsorbed layer thickness, δ, for a given particle radius, a and solid volume fraction, ϕ (Figure 4.10).

The Potential Energy Diagrams for Bridging Interparticle Interactions

At incomplete surface coverage, the free energy of interaction is a compromise between an attractive term due to polymer bridging and a repulsion which is caused by segment overlap and conformational entropy loss. There are essentially two ways to calculate these interactions (Vincent and Whittington 81). In the first case, polymer is assumed to be adsorbed in its equilibrium conformation on one surface, and the change in free energy is calculated when a second surface is brought to a distance d < L where L is the adsorbed layer thickness. In the second approach, a polymer molecule is generated between two surfaces separated by a distance d. Fleer has calculated the total interaction energy between covered and bare surfaces as follows (Fleer 71). He assumed the polymer is adsorbed in train-loop conformation (i.e., tails were ignored). The total interaction energy is divided into three contributions: (a) the adsorption attraction term, G^{AA}, (b) the configuration repulsion free energy, G^{Rb}, and (c) the free energy change due to mixing, G^{M}. To calculate G^{AA}, he assumed that all segments in loops in the region (L-d) are considered to be adsorbed on the bare surface in trains (Figure 4.11). Then, G^{AA} is given by:

$$G^{AA} = -N\epsilon \tag{4.40}$$
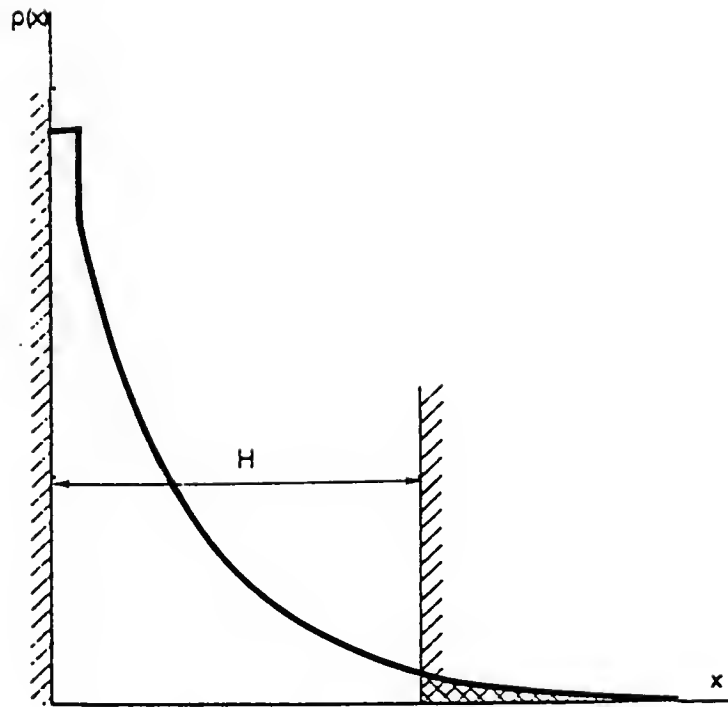
Figure 4.11   Schematic representation of the approach of a second
               (uncovered) particle to a covered one. It was assumed
               that, at large interparticle distance H, the number of
               segments which adsorb on the (originally) bare particle
               per unit area is equal to the number of segments per unit
               area which would lie beyond Hi in the absence of the
               second particle (i.e., shaded area) (Fleer, 1971).

where N is the number of segments per unit area in the region (L-d), and ε is the adsorption energy of the segment on surface. To evaluate, N, he assumed the exponential segment density distribution, $\rho(x)$, as given by Hoeve (Hoeve 65,70):

$$N = \int_b^\infty \rho(x) \, dx \qquad (4.41)$$

for homopolymer adsorption. At very short distances, the maximum adsorbed amount on the second surface was assumed to be a fraction of the adsorbed amount on the first surface.

The repulsive contribution to G^{Rb} which results from the reduction in the configurational entropy of the chains for d < L was calculated using Hesselink's equations (Hesselink 71). Hesselink et al. have derived the expression for the free energy of a loop and bridge on flat plate as a function of distance of separation between two flat plates. Schematic processes of bridging by a single loop consisting of i segments is shown in Figure 4.12.

The free energy associated with the above process is given by:

$$G_{Rb} = \int_{i=0}^\infty n_i \, [2\nu_B \, (i_H, d) - \nu_L \, (i, \infty)] \, di \qquad (4.42)$$

where n_i is the number of loops of size i per unit area and $\nu_b \, (i_H, d)$ is the configurational free energy of a bridge of i_H elements at an interparticle distance d. $\nu_i \, (i, \infty)$ is the configurational entropy of an unconfined loop of i elements. The total free energy of interaction between coated and uncoated plates as a function of distance of separation in the absence of electrostatic interactions is shown in Figure 4.13, where
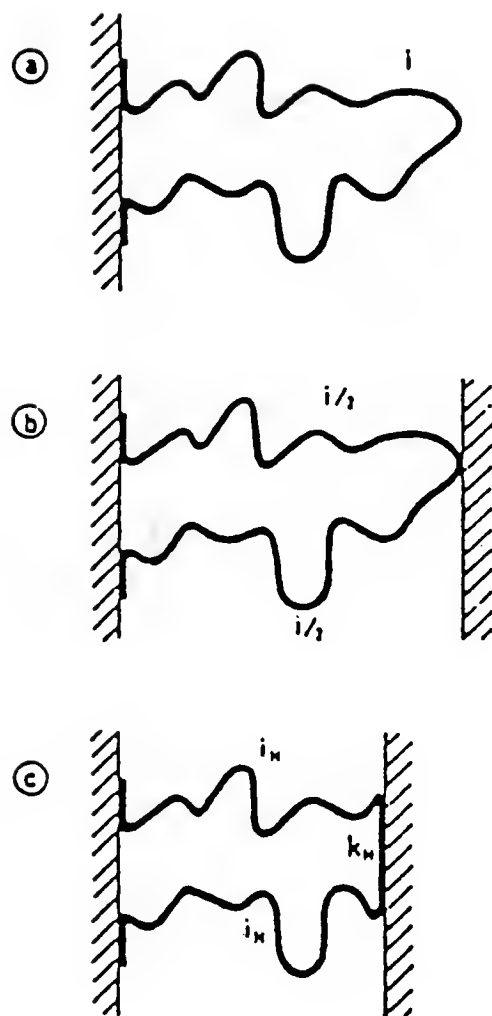
Figure 4.12   Schematic representation of the bridging process. (a) At
large distances, a loop of i segments has its unpurturbed
configuration. (b) After adsorption of the first
segment, two bridges of i/2 segments each are formed.
(c) At shorter distances, two bridges of i_H segments and
a train of K_H segments adsorbed on the second surface
(Fleer, 1971).
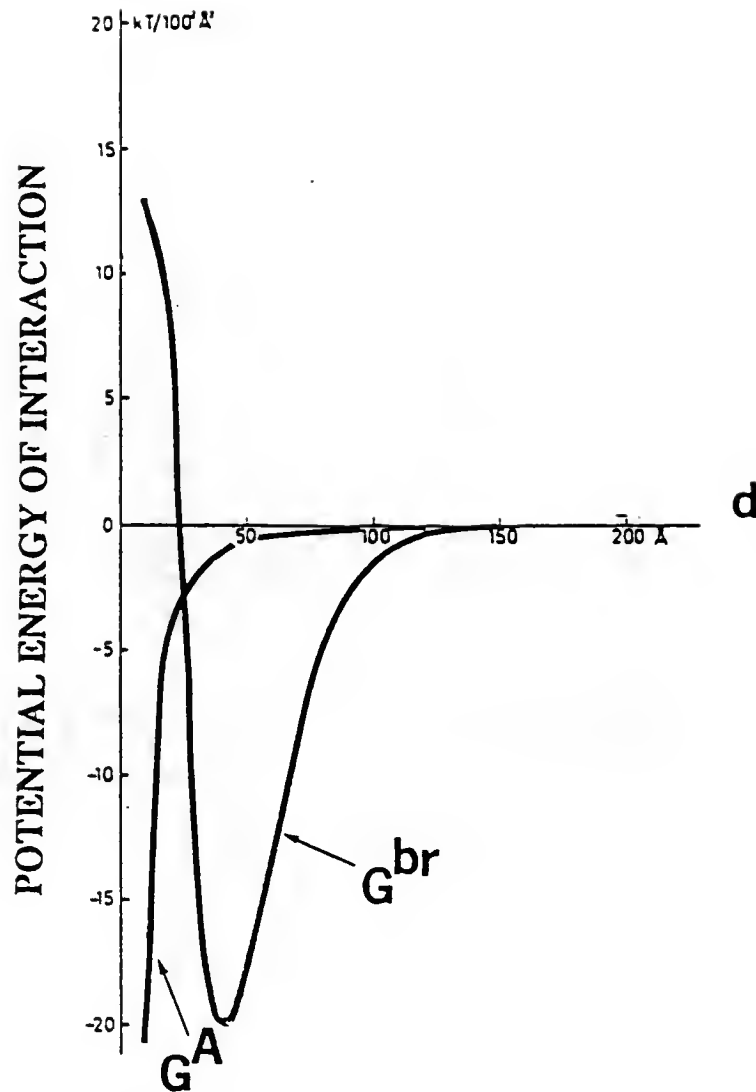
Figure 4.13   The total free energy of interaction between coated and
uncoated plates as a function of distance of separation
(Fleer, 1971).

$$G^{br}(d) = G^{AA} + G^{Rb} + G^A \qquad\qquad (4.43)$$

and G^A is the Van der Waal's attraction energy. It can be seen that there is a deep minima in the $G^{br}(d)$ plot, indicating strong flocculation. The magnitude, G_{min} and the position d_{min} of this potential energy minima will have an important effect on structure and the properties of the flocs formed. A perturbatory technique of monitoring suspension structure, such as rheological measurements, will be influenced strongly by these parameters.

In the second approach to calculate the free energy of interaction, the polymer molecule is generated between two confining surfaces at separation d. In the simple case of non-adsorbing polymer between two plates, the decrease in the configurational entropy of constrained polymer molecule compared to an equivalent unconstrained polymer leads to repulsion. The distance dependence of such repulsive interaction energy is given as G^{Rb} approximately d^{-2} from random walk and self-avoiding walk analysis between two plates (Richmond and Lal 74, Hesselink 69). If the polymer segments can adsorb on the approaching surface, the bridging of two surfaces by the polymer chain leads to attraction. Properties, such as the probability of bridging by the chain, the mean bridge length, etc., of the adsorbed chain have been determined as functions of segment-surface interaction energy and separation distance from the Monte Carlo simulation (Clark and Lal 82). Scheutjeans and Fleer have extended their polymer mean field adsorption theory to calculate the free energy of interaction for the case of bridging flocculation (Scheutjeans and Fleer 85; Fleer and Scheutjeans 86). They have considered two cases (a) restricted equilibrium--when the adsorbed amount remains constant and (b)

full equilibrium--when the polymer can freely enter or leave the gap between the surfaces. First, the segment density distribution in the gap was computed. From the known segment density distribution, the total free energy of interaction as a function of distance of separation was determined. deGennes also has employed scaling concept to calculate the energy of interactions at partial coverage (deGennes 82,87). The effect of various parameters (molecular weight, adsorbed amount, etc.) on bridging flocculation will be considered in the results and discussion section. The effect of these parameters on the rheological behavior of suspensions will be discussed with the help of total potential energy diagrams.

CHAPTER V
STRUCTURE OF SUSPENSIONS

Introduction

The total potential energy of interaction between two colloidal particles was reviewed in the last chapter. In the case of electrostatically stabilized dispersions (with no added polymer) under the conditions of high zeta potential and low ionic strength, the electrostatic repulsion leads to ordering of the particles in suspension. Ordering has been observed in suspensions of spherical monosized, particles (e.g., lattices, silica, etc.) and results in bright iridescent colors due to Bragg diffraction when the interparticle spacing is in the range of wavelength of visible light (e.g., Forsyth et al. 78, Hachisu and Takano 82, Hiltner and Krieger 69, Krieger and O'Neill 68, Ohtsuki, et al. 81, Takano and Hachisu 78, Tomita et al. 78, Yoshimura and Hachisu 83). This ordering of colloidal particles resembles liquid to solid transition of atomic systems and has been analyzed using statistical mechanics and Monte Carlo approach (Snook and Van Megan 82, Van Megan and Snook 84). It is important to note that the above techniques are valid under the equilibrium conditions. The order-disorder transition also has been observed in the case of sterically stabilized dispersions where the repulsion arises due to overlap of the adsorbed polymer layers.

For suspensions in which the potential between particles is strongly attractive (e.g., Van der Waal's attraction with no electrostatic repulsion, polymer induced bridging flocculation at low polymer

140

concentrations, particles coated with adsorbed polymer in a poor solvent, etc.) and the depth of the potential energy minima > ≈ 5 kT, encounters due to Brownian motion lead to aggregation of particles. This process of aggregation is random process, and the aggregate structure is not in thermodynamic equilibrium. The aggregation process is relevant to many scientific phenomena, e.g., dendritic growth, gel formation and flocculation of particles, kinetics of polymerization, tumor growth, etc. The resulting non-equilibrium structures (for example, dust, soot, cell colonies, electrolytic deposition, etc.) are not merely amorphous blobs but exhibit symmetry despite their random growth process (Sanders 86). These structures produced by the short-range forces are statistically well-defined on larger scales, and the long-range structure is independent of the details of the interparticle potential. These structures can be described using Mandelbrot's formulation of fractal geometry (Mandelbrot 82).

Fractal Geometry

The fractal dimension, d_f, of an object may be defined by the following equation:

$$M \propto l^{df} \tag{5.1}$$

where M is the mass of the object and l is a length which specifies the characteristic size of the object. For Euclidian objects, d_f, equals the dimension of the space, d (for example, in three dimensions, the mass of a sphere $M \propto R^3$, where R is the radius of the sphere and d = 3). Fractals are objects for which d_f is less than the dimensions of the space (i.e., $d_f \leq d$). For example, the mass of the polymer molecule

generated by random walk in three dimension is proportional to the square of the r.m.s. radius, i.e., $M \propto <r^2>$, hence, it is a fractal with $d_f = 2.0$. Fractal objects are scale invariant or self-similar (i.e., objects which look the same under different magnification) and do not exhibit any characteristic length scale. Since d_f has many properties of a dimension but is often a fractional, it is called the fractal (broken) dimension.

The fractal dimension of objects can be determined in several ways (Meakin 86). One way is to measure the radius of gyration, Rg, of the object as function of mass, M, as it grows. Alternatively, M and Rg might be measured for an ensemble of objects of different sizes, and d_f is determined by the relation $M \propto Rg^{df}$. The above mass-length relationship is observed over finite length scales in real systems. For example, in the case of colloidal aggregates, the scaling relation is observed between the lower length scale corresponding to the particle diameter and the upper length scale corresponding to the diameter of aggregate. Knowledge about the fractal geometry of colloidal aggregates is important since the physical behavior (e.g., rheology, sedimentation behavior, etc.) of dispersions will be directly related to its fractal geometry.

The fractal nature of the colloidal aggregates has been confirmed from x-ray scattering (e.g., see Schaefer et al. 84, Dimon et al. 86), small angle neutron scattering (Weitz et al. 85), direct observation under transmission electron microscope (Weitz and Olivera 84), and dynamic light scattering experiments. The fractal dimensionality is also important in studying the kinetics of aggregation since knowledge of d_f is essential in formulating the appropriate Smoluchowski equation for the

aggregation kinetics (Jullien and Kolb 84a, Jullien et al. 84b).
Kinetics give the cluster-size distribution as a function of time and
will be discussed later.

Models of Aggregate Formation

Computer simulation technique has been extensively used to study
aggregation and growth processes. This technique to generate ramified
structures can be broadly classified into two categories: (a)
simulations describing non-equilibrium irreversible growth processes
(such as flocculation) and (b) equilibrium models such as percolation to
describe critical phenomenon (for example, phase transition, sol-gel
transition, magnetization (M) near the curie point, etc.). In this
section, we will briefly describe various models proposed to described
the random growth processes.

Eden Growth

In Eden growth process, one starts with a seed (one lattice site on
a lattice) and randomly picks and occupies one of the neighboring sites
(Eden, 61). This process is repeated over and over, and the resulting
structure is shown in Figure 5.1. The structure grown in this fashion
has uniform interior and smooth surfaces relative to their radius, and
hence, is not a fractal object. This fact is important since it
demonstrates that not all random growth processes lead to ramified
fractal objects. The Eden growth is realized when growth occurs from
monomers with large functionality. This growth model has been proposed
by Keefer and Schaefer for the base-catalyzed polymerization of silicic
acid. They have modified the Eden's model (called Poisoned Eden growth

Figure 5.1   Eden cluster produced by monomer-cluster growth (Schaefer et al., 1984).
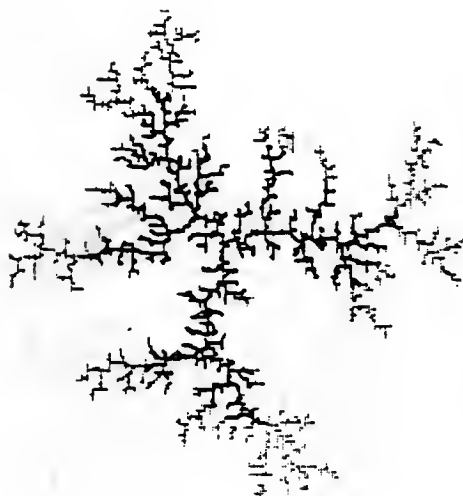
Figure 5.2   An aggregate grown by the DLA process (Sanders, 1986).

model) to account for the change in the mean functionality and the variance of the monomers (Keefer and Schaefer 86).

Diffusion Limited Aggregation (DLA)

Witten and Sanders developed a model for diffusion-limited aggregation process which produces complex random dendritic structures (Witten and Sander 81, Meakin 83a). This model provides the basis for obtaining a better understanding of a variety of diffusion limited processes such as random dendritic growth and flocculation of colloidal particles, etc. The growth starts from a single immobile growth site at the origin of a lattice. A single particle is then added at some random site at large distance from the origin and allowed to random walk (i.e., diffuse) until it comes into contact with the seed and sticks. Then, another random walker is released and allowed to walk until it sticks to either of the previous particles, and this process is continued. Figure 5.2 shows an example of an aggregate grown by this model. This model has been extensively investigated and aggregates grown show scale-independent correlations over an arbitrarily large range of distances with the fractal dimension of $d_f = 5/3$ for two-dimensional and $d_f \approx 2.5$ for three-dimensional clusters. The clusters grown using the DLA technique resemble objects such as snow flakes, coral, etc. In the DLA model, only one particle is allowed in the vicinity of growing cluster which is unrealistic for many colloidal systems. A variation of DLA model has been proposed by Meakin and Kolb et al. and will be discussed next (Meakin 83a,85 and Kolb et al. 83).

Cluster-Cluster Aggregation (CCA)

This model is more relevant to the study of flocculation of colloidal particles, hence, it will be discussed here in more detail. In this model, n_0, identical particles of radius R_0 and mass $m=1$ are initially distributed randomly in a volume V_0. The initial concentration $\rho_0 = n_0/V_0$ is considered sufficiently low so that the average distance between the particles is large. The particles are allowed to move randomly (i.e., by Brownian motion) and independently of one another. During the course of diffusion, if two particles come into contact, they will stick together due to strong short-range attractive interactions. In this way, two-particle clusters are generated, and these will diffuse randomly in a similar manner. The possibility of rotation of clusters is neglected. Also, some kind of mobility criterion can be introduced (for example, the mobility of cluster may vary with their mass) to mimic experimental physical conditions. If a cluster contacts another cluster, then, the contacting clusters can merge to form a single cluster; that is, a cluster of mass m_1 colliding with a cluster of mass m_2 forms a single new cluster of mass $(m_1 + m_2)$. In this process, the clusters formed never change their internal structure and all contacts are rigid. This process (if continued) results in a single large cluster (see Figure 5.3). The clusters grown with this model are also fractal objects with fractal dimension of $d_f \approx 1.45 - 1.5$ for two-dimensional simulations and $d_f = 1.75$ for three-dimensional clusters (Meakin 83a,83b, Kolb et al. 83). A number of modifications of the basic CCA model have been already carried out. The effect of sticking probability on the fractal dimensionality has been investigated by Jullien and Kolb and have shown
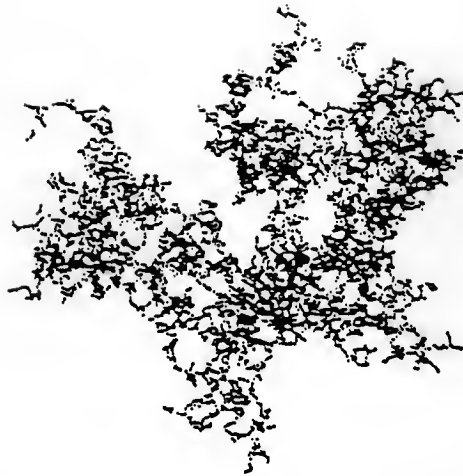
Figure 5.3   An aggregate grown by the CCA process (Jullien et al. 1984).

that a very small sticking probability raises the fractal dimensionality from about 1.45 to 1.55 in two-dimensional simulations and from about 1.75 to 2.0 in three-dimensional simulations (Jullien and Kolb 84a). Cluster formation process with a finite sticking probability is known as a Reaction Limited Cluster Aggregation, RLCA, process. Reorganization of the aggregate has also been considered, but no significant change in the effective fractal dimensionality was observed (Meakin 86a).

Hierarchial Model

Another simpler model used to investigate the structural properties of clusters is known as the Hierarchial Model (Jullien et al. 84b). In this model, one starts with $N_0 = 2^{k_0}$ particles. In step 1, $N_1 = N_0/2$ clusters are formed and each cluster consisting of two particles is formed by a process similar to DLA, i.e., one particle is kept fixed at the origin and the other particle is introduced at a random position far away from the particle and random walk of the second particle continues until it meets the immobile particle. In the next step, $N_2 = N_1/2$ clusters are formed and each cluster has four particles. Four-particle clusters are formed by contact between two two-particle clusters during random walk. Eventually, a single cluster with N_0 particles is formed having effective fractal dimensionality d_f approximately 1.42 for two-dimensional simulations.

Kinetics of Aggregation

The above described models, such as DLA and CCA deals with the structural (or morphology) properties of aggregates. The dynamics of cluster formation is also a very important problem and intensive research

efforts have been directed towards that goal (e.g., see Family and Landau 84, Pietronero and Tosatti 87). Essentially, there are two different ways to study the growth process. The first approach is a kinetic approach based one the Smoluchowski's equation. With this approach, under certain assumptions, the change in the cluster mass (size) distribution as a function of time can be described. The second approach is based on dynamic computer simulations to describe the time dependent cluster size distribution (e.g., DLA, CCA models). It is important to distinguish between two regimes of aggregation: (1) flocculation regime, i.e., where growing clusters stay far apart and (2) kinetically induced gelation phenomenon--where large network structures are formed (Jullien et al. 84b). This difference between these two cases can be seen more easily from a quantity known as the effective average cluster density, ρ_{eff}:

$$\rho_{eff} = \frac{N_c (\bar{R})^d}{V_o} = \rho_o \; \bar{m}^{(\frac{d-d_f}{d_f})} \tag{5.2}$$

where $\rho_o = n_o/V_o$ is the initial particle concentration, i.e., the total number of particles, n_o, contained in a volume V_o. N_c is the total number of clusters at a given time with average radius $\bar{R}$ and mass $\bar{m}$. For fractal objects, $\bar{m} \approx \bar{R}^{d_f}$ where d_f is the fractal dimension and d is the dimension of the space ($d_f < d$). From the above definition, it is clear that the effective cluster density increases with increasing average cluster mass. Thus, no matter how low the initial concentration ρ_o, eventually the cluster covers all space, i.e., $\rho_{eff} \approx 1$. This case is known as the kinetically induced gelation phenomenon. The gelation regime also exhibits scaling properties different from the scaling

properties of the flocculation regime. These two limiting scaling
regimes are separated by a crossover for intermediate concentration.

Smoluchowski's Equation

Kinetics of aggregation can be studied from the Smoluchowski's
equation as follows. These are two processes contributing to the kinetic
evolution of the cluster size distribution (a) the collisions of cluster
i and cluster j leading to the formation of cluster (i + j) and (b)
dissociation of a large cluster into two smaller ones. The
Smoluchowski's coagulation equation is given by:

$$\dot{C}_k = \frac{1}{2} \sum_{i+j=k} k_{ij} C_i C_j - C_k \sum_{j=1}^{\infty} k_{kj} C_j \tag{5.3}$$

where $C_k = C_k(t)$ is the time dependent concentration of clusters of
discrete mass k (k = 1, 2, . . .), and $\dot{C}_k(t)$ represents the time rate of
change of concentration $C_k(t)$ and k_{ij} is concentration-independent
collision kernel which determines the aggregation mechanism (Brownian
motion, gravitational settling, etc.). The above equation represents
that the population of k-clusters is increased by the collisions between
i clusters and j clusters where i + j = k and decreased when k cluster
combines with any other cluster. One needs to solve these coupled
differential equations to calculate $C_k(t)$. Equation 5.3 is based on the
assumption that all particles are randomly distributed and are
uncorrelated at all times. The kernel K_{ij} represents the probability of
meeting cluster i and j. The Equation 5.3 has been solved for some forms
of k_{ij} to arrive at complete time dependent solutions of $C_k(t)$ in closed
form (e.g., Bowen et al. 85, Ernst 86, Ziff 84). In some of these cases,

the solution is found to show a gelation transition after a finite period of time t_c at which an infinite cluster (the gel) is formed which manifests itself through a violation of the conservation law for the total number of finite size clusters, i.e., $\dot{M_i} = \Sigma\, kC_k \neq 0$ where M_1 is the first moment of the cluster size distribution $M_1 = \sum_{k=1}^{\infty} kC_k$ and represents the total mass of the system (Ziff 84).

The coagulation equation has been solved for the cases (a) where k_{ij} is assumed to be independent of the size of the reacting cluster, i.e., $k_{ij} = A =$ constant and (b) k_{ij} is proportional to the size of clusters, i.e., $k_{ij} = (i + j)B$ or $k_{ij} = (ij)C$ where B and C are constants (e.g., see Bowen et al. 85). Recently, the following forms of coagulation kernel have been considered: the product form $k_{ij} = (ij)^w$ and the sum form $k_{ij} = (i + j)^w$. For $w = 1$, the exact solution is available (e.g., see Ziff 84, Ernst 86). It has been shown that the product kernel describes a gelation transition provided $w > 1/2$ while product kernel with $0 < w \leq 1/2$ and the sum kernel with $0 < w < 1$ do not show gelation (e.g., see Ernst 86).

In conclusion, it can be said that the aggregation process is controlled by the mobility criterion (e.g., k_{ij} in Smoluchowski's equation) used. The information about structural properties (i.e., the fractal dimension) of the cluster or cluster aggregates have been obtained from computer simulation or experimentally from static or dynamic scattering (x-ray, light, neutrons) techniques. With regard to the dynamics of aggregation, the computer simulations are far ahead than the experimental observations. Techniques, such as flow cell have been applied to determine cluster size distribution and temporal evolution of

cluster size distribution during Brownian coagulation (e.g., see Bowen et al. 84b,85). Also, the importance of short-range forces (i.e., hydrophilic-hydrophobic interactions, steric effects, etc.) have been neglected in these treatments which may be important in real systems.

To control the properties of dispersion (such as rheological, sedimental behavior, etc.) adequate control over size, morphology, and strength of various aggregates (clusters) is essential. For full control of the properties of suspension, it is essential to consider the following points (Tadros 86):

(1) The aggregation mechanism (flocculation under Brownian motion, shear flocculation, bridging flocculation, etc.) should be known.

(2) The magnitude of the binding forces in aggregated structure (i.e., Van der Waal's coagulation, bridging flocculation, magnitude of the depth of minima in the total potential energy diagram, etc.) should be known.

(3) The time evolution of aggregation process (aging effects) should be understood.

(4) The mechanical properties of individual cluster or network (gel) and mechanism of structural breakdown under applied shear should be known.

(5) The reversibility of the aggregated structure (i.e., related to thixotropic behavior in rheology) and the properties of the subunit formed from the breaking process should be understood.

Very little is known regarding point 4 and 5, and hence, it is impossible at present to describe the rheological properties of flocculated concentrated suspensions quantitatively.

Equilibrium Properties of Suspension

It is well known that charged monodisperse particles, (lattices, silica, TiO_2, etc.) form ordered structures under certain conditions. In ordered state, particles form a three-dimensional crystalline structure and has a bright iridescent color due to Bragg diffraction of visible light. The order formation is related to the long-range electrostatic repulsion between particles. The secondary minima in the potential energy diagram (i.e., attraction, see Figure 3.6) cannot explain the long-range reversible order formation. It has been observed that additions of electrolyte results in order-disorder transition, opposite to behavior expected from the secondary minima explanations (as additions of electrolyte lead to increase in the depth of secondary minima, and hence, should promote ordering).

Since a colloidal dispersion consists of large number of particles (10^8-10^{19} / cm^3), correct formulation to describe equilibrium structure and ordering is based on the statistical mechanics principles. The importance of statistical mechanics is summarized as follows from the article by Israelachvili and Ninham:

> "a knowledge of the interaction free energy between two atoms or particles, taken in isolation, may tell us little of the properties of an ensemble of such particles . . . Thus, the first moral to be learned from statistical mechanics is that the existence of a minima in the two-particle interaction free energy in the associated or ordered state does not guarantee the formation of this state. Conversely, the existence of an associated or ordered state does not necessarily imply that the

particles are sitting at a separation where there is a minimum in two particle interaction free energy." (Israelachvili and Ninham 77)

From a known potential energy function (e.g., potential energy of interaction as a function of distance of separation given by DLVO theory), statistical mechanics can be applied to determine the excess thermodynamic properties of dispersion (e.g., radial distribution function, osmotic pressure, elastic constants, and phase equilibria, etc.--Snook and Van Megan 82). Within the framework of statistical mechanics, various approximate theories, such as integral equation methods, hard-sphere perturbation theory, and lattice models are available. Theoretically, exact Monte Carlo and molecular dynamics computer solutions are also available (Barker and Henderson 76).

The Order-Disorder Transition

The dispersion of monosized colloidal particles is modelled as a collection of hard spheres. From computer experiments, Alder et al. have shown that hard spheres will undergo a liquid-solid phase transition between volume fraction 0.5 - 0.55 (Alder and Weinright 62, Alder et al. 68). The volume fractions of co-existing disordered, ϕ^h_d, and ordered, ϕ_o^h, phases have been determined for the hard sphere model and are given as follows: $\phi^h_d = 0.494$ and $\phi^h_o = 0.540$ (e.g., see Hachisu and Takano 82).

In the case of electrostatically stabilized dispersions, the effective double layer thickness, Δa, is added to the particle radius, a, to calculate the effective hard sphere volume fraction of solids. It is

possible to construct real volume fraction hard spheres versus salt

concentration phase diagram from the following equations:

$$\phi^h_o = 0.55 = \phi_{o,true} \ (1 + \Delta a/a)^3, \text{ and}$$

$$\phi^h_d = 0.50 = \phi_{d,true} \ (1 + \Delta a/a)^3$$

(5.4)

As described in Chapter II, Δa is a strong function of electrolyte

concentration and valency of ions (i.e., $\Delta a \ \alpha \ \kappa^{-1}$). Schematic phase

diagram for electrostatically stabilized dispersions is shown in Figure

5.4. The volume fractions of coexisting ordered and disordered phases

are plotted as a function of electrolyte concentration in solution. From

Figure 5.4, it is clear that (i) $\phi_{d,true}$ and $\phi_{o,true}$ increases with the

increasing concentration of the electrolyte (as Δa decreases with

increases in electrolyte concentration). (ii) At high electrolyte

concentration $\phi_{o,true}$ and $\phi_{d,true}$ should approach the hard sphere limits

(i.e., $\phi_{o,true} \rightarrow 0.55$ and $\phi_{d,true} \rightarrow 0.50$). (iii) At low electrolyte

concentrations $\phi_{d,true}$ and $\phi_{o,true}$ becomes independent of the electrolyte

concentration, and (iv) the different between $\phi_{d,true}$ and $\phi_{o,true}$

decreases as the electrolyte concentration decreases. The detail

comparison between various statistical model in predicting order-disorder

transition is done by Van Megan and Snook (Van Megan and Snook 84). As

expected, hard sphere model gives semi-quantitative agreement with the

experimental observations regarding phase stability and more elaborate

model for the electrostatic potential energy at low ionic concentrations

($\approx \leq 10^{-5}$ moles/liter) is required. It has been reported that by

softening the interparticle repulsion (i.e., by decreasing the

electrolyte concentration), the transition in the ordered phase from face

centered cubic to body centered cubic structure has been observed (Megan
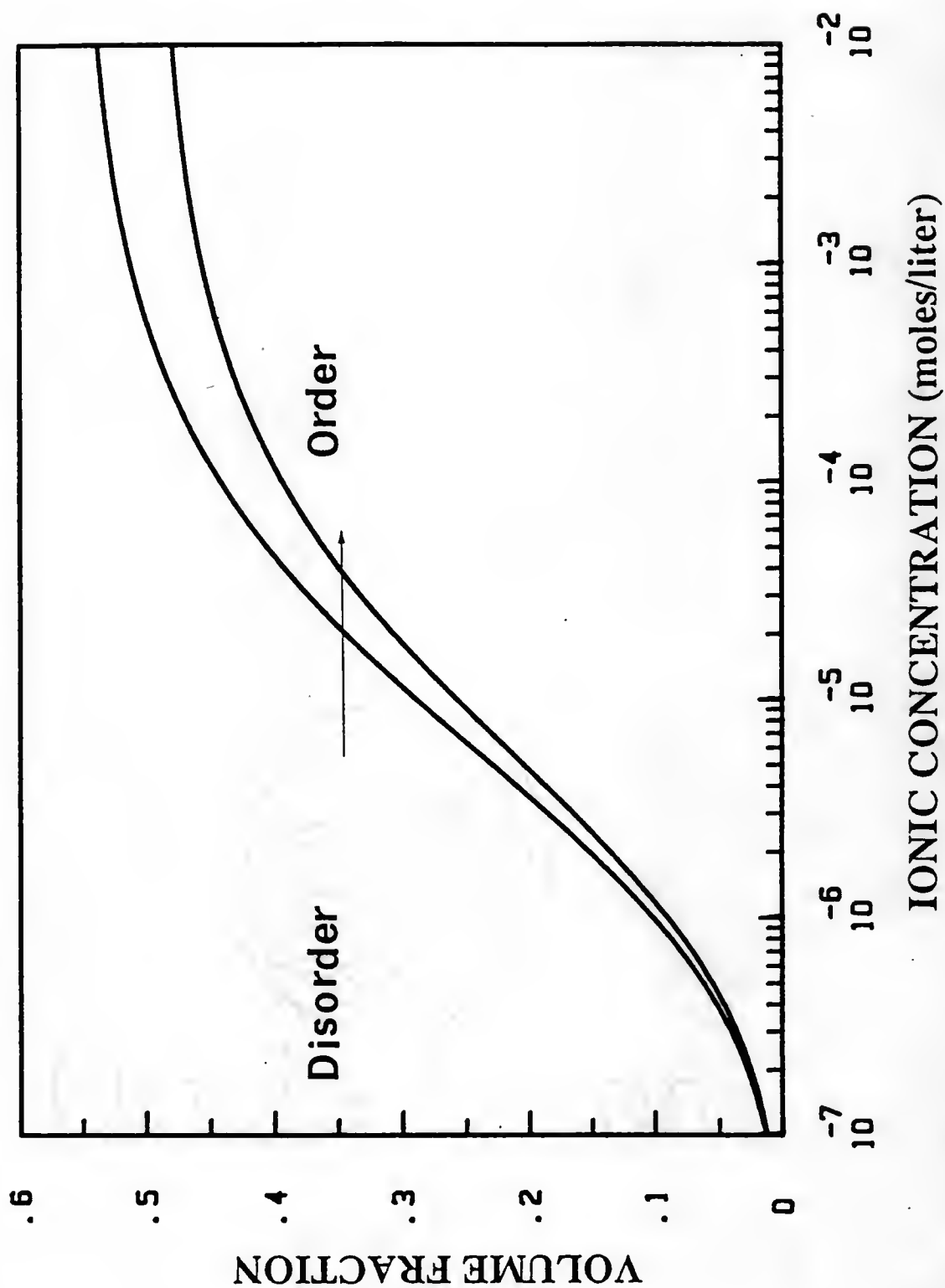
Figure 5.4   Schematic plot of phase diagram for monosized spherical particles.   The volume fraction of solids as a function of ionic concentration is plotted.   Solid lines are theoretical phase boundaries.

and Snook 84). The difference between the hard interactions and soft interactions is shown in Figure 5.5.

Other properties of dispersions, such as radial distribution function, coordination number (number of nearest neighbors), osmotic pressure, elastic constants, etc. show dramatic change near order-disorder transition. For example, the coordination number changes abruptly near order-disorder transition from $\approx$ 2 to 12 (Van Megan and Snook 84). The osmotic pressure versus volume fraction solids plot shows a discontinuity near order-disorder transition.

Another important feature of the ordered dispersion is its ability to sustain shear stress like a molecular crystal. Properties, such as viscoelastic behavior (shear modulus) or steady flow behavior (viscosity), show abrupt changes near order-disorder transition in the case of electrostatically stabilized latex dispersion (Van Megan and Snook 84). Order-disorder phenomenon has also been observed with the anisotropic particles. For example, dilute solution of rod shaped tobacco mosaic virus separates into two phases where the top layer is isotropic and the bottom is ordered phase (Forsyth et al. 78). Disk shaped clay particles under low electrolyte concentrations also separate into two phases. The effect of poly dispersity on order-disorder transition has been theoretically studied. From the molecular dynamics calculations, it has been found that ordered and disordered phases are distinguishable up to certain distribution width and $\phi_d{}^h$ is unaffected, but $\phi_o{}^h$ decreased with increasing distribution width (Van Megan and Snook 84).
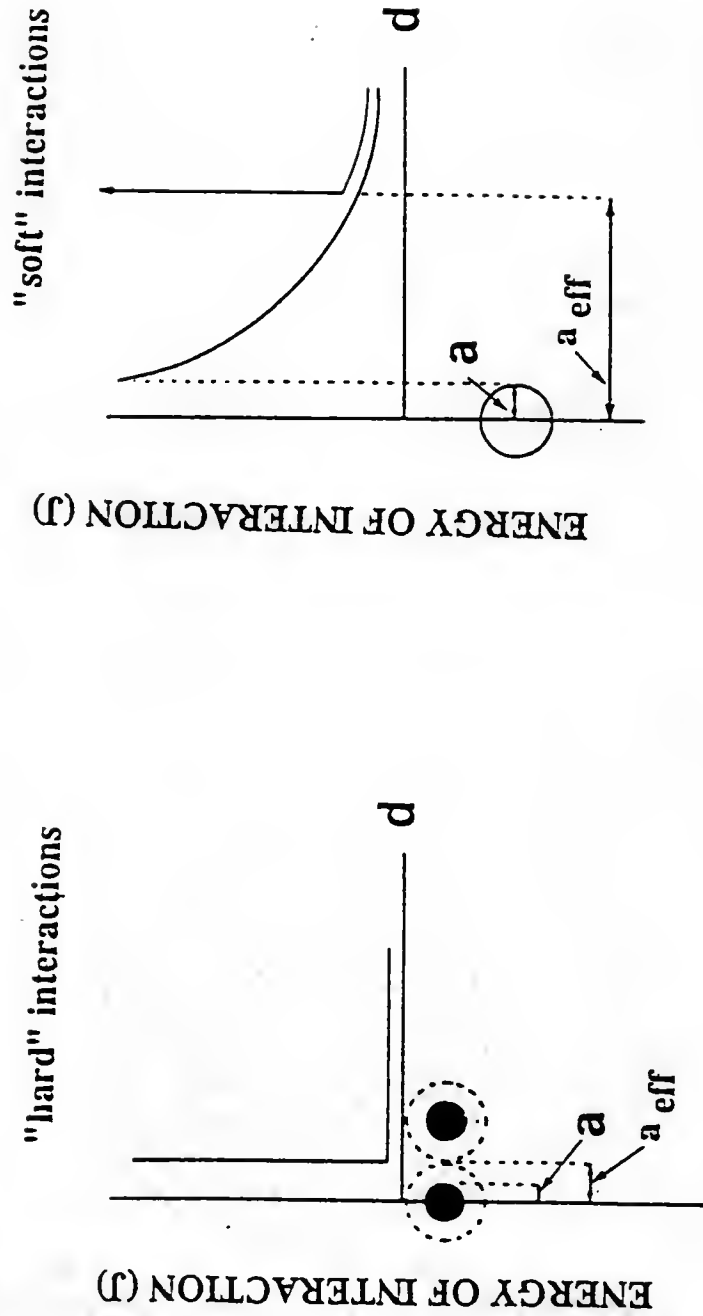
Figure 5.5   Schematic illustration showing (a) "hard" and (b) "soft" interactions between particles. The potential energy of interaction as a function of distance of separation is plotted (Tadros, 1986).

In summary, we considered two distinct mechanisms of structure formation in colloidal dispersions. The short-range attractive interactions lead to irreversible flocculation into primary minima. The structural properties of aggregates can be determined from fractal geometry principles, while kinetics of aggregation can be investigated from computer simulation experiments or from Smoluchowski's equation. The long-range ordering of the monosized colloidal particles, when repulsive forces are present, can be explained from the equilibrium statistical mechanics or from Monte Carlo computer calculations.

CHAPTER VI
RHEOLOGICAL BEHAVIOR OF COLLOIDAL DISPERSION

Introduction

Rheology is defined as the science of flow and deformation. The rheological properties of a colloidal dispersion are among its most important characteristics. Here, we will focus on the rheological properties of the concentrated suspensions. The distinction between "concentration" and "dilute" dispersion can be made as follows (Tadros 86). In a dilute dispersion, the average particle separation distance is much greater than the range of interparticle forces. In this case, colloidal particles are undergoing Brownian motion, and the particle interaction can be represented by two-body collisions. As the particle concentration in the suspension increased, the volume fraction occupied by the solid is increased and the forces of interactions (i.e., attraction or repulsion) plays an important role in determining the properties of the dispersion. As discussed in the last chapter, electrostatic repulsion under certain conditions (i.e., high surface potentials, low electrolyte concentrations) leads to ordering of the spherical particles. These long-range ordered suspensions are referred to as "solid" suspensions (Tadros 86). In between these two extreme cases of "dilute" and "solid" suspensions are systems defined as "concentrated" suspensions. With these suspensions, many body interparticle interactions are important, and the particle translational motions are restricted. In this case, the challenge is to correlate the

160

observed rheological properties to the structure of the dispersed phase
(Chapter IV) and to the interparticle forces (Chapters II and III). It
will be shown that the rheological techniques can provide information
about the stability of the dispersions. In the next section, we will
define various types of flow behavior encountered in rheological
experiments.

Viscosity Definition

The viscosity of a liquid is a property which defines the resistance
of liquid to flow. The viscous nature of a liquid is due to the
molecular attraction that offers resistance to shear, and consequently,
to the resulting flow induced by shear. To understand the concept of
viscosity more clearly, consider a model situation as shown in Figure
6.1. As shown in the figure, two parallel flat plates are separated by a
distance x, and the space between the plates is filled by a viscous
liquid. The bottom plate is stationary and force F is applied on top
plate of area A in a tangential direction, so that the top plate moves
with a constant velocity V in the given direction y, parallel to the
bottom plate. A thin layer of liquid adjacent to each plate will move at
the same velocity as the plate. (This is the "no slip" assumption and
holds true for most liquids.) Thus, the liquid molecules near the top
plate will be moving with the velocity V while velocity at the bottom
plate is zero. Molecules in liquid layers between these two extremes
will move at intermediate velocities. Under steady state conditions, the
force F required to produce the motion becomes constant and will be

162
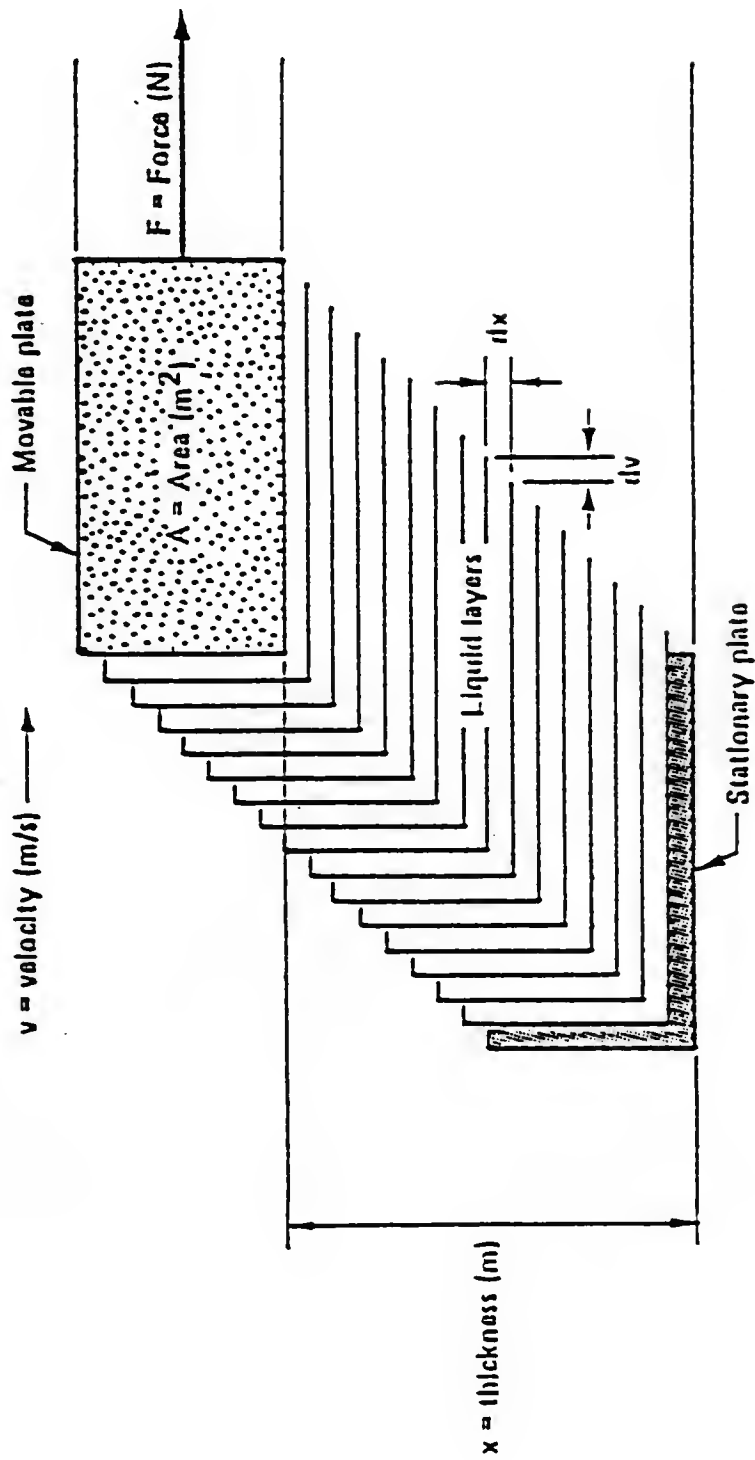
Figure 6.1   Schematic illustration of the concept of viscosity under laminar flow conditions.

related to the velocity gradient, dV/dx. The tangential force acting per

unit area i.e., the shear stress, τ, is given by the following equation:

$$\tau \text{ (shear stress)} = \frac{F \text{ (Force)}}{A \text{ (Area)}} \qquad (6.1)$$

and units of shear stress are dynes/cm^2 or N/m^2. Viscosity of the liquid

can be defined in terms of two measurable quantities, i.e., shear stress,

τ, and shear rate, $\dot{\gamma}$, as follows:

$$\eta \text{ (viscosity)} = \frac{\tau \text{ (Shear Stress)}}{\dot{\gamma} \text{ (Shear Rate)}} \qquad (6.2)$$

A liquid exhibiting a linear relationship between shear stress and shear

rate is called a Newtonian liquid. Newtonian flow behavior is exhibited

by single phase liquids with simple molecules, solutions of low

molecular-weight (non-polymeric) materials, and dilute suspensions of

spherical particles in simple liquids.

Classification of Rheological Behavior of Colloidal Dispersion

Colloidal dispersion is a two-phase mixture of solid particles

dispersed in a continuous liquid phase, and hence, the rheological

properties of the dispersion is dependent on the nature of the components

involved (i.e., solid and liquid) and also on the interactions between

these phases (solid-solid and solid-liquid). Based on the rheological

behavior, dispersions can be classified into two broad categories (a)

Newtonian and (b) non-Newtonian. Those dispersions that strictly follow

Newton's law of viscosity are called Newtonian dispersions. All other

types of rheological behavior are classified as non-Newtonian

dispersions. For non-Newtonian dispersions, it is convenient to define

an apparent viscosity η_a

TABLE 6.1

Classification of Flow Behavior

Suspensions				
Purely Viscous				**Viscoelastic**
Time-Independent			**Time-Dependent**	
No-Yield Stress	Yield Stress		Thixotropic	
Newtonian	Bingham		Rheopectic	
Pseudoplastic	Yield-pseudoplastic			
Dilatant	Yield-dilatant			

$$\eta_a = \tau/\dot{\gamma} \tag{6.3}$$

The apparent viscosity is a function of $\dot{\gamma}$ for non-Newtonian dispersions. (For Newtonian dispersions, η is independent of shear rate.) A colloidal dispersion can behave as a pure viscous substance (i.e., a substance which does not have the ability to recover its deformation imposed by the action of shear stress after the shear stress is removed) or show characteristics of viscoelastic materials (i.e., the ability of a substance to partially recover the deformation on removal of shear stress). The behavior of non-Newtonian pure viscous dispersions can also show time-dependent flow properties. The classification of flow behavior is shown in Table 6.1. We will discuss various types of flow behaviors with Figure 6.2, which shows the shear stress-shear rate and corresponding viscosity-shear rate plots (known as "rheograms" or "flow curves"). In this section, we will define the terms in Table 6.1. Various processes leading to flow behavior will be discussed later.

Newtonian Dispersions: As discussed earlier, Newtonian dispersions can be characterized by a linear relation between shear stress and shear rate and the ratio of shear stress to shear rate is independent of the shear rate. This type of behavior is exhibited by dilute dispersion of spherical particles where the interparticle interactions can be ignored. The viscosity of the dispersion is higher than the viscosity of the continuous liquid media since the perturbation of streamlines due to presence of particles leads to higher rates of energy dissipation during laminar flow of the dispersion.

Pseudoplastic Dispersions: Dispersions showing a decrease in viscosity with increased shear rate (shear thinning) are described as
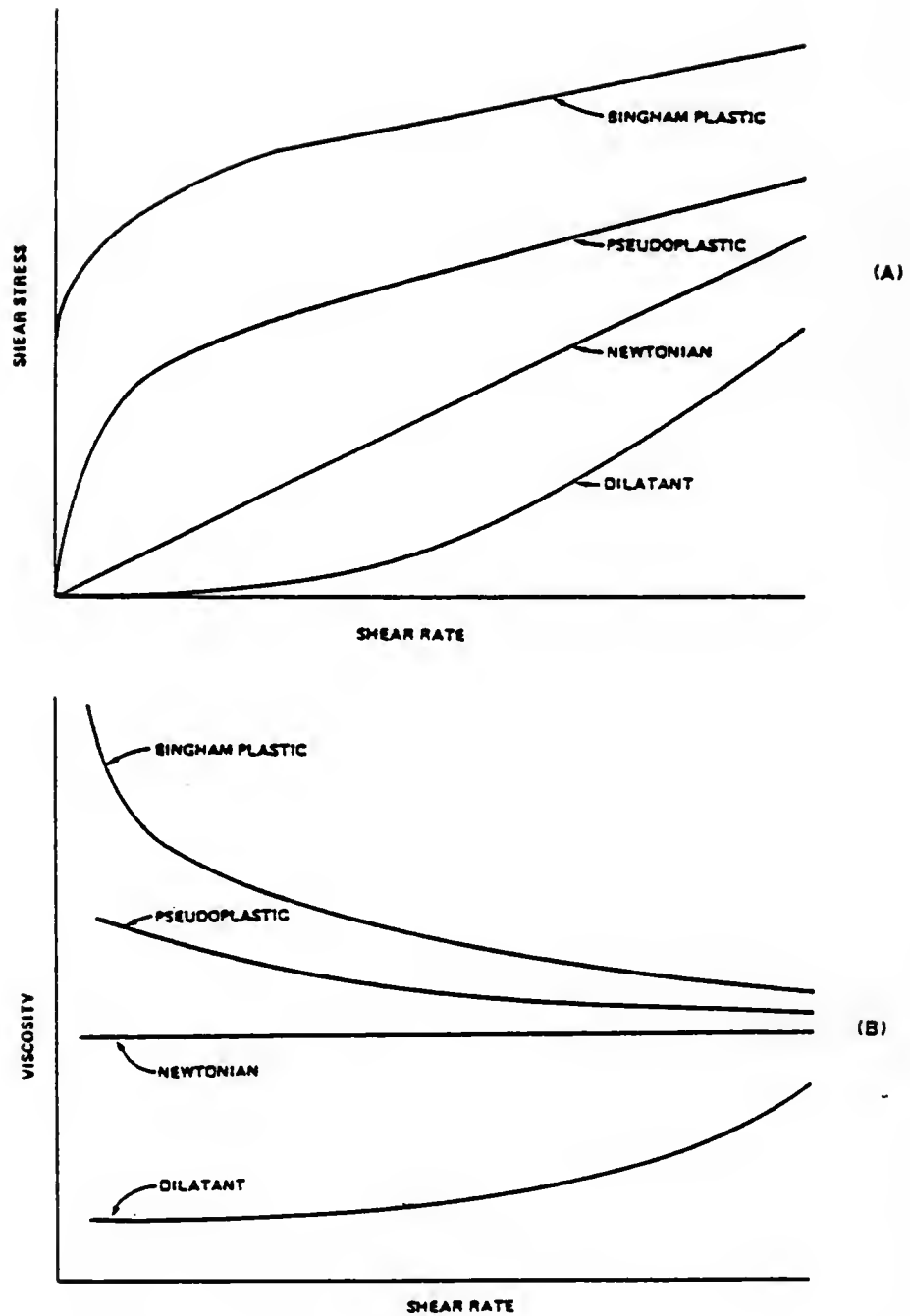
Figure 6.2   Schematic plots of (a) shear stress versus shear rate and
              (b) viscosity versus shear rate for various types of flow
              behaviors.

pseudoplastic. The shear thinning behavior is generally produced by the reversible breakdown of a three-dimensional network structures (formed by flocculation of the particles), alignment of anisotropic particles, etc.

Dilatant and Shear Thickening Dispersions: Dispersions showing increasing viscosity with increasing shear rate (shear thickening) are described as dilatant. This type of flow behavior is usually exhibited by dispersions of rigid particles at high concentration. Since this type of flow behavior was not exhibited by dispersions investigated in this study, it will not be discussed further.

Bingham Plastic Dispersions: Ideally, Bingham plastic dispersions exhibit a yield stress, τ_β, which is a certain minimum value of shear stress that must be exceeded before flow takes place. Once the critical shear stress is reached, flow starts and then the dispersion behaves as a Newtonian dispersion, i.e., shear stress is proportional to the shear rate. The slope of this straight line is called the plastic viscosity. The yield stress is indicative of the strong attractive interactions between particles. After the yield point, dispersions may show yield-pseudoplastic or yield-dilatant type of flow behavior. Pseudoplastic (or shear thinning) flow curves can be modeled as ideal Bingham dispersions and flow curve properties such as apparent yield stress and plastic viscosity can be related to the structural properties of dispersion.

Thixotropic Dispersions: For the dispersions discussed above, it was assumed that, for any given shear stress, there is only one associated shear rate (and viscosity) and, hence, the flow curves were independent of additional factors such as shear history, time scale, etc. In this type of dispersion, there is an instantaneous response to sudden changes

in shear. However, there exists a class of dispersions for which the response time is considerable. Pseudoplastic dispersions exhibiting time-dependent shear stress-shear rate are referred to as thixotropic. Thixotropy in a dispersion is generally due to breakdown of some loose network structure under applied shear stress. (This type of network structure is formed during flocculation stage.) Hence, the rate of rebuilding the structure after being destroyed by the shear stress is important in determining the thixotropic behavior. This structural rebuilding process is governed by the Smoluchowski's kinetic equation (Chapter IV). The presence of thixotropy can be detected either by measuring shear stress under constant shear rate conditions as a function of time or by studying the ascending and descending shear stress-shear rate curves under certain programmed conditions (i.e., shear rate is increased from zero to a certain peak value in a given time, and then decreased from a maximum shear rate to zero in the same time and the corresponding shear stress is measured). A thixotropic dispersion under such a program would produce a hysteresis loop for τ versus $\dot{\gamma}$ as shown in Figure 6.3. If the program time is kept constant, then, the hysteresis area can be related to the degree of thixotropy.

From the above discussion, it is clear that the interparticle forces (and, hence, stability) and the structure of the dispersion can be assessed from the rheological measurements. Since this study was aimed at correlating stability behavior to rheological properties of the dispersion, we will discuss this correlation in the next section. The main factors that affect the flow behavior of colloidal suspensions are Brownian motion, hydrodynamic interactions, and interparticle forces of attraction and repulsion.
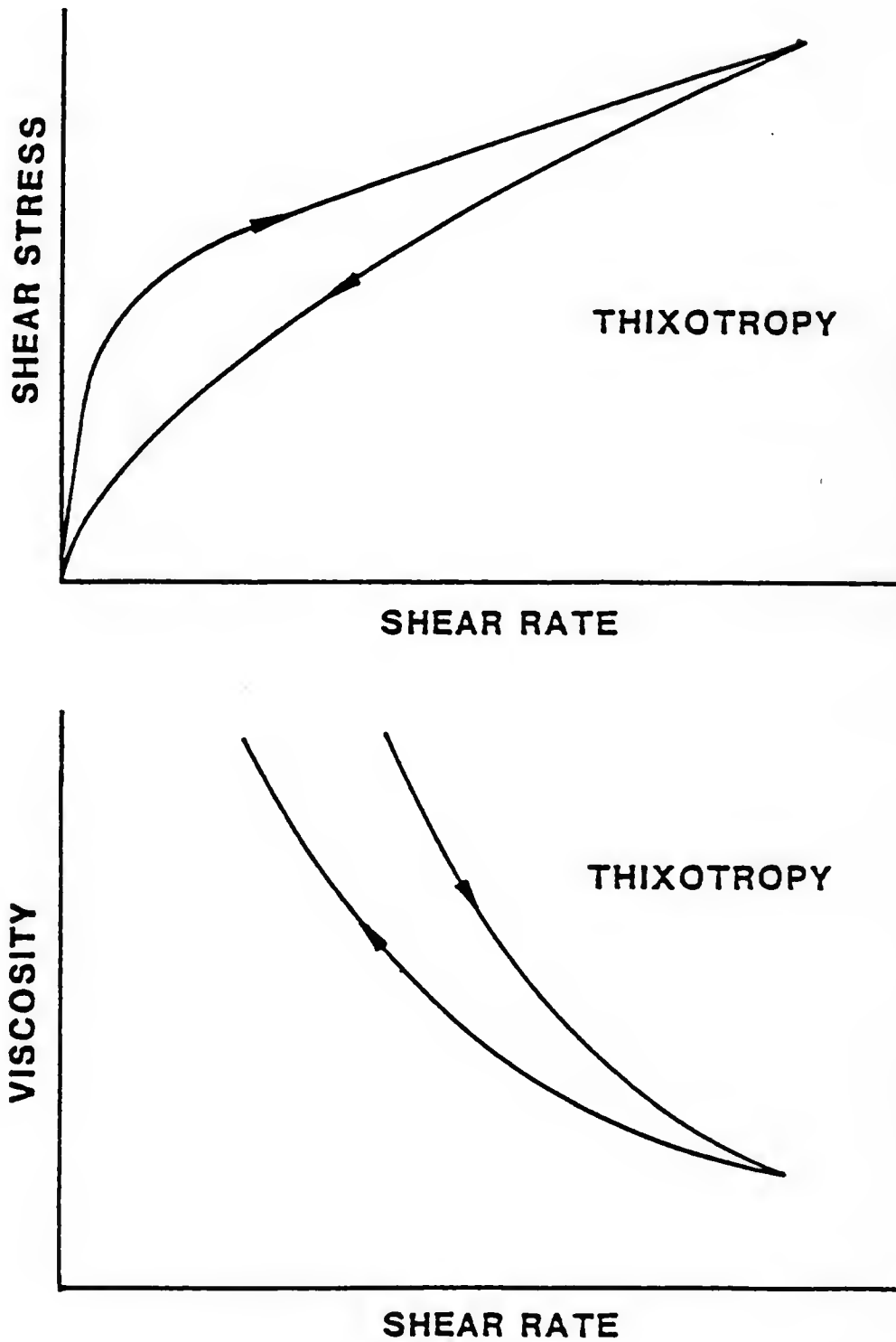
Figure 6.3   Schematic representation of thixotropic flow behavior,
(a) shear stress versus shear rate, and (b) viscosity
versus shear rate plots.

Factors Affecting Rheological Behavior of Colloidal Dispersions

Interparticle Interactions: Interparticle interactions are determined by the physicochemical bulk and surface properties of the components (Chapter II and Chapter III). We have already reviewed electrostatic and steric interactions (with adsorbed polymer) between two particles. We have shown that the repulsive interactions can be represented by hard sphere model or by soft interactions (Figure 5.9). The rheological behavior of colloidal dispersions can be classified into two categories: (1) Rheological properties of stable dispersions when (i) a net repulsion exists between two colloidal particles (such as electrostatically stabilized particles) or (ii) the depth of the pseudosecondary minima is much smaller than the thermal energy of particles (in the case of sterically stabilized dispersions). (2) Rheological behavior of flocculated dispersion, in this case, net attraction between particles, leads to structure formation (i.e., non-equilibrium aggregation) in dispersion. The origin of attraction can be due to Van der Waal's attraction, bridging attraction, flocculation under the condition of change in solvency, or flocculation in a good solvent in the pseudosecondary minima due to Van der Waal's attraction when the thickness of the adsorbed polymer is not sufficient. The effect of all of the above interactions on the rheological properties have been investigated in this study.

Brownian Motion: Colloidal particles distributed in a liquid undergo random motion which effectively acts as a dispersive mechanism. Brownian motion tends to oppose buildup of structure in the dispersion. This effect is more important in the rheology of dispersion of smaller

particles (usually ≤ 0.5 μm) when Brownian motion and shear field are superimposed during flow.

Hydrodynamic Interactions: Hydrodynamic effects result from the mere presence of solid particles in the flowing media. The presence of particles leads to perturbations of the flow field and a corresponding increase in the energy dissipation. The hydrodynamic interactions are determined by the geometrical and mechanical properties of the components. The continuous phase affects the flow through its viscosity, and rigid particles through their concentration, size distribution, and shape. The effect of these three factors on the rheological properties will be discussed in the next section.

Rheological Behavior of Stable Systems

First, we will consider the rheological properties of dispersions with hard sphere interactions, often called 'neutrally' stable dispersions. In this case, the effect of attraction and repulsion is minimized, and the main forces responsible for the rheological behavior are hydrodynamic and Brownian forces. This type of hard sphere system shows either Newtonian or non-Newtonian flow behavior depending on the particle concentration and the relative importance of Brownian motion and hydrodynamic interactions.

Einstein first described the dependence of the viscosity of a suspension on the volume fraction solid at low particle concentration by the following equation (Einstein 86):

$$\eta_{rel} = \eta/\eta_o = 1 + 2.5\phi \tag{6.4}$$

where η_{rel} is the relative viscosity, η is the suspension viscosity, and η_o is the viscosity of the suspending media, $\emptyset$ is the volume fraction of particles. The above equation is valid for rigid, uncharged, spherical particles at very low particle number concentrations (i.e., hydrodynamic interactions between particles were ignored). At higher particle concentrations, the dependence of relative viscosity η_{rel} on the volume fraction solid is shown in Figure 6.4. The slope of η_{rel} - $\emptyset$ curve reaches a limiting value of 2.5 only in the very dilute region. At intermediate concentrations, the η_{rel} increases more rapidly with $\emptyset$ than predicted by Einstein's equation (Equation 6.4). Above a certain volume fraction, the packing fraction $\emptyset_p$, the dispersed particles locks into a rigid structure and flow ceases (i.e., $\eta_{rel} \rightarrow \infty$). The fractional dependence of $\eta_{rel} = h(\emptyset)$ has been a subject of many studies both experimentally and theoretically.

For a monodisperse system, the dependence of Newtonian viscosity on $\emptyset$ can be represented by a power series expression (e.g., see Goodwin 75):

$$\eta_{rel} = \eta/\eta_o = 1 + k_1\emptyset + k_2\emptyset^2 + k_3\emptyset^3 + \ldots \tag{6.5}$$

In this expression, $k_1 = 2.5$ is similar to the Einstein's equation for rigid, uncharged, spherical particles. The coefficient k_2 is calculated from the perturbation of streamlines by collision doublets, and k_3, k_4, etc. are used to describe higher-order collisions. The range of values for k_2 is 4 - 14.1 depending on the assumptions involved and experimental estimates of the value of k_3 varying $\approx$ 16-50 (Goodwin 75). The power series expression is empirical in nature, and there is no theoretical justification for Equation 6.5. Thomas has suggested the following form
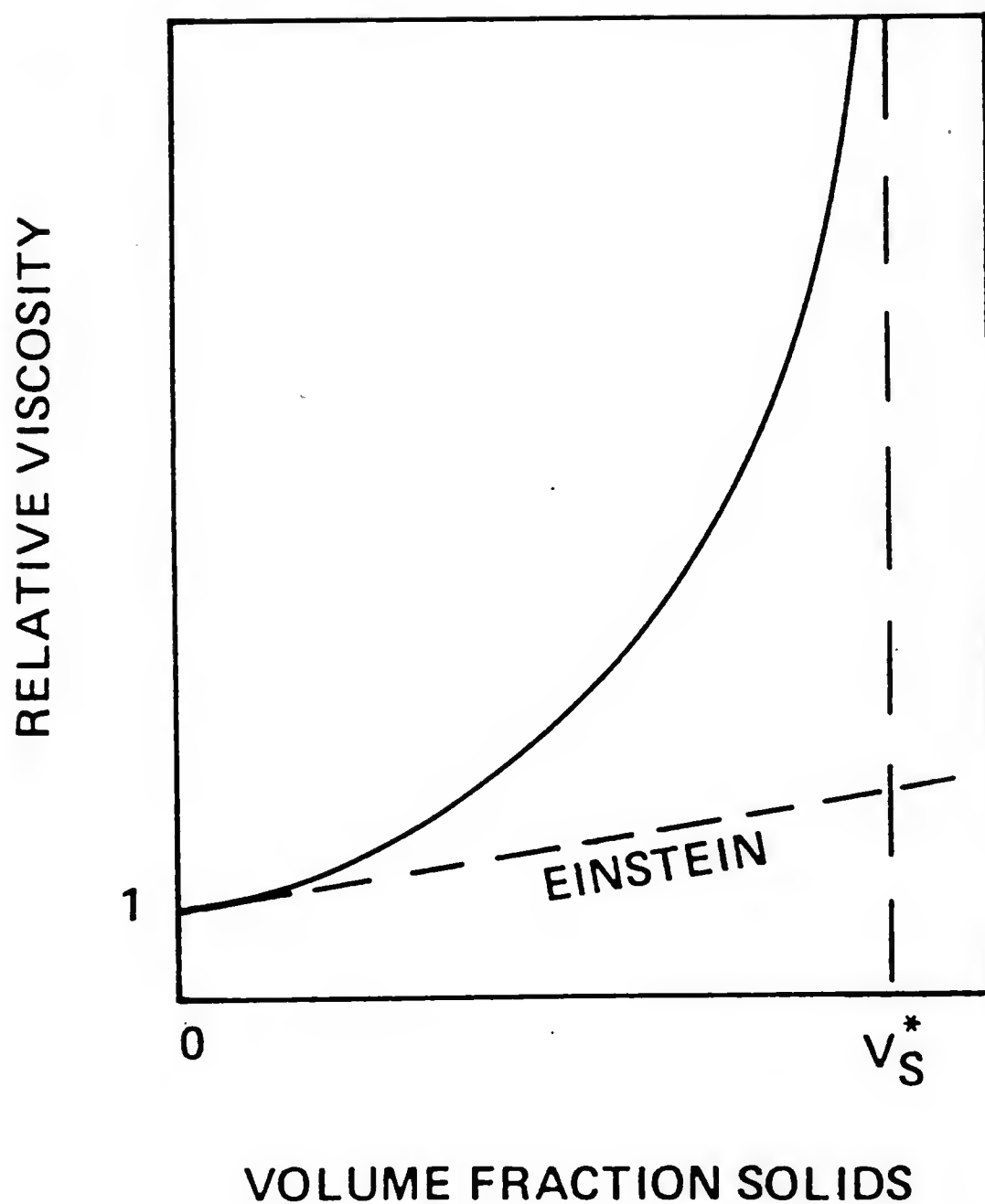
Figure 6.4   Schematic plot of dependence of relative viscosity on the volume fraction solid in suspension.

based on an analysis of extensive data on the relative viscosity of suspensions of spherical particles (Thomas 65):

$$n_{rel} = n/n_o = 1 + 2.5\phi + 10.05\phi^2 + A \exp (B\phi) \qquad (6.6)$$

where A and B are two adjustable parameters.

Mooney has derived the following equation based on purely geometric packing considerations (Mooney 51):

$$n_{rel} = n/n_o = \exp (\frac{2.5\phi}{1-k\phi}) \qquad (6.7)$$

The above equation is reduced to Einstein's equation when $\phi \to 0$. The value of parameter k is chosen such that the viscosity will become infinite when the packing of particles leads to complete mechanical interlocking, i.e., when:

$$k\phi_{max} = 1 \qquad (6.8)$$

Mooney argued that a simple cubic packed system will flow and a face-centered cubic packed system will not, and hence:

$$1.35 < k < 1.91 \qquad (6.9)$$

Various values of k have been suggested for different packing considerations. For example, for particles with net repulsive interparticle forces, k = 1.65 has been suggested (Goodwin 75). On the other hand, for the particles with net attraction, if one assumes that the highest volume fraction at which slip can occur is random packing of spheres, then, k = 1.56 (since $\phi_{max} = 0.64$ for random packing of spheres).

Krieger and Dougherty have suggested the following equations from the $n_{rel} - \phi$ studies of polymer lattices (Krieger and Dougherty 59):

$$n_{rel} = [1 - (\phi/\phi_p)]^{-[\eta]\phi_p} \qquad (6.10)$$

where ϕ_p is the so-called packing fraction and $[\eta]$ is the intrinsic viscosity defined as follows:

$$[\eta] = \underset{\phi \to 0}{\text{Lim}} \frac{(\eta_{rel} - 1)}{\phi} \qquad (6.11)$$

and $[\eta]$ = 2.5 for rigid, uncharged spheres. This equation fits the η_{rel} - ϕ data of lattices of different sizes stabilized by non-ionic surface active agent as shown in Figure 6.5.

The Effect of Adsorbed Layer

The hard sphere approximation can be applied to sterically stabilized colloidal dispersions if proper account is taken of the adsorbed layer volume. The adsorbed polymer layer thickness, δ, is usually added to the particle radius a to account for the increase in the effective volume fraction of solid. The effective volume fraction of solid, ϕ_{eff}, is related to the true solid volume fraction ϕ and the adsorbed layer thickness, δ, by the following relation:

$$\phi_{eff} = \phi_{true} \, (1 + \delta/a)^3 \qquad (6.12)$$

The value of ϕ_{eff} should be used in Equations 6.4, 6.5, 6.6, 6.10, etc. for ϕ in the case of sterically stabilized dispersion. This equation can also be used to evaluate the hydrodynamic thickness, δ, of the adsorbed polymer layer if ϕ_{true} and ϕ_{rel} is known (i.e., if ϕ_{eff} can be determined from the experimentally established η_{rel}-ϕ relation for a given system). Using this approach, the dependence of the effective hydrodynamic thickness on the molecular weight of the polymer has been determined in this study and the results will be discussed in Chapter VIII.
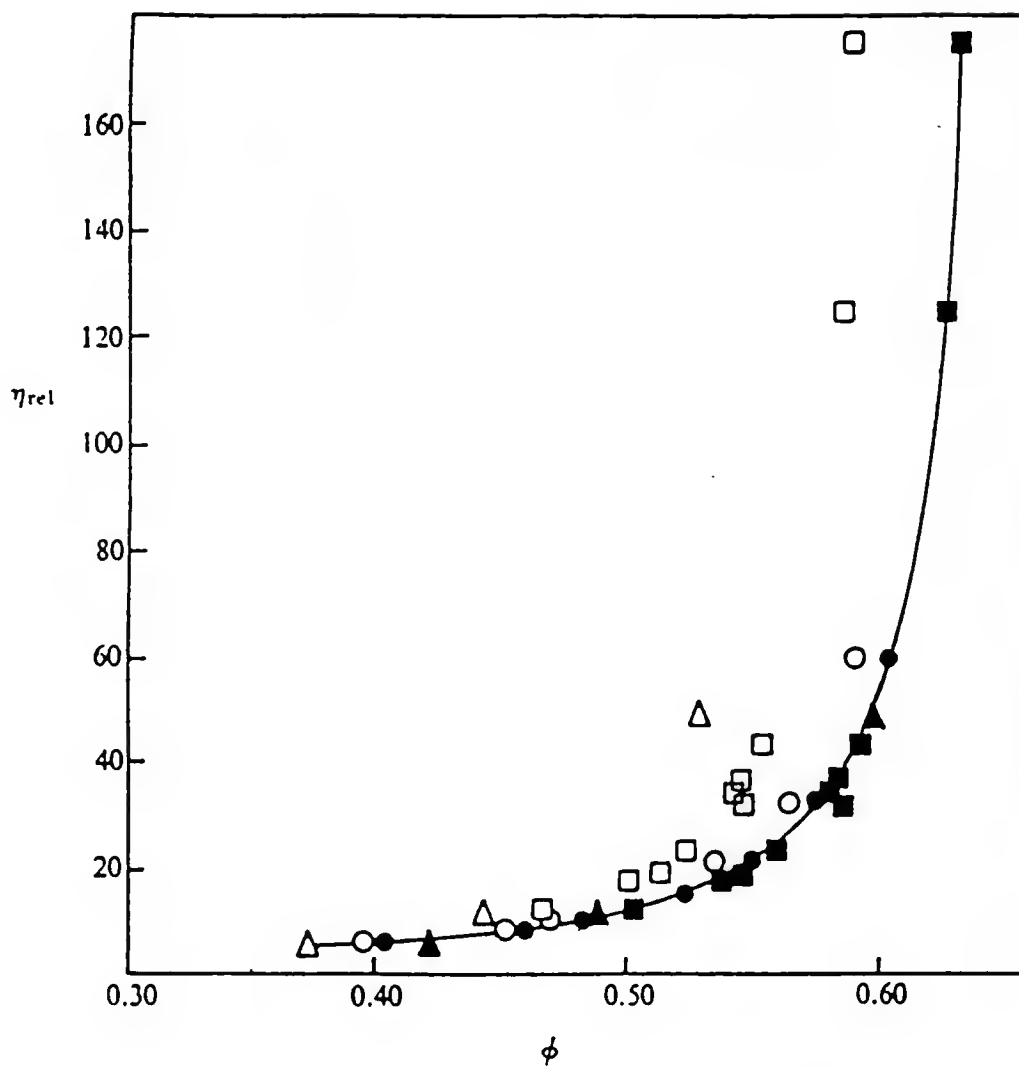
Figure 6.5   Plot of relative viscosity versus volume fraction latex
particles of different sizes.   Data was fitted using
Krieger equation (Krieger, 1972).

Equations 6.5, 6.6, 6.7, and 6.10 are generally used to relate relative viscosity to the volume fraction of solids at high shear rates where the rheological behavior is essentially determined by the hydrodynamic interactions. The case where Brownian and hydrodynamic interactions are important have been analyzed by Krieger using the principle of corresponding rheological states (Krieger 72). The appropriate dimensionless group characterizing the process is given by the product of shear rate $\dot{\gamma}$, and the time scale of Brownian diffusion, $t_r = 6\pi\eta_0 a^3 / kT$. This gives the dimensionless shear rate $\dot{\gamma}_r = 6\pi\eta_0 a^3 \gamma / kT$. According to the principle of corresponding state, the relative viscosity (under steady state and laminar flow conditions), of neutrally buoyant (i.e., density of particles = density of medium) particles is only a function of volume fraction of solid and dimensionless shear rate, i.e., $\eta_{rel} = f(\phi, \dot{\gamma}_r)$. Thus, at given volume fraction solids, η_{rel} is the unique function of $\dot{\gamma}_r$. Now, the same value of $\dot{\gamma}_r$ can be obtained by changing particle radius a or viscosity of the medium or shear rate γ. The validity of this approach has been proved by measuring the relative viscosity of latex dispersions at a fixed solids loading. The dimensionless shear rate $\dot{\gamma}_r$ was varied by either (i) changing the viscosity of medium (i.e., η_0) (Figure 6.6) or (ii) by changing the particle size (i.e., a), (Krieger 72). The superimposition of the rheological curves, where η_{rel} is plotted as a function of dimensionless parameter $\dot{\gamma}_r$, conclusively proves that the rheological behavior is affected by Brownian motion and hydrodynamic interactions in this case. The flow curve shown is shear thinning (i.e., η_{rel} decreases with
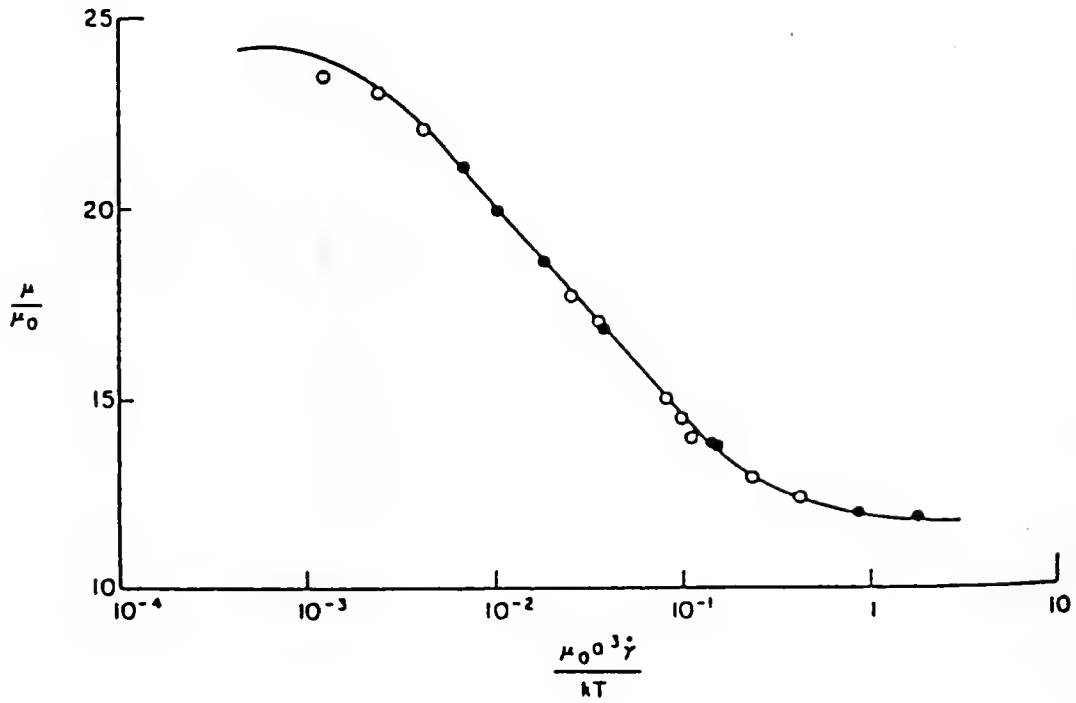
Figure 6.6   Plot of relative viscosity versus dimensionless shear
             rate, $\dot{\gamma}_r$, for monodisperse suspensions of polystyrene
             spheres at $\emptyset$ = 0.50 in different fluids (Krieger, 1972).

increasing $\dot{\gamma}_r$) which may be related to the structure of the suspension. At low shear rates, Brownian motion dominates and this tends to distribute particles randomly throughout the dispersion. The particles arranged in such a random way tend to jam the flow when forced to move in a shear field. Hydrodynamic forces tend to form ordered layered structural coinciding with the planes of constant shear. These layers can glide over one another in the flow direction, and hence, offers less resistance to flow, i.e., lower viscosity. A theory has been developed to explain non-Newtonian flow in hard spheres dispersions by Krieger. The relative viscosity as a function of dimensional shear stress τ_r is given by the following equation (Krieger 72):

$$\eta_{rel} = \eta_{1r} + (\frac{\eta_{2r} - \eta_{1r}}{1 + b \cdot \tau_r}) \qquad (6.13)$$

Hence, η_{2r} and η_{1r} are the low and high shear limiting viscosities. Dimensionless shear stress $\tau_r = a^3 \cdot \tau / kT$ where τ is the shear stress, a is the particle radius, and kT has the usual meaning. The parameter b is a concentration (ϕ) independent parameter.

For electrostatically stabilized dispersions, particle sizes up to approximately 0.5 μm follows the superposition as predicted by the rheological equation of state. For larger particles and at higher shear rates, the hydrodynamic interactions dominate the flow behavior and relative viscosity is essentially independent of particle size.

Important conclusions from the above discussion are: (1) Neutrally stable dispersions of colloidal particles at high solid concentrations may exhibit non-Newtonian flow behavior. (2) The suspension viscosity of concentrated dispersions of smaller particles will be higher at fixed low

shear rate and volume fraction solids than the dispersions of larger particles. (3) Sterically stabilized dispersions can be represented as hard spheres if the adsorbed polymer layer thickness is added to the particle radius to calculate effective volume fraction solids (ϕ_{eff}).

Stable Dispersions with Soft Interactions

This represents the case where the particle interactions are dominated by long-range interactions (either electrostatic or steric repulsion). The appropriate dimensionless group characterizing these types of suspensions is given by $\eta_o a^2 \dot{\gamma} / \epsilon \Psi_o^2$ where ϵ is the dielectric constant of the medium and Ψ_o is the surface potential (e.g., see Russel 80, Tadros 86). Here again, repulsive force plays an important role at low shear, while hydrodynamic forces play a dominate role at high shear. The effect of electrostatic forces on the viscosity of aqueous suspension of charged particles is classified into three categories (Krieger 72). (1) The primary electroviscous effect arises due to distortion under shear of the electrical double layer. (2) The secondary electroviscous effect arises due to electrostatic interactions between the double layers of different particles at finite concentrations. (3) The third electroviscous effect is due to the distortion of the particle itself due to the electrostatic forces. Clearly, this effect is not important in the case of rigid spherical particles.

As discussed in the last chapter, the thickness of the double layer is controlled by the ionic strength of the solution, and hence, electroviscous effects are more important under high charge, low ionic strength conditions. Long-range electrostatic interactions can lead to ordering of particles under certain conditions (see Chapter V) and

hence, higher viscosities and viscoelastic behavior can be observed. The amount of electrolyte added to suspension (ionic strength 1×10^{-2} M NaCl moles/liter) in the present investigation was sufficient for electroviscous effects to be neglected.

Rheological Behavior of Flocculated Dispersions

The rheological behavior of unstable dispersions (i.e., when net attraction exists between particles) is a more difficult problem from the theoretical as well as practical point of view. This is due to the formation of non-equilibrium structure at rest resulting from the weak Brownian motion. The quantitative description of the flow behavior of the flocculated dispersions is difficult because the role of interparticle forces on the properties of the non-equilibrium structures (e.g., structural properties such as average size, size distribution of particle-clusters, effect of shear on these structures, etc.) is not yet well understood, and the description of the structure itself is not a trivial problem.

Structure of Flocculated Suspensions

As mentioned in the last chapter, various types of non-equilibrium structures can be formed. Two extreme cases are the formation of chain-like structures or the formation of more spherically-shaped clusters of particles. These two shapes are the extreme simplifications of the real structures and are often used as a structural model for flocculated dispersions. In real systems, various intermediate structures are expected. At high particle concentrations, the difference between the

two cases must vanish. The structure of the dispersion has a profound effect on the properties of the dispersion such as its rheological behavior, sediment density and porosity, filterability, compressibility, etc. The properties of the flocculated suspension (and hence, its structure) are influenced by various factors, such as particle size and shape, solid surface characteristics, particle concentration, mixing conditions, shear history, interparticle forces, etc. In the case of electrostatically stabilized dispersions factors such as pH, electrolyte concentration, and ion type control the dispersion properties. If polymer is present, then additional parameters such as polymer concentration in solution (i.e., adsorbed amount of polymer or fractional coverage), polymer molecular weight, and polymer characteristics are important variables controlling the dispersion properties.

Various types of structural models have been used to describe the properties of flocculated dispersions. Here, only a brief summary is given. The recent developments in describing non-equilibrium structures have been discussed in Chapter V.

Michaels and Bolgers assumed that the basic flow units in flocculated dispersion are small particle clusters consisting of randomly packed spherical particles called flocs (Michaels and Bolgers 62). At low shear (or at rest), the flocs group into clusters of flocs called aggregates. The aggregates may form a network which can fill the entire volume of the dispersion and which can give the dispersion its plastic and structural properties. A similar model was also used by Vold (Vold 63) to explain the large sediment volume of silica sols in organic solvents. From computer simulation, she showed that flocs grown from successive random

additions of individual spherical particles have a roughly isometric "core" of slowly diminishing density and "tentacles" giving the floc a rough surface. Also, the mean density of the floc decreases with increasing size and is given by the following equation:

$$\rho = 69 \ N^{-0.29} \tag{6.14}$$

where ρ is the mean density of the core containing N particles. This functional dependence is very similar to the one used to describe a fractal object (Chapter V).

Firth and Hunter proposed an elastic floc model to describe the flow behavior of flocculated dispersions (Firth and Hunter 76a, Hunter 82, van de Ven and Hunter 79). In their model, a typical floc is assumed to consist of a string of particles linked together in a more or less regular three-dimensional network. A parameter known as the floc volume ratio $C_{FP} = \phi_F / \phi_p$ measures the compactness of the floc, and C_{FP} has been related to interparticle forces and shear history. Later, we will discuss the elastic floc model in more detail. From the above discussion, it is clear that the internal arrangement of particles in a given floc is either assumed to be uniform (random packing of spheres or some uniform low packing structure) or similar to a fractal object (mean density decreasing with floc size).

The information regarding the temporal evolution of the floc size distribution can be obtained from Smoluchowski's kinetic equations. Applied shear will have an effect on the collision frequency (i.e., kinetics of flocculation) (Zeichner and Schowalter 77). It will induce breakdown of aggregate network and flocs, and it can change stability conditions (van de Ven and Mason 76). It has been shown in the case of

dilute dispersions that the hydrodynamic interactions (which are ignored in Smoluchowski's equation) will retard the flocculation rate (Honig et al. 71). The effect of shear on the flow stability of dilute and electrostatically stabilized dispersions have been investigated (Zeichner and Schowalter 77, van de Ven and Mason 76). The stability diagram as shown in Figure 6.7 illustrates that, with increasing shear rate, weakly coagulated (in secondary minima) doublets can be separated into single particles. With further increases in shear rate (i.e., kinetic energy of particles), particles can surmount the potential energy barrier and particles can be coagulated into primary minima. Very little information is available regarding the rupture susceptibility of flocculated structures. Usually, the exponential type of relation between average stable floc radius and shear rate is assumed as shown below:

$$R \approx \dot{\gamma}^{-a} \tag{6.15}$$

where R is the average floc radius, $\dot{\gamma}$ is the shear rate and a is an empirical constant. Sonntag and Russel have modified Alder and Mills' treatment of uniform porous floc breakup to accounts for the breakup of flocs with fractal characteristics (Sonntag and Russel 87, Alder and Mills 79). They showed that the location of rupture approaches the surface as R becomes large due to the decreased strength of the network (i.e., flocs are assumed to be fractal objects, and hence, the local density is a decreasing function of distance from the center of gravity of the floc. Due to lower density, flocs are expected to be weaker near surface compared to core.)

Various methods have been used to characterize flocculated structures. The most simple is the direct observation of structure using
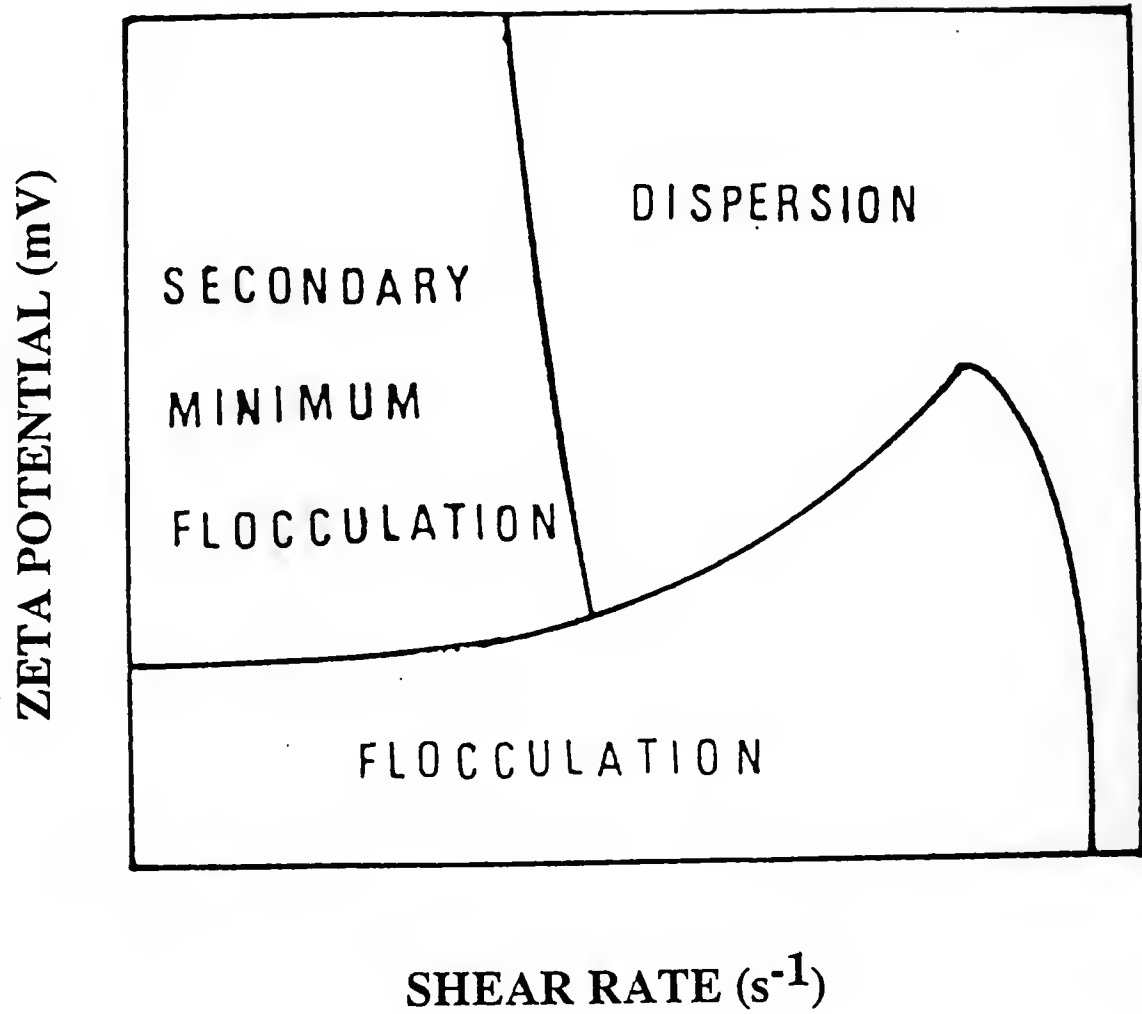
Figure 6.7   Schematic illustration of the effect of shear on the
              stability of suspensions (Zeichner and Schowalter, 1977).

optical microscopy or using scanning or transmission electron microscopy.
Freeze-fracture technique has been developed to observed concentrated
dispersions (for e.g., see, Menold et al. 76). It is obvious that these
techniques can be applied to obtain structural information by application
of quantitative microscopy if flat sections through the freeze-dried
dispersions can be prepared. Changes in structure can be detected and
analyzed by physical techniques such as electrical conductivity,
dielectric measurements, optical measurements, and scattering techniques
(Mewis and Spaull 76). For fractal clusters with fractal dimensionality,
$d_f < 2$, the two-dimensional projections can be used to determine d_f of
three-dimensional structures (Weitz et al. 84). Another method of
obtaining information on random structures is computer simulation.
Various cluster growth models, such as diffusion limited growth (DLA) and
cluster-cluster aggregation model (CCA), have been discussed in detail in
the last chapter. From the above discussion, it can be concluded that
detailed information regarding the properties of the structure is still
lacking. The recent applications of fractal geometry for irreversible
processes and the solutions of Smoluchowski's equation under different
kernel seems to be a step in the right direction.

Flow Behavior of Flocculated Dispersions

Flocculated dispersions show pseudoplastic (or shear thinning)
behavior at low volume fractions of solids, while more concentrated
dispersions display plastic behavior. Suspensions flocculated with
polymeric additives often show time dependent flow or thixotropic flow
behavior. There are a few equations which are commonly used to describe

shear thinning flow behavior (Goodwin 75, Tadros 80). Often these equations are derived based on the assumption that the shear thinning flow behavior results from the breakdown of three-dimensional network structure under shear, but the analysis is rarely carried out in detail to determine all the constants of the model. Hence, these equations are empirical in nature.

Flocculated Dispersion Showing No Time Dependence

As shown in Figure 6.8, three parameters are often used to characterize the pseudo plastic flow curve: (1) D_o, the critical shear rate at which the flow curve becomes linear, (2) n_{pl}, the plastic viscosity which is the slope of the linear portion of the shear stress-shear rate curve, and (3) τ_b, an apparent yield stress obtained by extrapolation of the linear portion of the shear stress-shear rate curve to $D = 0$.

We will briefly review some of the models put forward to relate the dependence of the flow curve parameters to the interparticle interactions and floc structure. To obtain a satisfactory model of the flow process, it is necessary to identify, at the microscopic level, various energy dissipation processes. From the characteristic fluid motion, it should be possible to calculate the forces necessary to produce postulated structural changes or deformations of flocculated dispersion.

In a flocculated system, it is assumed that dynamic equilibrium exists between aggregate growth and destruction at any shear rate. High shear rate shifts the equilibrium in the direction of better dispersion, whereas low shear favors aggregation. It is generally assumed that above

188
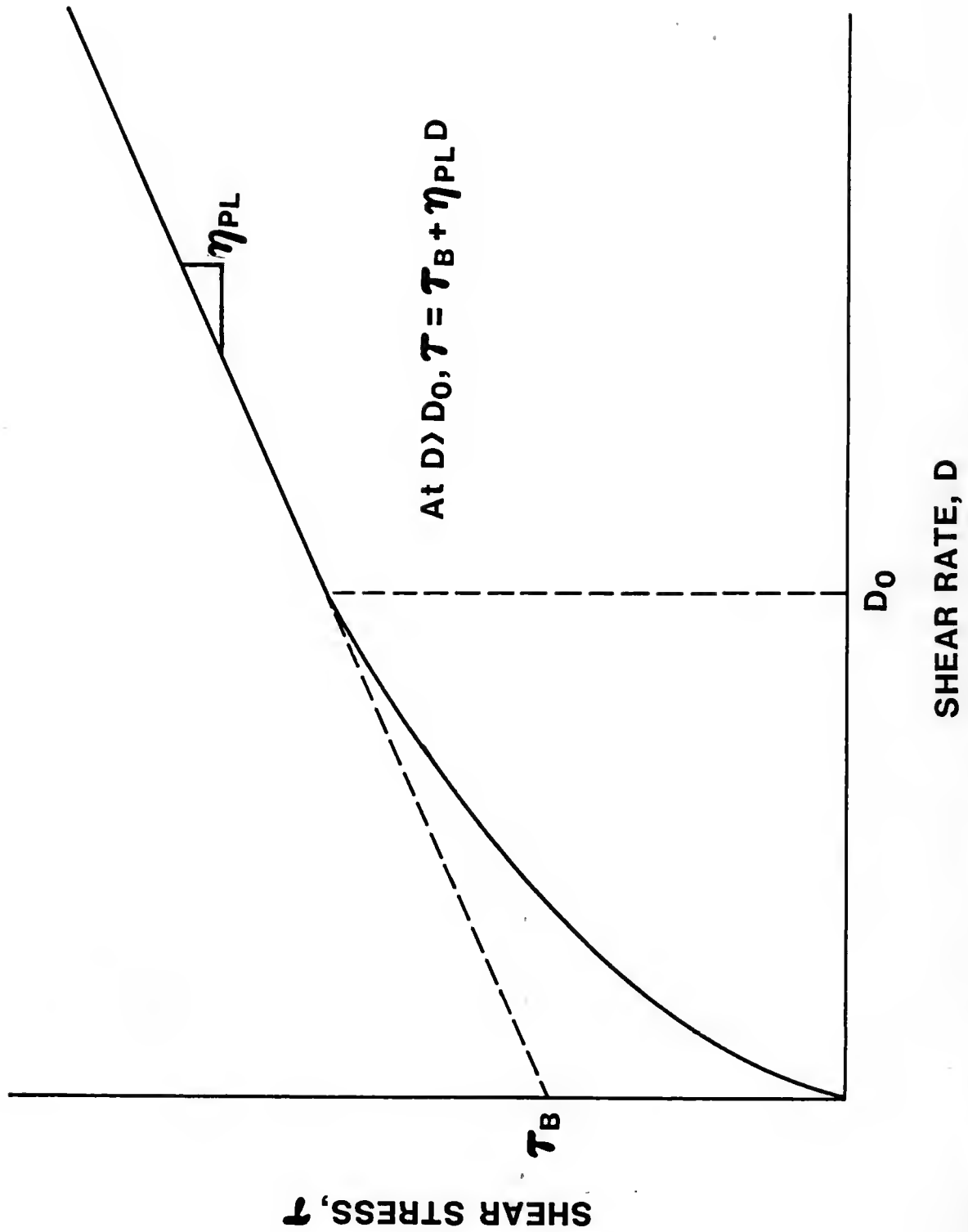
Figure 6.8   Schematic illustration of flow curve parameters for pseudoplastic flow behavior.

a critical shear rate, aggregates are broken down to individual particles
or at least to single floc.

Albers and Overbeek equated the maximum hydrodynamic force, F_H,
exerted on a pair of flow units (in their case, particle-doublet) with
the maximum interaction force, F_{max} (Albers and Overbeek 60). To
evaluate F_H, the expression derived by Goren for two "touching" spheres
in couette flow is used (Goren 71). The maximum hydrodynamic force is
given by the following equation:

$$F_H = 6.12 \ \pi \ \eta_o \ a^2 \ D \tag{6.16}$$

where a is the particle radius, η_o is the solvent viscosity, and D is the
shear rate.

The energy dissipation in the flow process can be divided into two
parts: (i) the part due to the flow of fluid around the flow units
(assuming the flow units are impermeable) and (ii) additional energy
dissipation due to attractive interactions within or between flow units.
This breakdown of total energy was first suggested by Goodeve and
developed by Gillespie who showed that the Bingham yield value could be
related to the interaction energy between the flow units by (Goodeve 39
and Gillespie 60):

$$\tau_b = \frac{3\phi^2}{2\pi^2} \ R^3 \ \cdot \ E_{SEP} \tag{6.17}$$

where ϕ is the volume fraction of flow units, R is the radius of the flow
unit, and E_{SEP} is the energy required to separate a doublet of flow
units. This model has been applied by Neville and Hunter for the case of
reversible flocculation of sterically stabilized dispersions (Neville and
Hunter 74, Tadros 84). The linear relationship between τ_b and ϕ^2

(Equation 6.13) has been confirmed experimentally by various investigators (see e.g., Firth 76a, Michaels and Bolgers 62, Hunter and Nicol 68).

Elastic Floc Model

Hunter et al. have shown that much of the flow behavior of dilute dispersions ($\phi \approx 0.01 - 0.1$) can be explained with the "elastic floc model." In this model, the basic flow units are considered to be "elastic" flocs which can undergo extension and compression during rotation in the shear field. The flocs are formed from the association of particles or "flocculi" (i.e., cluster of particles, or hard agglomerates, which cannot be broken by shear). The most important characteristic of the floc is the degree to which it can entrap liquid (i.e., the floc packing density). This is measured by a quantity called the floc volume ratio, C_{FP}, and given is by the following equation:

$$C_{FP} = \phi_F / \phi_P \tag{6.18}$$

where ϕ_F is the volume fraction of flocs and ϕ_P is the volume fraction of particles. A higher value of C_{FP} indicates a more open floc structure.

The flow curve parameters, such as extrapolated yield stress, τ_b, relative plastic viscosity, n_p, and critical shear rate, D_o, are related to floc structure and interparticle forces as follows.

To describe the flow behavior by the above parameters, the energy dissipation process was separated into two types, as described earlier, (1) energy dissipation, E_v, due to the viscous flow of medium around the flow units and (2) energy dissipated in overcoming interactions between

particles. The shear stress-shear rate relation can be described by the following equation above D_O:

$$\tau = \tau_\beta + \eta_{pl} \cdot D = \tau_\beta + \tau_v \tag{6.19}$$

and energy dissipation by:

$$E_{total} = \tau \cdot D = \tau_\beta \cdot D + \eta_{pl} D^2 \text{ and}$$

$$E_v = \eta_{pl} \cdot D^2 = \tau_v D \tag{6.20}$$

Coagulated systems often show a linear shear stress-shear rate relationship above D_O (Figure 6.8). This means that the relative plastic viscosity is constant (i.e., the effective volume fraction of flocs ϕ_F, does not alter during the measurement procedure above D_O). At high shear rate, the flocculi can be transferred from one floc to another during collisions, but the value of ϕ_F (or C_{FP}) remains constant for all $D > D_O$. Substituting for η_{pl} in Equation 6.20 in terms of ϕ_p (using Equations 6.4 and 6.18), we have:

$$E_v = \eta_{pl} D^2 = \eta_O D^2 (1 + 2.5 C_{FP} \phi_p) \tag{6.21}$$

In using the above equation, it is implicitly assumed that the flocs are spherical and are impervious to the suspension medium. At high shear rates, floc deformation due to rotation cannot be neglected. The energy associated with floc deformation and associated with the transfer of flocculi from one floc to another is estimated by considering detailed interactions between two flocs as they collide and get separated by the shear field (van de Ven and Hunter 79). The elastic floc model predicts how the value of C_{FP} (which is related to η_{pl}--Equation 6.21) depends on the colloidal properties of the dispersion. By equating the shear stress exerted by the applied shear field F_H, to the strength of the floc F_{max}, the following equation for C_{FP} is obtained:

$$C_{FP} = 1.5 + \frac{1}{5\eta_o D_{CFP} a} \left\{ \frac{A}{12d_1^2} - B(\epsilon, \kappa d_1)\zeta^2 \right\} \tag{6.22}$$

where D_{CFP} is the maximum shear rate to which the system is subjected, A is the Hamaker constant, d_1 is the distance between particles at which maximum interactive force occurs, B is a function determining dependence of electrostatic repulsion on the dielectric constant, ϵ, of the medium, Debye Huckel parameter κ, and zeta potential, ζ.

The minimum value of 1.5 for C_{FP} can be explained since any aggregate must trap some liquid. The dependence of C_{FP} on 1/a at constant zeta potential has been demonstrated by Firth (Firth 76b). The linear dependence of C_{FP} on zeta potential squared has also been demonstrated (Firth 76b, Hunter and Frayne 80). In addition, the calculated values of d_1 from the experimental data are reasonable (i.e., in the range of 1 to 10 °A). The decrease in the C_{FP} with increase in the repulsion indicates that the flocs formed under repulsive interactions are more compact. Although the above trends have been verified, the quantitative agreement is very poor.

In order to calculate the Bingham yield value (an apparent yield stress), following Michaels and Bolgers, Hunter considered, the energy dissipation during the rupture of the floc doublet. In the elastic floc model, it is assumed that two elastic flocs when collided can form a floc doublet. The energy required to break the floc doublet is supplied by the shear field. This energy consists of two parts: (i) the energy to break the bonds between two flocs forming a doublet and (ii) the energy required to stretch the bonds within the floc as the tension must be transmitted from the shear field to the floc-floc interface. Since the

number of bonds between flocs is relatively small, the energy required to break them is relatively small when compared with the energy due to bond stretching. The energy required to stretch one bond is smaller than that required to break it, but the number of bonds involved in stretching are much more than bond breaking. The energy needed to stretch bonds consists of several parts. (1) Elastic energy required to overcome the interparticle forces which are keeping the particles in a primary minima position; (2) Viscous energy dissipated to overcome the viscous drag as particles will be displaced during stretching; and (3) Viscous energy dissipation due to liquid movement inside flocs during collision.

Van de Ven and Hunter have derived the necessary equations to calculate the above energy terms. From the order of magnitude approximations, they showed that only the contribution due to fluid movement inside the floc is important. From the above analysis, Bingham yield is given by:

$$\tau_\beta = \frac{\beta' \lambda \eta_o D \; r^2 \; \delta_1 \; \phi_p^2 \; C_{FP}}{a^3} \tag{6.23}$$

where δ_1 is the increase in distance between the spheres as a result of stretching (a few angstrom units at the most), β' is a constant $(27/5)$, λ is the orthokinetic efficiency which depends weakly on shear rate $(\lambda \; \dot{\alpha} \; \gamma^{-0.18})$, r is the floc radius, and a is the particle radius.

The trends predicted by the above equation have been verified by the linear relations for (i) τ_β vs. ϕ_p^2 (Firth 76b, Michaels and Bolgers 62, Hunter and Nicol 68), (ii) τ_β vs. C_{FP} (or more correctly τ_β vs. $1/\zeta^2$) (Hunter and Frayne 80), and (iii) $a^3 \tau_\beta$ vs. $C_{FP} \phi_p^2$) (Hunter and Frayne 80).

The critical shear rate, D_O, is related to the number of floc/floc bonds, n_F, by the following relation:

$$D_O = \frac{n_F F_M}{5\eta_O} \qquad (6.24)$$

where F_M is the maximum force of attraction between particles. The elastic floc model also suggests following relation between C_{FP} and F_M:

$$C_{FP} = 1.5 + \frac{F_M}{b\eta_O a^2} \qquad (6.25)$$

where b is constant approximately equal to 10. Equation 6.25 is incorrect by orders of magnitude. A reasonable value for F_M is $\approx$ 1.6 x 10^{-9} N (i.e., force of attraction between two spherical partices of radius a = 0.5 μm, separated by distance of 5°A. The value of Hamaker constant A = 1 x 10^{-19} J). Substituting η_O = .001 Pas and C_{FP} in the range 2-7, we obtain (from Equation 6.25):

$$F_M = 1.25 \times 10^{-17} \text{ N } (C_{FP} = 2) \text{ and } F_M = 3.2 \times 10^{-16} (C_{FP} = 7)$$

If we compare F_M values (1.25 x 10^{-17} - 3.2 x 10^{16} N) predicted by Equation 6.25 with the resonable estimates ($F_M \approx$ 1.6 x 10^{-9} N), we observe that Equation 6.25 is in error by orders of magnitude.

The floc radius, r, is

$$E_v = \eta_{pl}D^2 = \eta_O D^2 (1 + 2.5 C_{FP} \phi_p) \qquad (6.21)$$

by the following equation:

$$r = (1.2 \pi n_F)^{-1/2} \qquad (6.26)$$

Hunter claims that the above equation predicts the correct order of magnitude of the floc radius (one to few microns) at D_O, but since the value of n_F used in the above equation is erroneous (as n_F was calculated

from Equation 6.25), the value of the floc radius cannot be assumed to be valid.

In summary, it can be said that the quantitative description of the flow behavior of the flocculate dispersion is clearly lacking. The model described above is one of the few models which tries to relate the colloidal parameters (i.e., particle radius, zeta potential, Hamaker constant, ϕ, etc.) of the dispersion to the flow parameters (i.e., τ_β, η_{pl}, etc.) of the dispersion and is successful in predicting certain trends. The whole treatment is based on the network floc model and dependence of C_{FP} on the interparticle forces. Since this link is not yet firmly established, the complete solution is not yet possible. Hunter's elastic floc model is developed for the dispersions with only electrostatic interactions. Flocculation with the adsorbed polymer introduces additional complications since the exact nature of the interaction forces at partial coverage is not yet known, and the kinetics of the polymer adsorption process also play an important role.

CHAPTER VII
MATERIALS: PROPERTIES AND CHARACTERIZATION/EXPERIMENTAL PROCEDURES

Introduction

In this chapter, we will review the characteristics of materials used in this investigation. All dispersions were prepared using spherical, narrow-sized silica particles in water. Poly (vinyl alcohol), PVA, having different molecular weights and acetate contents were used in this investigation.

Silica as a Model Material

Narrow-sized agglomerate-free spherical silica powder was used in this investigation. There are several advantages of using homogeneous particles of uniform size and shape (Overbeek 82b). The colloid stability (or interaction between particles) of dispersion is usually explained from the interactions between two particles, and if all particles are of the same size and shape, then, the explanations are more satisfactory. Spherical shape and narrow size distribution is important in studying various scientific phenomena, e.g., Brownian motion, coagulation, light scattering by colloidal particles, liquid-solid phase transition in concentrated dispersions, sintering, etc. Monosized spherical particles can be used as a calibration standard (for example, spherical latex particles are used to calibrate scanning electron microscope, SEM, magnification).

Polymer lattices with very narrow-size distribution can be made reproducible and have been used as a "model" material in testing various theories of colloidal stability (Hearn et al. 81). For such studies, the surface characteristics of the particles are very important, and hence, usually emulsifier-free systems are used (e.g., see Krieger 72, Vanderhoff et al. 70, Hearn et al. 81). The detailed surface characterization of latex particles is not yet possible (initiator use and efficiency of cleaning have influence on the surface characteristics). The stability of polymer lattices is usually explained from the electrostatic interactions, but the absence of steric contribution to stability is not yet conclusively proved (Hearn et al. 81, Killmann et al. 88).

The silica used in this investigation has certain advantages with respect to studying the factors affecting processing of ceramic powders. It is expected that the material characteristics, such as density, surface properties, Hamaker constant, etc., will have a significant effect on the properties of dispersion. The surface characteristics of silica are modified by calcination treatment and have been characterized using Fourier Transform Infrared Spectroscopy, (FTIR) (Sacks et al. 87). In ceramic processing operations, dispersions are usually made by mixing powders and additives in appropriate solvent. In contrast, latex dispersions are prepared by emulsion or suspension polymerization technique (i.e., latex particles are grown in-situ) and these dispersions are used to investigation the stability behavior under various conditions. Thus, additional complications due to the sequence of additions of various components and mixing conditions cannot be studied.

Also, the stability mechanism can be studied unambiguously (as initially, no polymer or surfactant is present on the silica surface). The surface of the precipitated silica is well-covered with hydroxyl groups, -OH. The surfaces of many oxides, such as alumina, zirconia, etc., and other technically important ceramics such as silicon carbide, silicon nitride, etc., are also covered with surface hydroxyl groups. Therefore, the effect of surface characteristics on the dispersion properties, investigated for silica in this study, may have applications in colloidal processing of other ceramics. Recently, there has been substantial interest in the processing of monosized powders using the colloidal processing route. Bowen and Barringer have stated two postulates to improve manufacturability of value added ceramics (Bowen, 84a):

(1) Powders with narrow-sized distributions are easier to process into uniform green microstructures (i.e., uniformity with respect to pore size and size distribution), which results in easier control of the microstructure during sintering. (2) To achieve uniform green microstructure, interparticle forces (electrostatic, solvation, or steric) between colloidal particles should be controlled by controlling surface chemistry. (Postulate 1 has been recently challenged by Sacks and coworkers (Sacks 88--unpublished work).

The effect of the green density (i.e., green microstructure) on the sintering behavior has been studied in the case of monosized titania, TiO_2, by Barringer (Barringer and Bowen 82), and for spherical monosized silica, SiO_2, by Sacks and Tseng (Sacks and Tseng 84, Shinohira et al. 78). They showed that the densely packed samples can be sintered at much lower temperatures (clear glass can be obtained at 1100°C, much below its

melting point). Also, TiO$_2$ can be sintered at 1050°C to greater than 99

percent of the theoretical density (Barringer and Bowen 82). In this

work, the effect of various factors on the stability of narrow-sized

silica dispersions of moderate silica concentration (twenty volume

percent) and on the green microstructure is investigated. The effect of

starting green density (packing) on the evolution of the microstructure

during sintering is under investigation (Vora and Sacks 88--unpublished

work).

Silica Preparation and Characterization

The silica used in this investigation was prepared using the Stober

et al. method (Stober et al. 68). Spherical silica particles of uniform

size are prepared by hydrolysis of tetraalkylsilicate and subsequent

condensation of silicic acid in alcoholic solutions containing water and

ammonia at room temperature. The hydrolysis of tetraethylorthosilicate

(Si(OC$_2$H$_5$)$_4$), TEOS, and subsequent condensation of resulting silanol

groups, ($\equiv$ SiOH), can be represented by the following reaction:

$$\equiv \text{SiOEt} + \text{H}_2\text{O} \rightarrow \equiv \text{SiOH} + \text{EtOH (Hydrolysis)} \qquad (7.1)$$

$$2 \equiv \text{SiOH} \rightarrow \equiv \text{Si-O-Si} \equiv + \text{H}_2\text{O (Condensation)} \qquad (7.2)$$
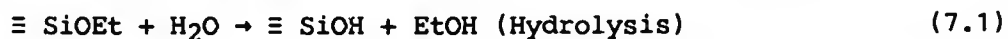
The rates of hydrolysis and condensation reactions are important in

determining the final form of the silica. If the above reaction is

carried out at low pH (acid catalyst) then, silica gel is obtained

(Keefer 84). In basic solution, the hydrolysis reaction proceeds by

nucleophilic substitution, i.e., negatively charged hydroxide ion attacks

the positively charged silicon atom (Keefer 84). In this reaction, TEOS

is hydrolysed at a slower rate to form monomeric hydrolysis product, OH-

$Si(OC_2H_5)_3$, and subsequent hydrolysis reaction proceeds at a faster rate to produce orthosilicic acid, $Si(OH)_4$. Subsequent condensation and cross-linking of orthosilicic acid polymers gives silica particles of which the interior consists essentially of silicon and oxygen atoms with hydroxyl groups attached to silicon only around the outside.

In the Stober method, ammonia acts as a catalyst for hydrolysis reaction and as a morphological modifier to make particles spherical (Stober 68). The final particle size depends mainly on the initial water and ammonia concentration, the particular silicon alkoxide (methyl, ethyl, pentyl esters, etc.) and alcohol (methyl, ethyl, butyl, pentyl alcohol, etc.) mixture that is used (Stober 68), and the temperature of the reactants (Tan et al. 87). To obtain monosized colloidal dispersions, nucleation and growth processes should be separated in time (Overbeek 82b, Sugimoto 87). In this method, all nucleation takes place in a very short period and additional material is supplied in such a way to growing nuclei that no supersaturation, and hence, no further nucleation takes place. Sometimes, early nucleation can be replaced by addition of seed material. Overbeek has shown that, if the nucleation takes place in a very short time, then, the growth process will decrease the relative width of the particle size distribution (compared to the relative width of the nuclei size distribution) or at worst will remain constant (Overbeek 82b). This controlled nucleation and growth technique has been applied for synthesizing monodispersed oxide powders besides silica, such as $Cr(OH)_3$ (Demchak and Matijevic 69), $AlOOH$ (Brace and Matijevic 73), and TiO_2 (Matijevic et al. 77). Silica powder used in this investigation was prepared as follows:

(i) <u>Materials</u>: Analytical grade chemicals were used. For initial silica batches, ethyl alcohol* was distilled. Tetraethylorthosilicate**, TEOS, was distilled under vacuum at approximately 55°C (lower than its boiling point at one atmosphere pressure 88°C). Concentrated ammonia solution*** with approximately 30 wt.% ammonia, (NH_3) was used as-received. From the trial experiments, it was found that the distillation of ethyl alcohol and TEOS is not necessary to obtain spherical powder, hence, distillation procedures were discontinued (but distillation of TEOS may have an effect on the average silica size obtained at the particular concentrations of TEOS, alcohol, and ammonia).

(ii) <u>Cleaning</u>: All glassware was first cleaned with soap solution. Then rinsed thoroughly with tap water. Then, it was cleaned with two percent hydrogen fluoride, HF, solution and then rinsed with distilled water. All glassware was rinsed with ethyl alcohol just before use. Since controlled nucleation produces monosized silica particles, thorough cleaning of the glassware is essential.

(iii) <u>Mixing</u>: An appropriate volume of alcohol was measured using a two liter measuring cylinder and added to a six-liter flask. Then, concentrated ammonia solution was added to the alcohol under the hood, and the mixture was stirred for approximately five minutes. TEOS was then added to the alcohol-ammonia mixture, and then, the flask was covered with a wax film.**** After an (invisible) hydrolysis reaction in

---

*Fisher Scientific Co., Fairlawn, NJ.

**Fisher Scientific Co.

***Fisher Scientific Co.

****Fisher Scientific Co.

which silicic acid is formed, the condensation reaction of the
supersaturated silicic acid was indicated by the increase in the
opalescence of the mixture starting approximately two minutes after the
addition of TEOS. The time at which opalescence first appears is related
to the final particle size. Generally, for the smaller sizes, the time
is longer. Stober has indicated that the above reaction is completed in
approximately fifteen minutes. To assure that the reaction was complete,
the mixture was kept stirring for at least one hour after the
precipitation of silica particles. Most of the silica powder used in
this was study was prepared using the following concentrations of the
chemicals:

TEOS: .063 liter TEOS/liter alcohol corresponding to .28 moles
TEOS/liter alcohol. (TEOS molecular weight: 208.34 and density at room
temperature: .9358 g/cm^3).

Ammonia: 0.189 liter concentrated ammonia/liter alcohol corresponding to
approximately 3 moles NH_3/liter alcohol and 6.5 moles H_2O/liter alcohol.
(Density of the 30 wt.% ammonium hydroxide solution is .89 grams/cm^3.)

Typically, four liters of alcohol was used per silica batch giving
approximately sixty grams of powder. After one hour, the silica powder
was separated using a teflon-coated filtration apparatus.* Millipore
GVHP filter paper* with .22 micron pore size was used. To increase the
filtration rate, the pressure was applied using compressed commercial
nitrogen gas. The filter cake was dried under the hood at room
temperature.

---

*Millipore Corp., Bedford, MA.

Silica Washing Procedures

Room temperature dried silica cake was ground using morter and pestle. To remove adsorbed ammonia and alcohol, silica powder was calcinated at 90°C for $\approx$ 24 hours. To remove soluble impurities and to remove remaining ammonia, silica was washed with deionized water[*] as follows.

An approximately five volume percent silica dispersion using deionized water was prepared. To facilitate dispersion, samples were sonicated[**] for at least 15 minutes. The dispersion was filtered using filtration apparatus and 0.22 μm filter paper. Fresh deionized water was added to the filtration apparatus and filtration was continued. The electrical conductivity of the filtrate was measured using a conductivity meter[***] (The measured conductivity gives a rough estimate of the concentration of the soluble impurities in water; higher conductivity corresponds to higher concentration of soluble impurities). When the conductivity of the filtrate was smaller than twice the conductivity of the fresh deionized water, filtration was discontinued. (Typically, conductivity values in the range of 0.5×10^{-6} - 1×10^{-6} 1/ohm cm were measured for the deionized water. Filtration was discontinued when the filtrate conductivity was $< 1.5 \times 10^{-6}$ 1/ohm cm. For comparison, the conductivity of a 1×10^{-2} M KCl solution at 25°C is 1.41×10^{-3} 1/ohm cm.) The above washing procedure is satisfactory since the ionic strength was kept constant at 1×10^{-2} moles/liter NaCl for most of the

---

[*]Continental water supply.

[**]Model W-375, Heat Systems, Ultrasonics, NJ.

[***]Model-70 CB, The Barnstead Company, Boston, MA.

dispersions prepared in this study. The filter cake was dried in the oven at 60°C and then it was crushed, and the powder was stored in plastic bottles.

Silica Calcination Treatment

To investigate the effect of silica-surface properties on the polymer adsorption (and hence, on the stability of dispersions), silica powders were calcined at various temperatures. Ground silica powder was calcined in a high purity (> 99%) dense alumina crucible[*] at the desired temperature for six hours. The sample was heated to calcination temperature in three hours and was cooled in three hours (i.e., total cycle time is three hours of heating, six hours of calcination, and three hours cooling, totalling twelve hours). Powder was loosely packed to avoid aggregate formation during the calcination treatment. After the calcination treatment was over, powder was transferred (while it was warm $\approx$ 50°C) to a cleaned and dried polypropylene bottle, and the cap was sealed using electrical tape.

Effect of Calcination Treatment on the Nature of the Silica Surface

Surface of the precipitated (and calcined at temperatures < 100°C) silica powder is covered with the densely packed surface hydroxyl groups called surface silanol groups, $\equiv$ Si-OH, and physically adsorbed water. Physically adsorbed water can be removed by degassing silica under vacuum at room temperature (Hair 67). At high temperatures, two adjacent

---

[*]Coors, alumina crucible.

silanol groups undergo a reversible condensation reaction to form a siloxane bond, $\equiv$ Si-O-Si $\equiv$, with evolution of water:

$$2 \equiv \text{SiOH} \rightarrow \equiv \text{Si-O-Si} \equiv + \text{H}_2\text{O} \qquad (7.3)$$

This reaction is completely "reversible" up to 400°C (Hair 67). Hence, a heat treatment of silica reduces the concentration of the surface hydroxyl groups. There are essentially two types of silanol groups present on the silica surface (i) 'Free' (or isolated) silanol groups which do not interact with other OH groups and (ii) 'bound' silanols which are close enough to other OH groups to form hydrogen bonds. The various types of surface groups present are shown in Figure 7.1. Heating silica above 400°C causes drastic irreversible elimination of bound hydroxyl groups, and at temperatures around 800°C, only isolated silanol groups remain on the silica surface (Hair 67). In the infrared spectrum, these two types of silanol groups appear as quite different species. Figure 7.2 shows the diffuse reflectance Fourier transform infrared (FTIR)* spectra of silica powders calcined at various temperatures (Sacks et al. 87). The uncalcined and 200°C calcined powders are extensively hydroxylated (and also have physically adsorbed water). The broad asymmetric absorption bond observed in the range $\approx$ 3000 to 3600 cm^{-1} in these materials is associated with OH stretching vibrations in hydrogen-bonded molecular water and to silanol groups bonded to molecular water (Hair and Hertl 69, Kiselev and Lygin 75). The broad absorption around $\approx$ 3660-3680 cm^{-1} is associated with weakly hydrogen bonded SiOH groups and adsorbed water molecules. A strong absorption peak develops at $\approx$ 3750 cm^{-1} for silica calcined at

---

*Model MX-1, Nicolet Analytical Co., Madison, WI.

SILOXANE
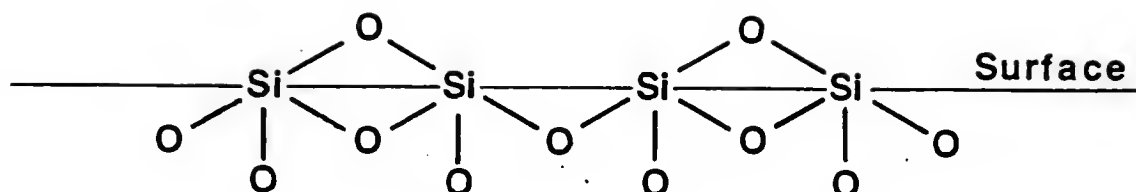
Surface

ISOLATED HYDROXYL GROUP
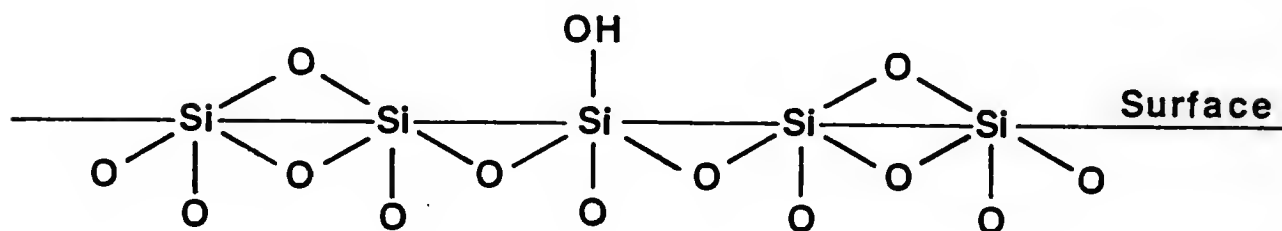
Surface

HYDROGEN BONDED HYDROXYL GROUP
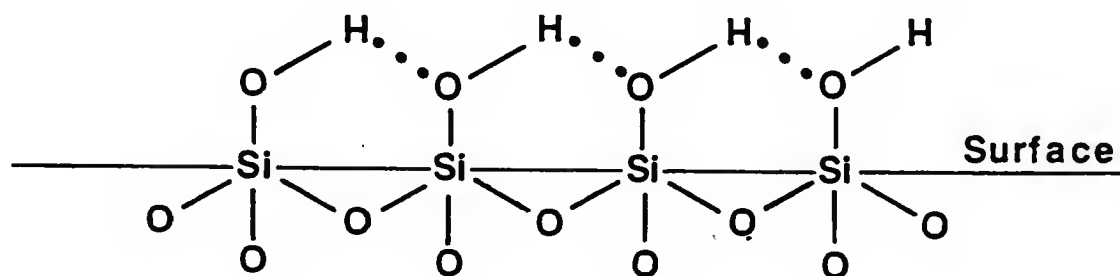
Surface

Figure 7.1   Schematic representation of various types of surface groups present on the silica surface.
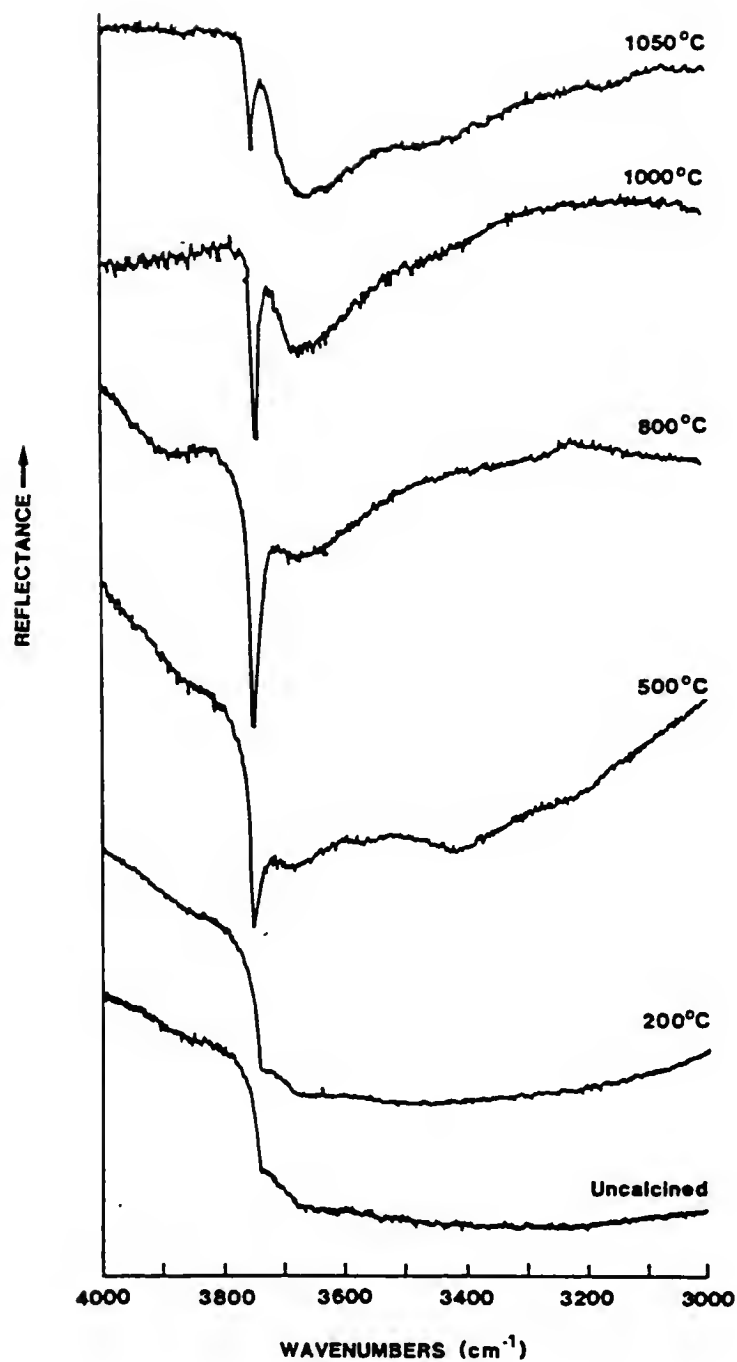
Figure 7.2   The diffuse reflectance Fourier transform infrared
              spectra of silica powders calcined at various
              temperatures (Sacks et al., 1987).

temperatures above 500°C. This peak has been associated with free
(isolated) SiOH groups on silica (Kiselev and Lygin 75). The
concentration of surface hydroxyl groups as a function of calcination
temperature has been studied by many investigators using techniques, such
as chemical and isotropic substitution, spectral methods, etc. (Hertl and
Hair 68). Figure 7.3 shows the compilation of results by Kiselev. From
the figures, it is clear that the hydroxyl group density decreases from
about 4.6 nm^{-2} at 180°C to values as low as 0.5 nm^{-2} at 900°C. The
importance of isolated silanol groups in polymer adsorption behavior has
been studied by various investigators (e.g., see Rubio and Kitchner 76,
Tadros 78). Although the heat treatment reduces the total concentration
of the surface silanol groups, the concentration of isolated silanol
groups is maximum in a certain range of calcination temperatures (usually
700-800°C) (see Figure 7.2). The effect of increasing the concentration
of isolated silanol groups on the polymer adsorption densities will be
discussed in detail later. However, it can be stated that the maximum
amount of adsorbed polymer on silica occurs after calcination at $\approx$ 700°C.
This result is consistent with observations by other investigators (Rubio
and Kitchner 76, Tadros 78, Moudgil and Cheng 86). The effect of surface
hydroxylation on dispersion stability will be described in the next
chapter. It is important to note that the silica surface is
heterogeneous with respect to adsorption and the degree of heterogeneity
depends on the calcination treatment. In the case of uncalcined silica
(i.e., the surface is well-covered with hydroxyl groups), hydrogen
bonding between surface hydroxyl groups and OH groups of poly (vinyl
alcohol), PVA, will be an important adsorption mechanism. For silica
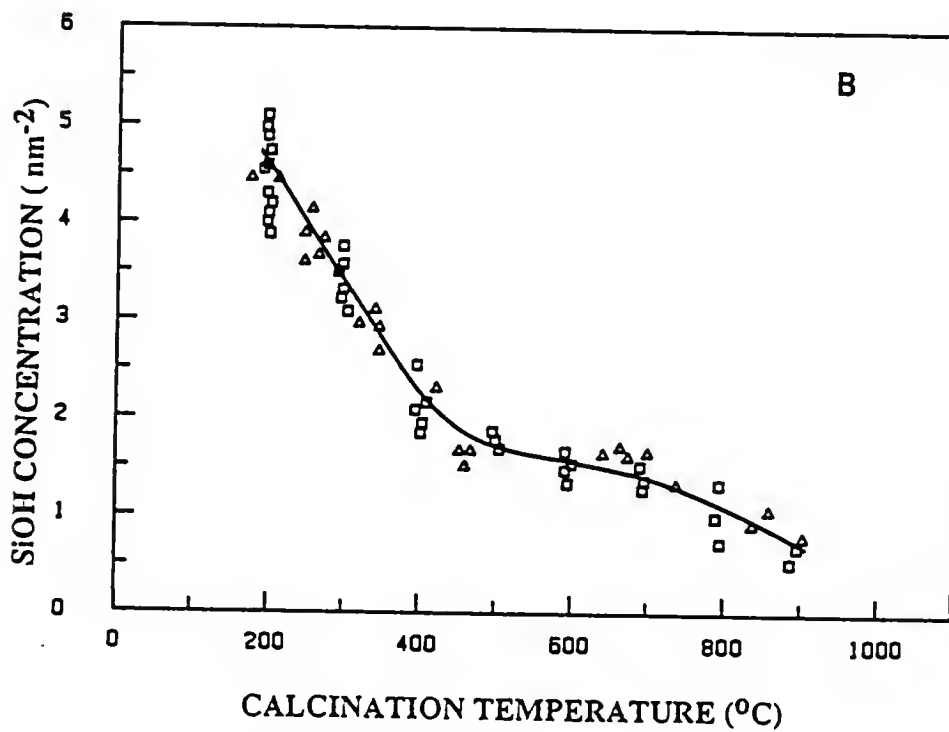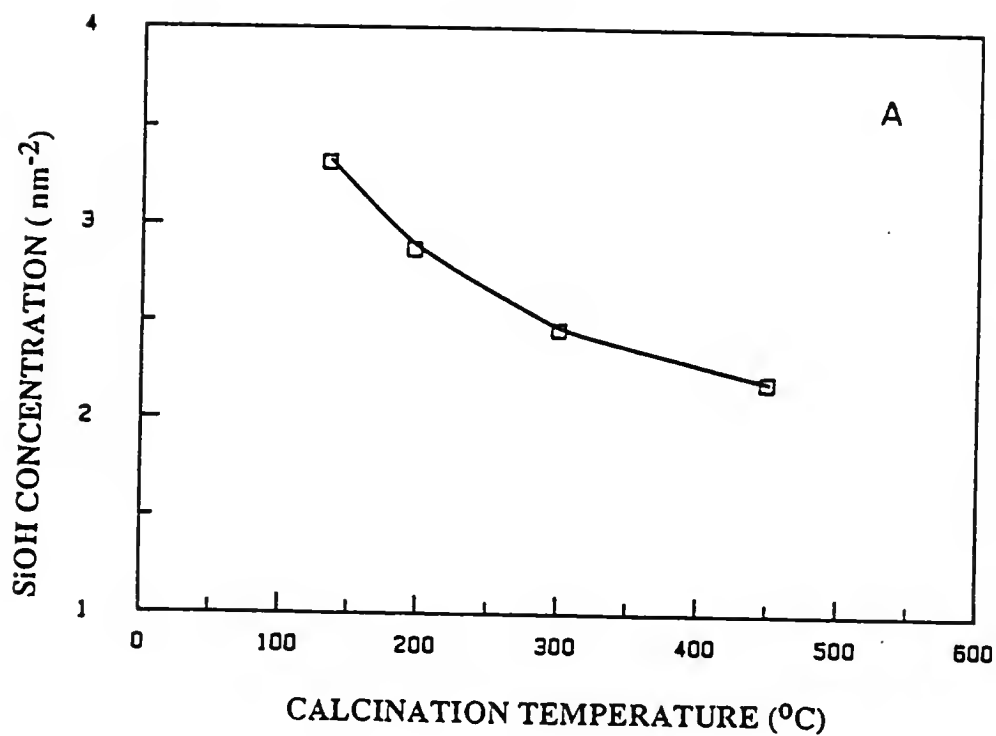
Figure 7.3   Concentration of surface silanol groups as a function of
the temperature of calcination ((a) Bode et al., 1967 and
(b) Kiselev, 1975).

calcined at higher temperature (i.e., for example, 700°C silica), the surface will be largely hydrophobic so that adsorption by means of hydrophobic bonding is also likely to occur. (At high temperature, hydrogen bonding between isolated silanol groups and -OH groups of PVA is still likely to be an important mechanism). The increase in the adsorption density of partially hydrolysed (88%) PVA has been associated with hydrophobic bonding between acetate groups and hydrophobic surface sites (Cohen Stuart 80a, Tadros 78). The silica surface can be made hydrophobic by chemically grafting polymers on to the silica surface by in-situ polymerization and stable non-aqueous silica dispersions can be prepared (Laible and Hamann 80). Since only aqueous silica dispersions were prepared in this study, we will not further discuss other techniques of rendering the silica surface hydrophobic.

Silica Size and Size Distribution

The average size and size distribution of the silica particles were determined using two techniques: (i) scanning electron microscopy, SEM, and (ii) x-ray sedimentation. Samples for SEM examination were prepared as follows.

A dilute dispersion (approximately 300 ppm silica) of silica in ethyl alcohol was prepared by ultrasonication treatment for fifteen minutes. A drop of this dispersion was placed on polished and cleaned (with alcohol) aluminum sample holder and was carefully dried. (To avoid dust pick up, a plastic cup was placed on sample holders, or alternatively, a glass slide cleaned with a Chormic Sulfuric acid cleaning solution was also used). All samples were sputter coated with

thin layers of gold (≈ 100 °A) to avoid charging of the sample during SEM examination. Several photomicrographs were analyzed for each silica batch to determine particle size and size distribution. Particle diameter was measured using a digitizing tablet* and a specially developed computer program. Figure 7.4 shows a SEM photomicrograph of silica particles used in this investigation. Spherical shape and narrow size distribution is quite evident from the photomicrograph. Since the particle size distribution exhibited nearly log-normal distribution characteristics, the geometric mean and standard deviation were used to characterize a silica batch. For perfectly monosized particles, the geometric standard deviation would be 1. For the silica batches in this study, the geometric standard deviation was ≈ 1.1 or less. Typically, two hundred particles were analyzed to obtain average size. (It was found that the difference in the mean between 50 and 1000 particles was statistically insignificant). To represent the particle size distribution, a histogram (number of particles in a given diameter class versus particle diameter) can be constructed. A typical histogram with a geometric mean ≈ 0.42 μm and geometric standard deviation, ln σ_g, = 1.1 is shown in Figure 7.5.

Median diameter and particle size distribution information was also obtained from the x-ray sedigraph. A plot of cumulative mass percent versus equivalent spherical diameter is shown in Figure 7.6. Samples for x-ray sedigraph was prepared as follows.

Silica powder was ground using a mortar and pestle. An approximately three volume percent silica dispersion at pH ≈ 7.5 was

---

*Model 9111A, Hewlett Packard, CA.
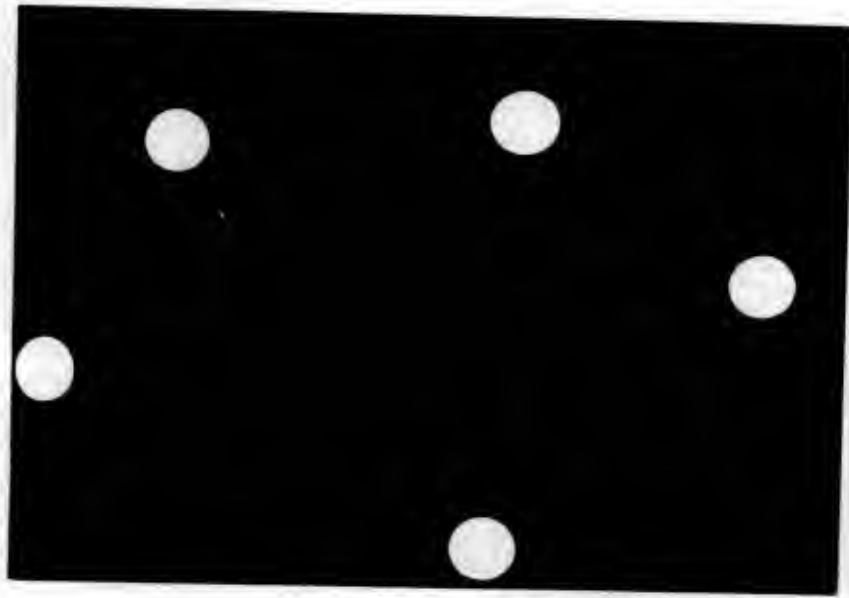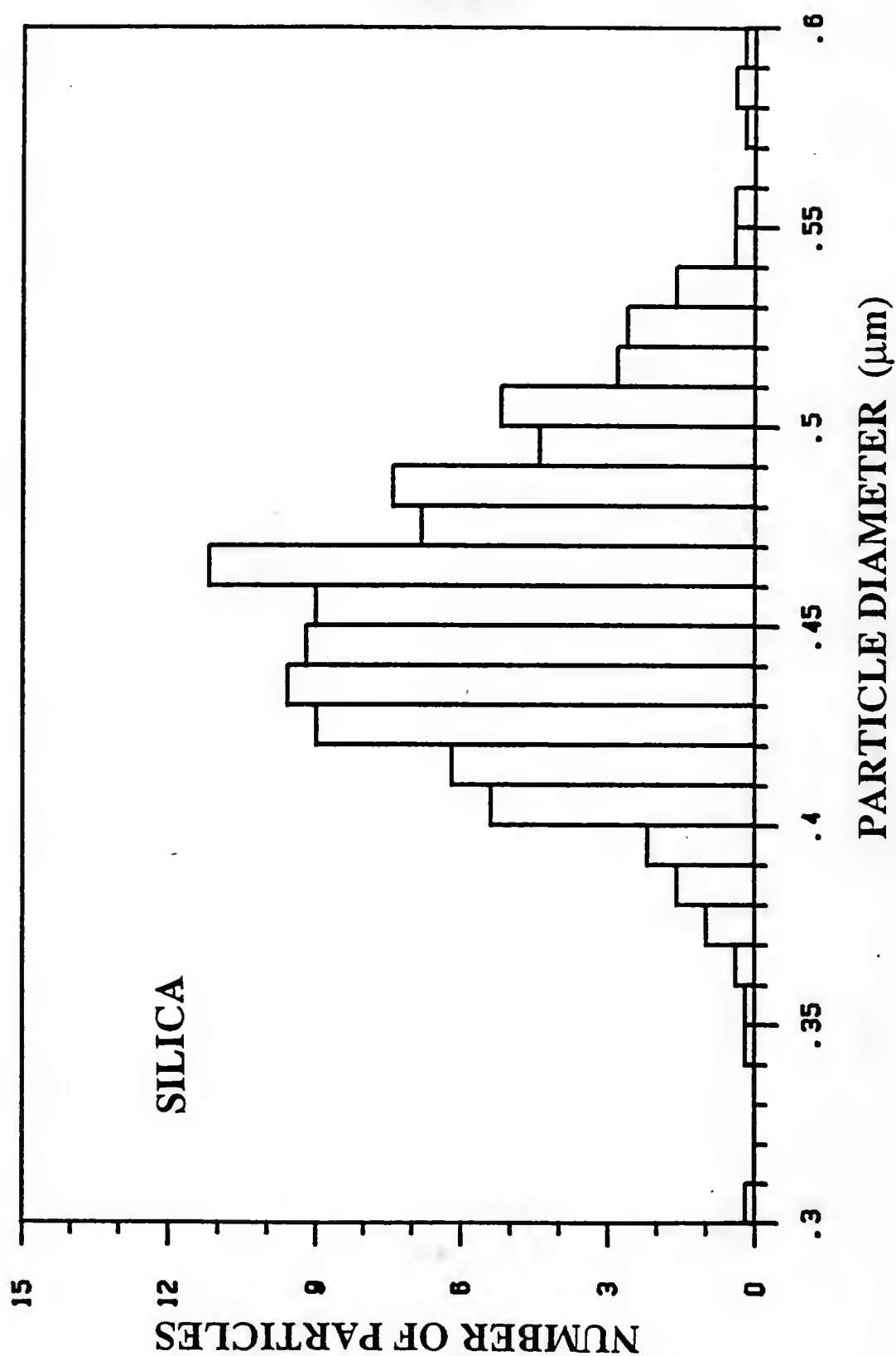
Figure 7.5   A histogram (number of particles in a given diameter class versus particle diameter) of a typical silica batch.
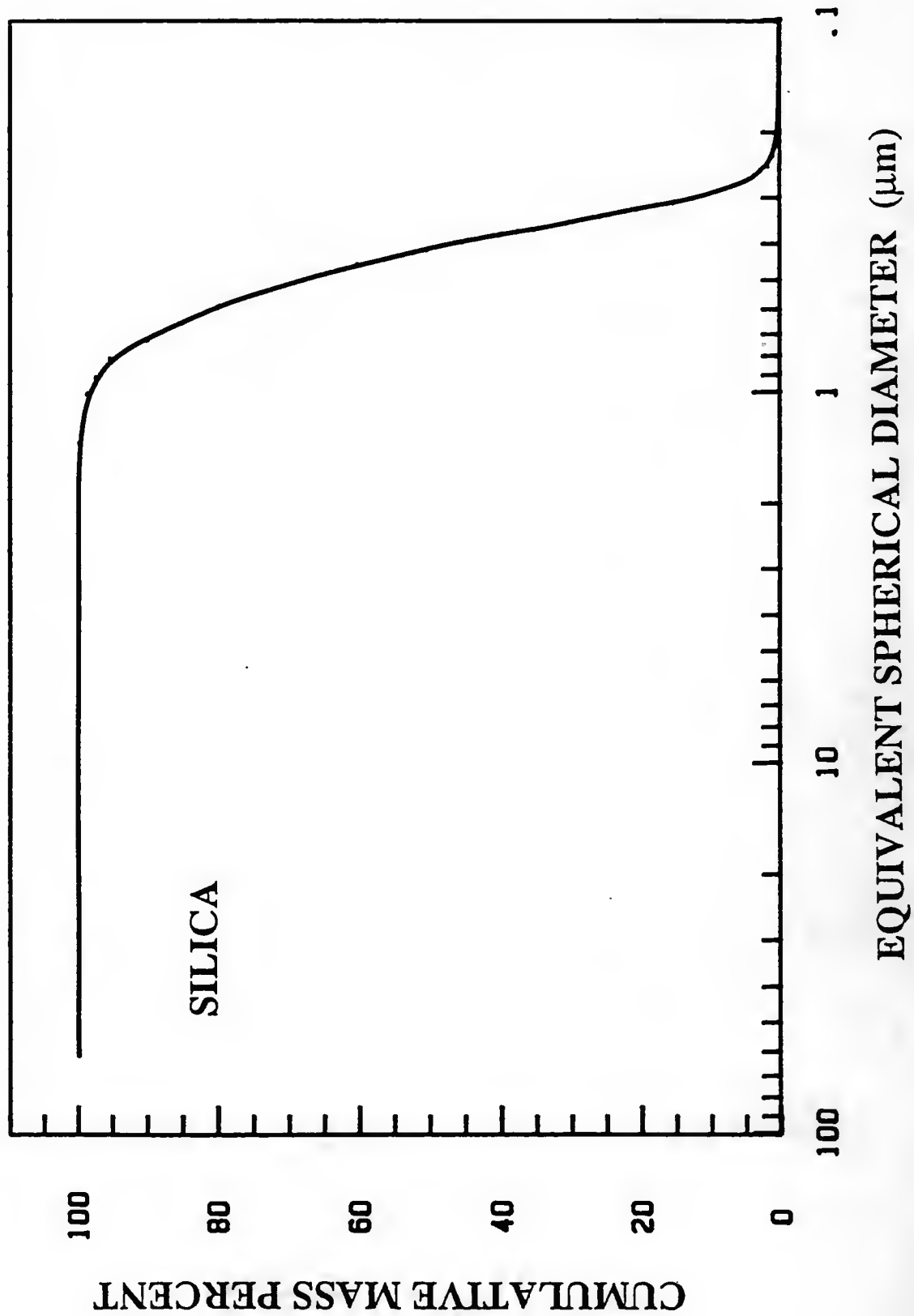
Figure 7.6   Plot of particle size distribution for silica determined by x-ray sedimentation.

prepared (to ensure electrostatic stabilization) and ultrasonicated for $\approx$ two hours to breakdown agglomerates. The x-ray sedigraph result shows (Figure 7.6) a small fraction of larger particles in the suspension (i.e., > 0.8 μm), compared to the SEM results. This may reflect the formation of temporary doublets, triplets (or higher order clusters), etc. during Brownian collisions at the relatively high ($\approx$ 3 vol. %) solid concentration and/or may indicate the presence of a small concentration of hard agglomerates that formed during processing (e.g., drying, pre-calcination treatment, etc.).

Silica Surface Area

The powder specific surface area (m^2/gram) was measured using nitrogen gas adsorption using the multipoint BET method[*]. Uncalcined powders were outgassed at temperatures $\approx$ 80°C (i.e., below the drying temperature of 90°C) under flowing nitrogen, and calcined samples were outgassed at the temperatures in the range 150 to 200°C for at least three hours. Surface area measurements were repeated at least two times, and the average surface area of a given silica lot was used to report the adsorbed amount of polymer in the units of mg polymer adsorbed/m^2 solid surface. Typical results for various silica lots are shown in Table 7.1. No significant change in the measured surface area with the calcination temperature was found by Sacks and Tseng indicating an absence of micropore formation during the dehydroxylation treatment (Sacks and Tseng 84). Also, close agreement was found between surface area calculated (Sp) from the average particle radius a, and the powder true density, ρ

---

[*]Model OS-7, Quantachrome Corp., Syosett, NY.

TABLE 7.1

Geometric Mean and Specific Surface Area of Various Silica Lots Used

Silica Lot #	Calcination Temperature (°C)	Geometric Mean from SEM (μm)	BET Surface Area (m^2/gram)	Calculated Surface Area (m^2/gram)
1	700	0.70	5.16	4.08
2	"	0.42	8.34	6.80
3	"	0.42	8.00	6.72
4	"	0.43	7.90	6.64
5	"	0.44	8.00	6.50
6	50	0.45	8.07	6.36
7	700	0.45	8.03	6.36
8	850	0.45	7.51	6.36

(i.e., Sp = 3/ρ.a) and the measured value obtained from BET. Van Helden et al. reported that uncalcined powder (dried at 25°C) is highly porous to nitrogen, i.e., it has a high surface area compared to powder heated to 90°C (Van Helden et al. 81). In both cases, area determined with OH⁻ ions was the same. Vrij et al. suggested that, upon heating the diameter of the surface micropores decrease and become impermeable to nitrogen. In summary, the powder used in this investigation (heated at temperatures > 90°C) has no significant amount of surface porosity.

Silica True Density

Powder true density of Stober silica has been measured using helium gas pycnometry[*]. The increase in the true density with calcination temperature is shown in Figure 7.7 (Sacks and Tseng 84). True density increases as water and ethoxy groups are removed during low temperature calcination. Density values for powders calcined at temperatures above 800°C (Figure 7.7) are slightly higher than the usual reported value for fused silica, 2.20 g/cm^3. The reasons for this observation is not yet clear (Sacks and Tseng 84). Thermogravimetric results show that ≈ 12 wt.% loss occurs on heating uncalcined silica samples (Sacks and Tseng 84). The endothermic peak (centered at ≈ 160°C) observed in Differential Thermal Analysis, DTA, shows that much of the bound water is removed at temperatures below 200°C.

---

[*]Model PY-5, Quantachrome Corp., Syosett, NY.
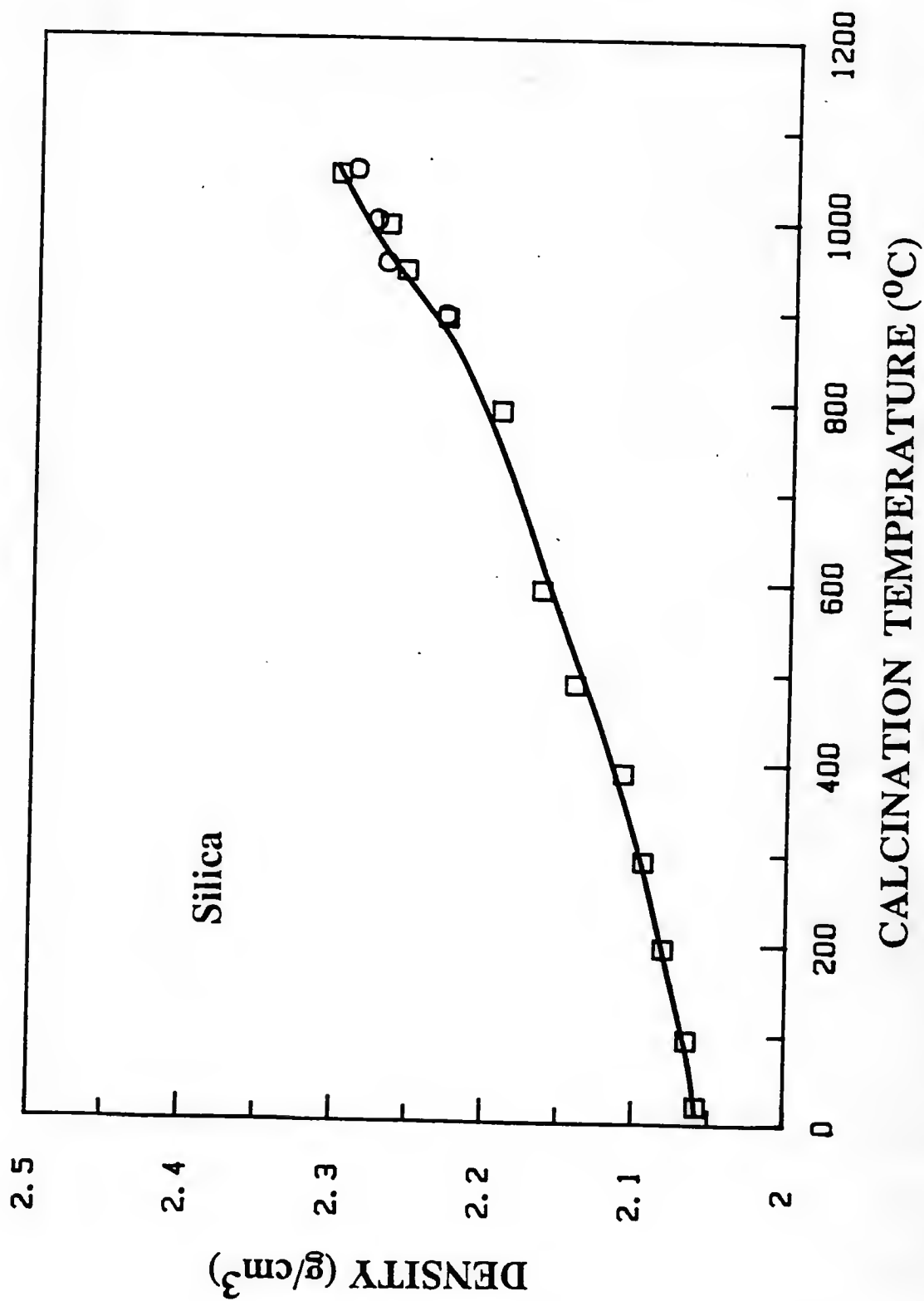
Figure 7.7 Gas pycnometer density versus calcination temperature for SiO_2 powders (Sacks and Tseng, 1984).

Poly (Vinyl) Alcohol

Synthesis and Properties

Poly (vinyl alcohol), PVA, is a water soluble polymer with simple chemical structure. The basic unit is $-(CH_2-CHOH)-$. Vinyl acetate is polymerized to form poly vinyl acetate, PVA_c, and the subsequent hydrolysis reaction forms PVA. In industrial practice, complete hydrolysis is seldom achieved, and the catalyst used determines the residual acetate distribution. An alkaline catalyst favors 'blocky' distribution whereas acidic promotes random distribution of acetate groups, (CH_3COO-) (Pritchard 70). The majority of samples used in this study were supplied by Air Products and Chemicals*. The following physical properties of PVA are important for adsorption studies.

Solubility, Solution Behavior and Interfacial Activity

These properties are dependent not only on the primary chemical structure of the molecules, but secondary effects, such as branching, end groups, irregularity in chain, stereoregularity, residual acetate content, distribution of acetate groups, and molecular weight of the polymer.

PVA is essentially an uncharged polymer. Structural impurities, such as carboxyl and sulphate groups, will result in a charged polymer (Pritchard 70, Koopal 78). Fleer has shown from electrophoresis and intrinsic viscosity measurements at various ionic strengths that PVA is an uncharged polymer (Fleer 71). PVAc is often a branched polymer, but most side chains may split off during saponification, and thus, the resulting PVA has little branching or is an unbranched polymer (Pritchard

_____

*Air Products and Chemicals, Inc., Allentown, PA.

70). Stereoregularity of the polymer affects properties such as crystallinity and solubility. Industrial samples are usually atactic and tacticity of a polymer is not an important factor in adsorption studies (Koopal 78).

The rate of dissolution and the solubility of PVA strongly depends upon the degree of hydrolysis. PVA containing approximately twelve percent acetate groups easily dissolves in cold water. More highly hydrolysed PVA ($< \approx 2\%$ acetate) dissolves quickly only at elevated temperature (e.g., $\approx 80°C$) and has a tendency to age and form aggregates at room temperature. The main reason for this phenomenon is the intra- and intermolecular hydrogen bonding between the hydroxyl groups which decreases the dissolution rate and the solubility. Residual acetate groups are hydrophobic in nature and prevent hydrogen bonding of hydroxyl groups and improve the solubility characteristics. To break the internal hydrogen bonds and to dissolve the PVA, a temperature above glass transition point ($\approx 75°C$) is required. The following procedure was used to prepare polymer solutions with known concentration.

To prepare 100 ml of polymer solution of known concentration, PVA was weighed using an analytical balance and polymer was added to a beaker with ≈ 75 cm^3 of deionized water (water was stirred using magnetic stirrer). PVA powder was slowly added to the vortex to avoid formation of lumps. Stirring was continued until the polymer particles were wetted. Then, the solution was heated for approximately thirty minutes at $\approx 85°C$ using a double walled jacket apparatus and a temperature controlled circulator. The solution was cooled to room temperature and

was transferred to a 100 ml volumetric flask. The beaker was thoroughly rinsed with deionized water and the solution was transferred to a 100 ml volumetric flask. Deionized water was then added to make 100 ml of polymer solution of known concentration. At room temperature, solutions prepared within completely hydrolysed PVA (> 2% acetate) are reasonably stable (Gruber et al. 74). Also, polymer concentrations used were relatively low (usually, at most, 3 g PVA/100 cc). Hence, polymer solutions with higher acetate content (> 10%) were used for up to three days before being discarded. Solution of PVA, hydrolysed > 98%, were discarded after twenty-four hours.

Fractionation of As-received PVA

As-received polymer samples were fractionated using a sequential precipitation technique to remove high and low molecular weight impurities (van den Boomgaard et al. 78). To obtain polymer samples with varying molecular weights and acetate contents, various commercial samples were fractionated. Preparative scale Gel Permeation Chromatography, GPC, has been used by Garvey et al. to obtain various molecular weight samples with narrow molecular weight distribution (Garvey et al. 74). But, the above method is not practical for our study since larger quantities of samples are necessary to study suspension properties. (Preparative scale GPC gives few mg of samples while approximately ten grams of PVA samples were used to study various aspects of dispersion stability.) The following procedure was followed to fractionate samples.

One liter of polymer solution with ≈ 5 w/v % PVA was prepared following the procedure described before (i.e., initially wetting the polymer beads while stirring, and then, heating the solution to ≈ 85°C for thirty minutes). The polymer solution was cooled to room temperature, and then, acetone was added to this polymer solution while stirring. When the solution became turbid, some more acetone was added (≈ 100 cc) in order to produce a sufficient amount of gel phase. The solution was stirred for one more hour and was left to sediment for three to four days. The precipitated polymer forms a strong gel-sediment at the bottom of the container. The top solution was transferred to another container, and more acetone was added to precipitate the next fraction. Each polymer was separated into four to five fractions. Each fraction was washed with excess acetone and dissolved in water and kept in an oven at ≈ 40°C for one day to remove the last traces of acetone. Then, films were cast from this viscous solution and dried at ≈ 60°C for two days. These films were stored in a plastic bottle and were useful for accurately weighing the required amount of polymer. These samples were then characterized for acetate content and molecular weight as follows.

Acetate Content of Polymer

The acetate content of the fractions was determined by a saponification technique (Garvey et al. 74, Pritchard 70). Approximately 0.13 grams of polymer was refluxed for 1/2 hour with 20 ml of 0.1 N NaOH solution. The unreacted amount of NaOH was determined by titration with 0.1N HCl using a phenol red indicator. From the amount of NaOH consumed, the acetate content was calculated using the following formula:

$$\text{Mol \% hydrolysed} = \frac{(w - 86 \times 10^{-4} \, y)}{(w - 42 \times 10^{-4} \, y)} \times 100 \qquad (7.4)$$

where w is the weight of the sample and y is the ml of 0.1 N NaOH consumed. Since the end point of the titration can be determined accurately within ± 0.1 ml, the acetate content can be determined within ± 1% of the true value. The results of polymer characterization are reported in Table 7.2.

Molecular Weight and Molecular Weight Distribution

Polymer samples were characterized for their molecular weight and molecular weight distribution using viscometry and Gel Permeation Chromatography, GPC.

Viscometry

Viscosity measurements were carried out at 30 ± .05°C using an Ubbelohde suspended level dilution viscometer. Polymer solutions were prepared following the procedure described earlier. The polymer concentration was typically ≈ 0.6 g PVA/dL. Samples were filtered using glass fiber filter paper. Special attention was paid to good temperature control, vertical alignment of the viscometer, filling of the viscometer, and cleanliness. After the experiment, the viscometer was thoroughly rinsed with deionized water using a peristaltic pump. Then, it was rinsed with filtered methanol and dried at 40°C. Ten ml of sample was introduced and flow time was measured using a stop watch. Three consecutive readings within ± .01 sec were used for calculations. Then,

three ml of deionized water was added and the sample was mixed and equilibrated for fifteen minutes. The above procedure was continued until four readings were recorded. The flow time for deionized water was periodically checked to ensure consistency. The flow time for water was about 159 seconds. Intrinsic viscosities, $[\eta]$, for each PVA sample were determined using the equation of Huggins:

$$\frac{\eta_{rel}}{C_p} = [\eta]_H + k'_H [\eta]_H^2 C_p \tag{7.5}$$

and Martin:

$$\ln \frac{\eta_{rel}}{C_p} = \ln [\eta]_M + k'_M [\eta]_M C_p \tag{7.6}$$

where η_{rel} is the viscosity excess ratio and $\eta_{rel} = (t - t_o)/t_o$ where t is the flow time for the polymer solution with concentration, C_p, and t_o is the flow time for water. k'_H and k'_M are the Huggins and Martin constants. Since water is only a poor solvent for PVA, $[\eta]_M$ was used to calculate the viscometric average molecular weight, M_υ (Koopal 78). (In good solvents, the arithmetic average of $[\eta]_M$ and $[\eta]_H$ gives best an estimate of $[\eta]$.) The intrinsic viscosities from Huggins or Martin plot for the same polymer differed by approximately six percent or less, with $[\eta]_M > [\eta]_H$.

From intrinsic viscosities, M_υ can be calculated with the Mark-Houwink-Sakurada (MHS) equation:

$$[\eta] = K M_\upsilon^a \tag{7.7}$$

if the constant K and a are known. The values of the constants depend on the nature of the polymer and solvent and on the temperature. Generally, a is a measure of polymer solvent interaction, and for a linear flexible

TABLE 7.2

Viscometric Molecular Weight and Acetate Content of PVA Fractions

| Sample | | Viscometry | | % Hydrolysed | Fractionation |
		$[\eta]$ dL g^{-1}	M_υ x 10^3 (g/mole)		% Acetone
PVA 203*	Unfrac- tioned	0.260	21	88	--
	F1	0.348	33	90	62
	F2	0.280	23	86	69
	F3	0.173	11	84	76
PVA 540*	Unfrac- tioned	0.913	153	88	--
	F1	1.132	215	90	50
	F2	0.985	173	87	56
	F3	0.781	120	85	60
PVA 20/30+	Unfrac- tioned	0.402	42	86	--
	F1	0.497	58	90	60
	F2	0.407	42	87	68
	F3	0.330	31	80	75
SPP 88/96$	Unfrac- tioned	0.841	135	86	--
	F1	1.024	184	90	55
	F2	0.937	160	86	58
	F3	0.816	129	82	61
	F4	0.700	100	80	64

* Air Products, PA, + Monsanto, $ Scientific Polymer Products.

M_υ is the viscometric molecular weight calculated from Equation 7.9.

polymer, a = 0.5 for θ solvent and a = 0.8 - 1.0 for very good solvent. The value of K depends mainly on the nature of the polymer. For PVA water systems, various pairs of constants have been reported (Koopal 78). For fully hydrolysed samples, the following equation has been suggested by Pritchard (Pritchard 70):

$$[\eta] = 4.67 \times 10^{-5} \, M_\upsilon^{0.64} \, (dm^3 \, g^{-1}) \tag{7.8}$$

The above relation is given at 25°C, but the constants K and a are similar to that reported by Kurata at 30°C (with K in the range 4.28 - 6.66 x 10^{-4} and a = 0.64), and hence, the above equation was used at 30 °C (Kurata et al. 75). For partially hydrolysed PVA ($\approx$ 88%), Koopal has given the following equation (Koopal 78):

$$[\eta] = 4.97 \times 10^{-5} \, M_\upsilon^{0.63} \, (dm^3 \, g^{-1}) \tag{7.9}$$

Nagy has determined the number average, M_n, and the weight average, M_w, of the unfractioned PVA similar to samples used in this study using Gel Permeation Chromatography, GPC (Nagy 86). From the plot of M_w (as reported by Nagy) versus [η] (determined in this study), the following values for the constants were obtained: K = 4.06 x 10^{-5} and a = 0.65 (i.e., similar to the values reported above). Intrinsic viscosities and viscometric molecular weights calculated using Equation 7.9 are shown in Table 7.2 for unfractioned and fractioned PVA samples.

Gel Permeation Chromatography

To obtain information about the molecular weight distribution and as an additional independent measure of the molecular weights, a Gel Permeation Chromatography, GPC, study was made.

<u>Experimental Procedure:</u> The instrument used was an LKB Gel Permeation Chromatograph[*] equipped with a differential refractive index detector, fitted with a 200 μL sample loop. Two Toyo Soda TSK-PW 4000 columns[**] of thirty cm length each were used. PVA solutions were prepared following the procedure described above and filtered using glass fibre filter paper. The polymer solution concentration was ≈ 0.5 g PVA/dL. The mobile phase was a deionized water which was deareated using vacuum and purged with nitrogen gas to remove dissolved gases. The GPC flow rate was 1 ml/min.

The relation between the molecular weight and elution volume is needed to determine molecular weight, which can be done using well-defined narrow PVA fractions. However, such fractions were not available, and therefore, poly ethylene oxide, PEO, calibration standards were used.[***] (The characteristics of the PEO standards used are listed in the Table 7.3.) In this case, the extra relation between the molecular weights of PVA and PEO at the same elution volume has to be determined. The following procedure, commonly used to determine such a relation, was followed (Doi 75, Dawkins, 72).

It was assumed that polymer molecules with equal hydrodynamic volumes were eluted at the same elution volume, irrespective of their chemical nature. The hydrodynamic volumes V_H, were found from Einstein's law:

$$V_H/K_H = [\eta]_{cal} \, M_{cal} = [\eta]_x \, M_x \tag{7.10}$$

---

[*]LKB, Stockholm, London.

[**]Toyo Soda Manufacturing Co., Japan.

[***]Toyo Soda Manufacturing Co.

TABLE 7.3

Molecular Characteristics and Elution Volume of
PEO Calibration Standards

Type	$[\eta]^*$ dl/g	M_υ^* x 10^{-5}	M_w^* x 10^{-5}	GPC* M_w x 10^{-5}	GPC* M_w/M_n	Elution Volume (cm^3)	AR/HT
SE-2	0.352	0.18	0.20	0.17	1.10	17.18	1.73
SE-5	0.566	0.39	0.40	0.35	1.07	15.82	1.74
SE-8	0.975	0.86	0.88	0.80	1.02	14.31	1.78
SE-15	1.430	1.45	1.53	1.35	1.03	13.42	1.86
SE-30	2.150	2.52	2.77	2.59	1.04	12.51	1.75
SE-70	3.910	5.94	6.63	6.68	1.04	11.89	1.16

* PEO Calibration Standard Characteristic Data, Toyo Soda Manufacturing Co.

M_υ - viscometric molecular weight, $[\eta] = (3.97 \times 10^{-4})\ M_\upsilon^{0.686}$.

M_w - weight average molecular weight from light scattering.

M_n - number average molecular weight from GPC.

AR/HT - Area to height ratio of chromatograms determined in this study.

TABLE 7.4

Gel Permeation Chromatography Data for Unfractioned Polymer Samples
The Relation Between PVA Molecular Weight and Elution Volume was Determined Using PEO Calibration Standards
(Equation 7.14)

PVA Type	% Hydrolysed	Viscometry $M_\nu \times 10^{-3}$	GPC			
			$M_w \times 10^{-3}$	$M_n \times 10^{-3}$	M_w/M_n	AR/HT
PVA 540[+]	88	154	107	25	4.4	4.5
PVA 523[+]	88	143	94	21	4.5	4.5
PVA 205[+]	88	--	24	7	3.5	4.4
PVA 203[+]	88	21	10	4	2.9	4.0
PVA 20/30[*]	86	42	15	5	2.9	4.3
PVA 20/60[*]	86	--	43	9	4.8	5.2
SPP 75/3000[**]	75	3	3	8	3.6	3.7
Vinol 107[+]	99	38	32	5	6.8	4.4
Vinol 165[+]	99	--	167	24	6.8	4.2

+ Air Products Co., Pa.   * Monsanto Co.   ** Scientific Polymer Products.

where K_H is the hydrodynamic constant and M is the molecular weight. The subscripts "cal" and "x" refer to the calibration standard (PEO) and the unknown sample (PVA), respectively. The intrinsic viscosity, [η] is related to M through the MHS Equation 7.7. Inserting Equation 7.3 into Equation 7.10 with K_{cal} and a_{cal} as the MHS constants for the calibration standard and k_x and a_x for the unknown, we obtain:

$$\log M_x = \frac{a_{cal} + 1}{a_x + 1} \log M_{cal} + \frac{\log(K_{cal}/K_x)}{1 \quad a_x + 1} \tag{7.11}$$

For PEO standards, the following MHS constants were used (Toyo Soda specifications):

$$K_{cal} = 3.97 \times 10^{-5} \quad (dm^3 \ g^{-1}) \quad a_{cal} = 0.686$$

and the following values of MHS constants for partially hydrolysed PVA were used:

$$K_x = 4.97 \times 10^{-5} \quad (dm^3 \ g^{-1}) \quad a_x = 0.64$$

Substituting these values in the Equation 7.11, the following relation is obtained:

$$\log M_x = 1.028 \log M_{cal} - 0.06 \tag{7.12}$$

Using PEO calibration standards, the relation between the elution volume, V_e, and M_{cal} (molecular weight of the PEO calibration standards) was established (Figure 7.8). This can be represented by the following equation:

$$\log M_{cal} = -0.272 \ V_e + 8.90 \tag{7.13}$$

where V_e is the elution volume. Substituting Equation 7.13 into the Equation 7.12, the following relation between PVA molecular weight and
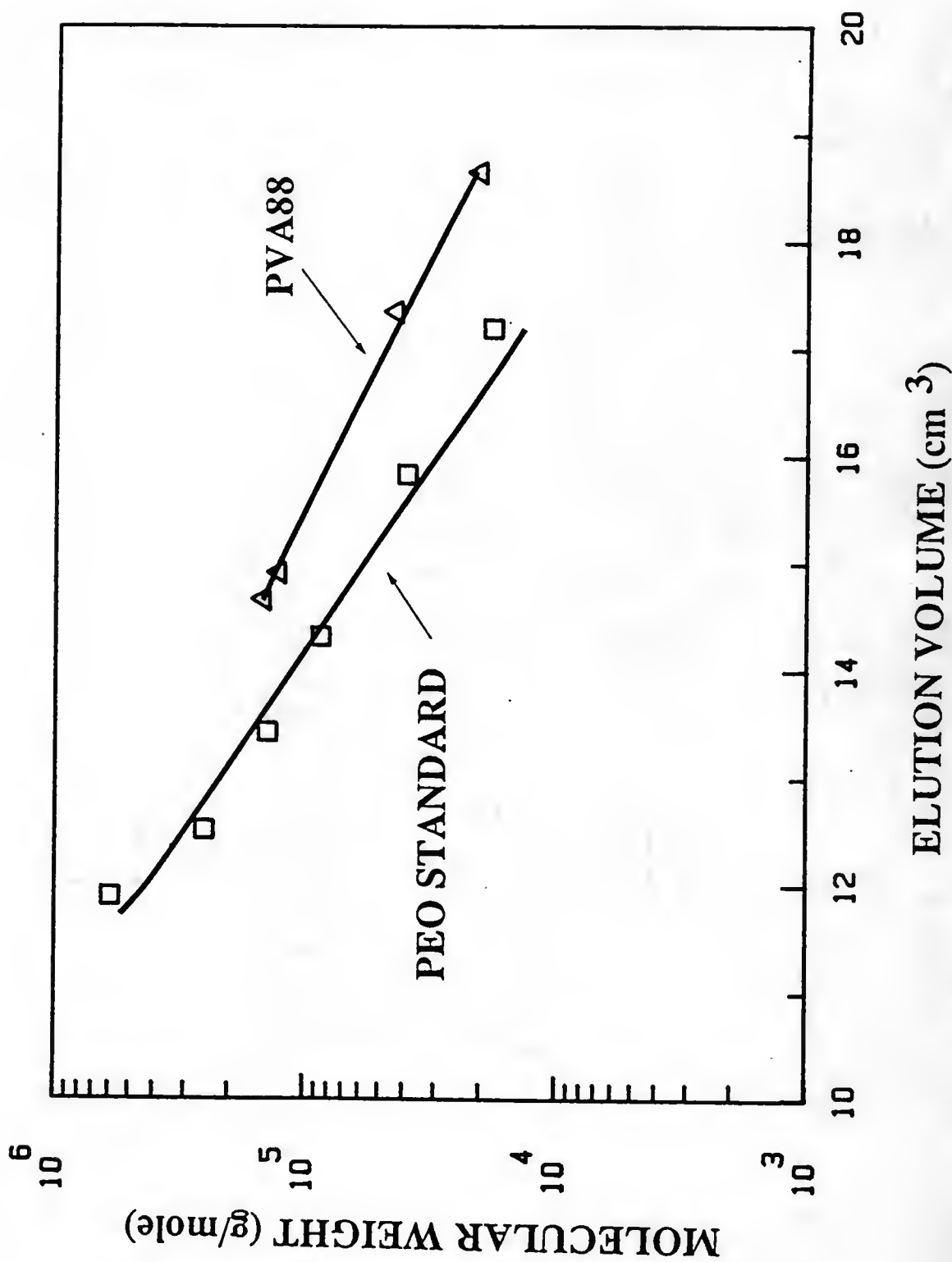
Figure 7.8 Molecular weight calibration curves for PEO standards and commercial PVA88. Log M is plotted as a function of elution volume.

the elution volume is obtained for our experimental conditions (temperature, given set of columns, flow rate, etc.):

$$\log M_x = -0.281 \, V_e + 9.15 \qquad (7.14)$$

Chromatograms for the unfractionated PVA polymers are shown in Figure 7.9. From the curves, number averaged, M_n, and weight averaged, M_w molecular weights, can be calculated using well-known equations (e.g., see Nagy 86). Values obtained for unfractioned polymer samples are reported in Table 7.4. Also, area/height ratio for chromatogram and polydispersity index M_w/M_n is reported in Table 7.3 and 7.4 for PEO calibration standards and PVA samples, respectively. As can be seen from the tabulated results, M_n, M_w values calculated from GPC are considerably lower (up to 100%) than the viscometric average molecular weights.

To improve the agreement between these two results, the calibration curve for PVA was established using PVA samples (commercial samples with broad-size distribution) whose molecular weights have been determined by GPC study by Nagy (Nagy 86). The relation between the peak retention volume, V_e, and M_w was established and can be represented by the following equation:

$$\log M_{PVA} = -0.21 \, V_e + 8.23 \qquad (7.15)$$

The effect of calibration curve on the calculations of M_w, M_n, and M_w/M_n is shown in Table 7.5 for three unfractioned samples. From Table 7.5, it is clear that the calibration curve determined using PVA samples (i.e., Equation 7.15) improved agreement between M_w and viscometric average molecular weight M_v. Also, the ratio M_w/M_n is dependent on the calibration method used. The values of M_w and M_n were still significantly different compared to viscometric molecular weight, M_v.
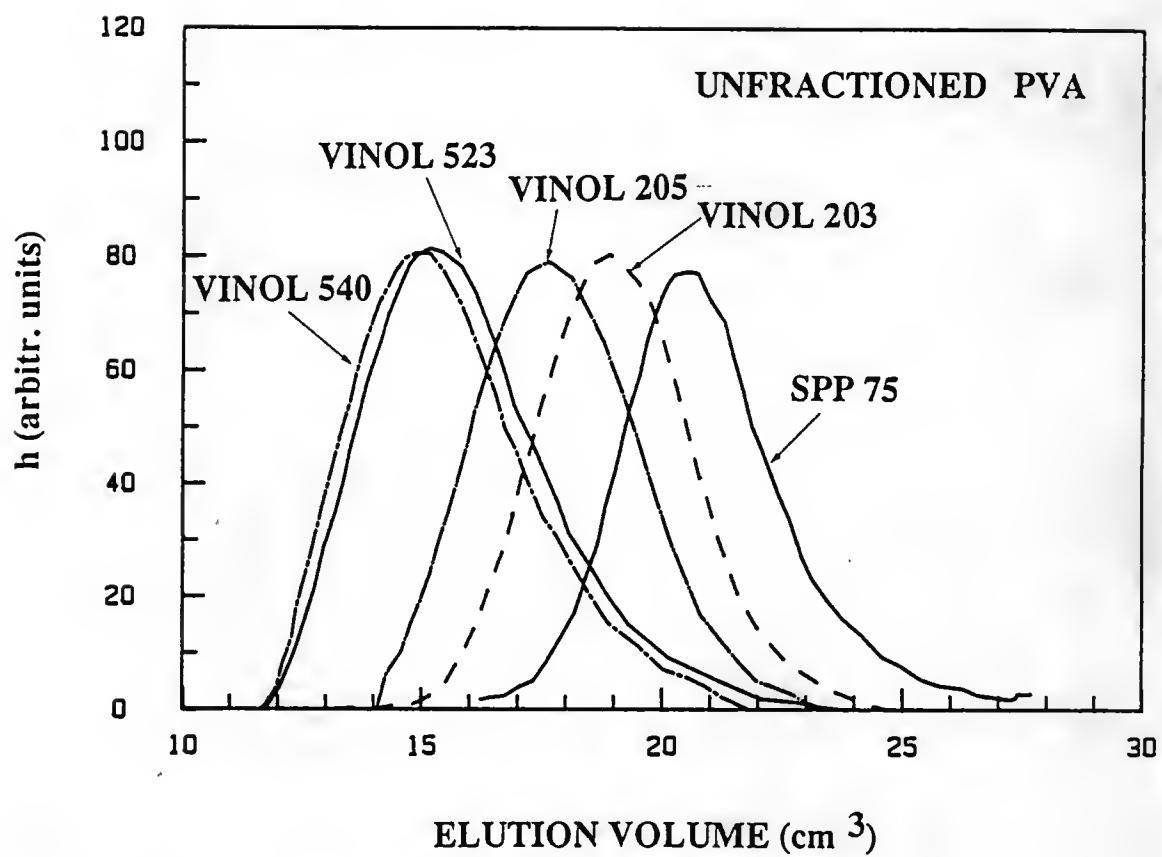
Figure 7.9   GPC chromatograms, showing refractive index detector
response, h, as a function of elution volume for several
unfractioned PVA samples.

The reasons for such a large discrepancy can be two-fold. (a) The method of converting molecular weight versus elution volume from the PEO standards to PVA standards is not suitable for these two water soluble polymers. (Koopal observed good agreement between the viscometric and GPC molecular weights when the GPA columns were calibrated using polystyrene standards.) (Koopal 78). (b) The length of columns used was not sufficient to obtain a good chromatographic separation of polymer molecules and to established log M versus V_e relation more accurately. (In our experimental setup, we used two 30 cm each long columns, while Nagy used four 60 cm each long columns, and Koopal used four 122 cm each long columns.)

Another motivation for conducting the GPC study was to obtain the information about the molecular weight distributions and the effect of fractionation on the distribution width. The width of the molecular weight distribution can be evaluated from the ratio M_w/M_n. These values are reported in Table 7.4 for as-received samples. Since the calculated M_w and M_n for a given polymer sample is dependent on the calibration curve (i.e., log M_w versus V_e), only a relative comparison between various polymer samples can be made (i.e., for a given sample, two different values of the ratio M_w/M_n can be obtained as shown in the Table 7.5). For comparison, the data on the PEO calibration standard is also shown in Table 7.3. Indirect comparison between the various fractions can be made by comparing the (area)/(peak height) ratios. These values are also listed in Table 7.3 and 7.4. The values of M_w/M_n (and area/peak height) indicate that the commercial PVA samples have broad molecular weight distributions. The effect of the acetone fractionation on the

TABLE 7.5

Effect of Molecular Weight - Elution Volume
Calibration Curve on the GPC Results

| PVA | GPC | | Viscometry | |
	Method 1 (Equation 7.14)	Method 2 (Equation 7.15)		
Vinol 540	M_n x 10^{-3} 25	58		
	M_w x 10^{-3} 107	133	M_v x 10^{-3}	154
	M_w / M_n 4.4	2.3		
Vinol 523	M_n x 10^{-3} 21	52		
	M_w x 10^{-3} 94	102	M_v x 10^{-3}	143
	M_w / M_n 4.5	2.3		
Vinol 203	M_n x 10^{-3} 4	13		
	M_w x 10^{-3} 10	23	M_v x 10^{-3}	21
	M_w / M_n 2.9	1.8		

Method 1:   Molecular weight - elution volume calibration was determined using PEO calibration standards.

Method 2:   Molecular weight - elution volume calibration was determined using PVA samples with broad-size distributions. Molecular weights, as reported by Nagy, were assumed (Nagy 86).

molecular weight distribution is shown in Figure 7.10 for the fractionation of two as-received polymers, Vinol 540 and Vinol 203, respectively. From the Figure 7.10 and Table 7.6, it is clear that the acetone fractionation procedure is more efficient for fractionation of low molecular weight as-received PVA (i.e., Vinol 203). Also, fractionation of fully hydrolysed PVA (> 98%) was not successful. Acetone addition and aging leads to the gelation of solution. This result is expected since the different molecular weight fractions are obtained due to differences in their solubility in the particular mixture of water and acetone. The solubility of PVA decreases with increasing molecular weight and more importantly with increasing degree of hydroxylation. Hence, the fractionation technique is less effective for fully hydrolysed PVA. Acetone fractionation decreases the width of the distribution slightly (Table 7.6). Thus, acetone fractionation did not produce "narrow" molecular weight fractions of PVA. Still, this fractionation procedure is important since it removes high and low molecular weight impurities from the samples. High molecular weight impurities are not desireable since the high molecular weight polymer preferentially adsorbs on the surface (Chapter II) and may have a significant effect on the flocculation behavior at low polymer concentrations. Due to the greater uncertainty associated with the GPC results, molecular weights calculated from the intrinsic viscosities (MHS equation) will be used for calculations of the solution properties of the PVA.

Also, with this choice, comparison with the literature results can be made on the same basis (for e.g., Koopal 78, Garvey et al. 74).
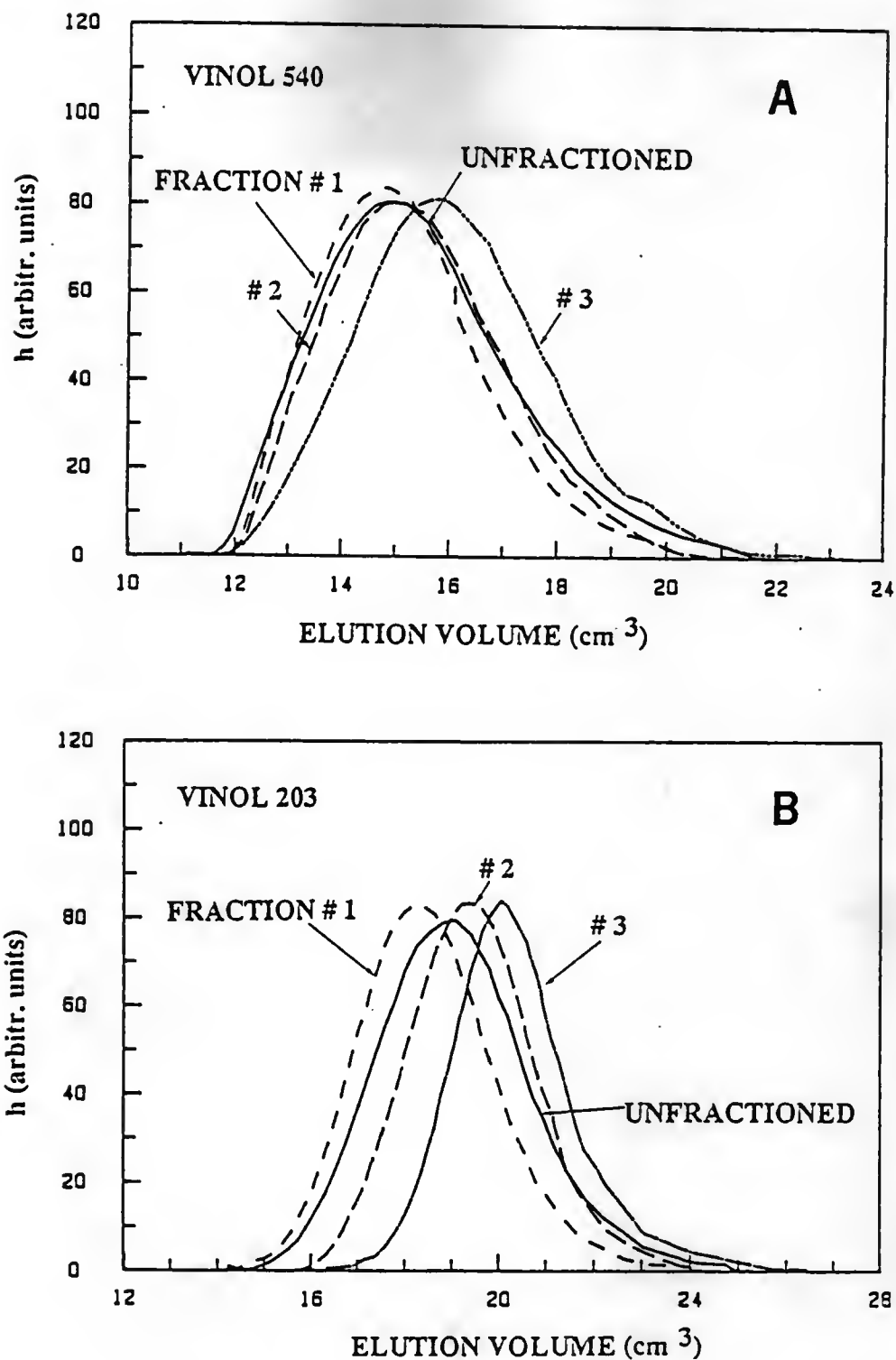
Figure 7.10   GPC chromatograms, showing the effect of acetone
                fractionation of Vinol 540 and Vinol 203 polymer samples
                on distribution widths.

TABLE 7.6

Comparison of Viscometric Molecular Weight and GPC Results for Various PVA Fractions

Sample		% Hydro-lysed	Viscometry		GPC*			
			$[\eta]$ dl/g	M_υ x 10^{-3}	M_w x 10^{-3}	M_n x 10^{-3}	M_w/M_n	AR/HT
Vinol 540	Unfrac-tioned	88	0.913	153	113	58	2.28	4.5
	F1	90	1.132	215	143	81	1.76	3.9
	F2	87	0.985	173	127	69	1.85	4.1
	F3	85	0.781	120	102	52	1.95	4.3
Vinol 203	Unfrac-tioned	88	0.260	21	23	12	1.86	4.0
	F1	90	0.348	33	30	19	1.57	3.7
	F2	86	0.281	23	17	11	1.60	3.4
	F3	84	0.173	11	12	7	1.85	2.9

* Molecular weight-elution volume calibration was determined using broad-sized PVA samples (Equation 7.15).

Conformation and Solution Parameters

In this section, the polymer conformation in solution and the solvent quality (measured by parameter χ) will be determined. The polymer conformation in solution is the initial conformation at the moment of polymer adsorption, and hence, it is expected that it can be correlated with the adsorption properties. This may be particularly important in the case of the flocculation regime (see Chapter V) when the time interval between Brownian collisions may be shorter than the reconformation time. The conformation of polymer molecules in solution is to a large extent determined by the solvent quality as measured by the Flory-Huggins parameter, χ (Chapter IV). The χ parameter is also important in determining the equilibrium conformation of the adsorbed polymer and stability of dispersions with the adsorbed polymer layer (Chapter V).

PVA Configuration Parameters

The unperturbed dimensions of a linear flexible polymer molecule can be obtained by using of the Stockmayer-Fixman equation (Stockmayer and Fixman 63):

$$[\eta] = K_o M^{1/2} + 0.51 \, \phi_o \, BM \tag{7.16}$$

where ϕ_o is the universal viscosity constant in a θ solvent (and has the value 2.6×10^{23} (Flory 69) when $[\eta]$ is expressed in dl/g) and K_o and B are constants.

From the measured intrinsic viscosities for PVA samples with varying molecular weights (with $\approx 88\%$ hydrolysed), a plot of $[\eta]/M^{1/2}$ versus $M^{1/2}$ was constructed (Figure 7.11). Linear regression of the data gave the
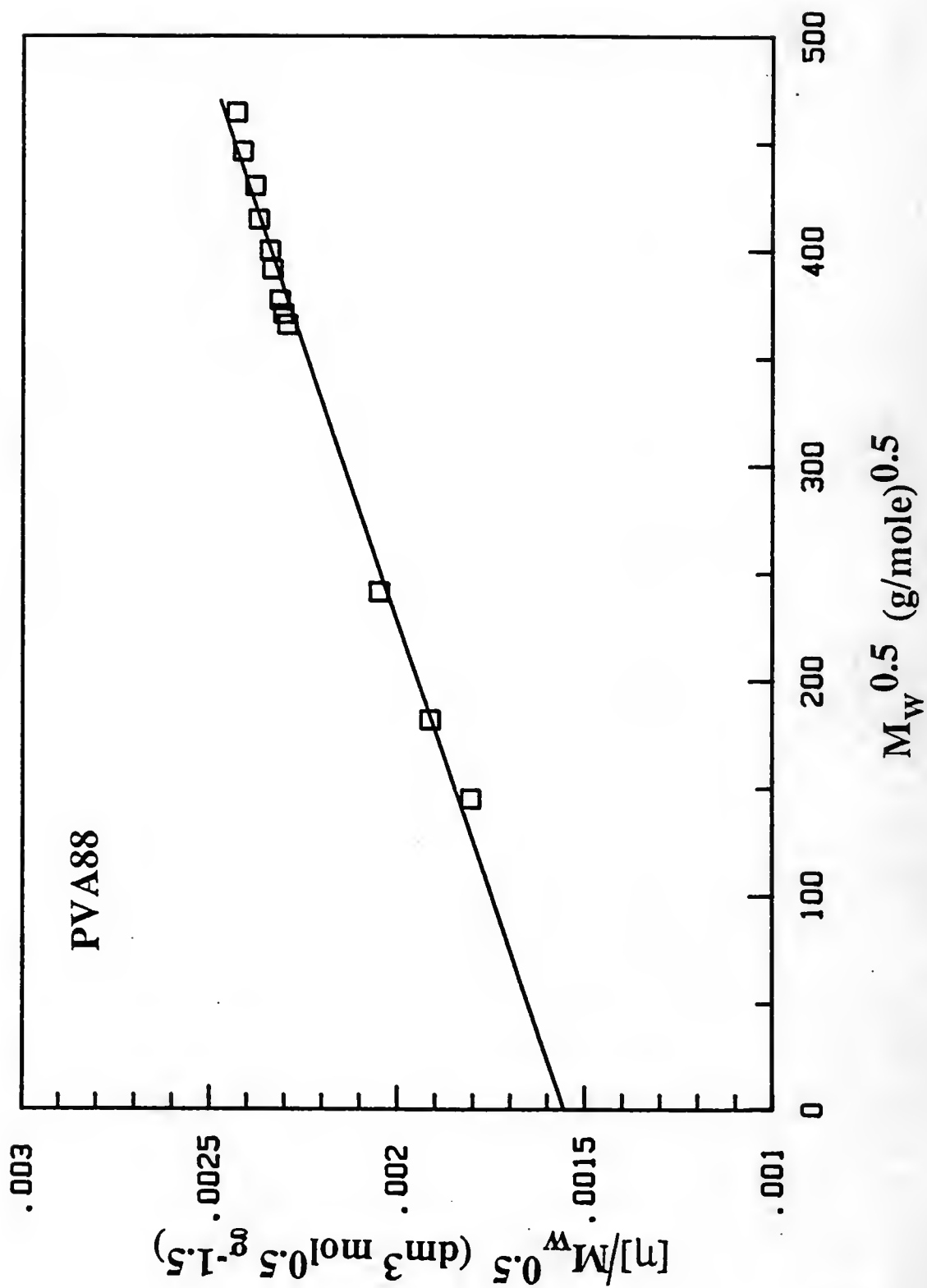
Figure 7.11   Stockmayer–Fixman plot for PVA88.

following values for constants: intercept $K_O = 1.55 \times 10^{-4}$, and slope,

$0.51\ B\phi_O = 1.958 \times 10^{-7}$. The value of K_O is in good agreement with the

value reported by Koopal, ($K_O = 1.58 \times 10^{-4}$) (Koopal 78) and by Garvey et

al. ($K_O = 1.52 \times 10^{-4}$) (Garvey et al. 74).

Flory-Fox showed that K_O is related to the root mean square end-to-

end distance of the unperturbed chain, $\langle h^2 \rangle_o^{1/2}$, by the following

equation (Flory and Fox 51):

$$K_O = \phi_o\ \langle h^2 \rangle_o^{3/2} /\ M^{3/2} \tag{7.17}$$

where $\langle h^2 \rangle_o^{1/2}$ is the rms end-to-end distance under θ conditions.   Under

non-θ conditions, an intrinsic viscosity-molecular weight relation is

represented by the (empirical) Flory-Fox equation:

$$[\eta] = K_o\ \alpha_n^3\ M^{1/2} \tag{7.18}$$

where α_n is the linear viscosity expansion factor and is defined by:

$$\alpha_n^3 \equiv [\eta][\eta]_o^{-1} \tag{7.19}$$

Kurata and Yamakawa developed the following equation to relate α_n

to the excluded volume parameter Z, for small values of Z (Yamakawa 71):

$$\alpha_n^3 = 1 + 1.55Z + \ldots \tag{7.20}$$

and Z is defined as follows:

$$Z = 0.330\ B\ A^{-3}\ M^{1/2} \tag{7.21}$$

where $A = \langle h^2 \rangle_o / M$.

In good solvents, the polymer chain tends to be more expanded

compared to θ conditions. The mean square end-to-end distance, $\langle h^2 \rangle^{1/2}$,

under these conditions is represented by:

$$\langle h^2 \rangle \equiv \langle h^2 \rangle_o\ \alpha_h^2,\ \text{and} \tag{7.22}$$

the mean square radius of gyration, $\langle s^2 \rangle$, by:

$$\langle s^2 \rangle \equiv \langle s^2 \rangle_o \, \alpha_S^{\,2} \quad \text{where} \tag{7.23}$$

$\langle s^2 \rangle_o$ is the mean square radius of gyration under θ conditions. The parameters α_h and α_S are the linear expansion factors for the polymer chain. The value of α_h and α_S increases with increasing solvent power.

The mean square end-to-end distance and the radius of gyration are related by the following equations:

$$\langle h^2 \rangle_o = \frac{1}{6} \langle s^2 \rangle_o \quad \text{(under θ conditions) and} \tag{7.24}$$

$$\langle h^2 \rangle_o \approx \frac{1}{6} \langle s^2 \rangle \quad \text{(under non-θ conditions)} \tag{7.25}$$

The parameters α_S and α_h are related to the excluded volume parameter Z by the Fixman equation (Fixman 55,62):

$$\alpha_h^{\,3} \approx \alpha_S^{\,3} = 1 + 2Z \tag{7.26}$$

From the measured intrinsic viscosities and the values of K_o and ϕ_o, the dimensions of the molecules in solution for the unfractioned PVA are shown in the Table 7.7. The values of dimensions in solution for fractioned polymers will be reported later.

The χ Parameter

The solvent-segment interaction parameter was determined from the Stockmayer-Fixman equation (Equation 7.16), (see Figure 7.11). The slope is related to second virial coefficient B by the following equation:

$$\text{slope} = 0.51 \, \phi_o \, B, \quad \text{and}$$

$$B = 2\nu_2^{\,2} \, (1/2 - \chi)/V_1 \, N_A \tag{7.27}$$

TABLE 7.7

PVA Dimensions in Solution

PVA Sample	$M_v \times 10^{-3}$	$\langle\alpha_h\rangle$	$\langle z\rangle$	$\langle\alpha_s\rangle$	$\langle h^2\rangle_o^{0.5}$ (nm)	$\langle s^2\rangle_o^{0.5}$ (nm)	$\langle s^2\rangle^{0.5}$ (nm)
Vinol 540	154	1.14	0.32	1.18	33.0	13.5	15.9
Vinol 523	143	1.14	0.31	1.18	31.8	13.0	15.3
Vinol 203	21	1.05	0.10	1.06	12.2	5.0	5.3
PVA 20/30	42	1.08	0.17	1.10	17.2	7.0	7.8

where ν_2 is the partial specific volume of the polymer (assumed to be equal to that of solid PVA, i.e., 0.788 cm^3/g (Pritchard 70)), V_1 is the partial molar volume of the solvent (i.e., 18 cm^3/mole for water), and N_A is Avogadro's constant. From linear regression, the slope was found to be equal to 1.958 x 10^{-7}. Substituting the above values in Equation 7.27, gave the value for the χ parameter for partially hydrolysed PVA in deionized water at 30°C:

$$\chi \text{ (partially hydrolysed, 30°C)} = 0.487$$

The χ value is similar to that determined by Koopal (Koopal 78). This is not surprising since the MHS constants reported by Koopal were used to calculate molecular weights from the intrinsic viscosities. Koopal has compared the literature value of χ parameter for fully (> 98%) and partially hydrolysed PVA's (Koopal 78). The χ parameter for fully hydrolysed PVA is similar to that for partially hydrolysed PVA (χ for 99% hydrolysed PVA is 0.488). This result is expected since the MHS constants for fully hydrolysed PVA are not too different from those for partially hydrolysed PVA (Equation 7.8 and 7.9). Thus, the solvent quality is about the same for both types of PVA, and water is a relatively poor solvent for both kinds of PVAs. Since the solvent quality is not different, it is expected that the conformation of the adsorbed PVA with varying acetate content is primarily determined by the amount adsorbed (see Chapter II).

Since water is a poor solvent, it is expected that intersegmental interactions occur in the polymer chain. The χ parameter can be changed by either (a) changing the temperature or (b) addition of electrolyte to water (see Chapter II).

Boomgaard et al. established MHS constants for PVA samples at various temperatures (van den Boomgaard et al. 78). From the Stockmayer-Fixman equation (Equation 7.16), the χ parameter at various temperatures was established. It was observed that, with increasing temperature from 25°C to 50°C, the value of the χ parameter changed from 0.464 to 0.485. Thus, the solvent power of water decreases with the increase in the temperature for PVA molecules. The values of χ parameters reported by various investigators should be compared with caution and should not be considered as absolute values. (The χ values determined depends on the MHS constants used.)

Tadros and Vincent have studied the effects of electrolyte type and concentration for PVA adsorption onto polystyrene latex particles (Tadros and Vincent 79, Barker and Garvey 80). From the adsorption and flocculation measurements, they concluded that the solvency conditions for the polymer worsen with increasing salt concentration. (However, they did not determine the χ parameter as a function of salt concentration.) This effect was the largest with Na_2SO_4 and the least with $CaCl_2$. The larger effect with Na_2SO_4 was related to the known water structure breaking effect by SO_4^{-2} anion (Tadros and Vincent 77). An SO_4^{-2} ion is generally assumed to be unhydrated in aqueous solution. Water molecules in the bulk phase are H-bonded to each other. Water structure in the region surrounding SO_4^{-2} ions is broken down and may be responsible for reduced solvency for PVA molecules. The effect of salt additions on the stability behavior of sterically stabilized silica dispersions will be reported in the next chapter.

The main focus of this study was correlating PVA adsorption behavior to model silica suspension properties. The adsorption procedure is described below.

Adsorption Measurements

The following procedure was used to establish the adsorption isotherms (i.e., the plot of the adsorbed amount of polymer as a function of the residual polymer concentration in solution at constant temperature and pressure). The total adsorbed amount of polymer was found from the difference in the polymer concentration before and after adsorption. All suspensions were prepared with a known initial polymer concentration in the solution. All suspensions were aged by rotating end-over-end for approximately twenty-four hours. The suspension was centrifuged[*] for approximately thirty minutes at an acceleration of 900 g to sediment the particles.

The PVA supernatant was appropriately diluted with 1×10^{-2} M NaCl solution to obtain a concentration in the range 0-0.1 mg/cm^3. Five cm^3 of the reagent containing 0.64 M H_3BO_3, 0.006 M I_2, and 0.018 M KI was added to ten cm^3 of diluted PVA solution of unknown concentration. A reaction between the reagent and PVA forms a green color complex. The reagent was added slowly to the PVA solution to avoid formation of 'blue specks' in solution. A green color solution was aged in the dark for at least half an hour to obtain a stable color. To determine the residual PVA concentration in solution, the solution was transferred to

---

[*]Model J2.21, Beckman, GA.

polystyrene cuvets[*] of 1 cm path length and absorbance was measured at 670 nm using a spectrophotometer.[**]

Calibration curves were measured under similar conditions. To do this, a known amount of PVA was dissolved ($\approx$ 0.1 gram) in a one liter volumetric flask. From this standard, the calibration curve was established for 0 - 0.1 mg/cm^3 concentration range using eight to ten dilution data points. The ionic strength of the solution was adjusted to 1 x 10^{-2} M NaCl/L. Plot of absorbance vs. concentration yield a good straight line (usually coefficient of regression > 0.99) (see Figure 7.12). Since the slopes of these lines depend on the molecular weight, acetate content, and ionic concentration, the calibration curve was established for each polymer sample used for the adsorption study.

Two samples in the concentration range of 0-0.1 mg/cm^3 were prepared from the supernatant by dilution. The absorbance at 670 nm was measured at least three times for each diluted supernatant. From the average of six absorbance measurements, the PVA concentration was calculated. The reagent was always used within two days and was always kept in the dark. Despite these precautions, the error in the analysis is about ± 2%, and the error in the adsorbed amount is ± 5% (Garvey et al. 74).

Suspension Preparation Procedure

The majority of suspensions were prepared at twenty volume percent solids loading. From the trial experiments, it was established that up to approximately 35 vol. % stable suspensions can be prepared in

---

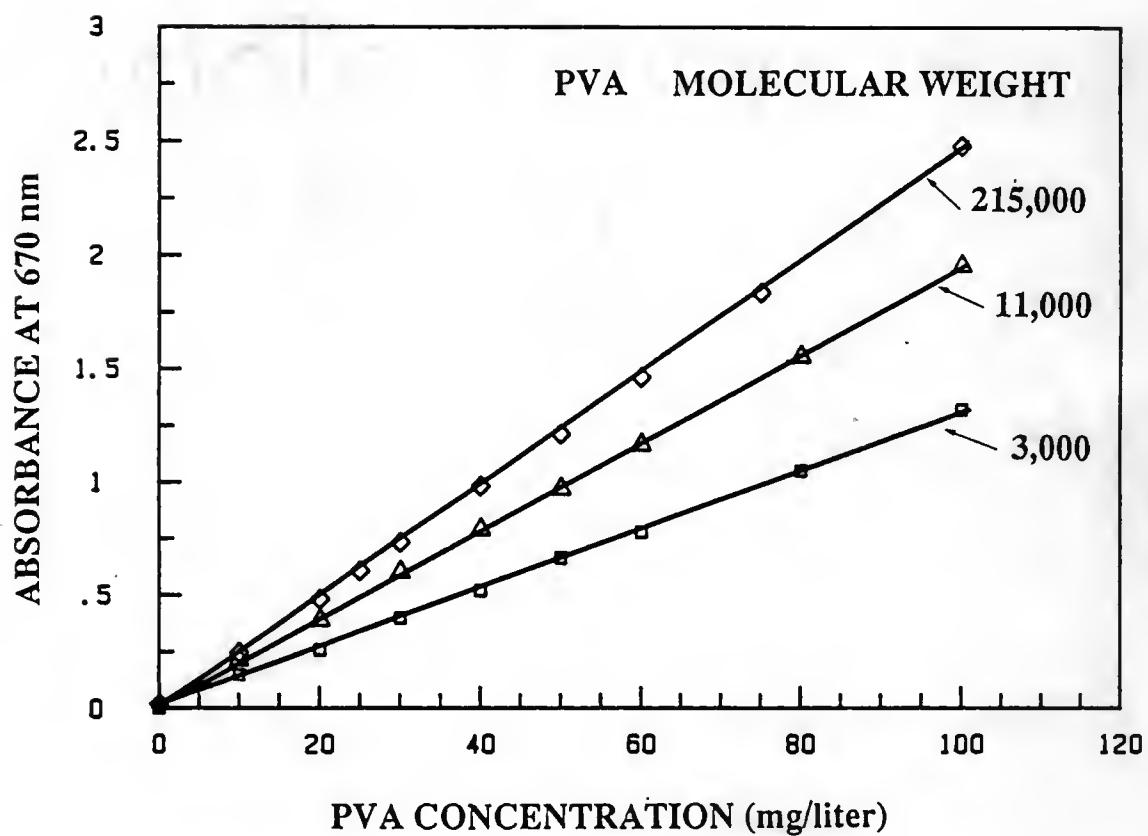[*]Fisher Scientific Co.

[**]Spectronic 2000, Bausch and Lomb.

Figure 7.12   Plot of absorbance versus PVA concentration in solution
                for various molecular weight polymers.

deionized water (pH ≈ 5.5 or greater). At solids loading > ≈ 35 vol. %, NaOH additions are required to raise the pH. (Due to silica being an acidic oxide, the pH drifts to lower pH values with increasing solids content.) To prepare sixty cm^3 of twenty volume percent silica suspension, the following steps were followed:

(a) To 23.2 grams of deionized water, approximately 26.4 grams of ground silica was added in two steps. Initially, approximately twenty grams of silica was added, and suspension was sonicated for approximately fifteen minutes. Then, the balance of silica (≈ 6.4 grams) was added and the sample was sonicated for two more hours. This results in a suspension with the ≈ 34 vol. % silica.

(b) After sonication, 4.8 ml of 0.1 M NaCl solution was added. This step makes the overall ionic concentration equals 10^{-2} M NaCl/L, and the silica vol. % is reduced to 30%.

(c) Twenty ml of polymer solution of known concentration was measured in a plastic bottle using volumetric pipet.* To this solution, the above silica suspension (40 cm^3) was transferred while stirring with a magnetic stirrer. The addition of a suspension to a polymer solution has been reported as the best way of mixing in order to achieve homogeneous distribution of polymer (Cohen Stuart et al. 86a).

(d) Immediately after adding the silica suspension to the polymer solution, a known amount of acid was added to the mixture in order to reduce the pH to the point of zero zeta potential, i.e., pH ≈ 3.7 (appropriate amount was predetermined from the trial experiments and was ≈ 0.2 ml of 0.1 M HCl for 60 ml of 20 vol. % silica suspension). The pH

---

*Fisher Scientific Co.

of the suspension was measured to ensure that the desired value was achieved.

(e) Mixing was continued for an additional five minutes. The suspension was then transferred to an end-over-end mixing device for aging. Rheological properties and adsorbed amounts were determined on suspensions aged for $\approx$ 24 hours.

A slight variation of the above procedure was adopted for experiments at high pH. To approximately 34 vol. % suspension (sonicated for two hours), NaOH was added to raise the pH of the suspension to $\approx$ 7.9 (usually $\approx$ 0.5 ml of 0.1 M NaOH was required). To this suspension, the balance of 0.1 M NaCl solution was added (4.8 ml minus the amount of 0.1 M NaOH that was added) and final silica concentration was reduced to 30 vol. %. This suspension was added to twenty ml of polymer solution of known concentration.

To investigate the effect of volume fraction, ϕ_p, of solids on the viscosity of electrostatically, stabilized suspensions, silica suspensions with $\approx$ 34 vol.% solids were initially prepared using the above procedure. To increase the solids loading above $\approx$ 34 vol.%, the pH of the suspension was adjusted to $\approx$ 7.9 and well-ground silica was added in steps of two grams. After each addition, the silica suspension was sonicated for $\approx$ fifteen minutes and the pH was measured. This procedure was continued until approximately fifty volume percent silica suspension was obtained. The ϕ values were redetermined by weighing (with the analytical balance) $\approx$ 1 gram of silica suspension in an aluminum dish, and then, drying in the oven for 24 hours at $\approx$ 60°C. From the dried

weight, ϕ_p values can be determined (i.e., from the measured wt fraction silica, the volume fraction silica could be calculated).

Suspension Characterization

Electrophoresis: To obtain information about surface potential, Ψ_0, electrokinetic measurements were carried out. As discussed in Chapter II, the experimentally determined near-surface potential, known as zeta potential, ζ, is generally substituted for Ψ_0 values. The zeta potential was calculated from the measured electrophoretic mobility. The electrophoretic mobilities were measured at 25°C using a microelectrophoresis apparatus.[*] A thin-walled cylindrical cell was used. The cell was washed thoroughly using deionized water between runs. The electrodes were blackened using a solution of 2% Hydrogen Hexa chloroplatinate hydrate and .02% lead acetate. All measurements were made using a constant current source. A He-Ne (3 mW) laser source was used to illuminate particles. Particle velocities were measured at the top stationary level. The particle velocity was calculated by measuring the time required to cross one grid length (28 μm). The field polarity was reversed after each measurement. At least one hundred readings were taken, and from these readings, the average velocity, U, was calculated. To calculate the field strength, X, the cell was calibrated for length. The cell length was calibrated from the cell diameter, the current flowing through the cell (measured using a volt meter and a known resistance used in series with the cell), and the specific conductance of the standard solution (1×10^{-2} M KCl). The field strength was

---

[*]Mark II, Rank Brothers, Cambridge, England.

calculated from the applied voltage and the cell length. The electrophoretic mobility is then defined as:

U_E = electrophoretic mobility = U/X (μm/sec)/(volt/cm)   (7.28)

or in SI units (meter/sec) / (volt/meter).

Samples for the electrophoresis were prepared as follows. Concentrated suspension were centrifuged at 900 g for approximately thirty minutes to obtain clear a supernatant. To this supernatant, a small drop of concentrated suspension was added. Typically, silica concentrations in the range of 100-500 ppm was used. The equation used for converting the value of electrophoretic mobility to electrokinetic ζ potential depends on the dimensionless parameter, κa, where κ is the Debye Huckel parameter (Chapter II), and a is the particle radius.

1. For $\kappa a > 200$, the Smoluchowski's formula was used:

$$U_E = \frac{\varepsilon_o \varepsilon_r \zeta}{\eta}$$ (7.29)

where ε_o is the permitivity of vacuum, ε_r is the relative dielectric constant, and η is the viscosity of the suspending media.

For aqueous dispersion at 25°C, Equation 7.29 can be written:

$$\zeta = 12.83 \ U_E$$ (7.30)

where ζ is the zeta potential in mV, and U_E is the electrophoretic mobility, (μm/sec) / (volt/cm).

2. $0.1 < \kappa a < 200$, the Henry equation was used for low zeta potentials (typically < 25.4 mV):

$$U_E = \frac{2\varepsilon_o \varepsilon_r}{3\eta} [1 + f(\kappa a)]$$ (7.31)

Tabulated values of function $f(\kappa a)$ for various κa values were used. For higher zeta potentials, a graphical solution published by Wiersema et al.

was used (Wiersema et al. 66). For most of our suspensions, the κa value was in the range of 15 to 70. The results of electrophoresis experiments will be discussed in the next chapter.

Rheological Measurements

Suspension rheological measurements were carried out at 25°C using a concentric cylinder Haake viscometer.[*] Shear history can affect the suspension flow behavior, hence, all samples had identical shear history (≈ five minutes mixing with a magnetic stir bar in identical bottles (125 ml) and 24 hours end-to-end mixing). The steady shear viscosity measurements were performed using the same sensor system (i.e., ZB 30 with inner cylinder O.D. (d_1) = 29.36 mm and outer cylinder I.D. (d_2) = 30 mm and gap size = $d_2 - d_1$ = 0.32 mm). The following shear rate program was used for all samples. After addition of ≈ 2 ml of suspension to the viscometer, the test was started immediately. The shear rate was increased from 0 to 1000 s^{-1} in two minutes (up curve) and was decreased from 1000 s^{-1} to 0 in another two minutes (back curve). Thus, the total time of one test was four minutes. At least four measurements were made by changing the sample after each run. The same procedure was followed to measure the supernatant viscosity. From the shear stress (τ) - shear rate ($\dot{\gamma}$) curve, the following flow curve parameters were determined as follows (Figure 6.8).

The viscosity at any shear rate can be calculated from the definition of the viscosity:

$$\eta \text{ (viscosity)} = \tau \text{ (shear stress)}/\dot{\gamma} \text{ (shear rate)} \quad (Pa \cdot S) \qquad (7.32)$$

[*]Model RV-100/CV-100 Viscometer, Haake, Inc., Suddle Brook, NJ.

The relative viscosity η_{rel} was calculated as follows:

$$\eta_{rel} = \eta_{susp.}/\eta_{sup.} \tag{7.33}$$

where $\eta_{susp.}$ is the suspension viscosity and $\eta_{sup.}$ is the viscosity of the supernatant.

If the τ-$\dot{\gamma}$ plot shows hysteresis (i.e., thixotropic behavior as described in Chapter VI), then the back curves were used to calculate the following flow curve properties:

(a) Extrapolated yield point τ_β: The linear portion of the τ - $\dot{\gamma}$ back curve was extrapolated to $\dot{\gamma} = 0$.

(b) Plastic viscosity, $\eta_{plastic}$: The plastic viscosity was calculated from the slope of the linear portion of τ - $\dot{\gamma}$ back curve, and relative plastic viscosity was calculated by dividing this number by the supernatant viscosity, i.e.,

$$\eta_{rel.\ plas.} = \eta_{plas.} / \eta_{sup.} \tag{7.34}$$

(c) Hysteresis Area, H_{area}: The hysteresis area (i.e., the area between the up curve and the back curve) was calculated using digitizing Tablet. The measured area (cm^2) was normalized using a proper shear stress scale. (The shear rate scale was the same for τ - $\dot{\gamma}$ curves, i.e., 0 - 1000 s^{-1}).

Consolidation and Green Microstructure

Suspensions were consolidated using two methods: (1) gravity sedimentation and (2) slip casting. For gravity sedimentation, approximately 2.5 ml of suspension (for i.e., $\approx$ 1 gram of silica for 20 vol.% silica suspension), was pipeted in an approximately two centimeter diameter plastic tube placed on a glass plate. Vacuum grease (only a

slight amount) was applied at the end of the tube to avoid slippage of the suspension. The tube was partially covered with a glass cover slip to prevent dust pickup. For slip casting, the plastic tubes were placed on a flat surface of the plaster of paris mold. Nylon filter paper ($\approx$ 0.22 μm pore size[*]) was placed between the tube and the mold. Filter paper prevents contamination of the bottom surface of the consolidated samples, but it also reduces the consolidation rate. Typically, water was removed in three to four hours by slip casting. For the sedimentation process, it took approximately one month for all the liquid to evaporate. Green compacts were dried at approximately 80°C for 24 hours to remove residual water. The residual polymer in the samples was removed by heating samples at approximately 550°C for three to four hours. The porosity characteristics of the consolidated samples were determined using Hg porosimetry.[**] Typically, 0.5 gram of sample was used, and pressure versus intruded volume plots were obtained. (The maximum applied pressure was $\approx$ 413 MPa.) From this plot, the pore size distribution (i.e., specific pore volume frequency versus pore radius) was obtained. The median pore radius was calculated from the following relation:

$$r(nm) = 735 / P_{0.5V} \tag{7.35}$$

where r is the median pore radius in micrometers and $P_{0.5V}$ is the pressure corresponding to the intruded volume = $V_{max}/2$, where V_{max} is the maximum intruded volume at $\approx$ 413 M PA.

---

[*]Fisher Scientific Co.

[**]Quantachrome Corp., Syosett, NY.

Summary

In this chapter, properties of materials used and various characterization tools employed were discussed.

The silica powder used was prepared by the Stober method. The precipitated powder was characterized for size, size distribution, density, surface area, and surface structure. From these results, it is clear that the powder used is narrow-sized and essentially free of surface porosity. The surface-chemical structure was characterized by FTIR.

The PVA used in this study was fractionated by sequential precipitation with acetone. The as-received and fractionated polymer samples were characterized for acetate content and molecular weight. The acetate content was determined using a saponification technique and molecular weights were calculated from the intrinsic viscosity measurements. GPC studies were carried out to obtain information regarding polydispersity of these samples. It was found that the GPC results were inconclusive in this respect, but that fractioned samples were polydispersed. From the measured intrinsic viscosities, the χ parameter for the PVA 88 was determined. The value of $\chi = 0.485$ was consistent with literature results. This value of χ parameter indicates that water is a relatively poor solvent for PVA. The PVA solution dimensions, such as end-to-end distance, $<h^2>^{0.5}$, and the radius of gyration $<S^2>^{0.5}$ were also calculated.

Finally, procedures used for suspension preparation, adsorption measurements, electrophoresis, rheology, and green microstructure characterization were described.

CHAPTER VIII
RESULTS AND DISCUSSION

Electrostatically Stabilized Dispersions

As discussed in Chapter III, the stability of electrostatically stabilized dispersion is controlled by two important parameters, i.e., the ionic strength of the solution and the surface potential, Ψ_0. First, we will describe the effect of zeta potential, ζ, (used for surface potential) on the rheological properties of ≈ 20 vol % silica ($\phi_p \approx 0.2$) suspensions. The geometric mean particle diameter was ≈ 0.35 μm, and the powder was washed and calcined at 300°C before preparing suspensions. As described in the last chapter, the zeta potential can be varied by changing the suspension pH. Figure 8.1 shows a plot of ζ potential as a function of suspension pH. (The ζ potential was calculated from the measured electrophoretic mobility.) At low pH (pH $< \approx 4$), the silica surface develops a small positive potential (≈ 5-10 mV), and at high pH, high negative potential is developed. The isoelectric point i.e.p., at pH ≈ 4 is evident from the Figure 8.1. This value is consistent with measurements reported previously for the Stober silica (Killmann et al. 86, Sacks and Tseng 84). This value is slightly higher than isoelectric points reported for other silicas which are typically in the range of pH ≈ 2-3 (Iler 79). Since i.e.p. is strongly dependent on various factors, such as silica preparation method, type and concentration of surface impurities, aging, surface treatment, etc., a direct comparison cannot be made.
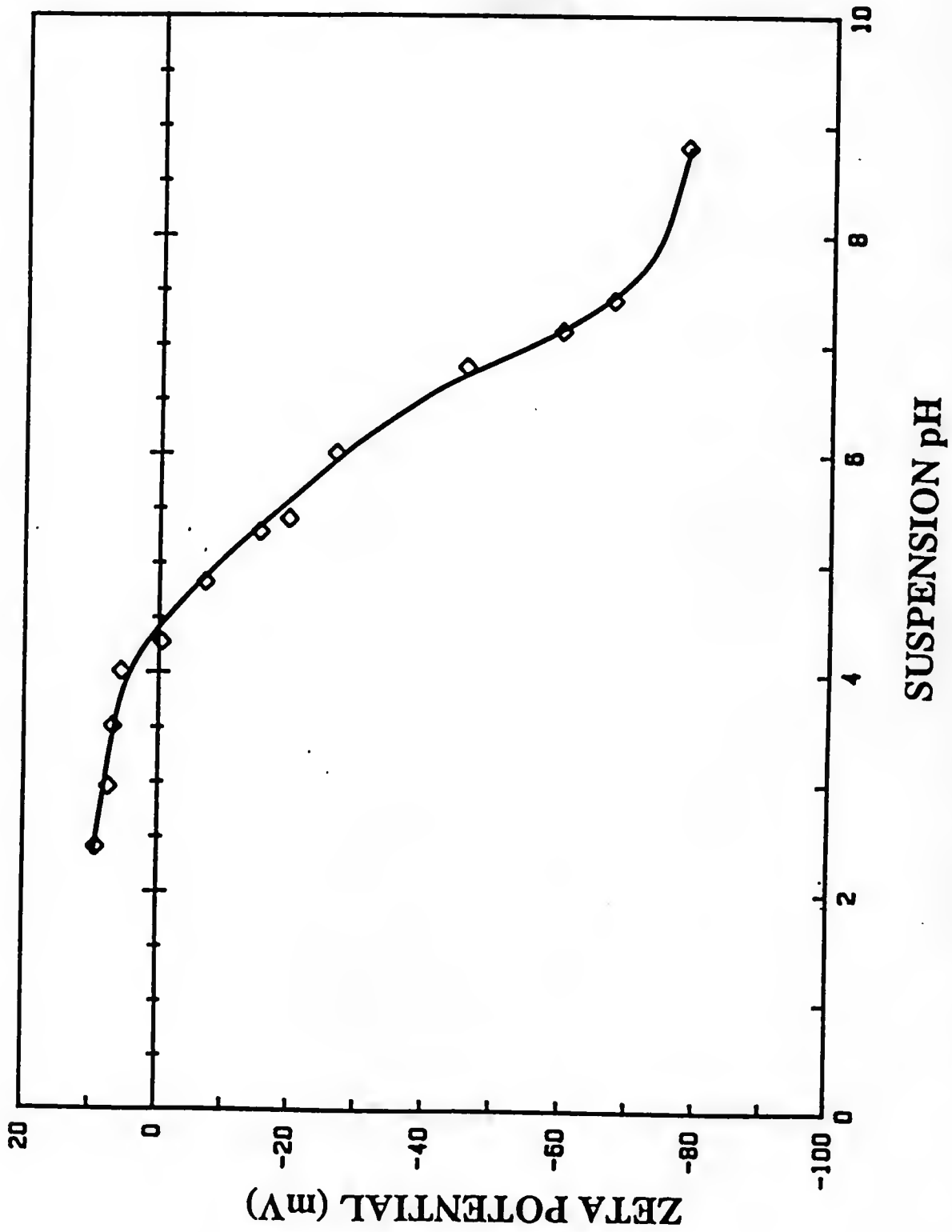
257

Figure 8.1   Plot of zeta potential versus suspension pH for 20 vol.% SiO$_2$ suspensions at ionic strength of 1 x 10^{-2} moles/liter NaCl.

The effect of ζ potential on the rheological flow behavior is shown in Figure 8.2. Figure 8.2A shows plots of shear stress versus shear rate and Figure 8.2B shows the corresponding plots of viscosity versus shear rate for suspensions with varying ζ potentials.

The shear stress versus shear rate plot for the suspension with approximately zero ζ potential exhibits pseudoplastic flow behavior. This can be more clearly seen from the corresponding viscosity versus shear rate plot. There is a significant decrease in the suspension viscosity with increasing shear rate. The higher suspension viscosities are due to higher effective volume fraction of solids in the suspension, and the shear thinning behavior can be associated with the breakdown of the floc aggregates with shear. The structural breakdown leads to liberation of occluded liquid from floc interstitials, and hence, the effective volume fraction of the suspension is decreased (Figure 8.3). At higher shear rates, a linear relation between shear stress and shear rate was observed (i.e., plastic viscosity was constant). This indicates that the effective volume fraction solids ϕ_{eff}, does not change beyond a critical shear rate. Thixotropic flow behavior was not observed with these flocculated suspensions. This indicates that there is essentially no difference in the rate of structural breakdown and the rate of structure reformation at a particular shear rate(i.e., the steady state suspension structure is instantaneously formed at a fixed shear rate).

To describe the pseudoplastic flow behavior of suspensions quantitatively, the following information is necessary: (i) description of suspension structure at rest (i.e., arrangement of particles in a suspension), (ii) effects of applied shear on suspension structures
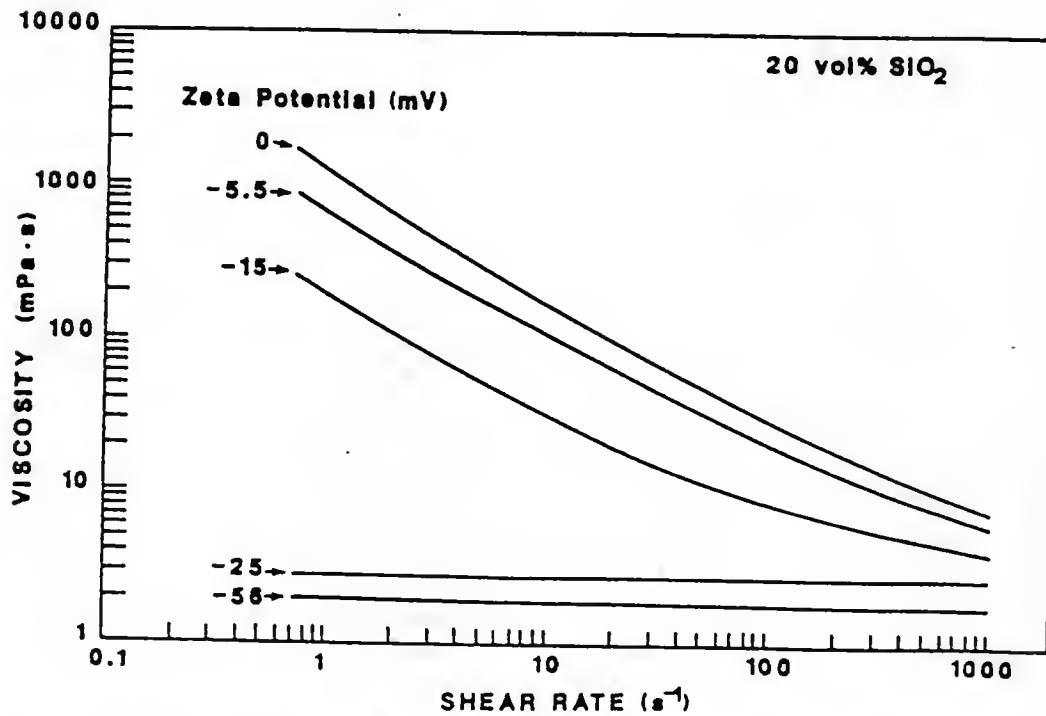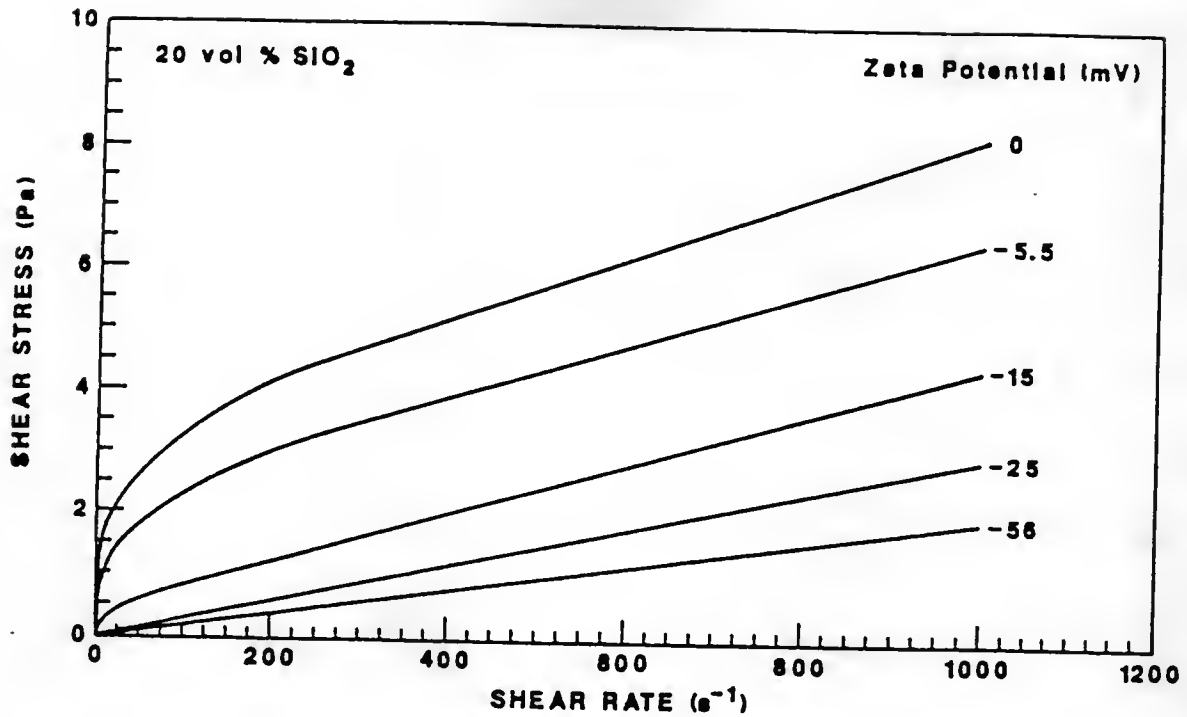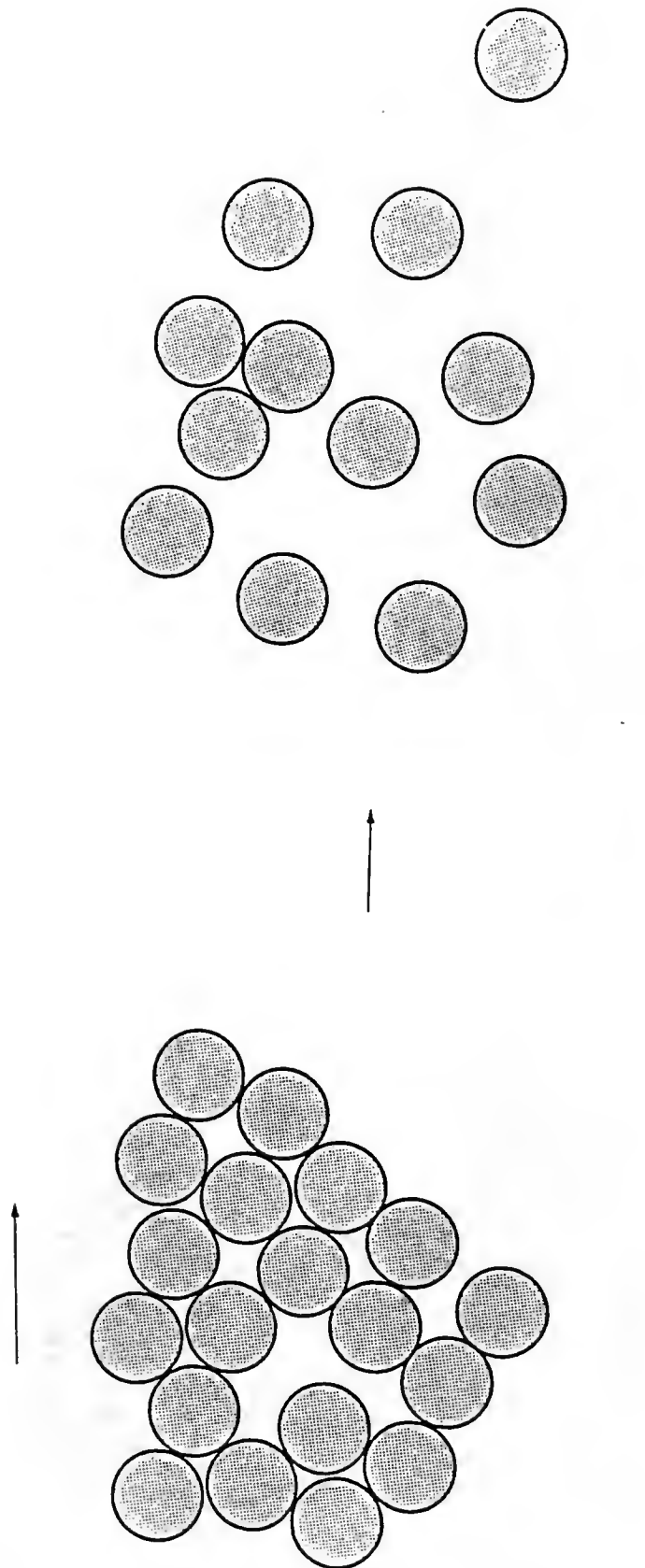
Figure 8.2   The effect of zeta potential on (a) shear stress versus shear rate and (b) viscosity versus shear rate plots.

8.3   Schematic illustration showing the structural breakdown of a floc due to applied shear.

(i.e., changes in the average cluster size and cluster size distribution), and (iii) interactions between clusters under shear, etc. Since the above information is not readily available, the quantitative description of flow curves is not possible.

With increasing ζ potential, there is a progressive decrease in the shear thinning behavior (i.e., lower viscosities at high and low shear rates compared to suspension with zero ζ potential). Newtonian flow behavior was observed for suspensions having ζ potential ≥ 25 mV. This can be more easily seen from Figure 8.2B which shows that the viscosity is independent of the shear rate. No significant decrease in the viscosity was observed for potentials ≥ -25 mV. The viscosity value of ≈ 2 mPa.s for suspensions with ζ potential ≈ -56 mV is very close to that predicted by various empirical equations (Thomas 65, Mooney 51, Krieger 72). This indicates that the flow units are essentially single particles. (However, the possibility of formation of temporary doublets and triplets, etc. under shear and Brownian motion cannot be eliminated.)

The effect of zeta potential on the stability of suspension can be also seen from the total interaction energy curves as shown in Figure 8.4. The value for the effective Hamaker constant $A_{131} = 0.85 \times 10^{-20}$ J was used. (This value is calculated by Hunter from the macroscopic approximation, Hunter 87). The height of the potential barrier V_{max} increases with increasing zeta potential (Figure 8.4). The value used for the effective Hamaker constant seems consistent with the experimental observation regarding the stability of silica suspensions from the rheological method. The total potential energy curve shows the potential energy barrier of ≈ 25 kT for ζ potential = -30 mV. At higher ζ
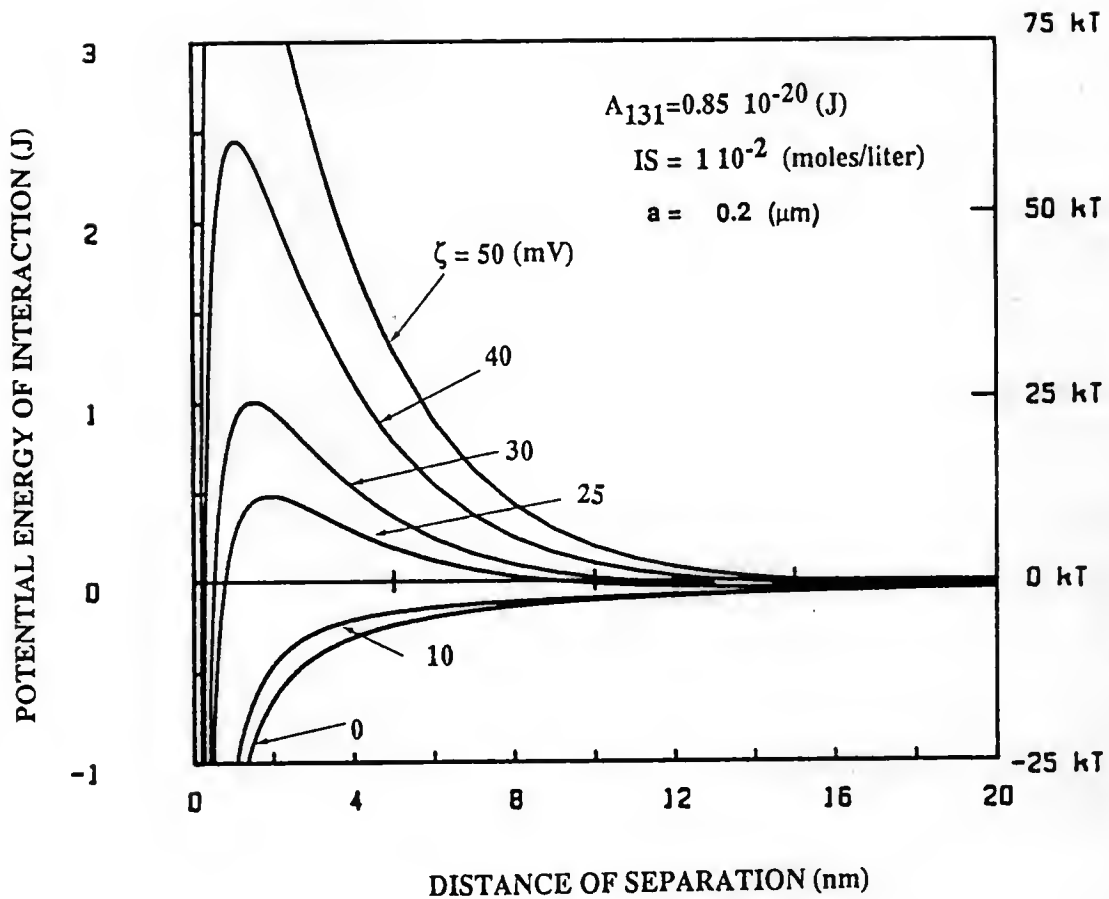
POTENTIAL ENERGY OF INTERACTION (J)

DISTANCE OF SEPARATION (nm)

$A_{131} = 0.85 \ 10^{-20}$ (J)

$IS = 1 \ 10^{-2}$ (moles/liter)

$a = 0.2$ (μm)

$\zeta = 50$ (mV)

Figure 8.4 DLVO plots of potential energy of interaction versus distance of separation at indicated ζ potentials.

potentials, the height of the potential barrier is increased which can prevent the aggregation of silica particles.

To gain more information about the flow units, parameters such as relative plastic viscosity, η_{pl}, critical shear rate, D_O, and extrapolated yield stress, τ_β, were determined from the flow curves. From the measured relative plastic viscosity, the effective volume fraction of flocs, ϕ_F, was calculated from the Thomas equation (Equation 6.6) (Thomas 65). These parameters (i.e., η_{pl}, $C_{FP} = \phi_F/\phi_P$ and τ_β) as a function of suspension ζ potential are shown in Figures 8.5 to 8.7, respectively.

As shown in Figure 8.5, the relative plastic viscosity decreases with increases in ζ potential. The effective volume fraction of flocs ϕ_F, was calculated from the measured relative plastic viscosity (Figure 8.5). Figure 8.6A shows a plot of C_{FP} (ie., floc openness parameter, $C_{FP} = \phi_F/\phi_P$) as a function of ζ potential. With increases in ζ potential, the effective volume fraction solids in dispersion decreases. This observation is consistent with computer simulation experiments which show that the clusters formed under Reaction Limited Aggregation, RLA, conditions are more compact (i.e., higher fractal dimensionality, d_f) than those formed without any potential barrier (Wietz et al. 84, Cohen 87). The exact dependence of C_{FP} on the total interaction energy is not yet clear. As discussed in Chapter VI, the elastic floc model predicts, $C_{FP} \alpha 1/\zeta^2$ (Hunter 82). To check this predicted behavior, C_{FP} as a function of ζ^2 is plotted in Figure 8.6B. The linear dependence of C_{FP} on ζ^2 was not observed. As discussed earlier, there can be several reasons for this observation.
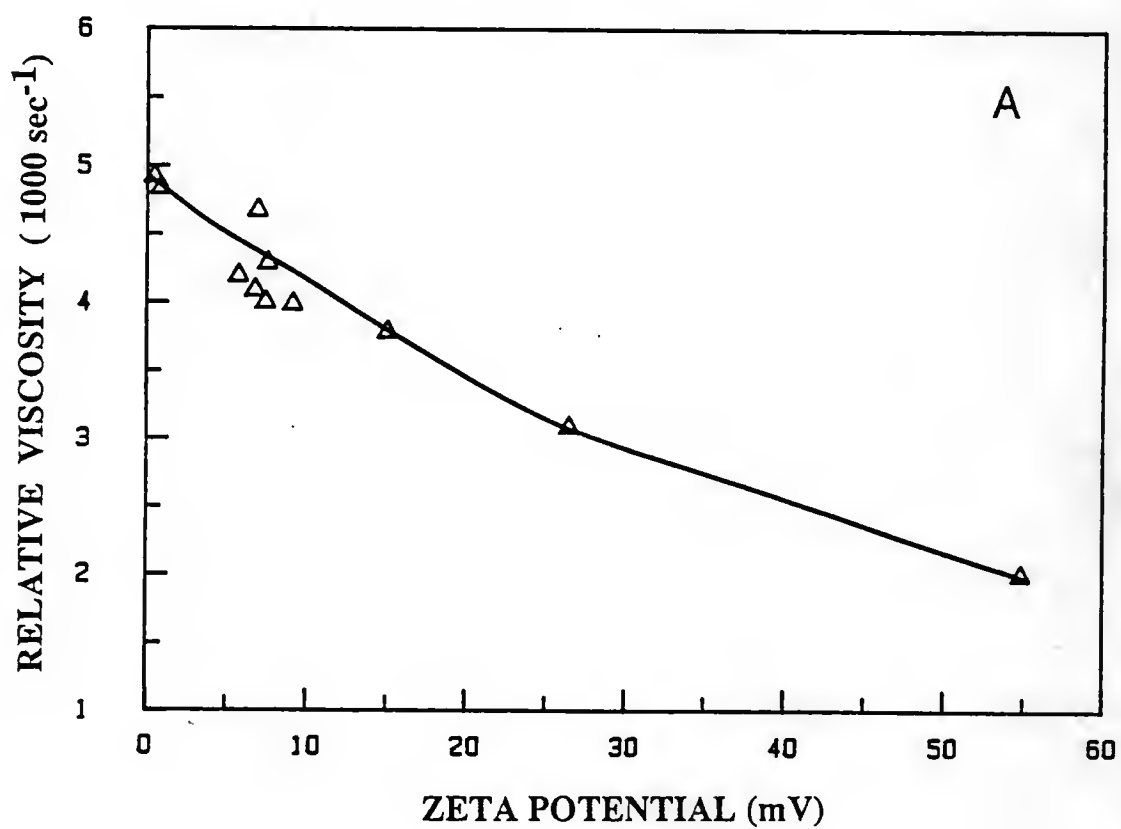
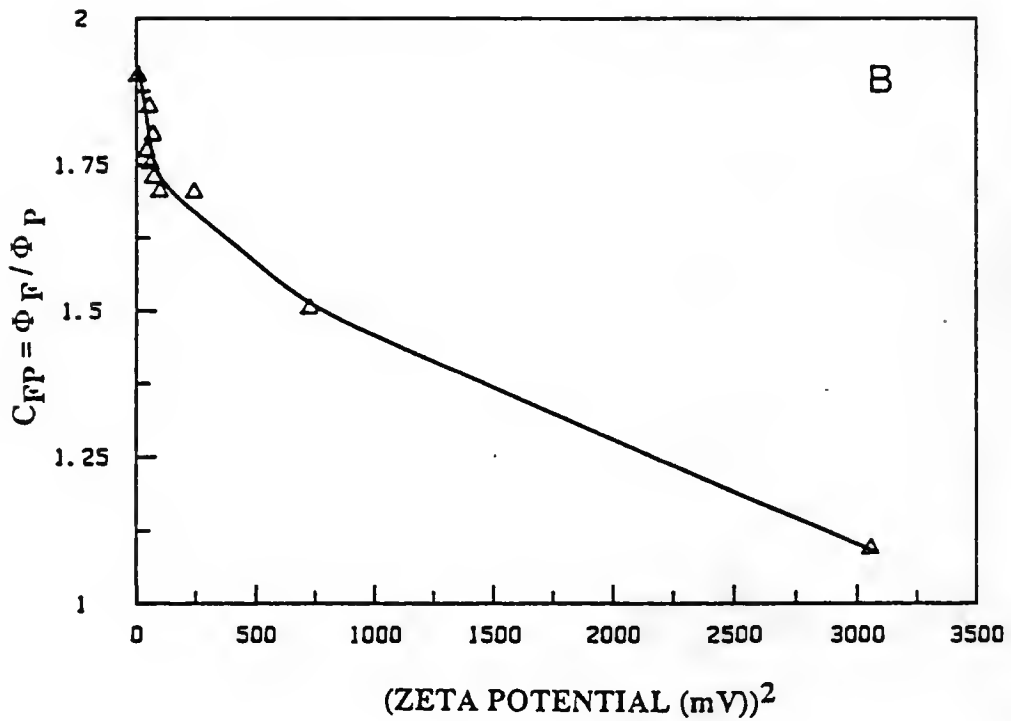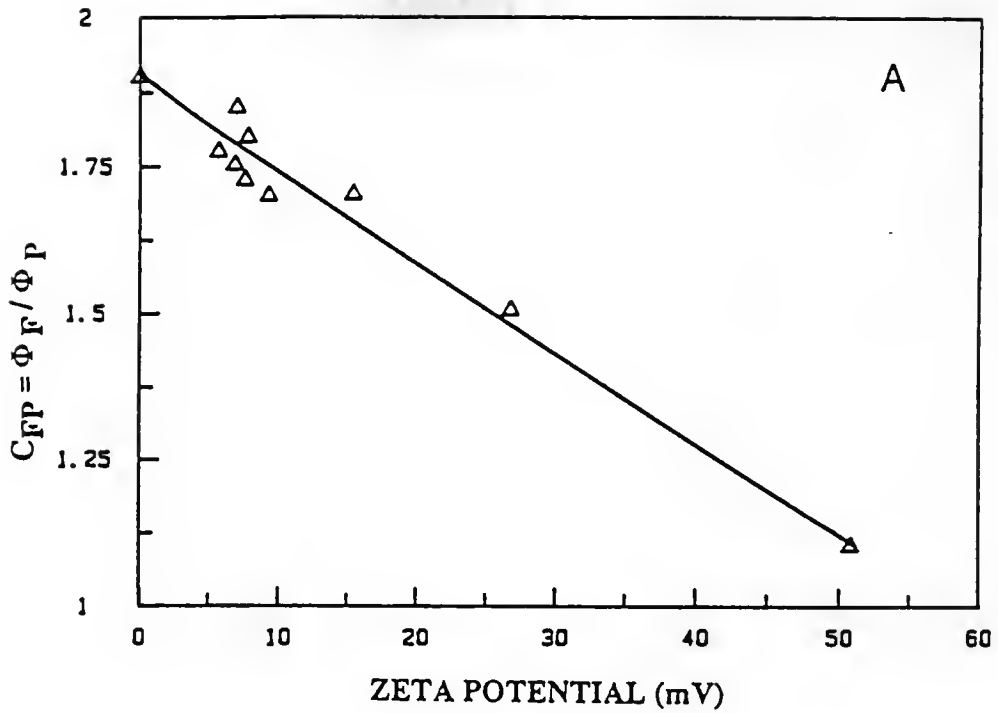Figure 8.5   Plot of relative viscosity versus zeta potential for 20 vol.% SiO_2 suspensions.

Figure 8.6   Plot of (a) C_{FP} versus zeta potential and (b) C_{FP} versus zeta potential square for 20 vol.% SiO_2 suspensions.

(i) Hunter et al. elastic floc model is valid for dilute suspensions, typically ϕ_p = .01 to 0.1. We employed suspensions with ϕ_p = 0.2. (ii) The elastic floc model assumes that the flocs have an open girder structure, where structure formed in our system may not form these chain-like structures. (It may be more appropriate to represent the floc structure as random packed spheres or as fractal object.) This can be also concluded from the low values of parameter C_{FP} (i.e., C_{FP} < 2.0) in Figure 8.6B. (Please note: C_{FP} = 1 i.e., ϕ_F = ϕ_p indicates that all particles are well separated, i.e., no flocculation of particles in suspension, C_{FP} = 1.28 indicates that the particles are arranged in a hexagonally close packed structure.) Also, if the suspension structure exhibits chain-like characters (i.e., large C_{FP}), it is usually not possible to prepare suspensions beyond a certain effective critical volume fraction of solids, ϕ_C. This critical value of ϕ_C has been correlated with the percolation threshold for elasticity of the network structure. The threshold for the elastic modulus for percolated structure on hexagonal lattice was observed when the volume fraction of solids is approximately 0.5, i.e., $\phi_C \approx 0.5$. With chain-like structures, the percolation threshold can be reached at true solids loading as low as ϕ = .01 (Mall and Russel 87). Another evidence for the existence of random aggregated (but not chain-like) is from the observation of sediment density. Typically, a relative sediment density of $\approx$ 55 to 58 % was observed (0.7 µm silica particles gave slightly higher density) for coagulated dispersions. This density is close to loose packing of spherical particles.

(iii) Short range interactions due to the "structural," "solvation," or "hydration" forces (i.e., due to solvent structure formation near the silica particle surface) were ignored in the elastic floc model. These forces may play an important role since they determine the distance of closest approach between particles.

Figure 8.7A shows a plot of the extrapolated yield stress, τ_β, vs. ζ potential, and Figure 8.7B shows corresponding plot of τ_β vs. ζ^2. The elastic floc model predicts a linear relation between τ_β and ζ^2 (Equation 6.19). The predicted linear relation between the τ_β and ζ^2 was not observed (Figure 8.7B). This observation again points out the inadequacy of elastic floc model for our system.

Sedimentation rates are often used to evaluate the state of particulates in dispersion. Generally, rapid sedimentation rates indicate flocculation of particles in suspension while slow rates of sedimentation indicate particles are well dispersed.

The flocculated silica suspensions did not undergo rapid sedimentation and flocculation could not be visually detected. (In the case of flocculation due to bridging by adsorbed polymer, rapid sedimentation was quite evident.) The observation of slow sedimentation rates of flocculated suspensions with no added polymer is consistent with results of Killmann et al. (Killmann et al. 86).

The slower rate of sedimentation for flocculated silica suspension indicates that conclusions regarding stability of silica suspensions cannot be reached from the sedimentation experiments alone. It also shows the importance of complimentary rheological measurements to evaluate the state of particulates in dispersion.
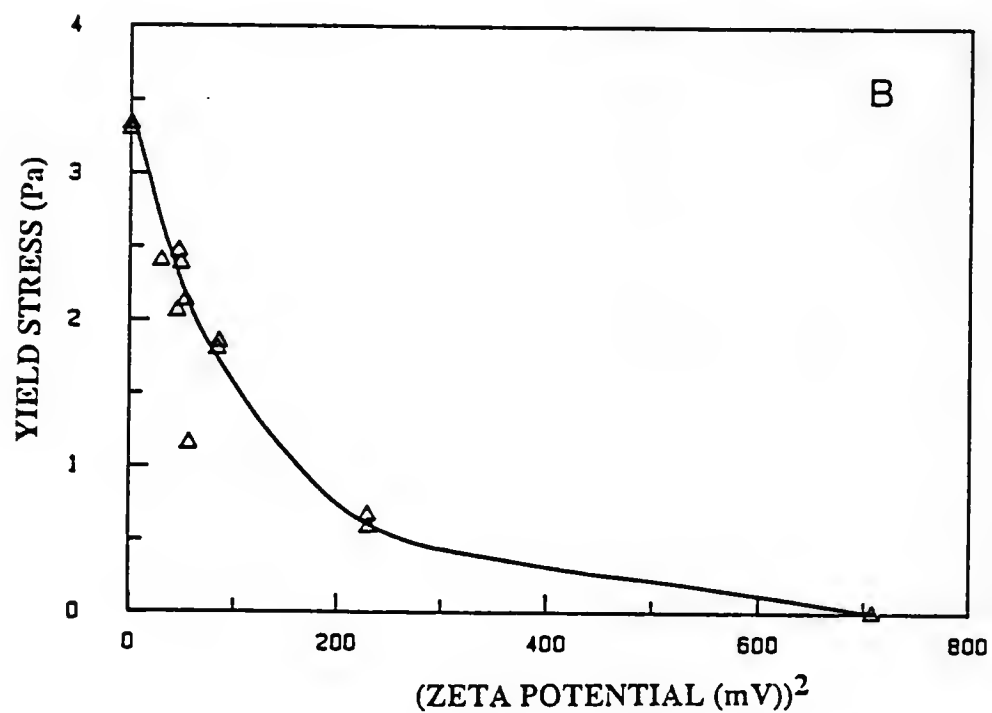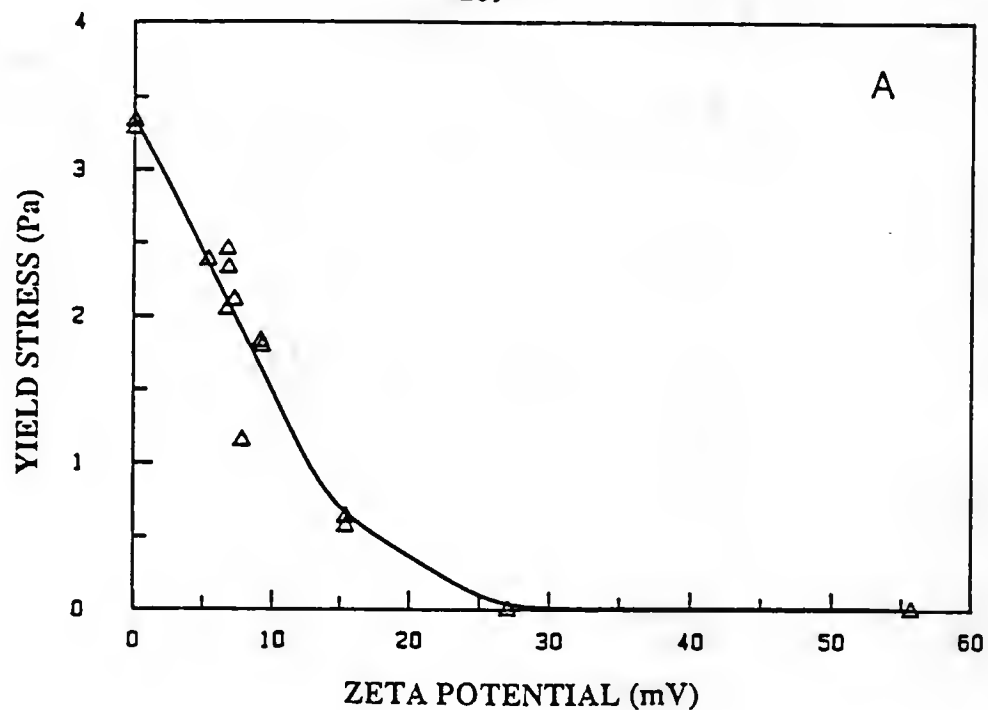
Figure 8.7   Plot of (a) extrapolated yield stress versus zeta
potential and (b) extrapolated yield stress versus zeta
potential square for 20 vol.% SiO_2 suspensions.

Suspensions with $\zeta \approx 0$ (i.e., pH approximately 3.7) and $\zeta \approx -60$ mV were consolidated using various techniques (i.e., gravity sedimentation, slip casting, centrifugal casting). Consolidation rate also plays a role in controlling the final green density of the sample and the pore size distribution obtained (Vora, Unpublished Work 88). Figure 8.8 shows the effect of suspension pH (or ζ potential) on the pore size distribution where specific pore volume frequency ($cm^3/g \cdot nm$) is plotted as a function of pore radius. The suspension with approximately zero ζ potential is flocculated and consolidation of suspension results in compacts with lower relative density (≈ 58 %) and larger average pore radius compared to suspension with high ζ potential. The strong electrostatic repulsion between silica particles leads to slow settling rates (as flow units are mainly single particles) and ordering of silica particles resulting in higher green density (≈ 64 %) and smaller average pore radius. The green density is approximately ten percent lower than the theoretical packing density of monosized spherical particles. This has been attributed to the formation of defects in the compact (i.e., grain boundary, point defect, stacking fault, etc.) and to development of pore channels (Sacks and Tseng 84, Aksay and Kikuchi 86). These channels can be developed during consolidation due to upward flow of water (Hunter and Ekdawi 86). Also, during the consolidation process, the volume fraction of solid increases in the settled bed and can reduce the diffusivity of the particles (i.e., "the structure is locked in") leading to lower density.

Thus, it can be concluded from the above discussion that the silica dispersions can be electrostatically stabilized at high pH and ionic strength of 1×10^{-2} NaCl moles/liter. At pH ≈ 3.7, i.e., near zero ζ
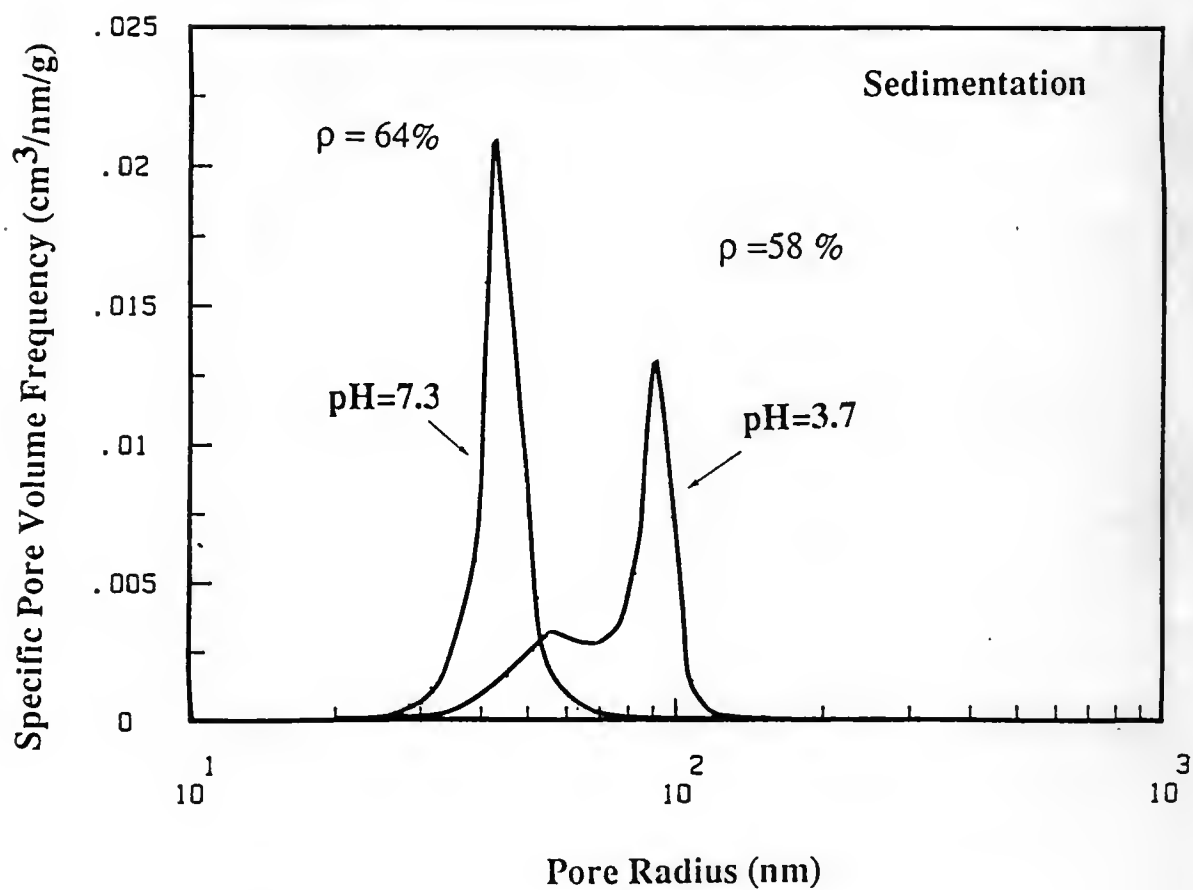
Figure 8.8   Plots of specific volume frequency versus pore radius
obtained by mercury porosimetry for sedimented samples
with indicated pH values.

potentials, the suspensions are coagulated due to Van der Waal's attraction. Flocculated suspensions showed shear thinning flow behavior and consolidation of suspensions resulted in compacts with lower densities and larger pore radii, compared to electrostatically stabilized suspensions. The elastic floc model was not adequate to describe our experimental observations. The Hamaker constant reported in literature (Hunter 87) for silica-water system (i.e., 0.85×10^{-20} J) appears consistent with our stability observations from the rheological method.

Effect of Adsorbed PVA on the Properties of Model Silica Dispersions

Our main aim of this study was to investigate the effect of adsorbed polymer on the stability of dispersions. The following scheme will be followed to discuss the effect of adsorbed polymer. First, the adsorption behavior of PVA on the silica particles will be described. The effect of the adsorbed amount of PVA on the rheological properties and the green microstructure will be reported. The information about the adsorbed polymer conformation (theoretical and experimental) and the total interaction energy diagram will be related to the observed flow behavior with the consistent model for the floc structure.

Effect of Amount Absorbed

The amount absorbed of polymer can be changed by varying polymer concentration in suspension. Figure 8.9 shows a typical high affinity adsorption isotherm of PVA onto the silica particles (Khadilkar and Sacks 88). The PVA and silica characteristics are listed on the Table 8.1. The initial additions of polymer are completely adsorbed and, as
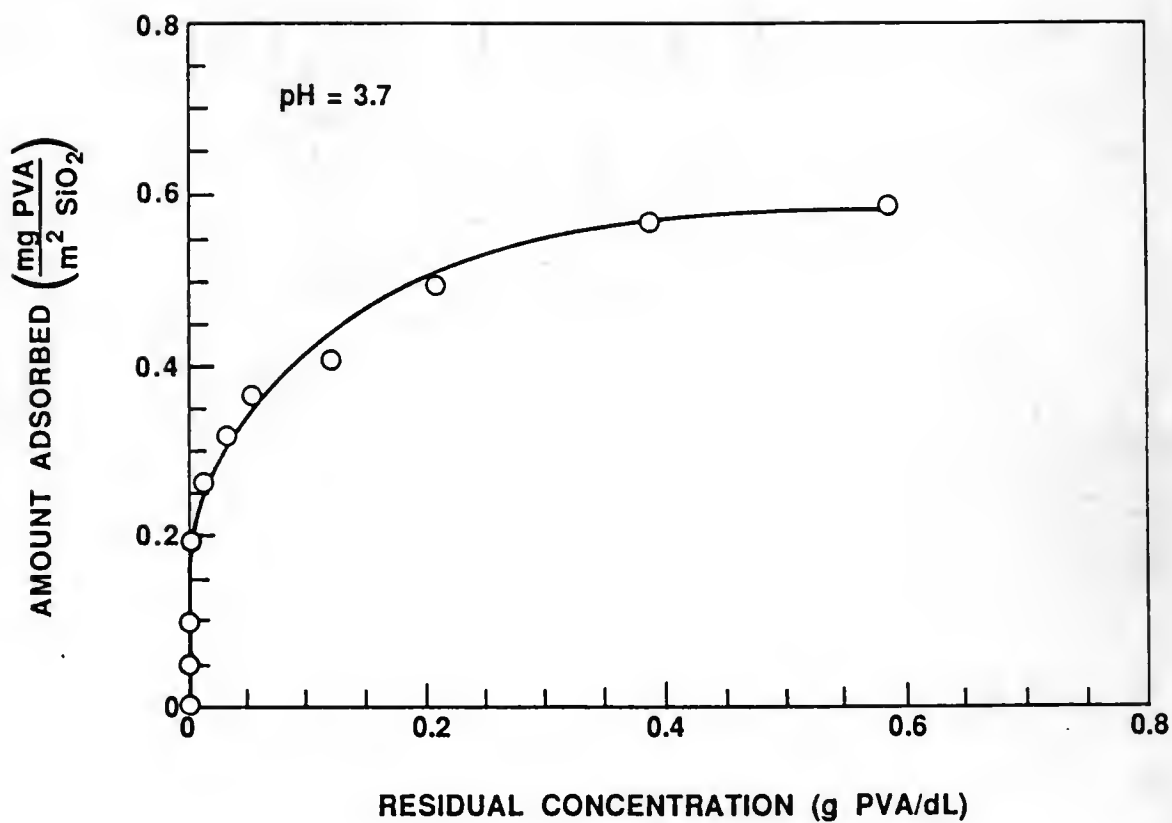
Figure 8.9   Adsorption isotherm for 20 vol.% SiO$_2$ suspensions
prepared with varying concentration of PVA with molecular
weight ≈ 24,000 at pH 3.7.

TABLE 8.1

Properties of Silica and PVA Used to Investigate the Effect
of Adsorbed Amount of PVA on the Suspension Properties

Silica

Geometric Mean Diameter	0.42	(μm)
Calcination Temperature	700	(°C)
Surface Area	8.0	(m^2/gram)

PVA

Viscometric Molecular Weight, M_ν	23,600	(g/mole)
% Hydrolysed	86	(%)
Radius of Gyration, $<s^2>^{0.5}$	7.8	(nm)

Suspension

Volume Fraction Silica, ϕ_p	0.2	
pH	3.7	
Ionic Concentration (NaCl)	1×10^{-2}	(moles/liter)

indicated in Figure 8.9, there is no residual polymer in the solution phase. With further increases in the overall polymer concentration, there is a more gradual increase in the amount adsorbed and also the residual polymer concentration increases. Eventually, the particle surfaces become "saturated" with adsorbed polymer as indicated by the "plateau" region of the isotherm in Figure 8.9. The rounded shape of the adsorption isotherm can be due to the preferential adsorption of large molecules at lower polymer concentrations (Koopal 81).

As discussed in Chapter II, the following changes in the conformation of the adsorbed polymer molecule with increase in PVA concentration in solution are expected.

At extremely low polymer concentrations ($\phi < 10^{-4}$), flatter conformation can be expected (where a relatively higher portion of segments can be adsorbed as trains and short loops with minimal portion in tails) under equilibrium conditions. With increasing polymer concentration in solution, the adsorbed amount is increased, and additional segments are accommodated into larger loops and tails giving a relatively thicker adsorbed polymer layer. Silica powder used for this study was calcined at 700°C and PVA was partially hydrolysed (Table 8.1). Hence, the hydrophobic bonding between the siloxane groups and the acetate groups and the hydrogen bonding between the isolated silanol groups and the alcohol groups may be involved in bonding of train segments to the silica surface.

Indirectly, some information on the conformation of adsorbed polymer can be obtained by comparison of the plateau adsorbed amount with the amount adsorbed in a close-packed monolayer. Koopal has estimated this

amount to be about 0.3 mg/m^2 (Koopal 78). Thus, at saturation adsorption, $\approx$ 50% of the adsorbed PVA is accommodated in the loops and tails. The saturated amount adsorbed is smaller than the PVA adsorption densities on AgI and PS-latex particles for comparable molecular weights. This reveals a significant importance of the chemical nature of the adsorbent surface on the plateau adsorbed amounts (and hence, on the conformation and on the layer thickness) (Killmann et al. 88).

The effect of the adsorbed amount of PVA on the suspension rheological behavior is illustrated in Figure 8.10. Figure 8.10A shows plots of relative viscosity versus shear rate with varying amounts of adsorbed polymer (0 - 0.19 mg PVA/m^2 SiO$_2$), while Figure 8.10B shows similar plots for larger adsorbed amounts (0.19 - 0.59 mg PVA/m^2 SiO$_2$). For comparison, the relative viscosity versus shear rate plot is shown for a suspension at pH = 7.3 with no added polymer. As discussed in the last section, at this pH, the suspension is extremely well dispersed due to the large zeta potential ($\approx$ -60 mV) which gives rise to strong electrostatic repulsive forces between the particles. Good dispersion is indicated by the low relative viscosity and the Newtonian flow behavior of the suspension. In contrast, the pH 3.7 suspension with no added PVA shows high relative viscosity and highly shear thinning behavior (Figure 8.10A). At this pH, the zeta potential is approximately zero and particles flocculate due to Van der Waal's attraction. The decrease in the viscosity with increasing shear rate can be attributed to the reversible breakdown of the flocculated network structure and the release of occluded liquid. With the initial additions of PVA (i.e., up to 0.19 mg PVA/m^2 SiO$_2$), the relative viscosity increases substantially and the
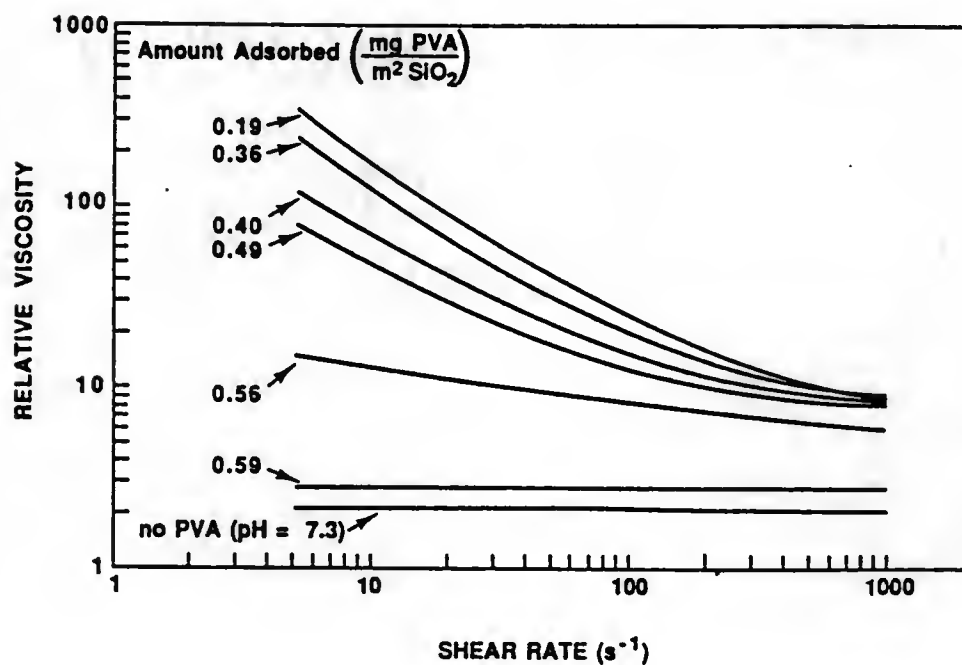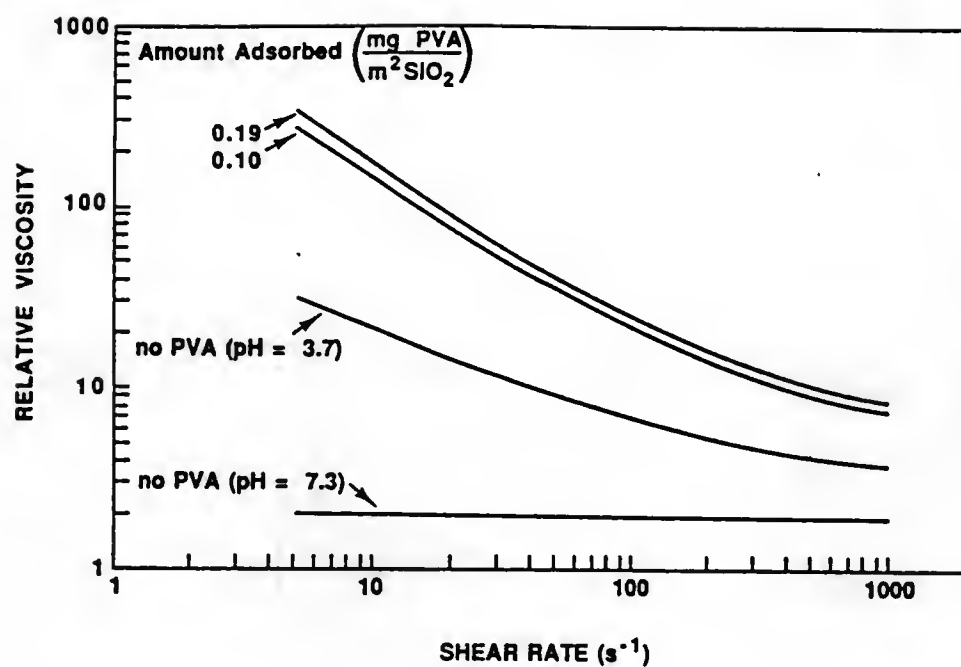
Figure 8.10   Plots of relative viscosity versus shear rate for 20
vol.% SiO$_2$ suspensions prepared at pH 3.7 with varying
PVA concentrations and pH 7.3 (-60 mV zeta potential)
with no PVA.

278

flow behavior is even more highly shear thinning. This indicates that a more open floc structure forms, i.e., due to polymer bridging flocculation.

As the amount of adsorbed polymer increases further (Figure 8.10B), there is a progressive decrease in the relative viscosities and the suspensions become less shear thinning. With increasing adsorbed amounts, the "mixing" and "elastic" contributions to the "elastic" contributions to the steric repulsive force increases, and close approach of particles is prevented (Chapter V). In addition, there is less chance for bridging flocculation to occur as the coverage of the particle surfaces increases. At the plateau coverage, the pH 3.7 suspensions show Newtonian behavior and low relative viscosity (Figure 8.10B). The viscosity is slightly higher compared to suspension with no added polymer. As discussed later in this chapter, this can be attributed to an increase in the "effective" volume fraction of solids in suspension due to adsorbed polymer layer.

The effects of the adsorbed amount of polymer on the rheological behavior can also be observed from the plots of extrapolated yield stress τ_β, relative viscosity η_{rel} (at shear rate 1000 s^{-1}), and hysteresis area H_{area} vs. absorbed amount of polymer (Figures 8.11, 8.12, and 8.13, respectively). Increases in τ_β, η_{rel}, and H_{area} with initial increases in the adsorbed amount of polymer is due to bridging flocculation of particles. With further increases in the surface coverage (i.e., adsorbed amount), a sharp decrease in the τ_β, η_{rel}, and H_{area} indicates improved stability of dispersion. At the plateau coverage, Newtonian flow behavior and lower relative viscosity were observed (i.e., τ_β and
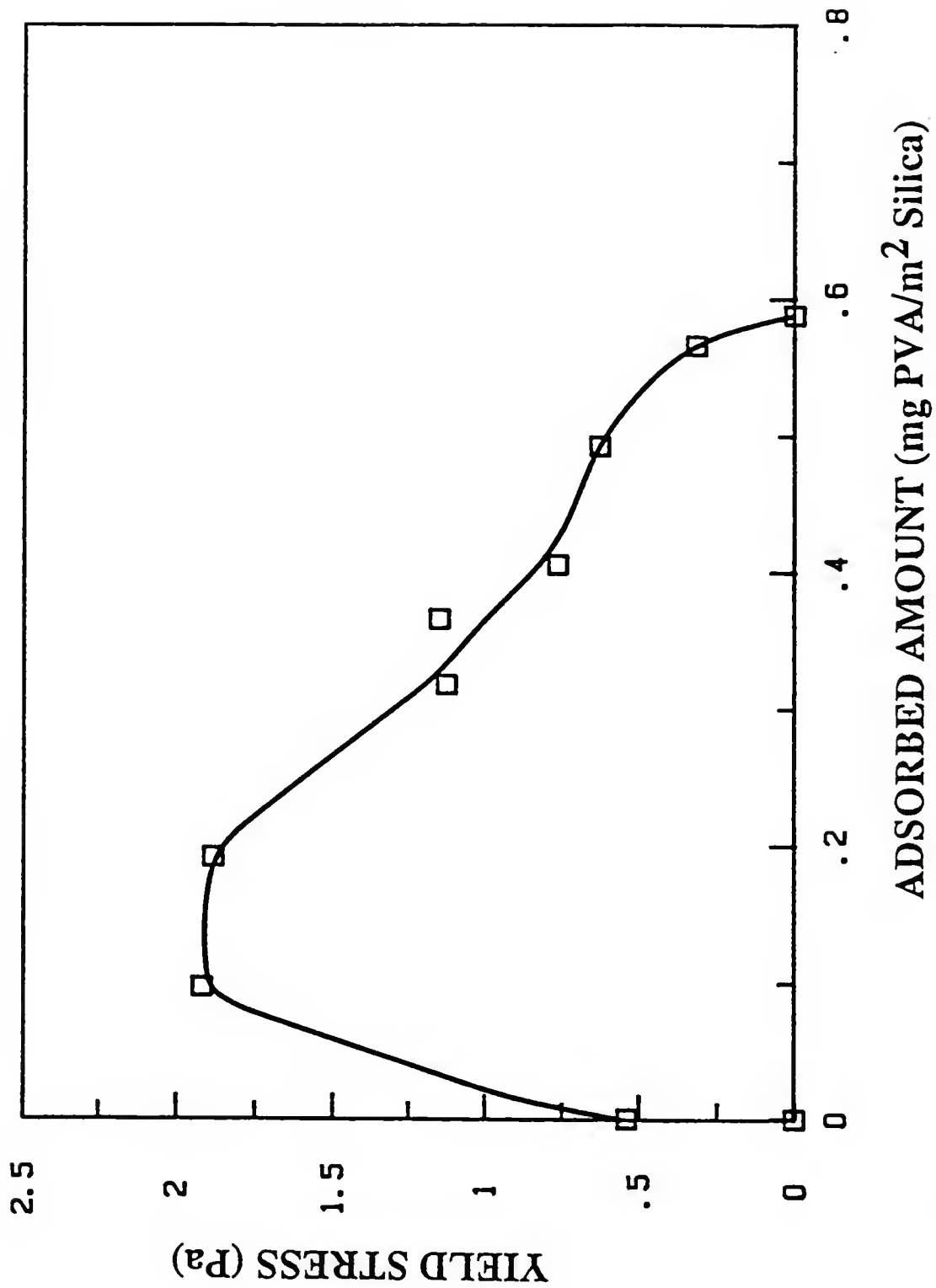
Figure 8.11 Plot of yield stress versus adsorbed amount of PVA with molecular weight ≈ 24,000 at pH 3.7.
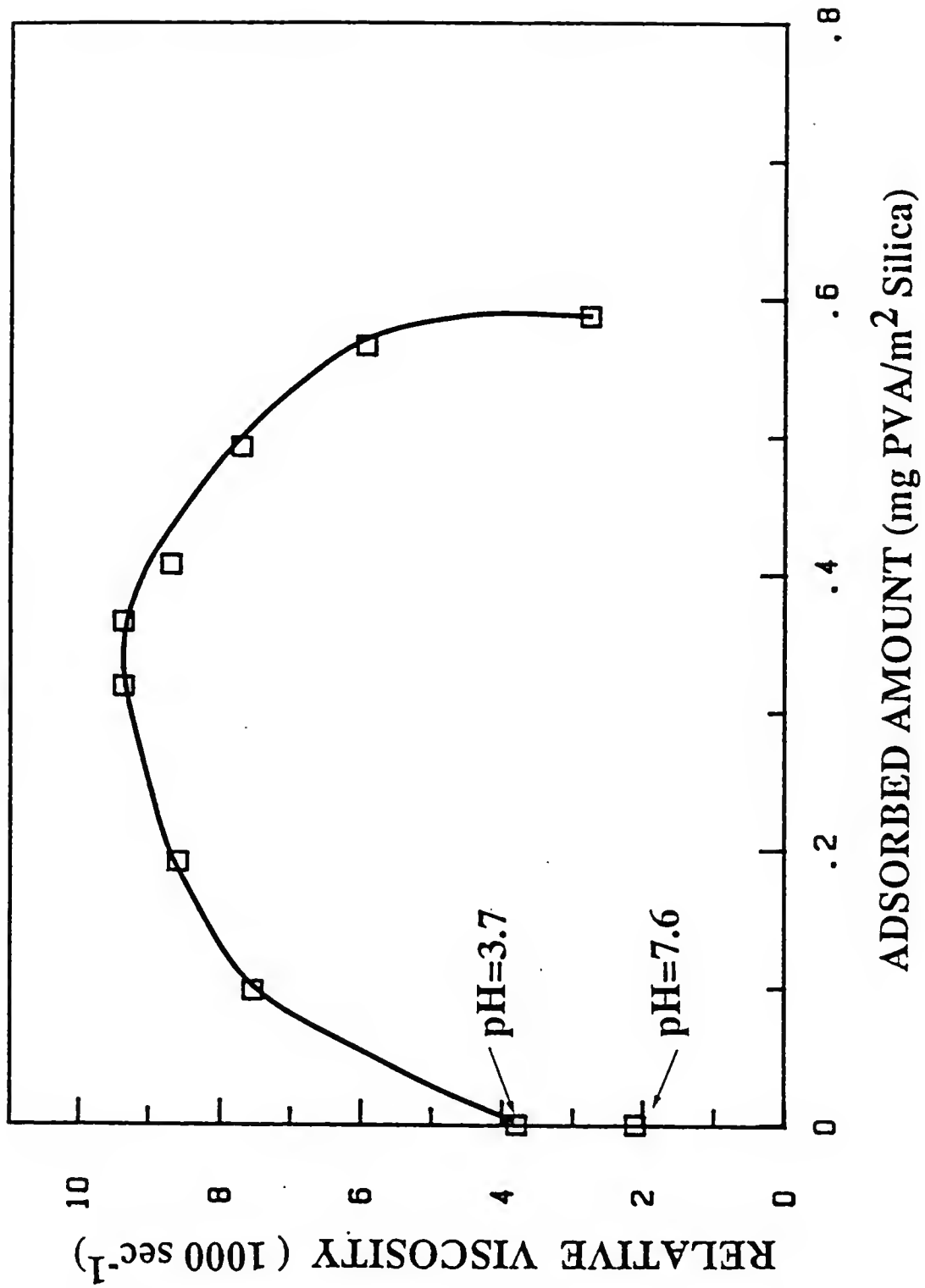
Figure 8.12   Plot of relative viscosity versus adsorbed amount of PVA for 20 vol.% SiO_2 suspensions prepared with varying PVA concentration.
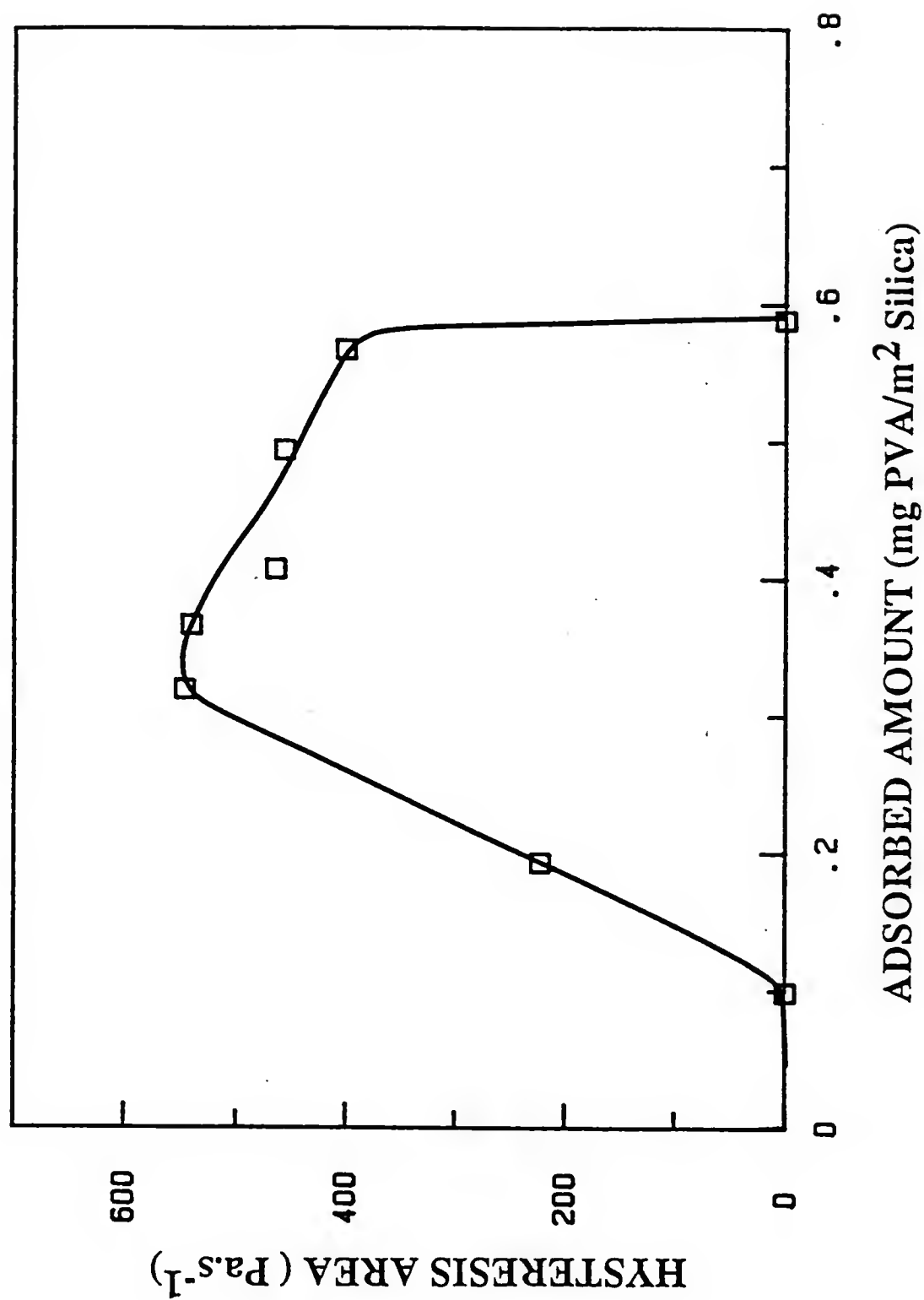
Figure 8.13   Plot of hysteresis area versus adsorbed amount of PVA of 20 wt.% SiO_2 suspensions.

$H_{area} = 0$ at the plateau coverage). We will discuss these results later in more detail.

The adsorption behavior and suspension rheology were correlated with the relative density of compacts formed by gravity sedimentation. Figure 8.14A shows the relative density as a function of the fraction of plateau coverage (i.e., the adsorbed amount divided by the plateau adsorbed amount. By doing so, as it will become clear later, it is possible to compare the effect of molecular weight, silica surface treatment, etc. on the same basis. The change in the conformation of polymer with adsorbed amount is ignored.) Figure 8.14B shows the corresponding plot of median pore radius vs. fraction plateau coverage. Figures 8.14A and 8.14B also show relative densities and corresponding median pore radii for compacts prepared from the suspensions without polymer. As described earlier, the electrostatically stabilized suspension (pH $\approx$ 7.3) produces highly ordered iridescent compacts with $\approx$ 64% relative density. Samples prepared from the flocculated (pH $\approx$ 3.7) suspension with no added polymer have lower relative density ($\approx$ 58%). With the initial additions of polymer, the relative density decreases ($\approx$ 53%) due to the more open floc structure formed due to bridging flocculation. This can be also seen from the increases in median pore radii with initial PVA additions (Figure 8.11B). As the surface coverage increases further, the relative density gradually begins to increase. This is consistent with the gradual decrease in the relative viscosity with increasing surface coverage that was observed in Figures 8.10 and 8.12. The relative density increases sharply (and median pore radius decreases sharply) as the amount of adsorbed polymer approaches the plateau coverage. Again,
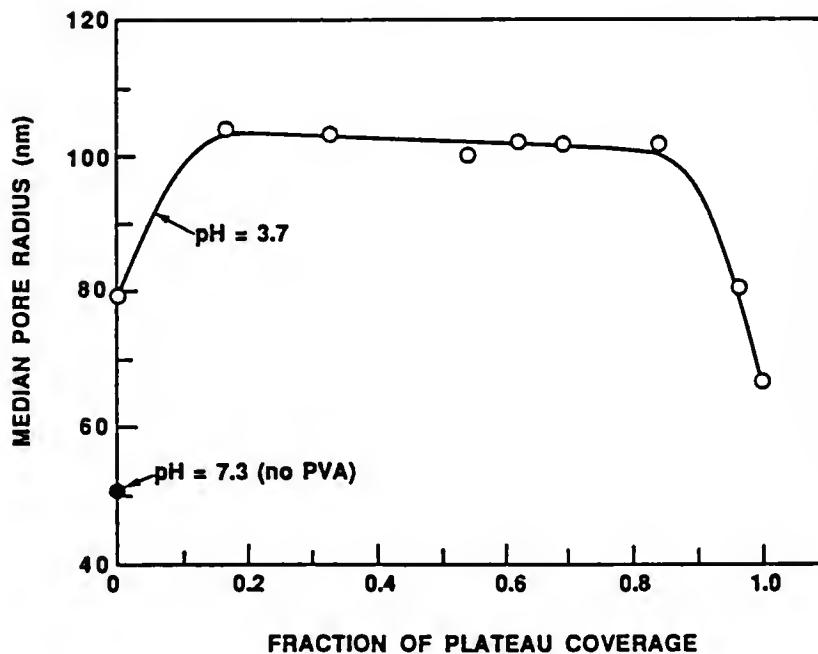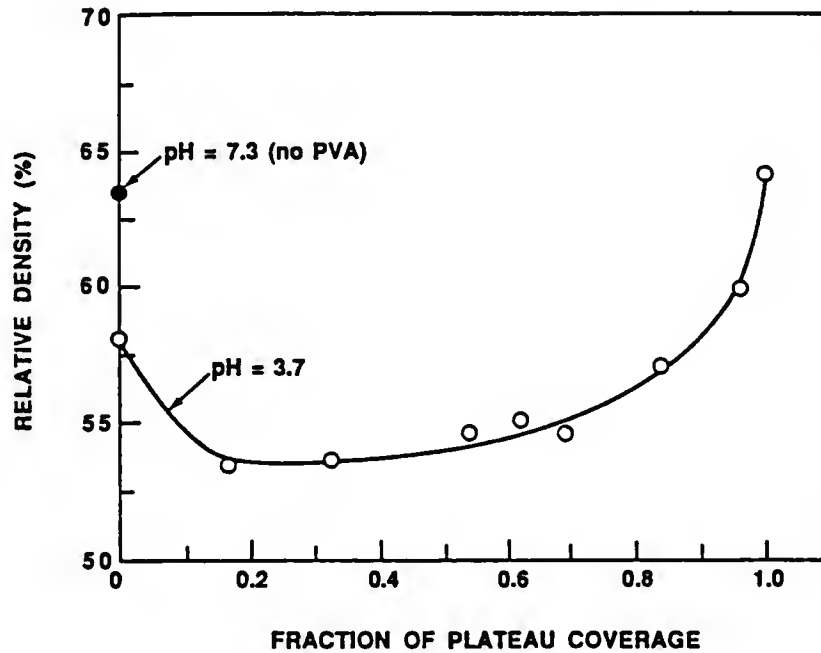
Figure 8.14   Plot of (a) sediment density versus
fraction plateau coverage and
(b) median pore radius versus fraction
plateau coverage for compacts prepared
from 20 vol.% SiO_2 suspensions with
varying PVA concentrations at pH 3.7
and pH 7.3 with no polymer.

this correlates well with the rheological data which shows that the particles are well-dispersed when plateau coverage is achieved. The relativity density obtained from the sterically stabilized suspensions is comparable ($\approx$ 63%) to the relative density from the electrostatically stabilized suspensions. From the above discussion, it is clear that the adsorbed amount (i.e., fraction of silica particles covered) is an important parameter controlling the rheological behavior of the suspension and the relative density of the compacts. This also shows that the silica particles can be sterically stabilized with the plateau adsorbed amount of polymer. As it will be shown later, complete coverage of particles is not a sufficient condition to achieve steric stabilization, but the adsorbed layer should be of sufficient thickness to overcome the Van der Waal's attraction.

Thus, in summary, two important factors controlling the stability of silica suspensions are (i) the fractional coverage and (ii) the thickness of the adsorbed polymer layer. The effect of various parameters (i.e., silica surface characteristics, particle size, PVA molecular weight, PVA degree of hydroxlyation, pH, ionic strength, etc.) will be described with reference to these two parameters.

Effect of Silica Calcination Treatment

Figure 8.15 shows the adsorption isotherms (mg PVA/m^2 SiO$_2$ versus residual polymer concentration) for silicas calcined at various temperatures for six hours. The properties of silica and PVA used are listed in Table 8.2. The adsorption isotherms are high affinity type. This can be due to high molecular weight PVA was used ($M_\nu \approx$ 215,000
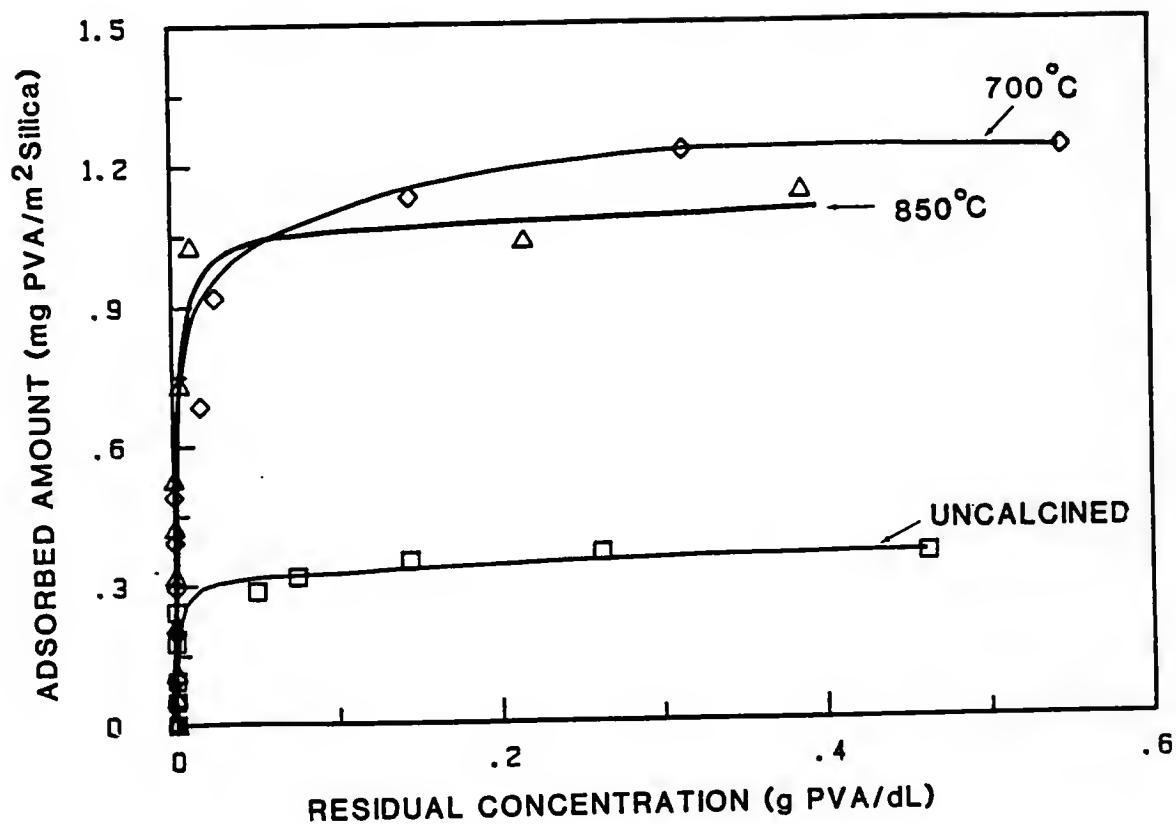
Figure 8.15   Adsorption isotherms for silicas calcined at various
temperatures with PVA molecular weight $\approx$ 215,000 at pH
3.7.

TABLE 8.2

Properties of Silica and PVA Used to Investigate the
Effect of Silica Calcination Temperature on the Suspension Properties

Silica

Geometric Mean Diameter	0.45	(μm)
Surface Area: Uncalcined, 300°C	8.07	(m^2/gram)
700°C Calcination	8.03	"
850°C "	7.51	"

PVA

Viscometric Molecular Weight, M_ν	215,000	(g/mole)
% Hydrolysed	90	(%)
Radius of Gyration, $<s^2>^{0.5}$	19.2	(nm)

Suspension

Volume Fraction Silica, ϕ_p	0.2	
pH	3.7	
Ionic Concentration (NaCl)	1×10^{-2}	(moles/liter)

g/mole). The plateau adsorbed amounts are the least for uncalcined silica, and the plateau adsorption was maximum for 700°C calcined silica. For silica calcined beyond 700°C, there was a decrease in the plateau adsorption density. This effect can be more clearly seen from Figure 8.16. Figure 8.16 shows a plot of plateau adsorbed amounts (mg PVA/m^2 SiO$_2$) as a function of silica calcination temperature. There was a more than three-fold increase between 300°C and 700°C. At higher temperatures, the adsorption density starts to decrease.

The observation of maximum in the plateau adsorption isotherm at 700°C is consistent with the observations of other investigators (i.e., PVA on silica-Tadros 78, poly acrylamide on silica-Griot and Kitchner 65, and PEO on silica-Rubio and Kitchner 76, Moudgil and Cheng 86). This maximum in the adsorption density has been correlated with the optimal concentration of isolated or "free" silanol groups (See Figure 7.1). The concentration of isolated silanol groups increases in the range of 300 to 700°C and decreases in the temperature range above approximately 700°C (Sacks et al. 87, Hair 67). The decrease in the plateau adsorption density beyond 700°C has been correlated with decrease in the concentration of "isolated" silanol groups for PEO adsorption on silica (Rubio and Kitchner 76). For PVA adsorption, the maximum adsorption density has been associated with the optimal concentrations of (i) siloxone groups and (ii) isolated silanol groups, (i.e., for the maximum in adsorption, the ratio = (concentration of silanol groups)/(concentration of silanol groups) should be optimal-Tadros 78). Tadros, Rubio and Kitchner have observed a sharp decrease in the adsorption density on Cab-O-Sil silica above 700°C (Tadros 78, Rubio and
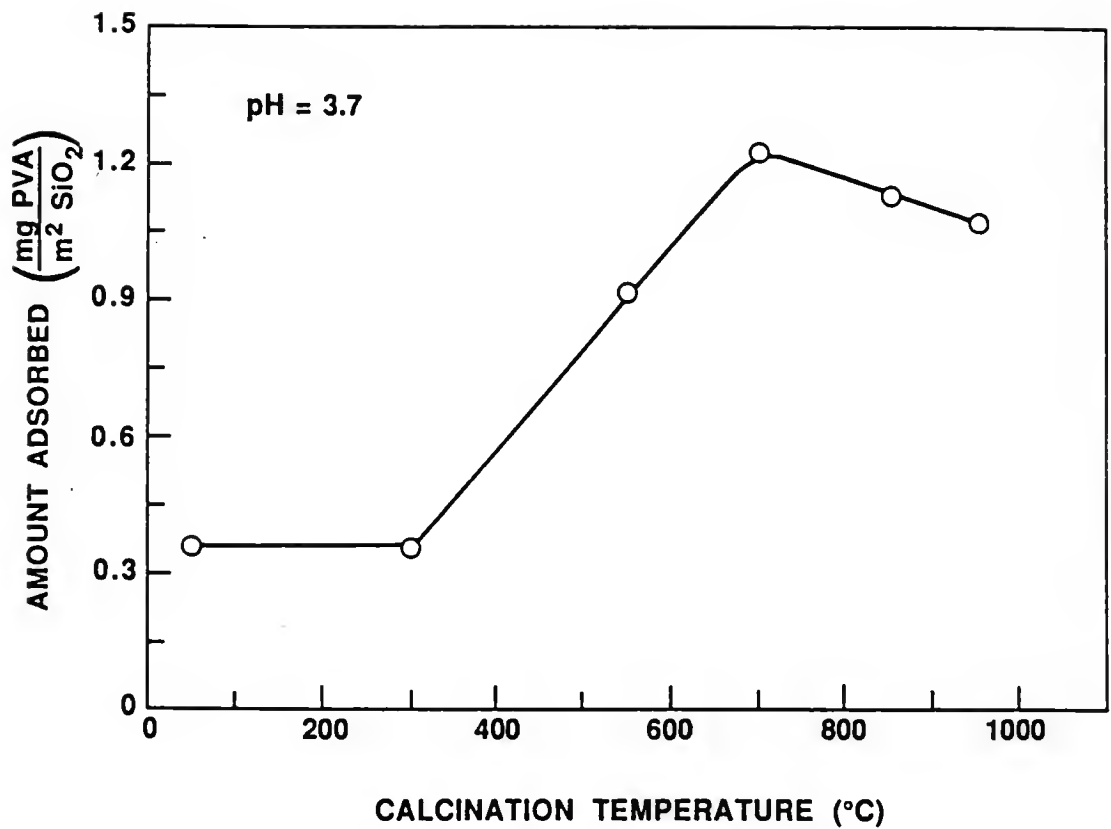
Figure 8.16 Plot of plateau adsorbed amount versus silica calcination temperature.

Kitchner 76). Their data is replotted in Figure 8.17. Our results also show a decrease in the adsorption density above 700°C. But, we did not observe a sharp decrease as reported in Figure 8.17. This difference may be due to differences in surface structures of these two silica (Tadros and Rubio and Kitchner used Cab-O-Sil silica, whereas we used Stober silica).

The silica surface of uncalcined powder is completely covered with silanol groups, and hence, silica surface is hydrophilic. Since the acetate groups are strongly hydrophobic (Cohen Stuart 80a, Koopal 78, Barnett et al. 82), it can be expected that the bonding mechanics involves the hydrogen bonding between the silica silanol groups and the hydroxyl groups of the polymer for uncalcined powder. For low temperature calcined silicas, the plateau adsorption densities are lower because most of the hydroxyl groups on the silica surface form hydrogen bonds with neighboring hydroxyl groups and physisorbed molecular water (i.e., silanol groups are "bonded") and therefore, are unavailable for bonding with PVA hydroxyl groups (Sacks et al. 87). With increase in the calcination temperature, more silanol groups are removed (Figures 7.2 and 7.3), rendering relatively hydrophobic character to silica surface (siloxane bonds $\equiv S_i - 0 - S_i \equiv$). Also, the concentration of "isolated" silanol groups increases with increases in calcination temperature between 300 to 700°C. Thus, for high temperature calcined silica, hydrophobic bonding (between acetate groups of polymer and siloxane groups) and hydrogen bonding (between hydroxyl groups of polymer and isolated silanol groups) are important mechanisms for PVA adsorption (Tadros 78).
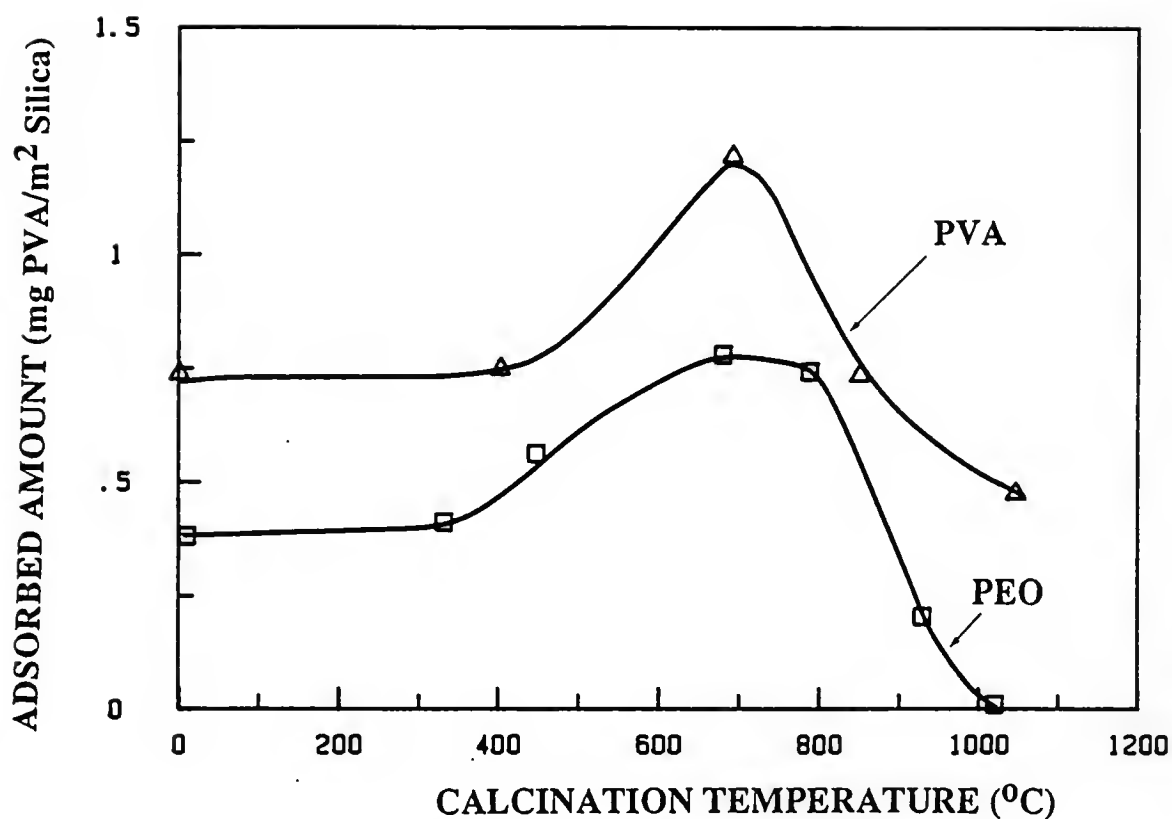
Figure 8.17   Plots of plateau adsorbed amount versus silica
calcination temperature for (a) PEO adsorption on Cab-O-
Sil (Rubio and Kitchner, 1976) and
(b) PVA adsorption on Cab-O-Sil (Tadros, 1978).

The effect of increasing adsorption density on the rheological behavior is illustrated in Figure 8.18 which show plots of relative viscosity versus shear rate for suspensions prepared with uncalcined and calcined powders. With uncalcined powders, the suspensions show high relative viscosities and highly shear thinning behavior indicating strong flocculation. In contrast, the suspension prepared with the powder calcined at 700°C has much lower relative viscosities and shows slight shear thinning behavior. The effect of calcination on rheological behavior can be also seen from plots of τ_β, relative viscosity, and hysteresis area vs. silica calcination temperature (Figures 8.19, 8.20, and 8.21, respectively). The decrease in τ_β, relative viscosity, and hysteresis area with increase in calcination treatment indicates improved suspension stability. The improved stability of 700°C calcined silica can be explained as follows:

With increase in the amount adsorbed, it can be assumed that the adsorbed layer thickness increases. From electrophoretic measurements, Koopal has shown that the adsorbed layer thickness is a unique function of amount adsorbed (i.e., it is independent of acetate content and molecular weight of the polymer, Figure 2.3--Koopal 78). The additional material is accommodated into larger loops and more importantly into longer tails with increasing adsorbed amounts. The effect of the adsorbed amount (hence, adsorbed layer thickness) on the total interaction energy curve is shown in Figure 8.22. Figure 8.22 shows the total interaction energy of interaction as a function of distance of separation plots with varying adsorbed amounts of polymers. These curves are plotted using equations developed by Bagchi for the interaction
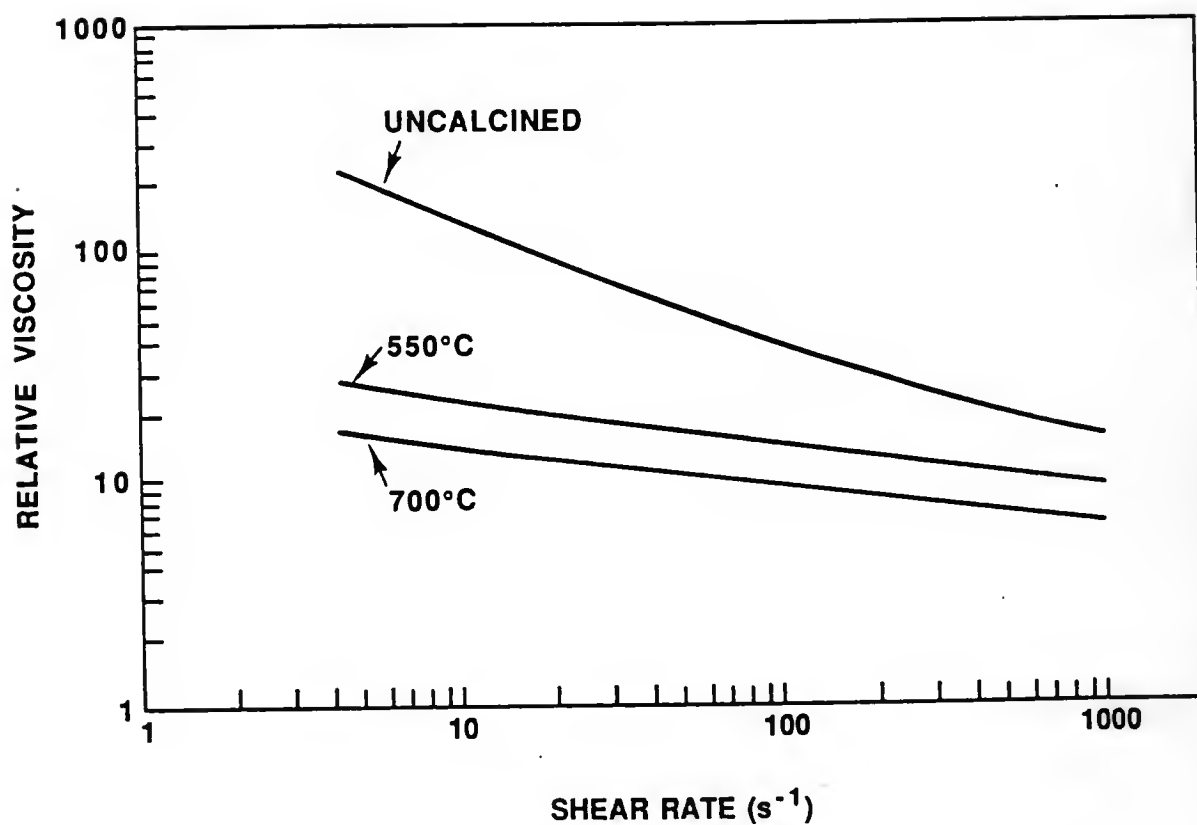
Figure 8.18   Plot of relative viscosity versus shear rate for 20 vol.%
                suspensions prepared with uncalcined silica and with
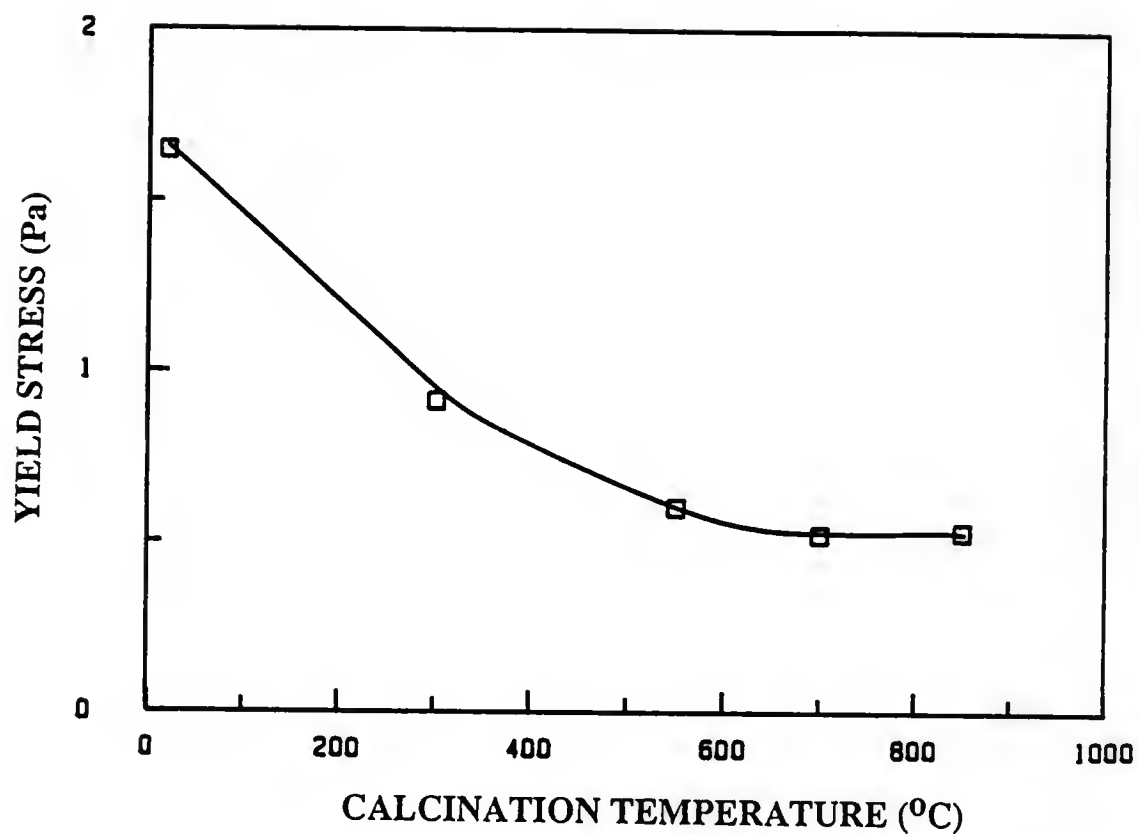   silica powder calcined at 500°C and 700°C.

Figure 8.19   Plot of yield stress versus calcination temperature for 20 vol.% silica suspensions at pH 3.7 prepared with silica particles calcined at various temperatures. PVA concentration in solution was sufficient to achieve plateau coverage of the silica particles.
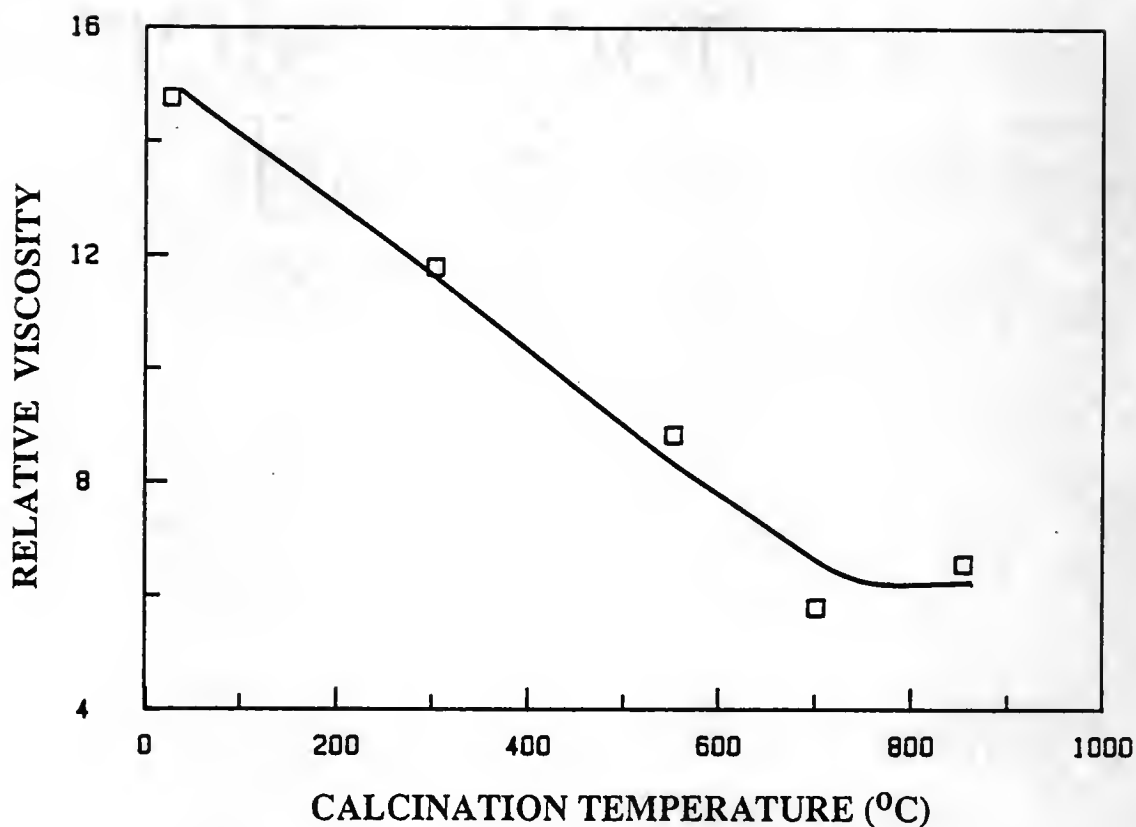
Figure 8.20   Plot of relative viscosity versus calcination temperature
for 20 vol.% silica suspensions at pH 3.7 prepared with
silica particles calcined at various temperatures. PVA
concentration in solution was sufficient to achieve
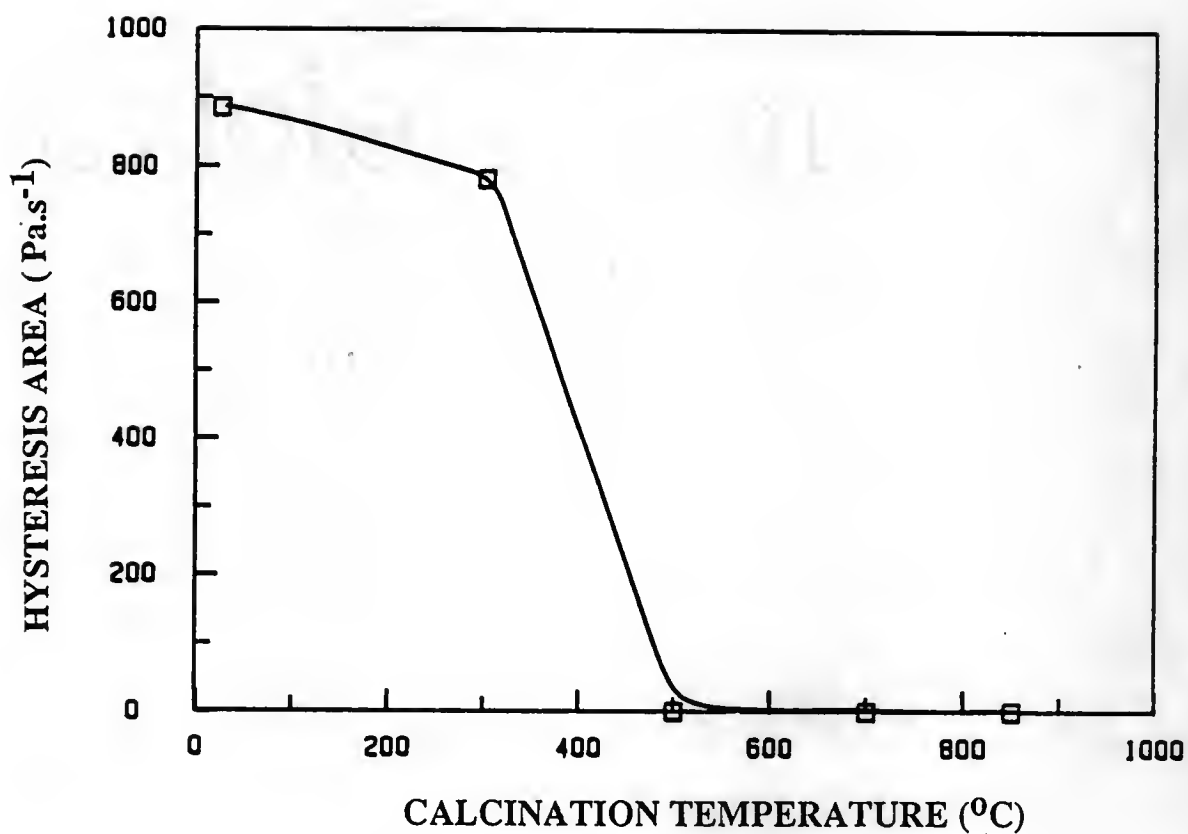plateau coverage of the silica particles.

Figure 8.21   Plot of hysteresis area versus calcination temperature
for 20 vol.% silica suspensions at pH 3.7 prepared with
silica particles calcined at various temperatures.   PVA
concentration in solution was sufficient to achieve
plateau coverage of the silica particles.

between particles under the assumption of constant segment density in the adsorbed polymer layer (Bagchi 74a). (Any other form of the segment density distribution will not affect the explanation.) With close approach of two particles under Brownian motion, "mixing" and "elastic" interactions will cause the repulsion between particles (water being better than the θ solvent). Direct force measurements between two adsorbed PVA layers has been measured by Lubetkin under "restricted" equilibrium conditions (i.e., no polymer is allowed to leave the gap between approaching surfaces) and under "dynamic" conditions (surfaces were brought together rapidly) (Lubetkin 88). It was observed that the repulsion measured under equilibrium was much smaller than that observed under dynamic conditions. Thus, under short duration involved during Brownian collision, the polymer may not have sufficient time for reconfiguration and strong repulsion will be felt due to overlap of the adsorbed layers. With sufficiently thick adsorbed polymer layer, the distance of close approach is reduced, and hence, the depth of the valley for the total interaction energy due to Van der Waal's attraction is decreased and suspension is sterically stabilized.

The flocculation of suspensions prepared with uncalcined silica with the plateau surface coverage can be explained as follows:
(i) The adsorbed layer thickness on uncalcined silica is not sufficient to prevent the flocculation due to Van der Waal's attraction. Killmann et al. have measured the hydrodynamic thickness of adsorbed PVA layer (for partially and fully hydrolysed PVA's) on precipitated silica (Stober) and PS latex particles (Killmann et al. 88). The measured hydrodynamic thickness for partially hydrolysed PVA at the plateau
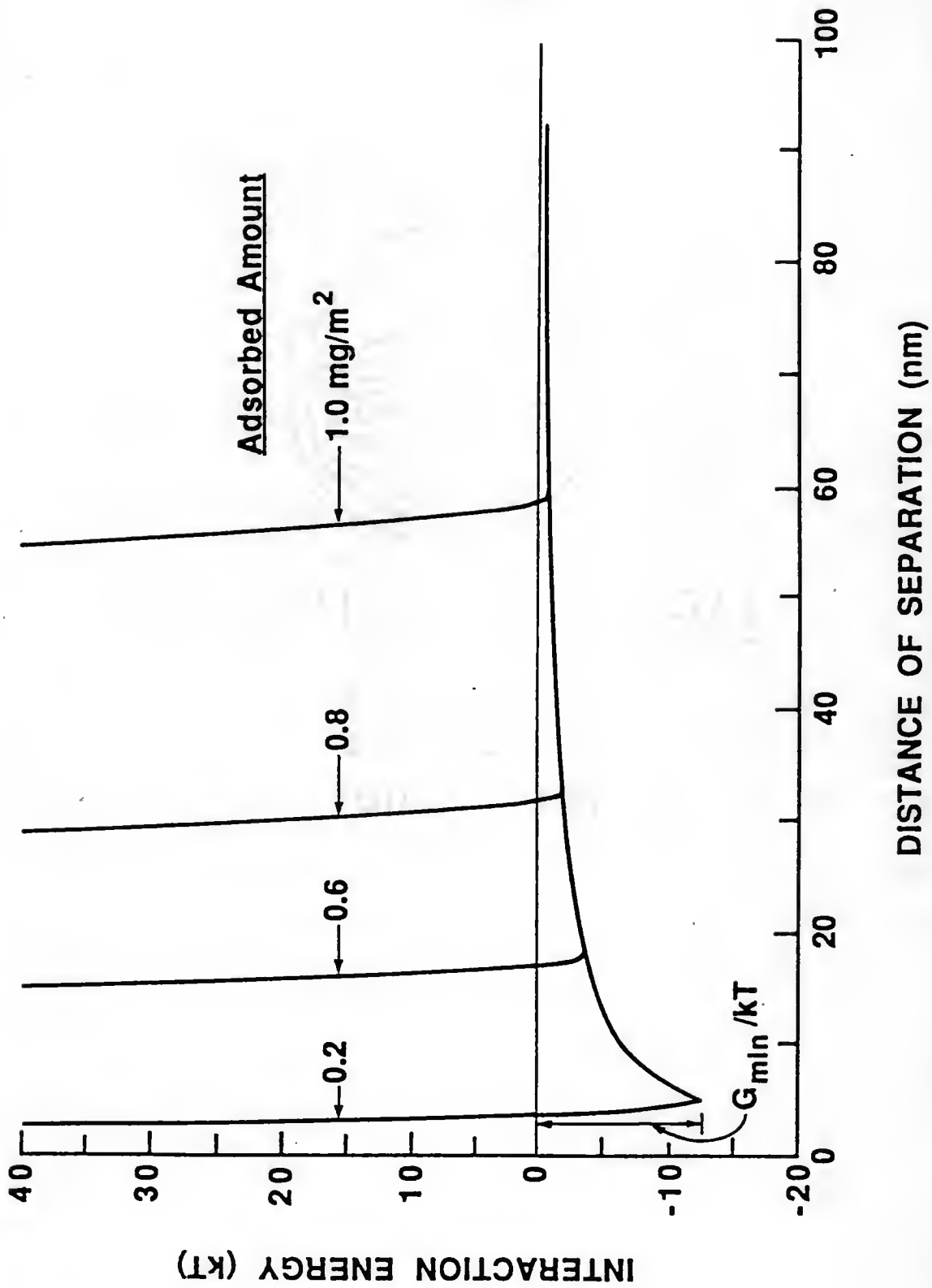
Figure 8.22   Schematic plot of the total interaction energy versus distance of separation between two polymer-coated particles with varying adsorbed amounts (Khadilkar and Sacks, 1988).

coverage was smaller on the precipitated silica surface (which is hydrophilic) compared to the latex surface (which is hydrophobic). Since the tails have a dominant influence on the hydrodynamic thickness (Cohen Stuart et al. 84a,84b,86a,86b), they concluded that there is a smaller fraction of segments in tails (and consequently, a higher fraction of segments in trains) on silica than latex (Killmann et al. 88). In our case, 700°C silica surface can be assumed to be more similar to the hydrophobic surface of latex particles, and different energetic interactions are responsible for different thicknesses on uncalcined and calcined silica powders.

(ii) Since the hydrogen bonding between silanol groups and alcohol groups of the PVA appears to be mainly responsible for the adsorption on uncalcined silica, it can be expected that the concentration of unadsorbed acetate groups (which are hydrophobic) at the outer side of the adsorbed layer remains relatively high. (In contrast, the preferential adsorption of hydrophobic acetate groups will lead to lower concentration of acetate groups at the periphery of the adsorbed layer for 700°C calcined silica.) The hydrophobic interaction between the acetate groups may give rise to additional attraction between particles.

The hydrophobic interactions are assumed to be responsible for 'cocervation' (i.e., phase separation of polymer solution) of PVA coated particles (Iler 75). The cocervation was observed when the adsorbed amount was just enough to form a monolayer with most of the OH groups of PVA oriented towards the silica surface and hydrogen bonded with the silanol groups on the silica surface as shown in Figure 8.23A. Externally, the particles are covered with the $-CH_2CH-$ backbone and
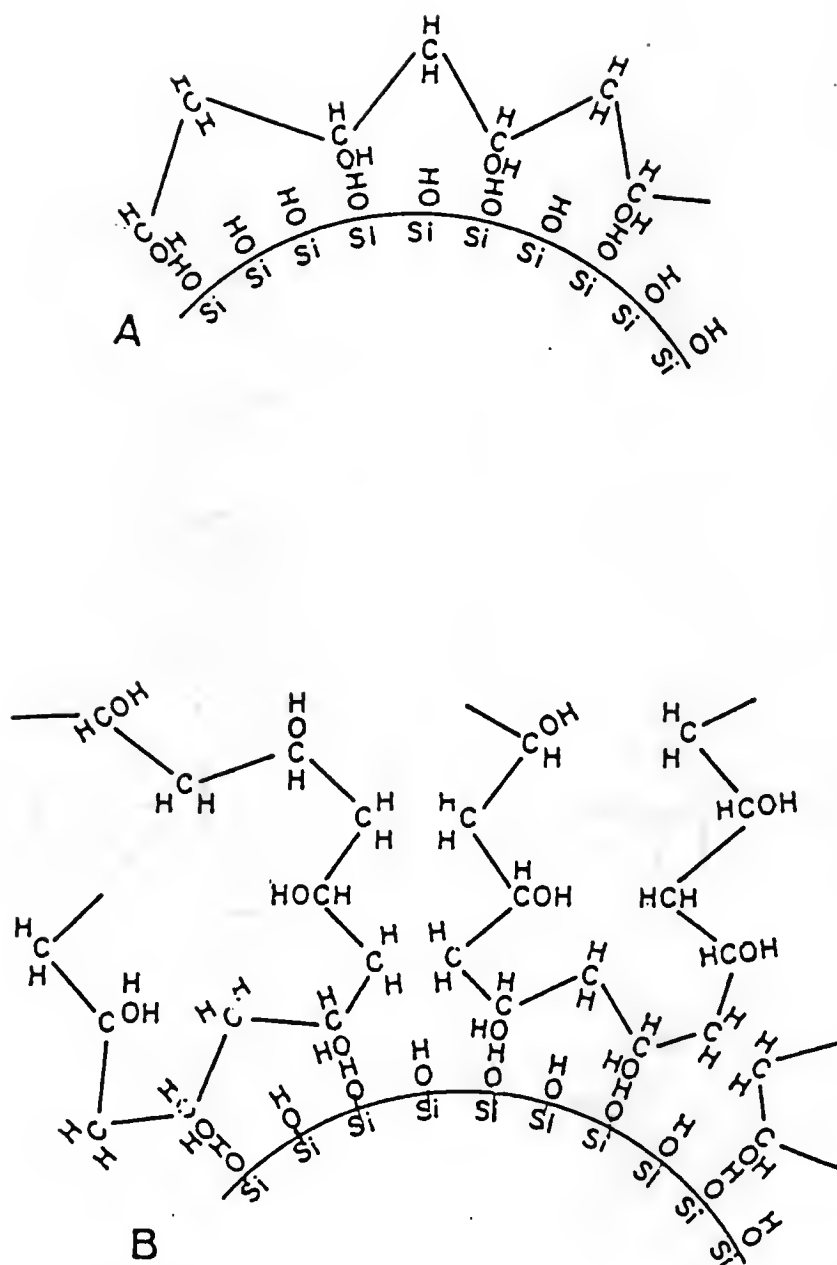
Figure 8.23   Schematic illustration (a) showing silica surface covered
with only enough PVA to make particles hydrophobic and
(b) excess of PVA adsorption prevents cocervation (Iler,
1976).

acetate segments of PVA chain which makes the silica surface somewhat hydrophobic. The hydrophobic bonding between particles leads to phase separation (Iler 75). The maximum yield of cocervation was observed by Iler when the adsorbed amount was $\approx$ 0.15 mg/m^2 (i.e., when three CHOH groups per square nonometer are present). Cocervation was not observed if there was an excess polymer present so that only a portion of each chain is attached to the surface (see Figure 8.23B). As shown in Figure 8.23B, excessively coated particles do not become hydrophobic and no cocervation was observed (Iler 76).

The hydrophobic attraction between acetate groups has been measured in the case of two liquid hepatene drops immersed in a PVA solution (Babak 88). The schematic of disjoining pressure as a function of distance of separation for two parallel water films stabilized with PVA is in shown in Figure 8.24. For comparison, the disjoining pressure curve for homopolymer is also shown in Figure 8.24. In the absence of specific interactions, repulsion is felt between two adsorbed layers due to "mixing" and "entropic" reasons. The specific attraction component (due to the hydrophobic interactions between acetate groups) in the case of PVA can lead to strong attraction between adsorbed layers upon compression, as shown in Figure 8.24. These hydrophobic interactions between the acetate groups may be responsible for a loss of stability of suspensions after compression, centrifugation or ultrafiltration (i.e., suspensions with adsorbed PVA after centrifugation cannot be redispersed easily).

The hydrophobic interactions between acetate groups does not seem to explain the flocculation of uncalcined silica suspension as we did not
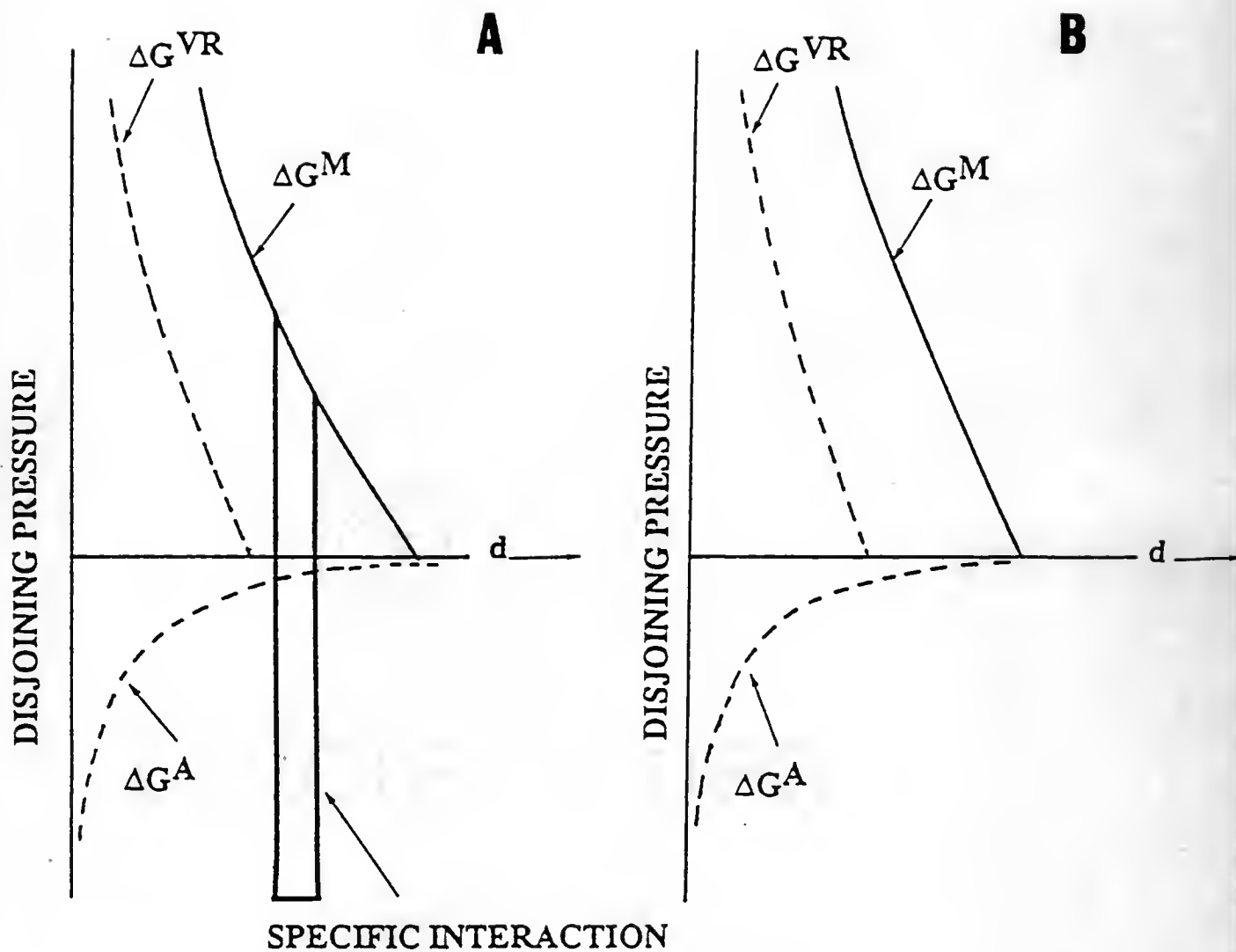
Figure 8.24   Schematic plot of (a) disjoining pressure as a function
of distance of separation for two parallel water films
stabilized with PVA film and (b) disjoining curve for
homopolymer. The specific attractive component in the
case of PVA derives from the hydrophobic interactions
between acetate groups (Babak, 1988).

observe the cocervation at any coverage, and suspensions prepared from uncalcined silica were unstable at partial as well as at complete coverage contrary to Iler's observation. This indicates that the insufficient adsorbed layer thickness seems to be the correct explanation for our experimental observations.

The effect of silica calcination temperature on the green compact characteristics is shown in Figure 8.25. Figure 8.25A shows the relative green density versus silica calcination temperature for slip cast samples. Relatively low slip cast sample density ($\approx$ 55 %) was obtained for samples prepared from the flocculated suspensions of uncalcined silica. In contrast, the higher relative density ($\approx$ 61%) was obtained from the well dispersed suspensions of 700°C calcined silica. Figure 8.26 shows plots of specific volume frequency as a function of pore radius for slip cast samples prepared with uncalcined and 700°C calcined silica. The cast samples of uncalcined silica have lower relative densities and relatively larger pore radii compared to compacts prepared from 700°calcined silica. Next, we will examine the effect of calcination temperature on the rheological behavior at partial coverages for uncalcined and 700°C calcined silica powders.

Figure 8.27 shows plots of relative viscosity (at moderate shear rate of 1000 sec^{-1}) versus adsorbed amount (mg PVA/m^2 SiO$_2$) and corresponding plots of relative viscosity versus fraction surface coverage (i.e., adsorbed amount/ plateau absorbed amount) for uncalcined and 700°C calcined silica powders. At low coverages (or adsorbed amounts), the relative viscosity of the 700°C calcined silica suspensions is higher than uncalcined silica suspensions. The relative viscosity at
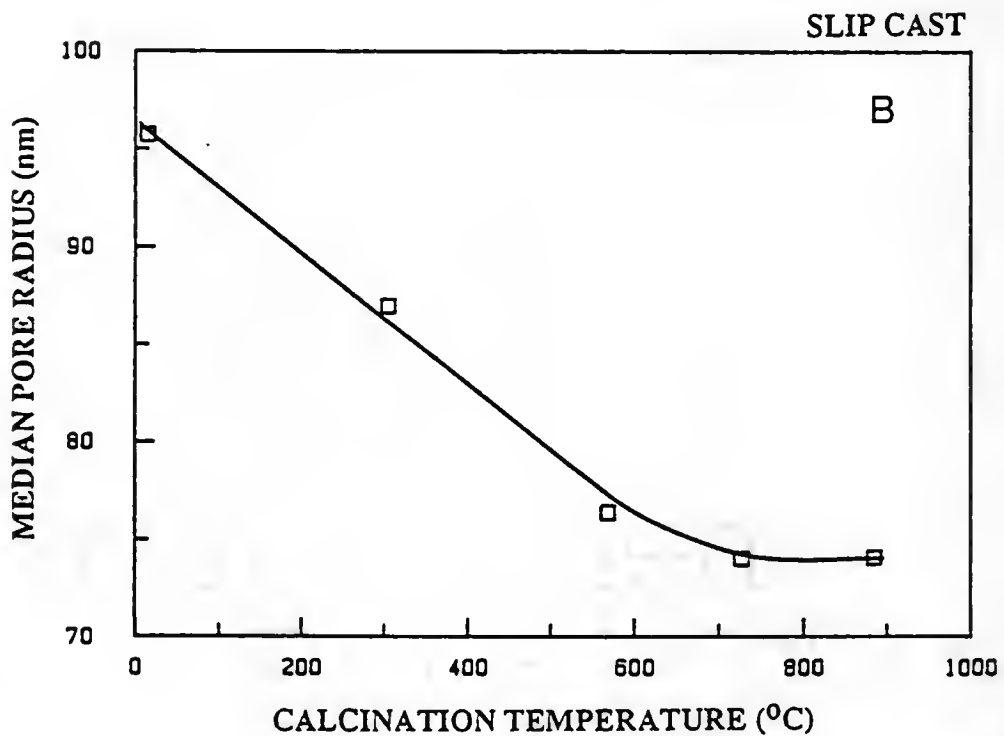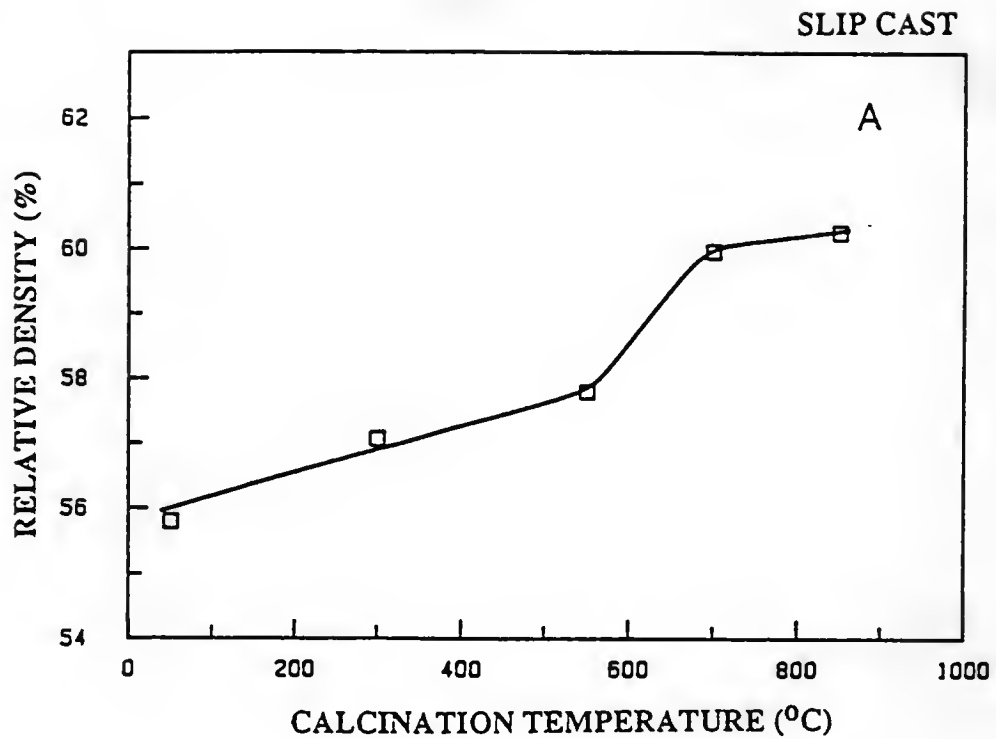
Figure 8.25   Plot of (a) relative density for slip cast samples versus silica calcination temperature and (b) median pore radius versus silica calcination temperature.
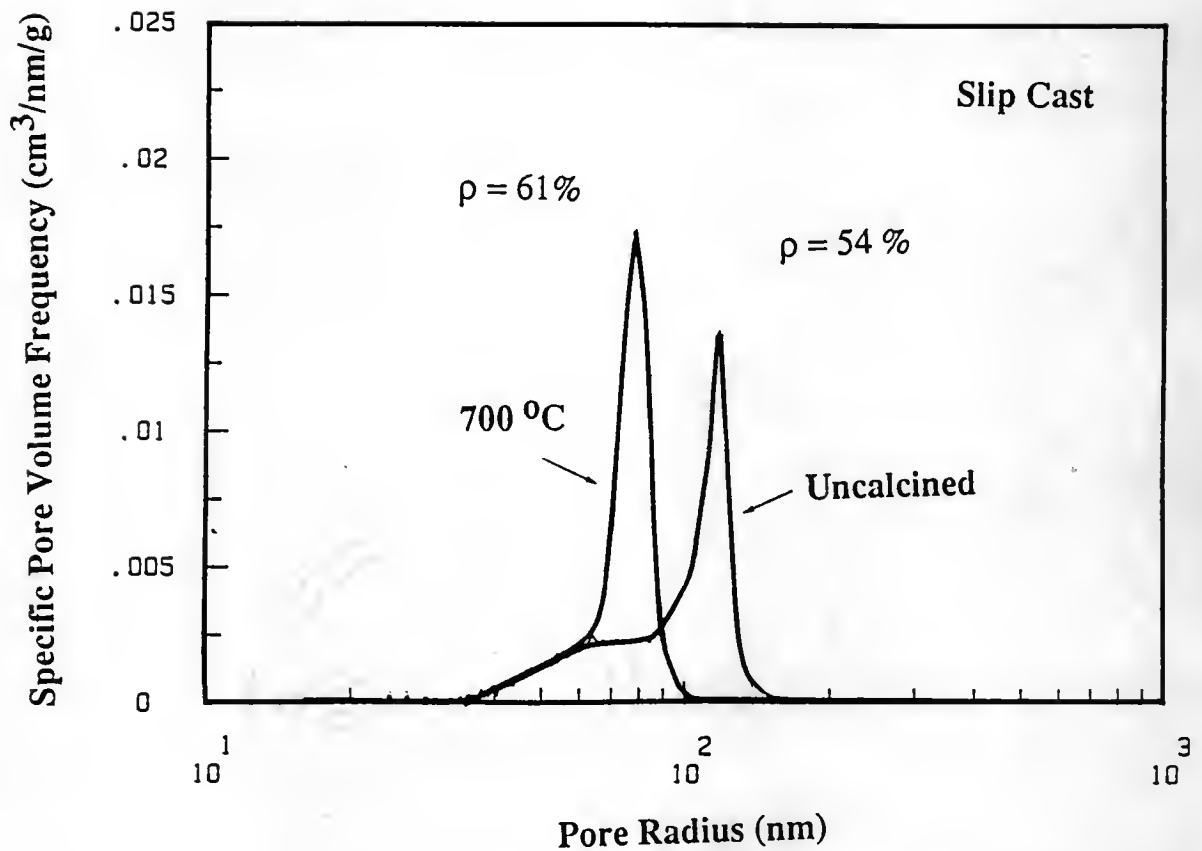
Figure 8.26   Plot of mercury porosimetry data for slip cast samples
prepared from uncalcined and 700°C calcined silica
powders.   Samples were prepared from 20 vol.% silica
suspensions at pH 3.7 with the plateau coverage of SiO_2
particles with PVA of molecular weight $\approx$ 215,000.

high shear rate can be used to estimate the effective volume fraction of solids in suspension. The higher relative viscosity (compared to viscosity of well dispersed suspension) indicates the higher effective volume fraction of solids, ϕ_F, in the suspension. Since both suspensions were prepared with ϕ_p = 0.2, it can be concluded that the flocs (or floc aggregates) formed for 700°C silica are relatively more open compared to flocs formed from uncalcined silica (see Figure 8.28). At partial surface coverages with adsorbed PEO, Killmann et al. also observed dense "granular" flocs with precipitated silica at pH ≈ 3.0 whereas more "structured" (i.e., open) flocs with calcined silica (Killmann et al. 86). Two factors can contribute to the formation of more open structures with 700°C calcined silica.

(i) PVA adsorbs more readily on the 700°C calcined silica and can bridge particles more effectively.

(ii) The adsorbed layer thickness is larger on calcined silica (due to relatively larger loops and tails) compared to uncalcined silica (relatively smaller loops and tails, i.e., flatter conformation). (Please note: the unique dependence of adsorbed layer thickness on the amount adsorbed (i.e., independent of PVA acetate content and molecular weight) has been demonstrated for the plateau adsorbed amounts of polymers, but this may not be true at partial coverage). As described earlier, specific surface interactions may play an important role in determining the adsorbed layer properties. Schematic of illustration of floc structures for calcined and uncalcined silica powders are shown in Figure 8.28. Wong et al. have applied the small angle neutron scattering, SANS, technique to study the aggregate structure of
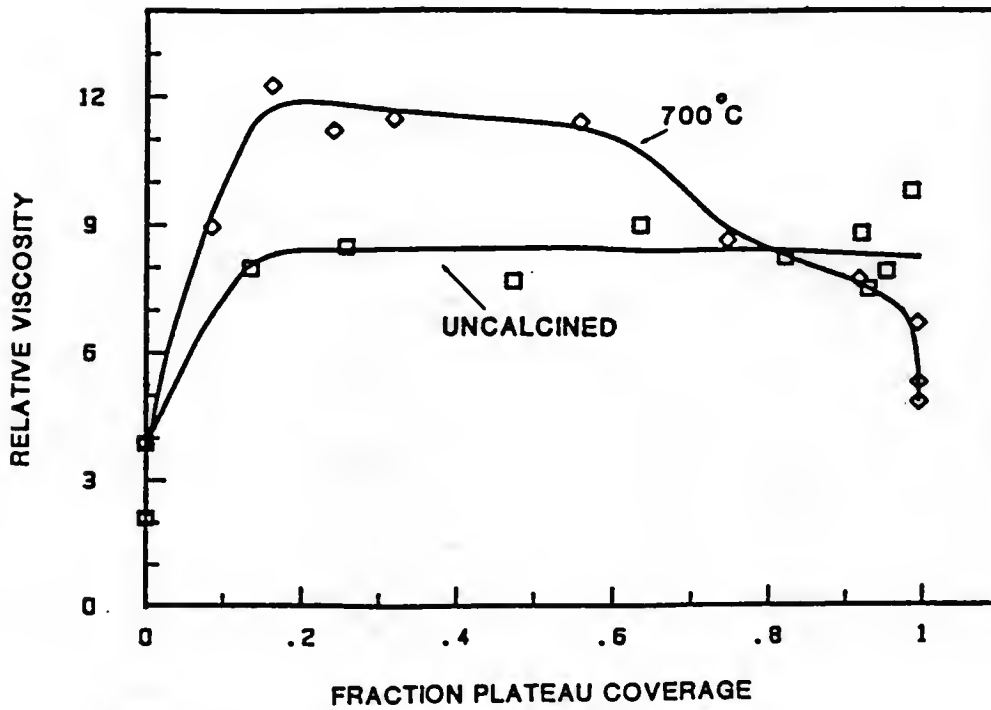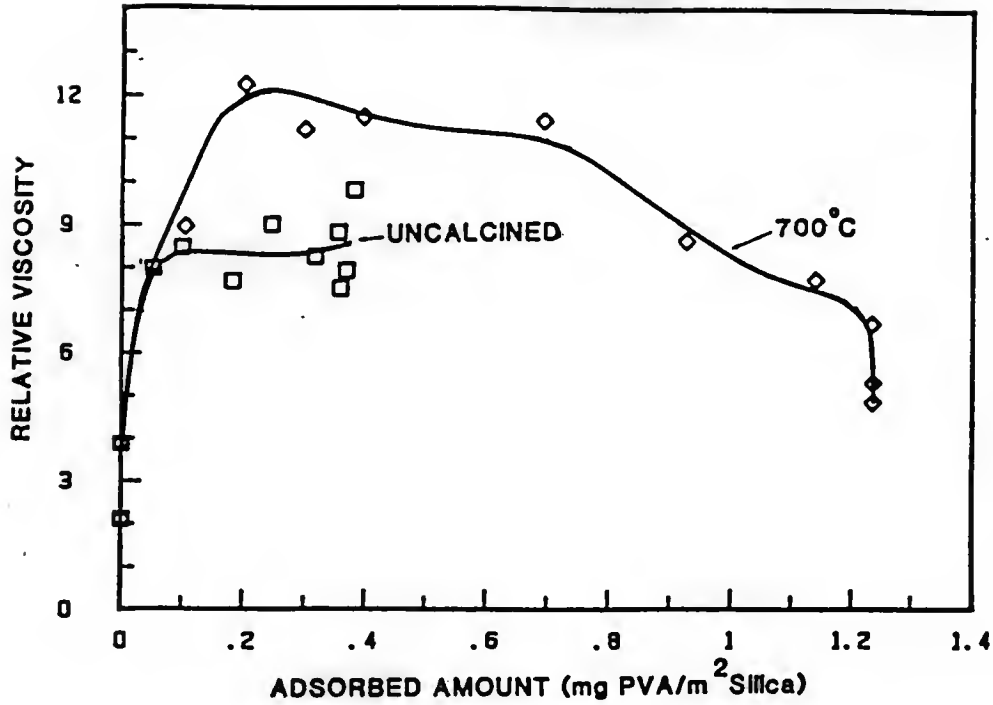
(SHEAR RATE 1000 SEC^{-1})

Figure 8.27   Plot of (a) relative viscosity versus adsorbed amount and (b) relative viscosity versus fractioned plateau coverage for 20 vol.% SiO_2 suspensions prepared with uncalcined and 700°C calcined powders.
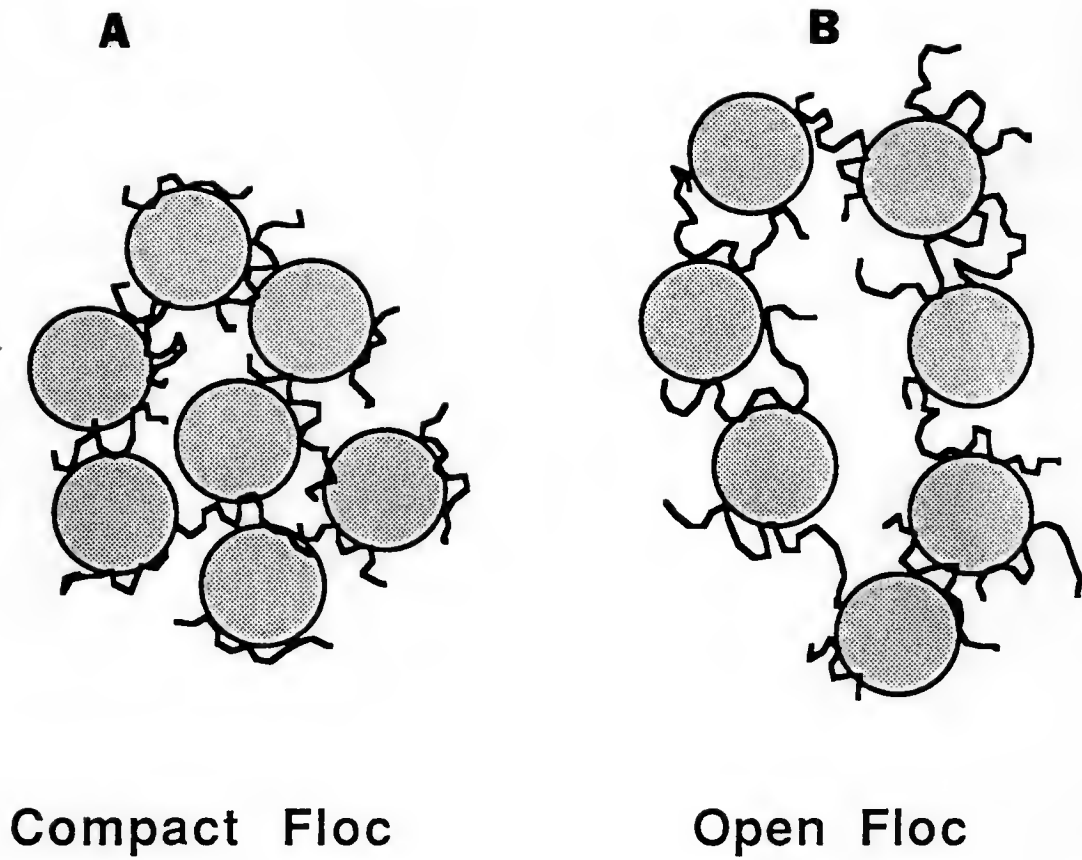
Compact Floc

Open Floc

Figure 8.28   Schematic illustration of floc structures formed with
a) uncalcined silica particles and b) with 700°C calcined
silica particles at low surface coverages with adsorbed
polymer.

precipitated silica (Stober silica of ≈ 0.04 μm size) flocculated with a cationic copolymer (acrylamide and trimethylamine ethyl acrylate five mol. percent) and suspension structure of coagulated silica (i.e., at i.e.p. or at high electrolyte concentration). They observed two distinct types of silica aggregate structures, (i) fractal structures (i.e., mass of aggregate α $R_g^{d_f}$ where R_g is the radius of gyration, d_f is fractal dimension, and $d_f < 3$) and (ii) a composite structure consisting of a short range ordered structure (i.e., at distances of the order of 4-5 particle diameters non fractal structure surrounded by fractal structure at larger distances). They observed that if no charge is present on the silica surface (i.e., coagulated dispersion), then aggregation results in a fractal structure. But, when a charge is present on the silica surface (due to SiOH dissociation or due to adsorbed polyelectrolyte), they observed ordering of particles at short distances while fractal structure at larger distances (i.e., type (ii) structure-Wong et al. 88a,88b). Also, the fractal nature of the flocs (at larger distances) was independent of the molecular weight of the polymer. These results should be applied with caution to the present study since the silica was of much smaller size (.04 μm where silica size we used was approximately 0.4 μm). The SANS investigation of our system would shed some light in this respect.

Figure 8.29 shows the general trends for stability of colloidal particles in the presence of polymers (Fleer et al. 88). In this figure, the depth Δf_{min} (ΔG_{min} in our notation) is plotted as a function of the total amount of polymer between plates for various solvency conditions (for χ = 0, 0.5 and 0.7) and for two chain lengths. All the curves have
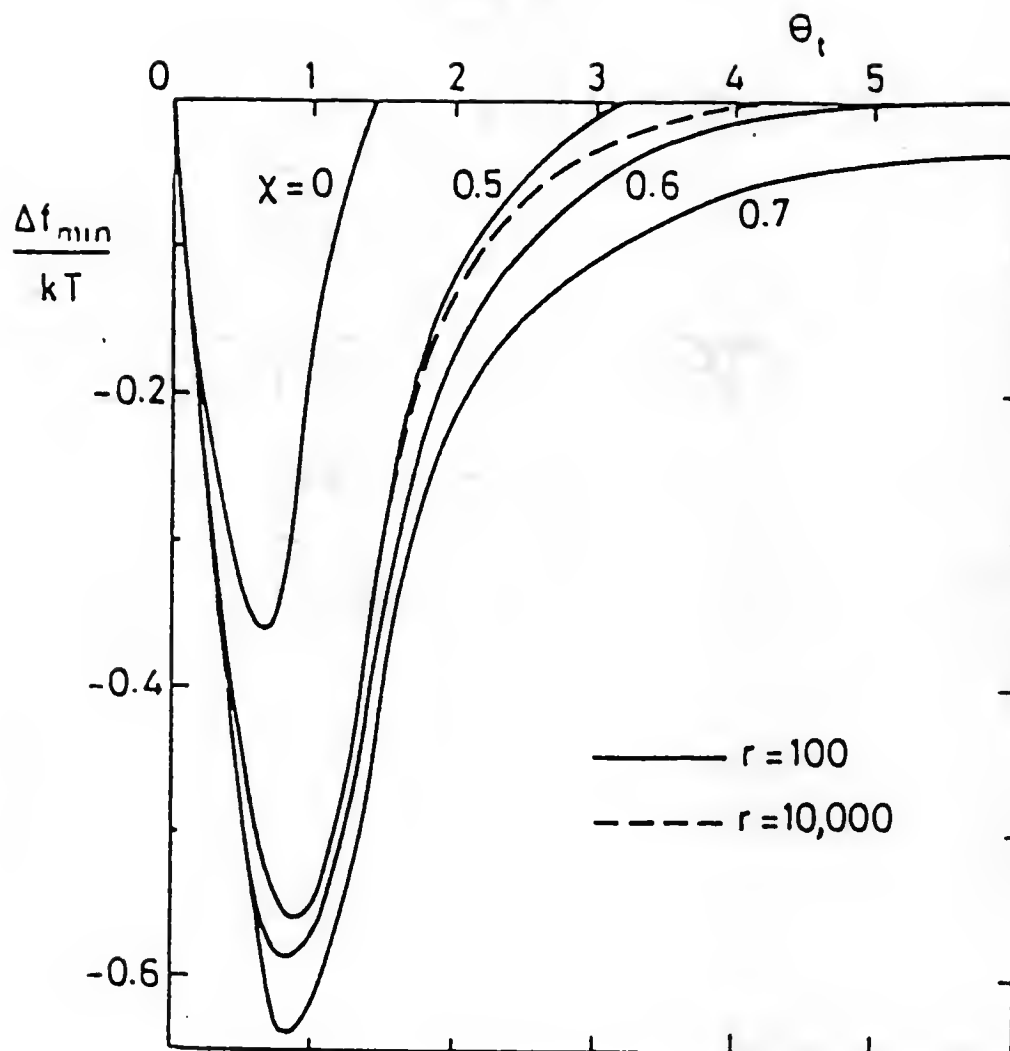
Figure 8.29   The depth of the free energy minimum as a function of the total amount of polymer between the surfaces at various solvency conditions for two molecular weights of polymer. θ^t is the total amount of polymer between the plates expressed as the number of equivalent monolayers, Δf_{min} is the interaction energy, and r is the number of segments per chain (Scheutjeans and Fleer, 1985).

the same general shape: with initial increase in the adsorbed amount, the attraction increases, and with the certain adsorbed amount (slightly below one monolayer, i.e., half monolayer per plate), the attraction reaches a maximum. At still larger amounts of polymer, the attraction becomes weaker and disappears (although Van der Waal's attraction is ignored in this figure) unless the solvent is extremely poor.

The depth of the attraction minimum (ΔG_{min}) can be related to extrapolated yield stress τ_β as follows. Figure 8.30 shows plots of extrapolated yield versus adsorbed amounts of PVA and corresponding plots of yield versus fraction coverage for uncalcined and calcined silica suspensions. The initial increase in the yield stress with increasing adsorbed amount can be related to increases in ΔG_{min} with adsorbed amount. At low adsorbed amounts of polymer, uncalcined silica suspensions have larger yield values. The larger value of ΔG_{min} for uncalcined silica suspension can arise due to:

(i) larger Van der Waal's attraction (since the adsorbed layer thickness is smaller, particles can approach closer),

(ii) adhesion due to hydrophobic interactions between acetate groups, and

(iii) more bridges can be formed between two particles due to the closer approach of particles. Scaling view point of polymer adsorption has been developed by de Gennes (de Gennes 87). He gave the following expression for the total number of bridges, n_{total}, formed between two particles of equal radii a, separated by a distance 2h (Figure 8.31).

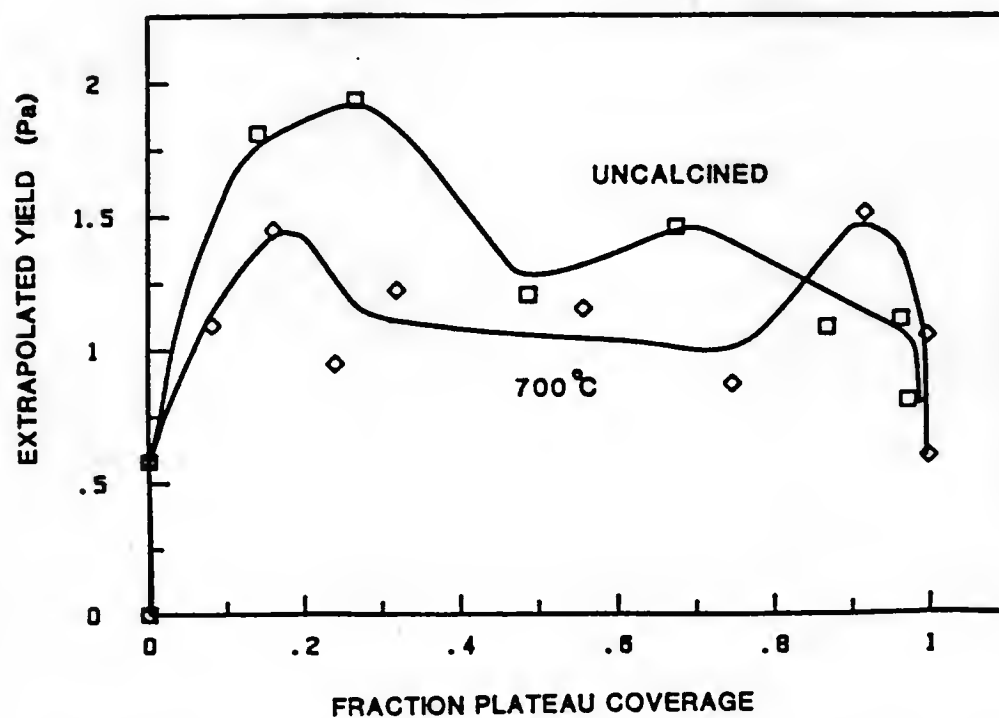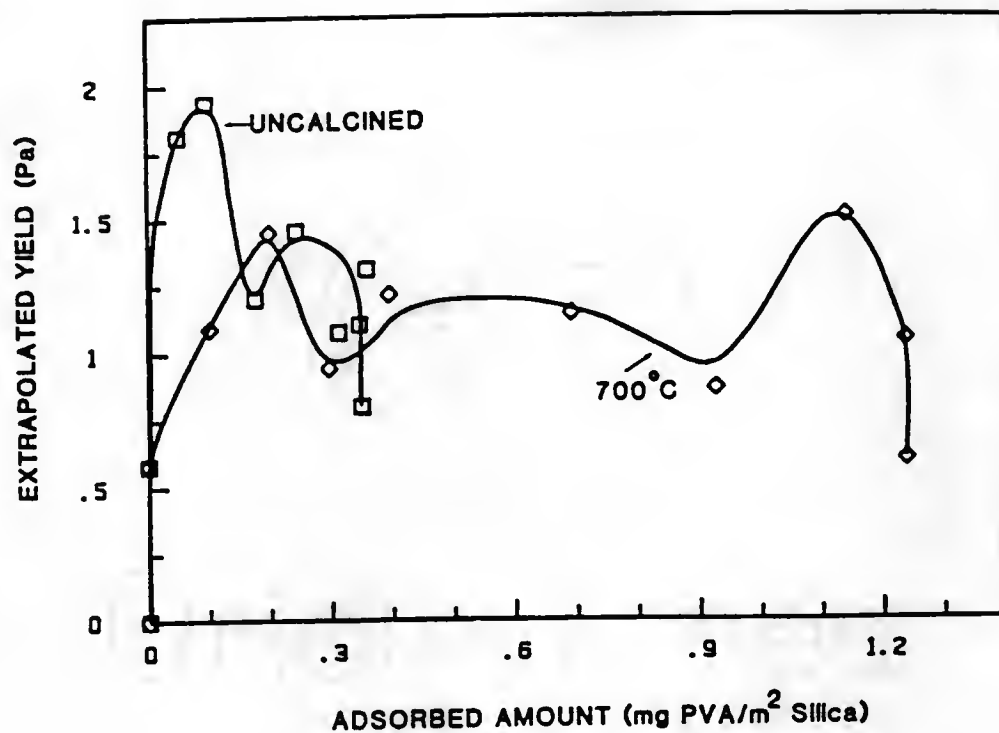$$n_{total} = \frac{a}{h} \tag{8.1}$$

Figure 8.30   Plots of (a) yield stress versus adsorbed amount and (b)
yield stress versus fractioned plateau coverage for 20
vol.% silica suspensions prepared with 700°C calcined and
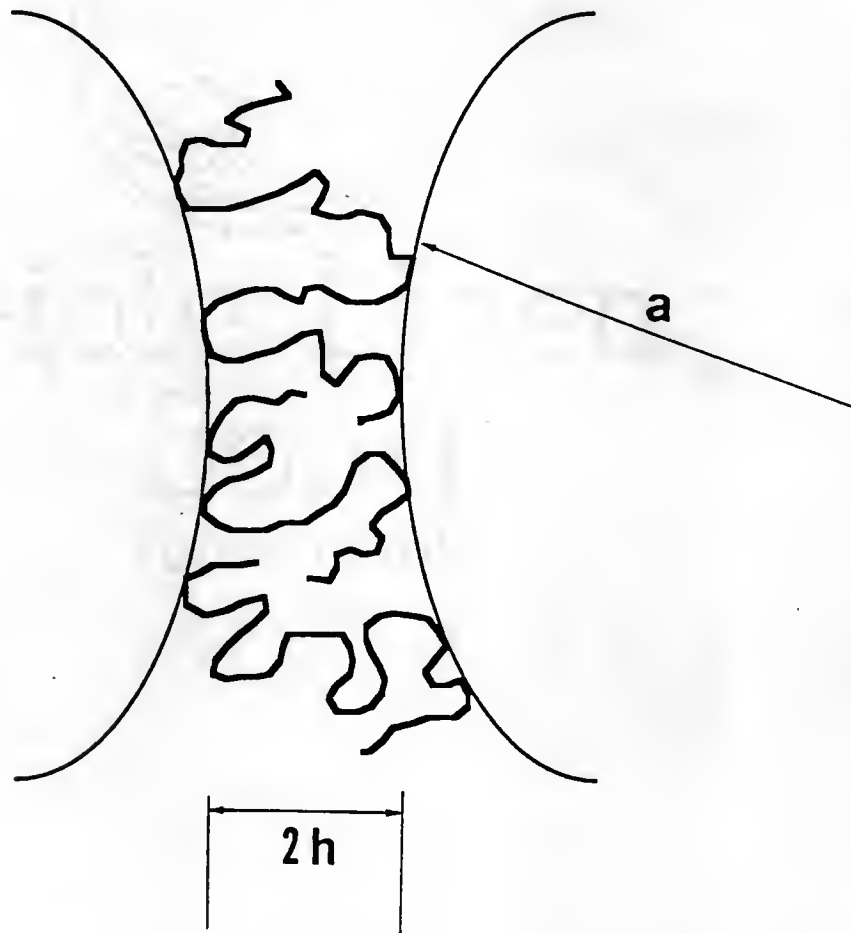uncalcined silicas with varying PVA concentration in
solution.

Figure 8.31   Schematic illustration shows the total number of bridges, n_{total}, formed between two spherical particles radii a separated by distance 2h.

From the equation 8.1, it is clear that the total number of bridges formed between two particles will be less for 700° calcined silica compared to uncalcined silica. (It is expected that relatively more open floc structure is formed with the calcined silica, i.e., larger h.) Eisenlauer et al. have also reported initial increase in the extrapolated yield stress with the coverage for Aerosil hydrosols flocculated with polyethylene glycols. They observed the maximum in the yield at approximately one-half surface coverage (Eisenlauer et al. 80). The appearance of a maxima in the yield stress at intermediate coverages indicates the tendency towards steric stabilization with increasing surface coverage. Not much significance can be attached to the surface coverage (e.g., half surface coverage) at which maxima in the yield stress is observed, since besides surface coverage the yield stress is also dependent on various other factors such as suspension structure, shear history, etc.

Near complete surface coverages, decreases in the yield stress was observed with increasing coverage. This indicates the improved dispersion stability with increases in the surface coverage. At the plateau coverages, both uncalcined and calcined silica suspensions show smaller yield. For 700°C calcined silica, the adsorbed layer thickness is rather large since PVA having high molecular weight was used ($M_\upsilon \approx$ 215,000 g/mole). The hydrodynamic volume of the particles is increased significantly by this adsorbed layer. The shear thinning behavior in Figure 8.18 and the appearance of small yield in Figure 8.30 can be attributed to the high "effective" solids loading in the suspension. In

contrast, uncalcined silica suspensions are highly flocculated (Figure 8.18) and have relatively lower green compact density (Figure 8.26).

This difference is also evident from Figure 8.32 which shows plots of relative sediment density versus the fraction plateau coverage for uncalcined and 700°C calcined silica. For uncalcined silica, the compact density is relatively low and does not change with the silica surface coverage. This observation is consistent with the rheological (i.e., extrapolated yield and relative viscosity) behavior of these suspensions. For 700°C calcined silica, the initial decrease in the green density can be associated with the bridging flocculation, and relatively high density ($\approx$ 61%) at complete coverages indicates steric stabilization under these conditions.

Figure 8.33 shows plots of hysteresis area versus adsorbed amount and corresponding plots of hysteresis area versus fractional coverages for uncalcined and calcined silica suspensions. For 700°C calcined silica, at very low and near full coverages, no hysteresis was observed. A maximum in the hysteresis area was observed at approximately one-fifth surface coverage. With further increase in the silica surface coverage, the hysteresis area is decreased. For uncalcined silica suspension, small increase and subsequent decrease in the hysteresis area was observed with increasing coverage. Also, the value of the maximum in the hysteresis area is smaller compared with the calcined powder. For Aerosil dispersions flocculated with PVA, Heath and Tadros observed a maximum in the plot of hysteresis vs. PVA concentration (Heath and Tadros 83). Since they did not measure the adsorption isotherm, our results cannot be directly compared. They also observed the thixotropic flow
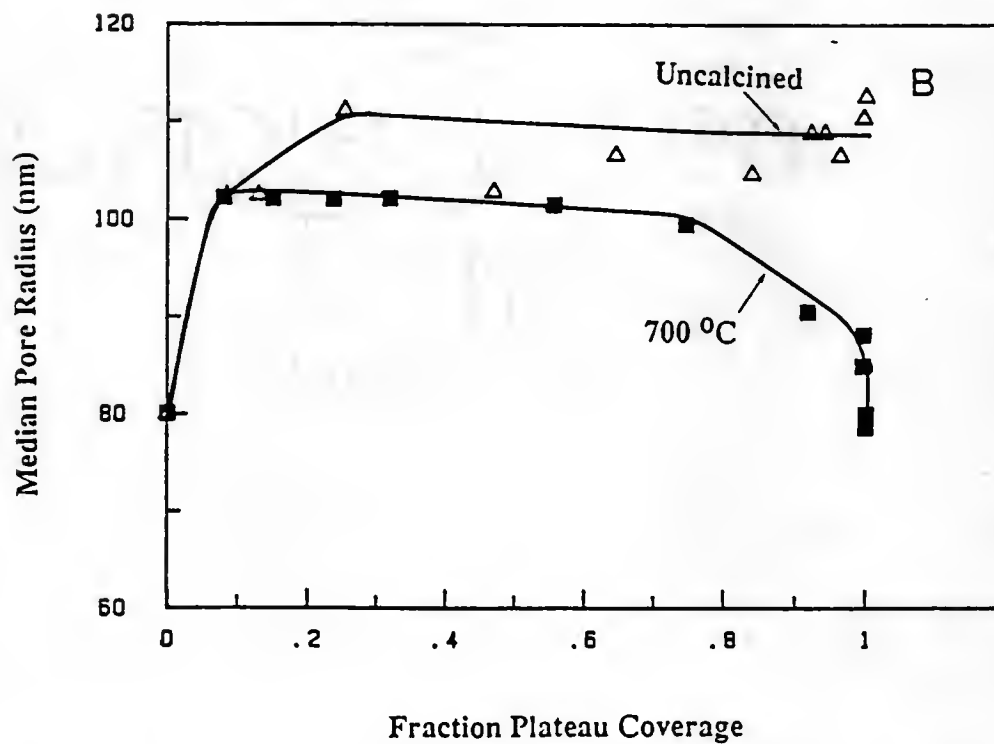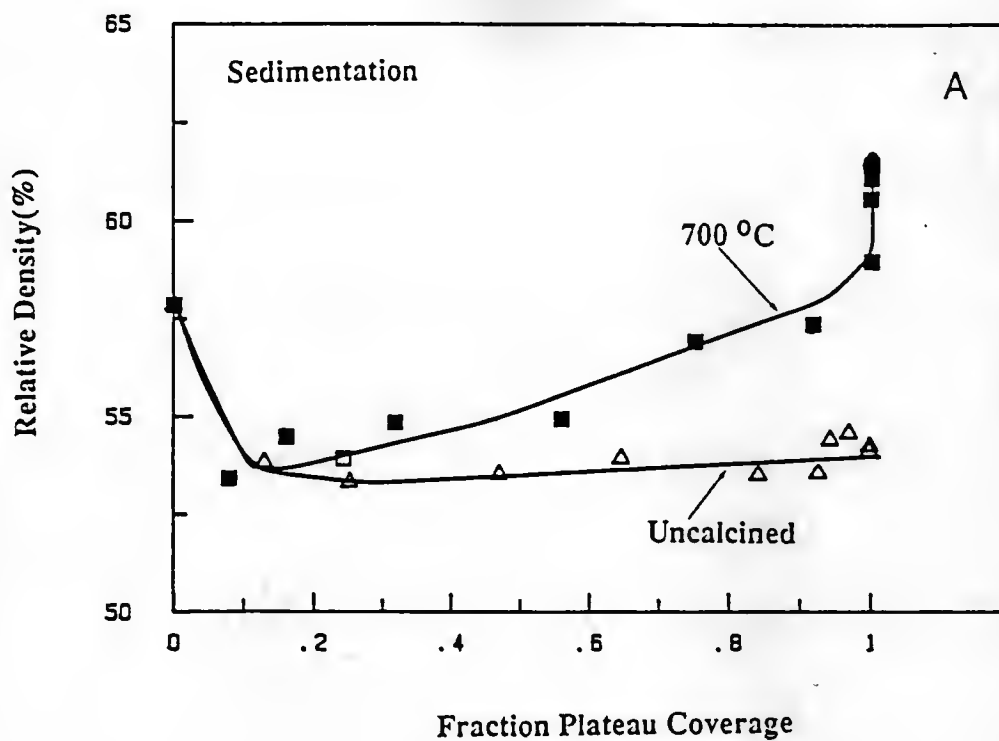
Figure 8.32   Plots of (a) relative density of gravity cast samples versus fraction plateau coverage and (b) median pore radius versus fraction plateau coverage for compacts prepared from 20 vol.% SiO_2 suspensions of uncalcined and 700°C calcined silicas with varying PVA concentrations.
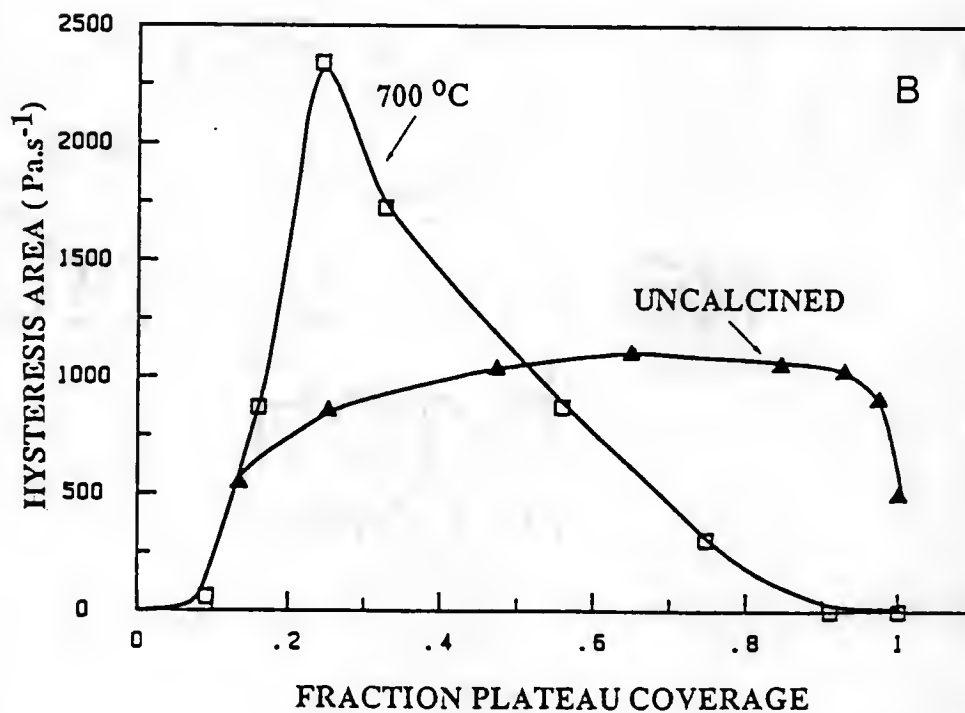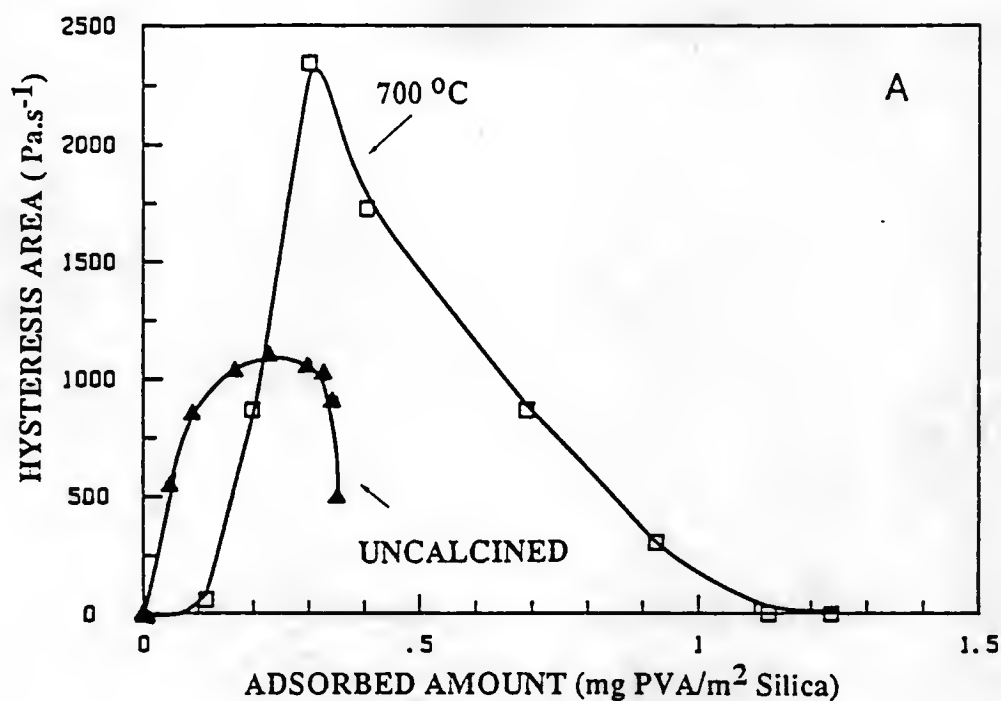
Figure 8.33   Plots of (a) hysteresis area versus adsorbed amount and
              (b) hysteresis area versus fraction plateau coverage for
              20 vol.% SiO_2 suspensions prepared with uncalcined and
              700°C calcined silicas with varying PVA concentrations.

behavior at sufficiently high PVA concentrations, consistent with our observations (i.e., their suspensions were flocculated at sufficiently high PVA concentrations). The observation of hysteresis indicates the formation of weak three-dimensional network structure in suspension with PVA additions. The larger hysteresis area indicates the formation of weak network structure which can be broken down under shear. To obtain the maximum in the hysteresis area, the structure should be more open (and weaker, i.e., ΔG_{min} is relatively small), and the rate at which the structure reforms (after breakdown by the applied shear) should be slower. Under certain coverages (or polymer concentrations), these two conditions are met and the maximum in the hysteresis is observed. Beyond the optimum concentration (i.e., with improved coverages), the stability of suspension is improved and the corresponding decrease in the hysteresis is observed.

From the above discussion, it is clear that the uncalcined silica (which is hydrophilic) and 700°C calcined silica (which is relatively hydrophobic) behaves differently with respect to the PVA adsorption behavior and rheological behavior (i.e., yield stress, relative viscosity, and hysteresis). The adsorption mechanism of PVA is expected to be different for these two powders. For uncalcined silica, it can be expected that the hydrogen bonding (i.e., bonding between the surface silanol groups and OH groups of PVA) is an important mechanism, while for calcined silica, both the hydrogen bonding and the hydrophobic bonding (i.e., bonding between the acetate groups and the silica siloxane groups) will be important adsorption mechanism. At partial coverages, relatively weak and more open floc structure with calcined silica powders and

relatively strong and more compact floc structure with uncalcined silica can be expected from the rheological measurements. Stable silica dispersions cannot be prepared with uncalcined silica with adsorbed PVA. This observation is consistent with the results of various investigators (Killmann et al. 86). Stable dispersions can be prepared with 700°C calcined silica, hence, for the rest of the investigation, calcined powder was used.

Effect of PVA Molecular Weight

In the last section, we described the effect of silica surface characteristics (i.e., calcination temperature) on suspension properties. Another important variable in controlling suspension properties is the PVA molecular weight. As we will show later, proper PVA molecular weight selection is important in achieving higher solids loading of suspensions, consistent with other criteria that are used in selecting polymer (e.g., green compact strength, etc.). First, we will discuss the effect of PVA molecular weight at fractional surface coverages.

Fractional Surface Coverage

Figure 8.34 shows plots of adsorption isotherms for two PVA samples with a similar degree of hydrolysis ($\approx$ 88%) but different viscometric molecular weights ($\approx$ 24,000 and 215,000) at pH $\approx$ 3.7 (i.e., near i.e.p. of silica). Both adsorption isotherms show a high affinity character. The plateau adsorbed amount is greater for the higher molecular weight PVA. The plateau adsorbed amount for high molecular weight PVA is approximately twice that of low molecular weight PVA. The adsorption density increases with molecular weight with proportionality $M_v^{0.2}$ (as
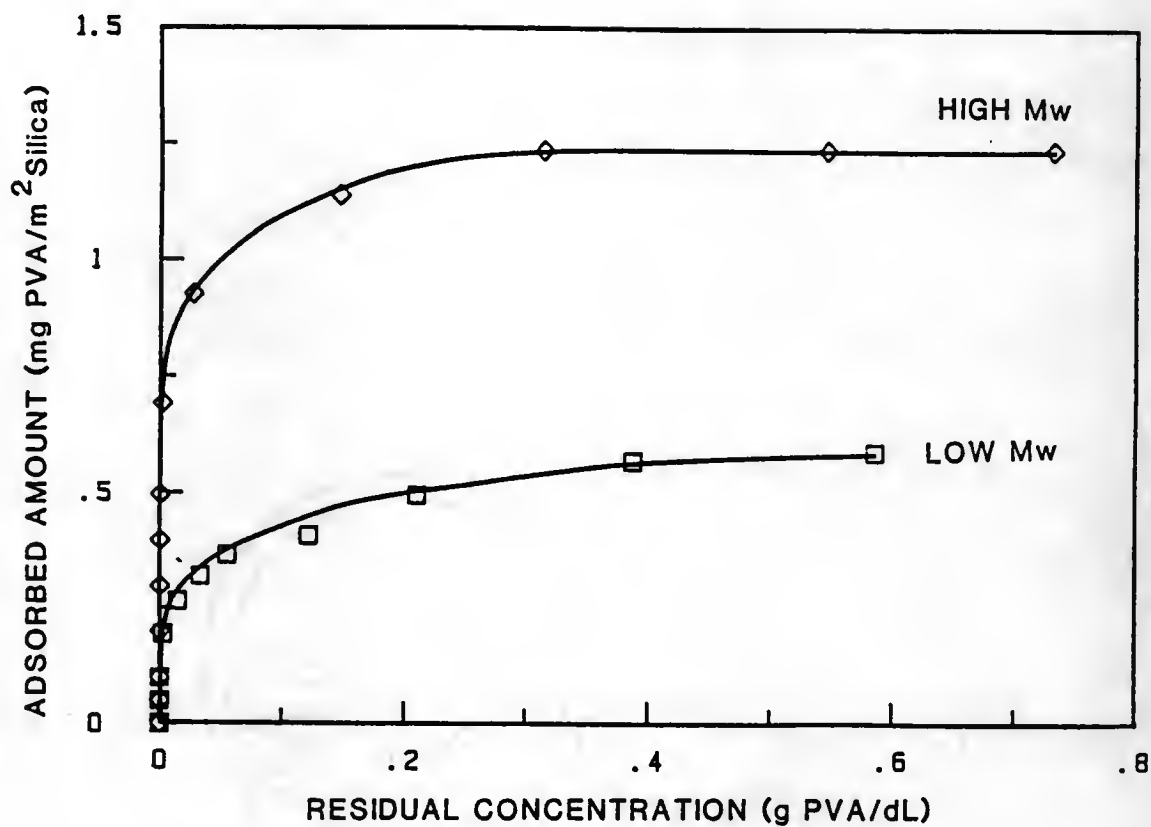
Figure 8.34   Plots of adsorption isotherms for two PVA samples with different molecular weights (i.e., 24,000 and 215,000 g/mole) determined using 20 vol.% SiO_2 suspensions at pH 3.7 with varying PVA concentrations.

shown in Figure 8.53). The small dependence of the plateau adsorbed amounts on molecular weight of PVA (i.e., A α $M_\nu^{0.2}$) indicates that the conformation of adsorbed polymer is mainly determined by the adsorbed amount, and hence, the molecular weight of PVA plays an indirect role in determining the adsorbed layer properties. This increase is similar to that reported by Koopal for the adsorption of partially hydrolysed PVA on AgI (Koopal 78). We will discuss these results later in more detail with reference to Figure 8.53.

Figure 8.35 shows plots of relative viscosity (at shear rate of 1000 s^{-1}) versus adsorbed amount (mg PVA/m^2 SiO$_2$) plots and corresponding relative viscosity versus fraction plateau coverage for two PVA samples. At low surface coverages, the relative viscosity is higher for the high molecular weight polymer. The effect of molecular weight on the relative viscosity at low coverages is more clearly illustrated in Figures 8.36 and 8.37. Figure 8.36 shows plots of relative viscosity versus shear rate for various molecular weights at fixed adsorbed amount of PVA ($\approx$ 0.15 mg PVA/m^2 silica) and Figure 8.37 shows a plot of relative viscosity versus molecular weight (log scale) at fixed adsorbed amounts of PVA ($\approx$ 0.15 mg PVA/m^2 SiO$_2$). (Please note: In this figure, the fraction plateau coverage is decreasing with increases in molecular weight since the plateau adsorbed amount increases with PVA molecular weight). The increased flocculation efficiency of higher molecular weight is evident from these results. The higher relative viscosity indicates the higher effective volume fraction solids in the suspension, i.e., the formation of more open floc structure for high molecular weight polymer (Figure 8.28). This trend is expected from the kinetics of polymer adsorption
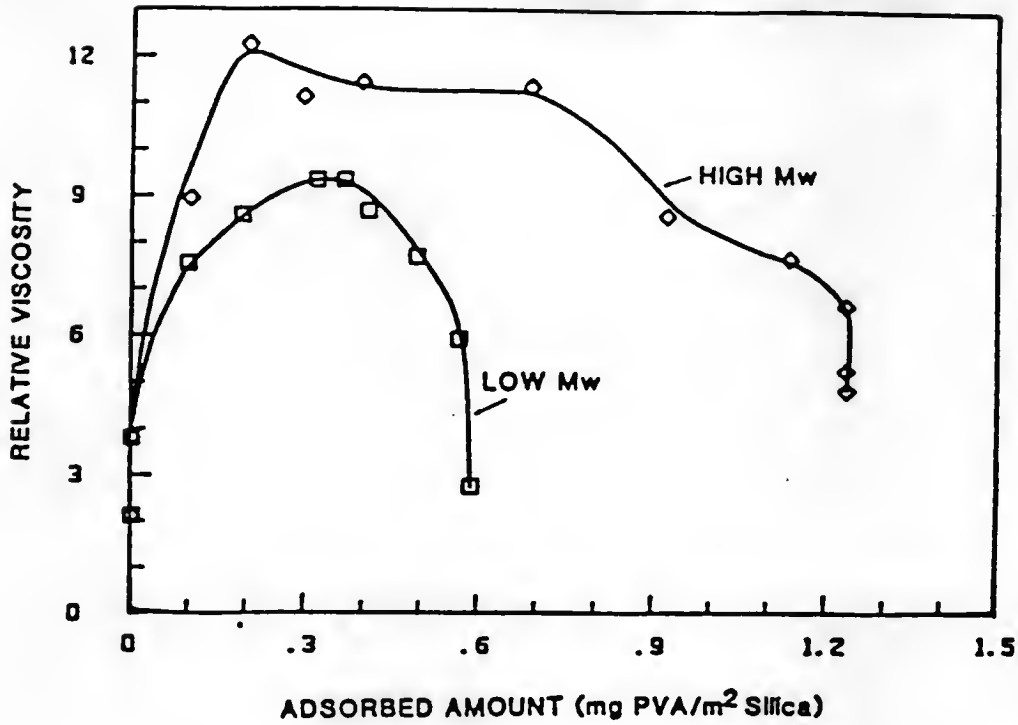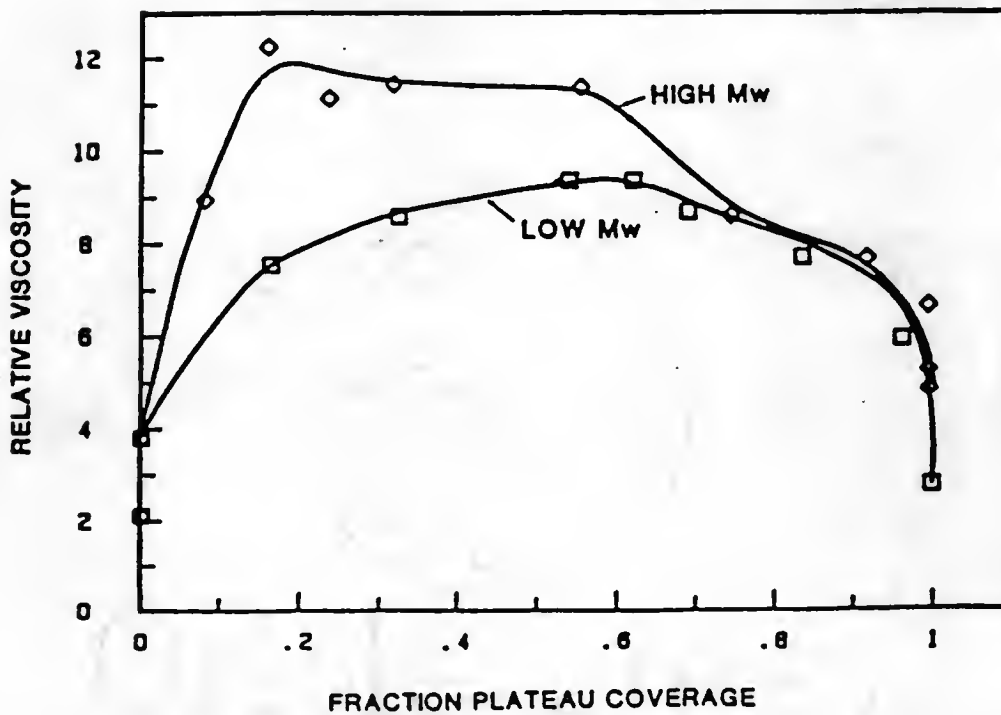
Figure 8.35   Plots of (a) relative viscosity versus adsorbed amount
and (b) relative viscosity versus fraction plateau
coverage for two PVA samples with different molecular
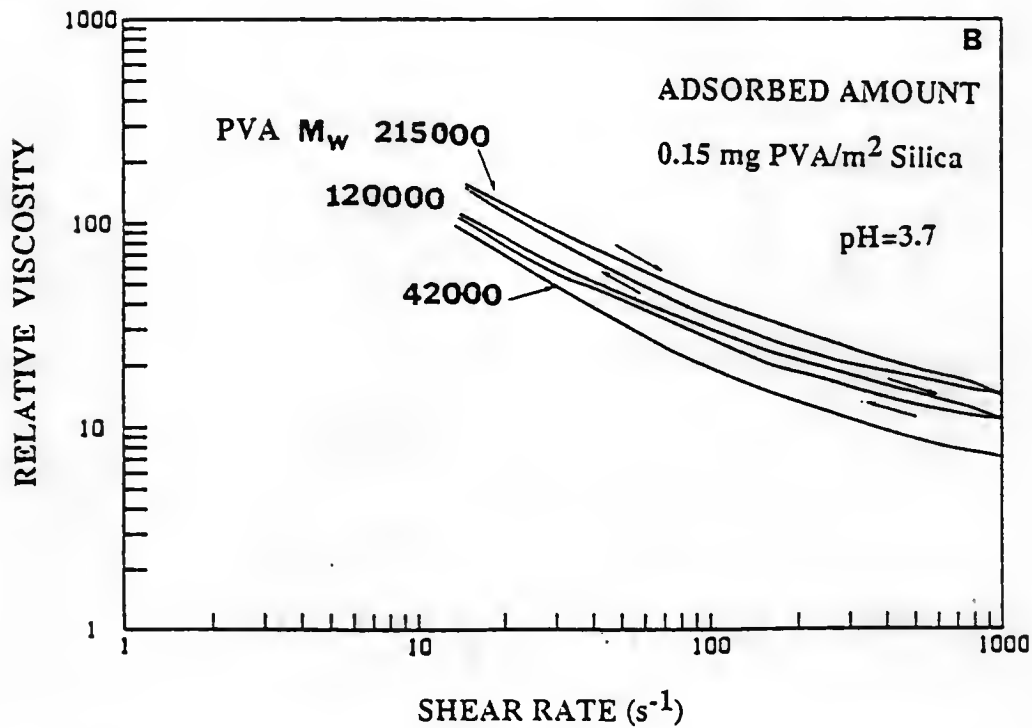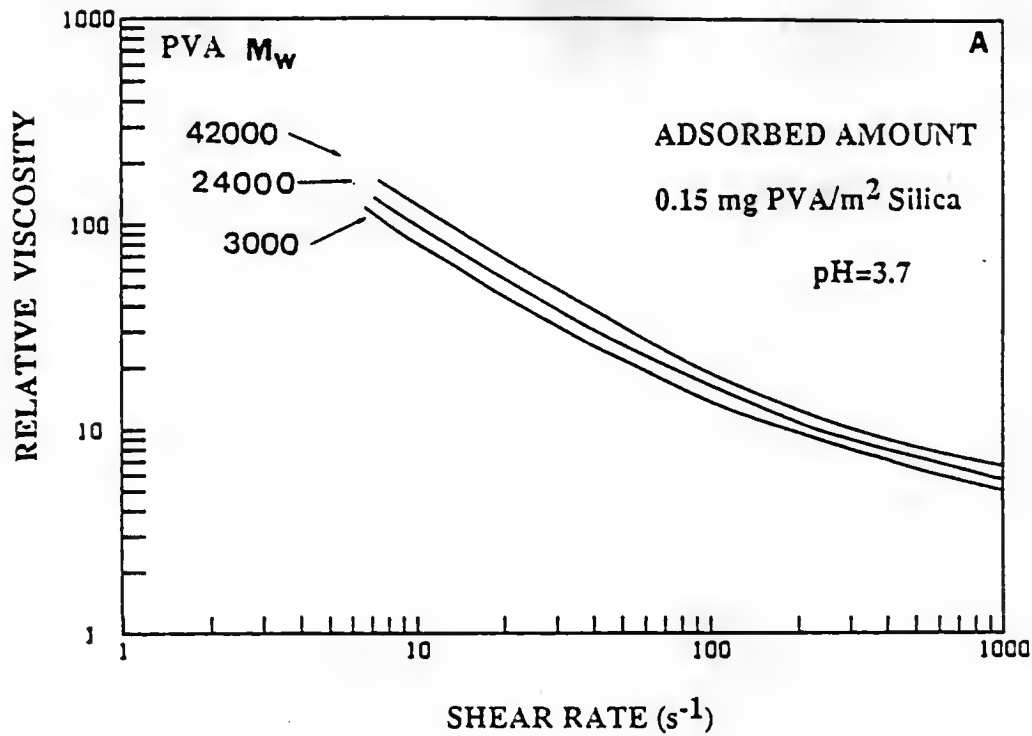weights.

Figure 8.36   Plots of relative viscosity versus shear rate for 20
vol.% SiO_2 suspensions prepared using different molecular
weight PVA samples at fixed PVA concentration in
solution.   Adsorbed amount was constant (0.15 mg PVA/m^2
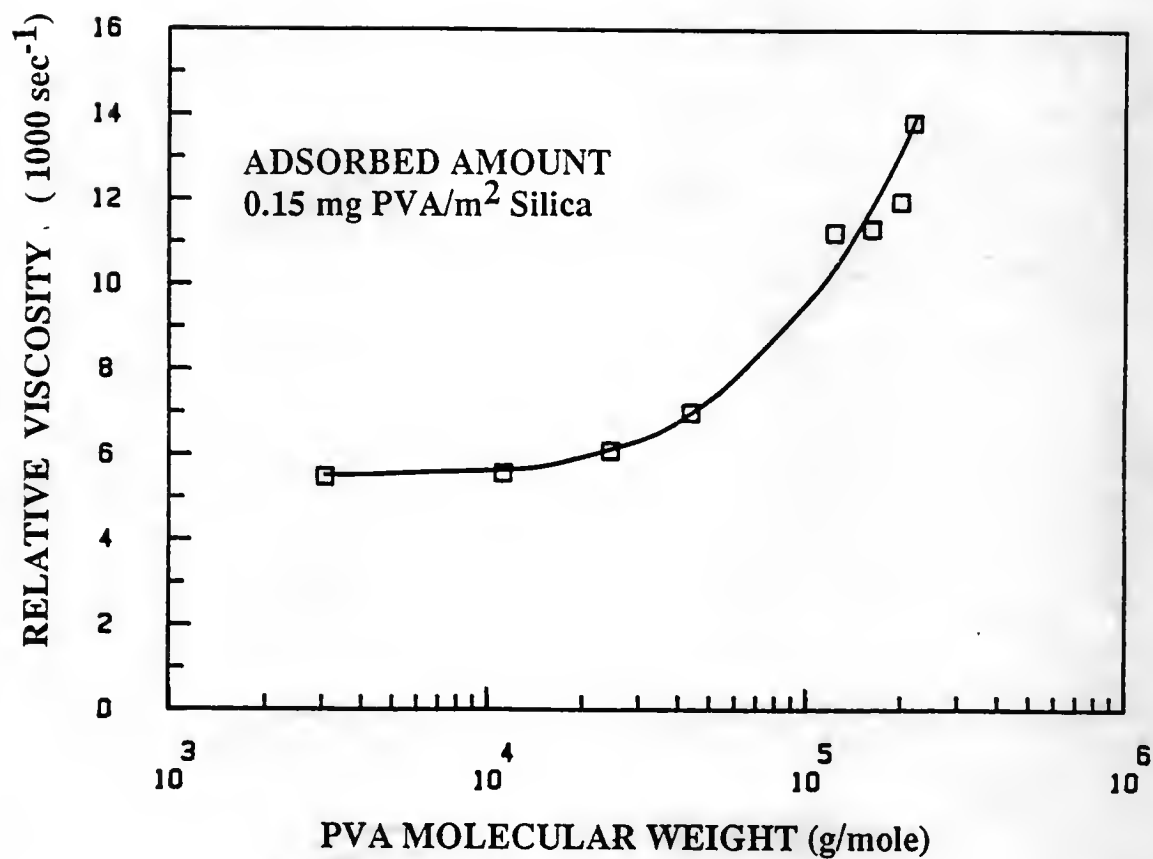SiO_2) for all suspensions.

Figure 8.37   Plot of relative viscosity versus PVA molecular weight
(log scale) at fixed adsorbed amount of polymer.

and flocculation. With increasing polymer molecular weight (and its dimensions in solution, i.e., $<h^2>^{0.5}$ or $<r^2>^{0.5}$ (1) the adsorption time increases (Equation 4.34), and (2) the number of collisions between bare and covered particles per unit time (Equation 4.38) increases. The strong dependence of the relative viscosity or molecular weight suggests that polymer molecules may not have achieved the equilibrium conformation during the time of flocculation ($\approx$ few seconds). (The equilibrium conformation predicted from the polymer adsorption theory such as SF does not indicate a sharp change in conformation (e.g., adsorbed layer thickness) with molecular weight at (small) constant adsorbed amounts-Fleer et al. 88).

The formation of a more open floc structure with higher molecular weight PVA is consistent with the extrapolated yield behavior. Figure 8.38 shows plots of yield stress versus adsorbed amount and corresponding plots of yield stress versus fraction plateau coverage for two PVA samples. The high yield stresses with low molecular weight polymer at low coverages indicates the formation of relatively stronger flocs (as described earlier). This can be also seen from a plot of yield stress vs. molecular weight at fixed amount of PVA (0.15 mg PVA/m^2 silica) (Figure 8.39). The higher yield stresses can be due to increased Van der Waal's attraction and an increased number of bridges between particles. As described earlier, the total number of bridges formed, n_{total}, increases with decreasing the distance of separation between particles (Equation 8.1). High molecular weight polymer shows small yield and higher relative viscosity at the plateau adsorption compared to low molecular weight PVA (Figures 8.35 and 8.38). This can be related to
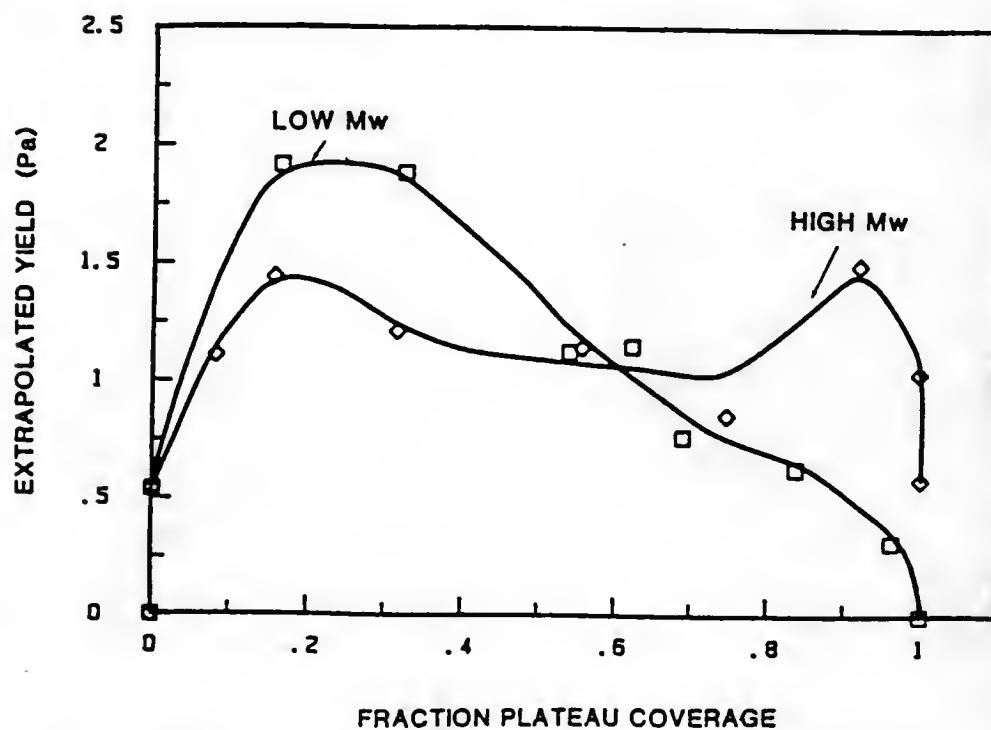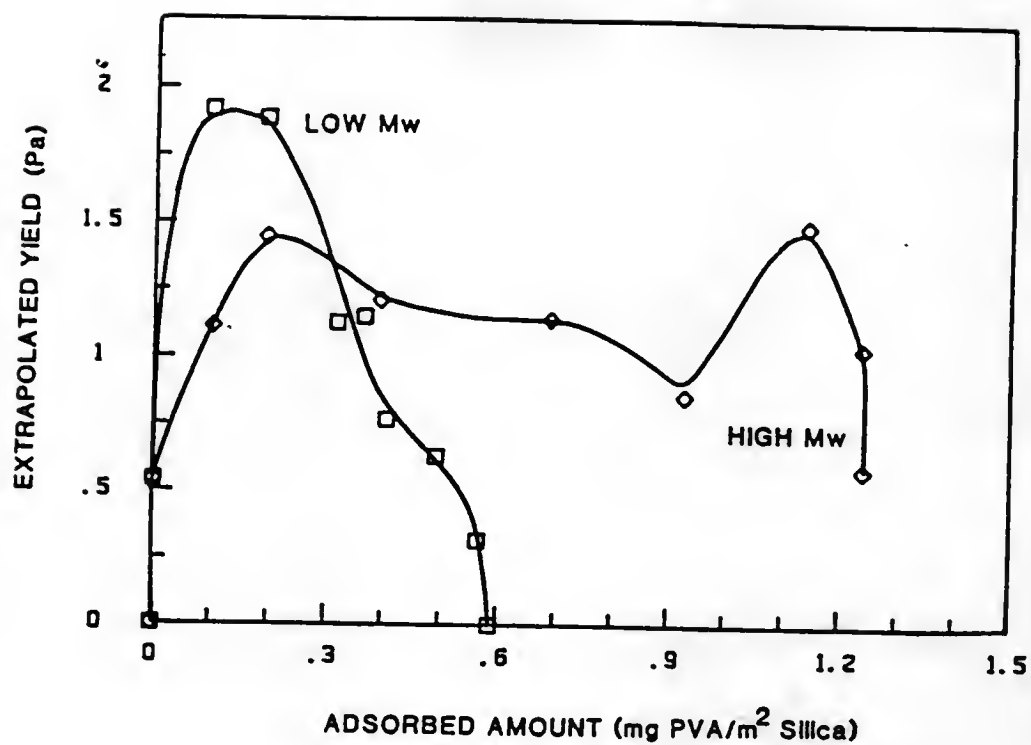
Figure 8.38   Plots of (a) yield stress versus adsorbed amount and (b)
yield stress versus fraction plateau coverage for 20
vol.% silica suspensions prepared with two PVA samples
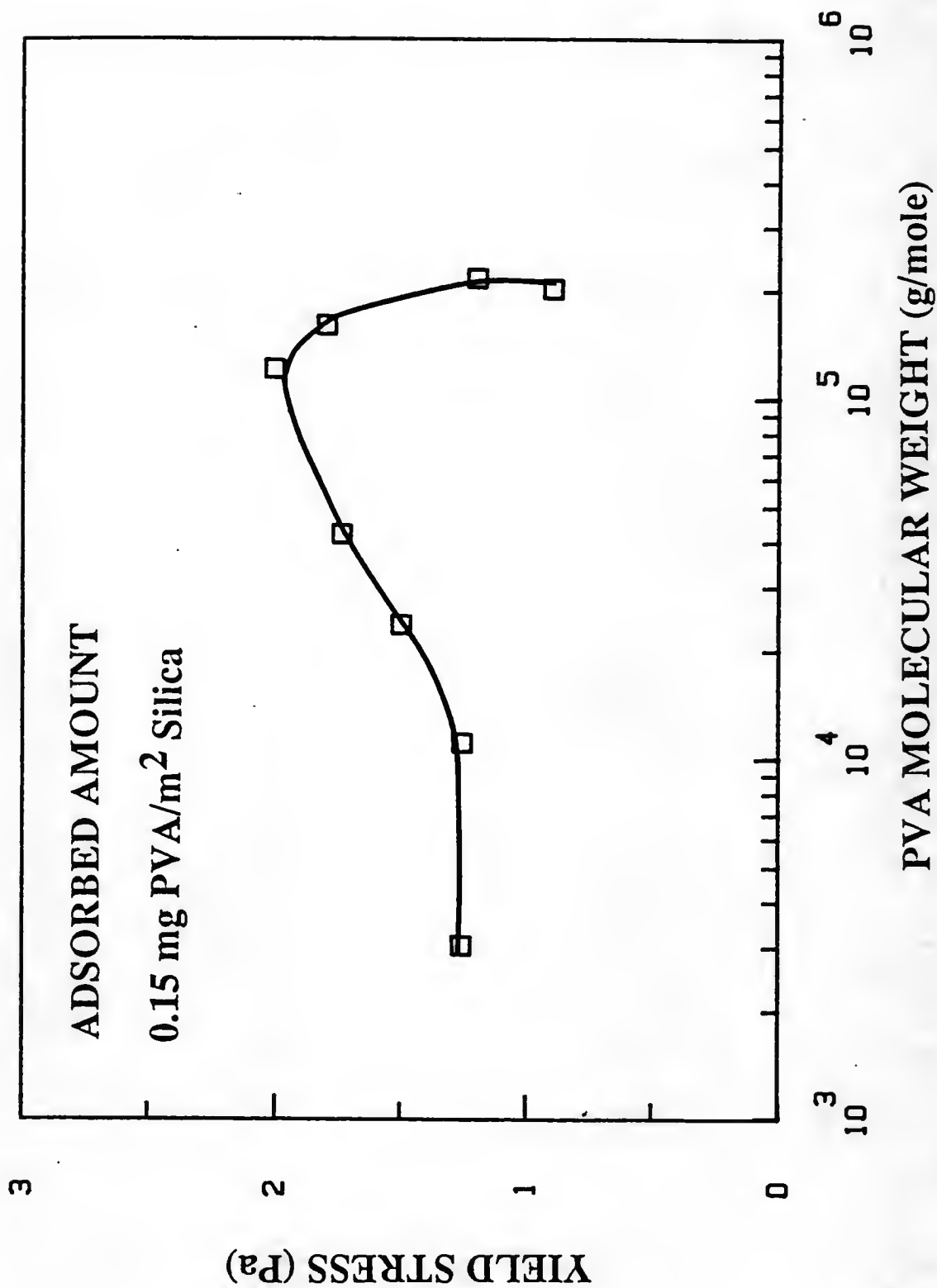with different molecular weights.

Figure 8.39   Plot of yield stress versus PVA molecular weight (log scale) at fixed adsorbed amount.

increasing hydrodynamic volume of particles with increasing adsorbed layer thickness. For low molecular weight PVA, no yield stress was observed at the plateau coverages (i.e., Newtonian flow behavior was observed).

The effects of molecular weight and surface coverage on the thixotropic flow behavior of silica suspensions is illustrated in Figure 8.40. Figure 8.40 shows plots of hysteresis area versus adsorbed amount and corresponding plots of hysteresis area versus fraction plateau coverage for two PVA molecular weight samples. The appearance of thixotropic behavior at lower coverages (≈ 0.1) and large hysteresis area is consistent with the open floc model for high molecular weight polymers. This can be seen more clearly from Figure 8.41. Figure 8.41 shows a plot of hysteresis area vs. molecular weight at a fixed adsorbed amount of polymer (i.e., 0.15 mg PVA/m^2 silica). From the Figure 8.41, it is clear that at the same adsorbed amount of polymer, higher molecular weight samples exhibited thixotropic flow behavior. (The appearance of hysteresis plot (Figure 8.40) for low molecular weight PVA is similar to the behavior observed for uncalcined silica suspensions-Figure 8.33). At complete coverages, the hysteresis area is zero, and silica suspensions are sterically stabilized.

Figure 8.42 shows plots of compact density (sedimented) versus fraction plateau coverage and corresponding median pore radius versus fraction plateau coverage for two PVA samples. The density and median pore radius data do not show significant difference with changing molecular weight from $\approx 24,000$ to $\approx 215,000$ g/mole. The effect of fraction plateau coverage on the compact density (i.e., the initial
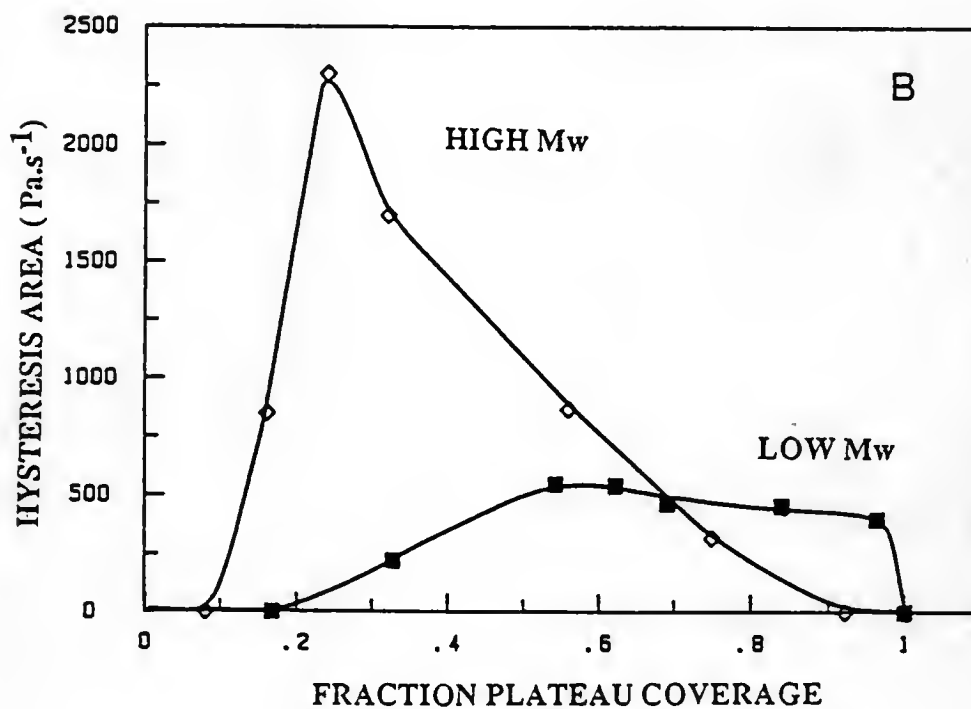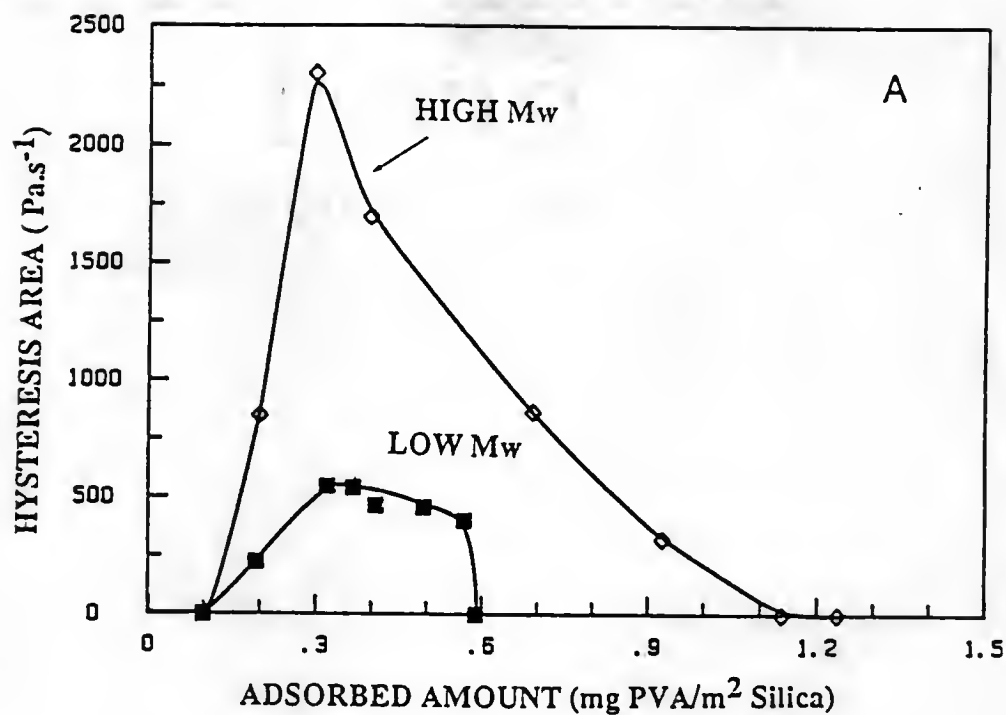
Figure 8.40   Plots of (a) hysteresis area versus adsorbed amount and (b) hysteresis area versus fraction plateau coverage for 20 vol.% SiO_2 suspensions prepared with two PVA samples of different molecular weights.
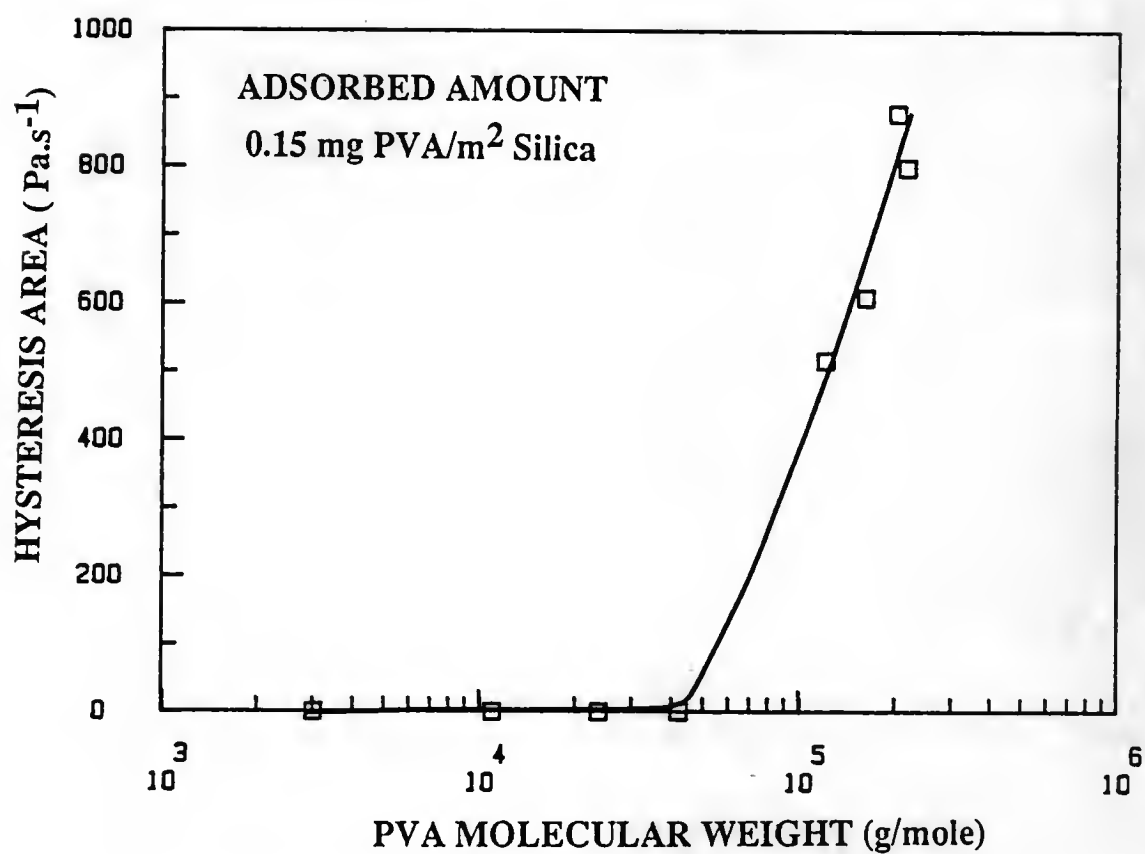
Figure 8.41   Plot of hysteresis area versus PVA molecular weight (log scale) at fixed adsorbed amount of polymer.
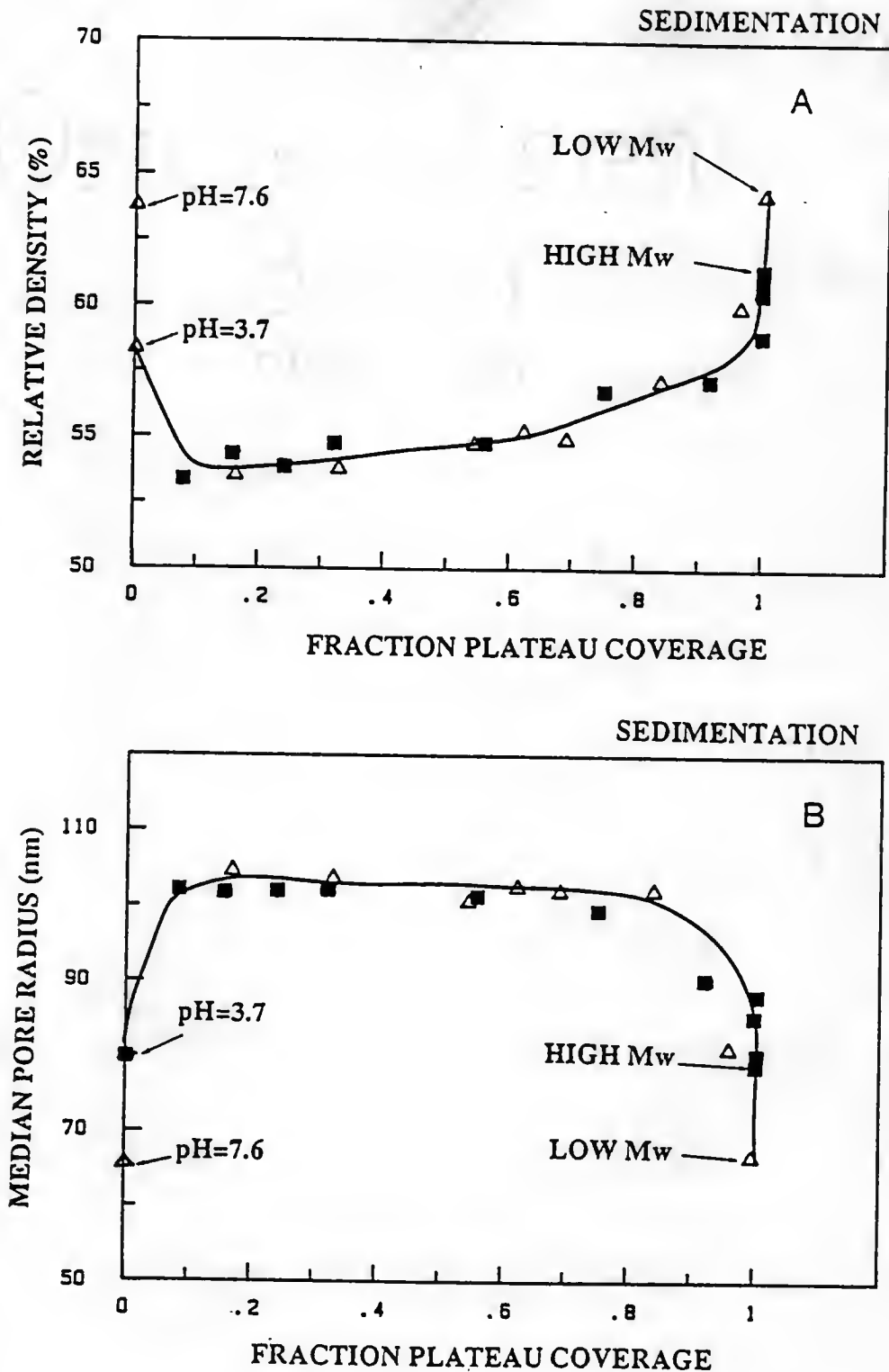
Figure 8.42   Plots of (a) relative density of sedimented samples versus fraction plateau coverage and (b) median pore radius versus fraction plateau coverages for compacts prepared using two PVA samples of different molecular weights.

decrease is due to bridging flocculation and the increased density near plateau coverage due to steric stabilization, etc.) has been already explained earlier. The effect of molecular weight on the compact density at partial coverage is shown in Figure 8.43. These samples were prepared from the flocculated silica suspensions with the same absorbed amount (0.15 mg/m^2) but increasing molecular weight of PVA. No significant difference in the green compact density (in this case, samples consolidated by slip casting and gravity sedimentation) with molecular weight was observed.

Figure 8.44 shows plots of sediment density vs. C_{FP} (= ϕ_F/ϕ_p) for high and low molecular weight PVA samples. The C_{FP} values were calculated from the measured relative plastic viscosities. (Higher value of C_{FP} indicates higher relative plastic viscosity or more open floc structure at fixed solids loading, ϕ_p). For comparison, results for electrostatically stabilized suspensions at pH $\approx$ 3.7 (i.e., $\zeta \approx 0$) and at pH $\approx$ 7.6 ($\zeta \approx$ -60 mV) are also shown in Figure 8.44. For electrostatically stabilized suspensions (i.e., pH $\approx$ 7.6) $C_{FP} \approx$ 1 (i.e., flow units are single particles) and consolidation of these suspensions results in compacts with $\approx$ 64% density. In contrast, suspensions at pH $\approx$ 3.7 are flocculated (i.e., $C_{FP} \approx$ 1.6) and consolidation results in compacts with lower green densities ($\approx$ 58%). For suspensions with adsorbed high and low molecular weight PVA's, the decrease in the compact density with increasing C_{FP} is evident. At the plateau coverages (indicated by smaller C_{FP} values) suspensions are sterically stabilized at pH $\approx$ 3.7 with high ($M_\upsilon \approx$ 215,000) and low ($M_\upsilon \approx$ 24,000) molecular weight PVA's. Since the hydrodynamic volume of particles covered with
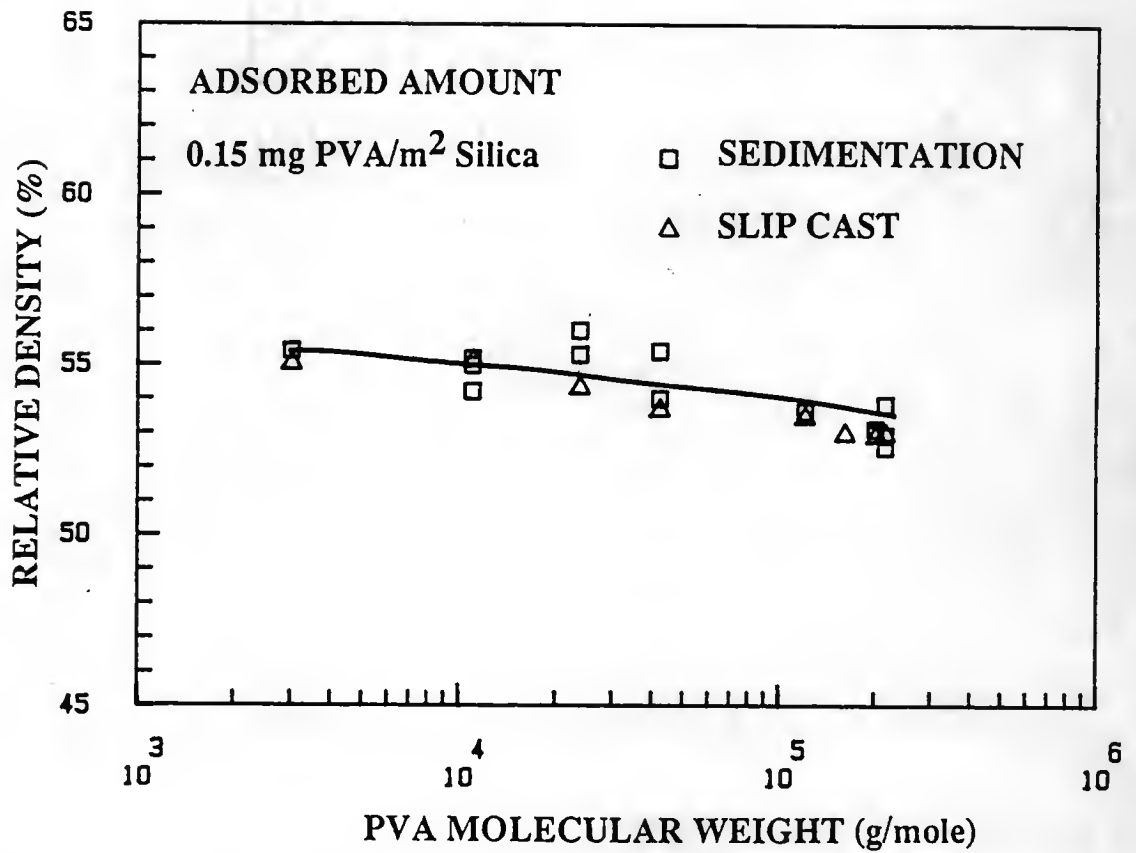
Figure 8.43   Plot of relative density of compacts prepared using gravity casting and slip casting versus PVA molecular weight at fixed adsorbed amount of polymer.
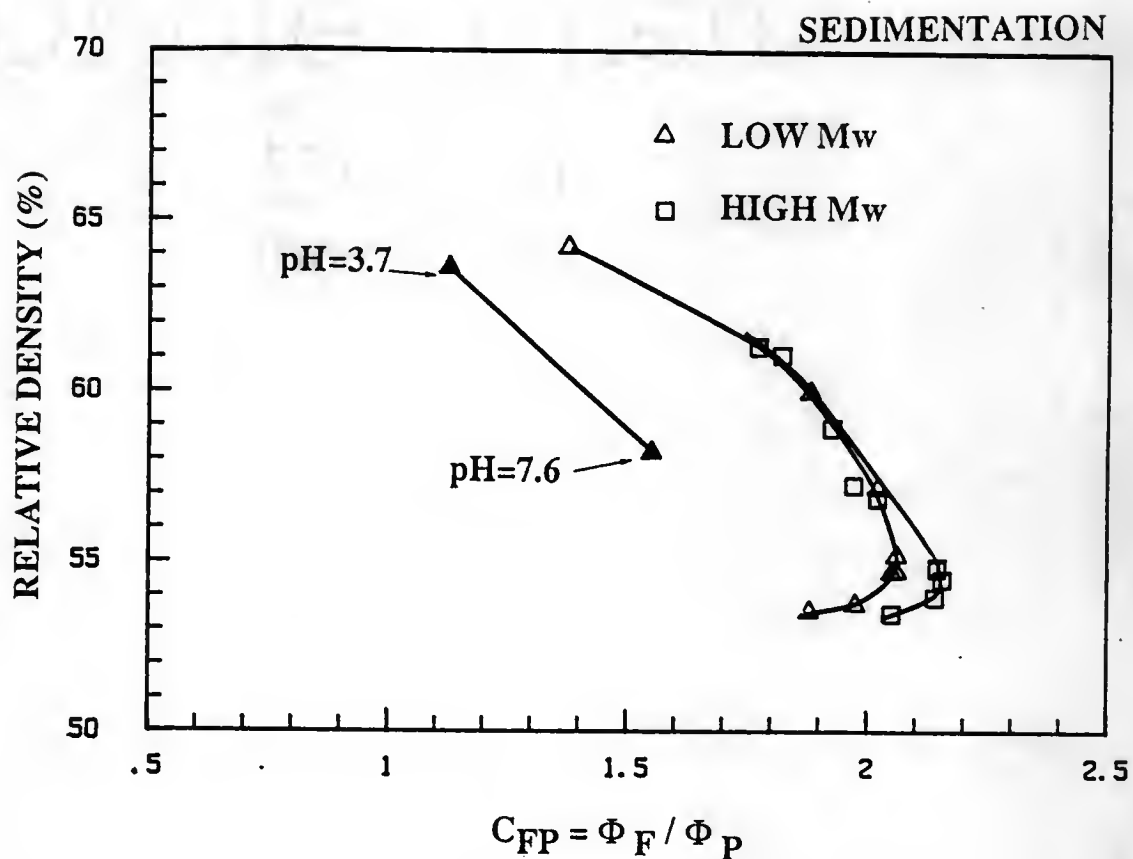
Figure 8.44   Plots of relative density versus C_{FP} (= ϕ_F/ϕ_P) for two
PVA samples with different molecular weights.   Results
for compacts prepared at pH 3.7 and pH 7.6 with no added
PVA are also shown.

high molecular polymer is expected to be larger, C_{FP} is larger of high molecular weight PVA. The higher compact density ($\approx 63\%$) was obtained with low molecular weight PVA compared to high molecular weight PVA (≈ 58-61%). This observation indicates the importance of molecular weight (or adsorbed layer thickness) on the density of sterically stabilized suspensions. The overlap of high and low molecular weight plots at partial coverages indicates that the density is directly influenced by the C_{FP} parameter (i.e., PVA molecular weight has an indirect effect on density).

Effect of Suspension pH

Before discussing the effect of PVA molecular weight with the plateau coverages on suspension properties, we will describe the effect of surface charge on PVA adsorption behavior at partial and plateau coverages. After that, the effect of PVA molecular weight and charge with the plateau adsorbed amounts will be described.

Charging of the silica surface has a significant effect on the adsorption behavior of PVA onto silica (Tadros 78). Figure 8.45 shows the plots of the adsorption isotherms for partially hydrolysed (88 mol %) PVA of molecular weight approximately 24,000 at two suspension pH values. The decrease in plateau adsorption density with increase in suspension pH was also observed for high molecular weight PVA ($M_{\upsilon} \approx 200,000$). As shown in Figure 8.46, decrease in the plateau adsorbed amount was observed above pH ≈ 6.0. As observed by other investigators, the plateau adsorption density is less when the pH is shifted away from the isoelectric point (Tadros 78). Tadros had suggested that the decrease in
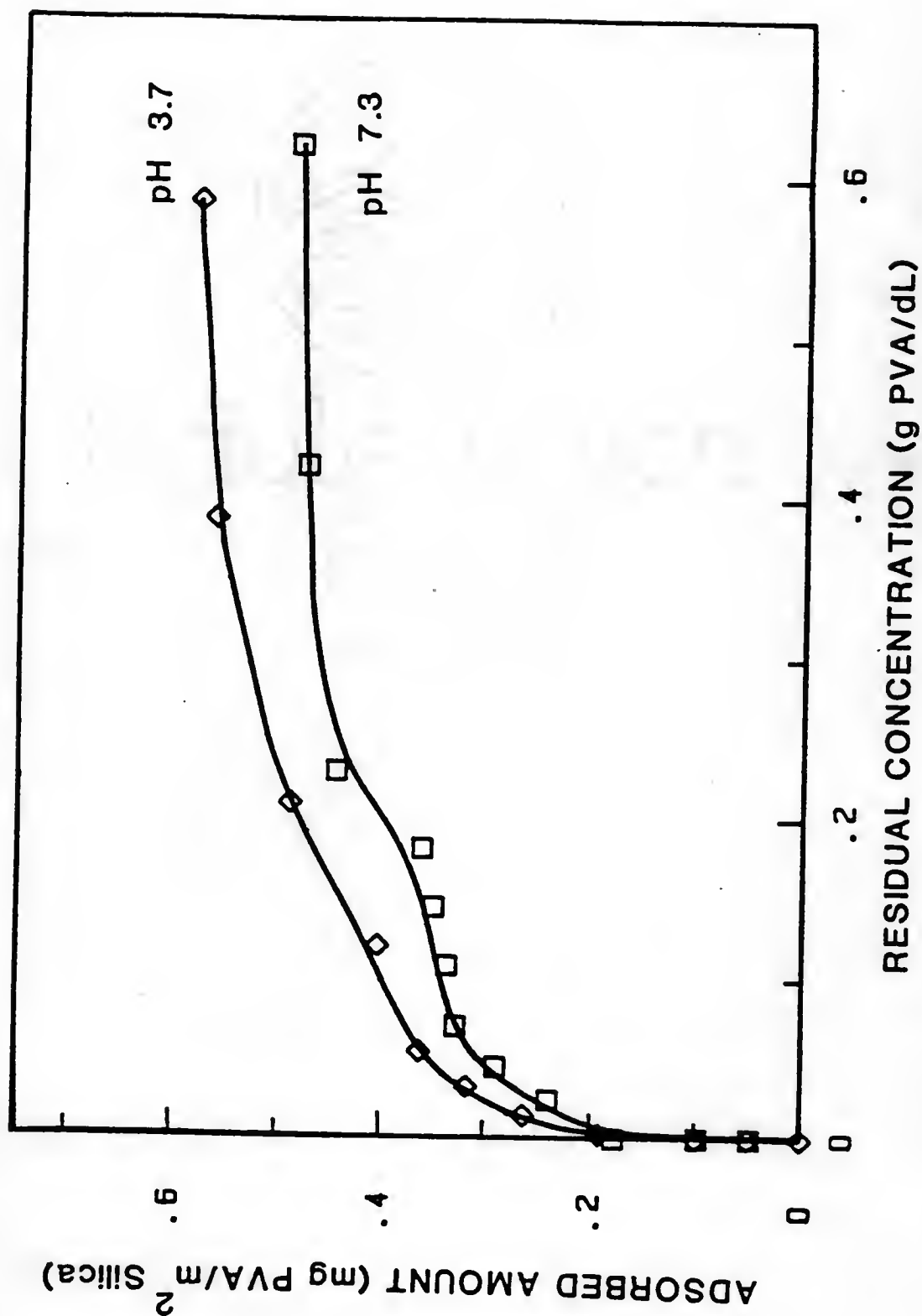
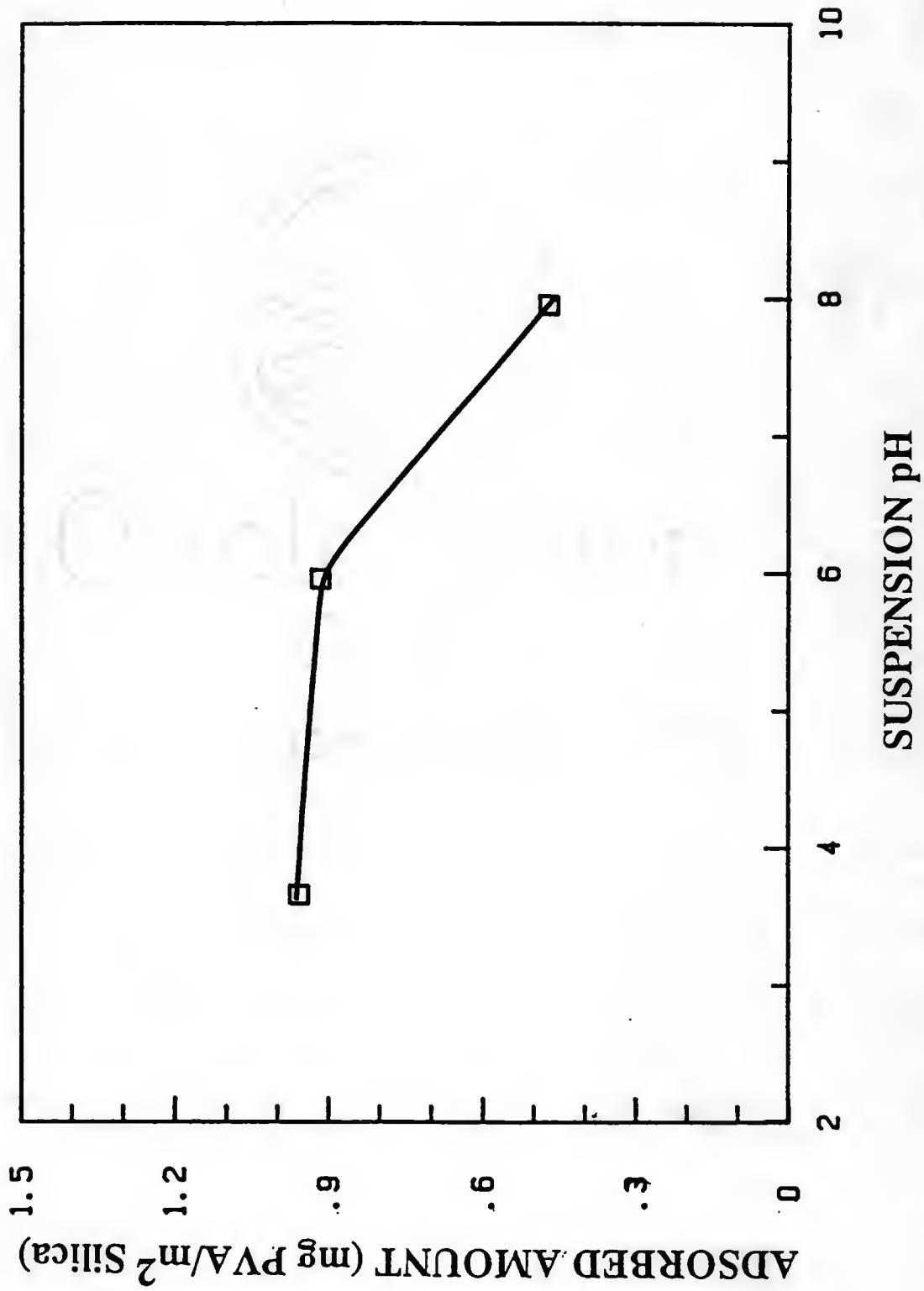Figure 8.45 Adsorption isotherm of PVA with molecular weight ≈ 24,000 at two different suspensions pH's.

Figure 8.46   Plot of plateau adsorbed amount of PVA with molecular weight ≈ 200,000 as a function of suspensions pH.

adsorption with increase in pH is due to reduction in the number of
surface silanol groups available for hydrogen bonding due to ionization
$(SiOH + OH^- \rightarrow SiO^- + H_2O)$ (Tadros 78). This explanation has been
criticized by Rubio and Kitchner on the basis of the fact that only very
small number (<< 1%) of silanol groups are ionized at modest pHs above
the isoelectric point (e.g., pH ≈ 6) (Rubio and Kitchner 76). However,
since the hydroxyl groups on silica have a range of Bronsted acid
strengths, they suggested that a certain minority type of silanol groups
(which are most important for hydrogen bonding) are most readily
dissociated. They also suggested that the decrease in adsorption is due
to general "double layer phenomenon" (i.e., reduction in affinity for
nonionic compounds due to electrostatic field near charged surface)
rather than loss of adsorption sites. This is consistent with the
observed increase in adsorption and flocculation with increasing neutral
salt concentration at constant pH (e.g., see Rubio and Kitchner 76,
Killmann 86). But the decrease in adsorption with increasing suspension
pH cannot be explained from the double layer phenomena (Tadros 78).
Other explanations, such as preferential adsorption of water molecules
and screening effect of hydrated counterions, have been suggested to
explain the decreased adsorbed amount with increasing suspension pH
(Tadros 78). Thus, the exact mechanism is not yet well understood.

Figure 8.47 shows the effect of suspension pH on the rheological
behavior. Figure 8.47A shows the plots of relative viscosity (shear rate
of 1000 s^{-1}) versus adsorbed amount, and Figure 8.47B shows corresponding
plots for relative viscosity versus fraction plateau coverage for
suspension at pH ≈ 3.7 and 7.6. Suspensions prepared at pH ≈ 3.7 (i.e.,
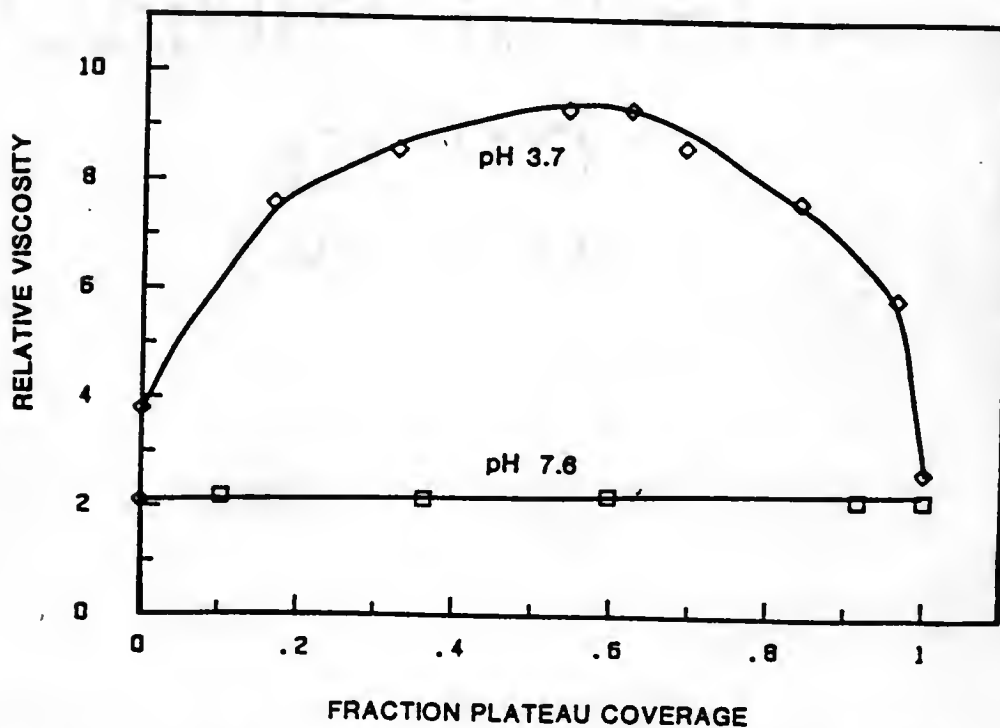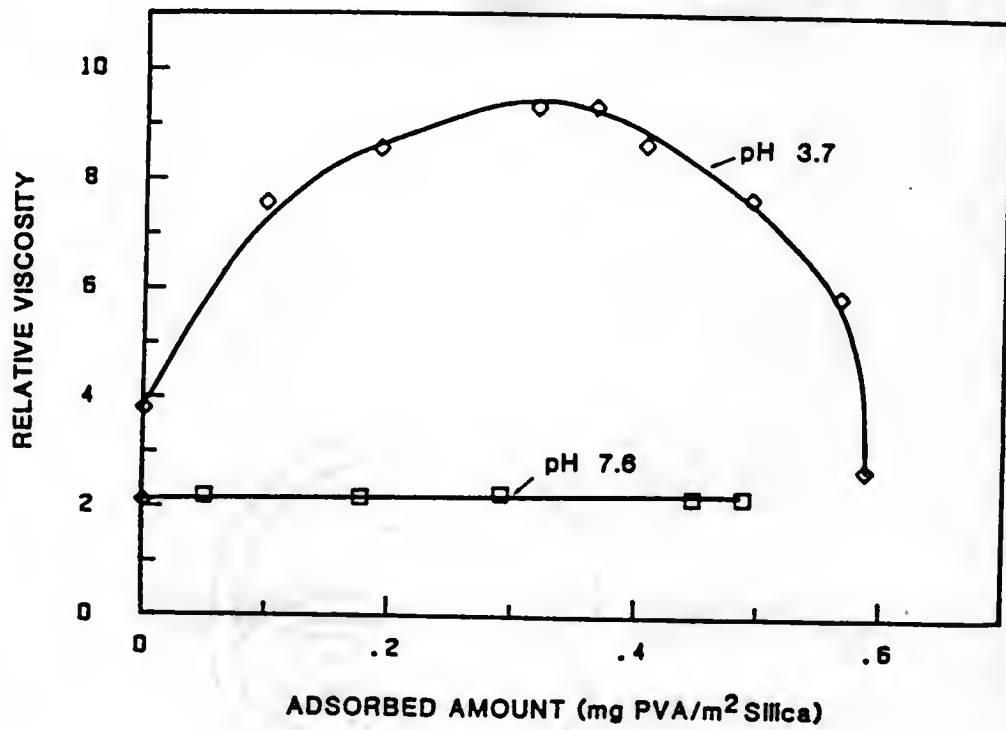
Figure 8.47   Plots of (a) relative viscosity of 20 vol.% suspensions
versus adsorbed amount of PVA with molecular weight ≈
24,000 and (b) relative viscosity versus fraction plateau
coverage for suspensions prepared at pH values 3.7 and
7.6 with varying PVA concentration.

at i.e.p.) showed higher viscosity and shear thinning flow behavior indicating bridging flocculation at partial surface coverages. These suspensions also exhibited considerable yield at partial coverages as shown in Figure 8.48. Figure 8.48A shows the plots of extrapolated yield stress versus adsorbed amount and extrapolated yield stress versus fraction plateau coverage plots (Figure 8.48B) for suspensions with pH ≈ 3.7 and 7.6. From Figures 8.47 and 8.48, it is clear that the adsorbed polymer can flocculate silica suspensions near i.e.p., while no significant change in the rheological behavior was observed for suspensions at pH ≈ 7.6. Killmann et al. have observed that precipitated silica can be flocculated with poly (ethylene oxide) at low polymer concentrations (i.e., low surface coverages) at low pH (pH ≈ 2-3) and at high electrolyte concentrations (Killmann et al. 86). Our (for 700°C calcined silica) low pH rheological results are consistent with the above observation. Suspensions at pH ≈ 7.6 showed low relative viscosities and Newtonian flow behavior at partial as well as at complete surface coverages with adsorbed PVA. These results indicate that the double layer repulsion prevents closer approach of particles, and if this distance of closest approach is larger than the span of the adsorbed polymer molecules (i.e., loop or tail extension), then the bridging flocculation can be prevented as shown schematically in Figure 8.49.

Figure 8.50A shows plots of sediment density versus fraction plateau coverages, and Figure 8.50B shows corresponding plots of median pore radius versus fraction plateau coverages for green compacts prepared from suspensions with pH ≈ 3.7 and 7.6. No changes in green density and median pore radius with varying surface coverage were observed for
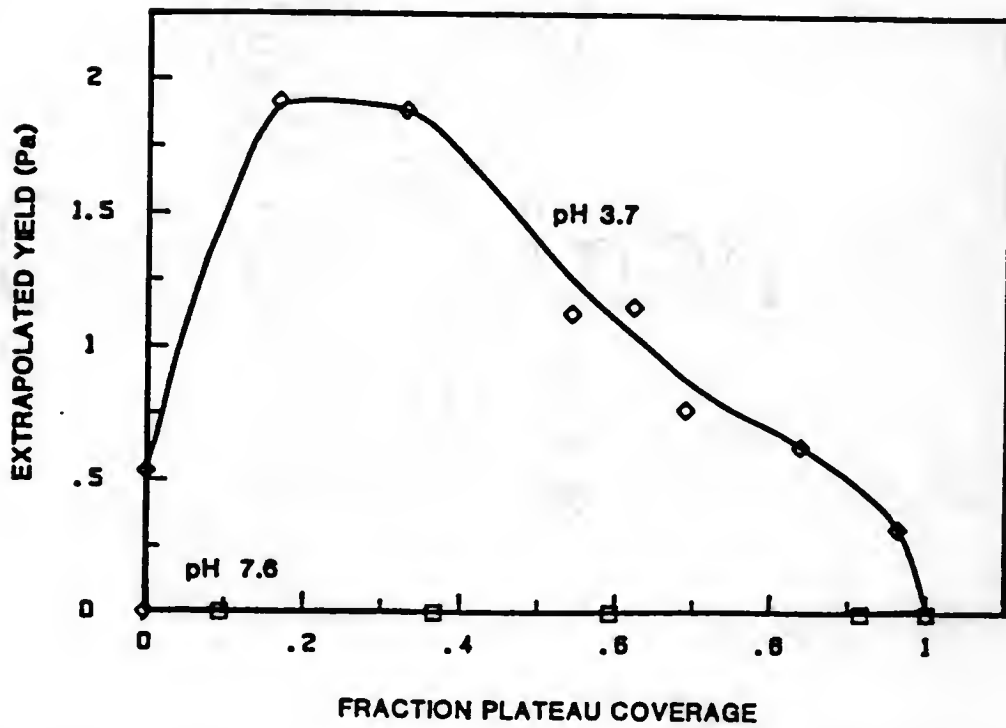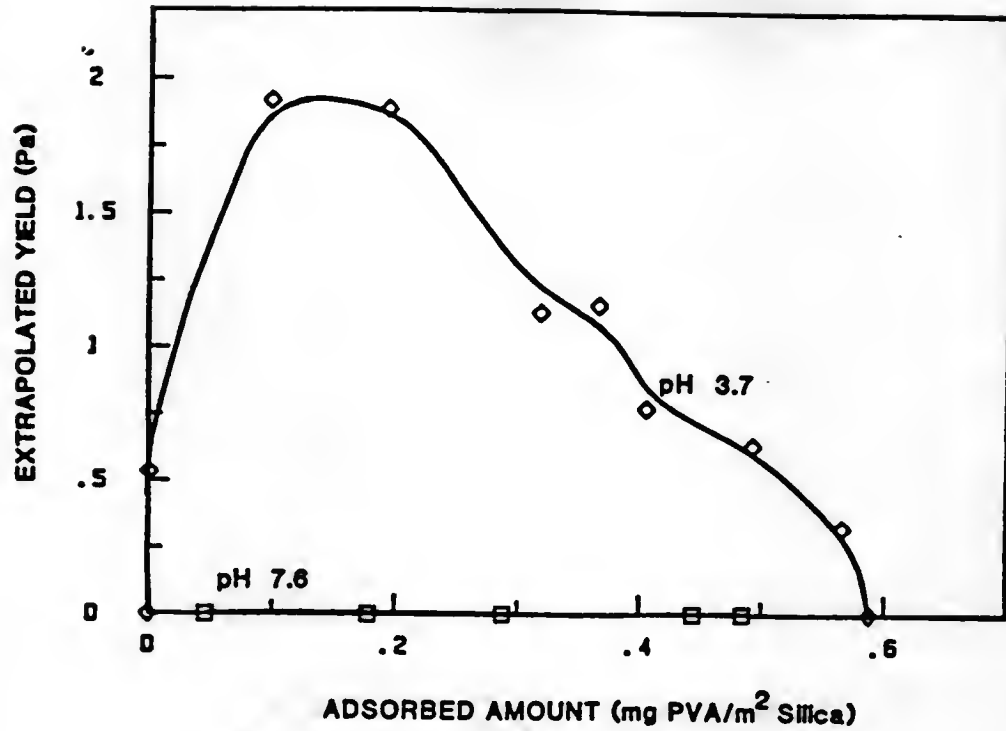
Figure 8.48   Plots of (a) yield stress versus adsorbed amount of polymer and (b) yield stress versus fraction plateau coverage for suspensions prepared at pH values 3.7 and 7.6.
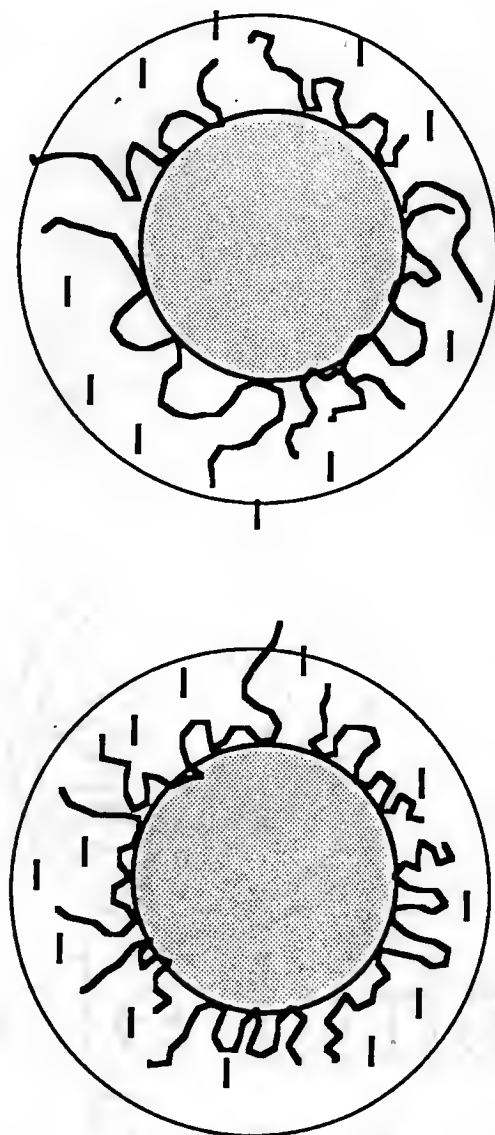
Figure 8.49   Schematic illustration showing the prevention of bridging flocculation due to diffuse electrical double layer.
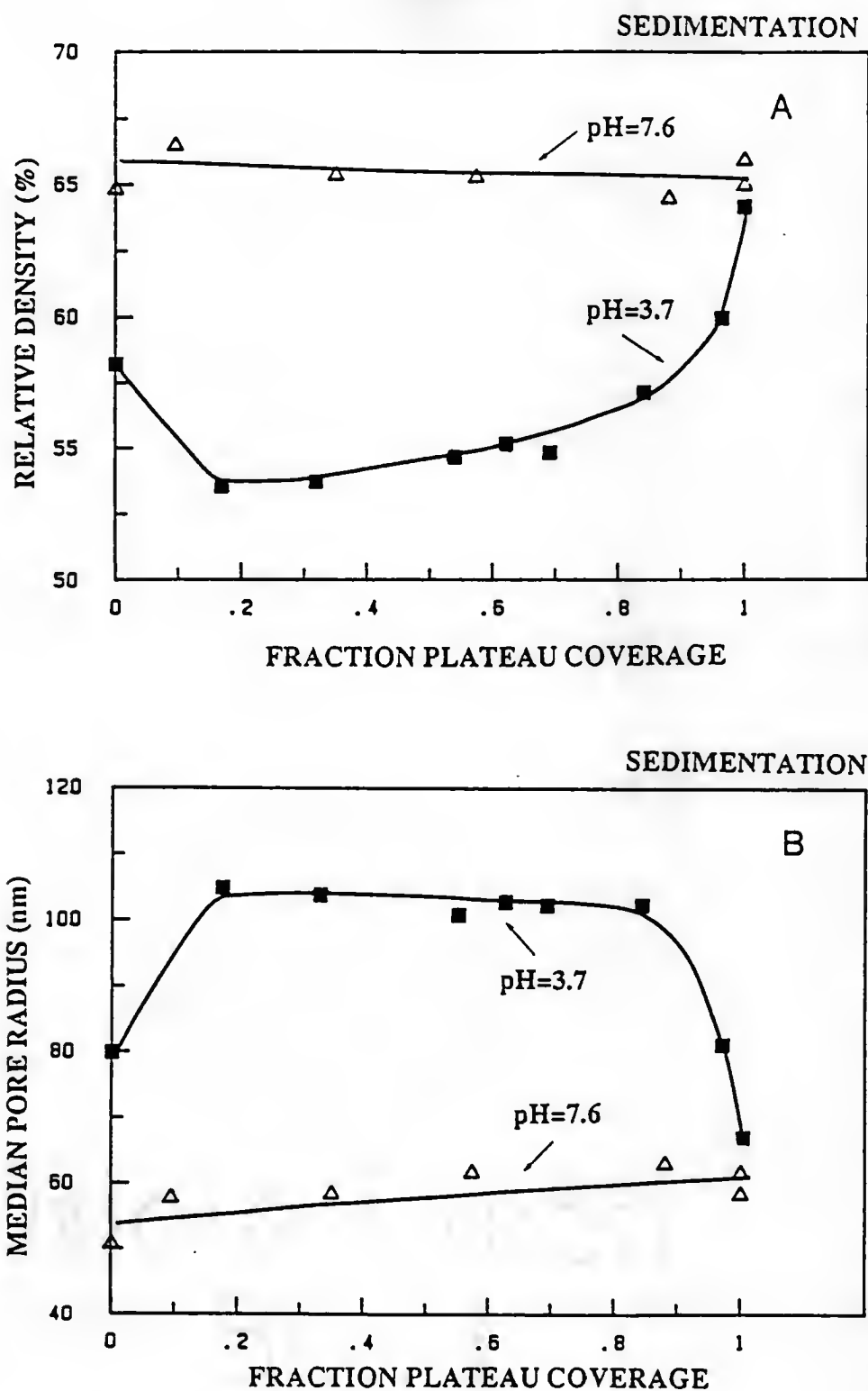
Figure 8.50   Plots of (a) sediment density versus fraction plateau coverage and (b) median pore radius versus fraction plateau coverage for compacts prepared from 20 vol.% SiO_2 suspensions with varying amounts of PVA concentrations at indicated suspension pH values.

compacts prepared from the high pH suspension. The compacts produced from the high pH suspensions were highly ordered and the compacts had green density of ≈ 64%. This observation is consistent with the rheological flow behavior of high pH suspensions (Figure 8.47), i.e., lower relative viscosities and the Newtonian flow behavior (indicating particles are well-dispersed in the suspension). In contrast, the compacts prepared from suspensions with pH ≈ 3.7 had lower green densities (and corresponding high median pore radii) at partial surface coverages. This indicates bridging of particles by the adsorbed polymer at partial coverages. At complete surface coverages, high green density (and smaller pore radius) indicates steric stabilization of suspensions (i.e., particles are well-dispersed in the suspension).

At pH ≈ 7.6, electrostatic repulsion contributes to the stability of suspensions at partial coverages. This can be seen more clearly from the plot of the zeta potential versus the adsorbed amount of polymer as shown in Figure 8.51. There is a decrease in the zeta potential with increasing adsorbed amount of polymer. When a nonionic polymer such as PVA is adsorbed at the solid surface, normally there is an outward shift in the "plane of shear" compared to its position in the absence of adsorbed polymer. From the observed decrease in the zeta potential, it is possible to calculate the hydrodynamic thickness of the adsorbed layer if one assumes that the adsorbed polymer does not affect (i) the surface charge density, (ii) the specific adsorption of ions in the stern plane, and (iii) the charge distribution in the diffuse layer (Koopal 78). The adsorbed polymer layer thickness, δ, can be calculated from the following equation:
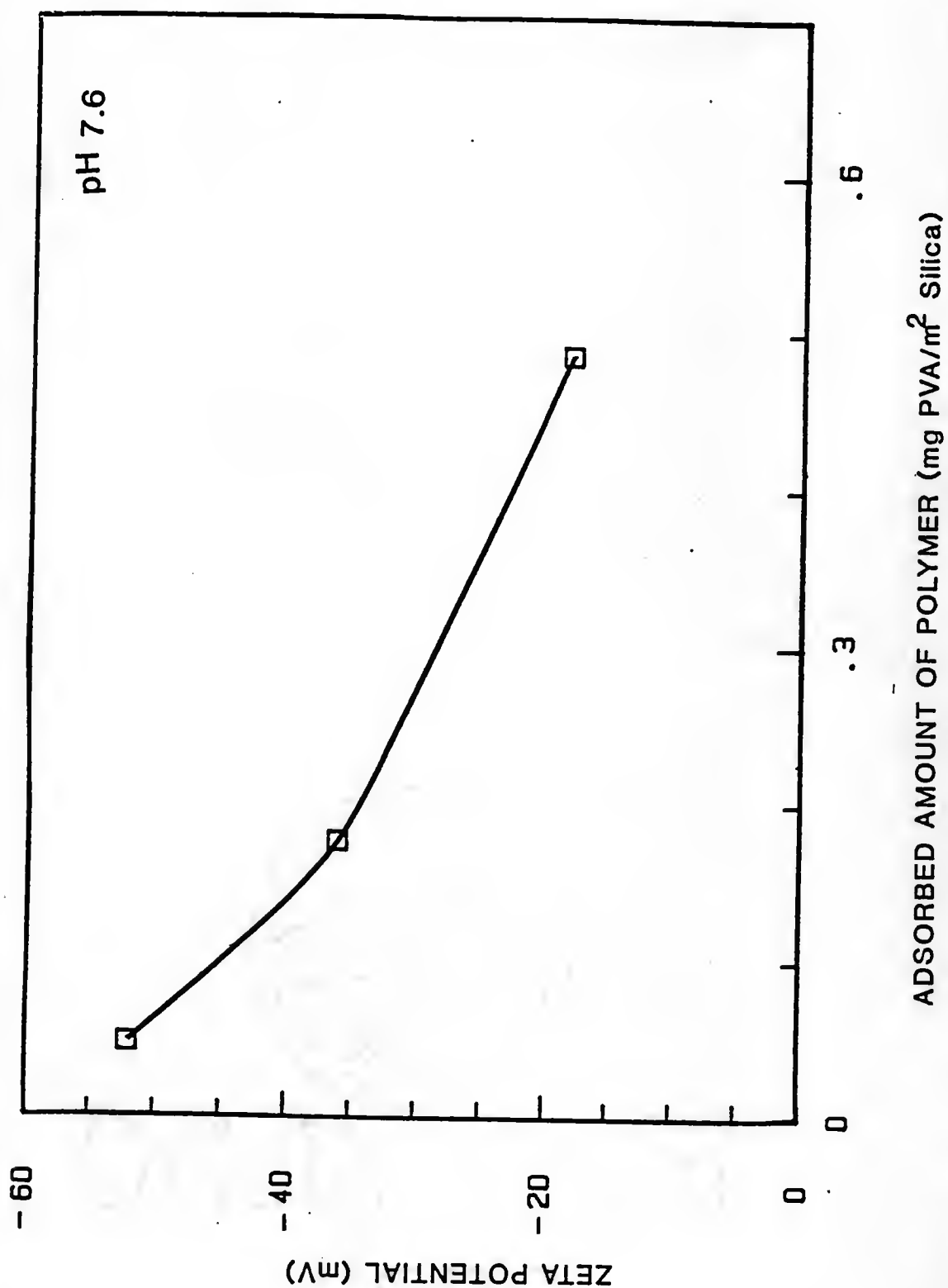
Figure 8.51   Plot of zeta potential versus adsorbed amount of PVA with molecular weight 24,000 at suspensions pH 7.6.

$\zeta_0 = -65$ (mV)

IONIC CONC.

(moles/liter)

10^{-4}

10^{-3}

10^{-2}

EFFECTIVE LAYER THICKNESS (nm)

MEASURED ZETA POTENTIAL (mV)

Figure 8.52   Schematic plots of effective adsorbed layer thickness, δ,
as a function of measured zeta potential at indicated
ionic strengths. The zeta potential with no adsorbed
polymer is ≈ -65 mV.

$$\tanh \left(ze\zeta/4kT\right) = \tanh \left(ze\zeta_o/4kT\right) \exp(-\kappa\delta) \qquad (8.2)$$

where ζ and ζ_o are the zeta potentials measured in the presence and in the absence of adsorbed polymer, z is the valency of the added electrolyte, e the electronic charge, and κ^{-1} is the Debye length. The calculated hydrodynamic thickness is also a strong function of the ionic strength of the solution since it controls the electrical double layer thickness (Figure 8.52) (Cohen Stuart and Mulder 85). The hydrodynamic thickness calculated from the decrease in the zeta potential was $\approx$ 4 nm which is similar to that measured for the viscometric technique ($\approx$ 5 nm) (Figure 8.64).

Effect of pH and Molecular Weight with the Plateau Adsorbed
Amount of Polymer

In this section, the effect of PVA molecular weight and suspension pH (with complete surface coverage of particles with adsorbed PVA) on suspension properties is described. Figure 8.53 shows the effect of PVA molecular weight on the plateau adsorbed amounts for suspensions prepared at pH $\approx$ 3.7 and pH $\approx$ 7.8. The plateau adsorbed amounts were less, as expected from the last section, for the suspensions prepared at pH $\approx$ 7.8. The increase in the plateau adsorption density with increasing molecular weights can be represented as $\alpha M_v^{0.2}$ for pH $\approx$ 3.7, as for well as pH $\approx$ 7.8. The values of plateau adsorption densitie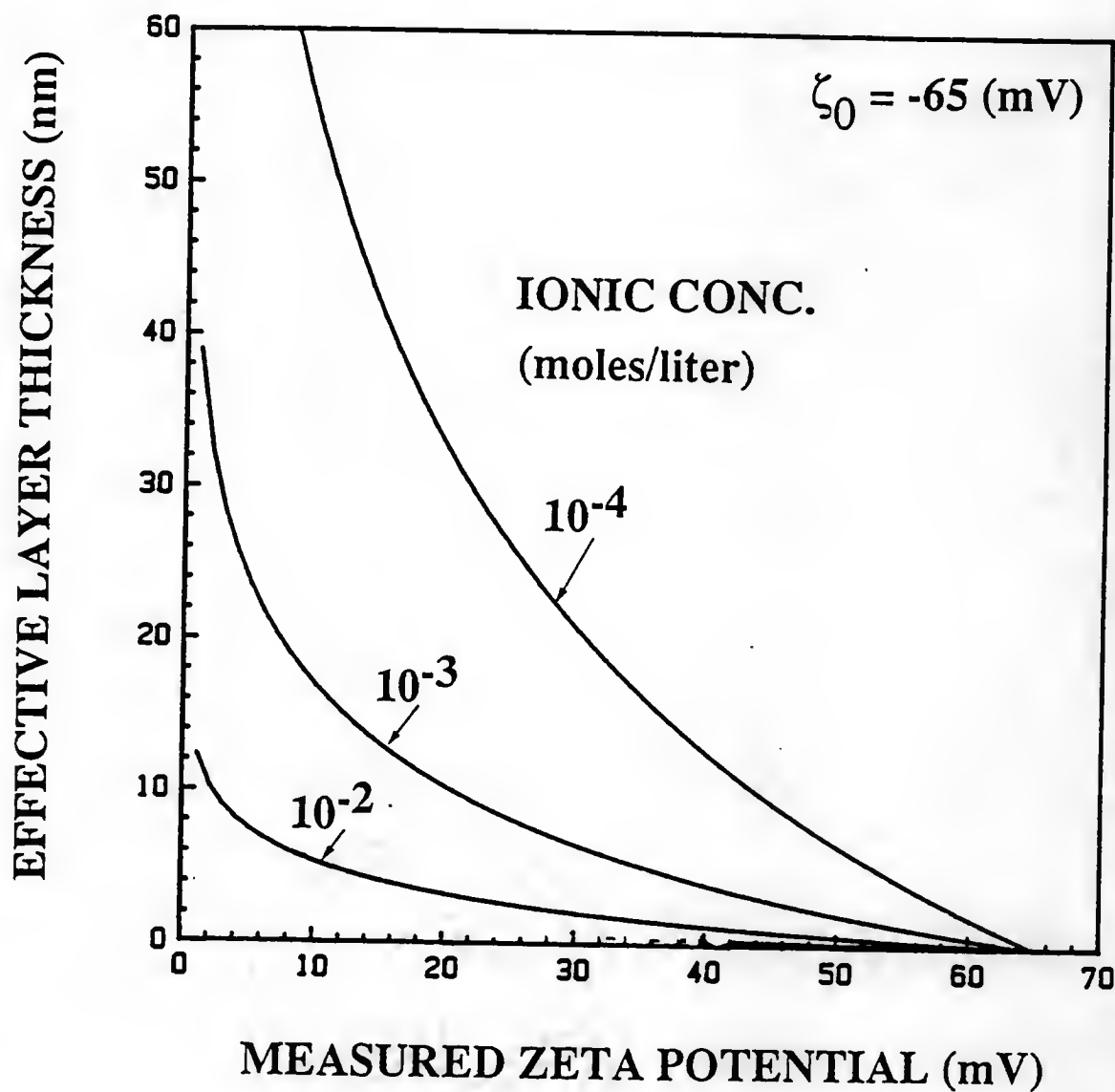s (0.6 - 1.25 mg PVA/m^2 SiO$_2$) were smaller than the plateau densities for PVA adsorbents for PVA adsorbed onto AgI (2 - 2.5 mg/m^2) (Koopal 78) or onto latex particles (1 - 3 mg/m^2) (Garvey et al. 74) indicating the importance of surface characteristics on the adsorption behavior. Garvey et al. observed the
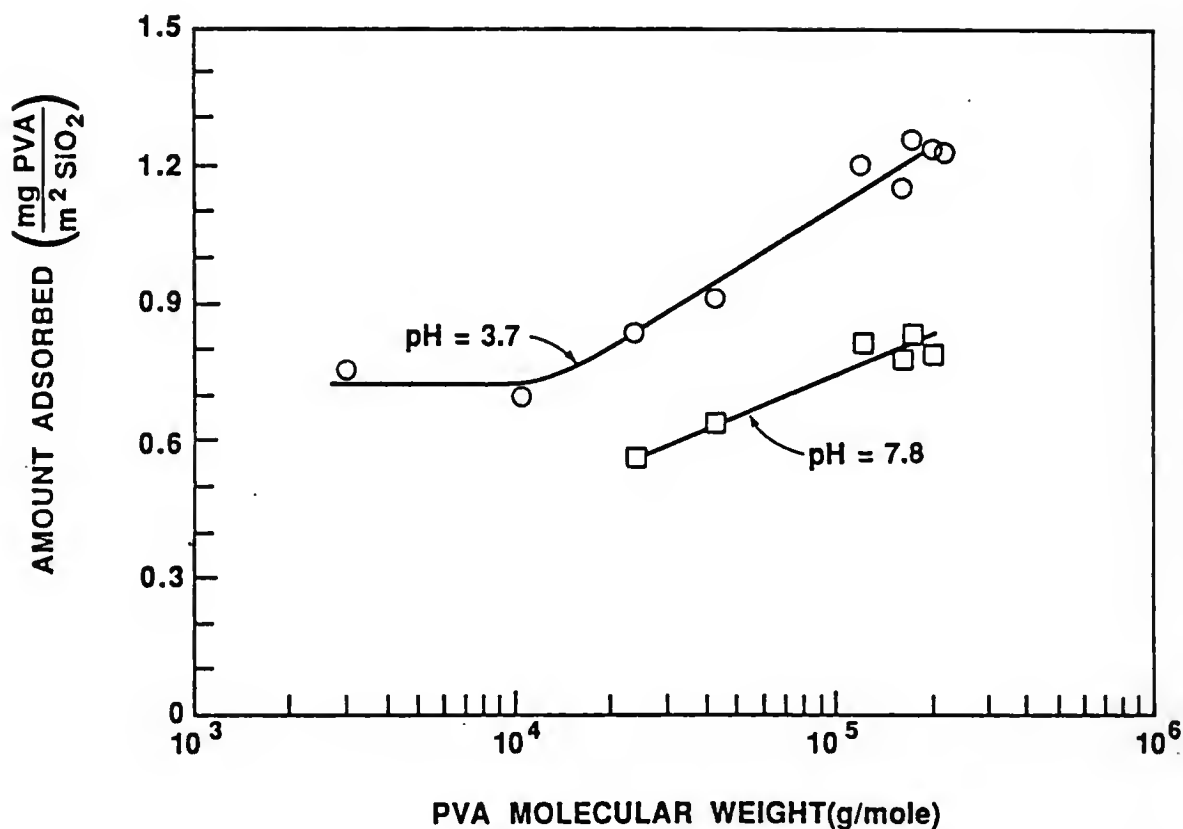
Figure 8.53   Plots of plateau adsorbed amounts of polymer versus PVA
molecular weight (log scale) at suspensions pHs 3.7 and
7.8.   Suspensions were prepared using 20 vol.% SiO₂ with
sufficient concentration of PVA in solution with varying
PVA molecular weights at indicated pH values.
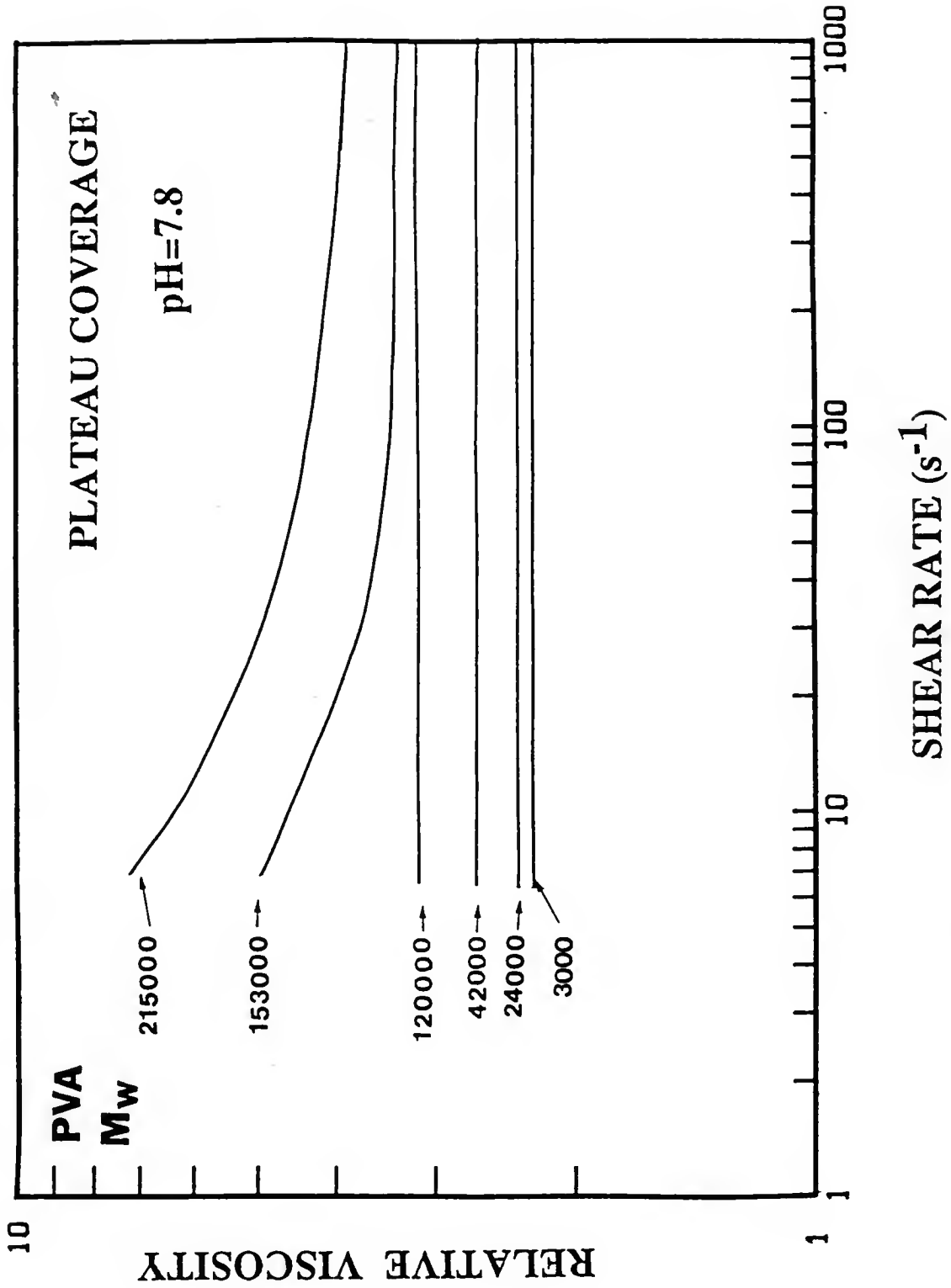
Figure 8.54   Plots of relative viscosity versus shear rate for 20 vol.% SiO₂ suspensions at pH 7.8 with plateau adsorbed amounts of PVAs of different molecular weights.
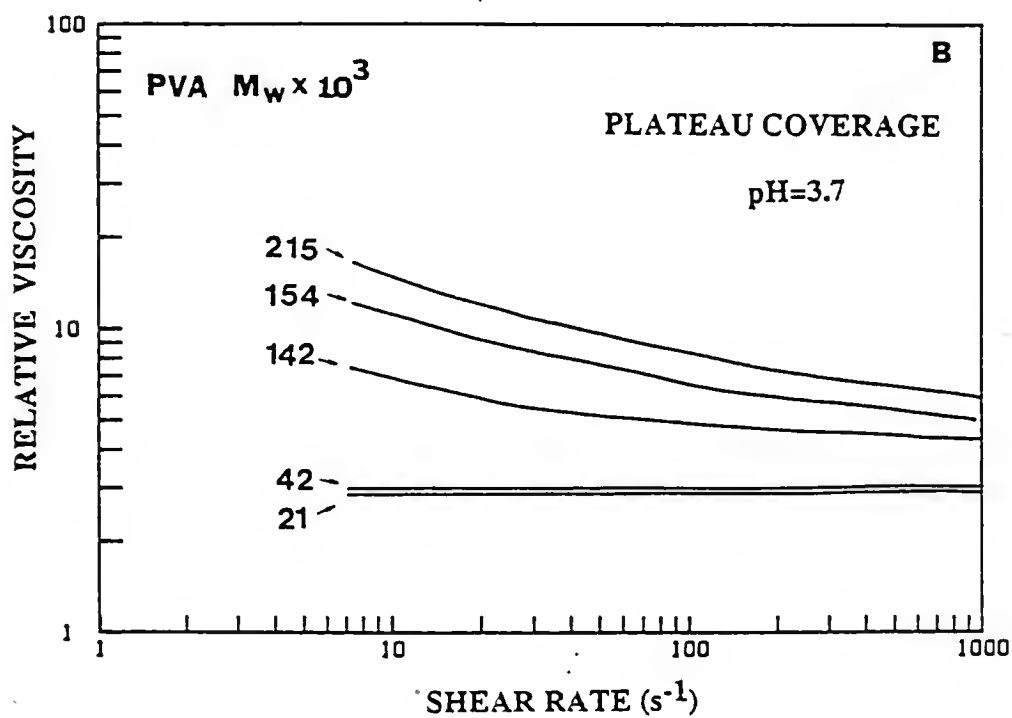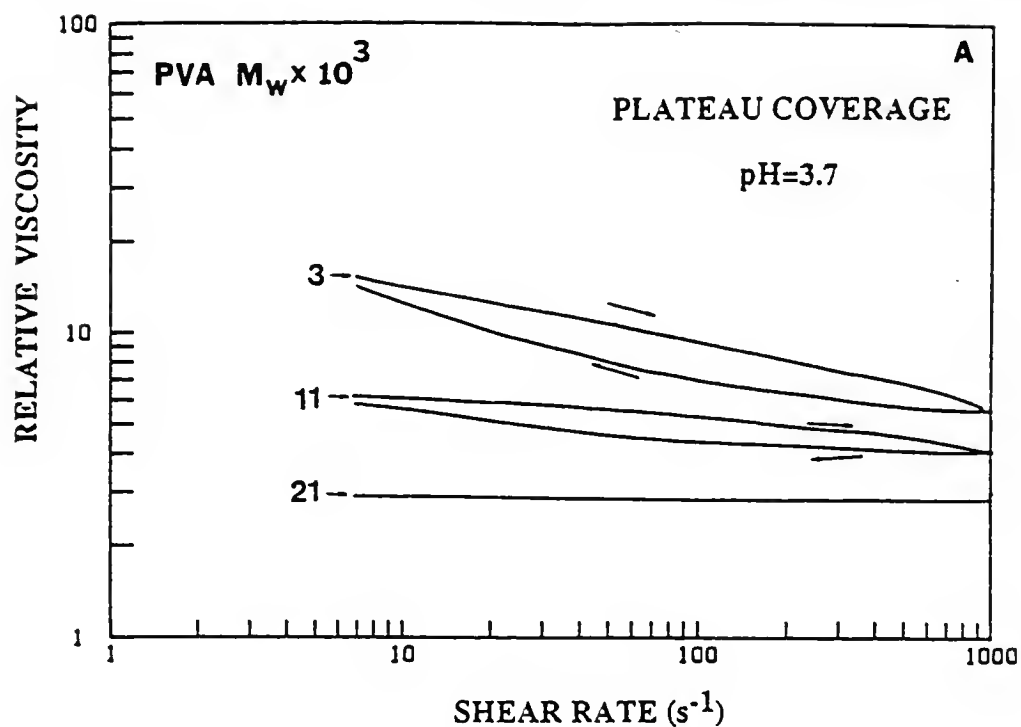
Figure 8.55 Plots of relative viscosity versus shear rate for 20 vol.% SiO_2 suspensions at pH 3.7 with plateau adsorbed amounts of PVAs of different molecular weights.

strong dependence of the plateau adsorbed amounts and the adsorbed layer thickness on PVA molecular weight, i.e., A and $\delta \propto M_\nu^{0.5}$. Also, the adsorbed layer thicknesses were approximately equal to the hydrodynamic diameters of polymer coils in solution (Garvey et al. 74). If one assumed that a polymer adsorbs as a rigid sphere of radius equal to radius of gyration, then the plateau adsorption density can be calculated. But, the plateau adsorption density was more than the calculated values. Hence, they concluded that the polymer molecules are adsorbed as an elongated coils. We observed the weak dependence of the plateau adsorbed amounts on the PVA molecular weight (i.e., A $\propto M_\nu^{0.2}$). This weak dependence of the plateau adsorbed amounts is similar to that observed by Koopal (Koopal 78). The weak dependence suggests that there is a significant change in the conformation of the adsorbed polymer (i.e., "train-loop-tail" conformation than random coil conformation) and that the conformation is not strongly dependent on PVA molecular weight (Koopal 78).

Figure 8.54 shows plots of relative viscosity vs. shear rate for suspensions at pH $\approx$ 7.8 with the plateau adsorbed amounts of PVA with varying molecular weights. Similar plots for suspensions at pH $\approx$ 3.7 are shown in Figure 8.55. The effect of molecular weight and suspension pH on the rheological behavior can be discussed more conveniently with Figure 8.56. Figure 8.56 shows the relative viscosity (at 1000 s^{-1}) as a function of molecular weight for suspensions prepared at two pH values with the plateau adsorbed amounts of PVA. Let us first consider the suspension behavior at pH = 7.8. In this case, the relative viscosity gradually increases with increasing molecular weight of the polymer.
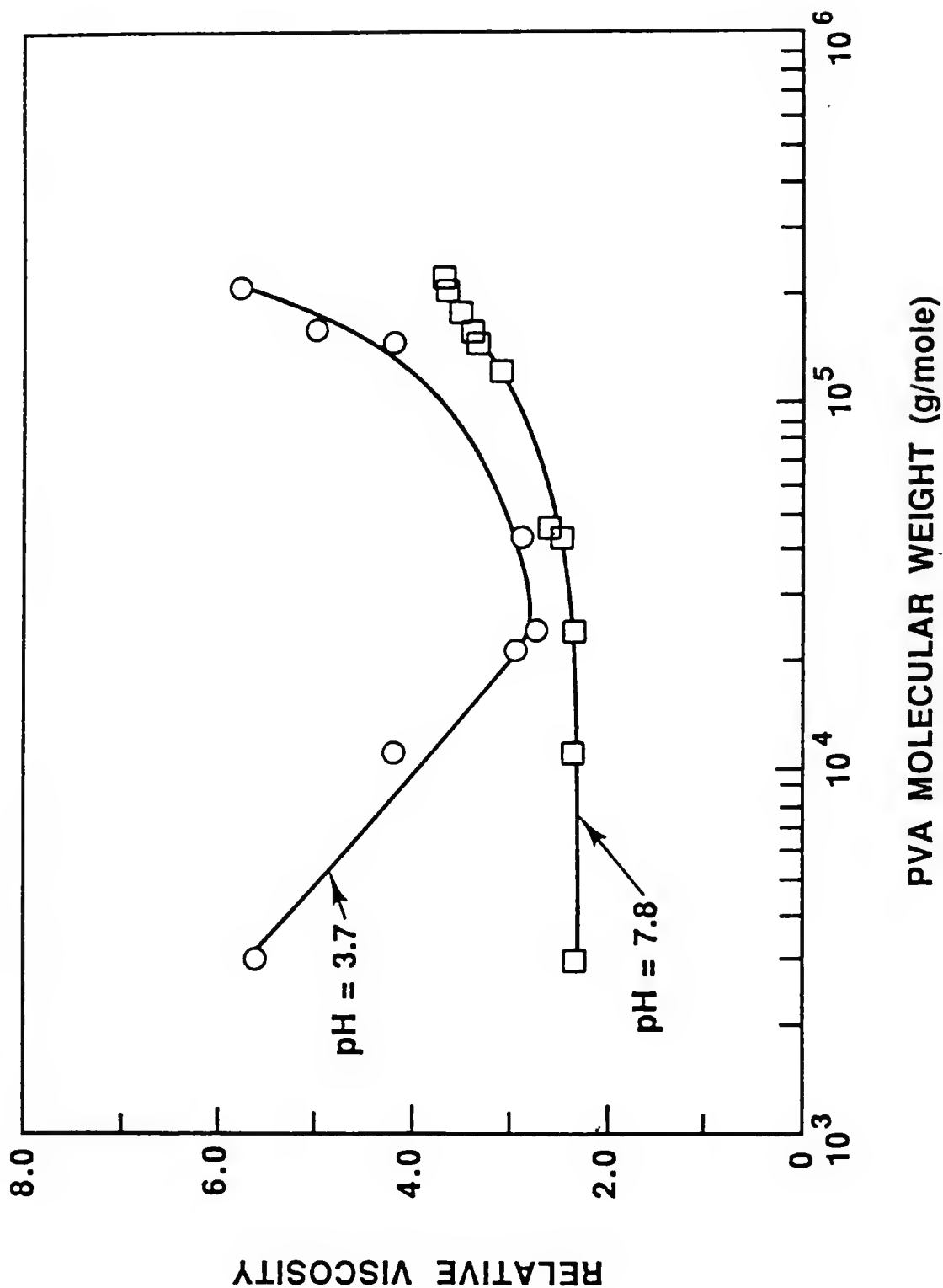
Figure 8.56   Plots of relative viscosity versus PVA molecular weight (log scale) for 20 vol.% SiO_2 suspensions with plateau adsorbed amounts of polymer at indicated pH values.

Suspensions remain well-dispersed as indicated by observations of approximately Newtonian flow behavior (Figure 8.54) and by high relative densities ($\approx$ 61 to 64 vol. %) of slip cast and sedimented samples as shown in Figures 8.59 and 8.60, respectively. With relatively low molecular weight polymers (i.e., approximately 3,000 to 24,000), both electrostatic and steric interactions contributes to suspension stability. The increases in the relative viscosity can be accounted for by increases in the "effective" volume fraction of solids in suspension. As described in Chapter II, the increased plateau adsorbed amount of polymer with increasing PVA molecular weight is accommodated by formation of larger loops and longer tails, i.e., there is an increase in the effective hydrodynamic thickness. (The degree of occupancy θ in the first layer is expected to be similar for all PVA samples (Koopal 78).) Thus, the increase in the relative viscosity can be related to increasing adsorbed layer thickness with increasing PVA molecular weight. We will expand on these results shortly.

In contrast to the suspensions behavior at pH = 7.8, the low pH suspensions showed a distinct minimum in the plot of relative viscosity versus PVA molecular weight (see Figures 8.55 and 8.56). It should be recalled that a suspension prepared at pH = 3.7 with no added polymer is extensively flocculated due to the approximately zero zeta potential, i.e., due to Van der Waal's attraction. The suspensions prepared with low molecular weight PVA (i.e., $\leq$ 20,000) were also flocculated to various extents as indicated by the higher relative viscosities and by observations of highly shear thinning behavior with low molecular weight PVA (Figure 8.55A). The flocculation of suspensions with low molecular

weight polymers (< 20,000 g/mole) is also clear from the plots of
hysteresis area and yield stress vs. PVA molecular weight (Figure 8.57
and 8.58, respectively). Although plateau adsorption was achieved in
these suspensions, the adsorbed layer thickness was too small to provide
sufficient steric repulsive forces to overcome the Van der Waal's
attractive forces. Thus, the flocculation occurs as particles fall into
the attractive minima as shown in Figure 8.22. At intermediate molecular
weights (i.e., approximately 20,000 to 40,000), the adsorbed layer
thickness is sufficient to stabilize suspensions against flocculation and
relative viscosity values are almost as low as the values for the pH $\approx$
7.8 suspensions with similar molecular weights (Figure 8.56). The
slightly higher relative viscosity values for the pH $\approx$ 3.7 suspensions
can be attributed to the larger amount of adsorbed polymer (Figure 8.53),
and hence, larger hydrodynamic volume of the polymer coated particles.
With further increases in molecular weight (i.e., greater than 40,000),
the relative viscosity of suspensions increases again. As in the pH $\approx$
7.8 suspensions, this is attributed primarily to increase in adsorbed
layer thickness with increasing PVA molecular weight. The explanations
given above are consistent with the observed relative density versus
molecular weight plot for pH $\approx$ 3.7 as shown in Figures 8.59 and 8.60.
The initial increase in the relative density with increasing molecular
weight indicates improved suspension stability with increasing PVA
molecular weight (i.e., adsorbed layer thickness). Relative densities
for PVA molecular weights in the range of 20,000 to 40,000 are close to
values obtained at pH $\approx$ 7.8. The gradual decrease in the relative
density with further increase in the PVA molecular weight (i.e., greater

Figure 8.57   Plots of hysteresis area versus PVA molecular weight (log
scale) for 20 vol.% SiO$_2$ suspensions at pH 3.7 with
plateau adsorbed amounts of polymers of different
molecular weights.

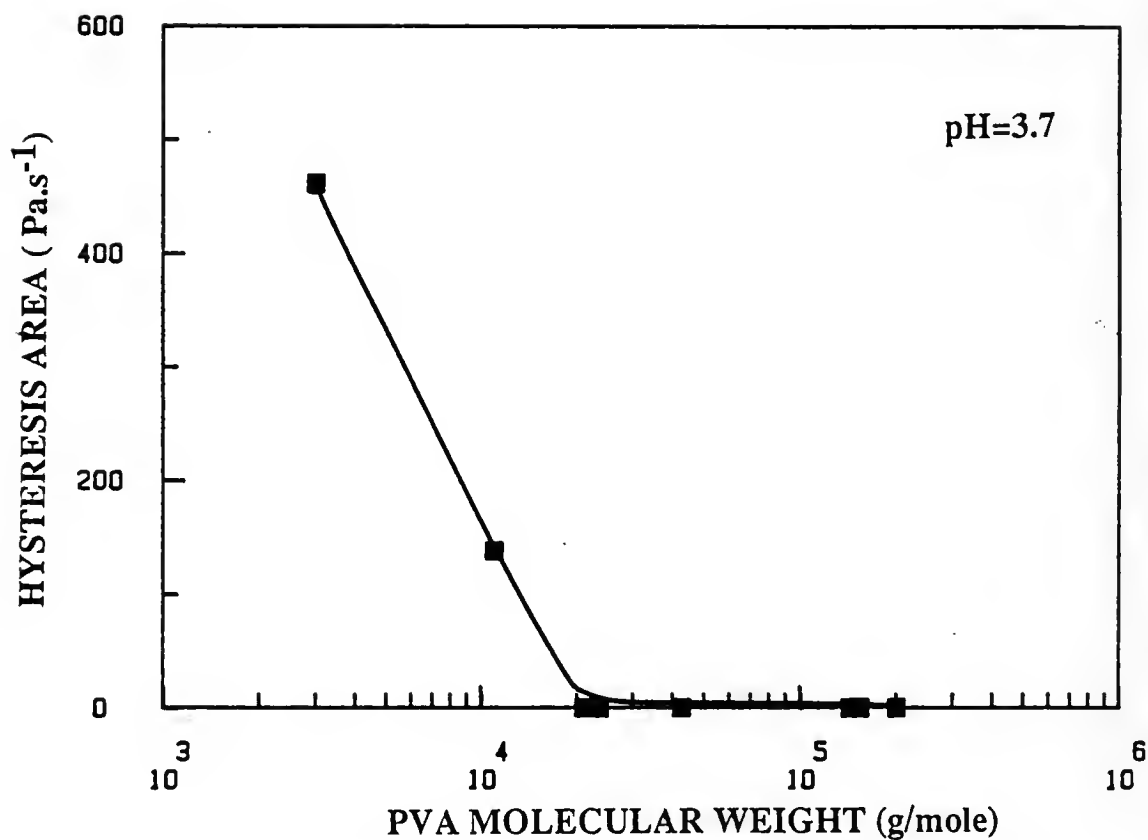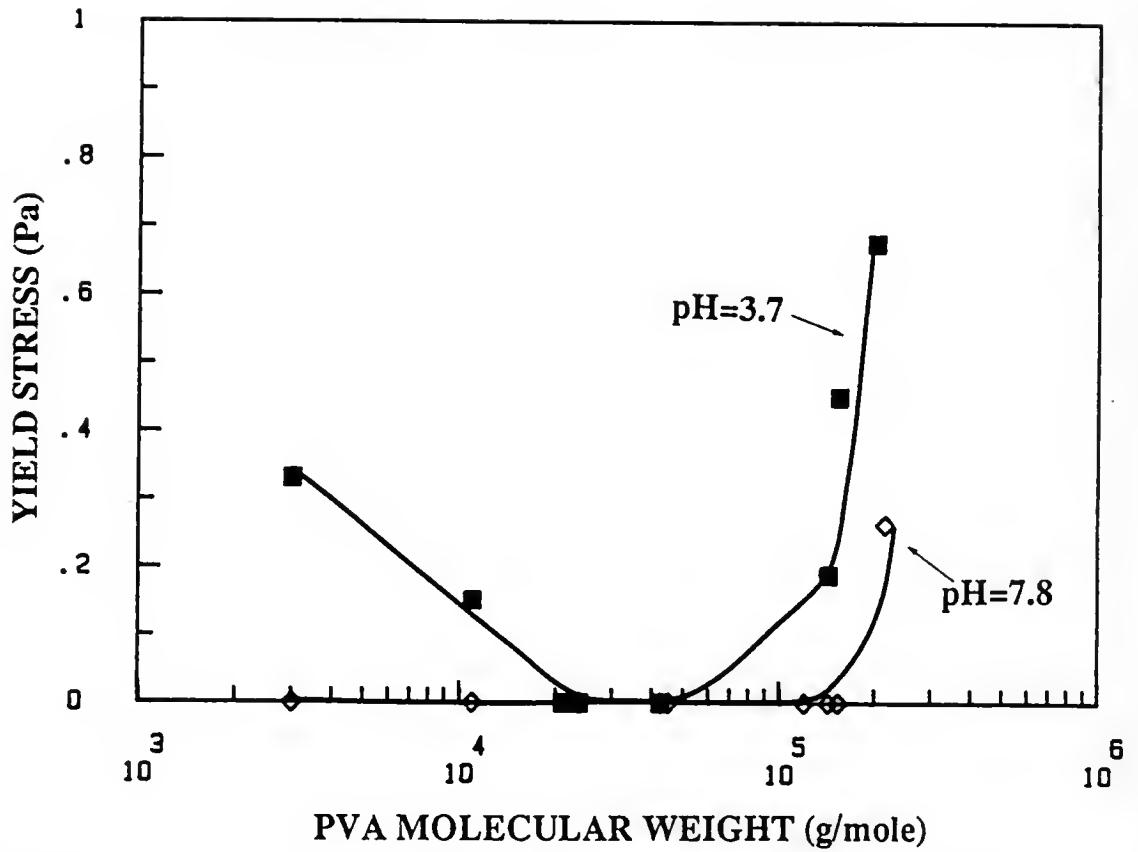

Figure 8.58   Plots of yield stress versus PVA molecular weight (log scale) for 20 vol.% SiO_2 suspensions with plateau adsorbed amounts of polymers of different molecular weights at indicated pH values.

than 40,000) indicates the effect of thicker adsorbed layers in consolidation of these samples. As described in Chapter V, suspension structures can be broadly classified into two categories (1) equilibrium structures (obtained when there is a net repulsion between particles) and (2) non-equilibrium structures (obtained when there is a net attraction between particles). Generally, the repulsive forces between particles leads to formation of high density ordered structures in the case of monosized particles. The adsorbed polymer layer thickness is not sufficient to prevent the Van der Wall's attraction between the particles, in the case of suspensions prepared at pH ≈ 3.7 with PVA molecular weights M_υ < 20,000 g/mole. The weak attraction between particles results in the formation of relatively low density after consolidation. Suspension compacts prepared at pH ≈ 7.8 with PVA molecular weight = < 20,000 g/mole, there is a net repulsion between particles, as the adsorbed layer thickness is insufficient to screen the electrostatic repulsion between particles (i.e., $\delta < \varkappa^{-1}$ where δ is the adsorbed layer thickness and $\varkappa^{-1}$ is the thickness of the electrical double layer (Figure 8.49). In this case, the repulsive interactions between particles results in the formation of higher density compacts. At sufficiently high molecular weight of PVA (M_υ > 30,000), the adsorbed layer thickness δ will be greater than the electrical double layer thickness (i.e., $\delta > \varkappa^{-1}$), and particles will be stabilized due to the adsorbed polymer layer (i.e., suspension is sterically stabilized). The gradual decrease in the compact density with increased PVA molecular weight was observed beyond M_υ ≈ 20,000 g/mole, for suspensions prepared at pH ≈ 3.7 (Figures 8.59 and 8.60). The slight lower compact densities

Figure 8.59   Plots of (a) relative density of gravity cast samples
versus PVA molecular weight (log scale) and (b) median
pore radius versus PVA molecular weight for compacts
prepared using 20 vol.% SiO_2 suspensions with plateau
adsorbed amounts of polymers with different molecular
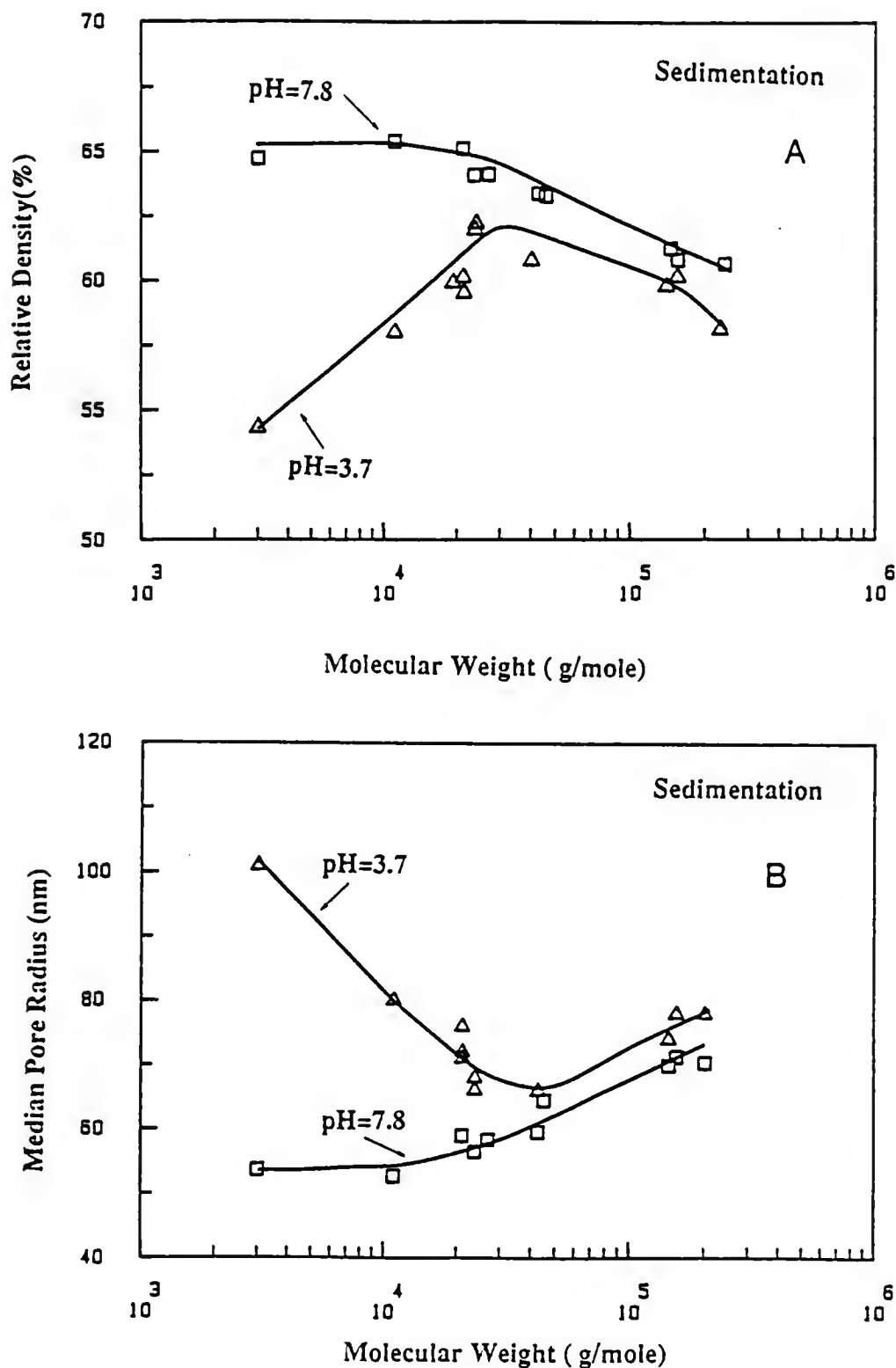weights at indicated pH values.
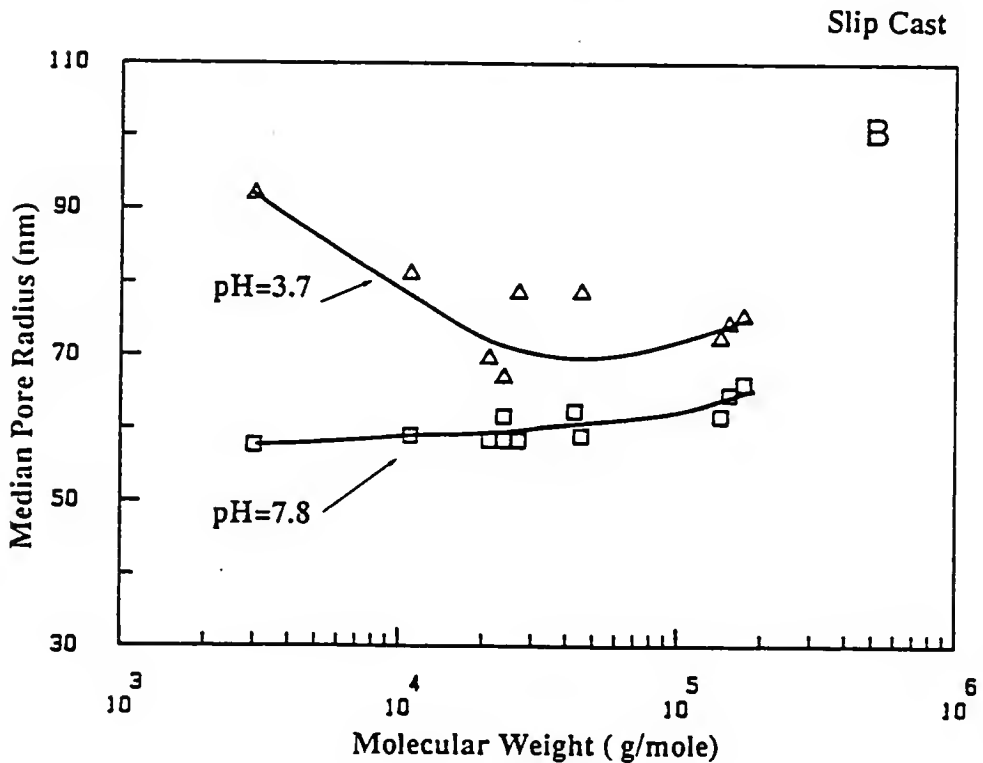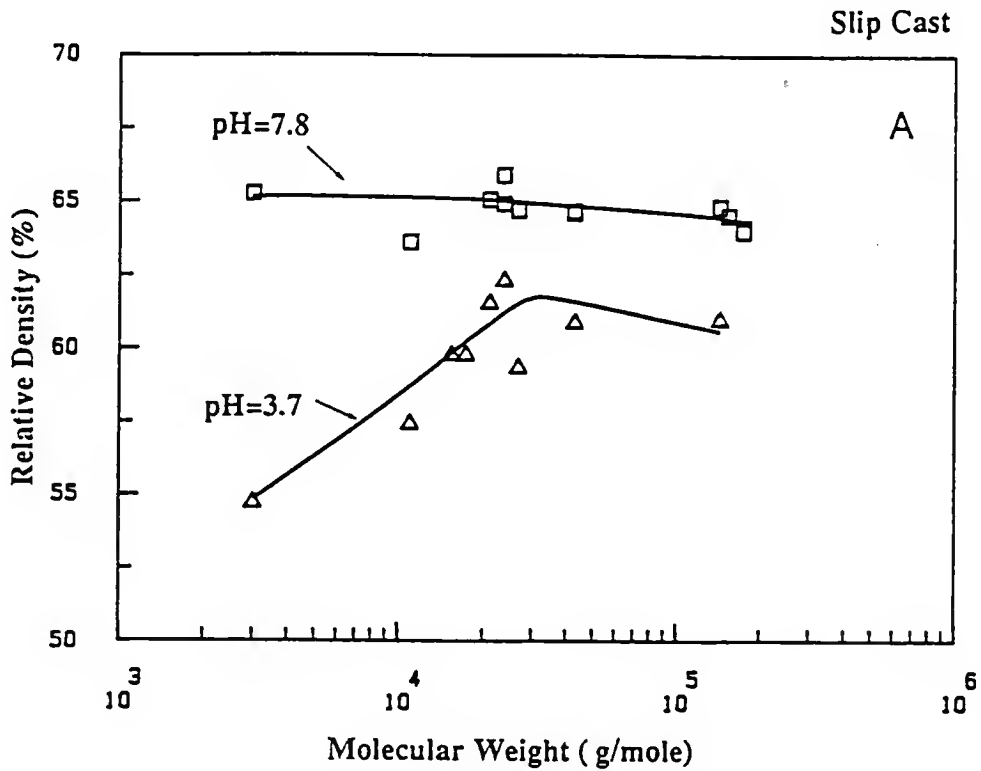
Figure 8.60   Plots of (a) relative density of slip cast samples versus
                PVA molecular weight and (b) median pore radius versus
                molecular weight for compacts prepared using 20 vol.%
                SiO_2 suspensions with plateau adsorbed amounts of PVAs
                with different molecular weights at indicated pH values.

($\approx$ 58-61%) at pH $\approx$ 3.7 can be related to the thicker adsorbed layer of PVA (Eirich 82).

The relationship between polymer layer thickness, δ, particle volume fraction, ϕ_p, and particle radius, a, on suspension stability (i.e., rheology and consolidated structures) was first pointed out by Long and Vincent (Long et al. 73). They showed that, for a system of PS-latex particles stabilized by non-ionic surfactant molecules (i.e., alkyl ethylene oxide), there exists a critical value of volume fraction solids, ϕ_c, below which the dispersion was thermodynamically stable (i.e., at ϕ_p < ϕ_c, the entropy of particles prevents aggregation), but above which a floc phase separates out. Moreover, the critical value of ϕ_c was dependent on a and δ, (i.e., ΔG_{min}) and ϕ_c decreases with increasing ΔG_{min}. This type of flocculation was reversible, i.e., on dilution of a system below ϕ_c results in stable dispersion (Long et al. 73, Garvey 77). Typical values of ϕ_c are << 1 vol. %, and since 20 vol. % silica dispersions were used in the above experiments, the observed flocculation behavior with low molecular weight PVA (i.e., thin δ) is consistent with the above results.

The critical molecular weight to stabilize suspensions of monosized spherical particles can be estimated if the relation between the adsorbed layer thickness and the PVA molecular weight can be established. Rheological data (Figure 8.56) can be used to calculate the thickness of the adsorbed polymer layer (Barsted et al. 71). When the particles have a polymer coating, the suspension liquid in the adsorbed layer is considered to be immobilized. (This is also true for the charged surfaces such as silica with no adsorbed polymer (Killmann et al. 88).)
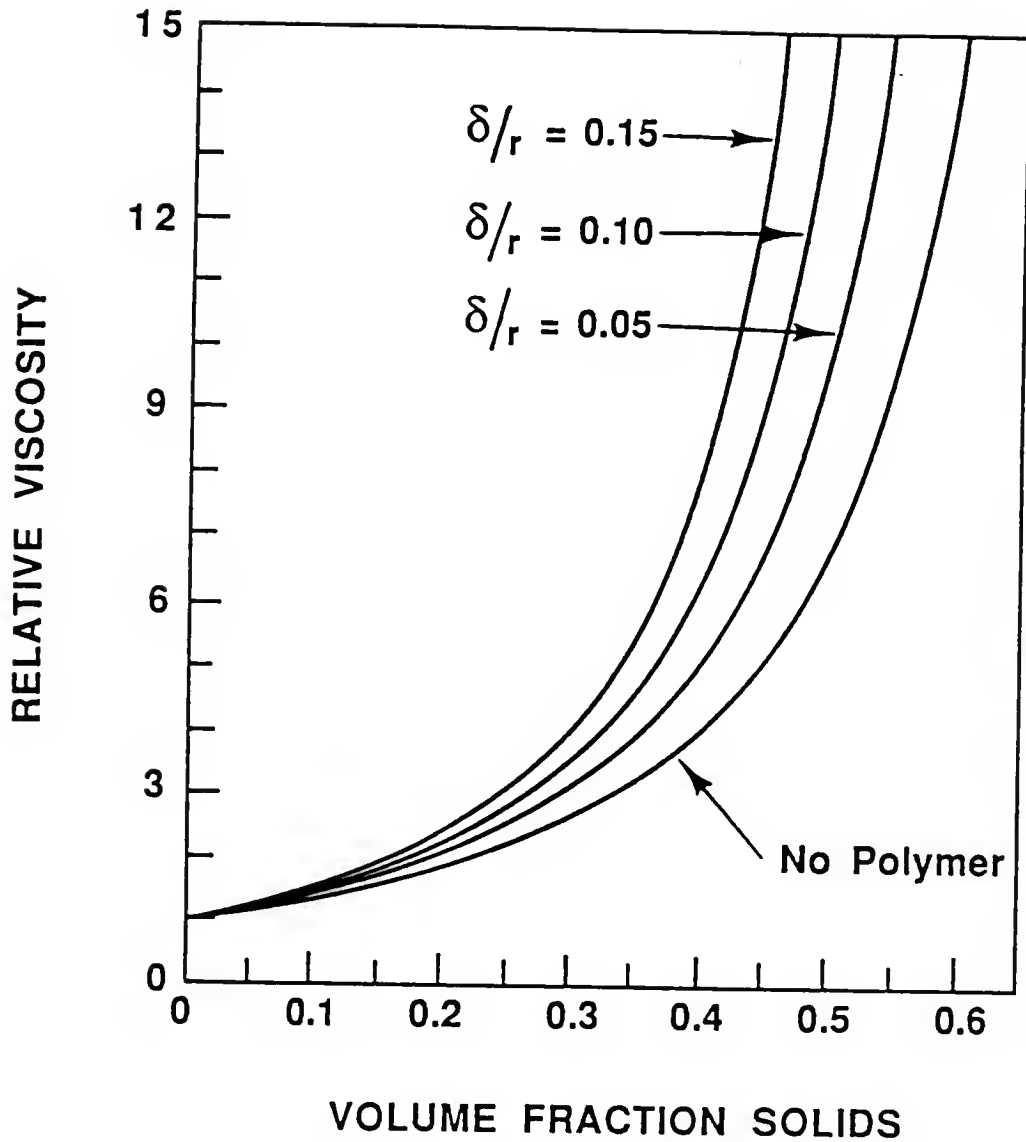
Figure 8.61   Schematic plots of relative viscosity versus the volume
                fraction of solids in suspensions for particles with the
                indicated thicknesses of adsorbed polymer. This
                thickness, δ, is indicated as a fraction of the particle
                radius.
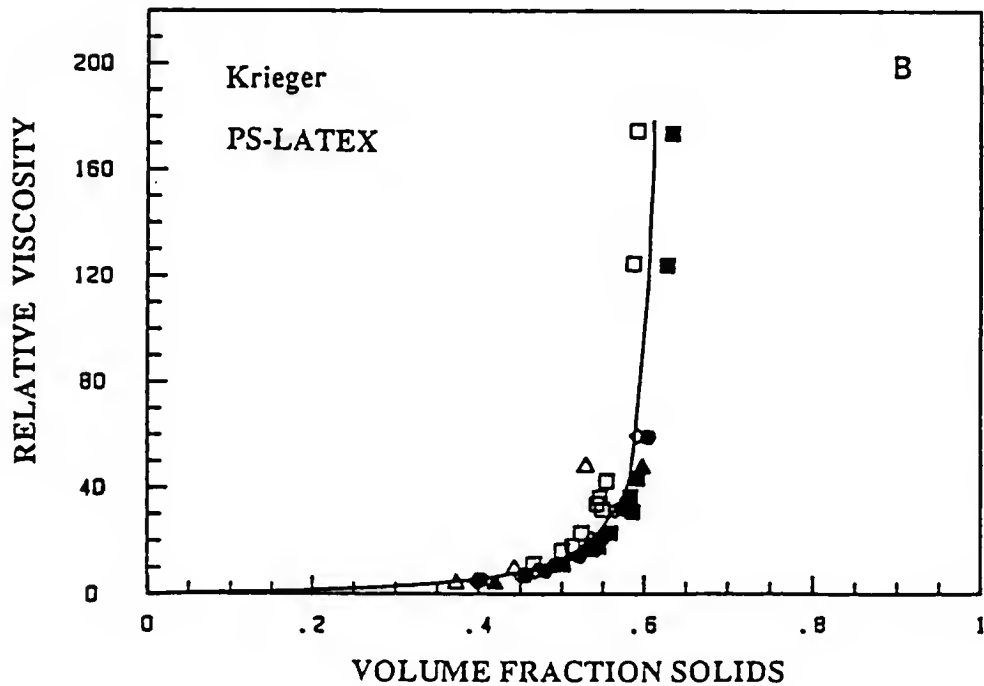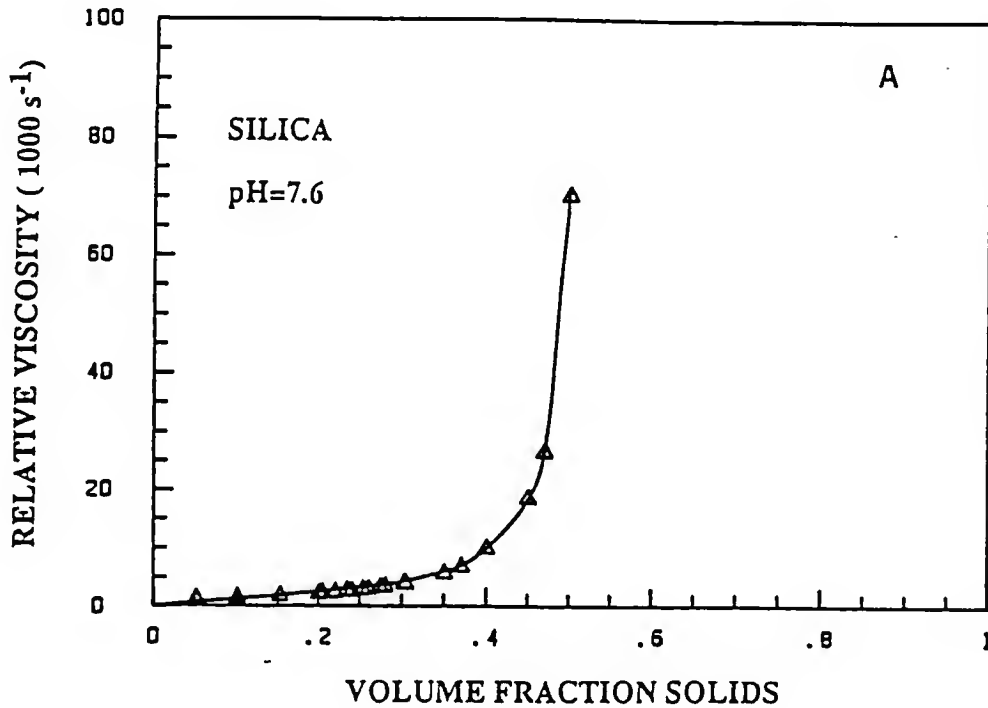
Figure 8.62   Plot of (a) relative viscosity versus volume fraction
              silica in suspensions prepared at pH 7.6 and (b) relati ⁄e
              viscosity versus volume fraction of latex particles as
              reported by Krieger (Krieger, 1972).
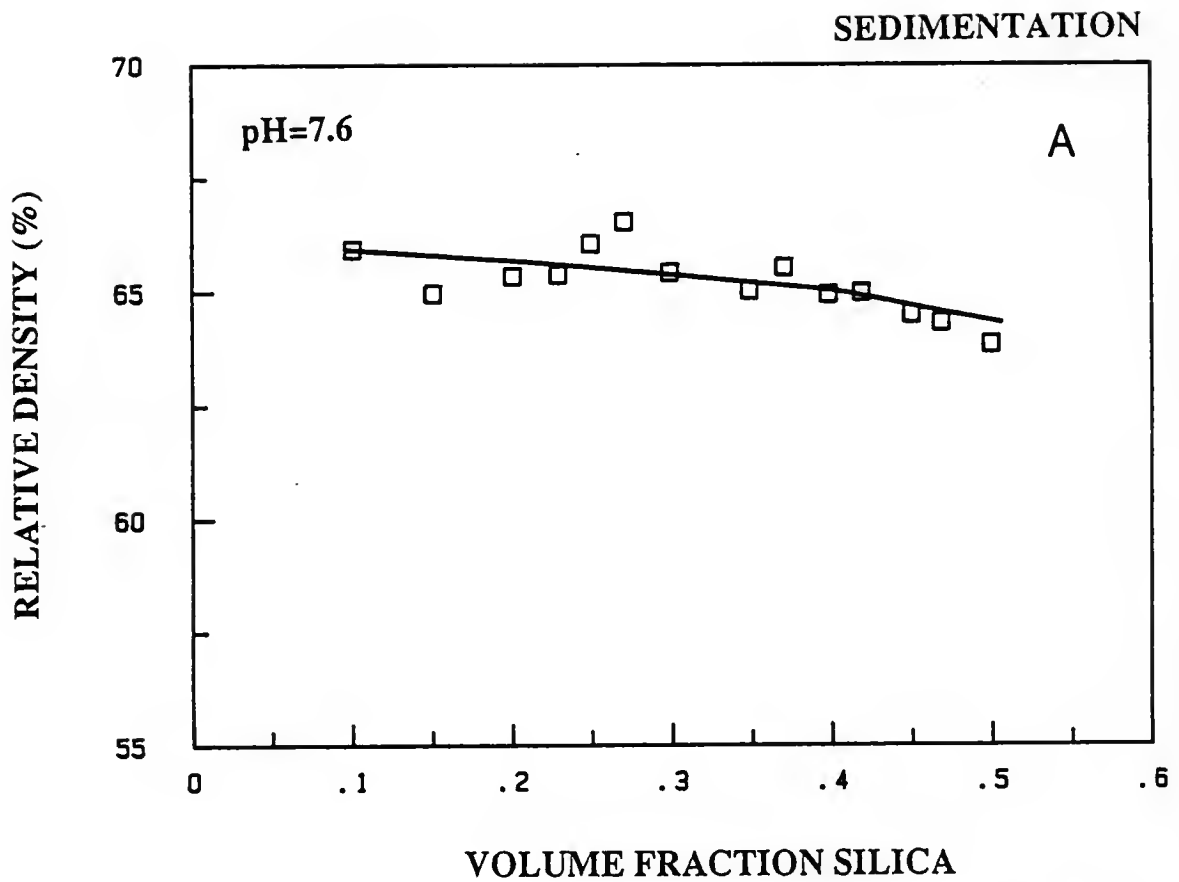
Figure 8.63   Plot of relative density of gravity cast samples versus
volume fraction silica at pH 7.6.

The shear plane is shifted away from the particle surface by the thickness of the adsorbed polymer layer, and therefore, the hydrodynamic volume of the particle is increased. As discussed in Chapter V, if one treats the particle plus adsorbed layer as a hard sphere, then the effective volume fraction of solids (ϕ_{eff}) can be related to the true volume fraction of particles (ϕ_p) by the relation:

$$\phi_{eff} = \phi_p [1 + (\delta/a)]^3 \qquad (8.2)$$

Figure 8.61 schematically illustrates the effect of the adsorbed layer thickness (which is represented as a fraction of the particle radius) on plots of relative viscosity versus solids volume fraction in suspension. The curve "no polymer" represents an empirical equation that was generated from data collected for model suspensions of monosized, spherical particles (e.g., see Thomas 65, Mooney 51, Krieger 72, etc.). It is evident from Figure 8.61 that the adsorbed layer can substantially increase the relative viscosity at higher solids loading.

For these calculations, an empirical curve of relative viscosity versus solids loading was initially generated for well-dispersed silica suspensions (Figure 8.62). Good dispersion was achieved by extensive sonication treatment to break down agglomerates and by pH adjustment to generate high zeta potential. (Electroviscous effects were minimized using solutions with 1×10^{-2} M NaCl. The stability of suspensions in the range of $\phi_p \approx 0.01$ to 0.5 is also evident from the high relative densities ($\approx 64\%$) as shown in Figure 8.63). For comparison, the η_{rel} – ϕ_p data of Krieger for monosized, spherical, and sterically-stabilized latex particles of various radii is also plotted in Figure 8.62B (Krieger 72). From Figure 8.62A, it is clear that there is a sharp increase in
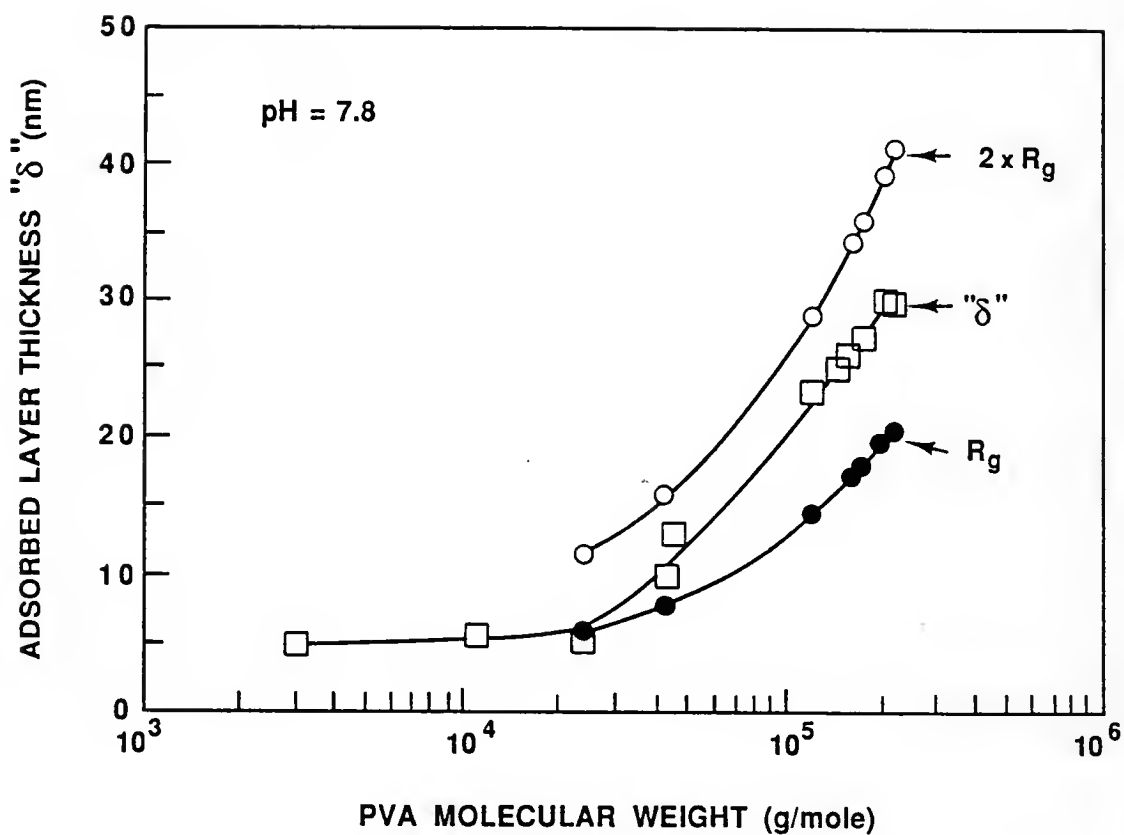
Figure 8.64   Plots of the adsorbed layer thickness, δ, versus PVA
molecular weight determined from the relative viscosity
values of 20 vol.% suspensions prepared at pH 7.8. Also
shown are the radius (R_g) and diameter ($2 \times R_g$) of
gyration of the polymers in solution as determined by
intrinsic viscosity measurements.

the relative viscosity with increasing silica volume fraction above $\phi \approx$ 0.4 and suspensions could not be prepared for $\phi > 0.5$. This maximum achievable solids loading for monosized spherical silica is smaller than the maximum solids loadings possible with latex particles ($\phi \approx 0.65$) (Figure 8.62B). The relative viscosity volume fraction silica data can be fitted equally well with Thomas' equation (Thomas 65) or Krieger's equation (Krieger 72):

Thomas Equation:

$$\eta_{rel} = 1 + 2.5\,\phi_{eff} + 0.186 \times 10^{(5.851\,\phi_{eff})} \qquad \phi_{eff} < 0.35$$

(8.3)

Krieger Equation:

$$\eta_{rel} = [1 - \phi_{eff}/0.51]^{-1.27} \qquad\qquad \phi_{eff} < 0.5$$

Thus, from the measured relative viscosity (Figure 8.56), ϕ_{eff} was determined using the above equations, and then, the adsorbed layer thickness δ was calculated using Equation 8.2. The calculated adsorbed layer thicknesses are shown in Figure 8.64 for various PVA molecular weights for suspensions with pH = 7.8. For comparison, the radius (R_g) and diameter ($2 \times R_g$) of gyration of polymer molecules in solution is also plotted in Figure 8.64. (The latter values were calculated from the measured intrinsic viscosities, Chapter VII.) The low thickness values at low molecular weights indicates the adsorbed polymer layer consists of smaller loops and shorter tails. With increasing molecular weight, the calculated thickness increases.

The fact that the calculated adsorbed layer thickness remains smaller than the diameter of the polymer coil in free solution indicates that there is a significant change in polymer conformation upon adsorption. Adsorbed polymer molecules are known to adopt a conformation

consisting of trains, loops, and tails. Tails extend farther into the solution and tails have a significant effect on the thickness of the adsorbed layer. As the polymer molecule is adsorbed in train, loop, and tail conformation, the number of segments remaining in the tail is smaller than the total number of segments in the macromolecule. Therefore, the hydrodynamic thickness (mainly determined by tails) is expected to be smaller than the random coil dimensions in solution. Figure 8.65 shows plots of adsorbed layer thickness versus (molecular weight)$^{0.5}$ for pH $\approx$ 7.8 and pH $\approx$ 3.7 for sterically stabilized suspensions (i.e., M_W > 24,000). An approximate linear relation is observed in both cases for M_v > 20,000. The adsorbed layer thickness was larger for pH $\approx$ 3.7 suspensions which is consistent with the larger adsorbed amounts of polymer at pH $\approx$ 3.7. The dependence of the hydrodynamic layer thickness, δ, on the molecular weight M_W can be represented by the following empirical equation: $\delta \propto M_W{}^{a'}$, where a is an empirical constant. The value of a' = 0.5 has been predicted by the SF theory for the homopolymer adsorption (Scheutjeans and Fleer 79,80). The hydrodynamic thickness calculated with the assumption of segment density profile of SF theory on the basis of a "porous layer model" results in $\delta \propto M_W{}^{0.8}$ (Cohen Stuart et al. 84b,84c,86a). From the scaling concepts, de Gennes gave, the following result: $\delta \propto M_W{}^{0.6}$ (de Gennes 87). The dependence of the hydrodynamic thickness on the molecular weight has been tested by various investigators (e.g., see Killmann et al., 85,88; Cohen Stuart et al. 84b,84c, Kato et al. 81, Cosgrove et al. 84). For the adsorption of PEO (i.e,. a homopolymer) on the PS latex from water, Kato et al. observed a = 0.56 whereas Cosgrove et al. obtained a = 0.8 and

Killmann et al. observed a = 0.46. No explanation has been given for the different values of exponent a', observed in the same system. PVA being a copolymer, the exponent a' cannot be compared directly with the theoretical predications. We observed a' = 0.5 for PVA adsorption on the 700°C calcined silica (Figure 8.65). The observation is similar to observations of Garvey et al. who measured the hydrodynamic thickness of PVA on the PS latex particles using photon correlation spectroscopy (Garvey et al. 74). Their results are compared with the hydrodynamic thicknesses determined in this study (Figure 8.65). The good agreement between these two techniques is evident from the Figure 8.65.

The importance of the adsorbed polymer layer thickness in preparing sterically stable dispersions and achieving maximum solids loading can be illustrated as follows:

Selection of Optimum Molecular Weight

In the absence of electrostatic repulsion, if the depth of the potential energy maximum due to Van der Waal's attraction is smaller than $\approx$ 1-2 kT, then the thermal energy of the particles can overcome this weak attraction and stable dispersions can be prepared. The Van der Waal's attraction energy at a distance of d is given by the following equation:

$$V_A = \frac{-A_{eff}}{12} \cdot \frac{a}{d} \qquad (8.4)$$

where A_{eff} is the effective Hamaker constant and a is the particle radius. As discussed above, the distance of closest approach d is related to the thickness of adsorbed polymer layer. It is reasonable to assume that the adsorbed layer thickness δ can be equated with the
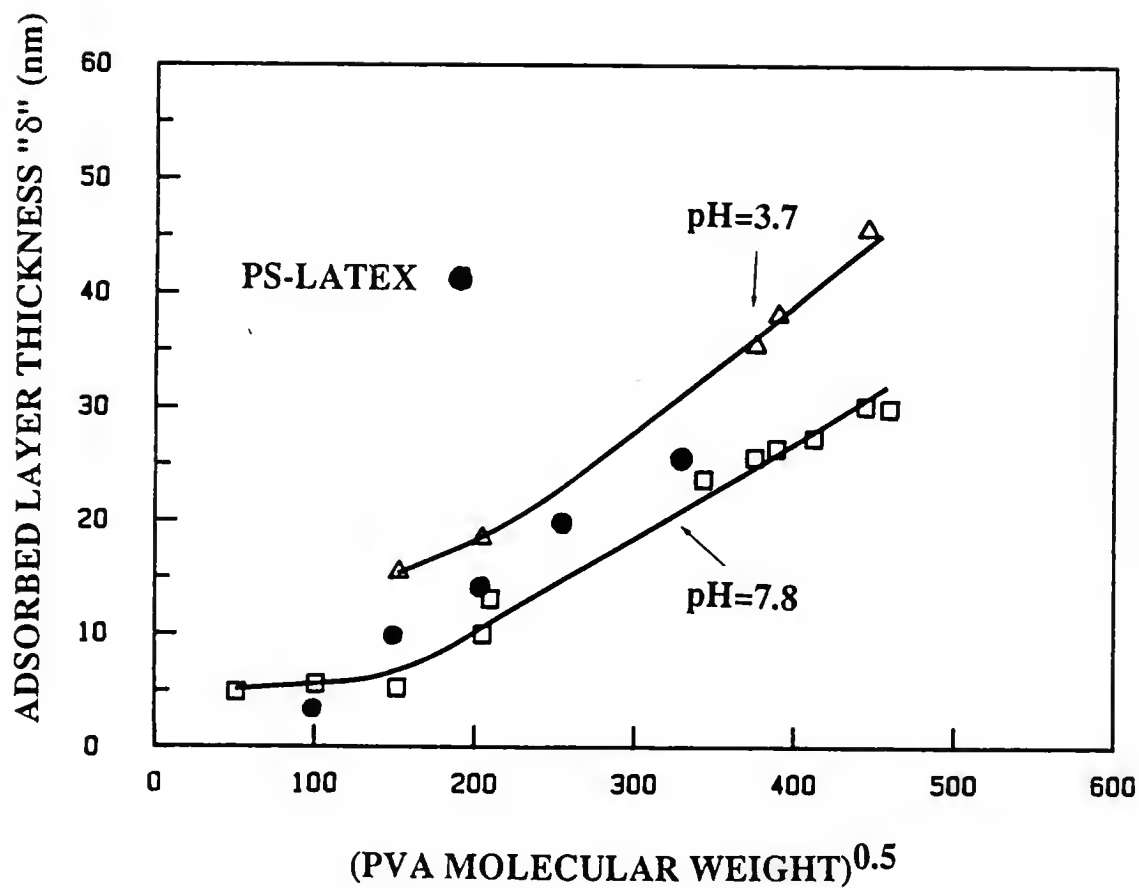
Figure 8.65   Plots of adsorbed PVA layer thickness, δ, on SiO$_2$
particles versus square root of PVA molecular weight.
Adsorbed layer thicknesses of PVA onto PS latex particles
is also shown as determined by Garvey et al.

diameter of polymer molecule in solution, i.e., $\delta = 2 \times R_g$, where Rg is the radius of gyration. (Alternatively, $\delta = K''M^{a''}$ where K'' and a'' are experimentally determined constants.) The adsorbed layer thickness δ and d are related as follows:

$$d = 2\,\delta \approx 4\,R_g, \text{ and} \tag{8.5}$$

the radius of gyration is related to molecular weight, M_w, of the polymer and for simplicity which can be represented as:

$$R_g \approx K'M_w{}^{a'} \tag{8.6}$$

where K' and a' are constants (depending on the solvent quality, chemical nature of the polymer, etc., see Chapter VI).

Substituting for d in terms of R_g in Equation 8.4, the following result is obtained:

$$M_w(min) = (\frac{1}{48K'} \cdot \frac{A_{eff}}{V_A} \cdot a)^{1/a'} \tag{8.7}$$

where k is the Boltzmann's constant, and T is absolute temperature, and V_A is $\approx kT$. Thus, the minimum polymer molecule weight $M_w(min)$, required to sterically stabilize dispersion (in a good solvent) is directly proportional to the effective Hamaker constant and the particle radius. Substituting K' and a' for partially hydrolysed PVA, we obtain:

$$M_w(min) = \{8.254 \times 10^8 \cdot \frac{A_{eff}}{V_A} \cdot a\}^{1.84} \tag{8.8}$$

Plots of log $M_w(min)$ versus particle radius for various values of (Hamaker constants/V_A) ratios are shown in Figure 8.66. The solid line separate stable and unstable regions based on the stability criterion used (i.e., the value assumed for A_{eff}/V_A). For example, for a given molecular weight of the polymer (for e.g., $M_w = 10^3$), there exists a
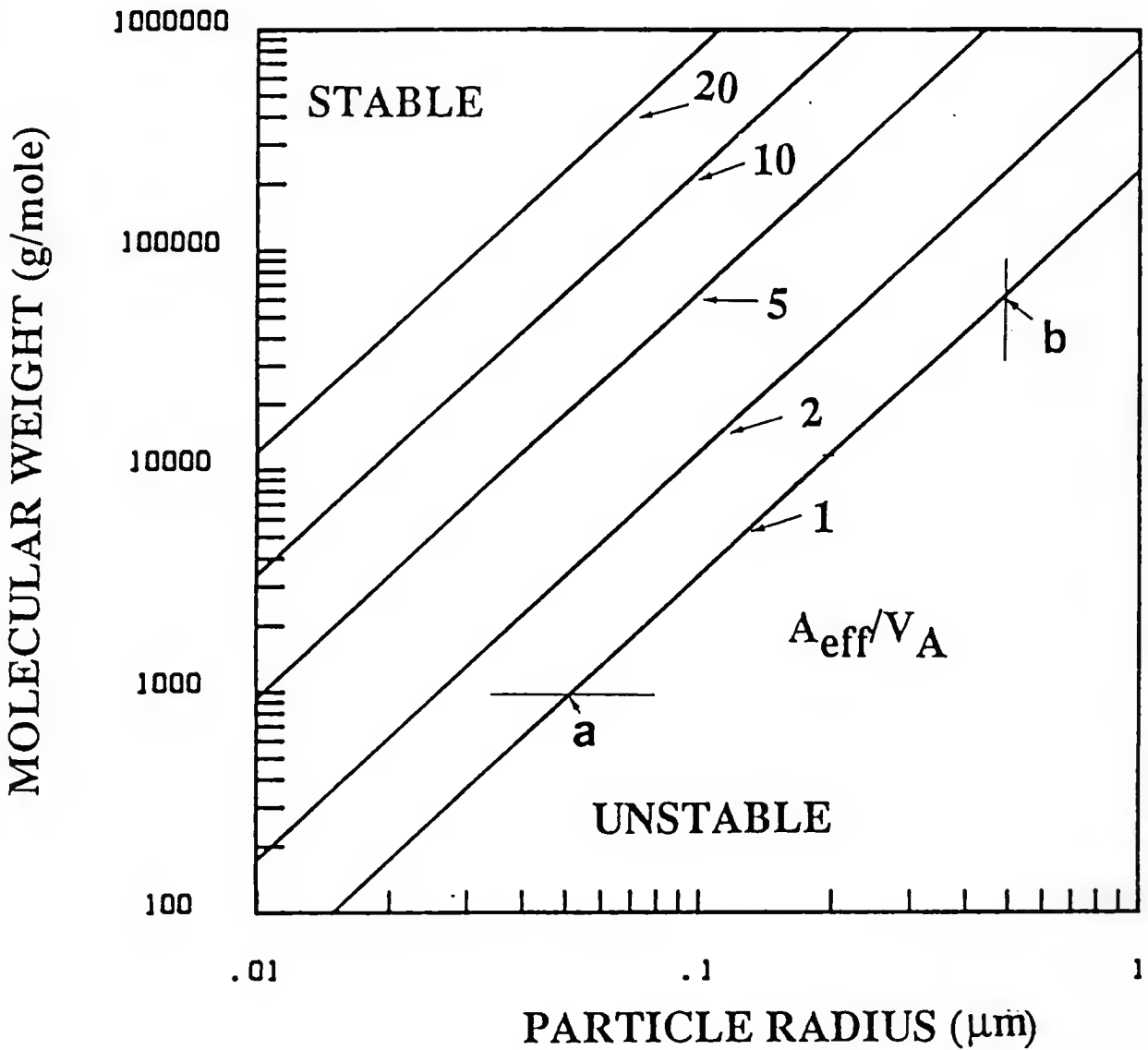
Figure 8.66   Schematic plots of minimum molecular weight (log scale)
              required to stabilize suspensions as a function of
              particle radius with different values of A_{eff}/V_A ratios.
              The solid lines separates stable and unstable regions of
              suspensions prepared with spherical particles of fixed
              size with varying molecular weight or suspensions
              prepared with fixed molecular weight and varying particle
              radius.

critical maximum particle size (i.e., 0.05 μm) above which stable

dispersion cannot be prepared as shown by point a in Figure 8.66 when

$A_{eff}/V_A = 1$. Similarly, to stabilize the suspension of a given particle

size (i.e., 0.5 μm), the minimum molecular weight required (i.e., $M_w(min)$

$\approx 10^4$) is evident (point b in Figure 8.66). Lower molecular weight will

result in weak flocculation as shown in Figure 8.56.

Alternatively, from the known $M_w(min)$ and particle radius a, it is

possible to estimate the value of the Hamaker constant. For example, for

≈ 0.2 μm silica particles, experimentally, we observed $M_w(min) \approx 24,000$

g/mole (Figure 8.56). Substituting these values into Equation 8.8, we

obtain:

$$\frac{A_{eff}}{V_A} = 1.45 \tag{8.9}$$

If we assume $V_A \approx 1$ kT, then, $A_{eff} \approx 0.6 \times 10^{-20}$ which is in close

agreement with the literature values of A_{eff} for silica in water. (We

assumed $A_{eff} = 0.850 \times 10^{-20}$, which was calculated by Hunter using the

macroscopic approach-Hunter 87). The adsorbed polymer layer also often

reduces the value of Hamaker constant (Vold 61), but it is not possible

to calculate theoretically the effective Hamaker constant for polymer

coated particles since the information regarding the segment density

distribution in the adsorbed layer is not available. The adsorbed

polymer layer will be a composite consisting of water molecules and PVA

segments. The effective Hamaker constant $A_{22}(eff)$, for the polymer layer

is given by the following equation (Vold 61):

$$A_{22}(eff) = [\phi_2 A_{22}^{1/2} + \phi_3 A_{33}^{1/2}] \tag{8.10}$$

where ϕ_2 and ϕ_3 are the volume fractions of the polymer and the medium, and A_{22}, A_{33} are the Hamaker constants for the polymer and the medium, respectively. The above equation is valid under the assumption of constant segment density distribution in the adsorbed layer. The value for the ϕ_2 can be estimated from the plateau adsorbed amounts and the adsorbed layer thickness and given by the following equation:

$$\phi_2 = \frac{\bar{V}_2 A \cdot 10^3}{\delta} \tag{8.11}$$

where $\bar{V}_2$ is the partial specific volume of PVA (0.77×10^{-6} m^3/g), A is the plateau adsorbed amount (mg/m^2) and δ is the adsorbed layer thickness (m). Substituting A = 1.25 mg/m^2 and δ = 50 nm into Equation 8.11 gives $\phi_2 = 0.02$. Since the adsorbed layer consisted mostly of water, the effect of adsorbed layer on the Hamaker constant can be ignored. Thus, the small difference between the calculated Hamaker constant (i.e., 8.5×10^{-20} J) and determined from the experiments (i.e., 0.6×10^{-20} J) can be associated with the experimental uncertainty in determining the Hamaker constant from the stability criterion.

Effect of Adsorbed Layer Thickness on the Maximum Solids Loading in Suspension

One of the often stated advantages of steric stabilization is its ability to achieve stable suspensions at higher solids loadings. As we will show shortly, this is not strictly correct if electrostatically stabilized suspensions of moderate viscosities can be prepared (i.e., under conditions of high zeta potentials and sufficient ionic strength to

minimize electroviscous effects). The effective solids loading ϕ_{eff} with adsorbed layer thickness δ can be represented as follows:

$$\phi_{eff} = \phi_p \, [1 + (\delta/a)]^3 \tag{8.12}$$

where ϕ_p is the true solids loading and a is the particle radius. Using Equations 8.5 and 8.6, we can substitute for δ in Equation 8.12:

$$\phi_{eff} = \phi_p \, (1 + \frac{2k' \, M_w^{a'}}{a}) \tag{8.13}$$

As described in Chapter VI, the dependence of relative viscosity on the volume fraction of solids ϕ_p, can be adequately described by an exponential relation (see Figure 8.61 and Equation 8.3). Beyond a certain critical volume fraction of solids, ϕ_{max}, the suspension will have an infinite viscosity (i.e., no flow will occur as the particles are "locked in"). The value for ϕ_{max} can be experimentally determined (for e.g., $\phi_{max} \approx 0.5$ for silica suspensions used in this study whereas $\phi_{max} \approx$ 0.62 for suspensions of latex particles as shown in Figure 8.62). In the case of monosized particles, ϕ_{max} can also be determined theoretically (e.g., if we assume that the suspension with hexagonally packed particles will not flow, then, we have $\phi_{max} = 0.64$). Now, if we equate ϕ_{max} with ϕ_{eff}, then, the <u>true</u> volume fraction of solids, $\phi_p(max)$, at which no flow will occur is given by the following equation:

$$\phi_p(max) = \phi_{max} \, [1 + \frac{2k' \, M_w^{a'}}{a}]^{-3} \tag{8.14}$$

The $\phi_p(max)$ in Equation 8.14 can be also considered as the maximum achievable volume fraction of solids in the suspension. The effect of molecular weight, M_w, and particle radius, a, on the $\phi_p(max)$ is shown in Figure 8.67. The curves in Figure 8.67 are plotted with $\phi_p(max) = 0.5$
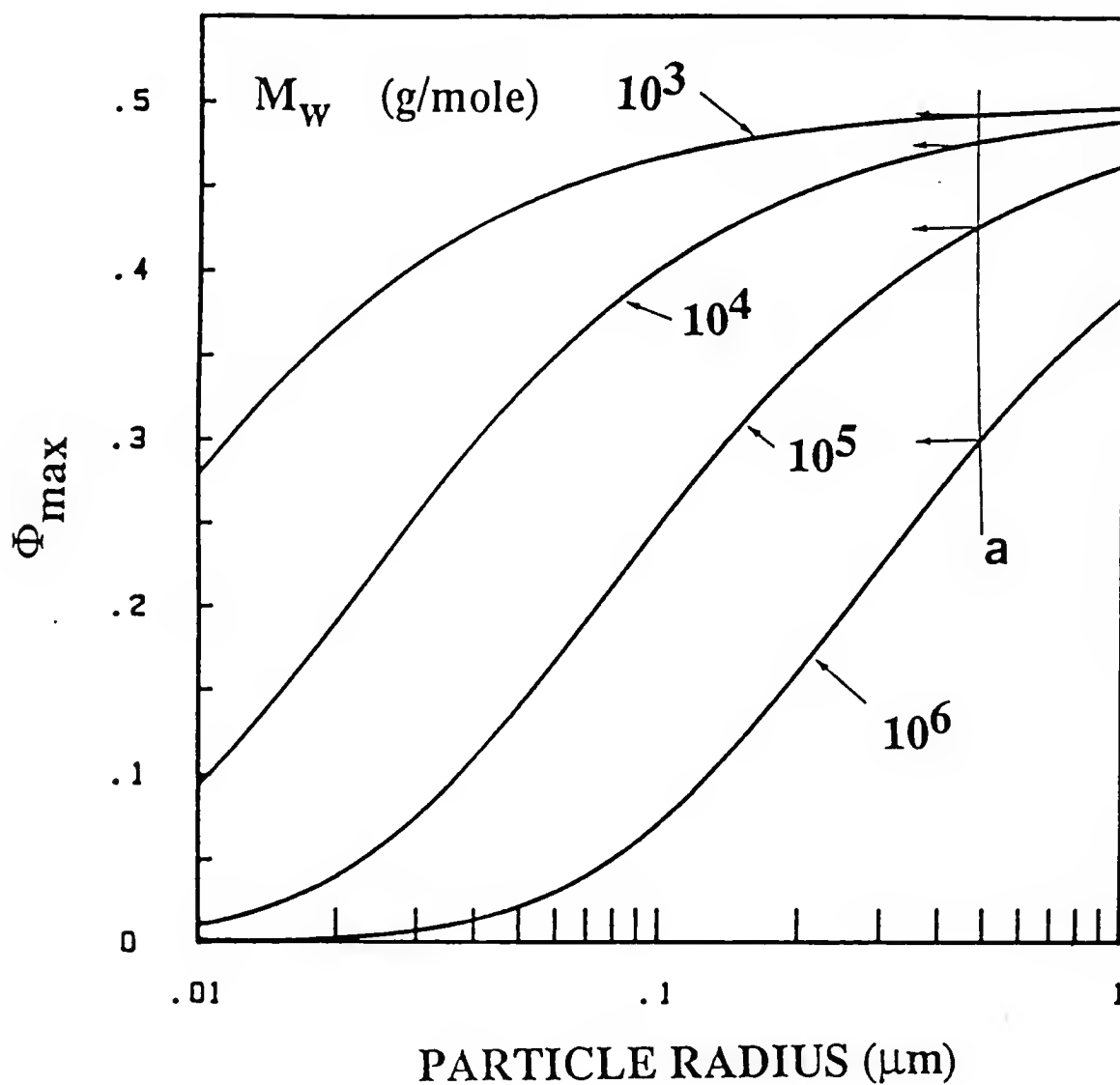
Figure 8.67   Schematic plots of maximum true solids loading, ϕ_{max}, achievable in suspensions prepared with spherical monosized particles of varying size using indicated molecular weights of polymer.

for different molecular weights of polymer: For a fixed molecular weight

of polymer (say, 10^5), there is increase in the ϕ_p(max) with particle

radius (i.e., the higher true solids loading can be achieved by increases

in particle radius at a fixed molecular weight of PVA). Also at a fixed

particle size (say, 0.5 μm), ϕ_p(max) increases with decreases in the

molecular weight of polymer (see line a in Figure 8.67). Thus, from the

Figure 8.67, the importance of larger particle size and smaller molecular

weight of the polymer in preparing highly loaded suspensions is clear.

The polymer molecular weight should be chosen in such a way that it

should be at least equal to the minimum molecular weight M_w(min) required

to stabilized the suspension (Equation 8.8 and Figure 8.66). However,

the above described considerations must be balanced against other

criterions that are used in selecting polymer for a particular processing

operation. For example, the higher molecular weight polymer may be

desirable in some cases in order to achieve higher green strength.

Effect of Silica Particle Size

In this section, we will describe the effect of silica particle size

on the suspension properties. The importance of small particle sizes in

sintering process is well recognized. With decrease in the particle

size, the solid-liquid interface area increases (at fixed ϕ_p) and

interfacial properties (e.g., PVA adsorption behavior) plays an

increasingly important role in controlling suspension properties.

Figure 8.68 shows plots of adsorption isotherms of high molecular

weight PVA ($\approx$ 215,000) on 700°C calcined silica powders of 0.4 μm and 0.7

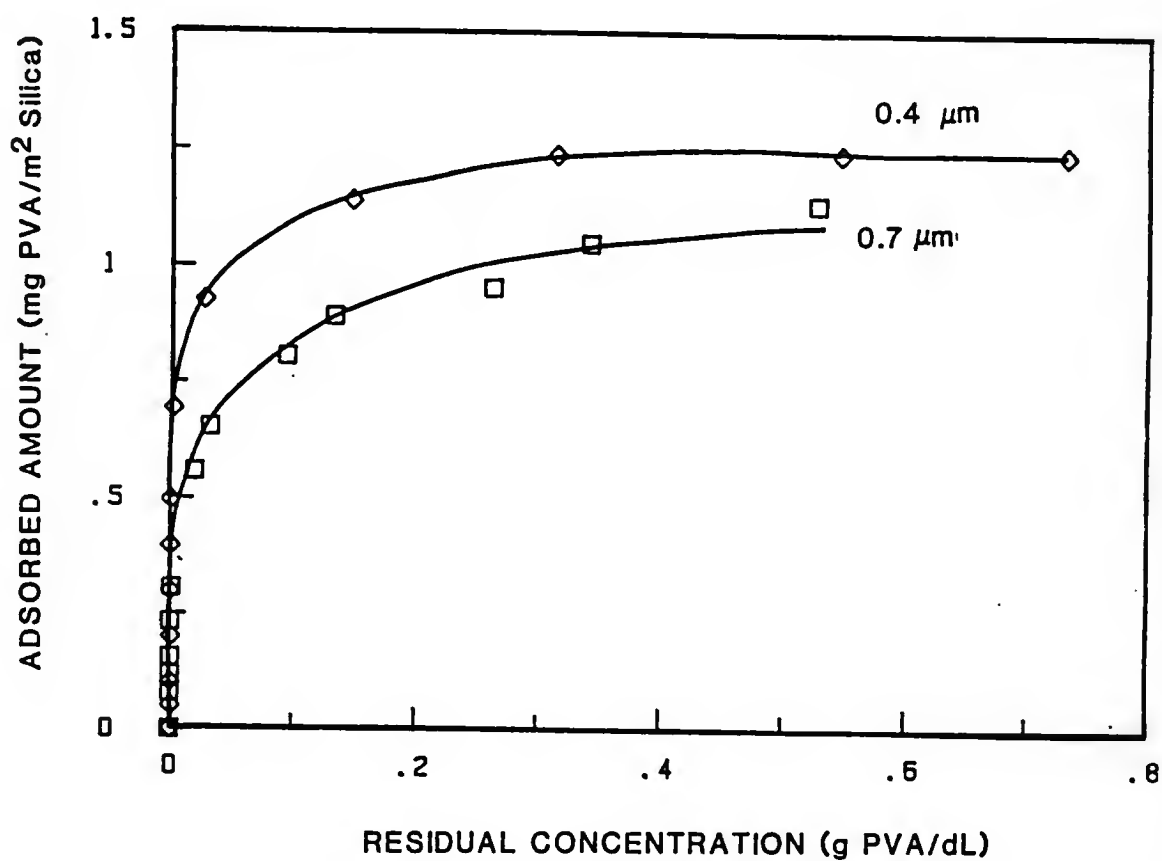μm diameter particles. Both size powders showed high affinity type of

Figure 8.68   Adsorption isotherms for PVA with molecular weight $\approx$ 215,000 for 20 vol.% SiO_2 suspensions prepared using 0.4 μm and 0.7 μm size particles with varying PVA concentrations.

adsorption isotherms. The plateau adsorbed amount was slightly larger

for the approximately 0.4 μm size particles. No difference in PVA

plateau adsorption density was observed by Garvey et al. and Ahmed et al.

for different size PS-latex particles (Garvey et al. 74; Ahmed et al.,

84). These investigators determined the plateau adsorbed amounts using

dilute dispersions (i.e., the volume fraction of latex particles < .02).

In this study, the volume fraction silica in suspension was the same (ϕ_p

= 0.2) for ≈ 0.4 as well as 0.7 μm size particles. Hence, the surface

area, S, per unit volume, V, of the suspension (m^2/cm^3) was almost double

for the 0.4 μm particle suspension (i.e., for 0.4 μm size particles, S/V

≈ 3.5 m^2/cm^3, whereas for 0.7 μm size particles, S/V = 2.1 m^2/cm^3 when ϕ_p

= 0.2). From the polymer adsorption theory developed for the adsorption

of polydispersed samples, it can be expected that with decreasing S/V,

the plateau adsorbed amount increases due to the preferential adsorption

of high molecular weight polymers (see Chapter II). But, we observed

slightly higher plateau adsorption for 0.7 μm particle suspensions. The

reasons for this difference were not investigated in this study.

The effect of particle size on the rheological properties is shown

in Figure 8.69. This figure shows plots of relative viscosity versus

adsorbed amount of PVA and corresponding plots of the relative viscosity

versus fractional coverages for 0.4 μm and 0.7 μm size particles. At

partial coverages, relative viscosities are higher for 0.4 μm size

particles indicating higher effective solids loading. As shown

schematically in Figure 8.70, for a given adsorbed layer thickness δ, the

effective increase in the hydrodynamic volume is larger for smaller

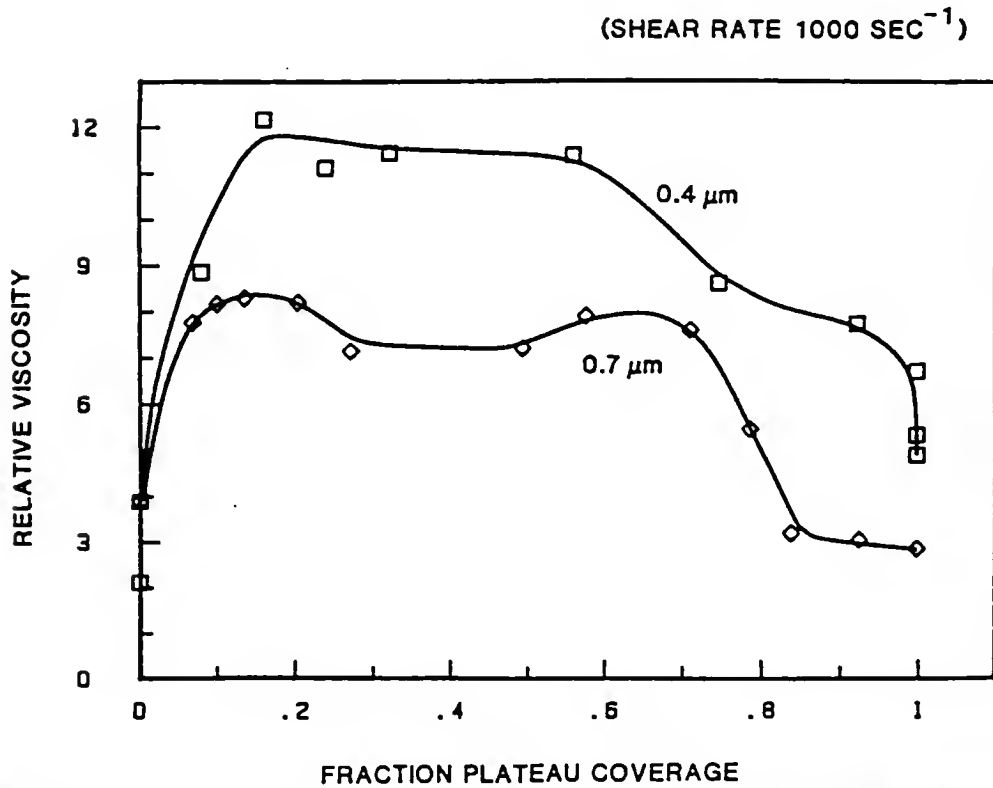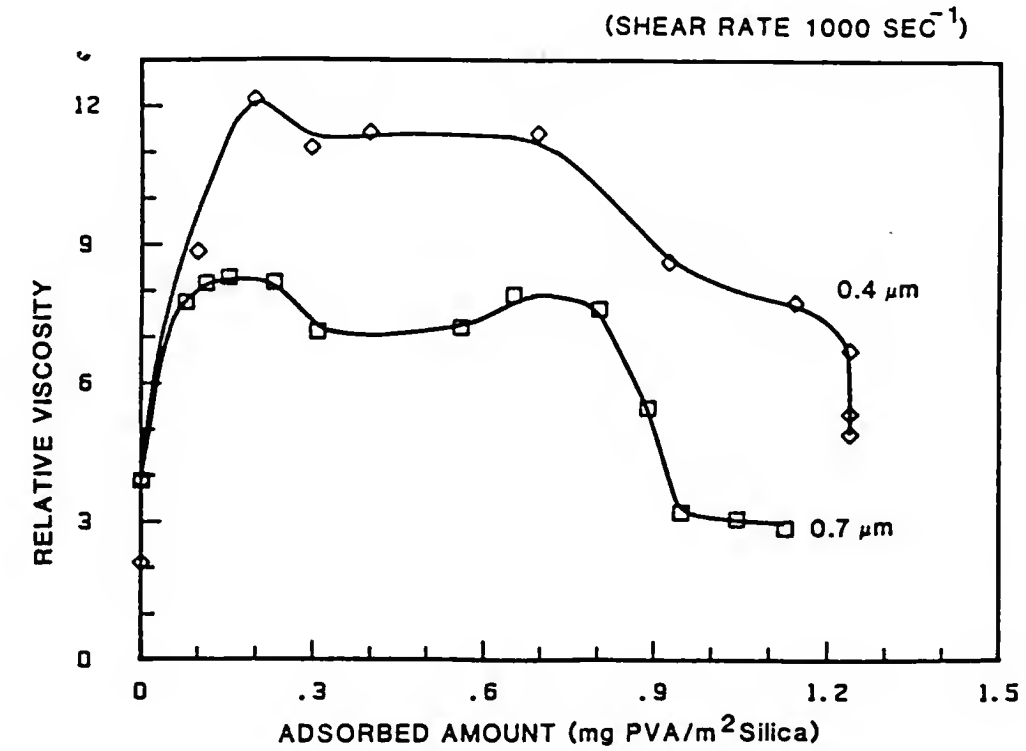Figure 8.69   Plots of (a) relative viscosity versus adsorbed amounts of PVA and (b) relative viscosity versus fraction plateau coverage for 20 vol.% SiO_2 suspensions prepared using 0.4 μm and 0.7 μm size particles.

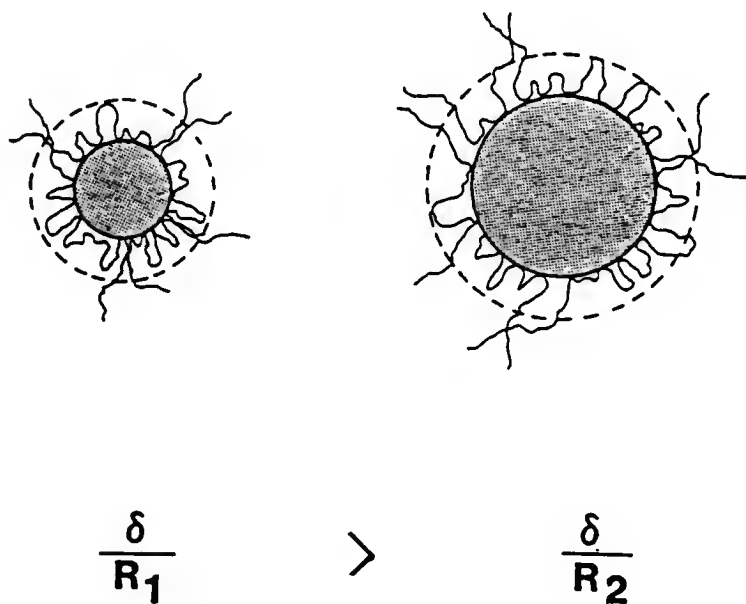$$\frac{\delta}{R_1} \quad > \quad \frac{\delta}{R_2}$$

Figure 8.70   Schematic illustration showing the effect of adsorbed layer thickness, δ, on the hydrodynamic volume of two different size particles.

particles compared to larger particles. If one assumes that there is no change in packing of the particles in a given floc, then:

$$\phi_{eff} = \phi_p [1 + (\delta/a)]^3 + \phi_{void} \qquad (8.15)$$

where ϕ_{void} is the volume fraction of voids. It is evident from the above equation that, with decrease in the particle radius a, there will be increase in the ϕ_{eff}, hence, the relative viscosity of the suspension. From the work of Hunter et al, it is well known that smaller size particles tend to produce more open floc structures, i.e., $C_{FP} = \phi_{eff}/\phi_p$ α 1/a (Firth 76), and hence, suspensions have higher relative viscosities. The elastic floc predicts linear relationship between τ_β versus 1/a (i.e., τ_β α C_{FP} α 1/a) for coagulated suspensions. But, the opposite behavior was observed at low coverages in this investigation. Figure 8.71 shows plots of extrapolated yield stress versus adsorbed amount of PVA and corresponding plots of yield versus fraction plateau coverage for 0.4 and 0.7 μm diameter particles. At low coverages (up to approximately 0.3), the yield values were higher for 0.7 μm size particles compared to 0.4 μm size particles. As explained earlier, the yield stress reflects the depth of interaction energy between particles at partial coverages. A larger depth of ΔG_{min} is expected for 0.7 μm size particles from two contributions (see Figure 8.31).

(i) For a given distance of separation h, the Van der Waal's attraction is greater for larger particles (see Equation 8.4).

(ii) The total number of bridges, n_{total}, formed between particles, are more for larger particles.

This can be seen more clearly from Figure 8.72. The scaling analysis has been applied to polymer adsorption by de Gennes (de Gennes
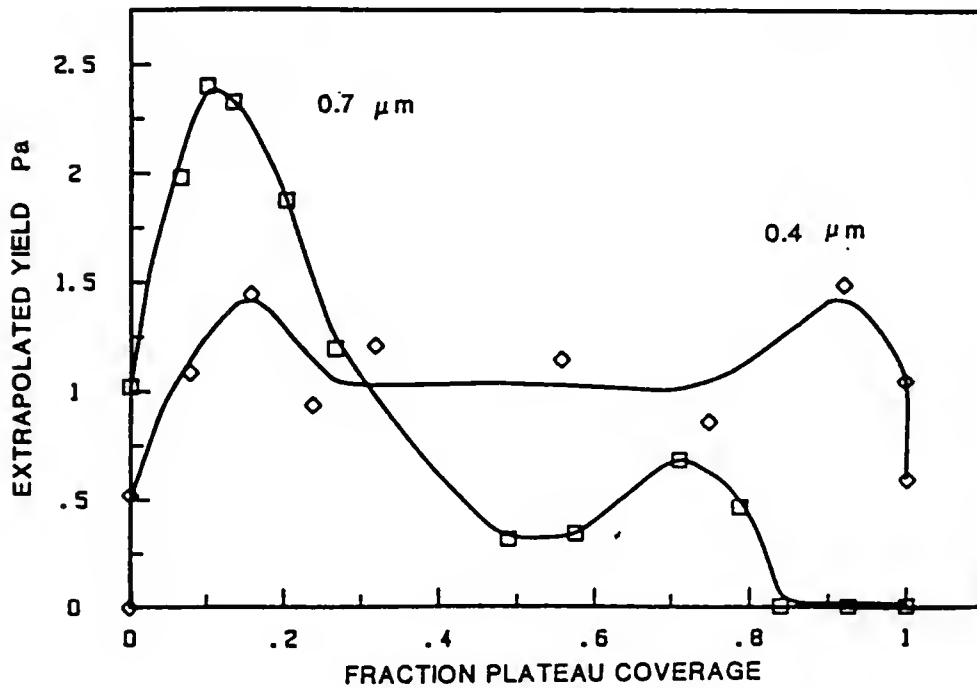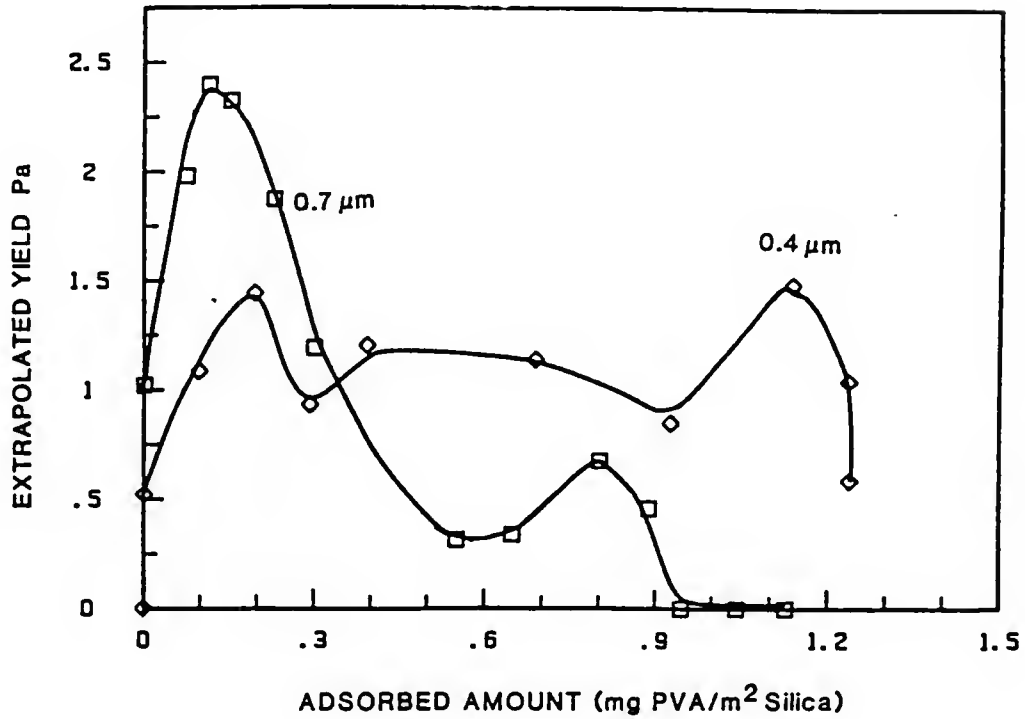
Figure 8.71   Plots of (a) yield stress versus adsorbed amount of PVA
                and (b) yield stress versus fraction plateau coverage for
                0.4 μm and 0.7 μm size particles.
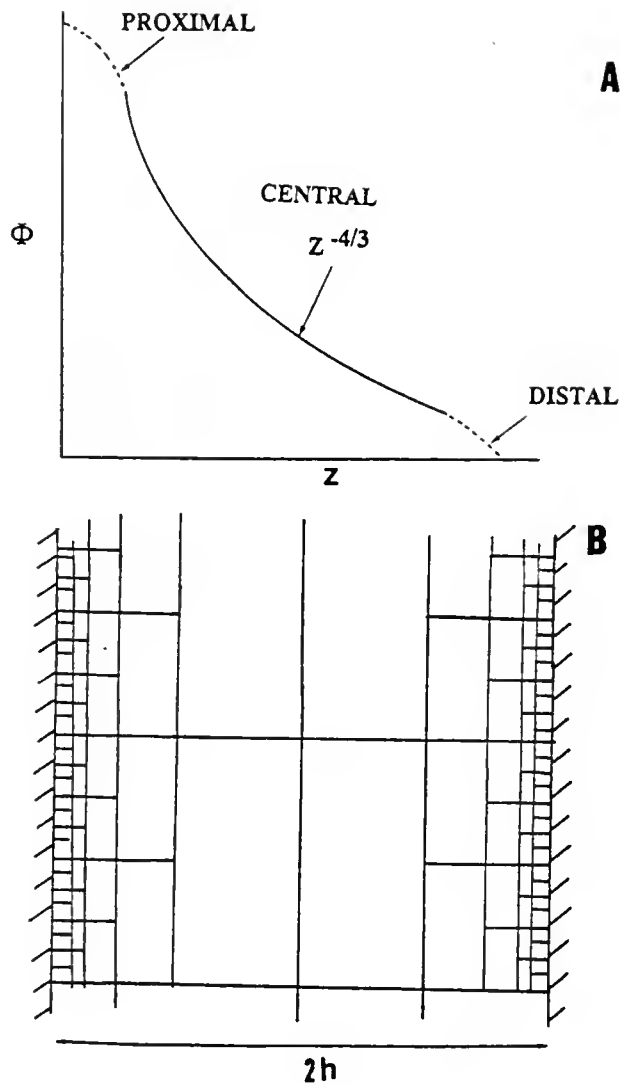
Figure 8.72   Schematic illustration showing (a) concentration profile,
                $\phi(Z)$, of adsorbed layer consisting of three regions (i)
                proximal (very sensitive to the details of the
                interactions), (ii) central (self-similar), and
                (iii) distal (controlled by a few loops and tails) and
                (b) "self-similar grid" presentation of an adsorbed
                polymer layer (de Gennes, 1987).

87). As shown in Figure 8.72A, he divided the adsorbed polymer layer into three regions (i) the "proximal regime" close the surface where the segment concentration profile is very sensitive to the details of the segment-surface interactions, (ii) a "concentration regime" where the profile has a self-similar structure" as shown in Figure 8.72B, (iii) a "distal regime" where the profile decays exponentially towards the density of the bulk solution. This regime is controlled by dilute large loops and tails. de Gennes gave the following expression for the equilibrium number of bridges per unit area, n_b (de Gennes 87):

$$n_b \approx 1/h^2 \qquad (h < Rg) \tag{8.16}$$

where Rg is the radius of gyration of polymer molecule. The total number of bridges formed, n_{total}, between two spherical particles of radius a, can be found if the area, A, involved in bridging is known:

$$n_{total} = A \cdot n_b \tag{8.17}$$

The area involved is given by $A = 2\pi ah$ from the geometric considerations. Substituting for n_b from Equation 8.16 and for A into Equation 8.17:

$$n_{total} = A \cdot n_b \approx 2\pi a/h \tag{8.18}$$

From Equation 8.18, it is clear that the total number of bridges formed increases with increasing particle radius at a fixed distance of separation h. de Gennes has predicted that these bridges should act as elastic springs, and keep particles together (de Gennes 87). Then, the larger yield with larger particles is consistent with the above proposed floc structure.

The formation of more open and weaker structures can be more clearly seen from the plots of hysteresis area versus fraction plateau coverages for 0.4 and 0.7 µm size particles (Figure 8.73). Appearance of the
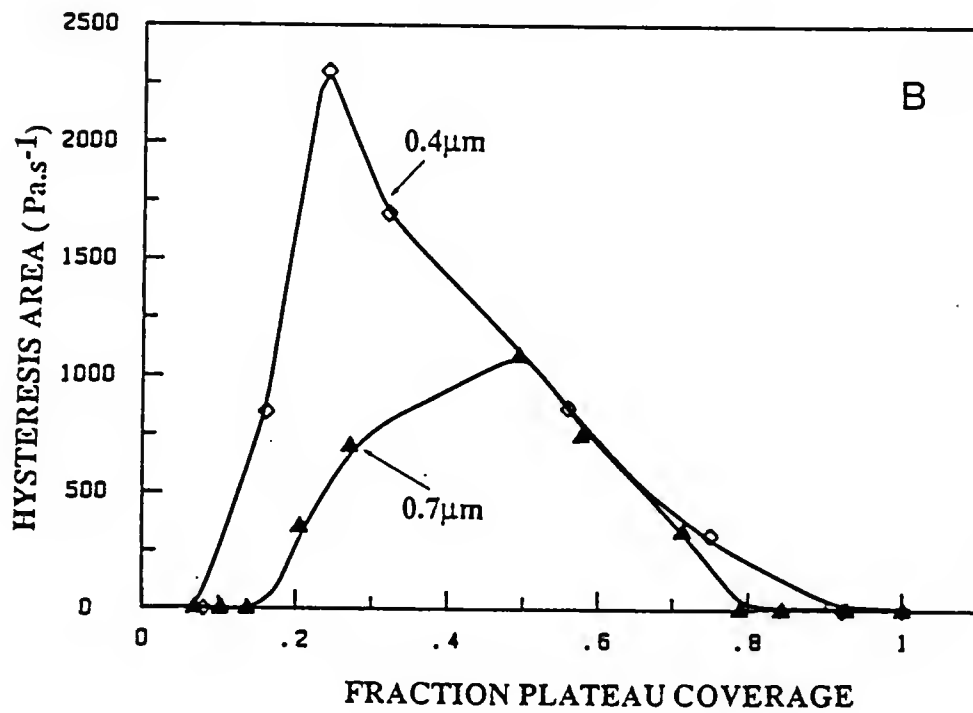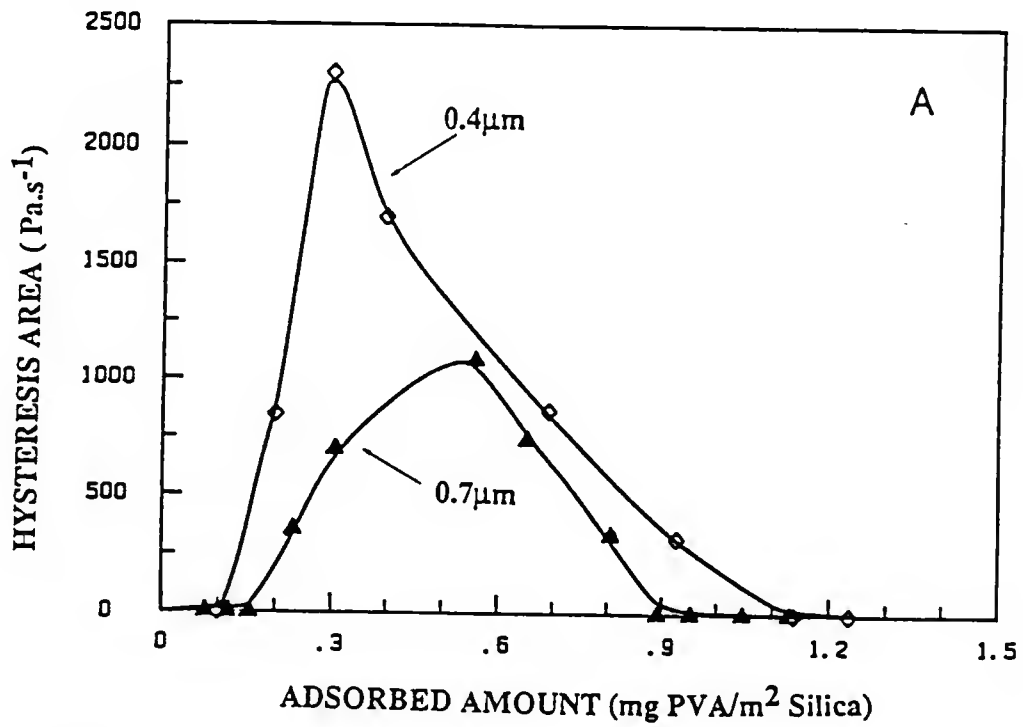
Figure 8.73   Plots of hysteresis area versus fraction plateau coverage
for 0.4 µm and 0.7 µm size particles.

hysteresis at slightly lower coverages (approximately 0.1) and also larger hysteresis areas for 0.4 μm size particles is consistent with the above presented floc picture.

At complete coverage, both suspensions (0.4 and 0.7 μm size particles) are sterically stabilized (as indicated by nearly Newtonian flow behavior and low viscosities of these suspensions), but the relative viscosity is higher for 0.4 μm size particles compared to 0.7 μm size particles. This can be expected since higher effective volume fraction of solids results for 0.4 μm size particles compared to 0.7 μm size particles (i.e., $\delta/a_1 > \delta/a_2$) for a given plateau adsorbed layer thickness δ. Here it is assumed that the δ is the same for both size particles. The effect of PS-latex particle radius on the hydrodynamic thickness, δ, has been studied by Garvey et al. and Ahmed et al. (Garvey et al. 74, Ahmed et al. 84). These investigator observed increases in δ with increasing particle radius, but the plateau adsorbed amount (i.e., mg PVA/m^2) remained the same. Garvey et al. assumed that there is no change in the conformation of the adsorbed polymer molecule with increases in particle radius and the adsorbed layer occupies same volume per unit area on different size particles. With these assumptions, Garvey defined the effective flat surface thickness δ_{eff}, and showed that δ_{eff} is independent of particle size (Garvey et al. 74). Hence, they concluded that the increase in thickness with increasing particle size is only due to the geometry of the system. On the other hand, later group explained increase in δ with particle radius assuming that there is a change in the conformation of the adsorbed polymer molecule with particle size (i.e., longer loops and tails are formed on larger particles). The
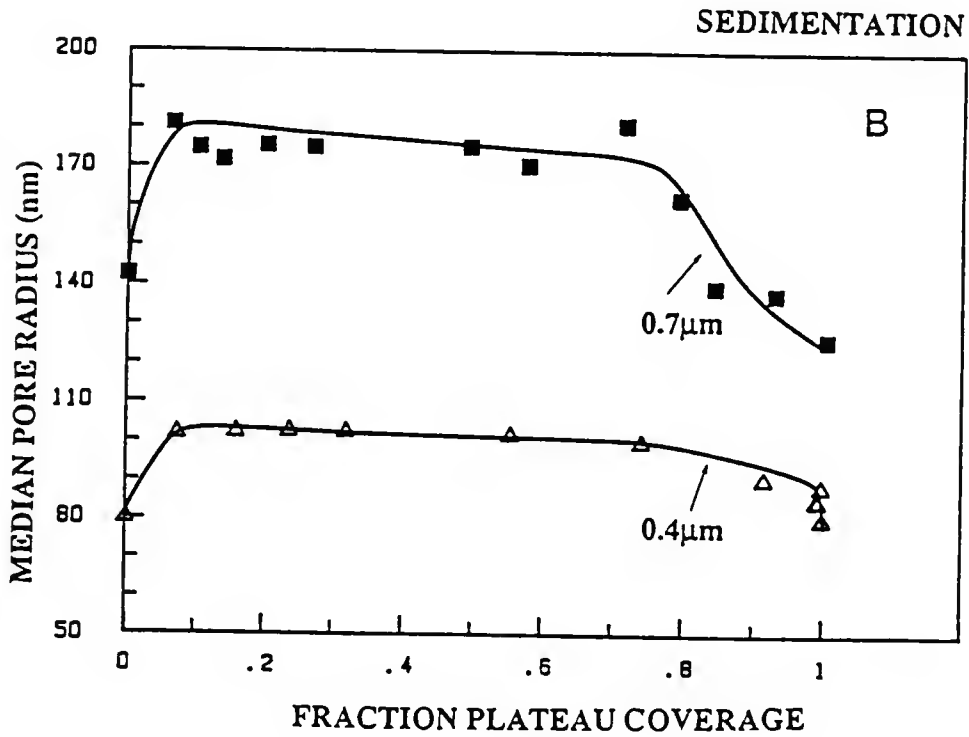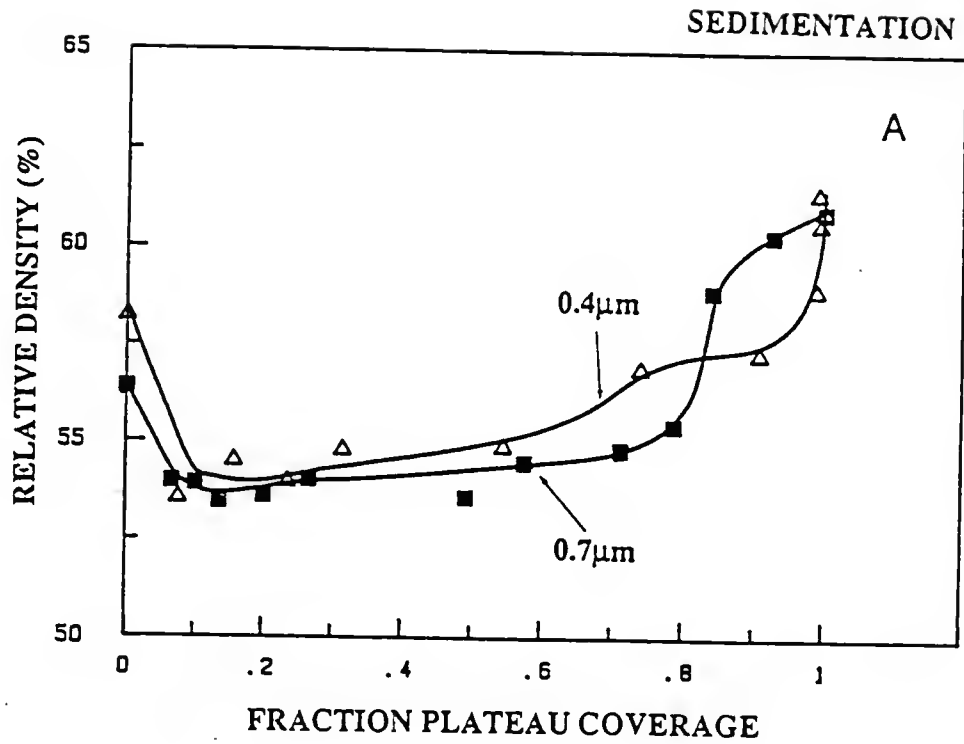
Figure 8.74   Plots of (a) relative density of sedimented samples versus fraction plateau coverage and (b) median pore radius versus fraction plateau coverage for 0.4 μm and 0.7 μm size particles.

387
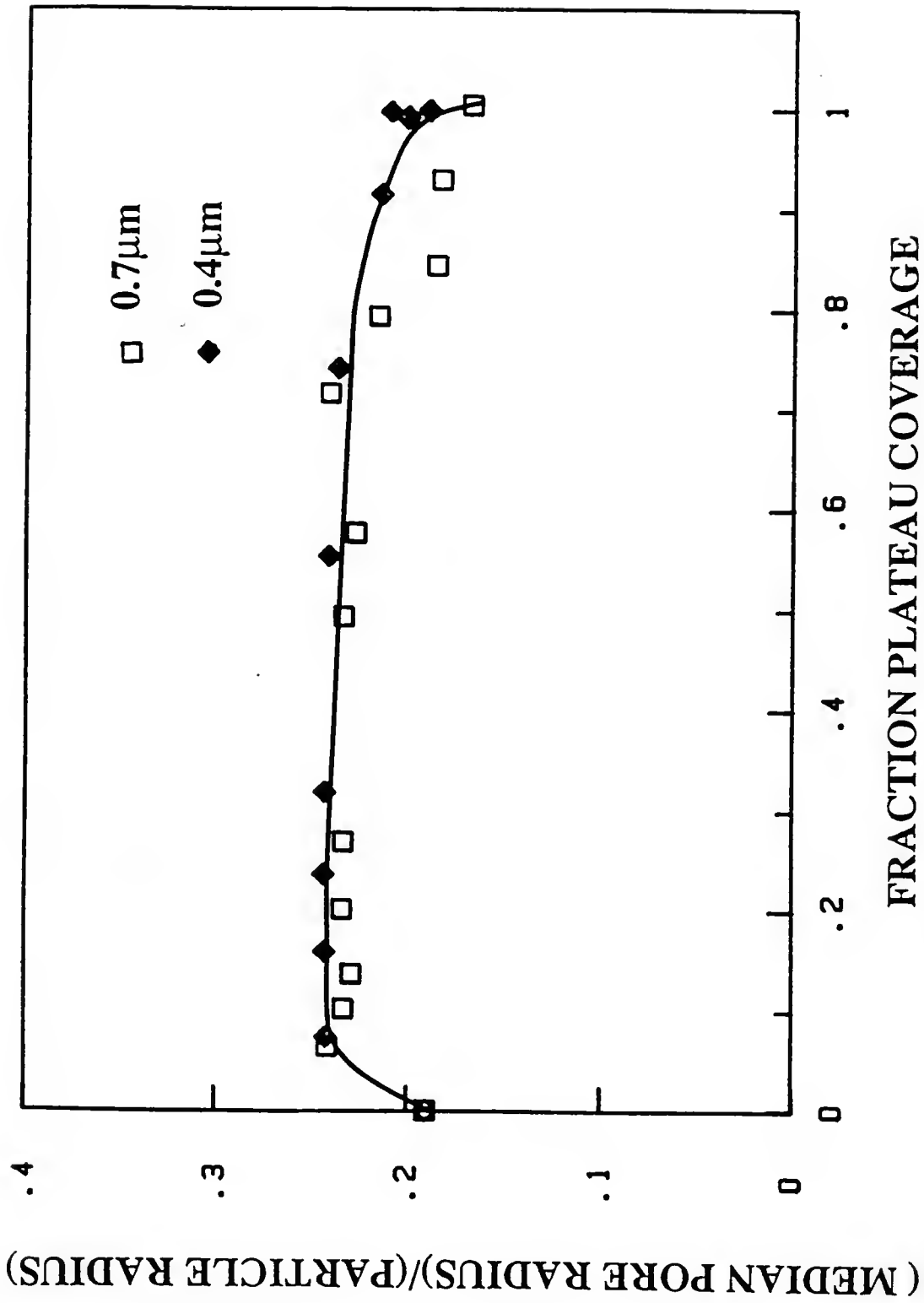
Figure 8.75   Plots of normalized median pore radius (i.e., median pore radius/particle radius) versus fraction plateau coverage for 0.4 μm and 0.7 μm size particles.

δ_{eff} calculated by these investigators increased with increasing particle radius. From the above discussion, it is clear that the effect of particle radius on the adsorbed layer thickness is not well understood.

Figure 8.74 shows plots of relative density of compacts (prepared by sedimentation) versus fraction plateau coverage and corresponding plots of median pore radius versus fraction plateau coverage for 0.4 and 0.7 μm size particles. No significant difference was observed for the density versus fraction plateau coverage plots for these two size particles. As expected (Figure 8.74B), larger median pore radii were observed for 0.7 μm size particles compared to 0.4 μm size particles at any given fractional coverage. The normalization of median pore radius by the particle radius results in the overlap of data for 0.4 and 0.7 μm size particles (Figure 8.75).

Effect of PVA degree of Hydrolysis on Adsorption Behavior

For the experiments described so far, the partially hydrolysed PVA of various molecular weights was employed. The polymer adsorption behavior is dependent on the chemical interactions between specific adsorption sites on the silica surface (i.e., isolated silanol groups and siloxane groups) and the chemical nature of the specific groups of the polymer (i.e., alcohol and acetate groups in the case of PVA). In this section, the effect of degree of hydrolysis of PVA will be described. Figure 8.76 shows plots of adsorption isotherms for three PVA samples of similar molecular weight and different degrees of hydroxylation. (The molecular weight and the degree of hydroxylation are reported in Table 8.3.) The plateau adsorbed amounts were larger for partially
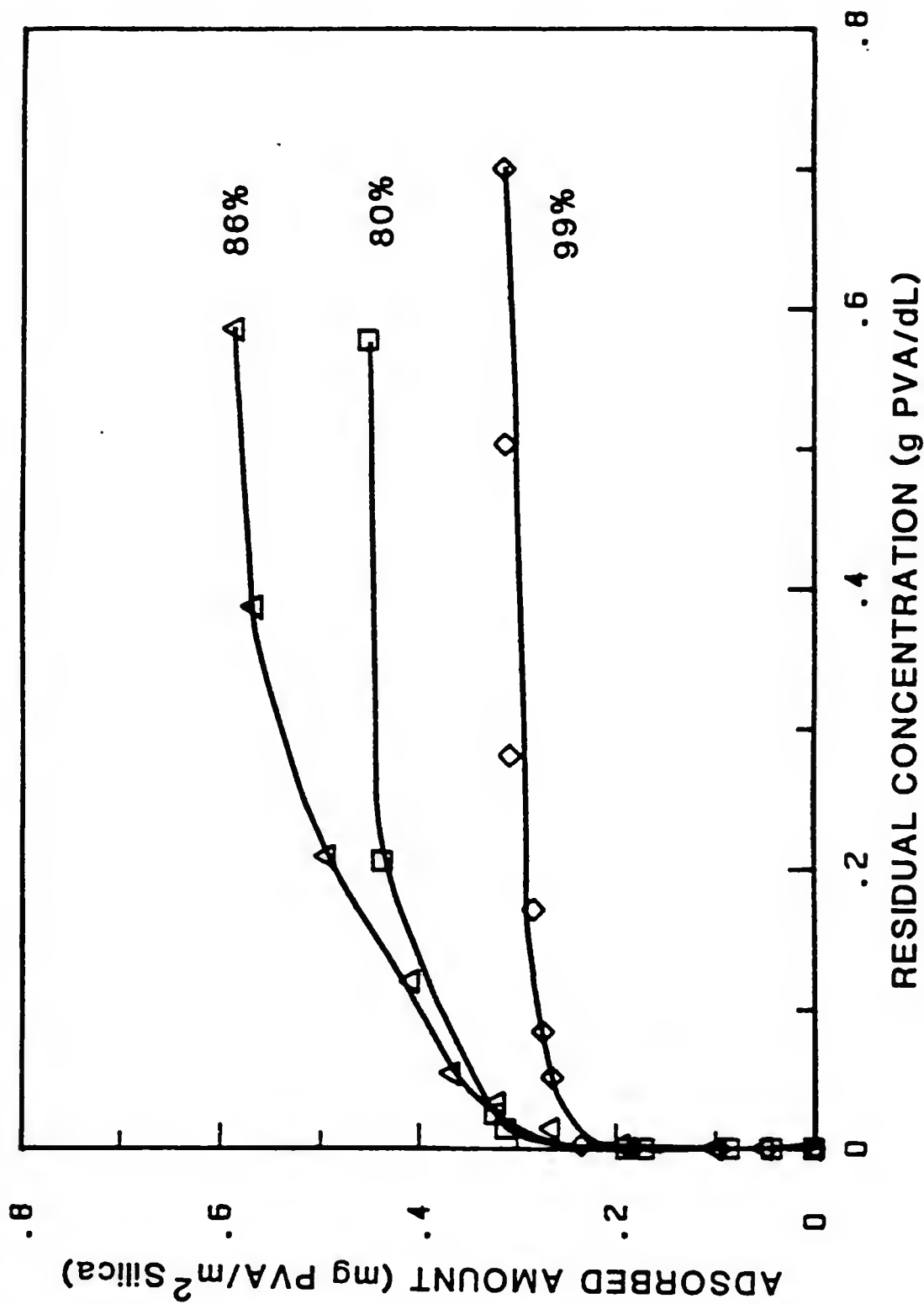
Figure 8.76   Adsorption isotherms for PVAs with similar molecular weights but varying degree of hydroxylation of 20 vol.% SiO_2 suspensions.

TABLE 8.3

Molecular Weight and Degree of Hydroxylation of PVA Samples to
Study the Effect of Degree of Hydroxylation on the Suspension Properties

	PVA 1	PVA 2	PVA 3
M_υ (g/mole)	30,000	24,000	38,000
% Hydrolysed	80	86	99
$<s^2>^{0.5}$ (nm)	6.5	5.8	6.9

hydrolysed (i.e., 80%, PVA80 and 86% PVA86) PVA's compared to "fully"

hydrolysed PVA ($\approx$ 98%, PVA98). The differences in adsorption behavior

may arise due to (i) the differences in solvency (i.e., the differences

is χ parameter for partially and fully hydrolysed PVA's) (ii) the

differences in the flexibility of polymers, or (iii) differences due to

the segment-surface interactions (i.e., χ_s parameter may be different for

acetate and alcohol groups of PVA). As described earlier (Chapter II and

VII), χ (PVA98) and χ (PVA88) are only slightly different, and the

differences in adsorption behavior cannot be explained by the solvency

effect. For PVA88, the acetate groups are generally assumed to be

distributed in blocks while PVA acetate groups are randomly distributed

(i.e,. PVA88 is a block copolymer whereas PVA98 is a random copolymer).

Hence, it can be expected that the flexibility of PVA88 is relatively

lower as bulky acetate groups are distributed as blocks. The lower

flexibility of partially hydrolysed PVA can set constrains on the minimum

loop size (i.e., the average loop size is expected to be larger for PVA80

and PVA86). The preferential adsorption of acetate group on AgI

particles (Koopal 78) and PS-latex particles (Barnett et al. 82) has been

confirmed. Since the adsorbed amount of polymer in the first layer

(i.e., A_{mono}) is expected to be similar for the partially and fully

hydrolysed PVA, the large adsorbed amount for PVA88 is due to formation

of larger loops and tails. From the electrophoretic measures, Koopal

found that the adsorbed layer thickness of AgI was larger for PVA88

compared to PVA98 of the comparable molecular weights (Koopal 78). This

observation is consistent with the formation of larger loops and tails

for partially hydrolysed PVA. With hydrodynamic thickness measurements

using PCS, Killmann et al. observed larger adsorbed layer thicknesses with PVA88 compared to PVA98 on precipitated silica as well as on PS-latex particles (Killmann et al. 88).

The effect of PVA degree of hydroxylation on the rheological behavior is shown in Figure 8.77. This figure shows the plots of relative viscosity versus shear rate plots for PVA's hydrolysed to various extents. The suspensions prepared with fully hydrolysed PVA with the plateau adsorbed amount of polymer were highly flocculated as indicated by highly shear thinning and thixotropic flow behavior. This behavior correlates well with the thinner adsorbed layer thickness (i.e., relatively low plateau adsorption density). As described before, thin adsorbed layer is insufficient to overcome the Van der Waal's attraction between particles leading to flocculation of particles (Figure 8.22). The stability of suspensions was not improved with increasing molecular weight of PVA98. Weaker dependence of the plateau adsorption density on molecular weight has been reported by Koopal (i.e., plateau density α $M_w^{0.1}$) (Koopal 78). Hence, there may not be significant increase in the adsorbed layer thickness with increasing PVA98 molecular weight. Stable dispersions, as indicated by the Newtonian flow behavior and low relative viscosity, could be prepared with the partially hydrolysed PVA.

Figure 8.78 shows plots of specific volume frequency versus pore size curves for green compacts prepared using PVA88 and PVA98. Samples were prepared by sedimentation of suspensions with the plateau adsorbed amounts. The lower relative density and corresponding relatively larger pore sizes for PVA98 is consistent with the rheological behavior (Figure 8.77). From this discussion, the importance of (i) strong adsorption and
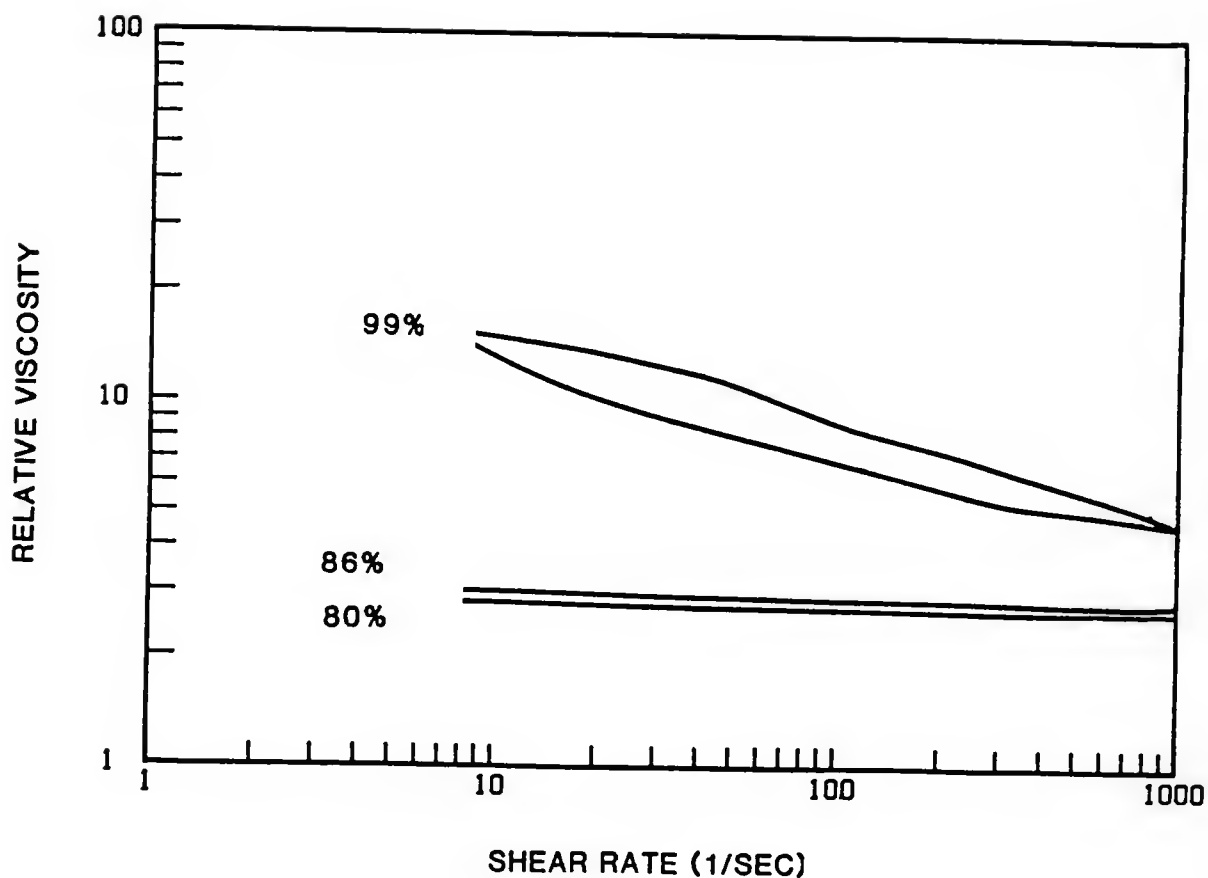
Figure 8.77   Plots of relative viscosity versus shear rate of 20 vol.%
                silica suspensions prepared with different PVAs with
                indicated degree of hydroxylation.   The suspensions are
                prepared at pH 3.7 with the plateau adsorbed amounts of
                PVAs.
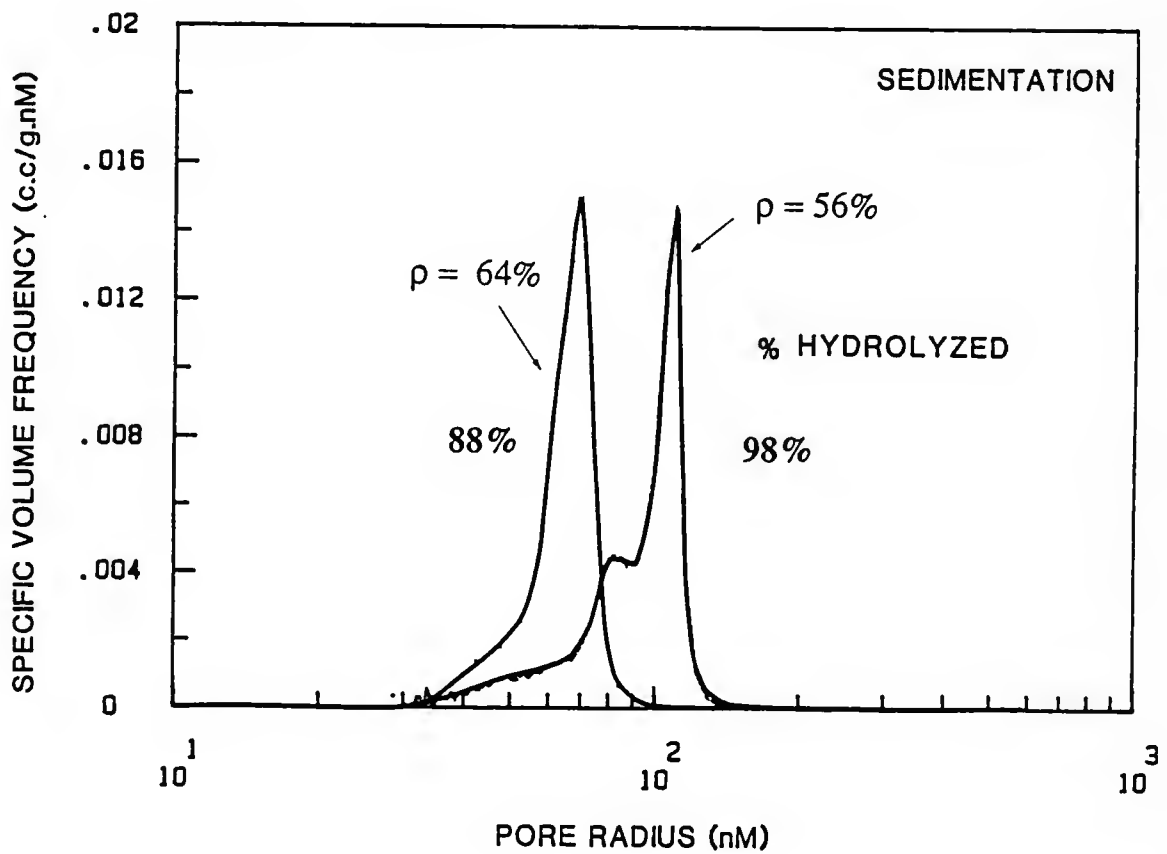
Figure 8.78   Plots of specific volume frequency versus pore radius for
gravity cast samples prepared from 20 vol.% SiO$_2$
suspensions with plateau adsorbed amounts of PVAs with
indicated degree of hydroxylation.

(ii) sufficient adsorbed layer thickness (i.e., proper selection of chemical characteristics of polymer to improve adsorption on a given solid surface) is evident.

Figure 8.79 shows plots of relative viscosity versus adsorbed amounts of polymer and corresponding plots of relative viscosity versus fractional plateau coverage curves for partially and fully hydrolysed PVA's of similar molecular weights. At partial coverages, the relative viscosity is higher for the partially hydrolysed PVA's compared to fully hydrolysed PVA indicates the higher effective solids loading, i.e., formation of relatively more open floc structures. This is consistent with the formation of longer loops and tails with partially hydrolysed PVAs. Formation of relatively more open floc structure is consistent with the greater hysteresis area (i.e., thixotropic behavior) of these suspensions (Figure 8.80). The lesser affinity for adsorption of fully hydrolysed PVA is also reflected in the extrapolated yield behavior. Figure 8.81 shows extrapolated yield versus adsorbed amount and corresponding fractional coverage plots for PVA's hydrolysed to various extents. The extrapolated yield values are slightly higher for PVA86 and PVA80 hydrolysed PVA's compared to PVA98 at similar coverages. This observation is not consistent with the previously described results. We observed higher yield stresses and lower relative viscosities at partial coverages with uncalcined silica, low molecular weight PVA or smaller size particles, i.e., conditions leading to lower plateau adsorption density resulted in larger yields and lower relative viscosities at partial coverages. As described earlier, the extrapolated yield behavior can be related to G_{min} in the potential energy diagram. The stronger
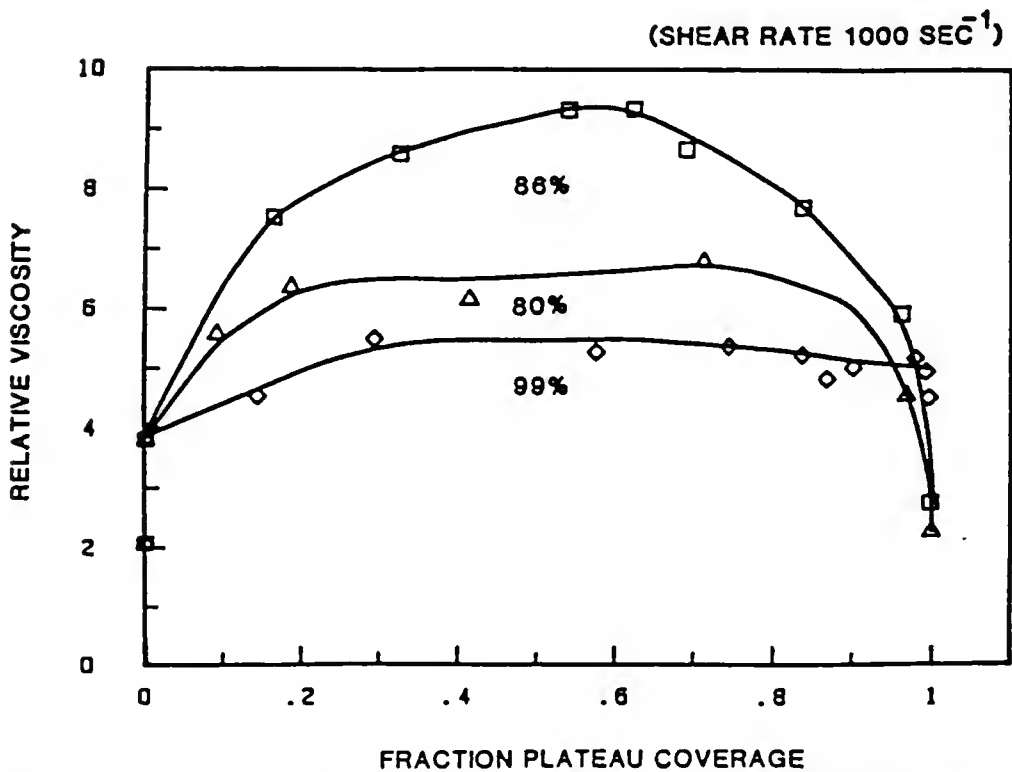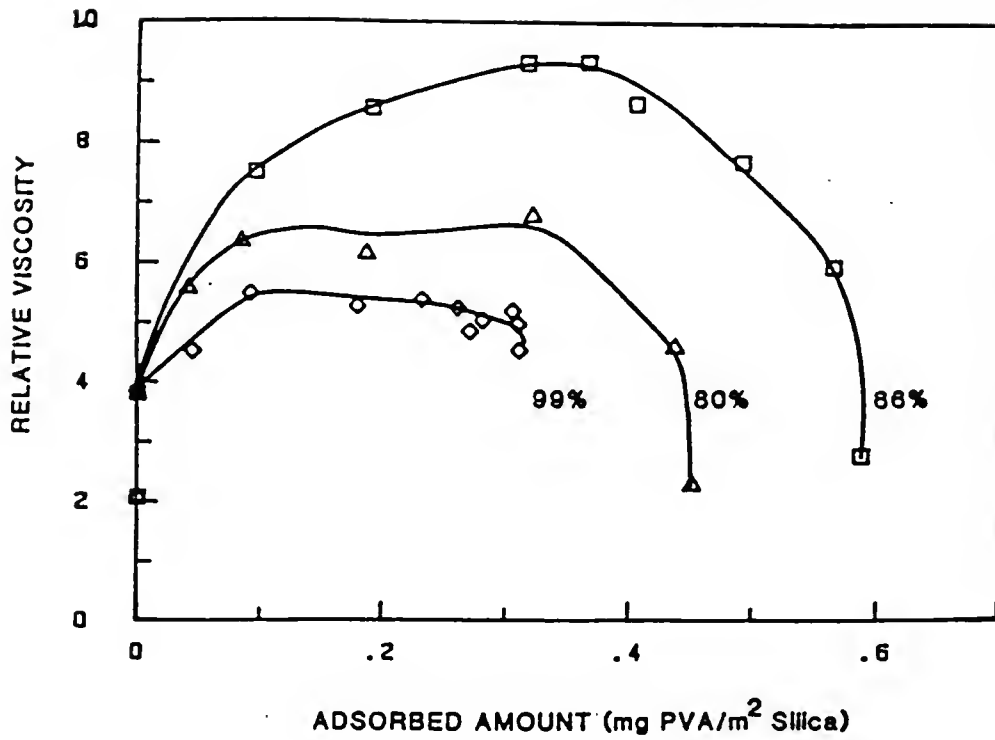
Figure 8.79   Plots of (a) relative viscosity versus adsorbed amounts
and (b) relative viscosity versus fraction plateau
coverage for 20 vol.% SiO_2 suspensions prepared using
varying PVA concentrations in solution. The degree of
hydroxylation of different PVAs used is shown in the
figure.
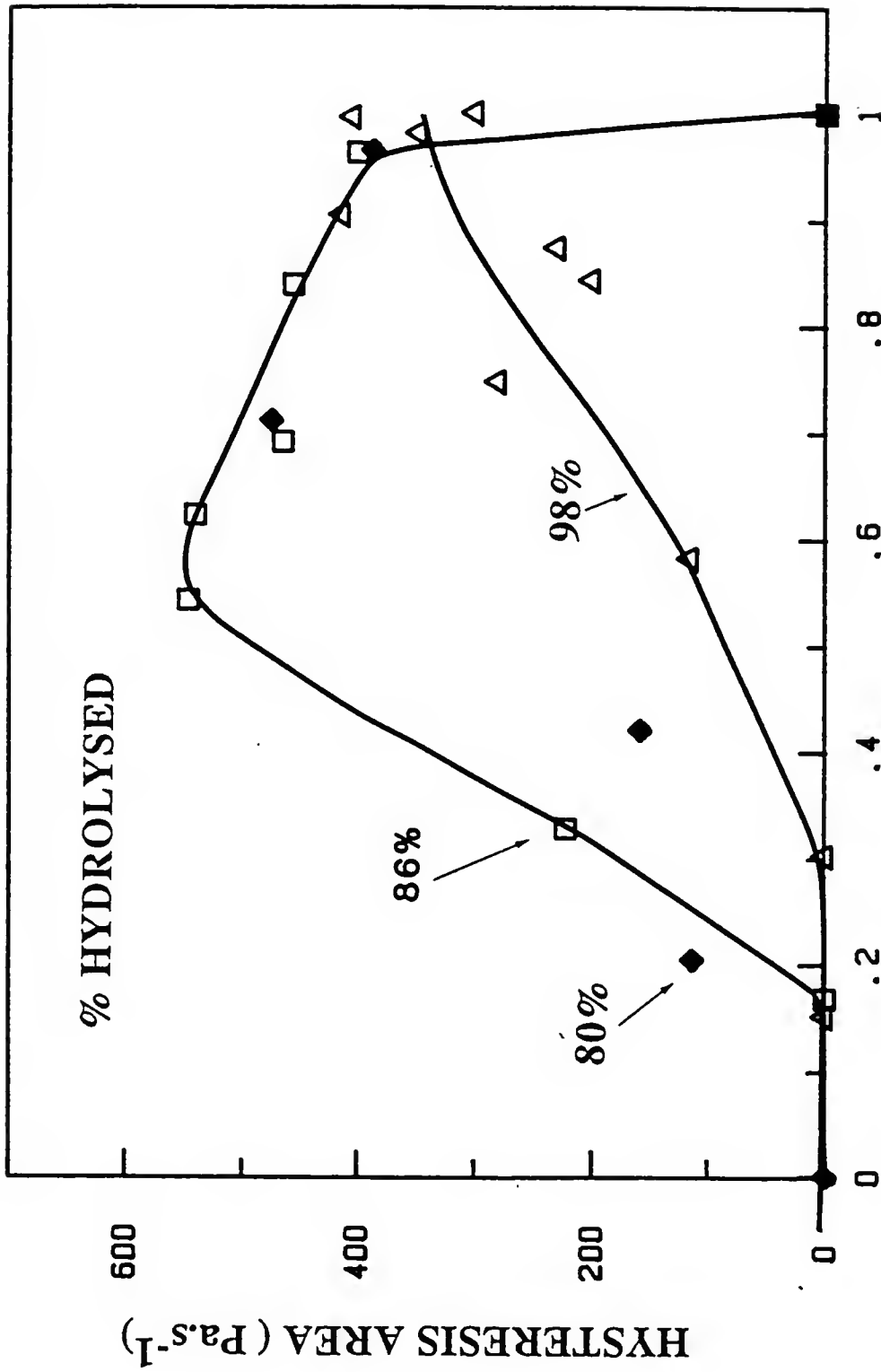
Figure 8.80   Plots of (a) hysteresis area versus adsorbed amount and (b) hysteresis area versus fraction plateau coverage for 20 vol.% SiO_2 suspensions prepared using PVAs with indicated degree of hydroxylation.
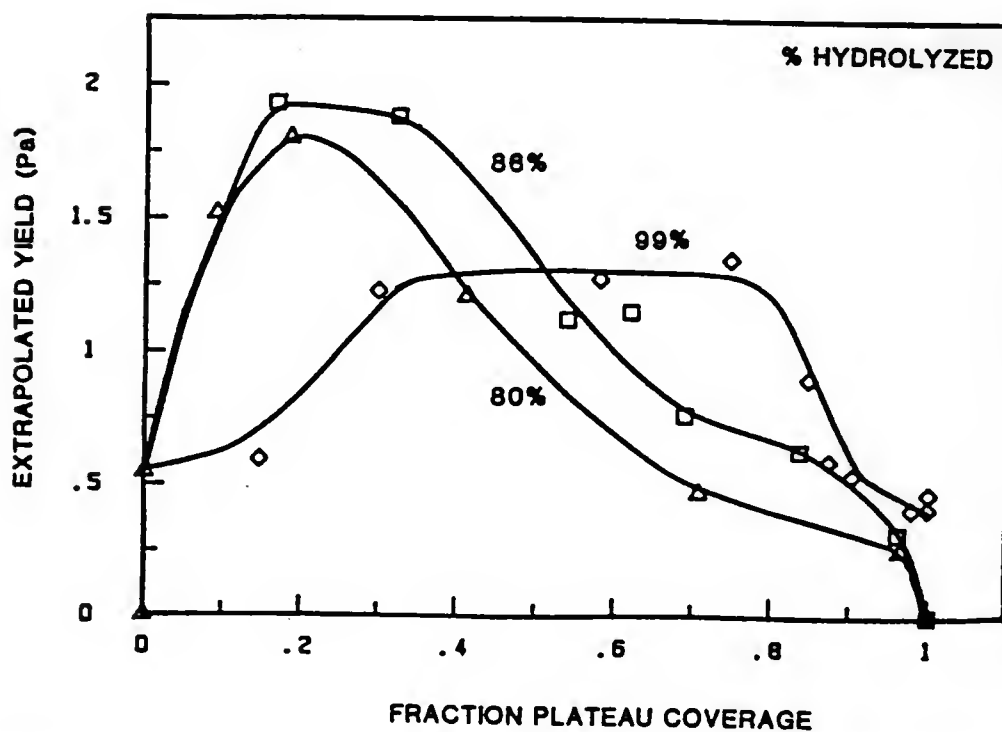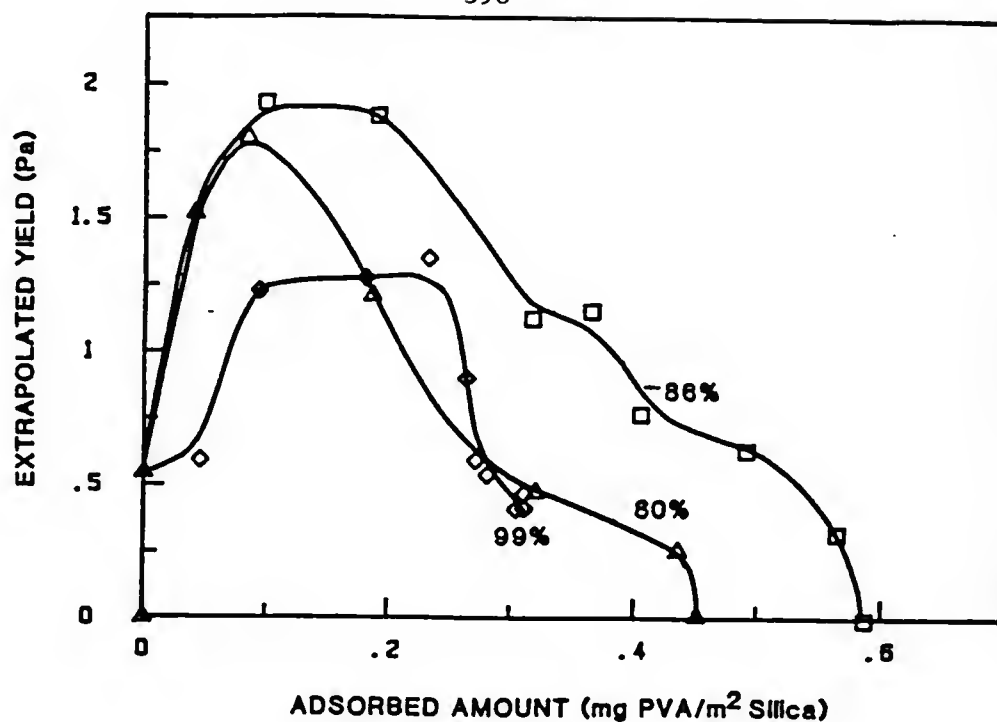
Figure 8.81   Plots of (a) yield stress versus adsorbed amount and (b) yield stress versus fraction plateau coverage for 20 vol.% SiO_2 suspensions prepared using PVAs with indicated degree of hydroxylation.
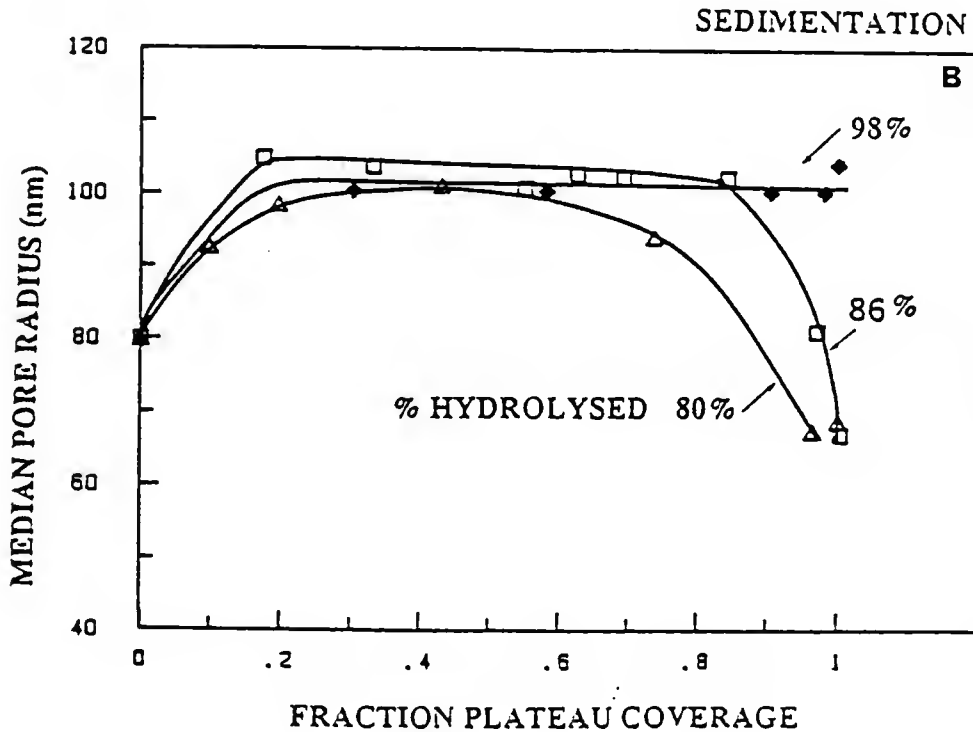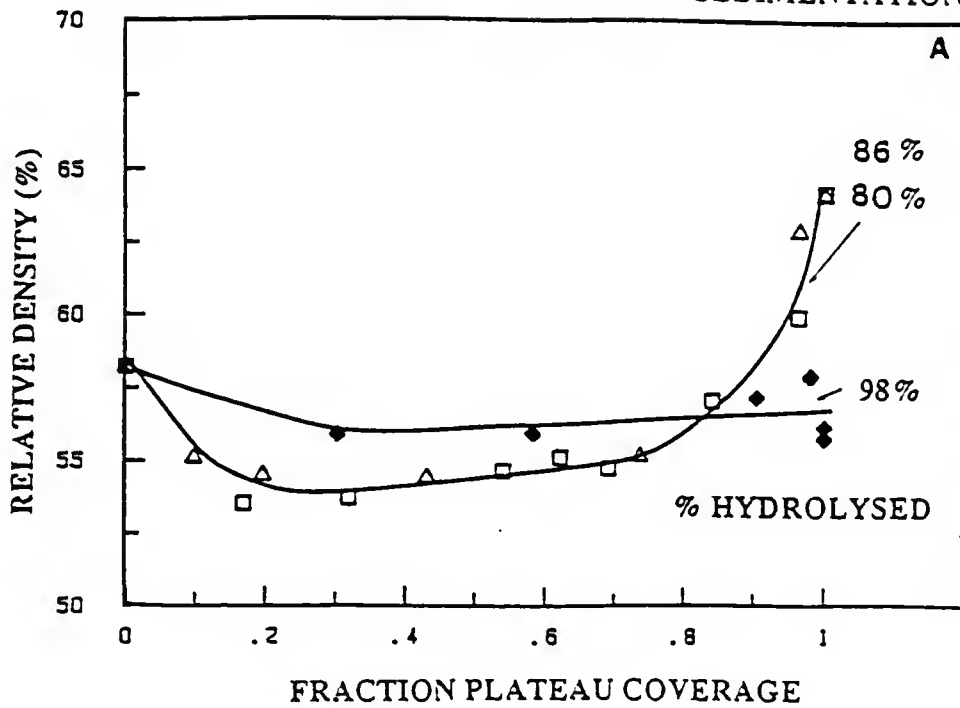
Figure 8.82   Plots of (a) relative viscosity of gravity cast sample
versus fraction plateau coverage and (b) median pore
radius versus fraction plateau coverage of compacts
prepared from 20 vol.% SiO_2 suspensions with varying PVA
concentration in solution.   The degree of hydroxylation
for various polymers is indicated in the figure.

adsorption of partially hydrolysed PVA (i.e., through acetate group blocks of longer lengths) seems responsible for slightly higher yield stresses for partially hydrolysed (i.e., 80% and 86%) polymers. With increasing surface coverages, for PVA80 and PVA86, decrease in the yield stress was observed (as less empty sites are available for bridging) and at the complete coverage, no yield stress was observed (indicating particles are sterically stabilized). A small yield was observed for fully hydrolysed PVA at complete coverages indicating flocculation due to insufficient adsorbed layer thickness.

Figure 8.82A shows plots of relative density of gravity cast samples versus fraction plateau coverage and 8.82B shows corresponding plots of median pore radius versus fraction plateau coverage for compacts prepared using PVA's hydrolysed to various extents. At partial coverages, slightly lower compact densities were obtained for PVA80 and PVA86 consistent with the higher relative viscosities under these conditions. With increasing surface coverages, higher density compacts ($\approx 63\%$) could be produced with PVA86 and PVA80. As described earlier, relatively lower green density ($\approx 56\%$) was obtained from suspensions prepared using PVA98 at complete coverages.

Effect of Solvent Quality on the Rheological Behavior

So far, we described the results for suspensions prepared at the constant ionic strength of 1×10^{-2} moles/liter NaCl. At this ionic strength, solvent is a slightly better than θ solvent for PVA86 and PVA98. As described in Chapter IV, by studying the stability to the instability transition by changing solvent quality at the plateau

coverages, the effect of solvent quality can be investigated which is the topic of this section.

The effect of changing solvent quality on the rheological behavior was investigated for 20 vol. % suspensions with the plateau coverage of particle surface with $\approx$ 86% hydrolysed PVA of $M_w \approx$ 200,000. The solvent quality for PVA (i.e., as indicated by χ parameter) can be changed by either (a) addition of electrolyte (Vincent 79,82, Tadros 84, Barker and Garvey 80, Tadros and Vincent 79), or (b) changing the temperature (Lambe et al. 78). As discussed in Chapter IV, the θ point for the polymer sets the limit for the thermodynamic stability of the suspensions if the following conditions are satisfied: (1) complete coverage of the particles, and (2) sufficiently thick adsorbed polymer layer to overcome the Van der Waal's attraction.

The complete coverage of particles was ensured by using sufficient concentration of PVA in solution. (The initial PVA concentration was $\approx$ 0.8 g PVA/dL which was necessary to achieve the plateau adsorbed amounts at pH = 7.8). High molecular weight PVA ($M_v \approx$ 200,000) was used to obtain sufficiently thick adsorbed layer to overcome the Van der Waal's attraction and to screen electrostatic interactions between particles.

Figure 8.83A shows a plot of relative viscosity versus Na_2SO_4 concentration (moles/liter) and Figure 8.83B shows a plot of extrapolated yield versus Na_2SO_4 concentration. The shear stress shear rate curves (Figure 8.84) for suspensions below critical electrolyte concentration showed nearly Newtonian behavior (i.e., slight shear thinning behavior and small yield due to higher effective solids loading resulting from relatively thick adsorbed polymer layer), but above a critical
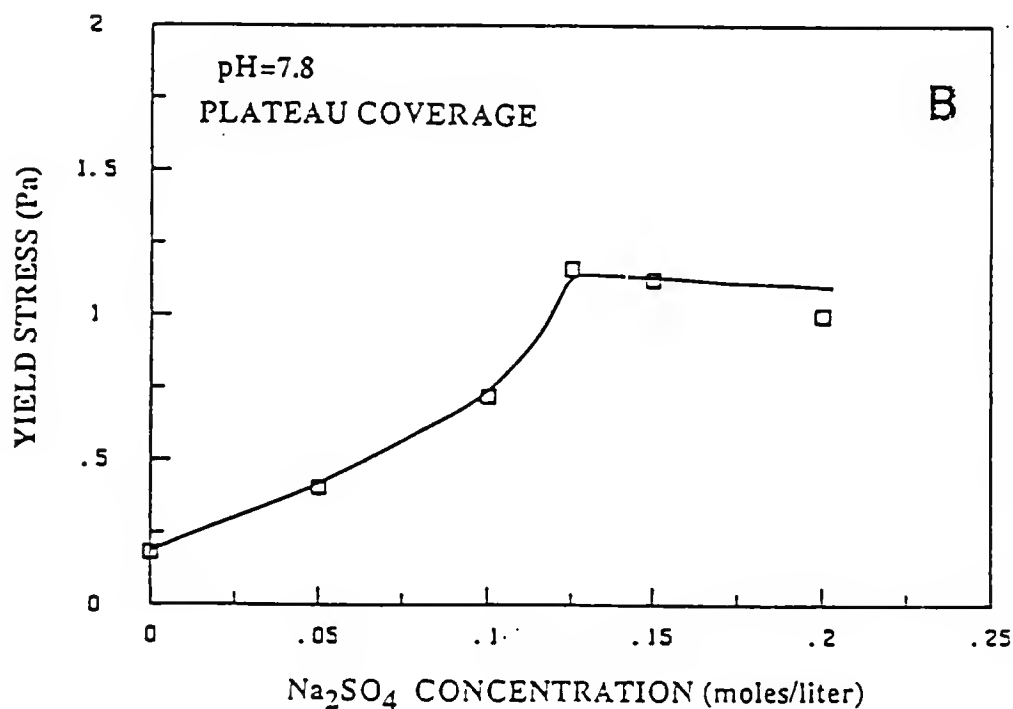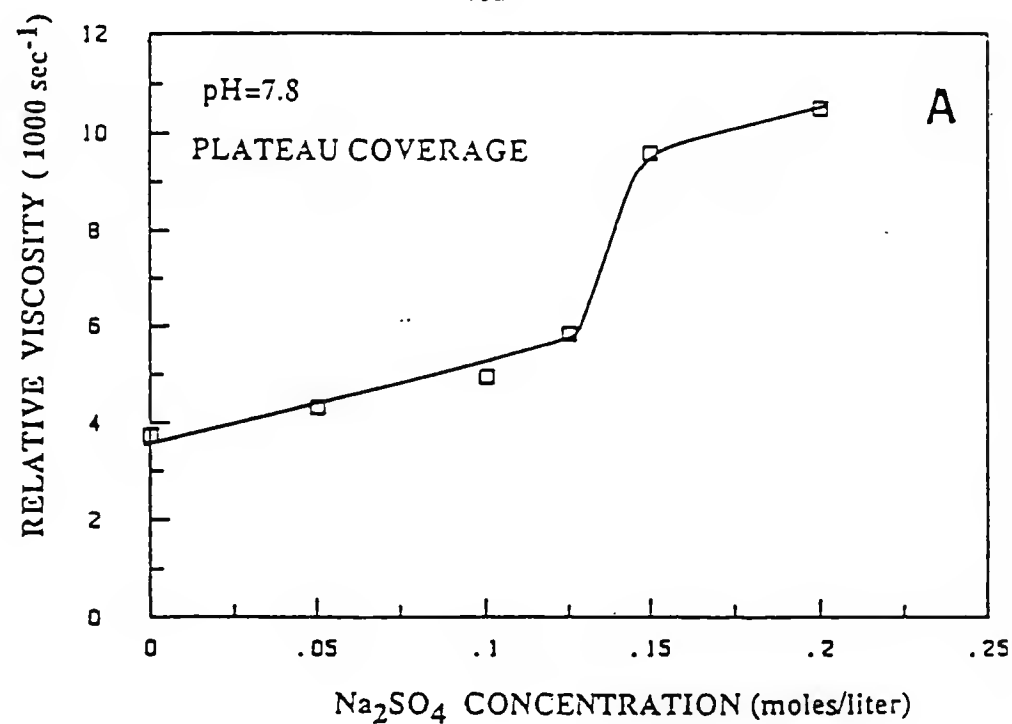
Figure 8.83   Plots of (a) relative viscosity versus Na_2SO_4 concentration and (b) yield stress versus Na_2SO_4 concentration for 20 vol.% SiO_2 suspensions with plateau coverages of particles with adsorbed polymer.
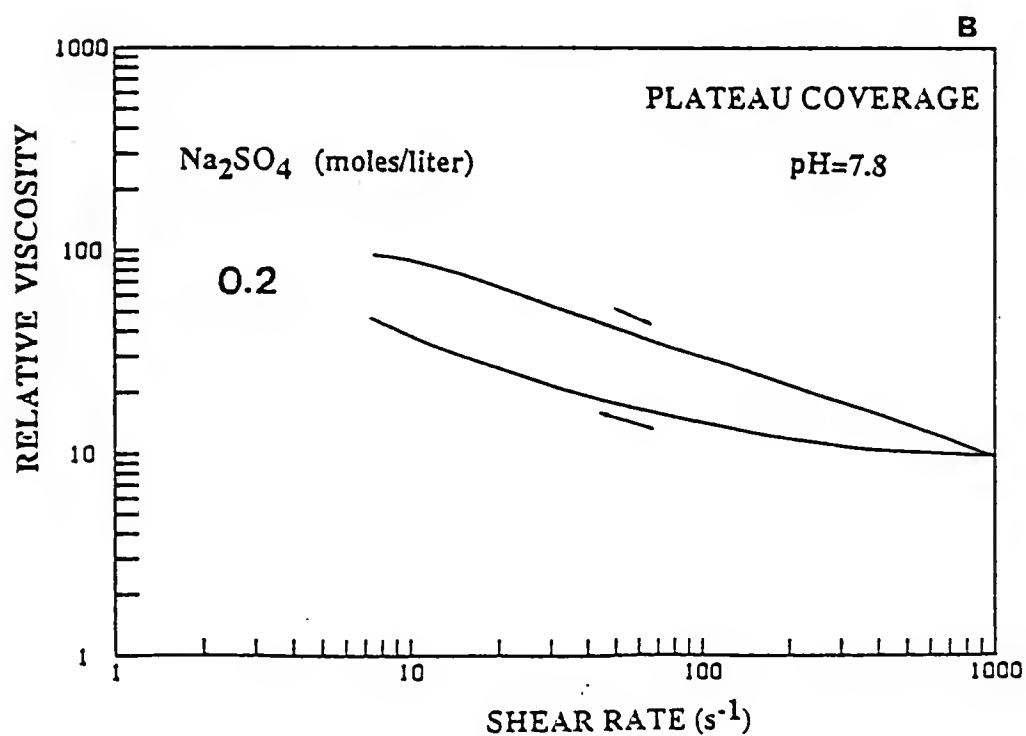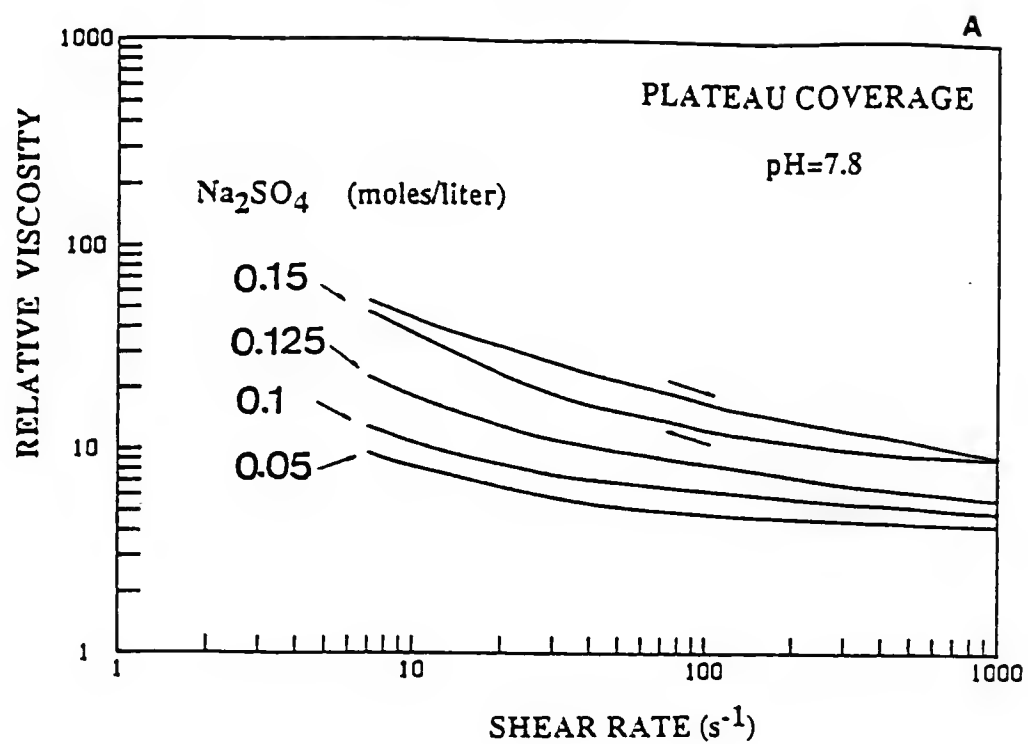
Figure 8.84   Plots of relative viscosity versus shear rate for 20
vol.% SiO$_2$ suspensions with varying Na$_2$SO$_4$ concentration.

electrolyte concentration, the flow curves became highly shear thinning and showed thixotropic flow behavior (Figure 8.85). A sharp increase in the relative viscosity and the yield stress with increases in the Na_2SO_4 concentration in the range 0.1 to 0.15 moles/liter was observed (Figure 8.83). In this Na_2SO_4 concentration range (i.e., 0.1-0.15 moles/liter), there is a dramatic change in the suspension properties (i.e., sterically stabilized suspension is catastrophically flocculated). The electrolyte concentration at which this sharp change occurs is called the critical flocculation concentration, C_{CFC}.

From the rheological observations, it can be concluded that the C_{FPC} for these silica suspensions is at $\approx$ 0.15 moles/liter for Na_2SO_4.

Figure 8.86A shows a plot of sediment density vs. Na_2SO_4 concentration and Figure 8.86B shows a corresponding plot of median pore radius vs. Na_2SO_4 concentration. Similar plots for slip cast samples are shown in Figure 8.87. Low relative densities were observed for the sedimented compacts produced from suspension with Na_2SO_4 concentration > 0.1 moles/liter (for slip cast samples, Na_2SO_4 concentration > 0.125 moles/liter produced low density compacts--Figure 8.87). The sharp change in the compact densities with increasing Na_2SO_4 concentration cannot be unambiguously associated with the C_{FPC} since during the drying stage as water evaporates, the concentration of Na_2SO_4 in the remaining solution increases which may lead to flocculation of the suspension. The C_{FPC} depends on the type of electrolyte (Barker and Garvey 80, Tadros and Vincent 79). The potency of an electrolyte in inducing flocculation is directly related to its ability to convert water into poorer solvent for the adsorbed polymer molecules. The effect of various types of
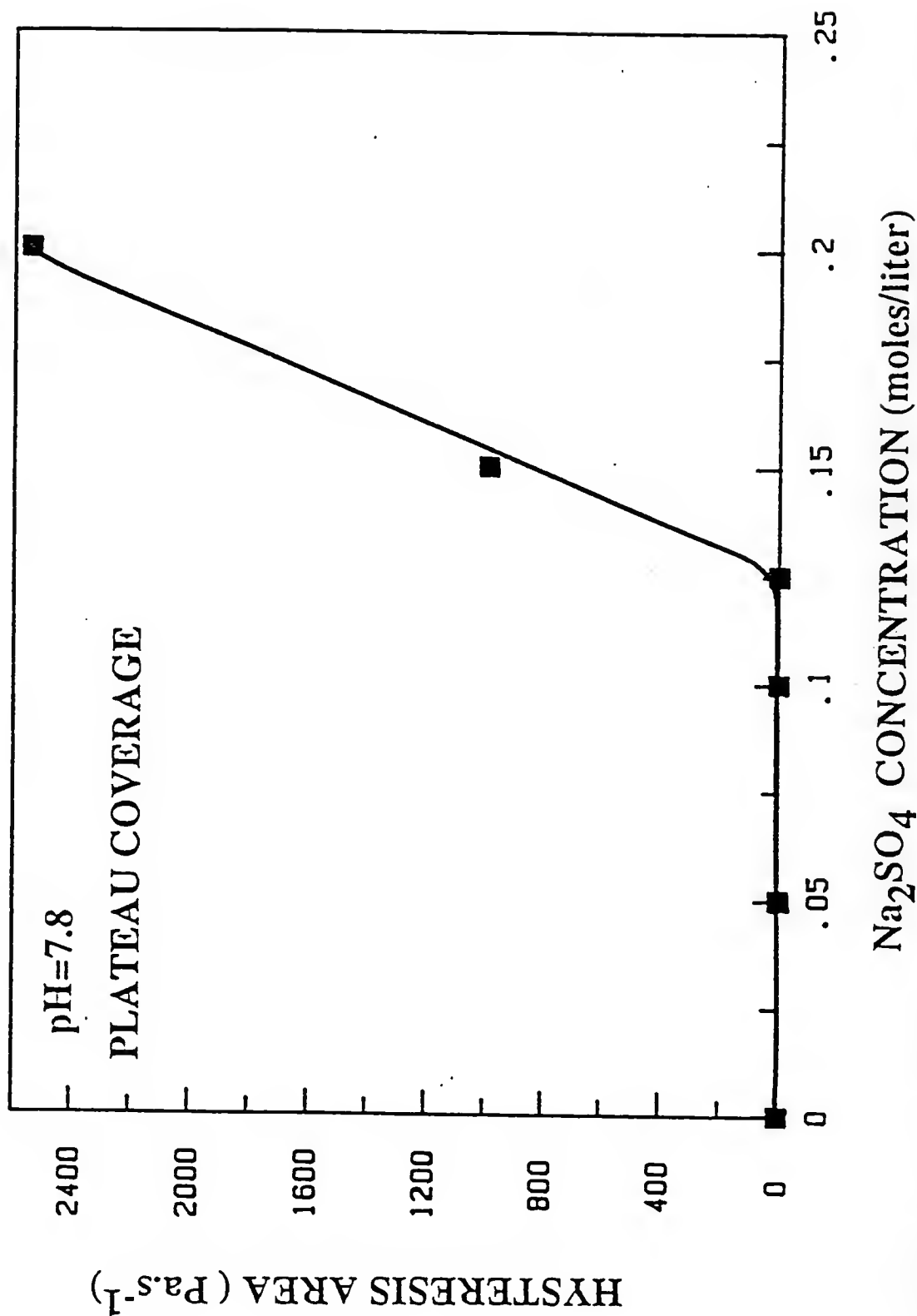
Figure 8.85 Plot of hysteresis area versus Na_2SO_4 concentration in solution suspensions were prepared at pH 7.8 with the plateau adsorbed amount of PVA with molecular weight ≈ 200,000.

Figure 8.86   Plots of (a) relative density of gravity cast samples versus Na_2SO_4 concentration and (b) median pore radius versus Na_2SO_4 concentration.
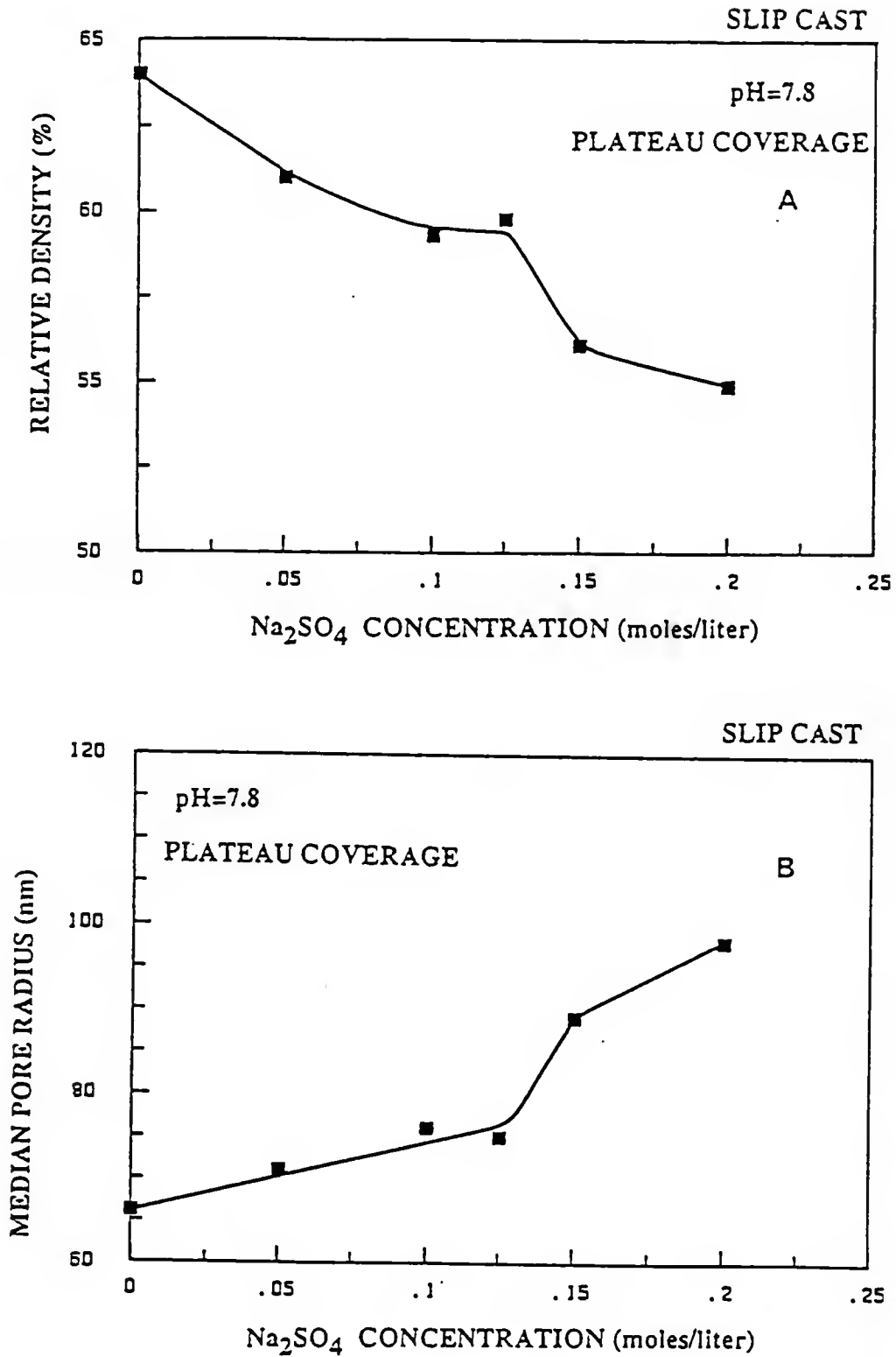
Figure 8.87   Plots of (a) relative density of slip cast samples versus
                Na$_2$SO$_4$ concentration and (b) median pore radius versus
                Na$_2$SO$_4$ concentration in solution.

electrolytes on the stability of the latex particles and on the force of interactions between two quartz filaments has been studied (Gotze and Sonntag 87,88, Sonntag et al. 82). It was observed that Na_2SO_4 was more effective (i.e., requires less concentration) compared to NaCl or KCl. This effect has been associated with the known water structure breaking properties of SO_4^{-2} anions. SO_4^{-2} is thought to be unhydrated in aqueous solution and to have extensive disordered region surrounding the ion. Thus, with Na_2SO_4 additions, normal water structure (i.e., relatively ordered structure due to hydrogen bonding between water molecules) is broken down. At sufficiently high Na_2SO_4 concentration, there will be an extensive breakdown of normal water structure, and hence, the solvency power of the medium for PVA is strongly reduced (Tadros and Vincent 79).

The C_{FPC} of $\approx$ 0.15 moles/liter observed for silica suspensions was smaller than the C_{FPC} of 0.22 moles/liter observed by Tadros for latex suspensions (Tadros 85). He also observed that the C_{FPC} depends on the particle concentration (i.e., $C_{FP} \approx$ 0.22 moles/liter was observed for $\approx$ 20 vol % latex dispersion whereas $C_{FP} \approx$ 0.28 moles/liter was observed for dilute dispersions).

The effect of particle concentration on the C_{FPC} was explained by Tadros as follows:

(i) He assumed that the adsorbed polymer layer close to the surface will exclude Na_2SO_4. This will lead to increases in the bulk Na_2SO_4 concentration. The increase in the bulk concentration will be larger for concentrated suspensions since with increasing solids loading the total adsorbed layer volume (which excludes Na_2SO_4) will increase.

(ii) There is a decrease in the entropy of particles upon flocculation. This entropy decrease will oppose the flocculation. The decrease in entropy upon flocculation will be more for a dilute suspensions compared to a concentrated suspensions. Hence, a larger Na_2SO_4 concentration is required to flocculate dilute suspension compared to more concentrated suspension.

The residual polymer in solution will also contribute to flocculation upon Na_2SO_4 additions. The Na_2SO_4 induced phase diagram has been determined by Barker and Garvey (Barker and Garvey 80). Their phase diagram is replotted and shown in Figure 8.88, which shows a plot of Na_2SO_4 concentration (moles/liter) vs. PVA concentration in solution (g PVA/dL). The solid line separates single phase region (i.e., true polymer solution) from the two phase region (i.e., precipitated polymer and solvent). With increases in Na_2SO_4 additions to PVA solution (of fixed concentration), phase separation will occur at the critical Na_2SO_4 concentration. The residual PVA concentration was ≈ 0.3 g PVA/dL in our suspensions (Tadros did not report whether latex dispersions were washed to remove residual polymer). From Figure 8.88, it can be expected that, if the PVA concentration in solution is ≈ 0.3 g/dL, then, the phase separation will occur when Na_2SO_4 concentration is ≈ 0.15 moles/liter. The C_{CFC} observed from the rheological experiments (i.e., 0.15 moles/liter) is similar to the concentration at which phase separation occurs. This suggests that the concentration of residual polymer in solution will be also important in determining C_{CFC}.

One of the often stated advantages of the sterically stabilized system is its ability to tolerate higher electrolyte concentrations
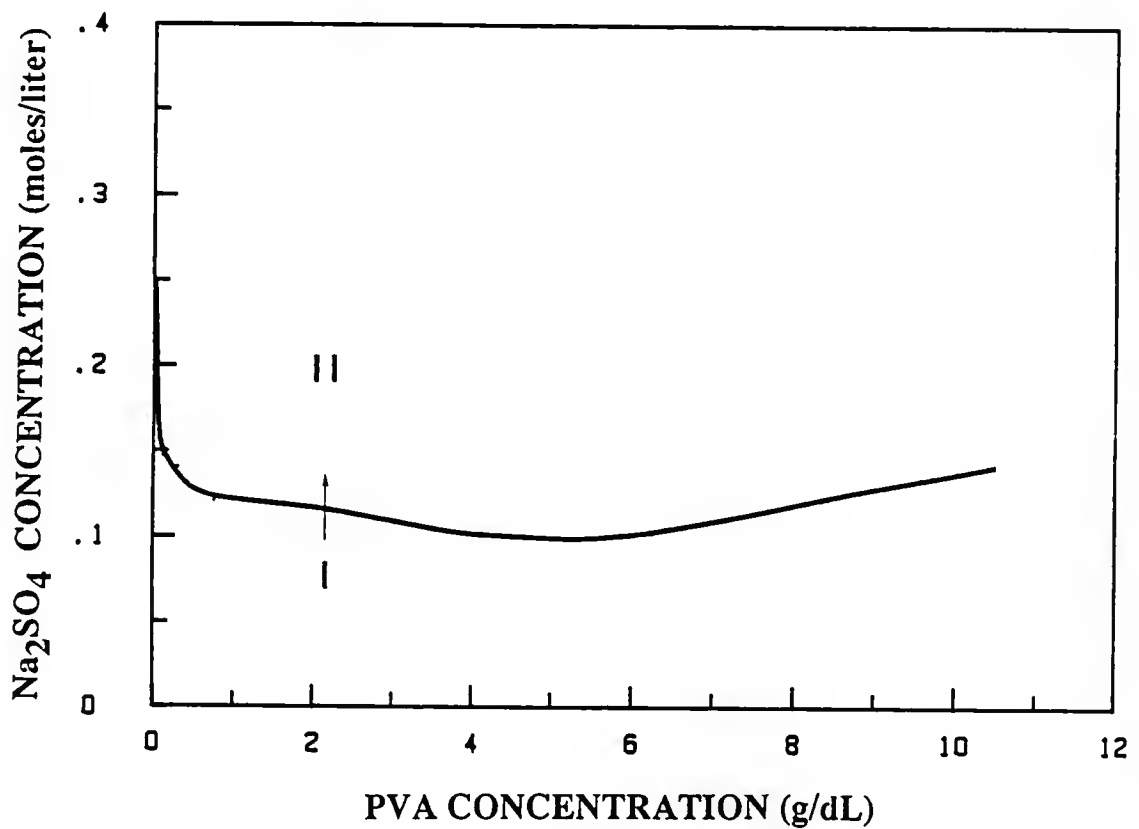
Figure 8.88   Plots of relative viscosity versus Na_2SO_4 concentration
                for suspensions of polymer coated particles and
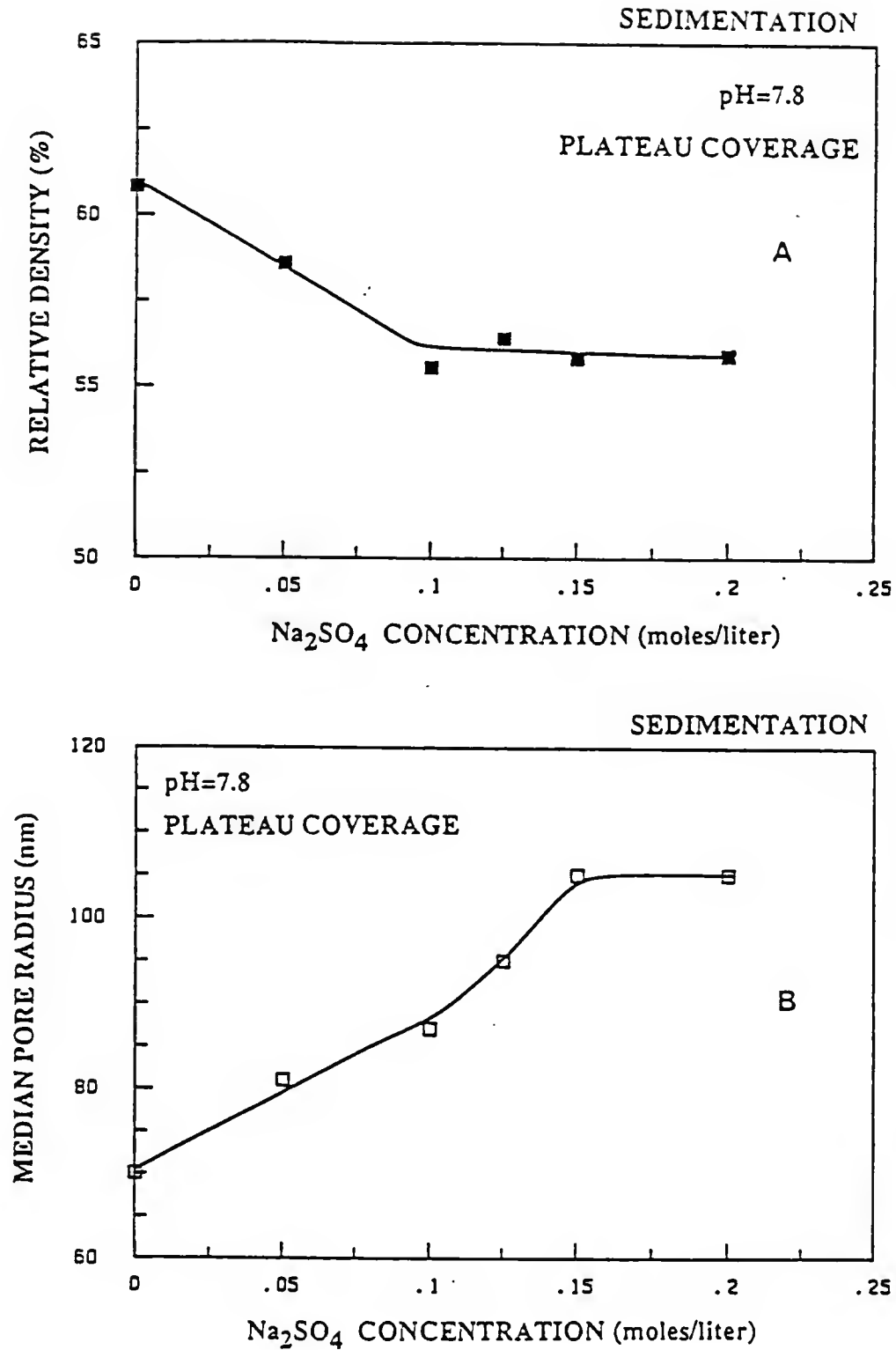   suspensions prepared with no added polymer at pH 7.8.
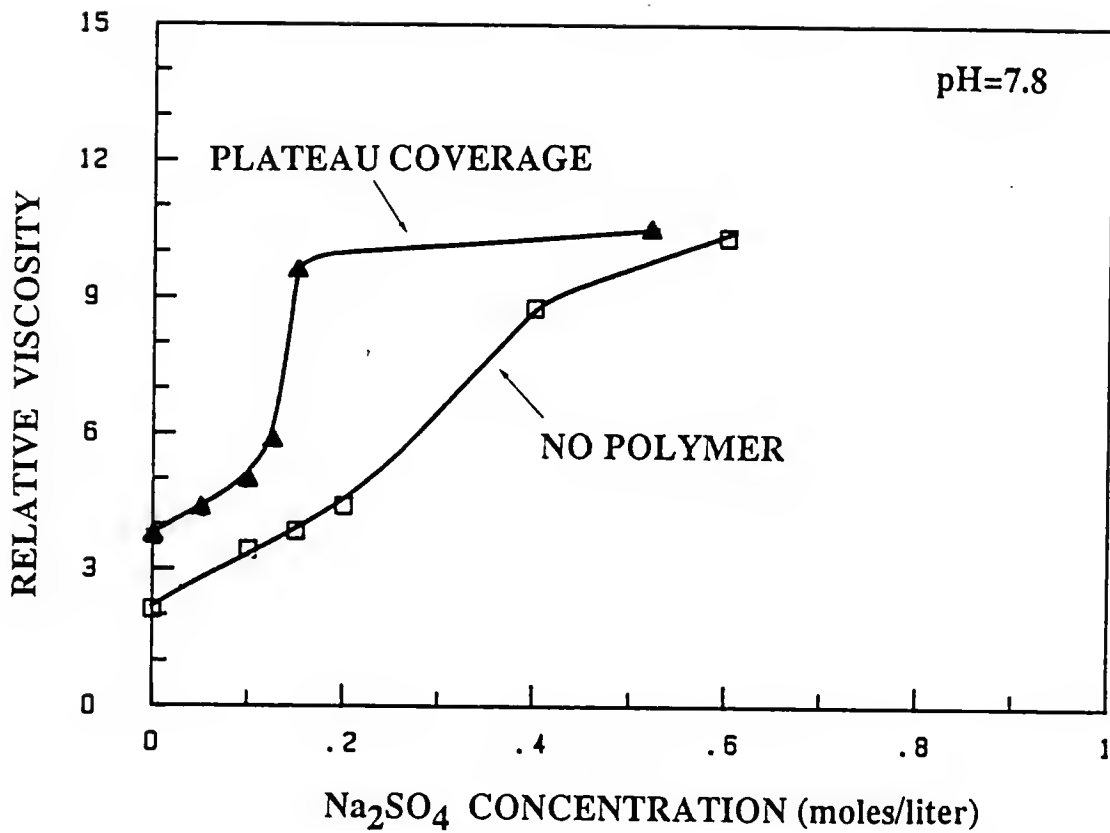
Figure 8.89   Plots of (a) relative density of gravity cast samples
                versus Na_2SO_4 concentration and (b) median pore radius
   versus Na_2SO_4 concentration of compacts prepared from
                suspensions of polymer coated particles and suspensions
                with no added polymer at pH 7.8.
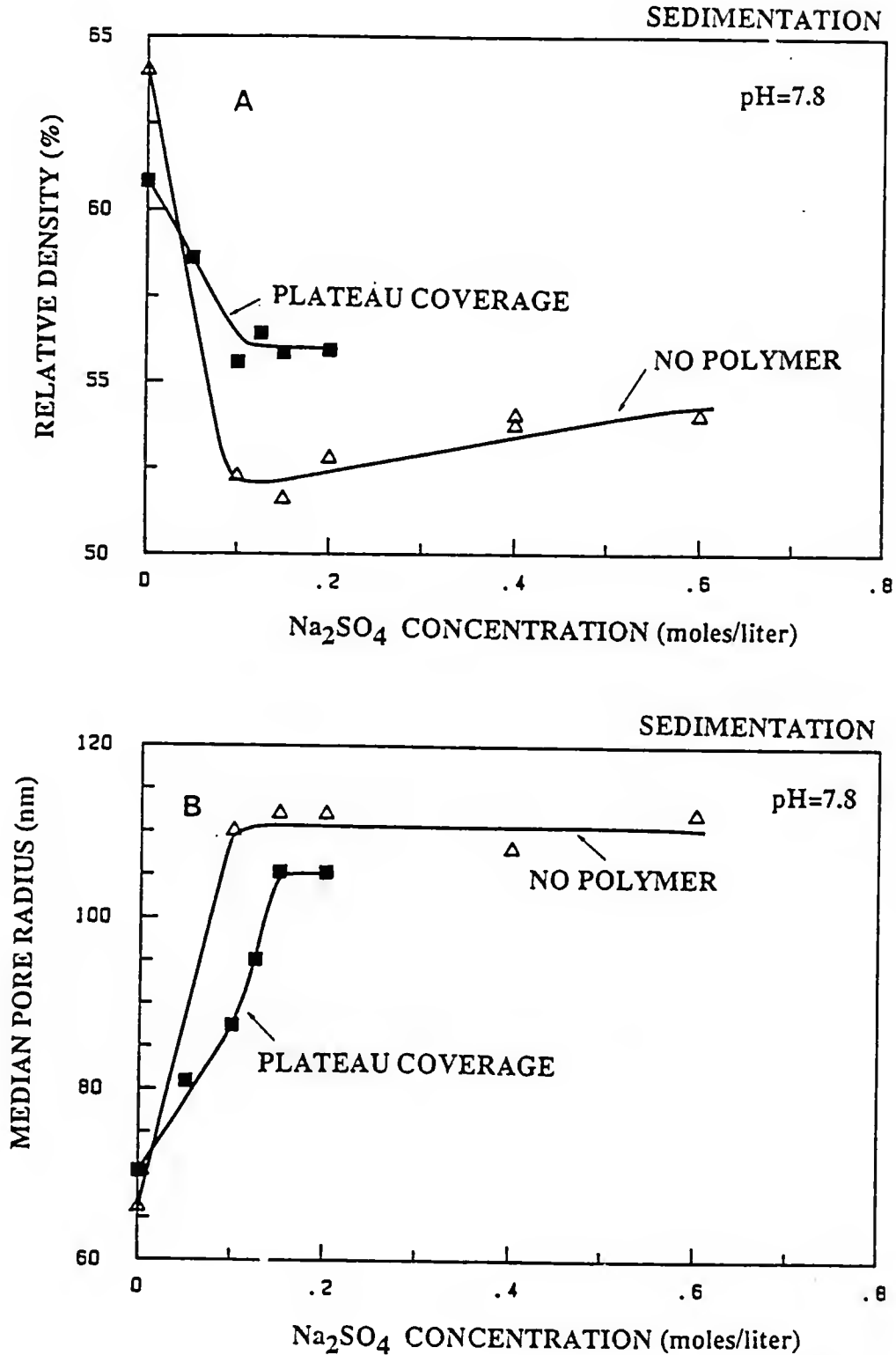
Figure 8.90   Plots of (a) relative density of gravity cast samples versus Na_2SO_4 concentration and (b) median pore radius versus Na_2SO_4 concentration of compacts prepared from suspensions of polymer coated particles and suspensions with no added polymer at pH 7.8.

compared to electrostatically stabilized suspensions (Napper 83, Tadros 80, Vincent 74). Figure 8.88 shows relative viscosity as a function of Na_2SO_4 concentration for suspensions of polymer coated particles, and suspensions prepared with no added polymer at pH = 7.8. As described earlier, the sharp increase in the relative viscosity with increasing Na_2SO_4 concentration (in the range of 0.1 to 0.15 moles/liter) for polymer coated particles is due to worsening of solvency with Na_2SO_4 additions. In contrast, flocculation of electrostatically stabilized suspensions (with no polymer) results from the decreases in the potential barrier (Figure 3.7, Chapter II) for flocculation with increases in Na_2SO_4 concentration. The stability of these two suspensions cannot be determined from the absolute values of relative viscosities since (i) the relative viscosity of polymer stabilized suspension is expected to be higher due to the adsorbed polymer layer and (ii) the flocculation results from different mechanisms, hence, the resulting suspension structure may be different in these two cases.

The green compacts prepared by sedimentation showed lower densities ($\approx$ 52% for suspensions with no polymer and $\approx$ 55% for suspensions with polymer) for Na_2SO_4 concentrations greater than $\approx$ 0.1 moles/liter (Figure 8.90). Thus, no significant improvement in the stability at higher electrolyte concentrations was observed due to adsorbed polymer layer.

CHAPTER IX
SUMMARY AND SUGGESTIONS FOR FUTURE WORK

Summary

In this study, the effect of interparticle forces on the dispersion

stability, rheological flow behavior, and consolidated density of model

silica suspensions was investigated.

Spherical, narrow-sized silica was prepared using Stober et al.

method and was characterized using various techniques (i.e., SEM, X-ray

sedimentation, BET, FTIR, etc.). All suspensions were prepared in

aqueous medium. The electrostatic interactions between particles were

varied by changing suspension pH. It was observed that near the

isoelectric point for the silica (i.e., pH ≈ 3.7), suspensions were

flocculated due to Van der Waal's attraction. At higher suspension pH's,

charge development at the solid liquid interface resulted in improved

suspension stability. An attempt to correlate the flow curve parameters

(i.e., yield stress, relative plastic viscosity, etc.) to zeta potential

using "elastic floc" model was not successful.

To investigate the effect of adsorbed polymer on the rheological

behavior of suspensions, non-ionic, water soluble, poly (vinyl alcohol),

PVA, was used. PVA was characterized for molecular weight (using

viscometry and Gel Permeation Chromatography, GPC), molecular weight

distribution (GPC), and degree of hydroxylation. The adsorbed amounts of

PVA onto silica were determined using the solution depletion technique.

The adsorption was dependent on a variety of factors including the

414

overall polymer concentration in suspension, PVA molecular weight, degree
of hydroxylation, suspension pH, and silica surface hydroxylation. The
adsorption characteristics were correlated with the state of the
particulate dispersion in suspensions using rheological measurements.
Suspension and green compact properties were highly dependent upon (i)
the fraction of silica surface covered with the adsorbed polymer and (ii)
the thickness of the adsorbed polymer layer.

Low surface coverages at pH $\approx$ 3.7 (i.e., with no electrostatic
repulsion) resulted in polymeric bridging flocculation while plateau
adsorption produced suspensions with improved stability against
flocculation.

At partial coverages, suspensions prepared with partially hydrolysed
PVA of higher molecular weight, with 700°C calcined powder (i.e.,
conditions leading to higher plateau adsorption density), or smaller size
silica exhibited higher relative viscosities at moderate shear rates.
This was attributed to more open, less dense floc structures under the
shear conditions. Yield stresses were lower in these systems apparently
due to (i) smaller Van der Waal's attraction (i.e., due to smaller
particle size and/or greater distances of separation between particles)
and (ii) less number of polymeric bridges formed between the particles.
The formation of more open (and weak) floc structure was also consistent
with highly thixotropic flow behavior observed under these conditions.
The consolidation under gravity sedimentation (and slip casting) resulted
in compacts of lower densities and larger pore radii.

When plateau coverage of silica particles with adsorbed polymer was
achieved, stable dispersions could be prepared under a variety of

conditions (i.e., under range of molecular weights, acetate contents, particle sizes, calcination temperatures, etc.). A certain minimum level of the adsorbed layer thickness was necessary to overcome the Van der Waal's attraction to stabilize the suspensions. Stable dispersions with the plateau coverage of silica could not prepared with low molecular weight partially hydrolysed polymers, fully hydrolysed PVAs, or with uncalcined silica (i.e., all these conditions resulted in lower plateau adsorption densities). A minimum molecular weight necessary to overcome the Van der Waal's attraction under variety of conditions of particle sizes and effective Hamaker constants was calculated.

With sufficiently thick adsorbed polymer layer, stable dispersions could be prepared. The consequence of thicker adsorbed layer is an increased "effective" solids loading of the suspension. The effect of molecular weight on the adsorbed layer thickness was determined using a viscometric technique. The observed adsorbed layer thicknesses were comparable to molecular dimensions (e.g., radius and diameter of gyration) in solution. The increased effective solids loading due to adsorbed polymer layer can limit the maximum true solids loading that can be used in suspension processing. It was concluded that the larger size particles with thin adsorbed layer thicknesses (consistent with the stability conditions) were necessary to obtain high true solids loading in suspensions.

Finally, the effect of Na_2SO_4 additions on the rheological behavior of polymer coated particles was investigated. It was observed that the additions of Na_2SO_4 beyond a certain critical concentration C_{FCP}, ($\approx$ 0.15 moles/liter) lead to catastrophic flocculation of suspensions. This was

attributed to worsening of the solvent quality for PVA with Na_2SO_4

additions. Generally, stated advantages of steric stabilization, i.e.,

(i) suspensions with higher solids loading can be prepared and (ii)

suspensions are generally stable against additions of higher electrolyte

additions were not realized with silica-PVA-water system studied in this

work. The electrostatically stabilized suspensions of higher solids

loading ($\phi_p \leq 0.5$) could be prepared and no significant improvement in

the stability against electrolyte additions was observed due to adsorbed

polymer layer.

Suggestions for Future Work

Agglomerate free, narrow sized, spherical silica powder used in this

study can be employed to study various aspects of suspension stability

and properties of green compacts produced. Suggestions for future work

are described below:

i) The hydrodynamic thickness δ, of the adsorbed polymer layer can be

measured using photon correlation spectroscopy, PCS, technique. The

effect of silica surface nature, particle size, PVA molecular weight,

etc., on δ can be measured at partial coverages (at pH $\approx$ 7.6) and at the

plateau coverages (at pH $\approx$ 3.7 and pH $\approx$ 7.6). PCS results then can be

compared with the viscometric thicknesses determined in this study.

Also, the effect of particle radius on the adsorbed layer thickness can

be determined.

ii) Recently small angle neutron scattering, SANS, technique has been

utilized to obtain structural information of particle clusters (e.g.,

fractal dimension d_f). Light, x-ray, and neutron scattering techniques

will be useful to determine the structural properties of silica

aggregates. It will be useful to investigate the effect of silica size,

silica surface nature, PVA molecular weight, etc. on the floc

characteristics.

iii) Stability map (i.e., minimum molecular weight required to stabilize

suspension vs. silica particle size) can be established.

iv) The effect of polymer adsorption on the viscoelastic properties of

model suspensions can be studied. In this case, important variables will

be fractional coverage, volume fraction of solids, along with the

properties of materials employed (e.g., silica size, PVA molecular

weight, etc.).

v) A correlation between polymer adsorption behavior and green compact

characteristics (e.g., green strength) can be established for PVA-

silica-water system.

vi) The stability of model spherical silica particles in non-aqueous

media can be investigated. The polymer adsorption behavior can be

correlated with the rheological behavior of suspensions. In this case,

it may be possible to demonstrate an importance of steric stabilization

in achieving higher solids loading (compared to suspensions prepared with

no added polymer). Also, it may be possible (with proper choice of

solvent and polymer) to determine polymer adsorption mechanism less

ambiguously using techniques such as IR, calorimetry, etc. The effect of

solvent quality on polymer adsorption behavior and rheological behavior

can be investigated.

vii) Since silica particles of different sizes (≈ 0.1 μm to 1 μm) can be

produced, the effect of size distribution width on the rheological

measurements (of stable dispersions) and packing characteristics of
particles will be useful in optimizing distribution width for processing
of commercial powders.

REFERENCES

Ahmed, M.S., El-Aasser, M.S., and Vander hoff, J.W., (1984), in "Polymer Adsorption and Dispersion Stability," Ed. Goddard, E.D., and Vincent, B., ACS Symposium Series 240, Washington, D.C., p. 77.

Akers, R.J., (1975), Flocculation, I. Chem. F. London.

Aksay, I.A. and Kikuchi, R., (1986), in "Ceramic Chemical Processing," Ed. L.L. Hench and D.R. Ulrich, John Wiley, New York, p. 513.

Albers, W. and Overbeek, J.Th.G., (1960), J. Colloid Sci., 15, 589.

Alder, B.J. and Weinright, T.E., (1962), Phys. Rev., 127, 359.

Alder, B.J. and Hoover, W.G., and Young, D.A., (1968), J. Chem. Phys., 49, 3688.

Alder, P.M. and Mills, P.M., (1979), J. Rheo., 23, 25.

Ali, S. and Zollars, R.L., (1987), J. Colloid Interface Sci., 117, 425.

Babak, V.G., (1988), Colloids and Surfaces, 30, 307.

Bagchi, P., (1974a), J. Colloid Interface Sci., 47, 86.

Bagchi, P., (1974b), J. Colloid Interface Sci., 47, 100.

Bagchi, P. and Vold, R.D., (1972), J. Colloid Interface Sci., 38, 652.

Barker, M.C. and Garvey, M.J., (1980), J. Colloid Interface Sci., 74, 331.

Barker, J.A. and Henderson, D., (1976), Rev. Mod. Phys., 48, 587.

Barnett K.G., Cosgrove, T., Gowley, T.L., Tadros, Th.F. and Vincent, B., (1982) in "The Effect of Polymers of Dispersion Stability," Ed. Th. F. Tadros, Academic Press, London, p. 183.

Barringer, E.A. and Bowen, H.K., (1982), J. Am. Ceram. Soc., 65, C-199-C-201.

Barsted, S.J., Nowakowska, J., Wagstaff, I., and Walbridge, D.J.,
    (1971), Trans. Faraday Soc., 67, 3598.

Booth, F., (1950), Proc. Roy. Soc., A203, 533.

Bowen, H.K., (1984a), in "Microstructure and Properties of Ceramic
    Materials," Ed. T.S. Yen and J.A. Pask, Science Press, Beijing,
    p. 48.

Bowen, M.S., Broide, M.L. and Cohen, R.J., (1984b), in "Kinetics of
    Aggregation and Gelation," Ed F. Family and D.P. Landau,
    Elsevier/North-Holland, Amsterdam, p. 185.

Bowen, M.S. Broide, M.L., and Cohen, R.J., (1985), J. Colloid
    Interface Sci., 105, 617.

Brace, R. and Matijevic, E., (1973), J. Inorg. Nucl. Chem., 35,
    3691.

Casimir, H.B.G. and Polder, D., (1948), Phys. Rev., 73, 360.

Chan, F.S. and Goring, D.A.I., (1966a), J. Colloid Interface Sci.,
    22, 371.

Chan, F.S., Blanchford, J., and Goring, D.A.I., (1966b), J. Colloid
    Interface Sci., 22, 318.

Clark, A.T. and Lal, M., (1982) in "The Effect of Polymers on
    Dispersion Properties," Ed. Tadros, Th.F., Academic Press,
    London, New York, p. 169.

Clayfield, E.J. and Lumb, E.C., (1966), J. Colloid Interface Sci.,
    22, 285.

Clayfield, E.J. and Lumb, E.C., (1968), Macromolecules, 1, 133.

Cohen Stuart, M.A., (1980a), Thesis, Agricultural University,
    Wagenigen, The Netherlands.

Cohen Stuart, M.A., Scheutjeans, J.M.H.M., and Fleer, G.J., (1980b),
    J. Poly. Sci., Polymer Physics Ed., 18, 559.

Cohen Stuart, M.A., Fleer, G.J., and Bijsterbosch, J., (1982),
    Colloid Interface Science, 90, 321.

Cohen Stuart, M.A., Fleer, G.J., and Scheutjeans, J.M.H.M., (1984a),
    J. Colloid and Interface Sci., 97, 515.

Cohen Stuart, M.A., van den Boomgaard, Th., Zourab, Sh., M., and
    Lyklema, J., (1984c), Colloids and Surfaces, 9, 163.

422

Cohen Stuart, M.A., Waajen, F.H.W.H., Cosgrove, T., Vincent B., and Crowley, T.L., (1984b), Macromolecules, 17, 1825.

Cohen Stuart, M.A. and Mulder, J.W., (1985), Colloids and Surfaces, 15, 49.

Cohen Stuart, M.A., Cosgrove, T., and Vincent, B., (1986a), Adv. Colloid Interface Sci., 24, 143.

Cohen Stuart, M.A., Keurentjeans, J.T.F., Bonekamp, B.C., and Franye, J.G.E.M., (1986b), Colloids and Surface, 17, 91.

Cohen, R.D., (1987), AIChE, J., 33, 1571.

Cosgrove, T. and Fergie-Woods, J.W., (1987), Colloids and Surface, 25, 91.

Cosgrove, T., Vincent, B., Crowley, T.L., and Cohen Stuart, M.A., (1984), ACS Symp. Ser., 240, p. 147.

Cowell, C., and Vincent, B., (1982), J. Colloid Interface Sci., 87, 518.

Davenas, J. and Rabette, P.M., (1982), Ed., "Contribution of Cluster Physics to Materials Science and Technology," NATO ASI Series, E104.

Dawkins, J.V., (1972), Brit. Polym. J., 4, 87.

Dawkins, J.V. and Taylor, G., (1980), J.C.S. Faraday I, 76, 1263.

de Gennes, P.G., (1980), Macromolecules, 13, 1069.

de Gennes, P.G., (1982), Macromolecules, 15, 492.

de Gennes, P.G., (1987), Adv. Colloid Interface Sci., 27, 189.

Demchak, D. and Matijevic, E., (1969), J. Colloid Interface Sci., 31, 257.

Dimon, P., Sinha, S.K., Weiltz, D.A., Safinya, C.R., Smith, G.S., Varady, W.A., and Lindsay, H.M., (1986), Phy. Rev. Lett., 57, 595.

Doi, M., (1975), J. Chem. Soc., Faraday II, 71, 1721.

Dolan, A.K. and Edwards S.F., (1974) Proc. Roy. Soc., A337, 509.

Dobroszkowski, A. and Lambourne, R., (1965), J. Colloid Interface Sci., 26, 914.

Dunn, A.S., (1980), Chem. and Ind. 20, 801.

Eden, H., (1961), in "Proceedings of the Fourth Berkeley Symposium on Mathematics, Statistics and Probability," Ed. J. Noyman, Univ. of California, Berkeley, 4, 223.

Einstein, A., (1986), in "Investigation on the Theory of Brownian Motion," Metheun Publishers, London.

Eirich, F.R., (1977), J. Colloid Interface Sci., 58, 423.

Eirich, F.R., (1982), in "The Effect of Polymers on Dispersion Properties," Ed Th.F. Tadros, Academic Press, London, New York, p. 125.

Eisenlauer, J., Killmann, E., and Korn, M., (1980), J. Colloid Interface Sci., 74, 120.

Ernst, M.H., (1986), in "Fractal in Physics," Ed. L. Pietronero and E. Tosatti, Elsevier/North-Holland, Amsterdam, p. 289.

Evans, R., Smitham, J.B., and Napper, D.H., (1977), Colloid Polymer Science, 255, 161.

Family, F., and Landau, D.P., (1984), Ed. "Kinetics of Aggregation and Gelation," Elsevier/North-Holland, Amsterdam.

Firth, B.A., (1976a), J. Colloid Interface Sci., 57, 257.

Firth, B.A., and Hunter, R.J., (1976b), J. Colloid Interface Science, 57, 248, 257, 266.

Fisher, E.W., (1958), Kolloid Z., 160, 120.

Fixman, M., (1955), J. Chem. Phys., 23, 1356.

Fixman, M., (1962), J. Chem. Phys., 36, 3123.

Fleer, G.J., (1971), Thesis, Agricultural University, Wageningen, The Netherlands.

Fleer, G.J., (1987), "Reagents in Mineral Technology," Ed. P. Somasun daran and B.M. Moudgil, Marcel Dekker, New York and Basel, p. 105.

Fleer, G.J. and Lyklema, J., (1983), "Adsorption from Solution at Solid/Liquid Interface," Ed. G.D. Parfitt and C.H. Rochester, Academic Press, London, New York, p. 153.

Fleer, G.J. and Scheutjeans, J.M.H.M., (1986), J. Colloid Interface Sci., 111, 504.

Fleer, G.J., Scheutjeans J.M.H.M. and Cohen Stuart, M.A., (1988), Colloids and Surfaces, 31, 1.

Flory, P.J. and Fox, T.G., (1951), J. Am. Chem. Soc., 73, 1904.

Flory, P.J., (1953), "Principles of Polymer Chemistry," Cornell University Press, Ithaca, New York.

Flory, P.J., (1969), "Statistical Mechanics of Chain Molecules," Wiley and Sons, New York, London.

Flory, P.J., (1970), Discuss. Faraday Soc., 49, 7.

Fontana, B., (1963), J. Phys. Chem., 67, 2360

Fontana, B., (1966), J. Phys. Chem., 70, 1801.

Fontana, B. and Thomas J., (1961), J. Phys. Chem., 65, 480.

Forsyth, P.A., Marcelja, S., Mitchell, D.J., and Ninhan, B.W., (1978), Adv. Colloid Interface Sci., 9, 37.

Furusawa, K., Yamashita, K., and Konno, K., (1982), J. Colloid Interface Sci., 86, 35.

Garvey, M.J., (1977), J. Colloid Interface Sci., 61, 194.

Garvey, M.J., Tadros, Th. F., and Vincent, B., (1974), J. Colloid Interface Sci., 49, 57.

Garvey, M.J., Tadros, Th.F., and Vincent, B., (1976), J. Colloid Interface Sci., 55, 440.

Gillespie, T., (1960), J. Colloid Sci., 15, 219.

Goodeve, C.F., (1939), Trans. Faraday Soc., 35, 342.

Goodwin, J.W., (1975), in "Colloid Science," Vol. 2, The Chemical Society, London, p. 246.

Goren, S.L., (1971), J. Colloid Interface Sci., 36, 94.

Gotze, Th. and Sonntag, H., (1987), Colloids and Surfaces, 25, 77.

Gotze, Th. and Sonntag, H., (1988), Colloids and Surfaces, 31, 181.

Greenland, D.J., (1962), J. Colloid Science, 18, 647.

Gregory, J., (1969), Adv. Colloid Interface Sci., 2, 396.

Gregory, J., (1973), J. Chem. Soc., Faraday Trans. II, 69, 1723.

Gregory, J., (1988), Colloids and Surfaces, <u>31</u>, 231.

Griot, O. and Kitchner, J.A., (1965), Trans. Faraday Soc., <u>61</u>, 1026, 1032.

Gruber, E.B., Soehendra, B., and Schurz, J., (1974), J. Polym Sci. Symp. Sev. <u>44</u>, 105.

Hachisu, S. and Takano, K., (1982), Adv. Colloid Interface Sci., <u>16</u>, 233.

Hair, M.L., (1967), in "IR Spectroscopy in Surface Chemistry," Marcel Dekker, Inc., New York.

Hair, M.L., (1977), J. Colloid Interface Sci., <u>59</u>, 532.

Hair, M.L. and Hertl, (1969), J. Phys. Chem., <u>73</u>, 4269.

Hamaker, H.C., (1937), Physica, <u>4</u>, 1058.

Healy, T.W. and La Mer, V.K., (1962), J. Phys. Chem., <u>66</u>, 1835.

Hearn, J., Wilkinson, M.G., and Goodall, A.R., (1981), Adv. Colloid Interface Sci., <u>14</u>, 173.

Heath, D. and Tadros, Th.F., (1983), J. Colloid Interface Sci., <u>93</u>, 320.

Heller, W. and Pugh, T.L., (1954), J. Chem. Phys., <u>22</u>, 1178.

Hertl, W. and Hair, M.L., (1968), J. Phys. Chem., <u>72</u>, 4676.

Hesselink, T.Th., (1969), J. Phys. Chem., <u>73</u>, 3488.

Hesselink, F. Th., (1971a), J. Phy. Chem., <u>75</u>, 65.

Hesselink, F.Th., (1977), J. of Polymer Science, Polymer Symposium, <u>61</u>, 439.

Hesselink, F.Th., Vrij, A., and Overbeek J.Th.G., (1971b), J. Phys. Chem., <u>75</u>, 2094.

Hiemenz, P.C., (1977), "Principles of Colloid and Surface Chemisty," Marcel Dekker, New York.

Hiltner, P.A. and Krieger, I.M., (1969), J. Phys. Chem., Vol. 73, <u>7</u>, 2386.

Hoeve, C.A.J., (1965), J. Chem. Phys., <u>42</u>, 2558.

Hoeve, C.A.J., (1966), J. Chem. Phys., <u>44</u>, 1505.

426

Hoeve, C.A.J., (1970), J. Polym. Sci., C, <u>30</u>, 361.

Hoeve, C.A.J., (1971), J. Polym. Sci., C, <u>34</u>, 1.

Hogg, R., (1984), J. Colloid Interface Sci., <u>102</u>, 232.

Homola, A. and Robertson, A.A., (1976), J. Colloid Interface Sci., <u>54</u>, 286.

Honig, E.P., Roebersen, G.J., and Wiersema, P.H., (1971), J. Colloid Interface Sci., <u>36</u>, 97.

Hunter, R.J., (1982), Adv. Colloid Interface Sci., <u>17</u>, 197.

Hunter, R.J., (1987), "Foundations of Colloid Science," Vol. 1, Clarendon Press, Oxford.

Hunter, R.J. and Ekdawi, N., (1986), Colloids and Surfaces, <u>18</u>, 325.

Hunter, R.J. and Frayne, J., (1980), J. Colloid Interface Sci., <u>15</u>, 589.

Hunter, R.J., Neville, P.C., and Firth, B.A., (1975), ACS Symposium Series, <u>9</u>, 193.

Hunter, R.J. and Nicol, S.K., (1968), J. Colloid Interface Sci., <u>28</u>, 250.

Iler, R.K., (1979), "The Chemistry of Silica," Wiley-Interscience, New York.

Iler, R.K., (1975), J. Colloid Interface Sci., <u>51</u>, 388.

Israelachvili, J.N. and Ninham, B.W., (1977), J. Colloid Interface Sci., <u>58</u>, 14.

Israelachivili, J.N. and Pasley, R.M., (1983), Nature <u>306</u>, 249.

Israelachivili, J.N. and Pasley, R.M., (1982), Nature <u>300</u>, 341.

Jenkel, E., Rumbach, B., (1951), Z. Electro Chem., <u>55</u>, 612.

Jullien, R. and Kolb, M., (1984a), J. Phys. A <u>17</u>, 2639.

Jullien, R., Kolb, M., and Botet, R., (1984b) in "Kinetics of Aggregation and Gelation," Ed F. Family and D.P. Landau, Elsevier/North-Holland, Amsterdam, p. 101.

Kato, T., Nakamura, N., Kawaguchi, M., and Takahashi, A., (1981), Polymer J., <u>13</u>, 1037.

Keefer, K.D., (1984), in "Better Ceramics Through Chemistry," Ed., C.J., Brinker, D.E. Clark, and D.R. Ulrich, MRS Symposia Proceedings, Vol. 52, North-Holland, New York, p. 15.

Keefer, K.D. and Schaefer, D.W., (1986), Phys. Rev. Lett., 56, 2376.

Khadilkar, C.S. and Sacks, M.D., (1988), Ceramic Transactions, Vol. 1, Part A, p. 397.

Killmann, E., (1976), Croat. Chem. Acta, 48, 463.

Killmann, E. and Eckart, R., (1971), Makromol. Chem., 144, 45.

Killmann, E., Eisenlauer, J., and Korn, M., (1977), J. Polym. Sci., Polymer Symp., 61, 413.

Killmann, E., Maier, H., and Baker, J.A., (1988), Colloids and Surfaces, 31, 51.

Killmann, E., Maier, H., Kaniut, P., and Gutling, N., (1985), Colloids and Surfaces, 15, 261.

Killmann, E., Wild, Th., Gutling, N., and Maier, H., (1986), Colloids and Surfaces, 18, 241.

Kiselev, A.V. and Lygin, V.I., (1975), "Infrared Spectra of Surface Compounds," Halsted Press, Wiley and Sons, New York, Toronto.

Klein, J., (1980), Nature, (London), 288, 248.

Klein, J., (1982), Adv. Colloid Interface Sci., 16, 101.

Kolb, M., Botet, R., and Jullien, (1983), J., Phys. Rev. Lett., 51, 1123.

Koopal, L.K., (1978), Thesis, Agricultural University, Wageningen.

Koopal, L., (1981), J. Colloid Interface Sci., 83, 116.

Korn, M., Killmann, E., and Eisenlauer, J., Colloid Interface Sci., (1980a), 76, 7.

Korn, M., Killmann, E., and Eisenlauer, J., Colloid Interface Sci., (1980b), 76, 19.

Kreiger, I.M. and O'Neill, F.M., (1968), J. American Chemical Society, 90:12, 3114.

Kreiger, I.M., (1972), Adv. Colloid Interface Sci., 3, 111.

Krieger, I.M. and Dougherty, T.J., (1959), J. Trans. Soc. Rheol., 3, 137.

Kuhn, W., (1934), Kolloid-Z. <u>68</u>, 2.

Kurata, M., Tsunashima, Y., Iwama, M., and Kamda, K., (1975), in "Polymer Handbook," Ed. J. Brandrup and E.H. Immergut, J. Wiley and Sons, New York.

Laible, R. and Hamann, K., (1980), Adv. Colloid Interface Sci., <u>13</u>, 65.

Lambe, R., Tadros, Th.F., and Vincent, B., (1978), J. Colloid Interface Sci., <u>66</u>, 77.

Levine, S., Thomlinson, M.L., and Robinson, K., (1978), Faraday Disc. Chem. Soc., <u>65</u>, 202.

Leyrvaz, F., (1984), in "Kinetics of Aggregation and Gelation," Ed. F. Family and D.P. Landau, Elsevier/North-Holldan, Amsterdam, p. 201.

Long, J.A., Osmond, D.W.J., and Vincent, B., (1973), J. Colloid Interface Sci., <u>42</u>, 545.

Lubetkin, S., (1988) Colloids and Surfaces, <u>31</u>, 203.

Lyklema, J., (1968), Adv. Colloid Interfac Sci., <u>2</u>, 65.

Lyklema, J., (1985) in "Flocculation Sedimentation and Consolidation," Ed. by B.M. Moudgil and P. Somasundaran, P. 3.

Mackor, J., (1951), J. Colloid Sci., <u>6</u>, 942.

Mall, S. and Russel, W.B., (1987), J. Rheology, <u>31</u>, 651.

Mandelbrot, B.B., (1982), "The Fractal Geometry of Nature," Freeman, New York.

Matijevic, E., Bundnick, M., and Meites, L., (1977), J. Colloid Interface Sci., <u>61</u>, 302.

Meakin, P., (1983a), Phys. Rev. A., <u>27</u>, 1495.

Meakin, P., (1983b), Phys. Rev. Lett., <u>51</u>, 1119.

Meakin, P., (1984), in "Kinetics of Aggregatin and Gelation," Ed. F. Family and D.P. Landau, Elsevier/North-Holland, Amsterdam, p. 91.

Meakin, P., (1985), J. Chem. Phys. <u>83</u>, 3645.

Meakin, P., (1986), J. Colloid Interface Sci., <u>112</u>, 187.

Meier, D.J., (1967), J. Phys. Chem., 71, 1861.

Menold, R., Luttge, B., and Kaiser, W., (1976), Adv. Colloid Interface Sci., 5, 281.

Mewis, J. and Spaull, A.J.B., (1976), Adv. Colloid and Interface Sci., 6, 173 (and references contained therein).

Michaels, A.S. and Bolger, J.C., (1962), Ind. Eng. Chem. Fund., 1, 3, 153.

Mooney, M., (1951), J. Colloid Sci., 6, 162.

Moudgil B.M. and Cheng, Y.C., (1986), in "Ceramic Chemical Processing," Ed. L.L. Hench and D.R. Ulrich, Wiley-Interscience, New York, p. 550.

Nagy, D.J., (1986), J. Polymer Science, Part C, Polymer Letters, 24, 87.

Napper, D.H., (1977), J. Colloid Interface Sci., 58, 390.

Napper, D.H., (1983), "Polymeric Stabilization of Colloidal Particles," Academic Press, London.

Neville, P.C. and Hunter, R.J., (1974), J. Colloid Interface Sci., 49, 204.

Ohtsuki, T., Kishimoto, A., Mitaku, S., and Okano, K., (1981), Jpn. J. Appl. Phys., Vol. 20, 3, 509.

Ottewill, R.H. and Walker, T., (1968), Kolloid Z.Z. Polym., 227, 108.

Overbeek, J.Th.G., (1952), "Colloid Science," Ed., H.R. Kruyt, Vol. 1, Elsevier, Amsterdam, p. 278.

Overbeek, J.Th.G., (1982a), Adv. Colloid Interface Sci., 15, 251.

Overbeek, J.Th.G., (1982b), Adv. Colloid Interface Sci., 16, 17.

Pashley, R.M., Belvuschek, P., Muller M.M., Muller, M.R., and Konig, R., (1982), Colloid and Polymer Science, 260, 444.

Pashley, R.M. and Quirke, J.P., (1984), Colloids and Surfaces, 9, 1.

Pietronero, L. and Tosattig, E., (1986), Ed., "Fractals in Physics," North-Holland, Amsterdam, Oxford, New York, Tokyo.

Priel, Z. and Silberberg, A., (1978), J. Polymer Sci., Polymer Physics, Ed. 16, 1917.

Pritchard, J.G., (1970), "Poly (vinyl alcohol), Basic Properties and Uses," Gorden and Breach Science Publication, London.

Reerink, H. and Overbeek, J.Th.G., (1954), Disc. Faraday Soc., 18, 74.

Richmond, P. and Lal, M., (1974), Chem. Phys. Lett., 24, 594.

Robb, I.D. and Smith, R., (1974), Eur. Poly. J., 10, 1005.

Roe, R.J., (1974), J. Chem. Phys. 60, 4192.

Rowland, F.W. and Eirich, F.R., (1966), J. Polymer Sci., A14, 2033, 2401.

Rubio, J. and Kitchner, J.A., (1976), J. Colloid Interface Sci., 57, 132.

Ruehrwein, R.A. and Ward, D.W., (1952), Soil Science, 73, 485.

Russel, W.B., (1980), J. of Rheology, 24, 287.

Sacks, M.D. and Tseng, T.Y., (1984), J. Am. Ceram. Soc., 67 (8), 526.

Sacks, M.D., Khadilkar, C.S., Scheiffele, G.W., Shenoy, A.W., Dow, J.H., and Sheu, R.S., (1987), in "Ceramic Powder Science Advances in Ceramics," Vol. 21, Ed., G.L. Messing, K.S. Mazdiyasni, J.W., McCauley, and R.A. Haber, p. 495.

Sanders, L.M., (1986), Nature, 332, 780.

Sato, T. and Ruch, R., (1980), "Stabilization of Colloidal Dispersions by Polymeric Adsorption," Dekker, New York.

Schaefer, D.W., Martin, J.E., Wiltzius, P., and Cannell, D.S., (1984), Phys. Rev. Lett., 52, 2371.

Scheutjeans, J.M.H.M, and Fleer, G.J., (1979), J. Phys. Chem., 83, 1619.

Scheutjeans, J.M.H.M, and Fleer, G.J., (1980), J. Phys. Chem., 84, 178.

Scheutjeans, J.M.H.M. and Fleer, G.J., (1985), Macromolecules, Vol. 18, 10, 1882.

Shinohira, T., Makishima, A., Kotoni, K., and Wakakuwa, M., (1978), in "Proceedings of the International Symposium of Factors in Densification and Sintering of Oxide and Non-Oxide Ceramics," Ed. S. Somiya and S. Saito, Tokyo Institute of Technology, Tokyo, Japan.

Silberberg, A., (1962), J. Phys. Chem., 66, 1884.

Silberberg, A., (1967), J. Phys. Chem., 46, 1105.

Silberberg, A., (1968), J. Chem. Phys., 48, 2835.

Smellie, R.H. and La Mer, V.K., (1958), J. Colloid Sci., 13, 589.

Smitham, J.B. and Napper, D.H., (1979), Colloid Polymer Sci., 257, 748.

Snook, I.K. and Van Megen, W., (1982), Adv. Colloid Interface Sci., 17, 33.

Sonntag, R.C. and Russel, W.B., (1987), J. Colloid Interface Sci., 115, 378.

Sonntag, H., Ehmke, B., Miller, R., and Knapschinsky, L., (1982), in "The Effect of Polymers on Dispersion Properties," Ed. Th.F. Tadros, Academic Press, London, New York, p. 207.

Stober, W., Fink, A., and Bohn, E., (1968), J. Colloid Interface Sci., 26, 62.

Stockmayer, W.H. and Fixman, M.J., (1963), J. Poly. Sci., Part C, 1, 137.

Stone-Masui, J. and Watillon, A., (1968), J. Colloid Interface Sci., 28, 187.

Sugimoto, T., (1987), Adv. Colloid Interface Sci., 28, 65.

Tadros, Th.F., (1984) in "Polymer Adsorption and Dispersion Stability," Ed. E.D. Goddard and B. Vincent, ACS Symposium Series 240, p. 411.

Tadros, Th. F., (1978), J. Colloid Interface Sci., 64, 36.

Tadros, Th.F., (1980), Adv. Colloid Interface Sci., 12, 141.

Tadros, Th.F., (1982), in "The Effect of Polymers on Dispersion Properties," Ed. Th.F. Tadros, Academic Press, London, p. 1.

Tadros, Th.F., (1985), Progr. Colloid Polymer Sci., 70, 101.

Tadros, Th.F., (1986), Colloids and Surfaces, 18, 137.

Tadros, Th.F. and Vincent, B., (1979), J. Colloid Interface Sci., 72, 505.

Takahashi, A., Kawaguchi, M., Hirota, M., and Kato, T., (1980),

Takahashi, A., Kawaguchi, M., Hirota, M., and Kato, T., (1980), Macromolecules, 13, 884.

Takano, K. and Hachisu, S., (1978), J. Colloid Interface Sci., 66, 124.

Tan, C.G., Bowen, B.D., and Epstein, N., (1987), J. Colloid Interface Sci., 118, 290.

Thomas, D.G., (1965), J. Colloid Sci., 20, 267.

Tomita, M., Takano, K., and Vande ven, T.G.M., (1983), J. Colloid Interface Sci., 92, 367.

van den Boomgaard, Th., King, T.A., Tadros, Th.F., Tang, H. and Vincent, B., (1978) J. Colloid Interface Sci., 66, 68.

Van de Ven, T.G.M. and Hunter, R.J., (1979), Rheol. Acta., 16, 534.

Van de Ven, T.G.M. and Mason, S.G., (1976), J. Colloid Interface Sci., 57, 505, 517.

Van Megen, W. and Snook, I., (1984), Adv. Colloid Interface Sci., 21, 119.

Van Helden, A.K., Jansen, J.W., and Vrij, A., (1981), J. Colloid Interface Sci., 81, 354.

vander Linden C. and van Leemput, R., (1978), J. Colloid Interface Sci., 67, 48.

Vanderhoff, J.W., Van Den Hul, H.J., Taask, R.M.J., and Overbeek, J.Th.G., (1970), in "Clean Surfaces," Ed., G. Goldginger, Dekker, New York, p. 15.

Verwey, E.J.W. and Overbeek, J.Th.G., (1948), in "Theory of the Stability of Lyophobic Colloids," Elsevier, Amsterdam.

Vicsek, T. and Family, F., (1984), in "Kinetics of Aggregation and Gelation," Ed. F. Family and D.P. Landau, Elsevier/North-Holland, Amsterdam, p. 111.

Vincent B., (1974), Adv. Colloid Interface Sci., 4, 193.

Vincent, B., (1982) in "The Effect of Polymers of Dispersion Stability," Ed. Th. F. Tadros, Academic Press, p. 183.

Vincent, B. and Whittington, S., (1981), in "Surface and Colloid Science," Vol. 12, Plenum Press, New York, p. 1.

Visser, J., (1972), Adv. Colloid Interface Sci., 3, 331.

433

Silberberg, A., (1962), J. Phys. Chem., 66, 1884.

Silberberg, A., (1967), J. Phys. Chem., 46, 1105.

Silberberg, A., (1968), J. Chem. Phys., 48, 2835.

Smellie, R.H. and La Mer, V.K., (1958), J. Colloid Sci., 13, 589.

Smitham, J.B. and Napper, D.H., (1979), Colloid Polymer Sci., 257, 748.

Snook, I.K. and Van Megen, W., (1982), Adv. Colloid Interface Sci., 17, 33.

Sonntag, R.C. and Russel, W.B., (1987), J. Colloid Interface Sci., 115, 378.

Sonntag, H., Ehmke, B., Miller, R., and Knapschinsky, L., (1982), in "The Effect of Polymers on Dispersion Properties," Ed. Th.F. Tadros, Academic Press, London, New York, p. 207.

Stober, W., Fink, A., and Bohn, E., (1968), J. Colloid Interface Sci., 26, 62.

Stockmayer, W.H. and Fixman, M.J., (1963), J. Poly. Sci., Part C, 1, 137.

Stone-Masui, J. and Watillon, A., (1968), J. Colloid Interface Sci., 28, 187.

Sugimoto, T., (1987), Adv. Colloid Interface Sci., 28, 65.

Tadros, Th.F., (1984) in "Polymer Adsorption and Dispersion Stability," Ed. E.D. Goddard and B. Vincent, ACS Symposium Series 240, p. 411.

Tadros, Th. F., (1978), J. Colloid Interface Sci., 64, 36.

Tadros, Th.F., (1980), Adv. Colloid Interface Sci., 12, 141.

Tadros, Th.F., (1982), in "The Effect of Polymers on Dispersion Properties," Ed. Th.F. Tadros, Academic Press, London, p. 1.

Tadros, Th.F., (1985), Progr. Colloid Polymer Sci., 70, 101.

Tadros, Th.F., (1986), Colloids and Surfaces, 18, 137.

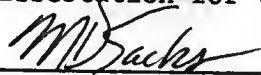Tadros, Th.F. and Vincent, B., (1979), J. Colloid Interface Sci., 72, 505.

Takahashi, A., Kawaguchi, M., Hirota, M., and Kato, T., (1980), Macromolecules, 13, 884.

Takano, K. and Hachisu, S., (1978), J. Colloid Interface Sci., 66, 124.

Tan, C.G., Bowen, B.D., and Epstein, N., (1987), J. Colloid Interface Sci., 118, 290.

Thomas, D.G., (1965), J. Colloid Sci., 20, 267.

Tomita, M., Takano, K., and Vande ven, T.G.M., (1983), J. Colloid Interface Sci., 92, 367.

van den Boomgaard, Th., King, T.A., Tadros, Th.F., Tang, H. and Vincent, B., (1978) J. Colloid Interface Sci., 66, 68.

Van de Ven, T.G.M. and Hunter, R.J., (1979), Rheol. Acta., 16, 534.

Van de Ven, T.G.M. and Mason, S.G., (1976), J. Colloid Interface Sci., 57, 505, 517.

Van Megen, W. and Snook, I., (1984), Adv. Colloid Interface Sci., 21, 119.

Van Helden, A.K., Jansen, J.W., and Vrij, A., (1981), J. Colloid Interface Sci., 81, 354.

vander Linden C. and van Leemput, R., (1978), J. Colloid Interface Sci., 67, 48.

Vanderhoff, J.W., Van Den Hul, H.J., Taask, R.M.J., and Overbeek, J.Th.G., (1970), in "Clean Surfaces," Ed., G. Goldginger, Dekker, New York, p. 15.

Verwey, E.J.W. and Overbeek, J.Th.G., (1948), in "Theory of the Stability of Lyophobic Colloids," Elsevier, Amsterdam.

Vicsek, T. and Family, F., (1984), in "Kinetics of Aggregation and Gelation," Ed. F. Family and D.P. Landau, Elsevier/North-Holland, Amsterdam, p. 111.

Vincent B., (1974), Adv. Colloid Interface Sci., 4, 193.

Vincent, B., (1982) in "The Effect of Polymers of Dispersion Stability," Ed. Th. F. Tadros, Academic Press, London, p. 183.

Vincent, B. and Whittington, S., (1981), in "Surface and Colloid Science," Vol. 12, Plenum Press, New York, p. 1.

Visser, J., (1972), Adv. Colloid Interface Sci., 3, 331.

Vold, M.J., (1961), J. Colloid Sci., 16, 1.

Vold, M.J., (1963), J. Colloid Sci., 18, 684.

von Smoluchowski, M., (1916a), Physik. Z. 17, 557, 585.

Von Smoluchowski, M., (1916b), Kolloid-Z., 18, 190.

von Smoluchowski, M., (1917), Z. Phys. Chem., 92, 129.

Walles, W.E., (1968), J. Colloid Interface Sci., 27, 797.

Weitz, D.A. and Olivera, M., (1984), Phys. Rev. Lett., 52, 1433.

Weitz, D.A., Huang, J.S., Lin, M.Y., and Sung, J., (1985), Phys. Rev. Lett., 54, 1416.

Whitten, T.A. and Sander, L.M., (1981), Phys. Rev. Lett., 47, 1400.

Wiersma, P.H., Loeb, A.L., and Overbeek, J.Th.G., (1966), J. Colloid Interface Sci., 22, 78.

Wong, K., Cobane, B., and Somasundaran, (1988a), Colloids and Surfaces, 30, 355.

Wong, K., Cabane, B., and Duplessix, R., (1988b), J. Colloid Interface Sci., 123, 466.

Yamakawa, H., (1971), "Modern Theory of Polymer Solutions," Harper and Row, New York.

Yoshimura, S. and Hachisu, S., (1983), Progr. Colloid and Polymer Sci., 68, 59.

Zeichner, G.R. and Schowalter, (1977), AIChE. J., 23, 243.

Ziff, R.M., (1984), in "Kinetics of Aggregation and Gelation," Ed. F. Family and D.P. Landau, Elsevier/North-Holland, Amsterdam, p. 191.

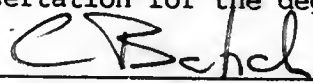Zwick, M.M., (1965), J. App. Polymer Science, 9, 2393.

BIOGRAPHICAL SKETCH

Chandrashekhar Sandanand Khadilkar was born in Pune, India, on July 27, 1959. He received his elementary and high school education at M.E.S. High School, Pune, India. He entered the Indian Institute of Technology, Bombay, India, in July 1976 and received the Bachelor of Technology in Metallurgical Engineering. He joined the University of Florida in August 1981 and received Master of Science in Materials Science in 1984. He married Dr. Vidula Paranjpe in September 1985. He will be joining industry as a ceramic research engineer.
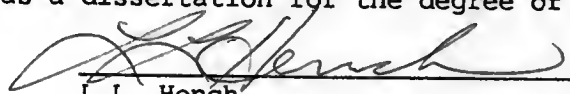
I certify that I have read this study and that in my opinion it conforms to acceptable standards of scholarly presentation and is fully adequate, in scope and quality, as a dissertation for the degree of Doctor of Philosophy.

Michael D. Sacks, Chairman
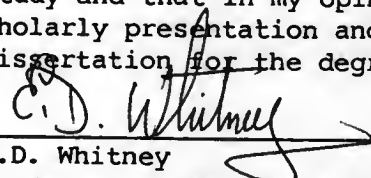Associate Professor of Materials
Science and Engineering

I certify that I have read this study and that in my opinion it conforms to acceptable standards of scholarly presentation and is fully adequate, in scope and quality, as a dissertation for the degree of Doctor of Philosophy.

C.D. Batich
Professor of Materials Science
and Engineering

I certify that I have read this study and that in my opinion it conforms to acceptable standards of scholarly presentation and is fully adequate, in scope and quality, as a dissertation for the degree of Doctor of Philosophy.

L.L. Hench
Graduate Research Professor of
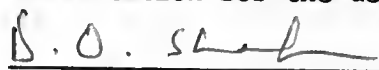Materials Science and Engineering

I certify that I have read this study and that in my opinion it conforms to acceptable standards of scholarly presentation and is fully adequate, in scope and quality, as a dissertation for the degree of Doctor of Philosophy.

E.D. Whitney
Professor of Materials Science
and Engineering

I certify that I have read this study and that in my opinion it conforms to acceptable standards of scholarly presentation and is fully adequate, in scope and quality, as a dissertation for the degree of Doctor of Philosophy.

D.O. Shah
Professor of Chemical Engineering

This dissertation was submitted to the Graduate Faculty of the College of Engineering and to the Graduate School and was accepted as partial fulfillment of the requirements for the degree of Doctor of Materials Science and Engineering.

December, 1988

Hubert C. Bever

Dean, College of Engineering

_____

Dean, Graduate School